N/0002653--063

Model Evaluation Report for Corrective Action Unit 97: Yucca Flat/Climax Mine, Nevada National Security Site, Nye County, Nevada

Revision No.: 1

July 2019

Prepared for U.S. Department of Energy under Contract No. DE-NA0002653.

Approved for public release; further dissemination unlimited.

Available for sale to the public from:

U.S. Department of Commerce
National Technical Information Service
5301 Shawnee Road
Alexandria, VA 22312
Telephone: 800.553.6847
Fax: 703.605.6900
E-mail: *orders@ntis.gov*
Online Ordering: *http://www.ntis.gov/help/ordermethods.aspx*

Available electronically at *http://www.osti.gov/scitech*

Available for a processing fee to U.S. Department of Energy and its contractors, in paper, from:

U.S. Department of Energy
Office of Scientific and Technical Information
P.O. Box 62
Oak Ridge, TN 37831-0062
Phone: 865.576.8401
Fax: 865.576.5728
Email: *reports@adonis.osti.gov*

Reference herein to any specific commercial product, process, or service by trade name, trademark, manufacturer, or otherwise, does not necessarily constitute or imply its endorsement, recommendation, or favoring by the United States Government or any agency thereof or its contractors or subcontractors.

Printed on recycled paper

N/0002653--063

MODEL EVALUATION REPORT FOR CORRECTIVE ACTION UNIT 97: YUCCA FLAT/CLIMAX MINE, NEVADA NATIONAL SECURITY SITE, NYE COUNTY, NEVADA

Revision No.: 1
July 2019
Navarro
c/o U.S. DOE
P.O. Box 98952
Las Vegas, NV 89193-8952

Prepared for U.S. Department of Energy under Contract No. DE-NA0002653.

Approved for public release; further dissemination unlimited.

MODEL EVALUATION REPORT FOR CORRECTIVE ACTION UNIT 97: YUCCA FLAT/CLIMAX MINE, NEVADA NATIONAL SECURITY SITE, NYE COUNTY, NEVADA

Approved by: /s/ Ken Rehfeldt Date: 07/16/2019

Ken Rehfeldt, UGTA Project Manager
Navarro

TABLE OF CONTENTS

List of Figures . . . vi
List of Tables . . . xv
List of Acronyms and Abbreviations . . . xvii

1.0 Introduction . . . 1-1

1.1 UGTA Strategy . . . 1-3
1.2 YF/CM Flow and Transport Model Background . . . 1-5
1.3 Classification Information . . . 1-7

2.0 Model Evaluation Data Collection . . . 2-1

2.1 Sampling LCA Completions for RNs . . . 2-2
2.1.1 Results Summary . . . 2-6
2.1.2 Historical Results . . . 2-10
2.1.3 WW C-1 . . . 2-11
2.1.3.1 Historical Results . . . 2-12
2.1.3.2 Potential Sources of ^{3}H In WW-C and WW C-1 . . . 2-14
2.1.4 Summary . . . 2-16
2.2 Interpreting Drilling Evidence from ER-2-2, ER-3-3, and ER-4-1 . . . 2-16
2.2.1 Evaluation of RNs Measured during Drilling . . . 2-18
2.2.2 ER-2-2 . . . 2-18
2.2.3 ER-3-3 . . . 2-20
2.2.4 ER-4-1 . . . 2-22
2.2.5 Permeability Estimates . . . 2-24
2.2.6 Summary . . . 2-26
2.3 Sampling Near-field Wells . . . 2-27
2.3.1 ER-3-3 . . . 2-27
2.3.2 ER-4-1 . . . 2-28
2.3.3 ER-7-1 . . . 2-29
2.3.4 U-3cn-5 . . . 2-31
2.3.5 UE-7nS . . . 2-34
2.3.6 Summary . . . 2-36
2.4 Sampling NASH Test Cavity at Satellite Well UE-2ce . . . 2-37
2.4.1 Historical Sampling . . . 2-38
2.4.2 Summary . . . 2-41
2.5 Performing WDT in the ER-4-1 LCA . . . 2-41
2.5.1 Summary . . . 2-44
2.6 Formalizing the ER-6-1-2 MWAT Reanalysis . . . 2-45
2.6.1 ER-6-1-2 MWAT . . . 2-45
2.6.2 Boundary Flow Estimation . . . 2-48
2.6.3 Yucca Flat Basin Flow Uncertainty Analysis . . . 2-49
2.6.3.1 NSMC Analysis . . . 2-51
2.6.3.2 Pareto-Based Hypothesis Testing Description . . . 2-52

TABLE OF CONTENTS (CONTINUED)

2.6.3.3 Comparison of Selected NSMC and Pareto Analyses Models to the Calibrated Model 2-56
2.6.3.4 DV3 Model Analysis of Flow Uncertainty Summary and Conclusions 2-59
2.6.4 Summary. 2-61
2.7 Evaluating ER-4-1 and Other Yucca Flat Groundwater Geochemistry 2-62
2.7.1 Predevelopment Hydraulic Heads in the LCA 2-67
2.7.2 Potential Sources of ER-4-1 Groundwater 2-67
2.7.2.1 Alkalinity versus pH 2-68
2.7.2.2 Calcium versus Sodium 2-68
2.7.2.3 Sulfate versus Chloride 2-70
2.7.2.4 Magnesium versus Potassium 2-70
2.7.2.5 δ^2H versus δ^{18}O 2-71
2.7.2.6 Carbon Isotopes 2-72
2.7.2.7 Summary Investigation of Source Area for ER-4-1 Groundwater 2-74
2.7.3 Downgradient Flow Paths from ER-4-1 2-74
2.7.3.1 Alkalinity versus pH 2-74
2.7.3.2 Calcium versus Sodium 2-75
2.7.3.3 Magnesium versus Potassium 2-76
2.7.3.4 Sulfate versus Chloride 2-77
2.7.3.5 δ^2H versus δ^{18}O 2-78
2.7.3.6 Carbon Isotopes 2-79
2.7.3.7 Estimating Effective Transport Porosity between ER-7-1 and ER-6-1-2 Based on ^{14}C 2-81
2.7.4 Summary. 2-82
2.8 Investigating LCA Surface Elevations 2-83
2.8.1 Summary. 2-87
2.9 Reviewing Historical Data for Detonations near or within the LCA 2-89
2.9.1 Exchange Volume Size and Shape 2-89
2.9.1.1 Phenomenology 2-90
2.9.1.2 Literature Review 2-93
2.9.2 Literature Review of Matrix Sorption Data for Cs and Sr in the LCA 2-96
2.9.3 Near-field ^{90}Sr and ^{137}Cs 2-98
2.9.4 Wells Drilled to the Saturated LCA 2-105
2.9.5 Containment Scientist Interviews. 2-106
2.9.6 Summary. 2-107

3.0 Model Evaluation Targets and Results 3-1

3.1 Basin Flux through Testing Area 3-1
3.1.1 Conclusions 3-2
3.2 Exchange Volume Size and Shape That Extends into the Saturated LCA. 3-2

TABLE OF CONTENTS (CONTINUED)

3.2.1 Exchange Volume Size and Shape 3-2
3.2.2 LCA Surface Uncertainty 3-3
3.2.3 Exchange Volume Intersecting the Saturated LCA 3-3
3.2.3.1 Identification of Detonations Intersecting the Saturated LCA 3-3
3.2.3.2 Estimating the Potential Impact on Transport from Identified Detonations 3-4
3.2.4 Conclusions 3-7
3.3 Extent of RN Contamination in the LCA 3-7
3.3.1 Conclusions 3-7
3.4 LCA Hydraulic Properties 3-8
3.4.1 Conclusions 3-12
3.5 ^{90}Sr and ^{137}Cs Mobility in the LCA 3-13
3.5.1 LCA Matrix Sorption of ^{90}Sr and ^{137}Cs. 3-16
3.5.2 Source Term Distribution Model 3-16
3.5.3 Conclusions 3-17
3.6 Fault Transport Properties 3-17
3.6.1 Conclusions 3-18
3.7 Permeability Anisotropy 3-19
3.7.1 Conclusions 3-20
3.8 Summary 3-21

4.0 Model Refinements 4-1

4.1 Introduction 4-2
4.2 Base Case Model Recalibration 4-4
4.2.1 Calibration Approach 4-4
4.2.2 Model Area and Mesh 4-6
4.2.3 Model Parameters 4-6
4.2.3.1 Pilot Points 4-8
4.2.3.2 Faults 4-8
4.2.3.3 Boundary Conditions 4-10
4.2.3.3.1 Estimated Boundary Flows 4-11
4.2.3.3.2 LCA Model Boundary Condition Assignments 4-11
4.2.3.4 Optimization “Super Parameters” 4-12
4.2.4 Observations Used for Model Calibration 4-13
4.2.4.1 Steady-State Water Levels and Gradients 4-14
4.2.4.2 ER-6-1-2 MWAT Pumping Responses 4-15
4.2.4.3 ER-4-1 WDT Pumping Responses 4-18
4.2.4.4 Transmissivity Measurements 4-18
4.2.4.5 Transmissivity Width Product Flux 4-21
4.2.4.6 Objective Function Formulation 4-21
4.2.5 Calibration Results 4-24

TABLE OF CONTENTS (CONTINUED)

4.2.5.1 Agreement with Observations 4-24
4.2.5.1.1 Steady-State Head and Gradient 4-25
4.2.5.1.2 ER-6-1-2 MWAT and ER-4-1 WDT Responses 4-28
4.2.5.1.3 Transmissivity 4-28
4.2.5.2 Calibrated Model Parameters 4-33
4.2.5.3 Calibrated Model Flow Paths 4-40
4.3 LCA Flow Model Uncertainty Analysis 4-43
4.3.1 Introduction 4-43
4.3.2 Alternative Flow Models with Extensive Transport 4-46
4.3.2.1 40-kg/s Basin Flux 4-46
4.3.2.2 High-K Yucca Fault 4-46
4.3.3 Global Uncertainty Analysis 4-50
4.3.4 LCA Flow Model Uncertainty Analysis Conclusions 4-74
4.4 Evaluation of Transient Pumping in Wells WW-C and WW C-1 on Transport 4-77
4.5 LCA Flow Modeling Summary and Conclusions. 4-79
4.6 LCA Model HST 4-82
4.6.1 HST Allocation to the LCA Model 4-83
4.6.2 NASH Source Term 4-87
4.7 Contaminant Boundary Forecasts 4-88
4.7.1 Transport Conceptual Model 4-89
4.7.2 Numerical Model Approach 4-89
4.7.3 Transport Parameters 4-91
4.7.3.1 Fracture Porosity 4-92
4.7.3.2 Fracture Aperture 4-95
4.7.3.3 Matrix Porosity 4-97
4.7.3.4 Matrix Diffusion Coefficient Parameters (Matrix Tortuosity and Free-Water Diffusion Coefficients) 4-100
4.7.3.5 Dispersivity 4-102
4.7.3.6 Fracture Retardation 4-102
4.7.3.7 Matrix Sorption 4-102
4.7.4 Results 4-102
4.7.4.1 LCA Flow Model Base Case Contaminant Boundary . . . 4-105
4.7.4.2 Comparison of LCA Flow Model Base Case with 2013 Base Case 4-111
4.7.4.3 Comparison of LCA Flow Model Base Case with Alternative Cases 4-111
4.7.4.4 Comparison of the Extents of Contamination Forecasted by the Model with Present Time Observations 4-121
4.7.4.5 CB Forecasts 4-122

TABLE OF CONTENTS (CONTINUED)

4.8 Transport Modeling Summary and Conclusions 4-127

5.0 Model Evaluation Team Recommendations 5-1

5.1 Model Refinements 5-2
5.2 Additional CADD/CAP Data Collection 5-4
5.3 Advancement to Closure Stage 5-4

6.0 PER Committee Recommendations 6-1

6.1 Background 6-1
6.2 Recommendations 6-2

7.0 References 7-1

Appendix A - Well Completion Diagrams and Tritium/Water Production Logs for Model Evaluation Wells

A.1.0 Well Completion Diagrams and Tritium/Water Production Logs for Model Evaluation Wells A-1

Appendix B - Nevada Division of Environmental Protection Comments

LIST OF FIGURES

NUMBER	TITLE	PAGE
1-1	UGTA Strategy Flowchart	1-4
1-2	Process Flow Diagram for CADD/CAP Model Evaluation Process	1-6
2-1	LCA Sampling Locations and Types	2-3
2-2	WW C-1 and WW-C ^{3}H Results (1964 to 2018)	2-13
2-3	Locations of Model Evaluation Wells and Detonations Potentially Intersecting the Saturated LCA	2-17
2-4	ER-2-2 Location with Respect to CALABASH Crater, Cavity, and Chimney	2-20
2-5	ER-3-3 Location with Respect to WAGTAIL Cavity and Chimney	2-21
2-6	ER-4-1 Location with Respect to STRAIT Crater, Cavity, and Chimney	2-23
2-7	Perspective View of STRAIT, ROUSANNE, TECHADO, and TOPGALLANT Detonations ($3R_c$) and Well ER-4-1	2-24
2-8	Field Water-Quality Measurements during ER-3-3 Pumping	2-28
2-9	Perspective View of TORRIDO and MICKEY ($2R_c$) Detonations and Well ER-7-1	2-30
2-10	Perspective View of BILBY Detonation ($2R_c$) and Wells U-3cn 5 and U-3cn PS 2	2-32
2-11	U-3cn-5 ^{3}H Results (1961 to 2018)	2-33
2-12	Perspective View of BOURBON Detonation ($2R_c$) and Nearby Observations Wells	2-35
2-13	RN Activities Relative to MCLs at Well UE-7nS	2-36
2-14	Perspective View of NASH Detonation ($2R_c$) and Well UE-2ce	2-38
2-15	Activity Relative to MCL for UE-2ce Samples	2-39
2-16	Plot of UE-2ce ^{3}H, ^{90}Sr, and ^{137}Cs Activities (1976 to 2016)	2-40
2-17	Activity Relative to ^{3}H for UE-2ce Samples (1976 to 2016)	2-40

LIST OF FIGURES (CONTINUED)

NUMBER	TITLE	PAGE
2-18	Pumping and Observation Wells for ER-4-1 WDT	2-43
2-19	Pumping and Observation Wells, Simulated Water-Level Contours, and Transmissivity and Physiographic Features	2-46
2-20	Simulated Transmissivity and Groundwater Flow Estimates	2-50
2-21	NSMC Model Objective Function Values before and after Null Space Adjustment	2-52
2-22	DV3 Model Objective Function versus Eastern Yucca Flat Flow from the NSMC Analysis	2-53
2-23	Pareto Front as (A) Objective Functions and as (B) Multipliers of Base Case Objective Function and Eastern Yucca Flat Flow for a 5-Times Flow Increase	2-54
2-24	Pareto Front as (A) Objective Functions and as (B) Multipliers of Base Case Objective Function and Eastern Yucca Flat Flow for a 5-Times Flow Decrease	2-55
2-25	Selected Drawdowns from the ER-6-1-2 MWAT for the Calibrated Model (1st column) and Flow Increase Pareto Iteration 11 (2nd column)	2-57
2-26	Selected Drawdowns from the ER-6-1-2 MWAT NSMC Realization 42 (1st column) and Flow Decrease Pareto Iteration 6 (2nd column)	2-58
2-27	LCA Flow near Yucca Flat from the NSMC/Pareto Analyses Uncertainty Models (A = Calibrated model, B = Flow increase Pareto iteration 11, C = NSMC realization 42, D = Flow increase Pareto iteration 6)	2-60
2-28	Expected and Simulated Water Budgets for the Calibrated Model	2-61
2-29	Estimated and Simulated Water Budgets for NSMC Realization 42 Model	2-62
2-30	Estimated and Simulated Water Budgets for the Pareto Analysis Flow Increase Iteration 11 Model	2-62
2-31	Expected and Simulated Water Budgets for the Pareto Analysis Flow Decrease Iteration 6 Model	2-63
2-32	Geochemistry Sampling Locations	2-65
2-33	Potentiometric Contours and Inferred Flow Paths	2-66
2-34	Alkalinity versus pH for Potential ER-4-1 Groundwater Source Area Wells	2-69

LIST OF FIGURES (CONTINUED)

NUMBER	TITLE	PAGE
2-35	Calcium versus Sodium for Potential ER-4-1 Groundwater Source Area Wells	2-69
2-36	Sulfate versus Chloride for Potential ER-4-1 Groundwater Source Area Wells	2-70
2-37	Magnesium versus Potassium for Potential ER-4-1 Groundwater Source Area Wells	2-71
2-38	δ^2H versus δ^{18}O for Potential ER-4-1 Groundwater Source Area Wells	2-72
2-39	δ^{13}C versus Alkalinity for Potential ER-4-1 Groundwater Source Area Wells	2-73
2-40	Carbon Isotopes for Potential ER-4-1 Groundwater Source Area Wells	2-73
2-41	Alkalinity versus pH for ER-4-1 and Other LCA and LCA3 Wells	2-75
2-42	Calcium versus Sodium for ER-4-1 and Other LCA and LCA3 Wells	2-76
2-43	Magnesium versus Potassium for ER-4-1 and Other LCA and LCA3 Wells	2-77
2-44	Sulfate versus Chloride for ER-4-1 and Other LCA and LCA3 Wells	2-78
2-45	δ^2H versus δ^{18}O for ER-4-1 and Other LCA and LCA3 Wells	2-79
2-46	δ^{13}C versus Alkalinity for ER-4-1 and Other LCA and LCA3 Wells	2-80
2-47	Carbon Isotopes for ER-4-1 and Other LCA and LCA3 Wells	2-80
2-48	Measured Data Used for Estimating LCA/LCA3 Surface Uncertainty	2-85
2-49	Total Surface Variability of 100 LCA/LCA3 Surfaces at Each Detonation Location	2-88
2-50	Histogram Showing Variability in Top of LCA/LCA3 at Each Detonation Location	2-89
2-51	Schematic Diagram for Geometry of Detonation-Altered Zones	2-92
2-52	K_d Distributions for ^{90}Sr and ^{137}Cs in Carbonate Mineral	2-96
2-53	Initial ^{3}H, ^{90}Sr, ^{137}Cs Activities Relative to MCL	2-104
3-1	Location of Detonations Potentially within $3R_c$ of the Saturated LCA/LCA3	3-6

LIST OF FIGURES (CONTINUED)

NUMBER	TITLE	PAGE
3-2	Transmissivity Plotted against the Open Interval Depth Range for LCA Detonations in Yucca Flat and Vicinity	3-10
3-3	Hydraulic Conductivity Plotted against Well Screen Length for LCA Detonations in Yucca Flat and Vicinity	3-12
3-4	Time-Cumulative Probability of MCL Exceedance for LCA Sources: (a) Base Case and (b) Alternative Matrix Sorption for Sr, Cs, C, and Ni	3-14
3-5	Fractional Exceedance Volume for LCA Sources Base Case and Alternative with Matrix Sorption for Sr, Cs, C, and Ni	3-15
4-1	Areal Extent and Faults Included in the LCA Flow Model	4-7
4-2	LCA Flow Model Pilot Point Locations	4-9
4-3	LCA Model Domain Boundary Locations, Permissible Ranges, and DV3 Predicted Flows	4-13
4-4	Hydraulic Heads at LCA Observation Wells in Yucca Flat	4-16
4-5	ER-6-1-2 MWAT Estimated Drawdowns for Wells ER-7-1, UE-7nS, ER-3-1-2, and U-3cn-5	4-17
4-6	Locations of Wells within Yucca Flat Evaluated for Possible Responses to the ER-4-1 WDT Pumping	4-19
4-7	ER-4-1-2 WDT Estimated Drawdowns for Wells ER-6-1-2, ER-7-1, U-3cn-5, UE-7nS, and WW-2	4-20
4-8	Transmissivity Measurements within the Yucca Flat LCA	4-22
4-9	Yucca Flat LCA Potentiometric Surface and Steady-State Head Residuals for the Base Case Flow Field	4-26
4-10	Modeled versus Measured Steady-State Heads for the Base Case Flow Field	4-27
4-11	Western and Eastern Yucca Flat Water-Level Profiles for the Base Case Flow Field	4-27
4-12	Simulated and Observed Drawdown Hydrographs at the Responding ER-6-1-2 MWAT Wells for the Base Case Flow Field	4-29

LIST OF FIGURES (CONTINUED)

NUMBER	TITLE	PAGE
4-13	Simulated and Observed Drawdown Hydrographs at the Responding ER-4-1 WDT Wells for the Base Case Flow Field	4-30
4-14	Modeled versus Measured ER-4-1 WDT Drawdowns for the Base Case Flow Field	4-31
4-15	Modeled versus Measured ER-6-1-2 MWAT Drawdowns for the Base Case Flow Field	4-31
4-16	Calibrated LCA Model Transmissivity Field with Observation Values for the Base Case Flow Field	4-32
4-17	Identifiability Index for Independent Parameters: (A) All Parameters and (B) Parameters with Identifiability Index Greater than or Equal to 0.5 for the Base Case Flow Field	4-34
4-18	Identifiability of Country Rock Hydraulic Conductivity and Specific Storage Pilot Points for the Base Case Flow Field	4-35
4-19	Cumulative Distribution Function of Calibrated Country Rock Pilot Point Hydraulic Conductivity for the Base Case Flow Field	4-36
4-20	Calibrated LCA and DV3 Model Transmissivity Comparison for the Base Case Flow Field	4-38
4-21	Travel Paths and Times from Particle Originating on the Model's Upper Perimeter for the Base Case Flow Field	4-41
4-22	Velocity Vectors at 0 m amsl for the Base Case Flow Field	4-42
4-23	Travel Paths and Times from Particle Originating at the 58 Detonations Included in LCA Flow and Transport Model for the Base Case Flow Field	4-44
4-24	Cumulative Particle Breakthrough near the LCA Model's Southern Boundary for the Base Case	4-45
4-25	Yucca Flat LCA Potentiometric Surface and Steady-State Head Residuals for a 40-kg/s Transmissivity-Width Flux Flow Field	4-47
4-26	Transmissivity Fields for a 40-kg/s Transmissivity-Width Flux Flow Field	4-48

LIST OF FIGURES (CONTINUED)

NUMBER	TITLE	PAGE
4-27	Travel Paths and Times from Particle Originating at the 58 Detonations Included in LCA Flow and Transport Model for a 40-kg/s Transmissivity-Width Flux Flow Field	4-49
4-28	Yucca Flat LCA Potentiometric Surface and Steady-State Head Residuals for a High-K Yucca Fault Flow Field	4-51
4-29	Transmissivity Fields for a High-K Yucca Fault Flow Field	4-52
4-30	Travel Paths and Times from Particle Originating at from the 58 Detonations Included in LCA Flow and Transport Model for a High-K Yucca Fault Flow Field	4-53
4-31	Western and Eastern Yucca Flat Water-Level Profiles for NSMC Model 99	4-56
4-32	Simulated and Observed Drawdown Hydrographs at the Responding ER-6-1-2 MWAT Wells for NSMC Model 99	4-57
4-33	Simulated and Observed Drawdown Hydrographs at the Responding ER-4-1 WDT Wells for NSMC Model 99	4-58
4-34	Calibrated Objective Functions (Sorted) for the NSMC Models	4-59
4-35	Flow through the Yucca Flat Sub-Basin for the NSMC Models	4-59
4-36	Mean Fault and Country Rock Hydraulic Conductivity for the NSMC Models	4-60
4-37	Transmissivity Fields for NSMC Models 3 (left) and 41 (right)	4-61
4-38	Topgallant and Yucca Fault Hydraulic Conductivity and Anisotropy Histograms for the NSMC Models	4-62
4-39	Country Rock, Carpetbag, and Tied Fault Hydraulic Conductivity and Anisotropy Histograms for the NSMC Models	4-63
4-40	Distribution and Histogram for Percentage of Particles Reaching the Northing Location of 4,090,000 m within 1,000 Years from 58 Detonations Potentially within $3R_c$ of the Saturated LCA	4-64
4-41	Perspective View of Particle Paths for NSMC Models 3 (top) and 41 (bottom) Flow Fields	4-66

LIST OF FIGURES (CONTINUED)

NUMBER	TITLE	PAGE
4-42	1,000-Year Time-Cumulative Probability of Exceedance of MCLs with NSMC 200-Year Particle Transport Extent	4-67
4-43	Particle Tracks and Transmissivity Field for Selected NSMC Models	4-69
4-44	Perspective View of Particle Paths for NSMC Model 28 Flow Field along with the Eastern Splay of Yucca Fault (purple surface)	4-75
4-45	Transmissivity Fields for NSMC Model 28 Flow Field	4-76
4-46	Production History for WW-C and WW C-1 Pumping Wells	4-78
4-47	Particle Paths and Times for Contamination Released at Each Detonation Included in the LCA Flow and Transport Model for the Base Case (left), 2 Times Eastern Yucca Flat Flow Rate (center), and High-K Yucca Fault (right)	4-80
4-48	Cumulative Distribution Function for RN Initial Concentrations within the Exchange Volume	4-87
4-49	Initial Particle Locations for the BOURBON Detonation	4-91
4-50	Fracture Porosity: (top) Distribution Sampled and (bottom) Distribution of the Model Values for the Country Rock and Fault Zones	4-96
4-51	Hydraulic Conductivity: (top) Distribution Sampled and (bottom) Distribution of the Sampled Values Used To Calculate Hydraulic Fracture Aperture for the Country Rock and Fault Zones	4-98
4-52	Calculated LCA Fracture Aperture	4-99
4-53	Sampled LCA Matrix Porosity	4-99
4-54	Calculated LCA Matrix Tortuosity	4-101
4-55	Calculated LCA Matrix Diffusion Coefficient	4-101
4-56	Sampled LCA Fracture Retardation Coefficient Distributions	4-103
4-57	Sampled LCA Matrix K_d Distributions	4-104
4-58	1,000-Year Time-Cumulative Probability of Exceedance of MCLs for the LCA Model Flow Base Case	4-106

LIST OF FIGURES (CONTINUED)

NUMBER	TITLE	PAGE
4-59	Probability of Exceedance of MCLs for the LCA Flow Model Base Case (left) at 50 Years, (center) at 100 Years, and (right) at 150 Years	4-107
4-60	Probability of Exceedance of MCLs for the LCA Flow Model Base Case (left) at 200 Years, (center) at 300 Years, and (right) at 400 Years	4-108
4-61	Probability of Exceedance of MCLs for the LCA Flow Model Base Case (left) at 500 Years, (center) at 600 Years, and (right) at 700 Years	4-109
4-62	Probability of Exceedance of MCLs for the LCA Flow Model Base Case (left) at 800 Years, (center) at 900 Years, and (right) at 1,000 Years	4-110
4-63	1,000-year Time-Cumulative Probability of Exceedance of MCLs for (left) LCA Flow Model Base Case and (right) 2013 Base Case	4-112
4-64	95th-Percentile 1,000-year Time-Cumulative Probability of Exceedance of MCLs for (left) LCA Flow Model Base Case and (right) High-K Yucca Fault	4-113
4-65	95th-Percentile 1,000-year Time-Cumulative Probability of Exceedance of MCLs for (left) Alternative Case with 40-kg/s Basin Flux and (right) NSMC Model 28	4-114
4-66	50th-Percentile 1,000-year Time-Cumulative Probability of Exceedance of MCLs for (left) LCA Flow Model Base Case and (right) High-K Yucca Fault	4-115
4-67	50th-Percentile 1,000-year Time-Cumulative Probability of Exceedance of MCLs for (left) 40-kg/s Basin Flux and (right) NSMC Model 28	4-116
4-68	5th-Percentile 1,000-year Time-Cumulative Probability of Exceedance of MCLs for (left) LCA Flow Model Base Case and (right) High-K Yucca Fault	4-117
4-69	5th-Percentile 1,000-year Time-Cumulative Probability of Exceedance of MCLs for (left) 40-kg/s Basin Flux and (right) NSMC Model 28	4-118
4-70	Distributions of Cumulative MCL Exceedance Volume for Model Evaluation Transport Runs Compared with 2013 Base Case	4-119
4-71	Average Fractional Exceedance Volume for (a) LCA Flow Model Base Case, (b) High-K Yucca Fault, (c) 40-kg/s Basin Flux, and (d) NSMC Model 28	4-120
4-72	50th-Percentile Probability of Exceedance of MCLs at 50 Years for (left) LCA Flow Model Base Case and (right) High-K Yucca Fault	4-123

LIST OF FIGURES (CONTINUED)

NUMBER	TITLE	PAGE
4-73	50th-Percentile Probability of Exceedance of MCLs at 50 Years for (left) 40-kg/s Basin Flux and (right) NSMC Model 28	4-124
4-74	1,000-Year Time-Cumulative Probability of Exceedance of MCLs CB Forecasts	4-125
4-75	50th-Percentile Probability of Exceedance of MCLs CB Forecasts at 50 Years	4-126
A-1	Well Completion Diagram for ER-2-2	A-2
A-2	Well Completion Diagram for ER-3-3	A-3
A-3	Well Completion Diagram for ER-4-1	A-4
A-4	Water Production and Tritium Log for ER-2-2	A-5
A-5	Water Production and Tritium Log for ER-3-3	A-6
A-6	Water Production and Tritium Log for ER-4-1 (TMWTA, TMLVTA, LTCU)	A-7
A-7	Water Production and Tritium Log for ER-4-1	A-8

LIST OF TABLES

NUMBER	TITLE	PAGE
1-1	Model Evaluation Targets and Associated Data Collection/Data Analysis Activities	1-2
2-1	Data Collection/Data Analysis Activities	2-1
2-2	Analyses for Each Location Type	2-4
2-3	Samples Collected from LCA Completions	2-5
2-4	RN Concentrations for Samples Collected from LCA Completions	2-7
2-5	ER-2-2 and ER-4-1 Depth-Discrete Bailer RN Results (pCi/L)	2-19
2-6	Permeability Estimates for WTA, TCU, and LCA	2-25
2-7	U-3cn-5 Hydraulic Testing Information	2-34
2-8	Estimated Drawdowns in ER-4-1 WDT Observation Locations	2-42
2-9	Estimated Drawdowns in Observation Wells from ER-6-1-2 MWAT	2-47
2-10	Summary of the RMS Errors for the Pareto and NSMC Models with Large Flow Changes in Eastern Yucca Flat Simulated by the Calibrated and NSCM/Pareto Analyses Uncertainty Models	2-56
2-11	Lateral Flow into and out of the Eastern LCA in Yucca Flat Simulated by the Calibrated and NSCM/Pareto Analyses Uncertainty Models	2-59
2-12	Recharge to the DV3 Model Domain Basins Simulated by the Calibrated and NSMC/Pareto Analyses Uncertainty Models	2-61
2-13	LCA Groundwater Compositions Used for Flow Path Analysis	2-64
2-14	Wells Sampling Vicinity of an Underground Nuclear Detonation	2-99
2-15	Near-field ^{3}H, ^{90}Sr, and ^{137}Cs Concentrations (pCi/L)	2-100
2-16	Wells Drilled to the Saturated LCA	2-105
3-1	Exchange Volume Size (Defined by R_c Mulitplier)	3-3
3-2	Detonations within $3R_c$ of the Saturated LCA Based on the HFM and Statistically Derived Surfaces	3-5

LIST OF TABLES (CONTINUED)

NUMBER	TITLE	PAGE
3-3	Transmissivity Data	3-10
3-4	LCA Transport Model K_d Distributions (mL/g)	3-16
3-5	Model Evaluation Target Summary and Resolution	3-22
4-1	Observation Group Contribution to the Measurement Objective Function and RMS Error for the Base Case	4-24
4-2	Calibrated Fault Permeability and Anisotropy for the Base Case Flow Field	4-36
4-3	Calibrated LCA Model Boundary Fluxes for the Base Case	4-39
4-4	Hydraulic Conductivity Parameters for Select NSMC Models	4-70
4-5	Basin Flux and Anisotropy Parameters for Select NSMC Models	4-71
4-6	Detonations in NSMC Models with Greater Particle Transport	4-72
4-7	Parametric Uncertainty Distribution for Melt-Glass Partitioning Factors	4-84
4-8	Parametric Uncertainty Distributions for the Finnegan RST	4-85
4-9	Parametric Uncertainty Distributions for HSU-Specific K_ds	4-85
4-10	Source Data Distributions and Methodology for Developing Fracture Parameters, Matrix Porosity, and Tortuosity Distributions	4-93
4-11	LCA Transport Model Fracture Retardation Distributions	4-95
4-12	LCA Transport Model K_d Distributions	4-95
4-13	Comparison of 50-Year, 50th-Percentile CB Forecasts to Present Time Observations	4-122

LIST OF ACRONYMS AND ABBREVIATIONS

General Acronyms and Abbreviations

2-D	Two-dimensional
3-D	Three-dimensional
acre-ft/yr	Acre feet per year
amsl	Above mean sea level
bgs	Below ground surface
BN	Bechtel Nevada
°C	Degree Celsius
CADD	Corrective action decision document
CAI	Corrective action investigation
CAIP	Corrective action investigation plan
CAP	Corrective action plan
CAU	Corrective action unit
CB	Contaminant boundary
CDF	Cumulative distribution function
CEV	Cumulative exceedance volume
Ci	Curie
cm	Centimeter
COC	Contaminant of concern
COPC	Contaminant of potential concern
CR	Closure report
CS	Carbon steel
D_m	Matrix diffusion coefficient
DOE	U.S. Department of Energy
DTW	Depth to water
DV3	Death Valley version 3
ES	Electric submersible

LIST OF ACRONYMS AND ABBREVIATIONS (CONTINUED)

FEHM	Finite element heat-mass
FEV	Fractional exceedance volume
FFACO	*Federal Facility Agreement and Consent Order*
ft	Foot
ft/day	Feet per day
ft^2/day	Square feet per day
ft^3/day	Cubic feet per day
gal	Gallon
GMWL	Global meteoric water line
gpm	Gallons per minute
HDD	Hydrologic data document
HFM	Hydrostratigraphic framework model
HGU	Hydrogeologic unit
HST	Hydrologic source term
HSU	Hydrostratigraphic unit
IAEA	International Atomic Energy Agency
K_d	Distribution coefficient
kg/m^3	Kilograms per cubic meter
kg/(m·s)	Kilograms per meters per second
kg/s	Kilograms per second
km	Kilometer
km/yr	Kilometers per year
kt	Kiloton
LANL	Los Alamos National Laboratory
LLNL	Lawrence Livermore National Laboratory
LTHMP	Long-Term Hydrologic Monitoring Program
m	Meter
m^2	Square meter

LIST OF ACRONYMS AND ABBREVIATIONS (CONTINUED)

m^3	Cubic meter
MCL	Maximum contaminant level
MDC	Minimum detectable concentration
MDL	Minimum detection limit
MER	Model Evaluation Report
mg/L	Milligrams per liter
mi	Mile
mi^2	Square mile
mL	Milliliter
mL/g	Milliliters per gram
mm/yr	Millimeters per year
mrem/yr	Millirem per year
m/s^2	Meters per square second
m/s	Meters per second
MWAT	Multiple-well aquifer test
m/yr	Meters per year
N/A	Not applicable
NAD	North American Datum
NDEP	Nevada Division of Environmental Protection
N-I	Navarro-Intera, LLC
NNSA/NFO	U.S. Department of Energy, National Nuclear Security Administration Nevada Field Office
NNSS	Nevada National Security Site
NSMC	Null Space Monte Carlo
NSPC	Nevada State Plane Coordinate
NTU	Nephelometric turbidity unit
pCi/L	Picocuries per liter
PER	Preemptive review

LIST OF ACRONYMS AND ABBREVIATIONS (CONTINUED)

ppb	Parts per billion
PS	Post-shot
QAP	Quality Assurance Plan
R^2	Coefficient of determination
R_c	Cavity radius
R_f	Retardation factor
RMS	Root mean square
RN	Radionuclide
RREMP	Routine Radiological Environmental Monitoring Plan
RST	Radiologic source term
SDWA	*Safe Drinking Water Act*
SEC	Specific electrical conductivity
SNJV	Stoller-Navarro Joint Venture
SS	Stainless steel
SU	Standard unit
SZ	Saturated zone
UDI	United Drilling, LLC
UGTA	Underground Test Area
USGS	U.S. Geological Survey
UTM	Universal Transverse Mercator
UZ	Unsaturated zone
WDT	Well development and testing
WP	Working point
WW	Water Well
YF/CM	Yucca Flat/Climax Mine
µCi/mL	Microcuries per milliliter
µg/L	Micrograms per liter
µm	Micrometer

LIST OF ACRONYMS AND ABBREVIATIONS (CONTINUED)

Stratigraphic, Geologic, Hydrostratigraphic, and Hydrogeologic Unit Abbreviations and Symbols

AA	Alluvial aquifer
AA3	Alluvial aquifer
ATCU	Argillic tuff confining unit
BFCU	Bullfrog confining unit
CHLFA	Calico Hills lava-flow aquifer
CHLFA3	Calico Hills lava-flow aquifer 3
CHLFA4	Calico Hills lava-flow aquifer 4
CHLFA5	Calico Hills lava-flow aquifer 5
CHVTA	Calico Hills vitric-tuff aquifer
CHZCM	Calico Hills zeolitic composite unit
LCA	Lower carbonate aquifer
LCA3	Lower carbonate aquifer-thrust plate
LCCU	Lower clastic confining unit
LTCU	Lower tuff confining unit
MGCU	Mesozoic granite confining unit
OSBCU	Oak Spring Butte confining unit
PLFA	Paintbrush lava-flow aquifer
Pz	Paleozoic (undivided)
QTa	Quaternary/Tertiary alluvium
Tbgb	Grouse Canyon bedded tuff
Tc	Crater Flat Group
Tclt	Crater Flat lower tuff
TCU	Tuff confining unit
Tlc/To	Paleocolluvium and older tuffs
Tma	Ammonia Tanks Tuff
Tmab	Ammonia Tanks bedded tuff

LIST OF ACRONYMS AND ABBREVIATIONS (CONTINUED)

TMLVTA	Timber Mountain lower vitric-tuff aquifer
Tmrh	Tuff of Holmes Road
Tmrp	Rainier Mesa mafic-poor Tuff
Tmrr	Rainier Mesa mafic-rich Tuff
Tm/Tw	Pre-Timber Mountain - Post Wahmonie Tuff (undifferentiated)
TMUVTA	Timber Mountain upper vitric-tuff aquifer
TMWTA	Timber Mountain welded-tuff aquifer
Tn	Tunnel Formation
Tn3	Tunnel Formation, Tunnel 3 Member
Tn3A	Tunnel 3 Member, bed 3A
Tn3&4	Tunnel 3&4 Members, Tunnel Formation
Tn4	Tunnel Formation, Tunnel 4 Member
Tn4K	Tunnel 4 Member, bed 4K
Ton	Older tunnel beds
Ton1	Tunnel bed 1
Ton2	Tunnel bed 2
Toy	Yucca Flat Tuff
Tp	Paintbrush Group (undivided)
TSA	Topopah Spring aquifer
TUBA	Tub Spring aquifer
Tv	Tertiary Volcanics
Tw	Wahmonie Formation
UCCU	Upper clastic confining unit
UCA	Upper carbonate aquifer
UTCU	Upper tuff confining unit
VA	Volcanic aquifer
VCU	Volcanic confining unit
WTA	Welded-tuff aquifer

LIST OF ACRONYMS AND ABBREVIATIONS (CONTINUED)

Symbols for Elements and Compounds

Am	Americium
Ar	Argon
C	Carbon
Ca	Calcium
Cl	Chlorine
CO_2	Carbon dioxide
Cs	Cesium
Eu	Europium
^2H	Deuterium
^3H	Tritium
H_2O	Water
HCO_3	Bicarbonate
I	Iodine
K	Potassium
Kr	Krypton
Mg	Magnesium
Na	Sodium
Ni	Nickel
Np	Neptunium
O	Oxygen
pmc	Percent modern carbon
Pu	Plutonium
Ru	Ruthenium
SiO_2	Silicon dioxide
Sm	Samarium
SO_4	Sulfate

LIST OF ACRONYMS AND ABBREVIATIONS (CONTINUED)

Sr	Strontium
Tc	Technetium
U	Uranium
Xe	Xenon
δ^2H	Delta deuterium
$\delta^{13}C$	Delta carbon-13
$\delta^{18}O$	Delta oxygen-18

1.0 INTRODUCTION

This Model Evaluation Report (MER) has been prepared for Corrective Action Unit (CAU) 97, Yucca Flat/Climax Mine (YF/CM), Nevada National Security Site (NNSS), Nevada. The YF/CM CAU is located in the northeastern portion of the NNSS and comprises 720 corrective action sites. A total of 747 underground nuclear detonations took place within this CAU between 1957 and 1992 and resulted in the release of radionuclides (RNs) in the subsurface in the vicinity of the detonation cavities.

The corrective action process for the YF/CM CAU is implemented by the U.S. Department of Energy (DOE), Environmental Management Nevada Program's Underground Test Area (UGTA) Activity in accordance with the *Federal Facility Agreement and Consent Order* (FFACO) (1996, as amended). The FFACO strategy for UGTA assumes that active remediation of subsurface RN contamination is not feasible with current technology. As a result, the corrective action is based on a combination of characterization and modeling studies, monitoring, and institutional controls. The strategy is implemented through a four-stage approach, proceeding from one stage to next upon approval by Nevada Division of Environmental Protection (NDEP) (see Section 1.1). The YF/CM CAU has progressed through the first two stages (corrective action investigation plan [CAIP] and corrective action investigation [CAI]) culminating in the development of the YF/CM flow and transport model (N-I, 2013). The CAU is currently in the third stage, the corrective action decision document (CADD)/corrective action plan (CAP).

The CADD/CAP stage for YF/CM is focused on model evaluation designed to build confidence in the site conceptual model and model forecasts to guide development of the long-term monitoring network and institutional controls. The CADD/CAP (DOE/EMNV, 2017d) identified key model uncertainties thought to impact forecasts of contaminant transport and model evaluation targets associated with these uncertainties. The CADD/CAP identified multiple data collection/data analysis activities deemed suitable for addressing each of the model evaluation targets (Table 1-1). Most of the data collection/data analysis activities contributed toward addressing multiple targets. It was recognized in the CADD/CAP that model acceptability could be achieved, even if some of the individual model evaluation targets are not met, by reducing the overall model uncertainty. The

Table 1-1
Model Evaluation Targets and Associated Data Collection/Data Analysis Activities

Model Evaluation Target	Data Collection/Data Analysis Activities
Basin flux through testing area	• Formalizing ER-6-1-2 MWAT reanalysis • Performing WDT in the ER-4-1 LCA
Exchange volume size/shape that extends into the LCA	• Sampling LCA completions for RNs • Sampling near-field wells • Interpreting drilling evidence from ER-2-2, ER-3-3, and ER-4-1 • Investigating LCA surface elevations • Reviewing historical data for detonations near or within the LCA
Extent of RN contamination in the LCA	• Sampling LCA completions for RNs • Sampling NASH test cavity at satellite Well UE-2ce • Interpreting drilling evidence from ER-2-2, ER-3-3, and ER-4-1
LCA hydraulic properties	• Formalizing ER-6-1-2 MWAT reanalysis • Performing WDT in the ER-4-1 LCA • Interpreting drilling evidence from ER-2-2, ER-3-3, and ER-4-1
^{90}Sr mobility in the LCA	• Sampling LCA completions for RNs • Sampling NASH test cavity at satellite Well UE-2ce • Reviewing historical data for detonations near or within the LCA
^{137}Cs mobility in the LCA	• Sampling LCA completions for RNs • Sampling NASH test cavity at satellite Well UE-2ce • Reviewing historical data for detonations near or within the LCA
Fault transport properties	• Sampling LCA completions for RNs • Sampling near-field wells • Interpreting drilling evidence from ER-2-2, ER-3-3, and ER-4-1
Permeability anisotropy	• Evaluating ER-4-1 and other Yucca Flat geochemistry • Performing WDT in the ER-4-1 LCA

Source: DOE/EMNV, 2017d

Cs = Cesium
Sr = Strontium
LCA = Lower carbonate aquifer
MWAT = Multiple-well aquifer test
WDT = Well development and testing

CADD/CAP stated that it would be necessary to refine and recalibrate the model (N-I, 2013). The refined and recalibrated LCA model, referred to as the "LCA flow model" in this report, supersedes the N-I (2013) model.

The scope of this MER is to summarize the model evaluation required by the YF/CM CADD/CAP (DOE/EMNV, 2017d) and provide recommendations regarding model adequacy for advancing to the closure report (CR) stage of the UGTA Strategy. The MER encompasses the following:

- Data collection and analysis description, and results with respect to model evaluation targets
- Data impact assessment and model refinements (i.e., contaminant boundary [CB] forecasts)

- Recommendations from the Model Evaluation Team and Preemptive Review (PER) Committee to either collect additional data or proceed to the CR stage

As seen in Table 1-1, while multiple data collection activities are required to address each of the model evaluation targets, most of the data collection activities apply to multiple targets. This complexity is accommodated in the MER by first describing the data collection activities in Section 2.0 and then discussing how each target is addressed in Section 3.0. The MER is structured as follows: Section 1.0 is the introduction with a brief background summarizing the scope of the MER, the UGTA corrective action strategy as defined by the FFACO, and the N-I (2013) flow and transport model. A summary of classification information is also provided. Section 2.0 describes the work performed under each of the data collection activities. Section 3.0 addresses the model evaluation targets and presents supplementary analyses as needed. Section 4.0 presents the LCA flow model refinement and recalibration, uncertainty analysis of the LCA flow models, selection of flow models chosen for forecasting CBs, hydrologic source term (HST) allocation to the model, transport model activities, and results. Section 5.0 provides the recommendation from the Model Evaluation Team for advancement to the CR stage, and Section 6.0 provides recommendation for advancement to CR stage from the PER Committee.

1.1 UGTA Strategy

The FFACO (1996, as amended), the governing agreement between DOE and NDEP, has four stages for UGTA Activity CAUs (Figure 1-1):

- CAIP
- CAI
- CADD/CAP
- CR

The YF/CM CAIP stage was completed with the publication of the CAIP in 2000 (DOE/NV, 2000a). The CAI stage was completed in 2017 when NDEP accepted the YF/CM flow and transport model for CADD/CAP studies and approved proceeding to the CADD/CAP stage (Andres, 2017a). NDEP acceptance occurred once all comments by an external peer review committee were resolved (N-I, 2015; Navarro, 2016b). The CADD/CAP studies focus on model evaluation to ensure that the groundwater flow and contaminant transport modeling results can be used for the regulatory decisions required for CAU closure.

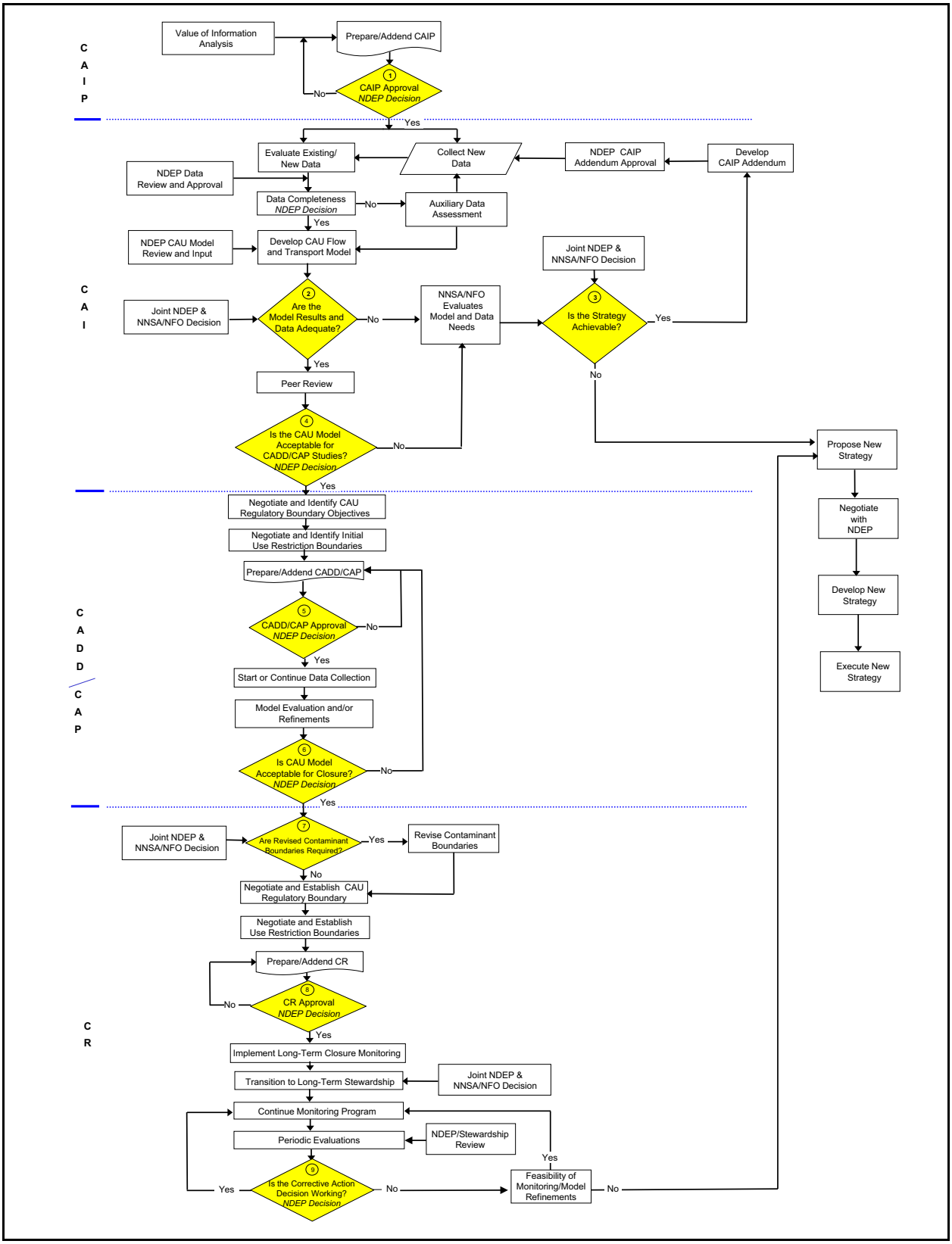

Figure 1-1
UGTA Strategy Flowchart
Source: FFACO, 1996 as amended

There are five steps in the CADD/CAP stage, as shown in Figure 1-2. In Step 1, an expert elicitation panel identified and ranked a set of model uncertainties in order of importance based on their potential impact on the CB (Kwicklis, 2016). Model evaluation targets were then identified, and data collection activities were selected to address these targets (Table 1-1). This information was included in the CADD/CAP (DOE/EMNV, 2017d), which was approved by NDEP in 2017 (Andres, 2017b), completing Step 2. To fulfill Step 3, data collection and/or data analysis activities (Section 2.0) were performed.

As part of Step 4, the data, analysis and results from each of the model evaluation activities were reviewed by the YF/CM PER Committee composed of subject matter experts in the areas of hydrology, geology, geochemistry, source term, flow and transport modeling, and site history. The PER Committee assessed whether each model evaluation target was sufficiently addressed, and advised whether the model refinements appropriately incorporated the knowledge and insights gained from the evaluation activities. A total of six meetings were conducted with the PER Committee and the Model Evaluation Team, each meeting consisting of technical presentations with questions and answers, followed by detailed technical discussions. The PER Committee provided the Model Evaluation Team with extensive comments, which were addressed during the ongoing work. (Figure 1-2). The decision that model refinements will be performed, with the goal to produce more realistic models, is documented in the CADD/CAP (DOE/EMNV, 2017d). Throughout Step 4, the decision to continue refining the model(s) was made until the Model Evaluation Team and PER Committee agreed that no additional model refinements were necessary (Figure 1-2). This MER is the final part of Step 4 and supports NDEP Decision 6 in the FFACO strategy, “Is CAU Model Acceptable for Closure?” (Figure 1-1). If NDEP determines that the model is acceptable, the CAU advances to the CR stage of the FFACO strategy.

1.2 YF/CM Flow and Transport Model Background

The YF/CM flow and transport model (N-I, 2013) addressed the fate of the entire YF/CM RN inventory in three coupled sets of flow and transport models: the unsaturated zone (UZ) models, the saturated zone (SZ) alluvial aquifer (AA)/volcanic aquifer (VA) models, and the saturated LCA models. The critical lateral transport processes of regulatory concern—those that define the CB for the YF/CM CAU—were shown to eventually occur in the saturated LCA system. Although the coupled set of three models was set up to consider RN migration to the LCA from the UZ and SZ

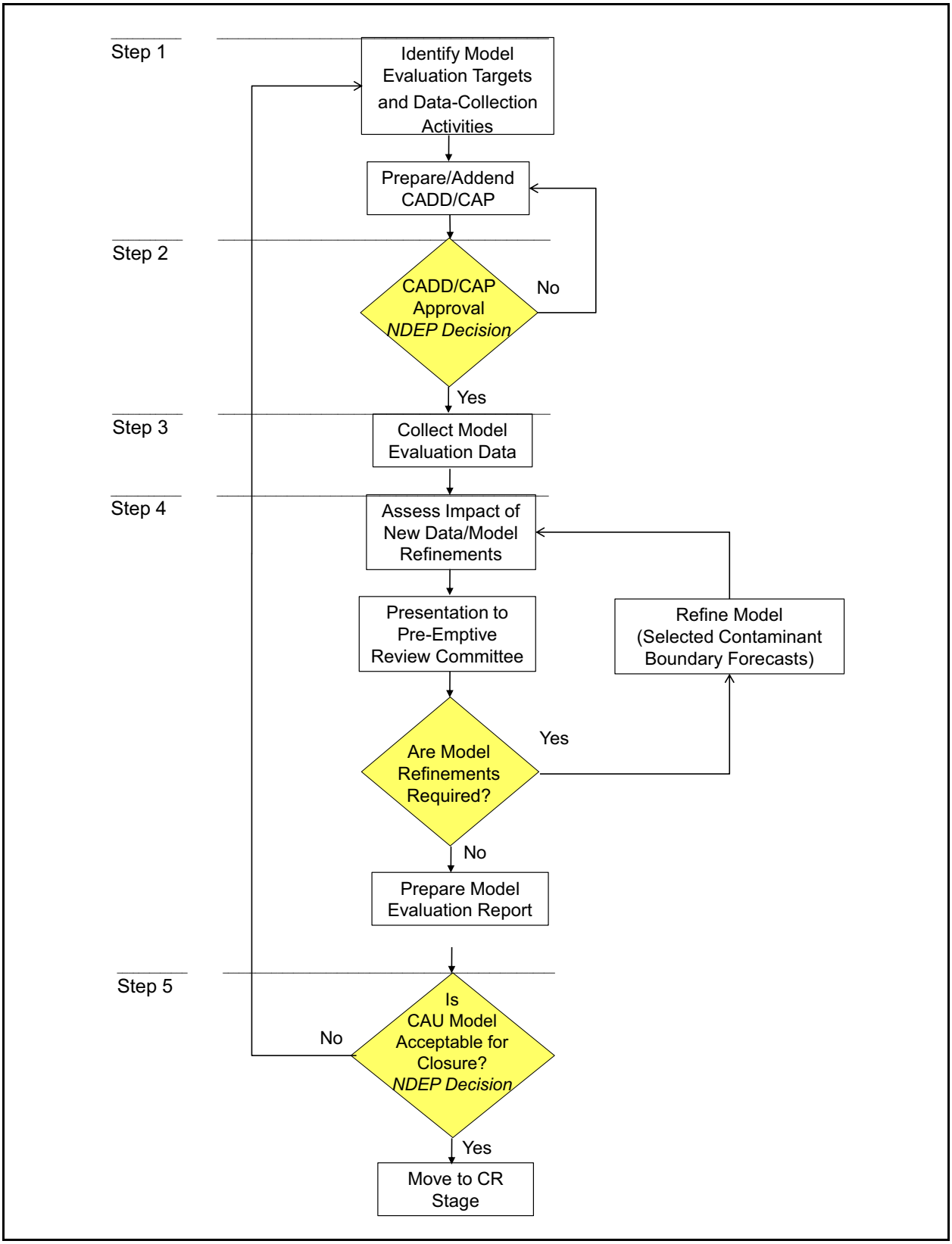

Figure 1-2
Process Flow Diagram for CADD/CAP Model Evaluation Process
Source: DOE/EMNV, 2017d

models and RN migration within the LCA (from either contaminant sources directly emplaced in the LCA or from RN influxes provided by the other models), the integrated analysis showed that the most significant contributors of contaminants to the LCA were deeply buried detonations near or in the LCA whose exchange volumes extended into the saturated LCA. In this case, a fraction of the contaminants from these detonations were introduced directly into the saturated LCA without any time delay for radioactive decay or significant sorption in the overlying tuffs. Although contaminant fluxes from the UZ and SZ AA/VA models to the LCA did occur—and, in some cases, at concentrations greater than the maximum contaminant levels (MCLs) stipulated in the *Safe Drinking Water Act* (SDWA) (CFR, 2018)—the effect of these RN sources on the CB was secondary compared to the RN sources introduced directly into the saturated LCA. This was especially true for UZ and SZ AA/VA models for the preferred recharge scenarios in which the long-term background recharge was assumed to be 1 millimeter per year (mm/yr) or less, which resulted in very small RN fluxes to the LCA from the overlying models. As a result, the model evaluation activities described in the CADD/CAP (DOE/EMNV, 2017d) focused on addressing key uncertainties in the LCA models, with uncertainties associated with the UZ and SZ AA/VA models viewed as insignificant from the perspective of defining the CB (Kwicklis, 2016). Therefore, in this MER, emphasis is placed on identifying the subset of the original 747 detonations in the YF/CM CAU that are deep enough to potentially intersect the saturated LCA. It was also intended that model evaluation targets would address model uncertainties that led to conservative assumptions made in the N-I (2013) LCA models that resulted in forecasts of contamination that were far more extensive than current data on groundwater contamination in Yucca Flat would indicate is possible.

1.3 Classification Information

The cavity radii (R_c) presented within this report are either measured, as reported in Zavarin (2014), for detonations with an announced yield (NNSA/NFO, 2015b); or estimated based on the maximum announced yield (NNSA/NFO, 2015b) and Equation 1 in Pawloski (1999). The Boardman (1970) equation may be used instead of Pawloski (1999) for detonations with carbonate rock working points (WPs).

All RN source term data are based on the unclassified inventory reported in Finnegan et al. (2016).

2.0 MODEL EVALUATION DATA COLLECTION

The model evaluation plan for the YF/CM CAU is described in the CADD/CAP (DOE/EMNV, 2017d). Model evaluation includes nine data collection/data analysis activities planned to address the model evaluation targets as described in Section 1.0. Table 2-1 presents these activities along with the model evaluation targets that they address. These activities were performed according to the UGTA Quality Assurance Plan (QAP) (NNSA/NFO, 2015a). As shown in Table 2-1, most activities address multiple model evaluation targets. This section describes and presents results for each data collection/data analysis activity identified in the CADD/CAP. The application of these results toward the model evaluation targets is presented in Section 3.0.

Table 2-1
Data Collection/Data Analysis Activities

Data Collection/Data Analysis Activities	Model Evaluation Target
Sampling LCA completions for RNs (Section 2.1)	• Exchange volume size/shape that extends into the LCA • Extent of RN contamination in the LCA • Fault transport properties • ^{90}Sr mobility in the LCA • ^{137}Cs mobility in the LCA
Interpreting drilling evidence from ER-2-2, ER-3-3, and ER-4-1 (Section 2.2)	• Exchange volume size/shape that extends into the LCA • Extent of RN contamination in the LCA • LCA hydraulic properties • Fault transport properties
Sampling near-field wells (Section 2.3)	• Exchange volume size/shape that extends into the LCA • Fault transport properties
Sampling NASH test cavity at satellite Well UE-2ce (Section 2.4)	• Extent of RN contamination in the LCA • ^{90}Sr mobility in the LCA • ^{137}Cs mobility in the LCA
Performing WDT in the ER-4-1 LCA (Section 2.5)	• Basin flux through testing area • LCA hydraulic properties • Permeability anisotropy
Formalizing ER-6-1-2 MWAT reanalysis (Section 2.6)	• Basin flux through testing area • LCA hydraulic properties
Evaluating ER-4-1 and other Yucca Flat groundwater geochemistry (Section 2.7)	• Permeability anisotropy • LCA hydraulic properties
Investigating LCA surface elevations (Section 2.8)	• Exchange volume size/shape that extends into the LCA
Reviewing historical data for detonations near or within the LCA (Section 2.9)	• Exchange volume size/shape that extends into the LCA • ^{90}Sr mobility in the LCA • ^{137}Cs mobility in the LCA

Source: DOE/EMNV, 2017d

2.1 Sampling LCA Completions for RNs

LCA completions were sampled for RN analysis to address several model evaluation targets: (1) *Exchange volume size/shape that extends into the LCA*, (2) *Extent of RN contamination in the LCA*, (3) *Fault transport properties*, (4) *^{90}Sr mobility in the LCA*, and (5) *^{137}Cs mobility in the LCA*. This section primarily supports the *Extent of RN contamination in the LCA* model evaluation target. This section also summarizes available ^{90}Sr and ^{137}Cs concentrations in the LCA to support the *^{90}Sr and ^{137}Cs mobility in the LCA* targets. Details supporting the *Exchange volume size/shape that extends into the LCA* and *Fault transport properties* model evaluation targets, with respect to RN analyses, are primarily presented in Section 2.2, "Interpreting Drilling Evidence from ER-2-2, ER-3-3, and ER-4-1"; and Section 2.3, "Sampling Near-field Wells."

A total of 15 sampling locations, shown in Figure 2-1, were sampled for this activity from 2014 to 2018. Samples were collected from wells accessing the saturated LCA and analyzed for RNs according to the NNSS Integrated Groundwater Sampling Plan (DOE/EMNV, 2018). The sampling plan categorizes YF/CM sampling locations into three types: characterization, source/plume, and early detection. The location type determines the analytical suite for each sample (Table 2-2). In addition to analyses performed by commercial laboratories certified by the State of Nevada, specialized analyses that result in low-level detection and analyses that are not available from commercial laboratories are performed by Lawrence Livermore National Laboratory (LLNL) (Table 2-2). Sample information including location type; sampling date and depths; collection method; and results for bromide, pH, and turbidity field measurements is provided in Table 2-3. As shown in Table 2-3, the majority of the samples were collected using a pump (electric submersible or rod pump), with three samples collected using a bailer and one sample collected from the well discharge line.

Water samples are generally collected in a manner that best ensures they represent ambient formation water. While the well is not purged when sampled using a bailer, purging of the well is required for collecting samples using a pump. Purging is considered adequate once a minimum of three effective well volumes are discharged and the water-quality parameters meet the following criteria: (1) the pH has stabilized, and measurements remained constant within 0.1 standard unit (SU); (2) specific electrical conductance (SEC) and temperature have stabilized, and vary by no more than 10 percent for at least three consecutive readings; and (3) the turbidity has stabilized. Stabilization of these water-quality parameters indicates that formation water is being sampled instead of stagnant water

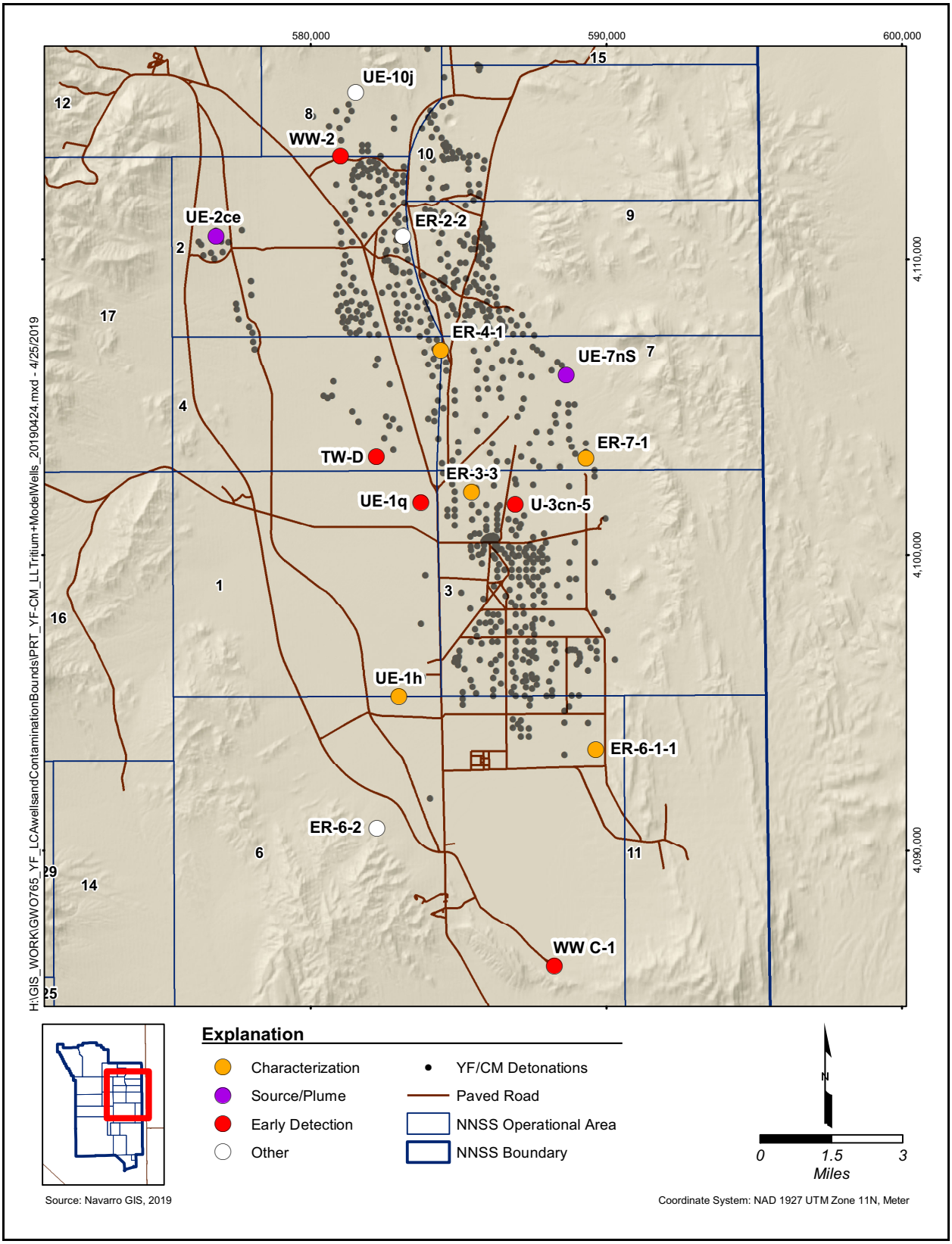

Figure 2-1
LCA Sampling Locations and Types

Table 2-2
Analyses for Each Location Type

Location Type	Commercial Laboratory	LLNL
Characterization	• Alkalinity, pH, specific conductance • Anions, total metals • Gross alpha and gross beta • Gamma emitters (e.g.,^{137}Cs) • ^{3}H, ^{14}C, ^{36}Cl, ^{90}Sr, ^{99}Tc, ^{129}I, ^{238}Pu,$^{239/240}$Pu	• ^{14}C and ^{36}Cl • δ^{2}H and δ^{18}O • Total inorganic carbon and δ^{13}C • Noble gases • ^{3}H (low level) if ^{3}H <300 pCi/L • ^{99}Tc, ^{129}I, and Pu if ^{3}H >5,000 pCi/L
Source/Plume	• ^{3}H,^{14}C, ^{36}Cl, ^{90}Sr, ^{99}Tc, ^{129}I, ^{137}Cs	• ^{14}C, ^{36}Cl, ^{99}Tc, ^{129}I
Early Detection	• ^{3}H	• None

Source: DOE/EMNV, 2018

C = Carbon
Cl = Chlorine
^{3}H = Tritium
I = Iodine
Pu = Plutonium
Tc = Technetium
δ^{2}H = Delta deuterium
δ^{13}C = Delta carbon-13
δ^{18}O = Delta oxygen-18

pCi/L = Picocuries per liter

from within and surrounding the well. All locations met the purging requirement with the exception of ER-3-3 (Table 2-3). Sampling ER-3-3 is discussed further in Section 2.3.1.

Although ER-6-1-2 was the well planned for sampling in the CADD/CAP (DOE/EMNV, 2017d), ER-6-1-1 was sampled instead. ER-6-1-1 and ER-6-1-2 are expected to sample equivalent LCA waters because they are located 167 ft from each other; both sample the LCA and are positioned in rough alignment with the dominant local fracture orientation (SNJV, 2005a). ER-6-1-1 has 300 ft open to the LCA versus the much longer 1,300 ft open in ER-6-1-2; thus, the volume of wellbore open to LCA in ER-6-1-1 is much smaller than that in ER-6-1-2. Sampling was conducted using a low-flow jack pump; hence, it was more practical to purge this well rather than ER-6-1-2 using this pump.

Well UE-1r, also planned for sampling, was not sampled in support of model evaluation because the water sampled from this well is not representative of LCA groundwater. This is because the Timber Mountain welded-tuff aquifer (TMWTA) and Timber Mountain lower vitric-tuff aquifer (TMLVTA) are thought to preferentially provide the majority of the groundwater production at this well. In addition, an obstruction inhibiting access to the LCA was observed.

Table 2-3
Samples Collected from LCA Completions

Well Name	Collection Method	Sample Depth (ft)	Sample Date	Volume Purged (gal)	Pump Rate (gpm)	Bromide (mg/L)	pH	Turbidity (NTU)
Characterization								
ER-3-3	ES Pump	2,630 – 3,193	12/15/2016	9.5E+03	13.0	0.17	10.1	316
ER-4-1	ES Pump	2,812 – 2,956	02/17/2017	1.7E+06	70.3	0.35	6.8	0.6
ER-6-1-1	Rod Pump	1,835 – 2,085	03/14/2018	5.6E+03	2.0	1.2 (J <0.06) [a]	7.6	6.3
ER-7-1	ES Pump	1,852 – 2,500	06/20/2014	2.4E+04	23.8	0.11	7.1	9.9
UE-1h	Rod Pump	2,349 – 3,358	12/06/2017	1.1E+04	2.5	<0.06 [a]	7.6	22
Source/Plume								
UE-2ce	ES Pump	1,455 – 1,650	12/14/2016	2.0E+04	14.2	--	7.1	16
			12/15/2016(a)	3.7E+04	14.2	--	7.2	25
			12/15/2016(b)	4.0E+04	14.0	--	7.2	24
			12/16/2016	5.6E+04	14.1	--	7.2	17
UE-7nS	Bailer	2,018	06/10/2015	N/A	N/A	--	6.8	62
Early Detection								
TW-D	Bailer	1,800	03/22/2018	N/A	N/A	--	8.0	17
UE-1q	Bailer	2,475	03/27/2018	N/A	N/A	--	8.0	3.8
U-3cn-5	ES Pump	2,835 – 3,028	11/13/2017	5.9E+03	50.7	--	7.5	16.1
WW C-1	ES Pump	1,543 – 1,707	02/15/2018	3.0E+04	21.6	--	7.0	9.9
WW-2	ES Pump	2,700 – 2,950 3,166 – 3,414	04/22/2015	7.3E+04	28.5	0.13	7.8	11.1
Other								
ER-2-2	Discharge Line	3,200 [b]	02/06/2016	N/A	N/A	--	9.2	--
ER-6-2	ES Pump	1,746 – 3,430	06/19/2014	2.5E+04	20.8	0.17	7.0	16
UE-10j [c]	Rod Pump	2,232 – 2,297	01/04/2018	2.8E+03	2.2	<0.06 [a]	7.3	83

Source: Navarro, 2019a

[a] Laboratory result.
[b] Sample was collected while the drill was circulating in the borehole at 3,200 ft bgs.
[c] UE-10j was categorized as a characterization well at the time of sampling (NNSA/NFO, 2014).

bgs = Below ground surface
ES = Electric submersible
ft = Foot
gal = Gallon
gpm = Gallons per minute
mg/L = Milligrams per liter
N/A = Not applicable
NTU = Nephelometric turbidity unit

J = Result is estimated.

2.1.1 Results Summary

Laboratory results for contaminants of concern (COCs) and contaminants of potential concern (COPCs) (as defined in the sampling plan [DOE/EMNV, 2018]) are presented in Table 2-4. Gross alpha and gross beta results are also provided when available (Table 2-4). Results for the remaining analyses listed in Table 2-2 are reported in the UGTA Chemistry Database (Navarro, 2019a). Table 2-4 also presents the SDWA MCLs (EPA, 2002). The MCL for gross alpha (15 pCi/L) includes the total of all alpha emitters except uranium and radon. The MCL for beta and photon emitters is based on a calculated dose of 4 millirem per year (mrem/yr). This means that the combined dose from all beta and photon RNs present in a particular water source must be less than 4 mrem/yr. Each single RN has a unique concentration of radioactivity (measured in pCi/L), which, when in isolation, equates to a 4-mrem/yr dose (EPA, 2002). The corresponding EPA-derived MCLs in Table 2-4 are the concentration of that single RN (^{14}C, ^{36}Cl, ^{90}Sr, ^{99}Tc, ^{129}I and ^{137}Cs) which, when in isolation, will result in a 4-mrem/yr dose. Thus, the concentrations of all RNs in a water source must be considered to determine compliance with the 4-mrem/yr MCL. If gross beta results are greater than 50 pCi/L, samples must be analyzed for the individual RNs (EPA, 2002).

No gross alpha or gross beta values exceeded the MCLs (Table 2-4). The gross alpha values reported in Table 2-4 were not adjusted based on the uranium or radon concentrations and, in all cases except ER-4-1 samples, the gross alpha values were still below the 15-pCi/L MCL. The uranium concentration in the ER-4-1 sample and its duplicate was reported as 6.12 micrograms per liter (µg/L) or 4.1 pCi/L. The adjusted gross alpha for the sample (13.3 pCi/L) and its duplicate (12.4 pCi/L) are below the 15-pCi/L MCL.

None of the RNs presented in Table 2-4 (with the exception of natural levels of ^{14}C and ^{36}Cl, measured using LLNL's highly sensitive analytical methods) were detected above their MDC in 10 of the 15 sampling locations (ER-3-3, ER-4-1, ER-6-1-1, ER-6-2, ER-7-1, TW-D, UE-1h, UE-1q, UE-10j, and WW-2). Low-level ^{3}H analysis was performed on these samples by the commercial lab (MDC ranges from 1.8 to 2.9 pCi/L) or LLNL (MDC ranges from 0.2 to 1.1 pCi/L), or both (Table 2-4).

Low levels of ^{3}H were detected in 4 of the 15 sampling locations (ER-2-2, U-3cn-5, UE-7nS, and WW C-1). No other RNs were measured for these samples (Table 2-4). Three of these locations (ER-2-2, U-3cn-5, UE-7nS) are near an underground nuclear detonation cavity; discussions of these

Table 2-4
RN Concentrations for Samples Collected from LCA Completions
(Page 1 of 3)

Location	Date	Type [a]	^{3}H	Gross Alpha	Gross Beta	^{14}C	^{36}Cl	^{90}Sr	^{99}Tc	^{129}I	^{137}Cs
			(pCi/L)								
MCL			**2.0E+04**	15 [b]	50 [c]	**2.0E+03**	**700**	**8**	**900**	**1**	**200**
Characterization											
ER-3-3	12/15/2016	S	<310	5.6	J 19.6	<410	<2.8	<0.23	<7.5	<0.64	<7.7
		D	<310	13.1	J 19.8	<390	<3.1	<0.26	<7.2	<0.74	<8.0
		SP [d]	<1.0	--	--	0.020	J 1.35E-04	--	--	--	--
ER-4-1	02/17/2017	S	<2.84	17.4 [b]	12.8	<347	<20.1	<0.96	<5.0	<0.62	<7.8
		D	<2.83	16.5 [b]	12.9	<347	<18.9	<0.95	<5.1	<0.92	<5.2
		SP [d]	<1.0	--	--	0.034	J 1.63E-04	--	--	--	--
		SPD [d]	<1.0	--	--	--	J 1.75E-04	--	--	--	--
ER-6-1-1	03/14/2018	S	<3.0	< 1.8	6.6	<420	<3.0	<0.46	<7.1	<0.75	<4.7
		D	<3.2	< 1.8	6.9	<410	<2.9	<0.51	<7.1	<0.79	<9.5
		SP [d]	<1.0	--	--	0.024	1.66E-04	--	--	--	--
ER-7-1	06/20/2014	S	<2.3	6.2	8.0	<470	<3.1	<0.52	<6.7	<0.75	<6.7
		D	<2.2	5.6	8.1	<470	<4.0	<0.59	<7.1	<0.74	<7.1
		SP [d]	<1.1	--	--	0.079	1.46E-04	--	--	--	--
UE-1h	12/06/2017	S	<2.5	4.7	7.4	<390	<3.2	<0.43	<7.2	<0.75	<6.0
		D	<2.8	8.1	12.3	<400	<3.1	<0.46	<7.4	<0.79	<8.0
		SP [d]	<1.0	--	--	J 0.035	--	--	--	--	--

Table 2-4
RN Concentrations for Samples Collected from LCA Completions
(Page 2 of 3)

Location	Date	Type [a]	^{3}H	Gross Alpha	Gross Beta	^{14}C	^{36}Cl	^{90}Sr	^{99}Tc	^{129}I	^{137}Cs
			(pCi/L)								
Source/Plume											
UE-7nS	06/10/2015	S	J 45.2	--	--	--	--	--	--	--	--
		SP [d]	53.3	--	--	--	--	--	--	--	--
UE-2ce	12/14/2016	S	120,000	--	--	--	--	<0.86	--	--	<4.7
		SP [d]	--	--	--	0.93	J 0.95	<2.8	<2.3E-04	1.0E-02	2.1
	12/15/2016	S(a)	134,000	--	--	--	--	<0.89	--	--	<6.1
		SP(a) [d]	--	--	--	0.95	1.14	<2.2	<2.3E-04	9.6E-03	2.2
		S(b)	134,000	--	--	--	--	<0.91	--	--	<6.8
		SP(b) [d]	--	--	--	0.96	1.13	<4.3	<4.7E-04	0.01	0.72
	12/16/2016	S	143,000	--	--	<318	<24.9	<0.96	<7.4	<1.0	<6.3
		D	--	--	--	<318	<24.8	--	<7.6	<0.64	--
		SP [d]	--	--	--	0.96	J 1.01	<1.1	<2.3E-04	9.3E-03	0.28
Early Detection											
TW-D	03/22/2018	S	<2.9	--	--	--	--	--	--	--	--
		D	<2.8	--	--	--	--	--	--	--	--
U-3cn-5	11/13/2017	S	10.2	--	--	--	--	--	--	--	--
		D	12.3	--	--	--	--	--	--	--	--
UE-1q	03/27/2018	S	<2.2	--	--	--	--	--	--	--	--
		D	<2.9	--	--	--	--	--	--	--	--
WW C-1	02/15/2018	S	12.2	--	--	--	--	--	--	--	--
		D	13.5	--	--	--	--	--	--	--	--
WW-2	04/22/2015	S	<2.2	U 2.3	5.0	<480	<2.6	<0.34	<8.6	<0.61	<7.6
		D	<2.2	U 1.7	7.3	<480	<2.7	<0.38	<7.0	<0.69	<9.2
		SP [d]	<0.2	--	--	J 0.04	1.3E-04	--	--	--	--
		SPD [d]	<0.2	--	--	J 0.04	1.4E-04	--	--	--	--

Table 2-4
RN Concentrations for Samples Collected from LCA Completions
(Page 3 of 3)

Location	Date	Type [a]	^{3}H	Gross Alpha	Gross Beta	^{14}C	^{36}Cl	^{90}Sr	^{99}Tc	^{129}I	^{137}Cs
			(pCi/L)								
Other											
ER-2-2	02/06/2016	S	J 13.3	--	--	--	--	--	--	--	--
ER-6-2	06/19/2014	S	<1.8	3.6	10.0	<470	<2.7	<0.47	<7.0	J <0.68	<8.6
		D	<2.2	3.1	10.5	<470	<3.6	<0.40	<7.0	J <0.78	<6.4
		SP [d]	<1.1	--	--	0.07	<1.3E-04	--	--	--	--
UE-10J	01/04/2018	S	<2.5	< 1.9	7.6	<380	<3.0	<0.48	<7.6	<0.74	<6.8
		D	<2.2	< 2.1	8.3	<390	<3.0	<0.49	<8.3	<0.80	<8.3
		SP [d]	<1.0	--	--	J 0.05	2.4E-04	--	--	--	--

Source: Navarro, 2019a

[a] S = Sample, D = Field duplicate, SP = Specialized laboratory analysis, SPD = Specialized laboratory analysis field duplicate sample.
[b] Gross alpha MCL (15 pCi/L) includes all alpha emitters except uranium and radon (CFR, 2018). The uranium concentration in the ER-4-1 sample and duplicate is 4.1 pCi/L (6.1 µg/L) (Navarro, 2019a); thus, the adjusted gross alpha values (13.3 and 12.4 pCi/L) are below the MCL.
[c] Value is a screening level and not the MCL; MCL is 4 mrem/yr. See text for further explanation.
[d] Sample analyzed by LLNL with the exception of ^{90}Sr and ^{137}Cs samples from UE-2ce. UE-2ce ^{90}Sr and ^{137}Cs samples were analyzed by LANL.

LANL = Los Alamos National Laboratory
MDC = Minimum detectable concentration

J = Result is estimated.
U = Compound was analyzed for, but was not detected ("Non-detect").
-- = Not analyzed.

Note: Values reported with "<" were below the MDC and therefore reported as "<MDC."

locations are provided in later sections. The ER-2-2 sample is discussed in Section 2.2, and the U-3cn-5 and UE-7nS samples are discussed in Section 2.3. The WW C-1 sampling results are discussed in Section 2.1.3.

Exceedance of the ^{3}H MCL was observed at a single location, UE-2ce. The ^{3}H concentration ranged from 120,000 to 143,000 pCi/L in time series samples collected from UE-2ce. No other RNs were detected in these samples by the commercial laboratory (Table 2-4). Concentrations well below the MDC were observed using the specialized analyses (Table 2-4). These results are further discussed in Section 2.4. These results focus on addressing the model evaluation target *^{90}Sr and ^{137}Cs mobility in the LCA*.

2.1.2 Historical Results

Historical results are presented in this section to further support the observation of the general lack of contamination in most Yucca Flat sampling locations (Table 2-4). Results for locations sampling near an underground nuclear detonation cavity (ER-2-2, ER-3-3, ER-4-1, ER-7-1, UE-2ce, UE-7nS, U-3cn-5) are not presented within this section. They are presented in the context of their proximity to the nearby detonation cavity in Sections 2.2, 2.3, or 2.4.

There have been significant differences in sampling and analytical protocols over the years; some samples were collected using pumps and some using depth-discrete bailers. Some analyses used the enrichment process for ^{3}H analysis, which reduced the MDC an order of magnitude. When analytical records for historical sampling are not complete, the analytical MDC is estimated based solely on the reported measurement error. In other cases, neither the MDC nor the measurement error is reported. In these cases, the reported value may or may not be above the MDC, and therefore the actual presence of the RN is uncertain.

Low levels of ^{3}H were previously reported at four locations (ER-6-1-2, ER-6-2, UE-1h, and WW C-1). The ^{3}H concentrations at ER-6-1-2 (31 pCi/L) and ER-6-2 (92 pCi/L) in samples collected in 2003 and 2004, respectively, were considered to be upper limits due to possible contamination after sampling (Rose, 2003; LLNL, 2005). No ^{137}Cs or ^{90}Sr was detected in these ER-6-1-2 and ER-6-2 samples above the 4- to 9.5-pCi/L MDCs for ^{137}Cs and the 0.43- to 0.52-pCi/L MDCs for ^{90}Sr. UE-1h was sampled in 1993 using a bailer, and the ^{3}H activity was reported as 6.08 pCi/L (2,136 ft bgs) and 10.9 pCi/L (1,978 ft bgs). The MDC is not reported with these results; therefore, the presence of ^{3}H in

these samples is uncertain. No ^{137}Cs or ^{90}Sr analyses were performed on these samples. Tritium has been observed in WW C-1 since the early 1960s; a discussion of these results is provided in Section 2.1.3

Three additional locations (TW-D, UE-1q, and WW-2) were routinely sampled as part of the Long-Term Hydrologic Monitoring Program (LTHMP), initiated in the early 1970s; and/or later under the Routine Radiological Environmental Monitoring Plan (RREMP), initiated in 1998. TW-D was sampled routinely since the early 1970s using a bailer within the slotted casing (1,800 to 1,880 ft bgs). UE-1q was sampled annually between 1999 and 2013 using a bailer at a depth of 2,475 ft. WW-2, a water supply well, was pumped through December 2008 with total withdrawals estimated to be about 1.0E+09 gal (Elliot and Moreo, 2011). WW-2 was sampled monthly to biannually from 1973 to 2006. No ^{3}H above MDCs (typically between 10 and 30 pCi/L) was reported in the majority of the historical samples from these wells (Navarro, 2019a). A few ^{3}H detections (5 to 150 pCi/L) were reported over the sampling period. No ^{137}Cs or ^{90}Sr was detected in the historical samples above the 1.9- to 9.8-pCi/L MDCs for ^{137}Cs and the 0.36- to 1.4-pCi/L MDCs for ^{90}Sr. The sporadic detections of low ^{3}H in the historical samples are viewed as uncertain, and are likely a result of sampling or laboratory cross contamination or uncertainty in the MDC. Groundwater contamination is suspected primarily when trends in the ^{3}H concentrations are observed as opposed to sporadic detections that are not repeated in subsequent samples from the same location.

UE-10j was previously sampled only in 1993. No ^{3}H was detected above the 190- to 210-pCi/L MDCs in these samples. Low-level ^{3}H analysis was not performed. No ^{137}Cs or ^{90}Sr was detected above the 4- to 8-pCi/L MDCs for ^{137}Cs and the 0.47- to 0.52-pCi/L MDCs for ^{90}Sr.

2.1.3 WW C-1

WW C-1 is open to about 170 ft of LCA, and about 1.1E+09 gal of water has been pumped from this well for water supply (Elliott and Fenelon, 2014). Additionally, nearby hole WW-C, located 30 meters (m) from WW C-1, which also is open to the LCA, pumped about 1.3E+09 gal from 1961 to 1995 (Elliot and Moreo, 2011). Tritium has been observed in WW C-1 and WW-C since the early 1960s (Navarro, 2019a). WW C-1 has been sampled quarterly between 1999 and 2012 in support of RREMP and before that was sampled monthly to quarterly in support of LTHMP. The sampling pump broke in 2012, and sampling was stopped until 2018 when a new pump was installed and sampling was performed in support of model evaluation.

WW C-1 is an early detection location and is sampled for low-level ^3H as stated in the NNSS Integrated Groundwater Sampling Plan (Table 2-2). WW C-1 is located at the southern edge of Yucca Flat (Figure 2-1). Concentrations were reported as 12.2 and 13.5 pCi/L for a sample and its duplicate in 2018 (Table 2-4). The MDCs for these analyses were 3.04 and 3.12 pCi/L, and the measurement errors were reported as 4.53 and 4.21 pCi/L for the sample and its duplicate, respectively.

This section will summarize the ^3H results historically reported and present potential sources of the ^3H in WW C-1 and also in the nearby well, WW-C.

2.1.3.1 Historical Results

The historical ^3H results for WW-C and WW C-1 are presented in Figure 2-2. The entire sampling period is presented in Figure 2-2a, and a zoomed-in view of the majority of the data is presented in Figure 2-2b for visualization purposes. The 13.5-pCi/L ^3H result for the 2018 sample was decay corrected over the sampling period to show the ^3H concentration expected if decay is the only process responsible for its decrease (see dashed line in Figure 2-2). General declines in ^3H activities are observed over time that are greater than would be expected by ^3H decay alone. The large variations in ^3H activity, particularly for samples collected from WW-C, may result from the interplay between pumping rate, pumping history, and well/aquifer dynamics; inconsistent sampling methods; variations in laboratory analytical error; and/or other factors (Pohlmann, 2018). Interestingly, the ^3H concentration decay corrected to 1964 is nearly identical to one of the 1964 samples (Figure 2-2).

The earliest ^3H results (1964 to 1971) were reported by Claassen (1973), who reported ^3H concentrations as high as 2,673 and 222 pCi/L in 1964 samples from WW-C and WW C-1, respectively. Neither the MDC nor the error are reported with these data, and no discussion of these results is included in the report. The ^3H for a WW C-1 sample collected in 1966 was reported as fewer than 700 ^3H units (<2,254 pCi/L), indicating an MDC nearly 3 orders of magnitude greater than that for most subsequent analyses reported by others (Figure 2-2). While elevated ^3H concentrations are reported for WW-C and WW C-1 by Claassen (1973), many other samples collected from other water supply wells around the same time (and likely analyzed within the same batches) showed anomalous ^3H detections, making these results highly uncertain. For instance, a ^3H concentration of 1,224 pCi/L was reported for a WW-8 sample collected the day before the WW C-1 sample with ^3H reported as 2,673 pCi/L. The other high ^3H result (and the highest reported for WW C-1) was for a sample collected on March 29, 1971 (1,095 pCi/L). A sample collected from Army 1 well (March 18, 1971)

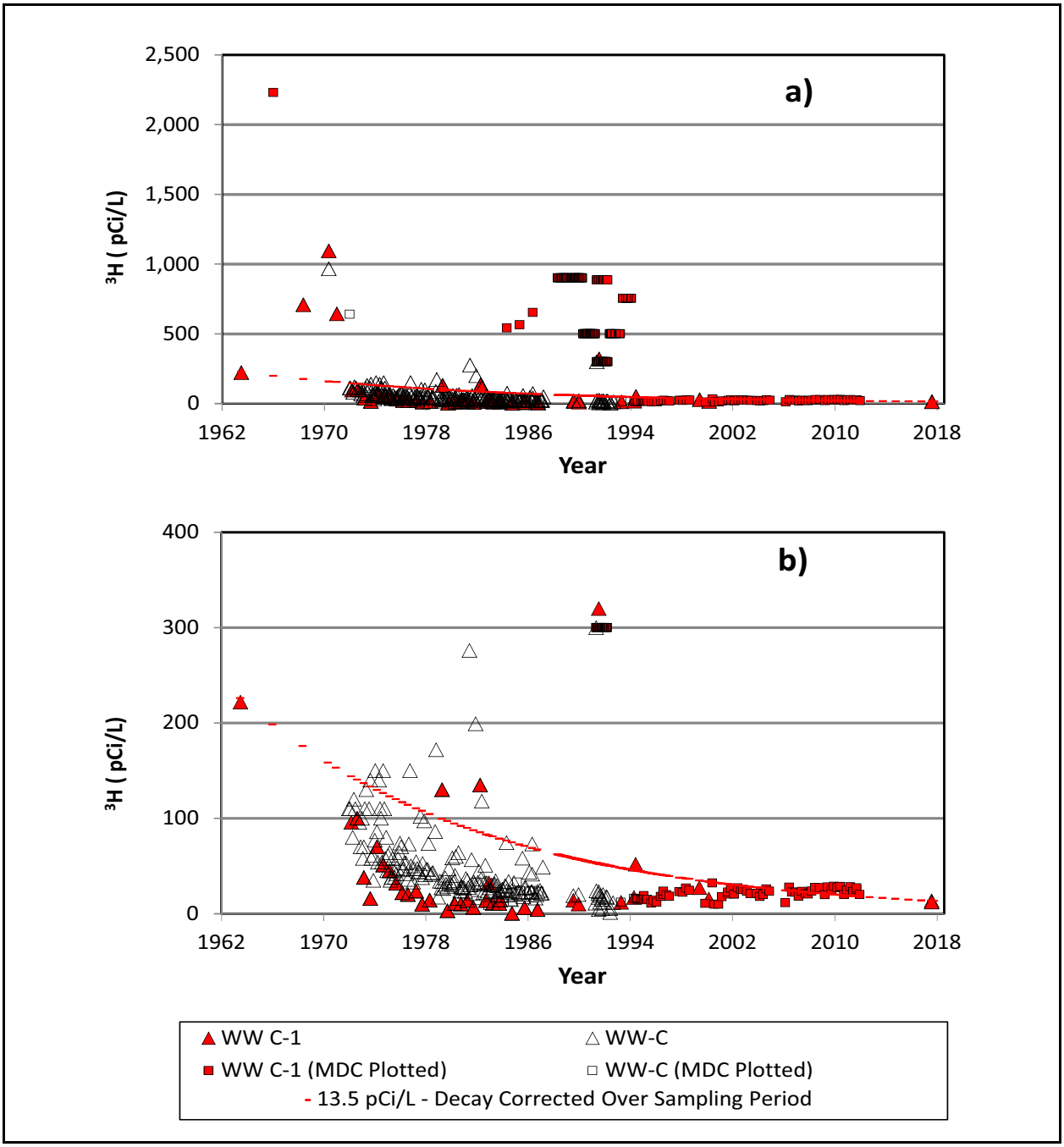

Figure 2-2
WW C-1 and WW-C ^{3}H Results (1964 to 2018)
Note: a = Full dataset, b = Zoomed-in view of lower ^{3}H concentrations.

within a couple of weeks of WW-C and WW C-1 (March 29, 1971) also reports a similar high ^{3}H concentration (869 versus 1,095 pCi/L). Both WW-8 and Army 1 wells are water supply wells with no detectable ^{3}H present. These results suggest a high positive bias in some ^{3}H results reported by Claassen (1973).

Lyles (1990) reports a declining trend in ^3H concentrations between 1973 and 1987. The reported ^3H concentrations ranged from -148 pCi/L (value is less than the MDC) to 135 pCi/L for WW C-1, and from -1.97 (value is less than the MDC) to 276 pCi/L for WW-C (Lyles, 1990). The ^3H concentration decreased approximately 70 pCi/L over this time period (Lyles, 1990).

Lantz (1978) documented LTHMP results for fiscal years 1971 through 1976. The nominal ^3H minimum detection limit (MDL) was 3E-07 microcuries per milliliter (µCi/mL) (300 pCi/L); the ^3H MDL was 600 pCi/L in 1970 and 1971, and decreased steadily through 1973 (Lantz, 1978). Lantz (1978) reported that "although infrequent positive samples of ^3H and plutonium were found, the evaluation of spot checks by other groups and the type of analysis involved indicated that none was detected." Reasons for the positive results were given as statistical fluctuations about the MDL or cross contamination in the laboratory. Lantz (1978) reported a ^3H concentration for a WW-C sample collected in 1972 of 100,000 pCi/L, which is considered to be a result of cross contamination in the laboratory.

Detectable ^3H was reported in 1993 as a maximum of 25.0 pCi/L for WW-C and 11.0 pCi/L for WW C-1 (EPA, 1996). Subsequent reported ^3H results were generally below the 10- to 30-pCi/L MDCs, with some sporadic detections ranging from 12 to 52 pCi/L (Navarro, 2019a; Russell, 2018).

2.1.3.2 Potential Sources of ^3H In WW-C and WW C-1

Several potential sources of ^3H at WW-C and WW C-1, both related and unrelated to underground testing, have been hypothesized. Lyles (1990) suggests that ^3H presence in these wells resulted from the accidental spillage of 0.1 to 0.2 curies (Ci) of ^3H, intended as an RN tracer, into WW C-1 in 1964. The planned tracer experiment was canceled, and little further data are available (Lyles, 1990). Additional sources were evaluated by Russell (2018) and Pohlmann (2018). Russell (2018) examined site-specific data and models to evaluate the feasibility of potential sources. Pohlmann (2018) summarized the YF/CM PER Committee discussions regarding these ^3H observations and their potential sources. These potential sources are described within this section.

Russell (2018) examined localized infiltration of precipitation through cracks in Yucca Lake, located a few kilometers (km) north of WW C-1 and WW-C, as a potential source for the ^3H. Large cracks that periodically develop in the playa deposits in southern Yucca Flat have been observed to drain substantial volumes of surface water into underlying sediments, possibly leading to recharge of the

LCA. For example, Doty and Rush (1985) measured more than 140,000 cubic meters (m^3) entering a single crack in 1974 to 1977, and Colton (1965) measured about 43,000 m^3 entering a crack during a single infiltration event in 1963. Using estimates of atmospheric ^3H content during these periods, Russell (2018) estimates about 0.02 Ci may have infiltrated in association with the events in 1974 to 1977 and about 0.31 Ci during the 1963 event alone, which occurred when atmospheric ^3H content was higher.

Russell (2018) also evaluated the potential for underground nuclear testing within Yucca Flat as the source for the ^3H. Only four detonations (BILBY, KLICKITAT, BYE, and AUK) within Yucca Flat were identified that have the potential to impact the LCA and that were detonated before ^3H was detected in WW-C and WW C-1 (1964). All were more than 15 km north and detonated within nine months of the ^3H observations, which requires groundwater flow velocities between 14.4 kilometers per year (km/yr) (BILBY) and 460 km/yr (AUK) (Russell, 2018). These unrealistically high velocities suggest that underground nuclear testing within Yucca Flat is not likely to be responsible for the first detections at WW-C and WW C-1 (Russell, 2018). In addition, the lack of ^3H in four wells (ER-7-1, ER-3-3, UE-1q, and ER-6-1) located directly downgradient of the majority of the LCA detonations, combined with the many years of pumping at WW-C and WW C-1, suggests that it is unlikely that large-scale ^3H migration extends south of these locations to WW C-1.

Pohlmann (2018) suggests that the decay-corrected signal may show a rising trend beginning around 1992 that could be interpreted as the arrival of a dispersed plume at WW C-1 and WW-C. The validity of this interpreted trend is difficult to assess because of the variability in the reported ^3H concentrations (Figure 2-2b). These variabilities are caused by the fact that many of the data are at or below their MDC and also result from variations in pumping schedules, sampling techniques, and analytical laboratories over the period of data collection.The majority of these results are well below the 1,000-pCi/L detection limit required for SDWA monitoring (CFR, 2018). Groundwater produced from WW-C and WW C-1 is possibly a mixture of water inflow from the eastern area that hosted few or no underground detonations, and groundwater from the testing area in the north. Therefore, ^3H concentrations measured at WW-C and WW C- 1 could be diluted compared to the concentrations in the testing area. Continued monitoring at this location will ensure potential MCL exceedances are known well in advance, and will confirm or refute a potential ^3H trend at this well.

2.1.4 Summary

Sampling for model evaluation from the LCA at ER-6-1-1, ER-6-2, TW-D, UE-1h, UE-1q, UE-10j, WW-2, and WW C-1 led to results consistent with historical samples. No ^{3}H was detected at these locations with the exception of WW C-1, where low values (12.2 and 13.5 pCi/L) were reported. The source of this low ^{3}H in groundwater at WW C-1 (<0.08 percent of the 20,000-pCi/L MCL for ^{3}H) is not known at this time. Several potential sources have been hypothesized, both related and unrelated to underground testing, and combinations of sources are also possible. Continued monitoring at this location will ensure potential MCL exceedances are known well in advance, and will confirm or refute any potential ^{3}H trend at this well. A better understanding of the ^{3}H sources may be useful for interpreting any observed future trends. Note that no other RNs except natural levels of ^{14}C, ^{36}Cl, and ^{129}I were detected in these samples (Table 2-4).

2.2 Interpreting Drilling Evidence from ER-2-2, ER-3-3, and ER-4-1

Three wells (ER-2-2, ER-3-3, and ER-4-1) were drilled in Yucca Flat to support model evaluation. The model evaluation well locations focused on the central corridor of Yucca Flat, where many deep, large-yield detonations were conducted (Figure 2-3). The wells were sited near detonations that potentially impacted the LCA. These detonations—CALABASH, WAGTAIL, and STRAIT—were thought to be within approximately $3R_c$ of the saturated LCA, or within $3R_c$ of a major fault. These locations were considered to have the greatest likelihood for encountering RNs in the LCA from testing (Kwicklis, 2015). Combinations of faulted and unfaulted locations were targeted to determine the impact of faults in the tuff confining unit (TCU) and LCA as transport pathways (Kwicklis, 2015).

Drilling evidence for these wells was intended to provide information to address four model evaluation targets (Table 2-1):

- *Exchange volume size/shape that extends into the LCA*
- *Extent of RN contamination in the LCA*
- *Fault transport properties*
- *LCA hydraulic properties*

The first three targets are addressed by evaluating RN concentrations observed during drilling. Concentrations of RNs with respect to the WP and cavity location and also with respect to nearby faults are evaluated to address these targets. Although little information regarding fault transport properties was acquired during drilling, the impact of faults on transport can be inferred by

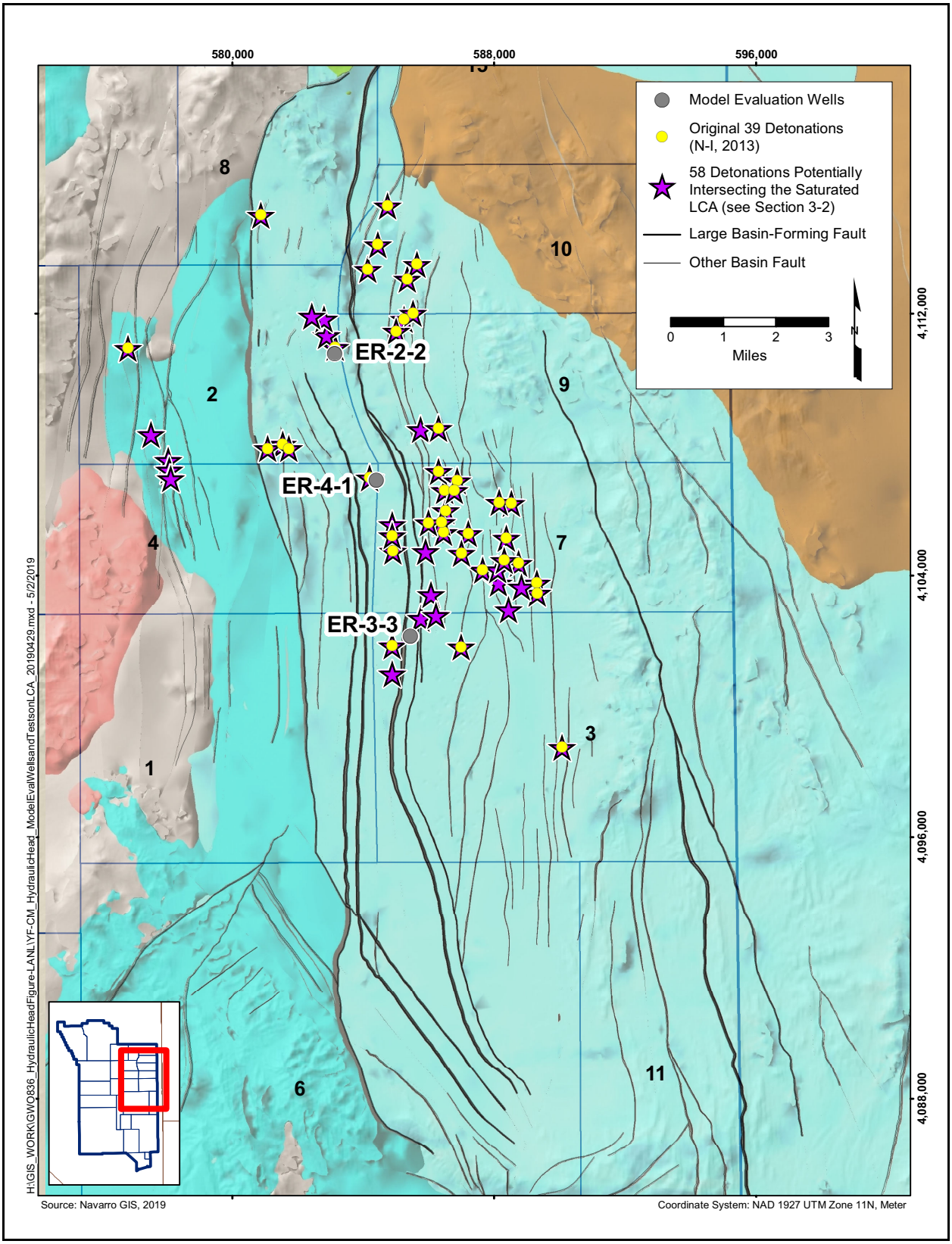

Figure 2-3
Locations of Model Evaluation Wells and Detonations Potentially Intersecting the Saturated LCA

evaluating RN concentrations in the LCA at locations near a fault (ER-2-2/CALABASH, ER-3-3/WAGTAIL) in comparison to locations without nearby faults (ER-4-1/STRAIT). The fourth target, *LCA hydraulic properties*, is addressed by estimating permeabilities/transmissivities using the drilling data (Section 2.2.5).

2.2.1 Evaluation of RNs Measured during Drilling

Details of drilling the model evaluation wells are provided in published well completion reports (DOE/EMNV, 2017a, b, and c). The well completion reports also present details regarding the RN sampling that took place during drilling. Two types of samples were collected during the drilling process: well discharge and discrete-depth bailer samples. Well discharge samples are collected periodically once drilling has advanced near the predicted water table and analyzed on site for ^{3}H. Select discharge samples are also sent to the laboratory if a lower detection limit is desired or to verify an onsite result. The average MDC for the onsite ^{3}H analyses were reported to be between 1,580 and 1,860 pCi/L (DOE/EMNV, 2017a, b, and c). The ^{3}H logs, presented in Appendix A, illustrate the results of the onsite ^{3}H analysis. Samples were also collected from ER-2-2 (TMLVTA) and ER-4-1 (lower tuff confining unit [LTCU]) using a depth-discrete bailer (Table 2-5).

This section provides background information for the model evaluation wells and describes the RN data collected during drilling. ER-4-1 and ER-3-3 samples collected after well development and testing are described in Section 2.3, “Sampling Near-field Wells.”

2.2.2 ER-2-2

ER-2-2 is located 194.2 m (637.1 ft) south of the CALABASH (U2av) detonation. CALABASH is located west of the Yucca fault in the central corridor in the northern part of the basin (Figure 2-3). CALABASH was detonated in 1969 at a depth of 2,050 ft (625 m) bgs. The CALABASH detonation has an announced yield of 110 kilotons (kt) (NNSA/NFO, 2015b) and an R_c of 56.3 m (Zavarin, 2014). The location of the CALABASH detonation with respect to ER-2-2 (i.e., within $3.4R_c$ at the WP) is shown in Figure 2-4.

CALABASH was originally thought to be within $2R_c$ of both the saturated LCA and a major fault, and studies of this detonation were thought to complement the findings of ER-4-1 located near STRAIT, a detonation with a similar R_c distance from the saturated LCA but located farther ($>5R_c$)

Table 2-5
ER-2-2 and ER-4-1 Depth-Discrete Bailer RN Results (pCi/L)

Analyte	ER-2-2		ER-4-1			
	01/24/2016 1,858 ft bgs TMLVTA		03/30/2016 1,768 ft bgs LTCU		03/30/2016 2,120 ft bgs LTCU	
Gross Alpha	J 216	J 193	880	840	331	680
Gross Beta	411	385	2,210	1,740	620	1,590
^{3}H	23,400,000	23,300,000	58,400	59,600	5,130	5,330
^{14}C	J+ 900	J+ 1,270	<370	<350	<400	<360
^{137}Cs	<7.2	<7.1	<8.7	<12	<10.6	<6.5
^{238}Pu	<0.023	<0.027	<0.033	<0.013	<0.035	<0.033
$^{239/240}Pu$	U 0.022	<0.021	<0.011	U 0.014	<0.035	<0.027

Source: Navarro, 2019a

Notes:
(1) Sample and field duplicate are reported for each location.
(2) Gamma-emitting RNs were not detected in the samples. ^{137}Cs is the only gamma emitter that is a COPC and therefore the only RN reported in this table.

J = Result is estimated.
J+ = Spectral problems prevented accurate quantitation. Result is estimated bias high.
U = Value was less than the MDC (0.009 pCi/L) plus error (0.017 pCi/L) and is considered a nondetect.
-- = Not analyzed

from major faults (Kwicklis, 2015). In reality, the LCA was approximately 160 m deeper than expected and is therefore likely to be greater than $3R_c$ below the CALABASH WP (Figure 2-4).

Elevated ^{3}H activities, approximately 9,300 to 24,800,000 pCi/L, were observed in grab samples collected from the TMLVTA and LTCU between 566.93 m (1,860 ft) bgs and 675.13 m (2,215 ft) bgs (see Figure A-4). These results are consistent with the 23,400,000- and 23,300,000-pCi/L ^{3}H activities reported for a sample and duplicate collected using a depth-discrete bailer at 566.3 m (1,858 ft) bgs (Table 2-5). A fluid discharge sample, collected while the drill was circulating in the borehole at 975.4 m (3,200 ft) bgs in the LCA (accessing the LTCU, Oak Spring Butte confining unit [OSBCU], argillic tuff confining unit [ATCU], and LCA), was analyzed for ^{3}H. The reported ^{3}H concentration, 13.31 pCi/L, was qualified by the laboratory as an estimate because quality control criteria were outside acceptable limits (Table 2-4). This is consistent with the lack of ^{3}H observed in the ^{3}H log for these hydrostratigraphic units (HSUs) (Figure A-4). As shown in Figure 2-4, the elevated ^{3}H is observed adjacent to the CALABASH chimney slightly outside the $3R_c$ sphere surrounding the WP. Very low ^{3}H (13.3 pCi/L) was detected in the LCA despite the close proximity of

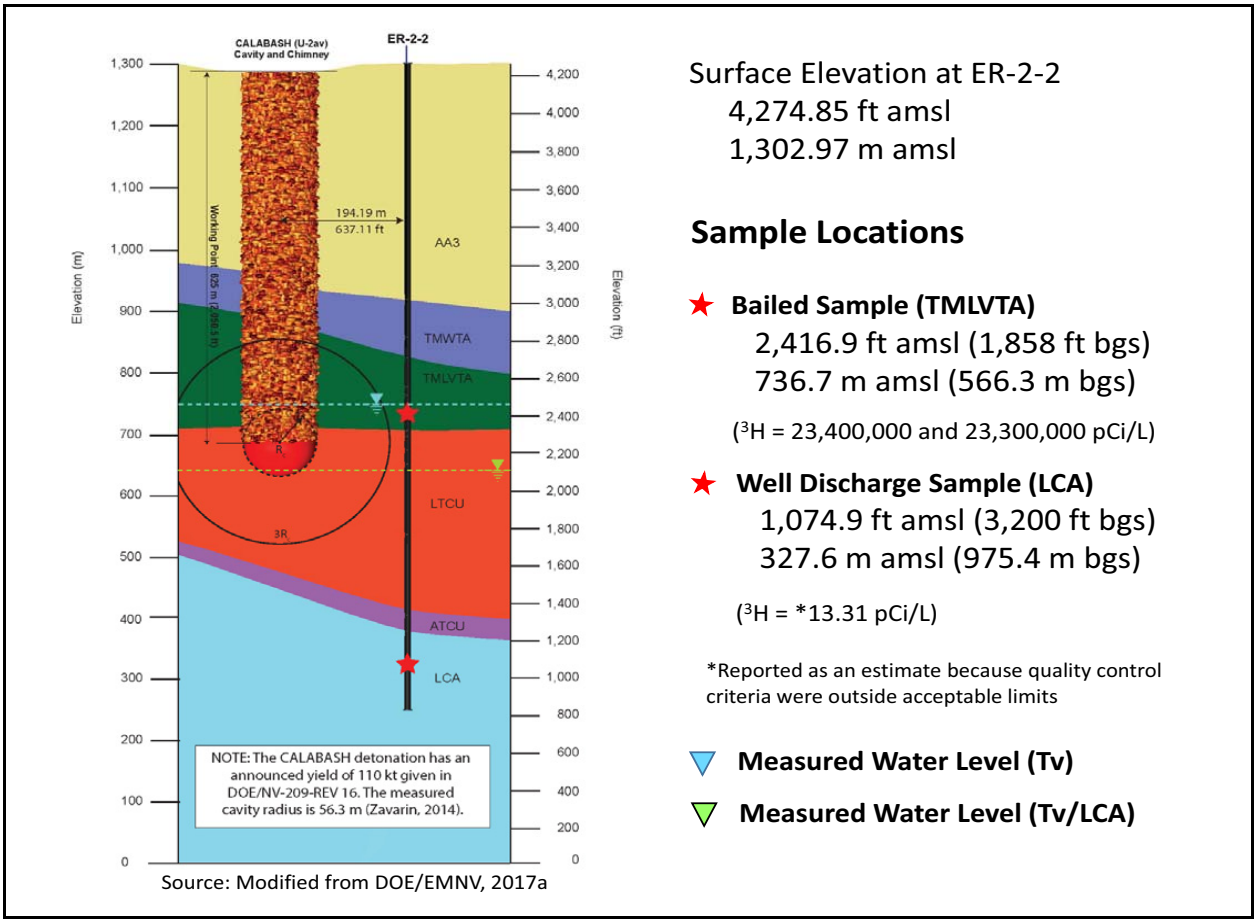

Figure 2-4
ER-2-2 Location with Respect to CALABASH Crater, Cavity, and Chimney

a fault and the CALABASH detonation and the greater than 20-million-pCi/L ^{3}H present in the overlying units. Due to unstable borehole conditions, ER-2-2 was plugged below a depth of 836 m (2,743 ft) bgs. The borehole is now open to the LTCU and OSBCU (see Figure A-1).

2.2.3 ER-3-3

ER-3-3 is located 196.4 m (644.3 ft southwest of the WAGTAIL (U3an) detonation. WAGTAIL was detonated in 1965 at a depth of 749.5 m (2,459 ft) bgs. The WAGTAIL detonation has an announced yield of 20 to 200 kt (NNSA/NFO, 2015b) and an estimated R_c of 65 m based on the maximum of the announced yield (200 kt) and Equation 1 in Pawloski (1999). WAGTAIL was selected for investigation as part of model evaluation because it is located within $1R_c$ of the eastern strand of the Yucca fault based on the YF/CM hydrostratigraphic framework model (HFM). The location of the WAGTAIL detonation with respect to ER-3-3 (i.e., within $3.0R_c$ at the WP) is shown in Figure 2-5.

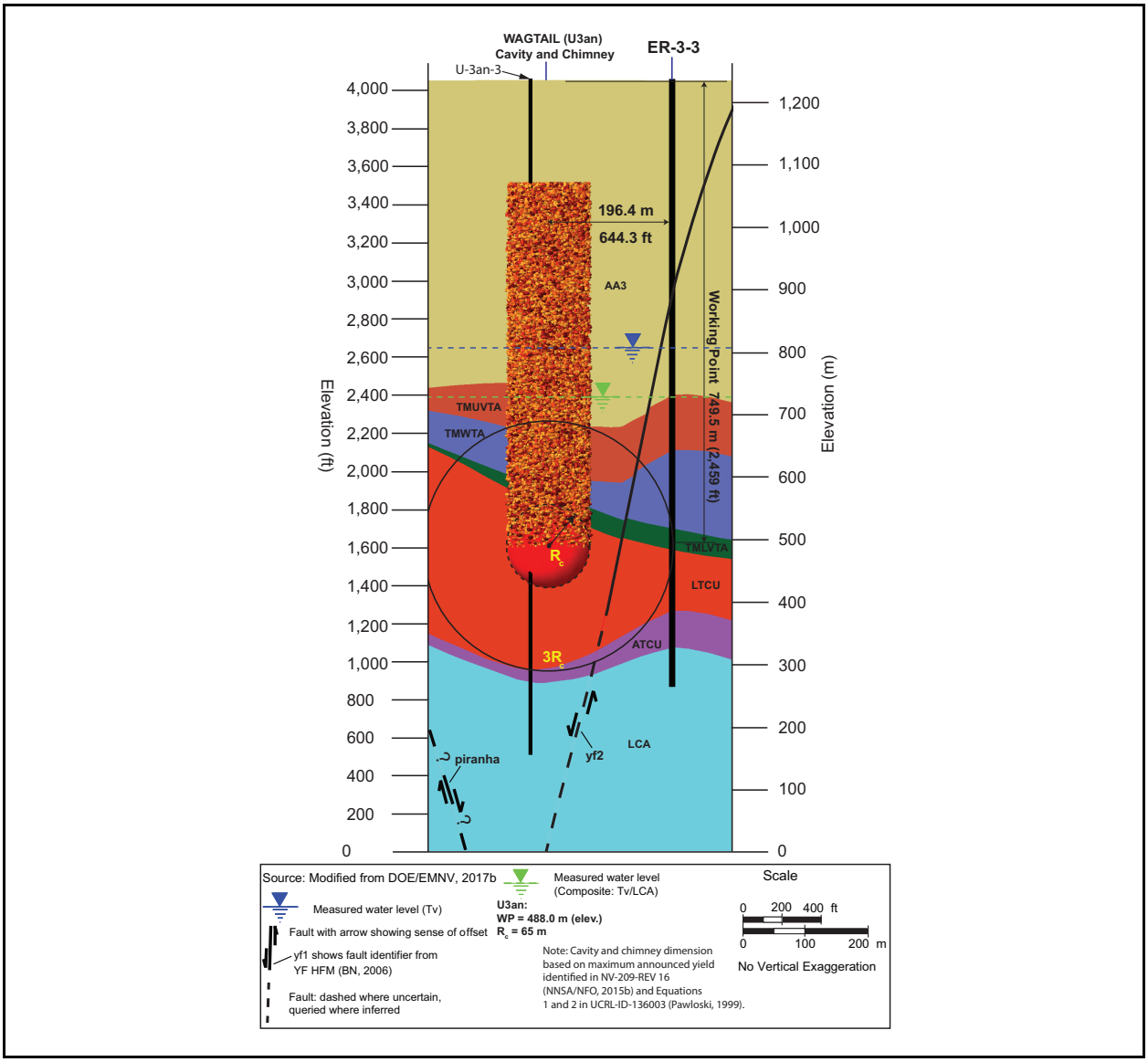

Figure 2-5
ER-3-3 Location with Respect to WAGTAIL Cavity and Chimney

The LCA is likely to be approximately 3.6R_c below the WAGTAIL WP. Although the LCA was encountered at 910 m bgs at ER-3-3, the LCA was deeper (984 m bgs) at Well U-3an-3, which is located 49.1 m from the WAGTAIL detonation (Figure 2-5). The distance of the WP depth to the LCA at ER-3-3 and U-3an-3 are 160.5 m (2.5R_c) and 234.4 m (3.6R_c), respectively. Because U-3an-3 is located closer to the WAGTAIL detonation (0.76R_c) it is likely a better indicator for the location of the LCA at WAGTAIL.

Figure A-5 shows ^{3}H activities ranging from 0 to 4,558 pCi/L measured during drilling. The majority of the ^{3}H spikes shown in Figure A-5, including the 4,558-pCi/L result, are analytical noise and not actual ^{3}H detections because most reported values are near or below the MDC. The MDCs ranged from 1,168 to 10,047 pCi/L, with an average of 1,860 pCi/L. The 4,558-pCi/L result was below the associated 10,047-pCi/L MDC and therefore represents analytical noise instead of an actual detection. Due to borehole instability and the injection of large amounts of mud, bailer samples were not collected in ER-3-3 until well after drilling was completed.

2.2.4 ER-4-1

ER-4-1 is located 220 m (722 ft) east of the STRAIT (U4a) detonation. STRAIT was detonated in 1976 at a depth of 782.4 m (2,566 ft) bgs. The STRAIT detonation has an announced yield of 200 to 500 kt (NNSA/NFO, 2015b) and an estimated R_c of 87 m based on the maximum of the announced yield (500 kt) and Equation 1 in Pawloski (1999). The location of the STRAIT detonation with respect to ER-4-1 (i.e., within 2.5R_c at the WP) is shown in Figure 2-6. The depth of the LCA at ER-4-1 is 859 m (2,818 ft) bgs and is less than 2R_c below the STRAIT WP based on the YF/CM HFM (Figure 2-6).

STRAIT was selected for investigation as part of model evaluation because it is located within 1R_c of the saturated LCA and was identified to be one of the most likely detonations to have impacted the LCA. Because STRAIT is more than 5R_c from any nearby faults, ER-4-1 can assess the exchange volume and integrity of the TCU near a major detonation away from faults.

Two high-amplitude gamma spikes were observed from 472.44 to 481.48 m (1,550 to 1,580 ft) bgs and at approximately 539.50 m (1,770 ft) bgs in the LTCU (DOE/EMNV, 2017c). The depth of these peaks and the depth of the STRAIT WP suggest that these anomalies may be associated with one of the other nearby underground nuclear detonations (Figure 2-7). The 3R_c extent for each detonation in the plane cut through ER-4-1 is shown in Figure 2-7. Two nearby detonations, TECHADO (U4o) and ROUSANNE (U4p), may be considered sources, as these detonations are located within approximately 2.5R_c of the STRAIT detonation but have WPs that are approximately 250 m (820 ft) shallower than the STRAIT detonation (Figure 2-7).

Two zones in Well ER-4-1 with elevated levels of ^{3}H were encountered during drilling (Figures A-6 and A-7). The first zone was in the TMLVTA and LTCU at 367 to 390 m (1,204 to 1,280 ft) bgs; ^{3}H

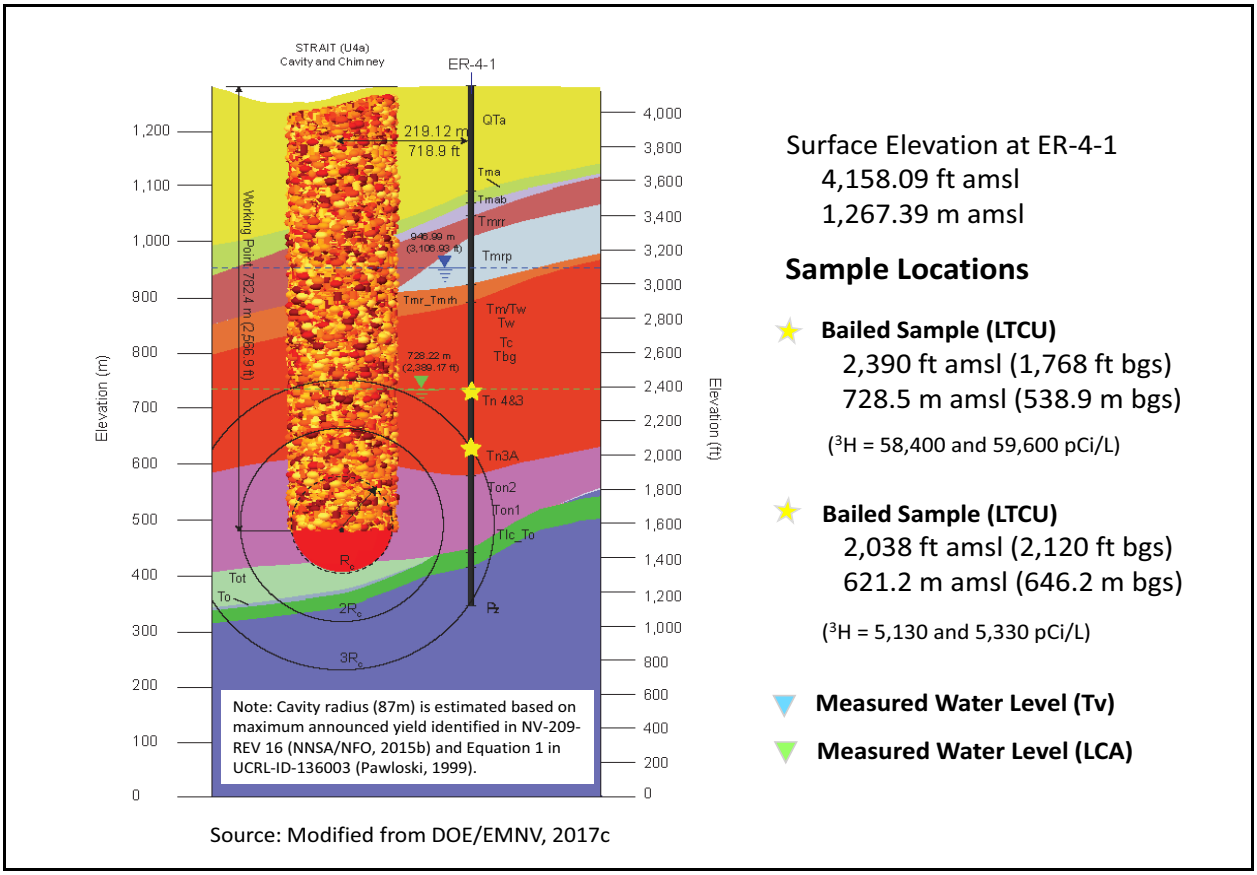

Source: Modified from DOE/EMNV, 2017c

Figure 2-6
ER-4-1 Location with Respect to STRAIT Crater, Cavity, and Chimney

activities ranged from 21,825 to 239,022 pCi/L. The second zone was in the LTCU at 542 to 575 m (1,778 to 1,886 ft) bgs; ^{3}H activities ranged from 8,739 to 100,680 pCi/L. The gamma spike was also observed at this depth. Elevated ^{3}H was also reported for bailer samples collected in the LTCU (Table 2-5). The location of these samples is shown on Figure 2-6. As shown in Figure 2-6, the elevated ^{3}H is observed adjacent to the STRAIT chimney slightly outside the $3R_c$ sphere surrounding the WP. The ^{3}H activity is nearly 3 orders of magnitude less than observed at ER-2-2 and may likely be attributed to the two more shallow detonations, TECHADO and ROUSANNE, which are within $3R_c$ of ER-4-1 at the locations with elevated ^{3}H and observed gamma activity (Figure 2-7). Although some spikes are observed within the LCA in the ^{3}H logs (Figure A-6), the reported values are near the MDC for these field analyses and therefore do not likely represent ^{3}H presence.

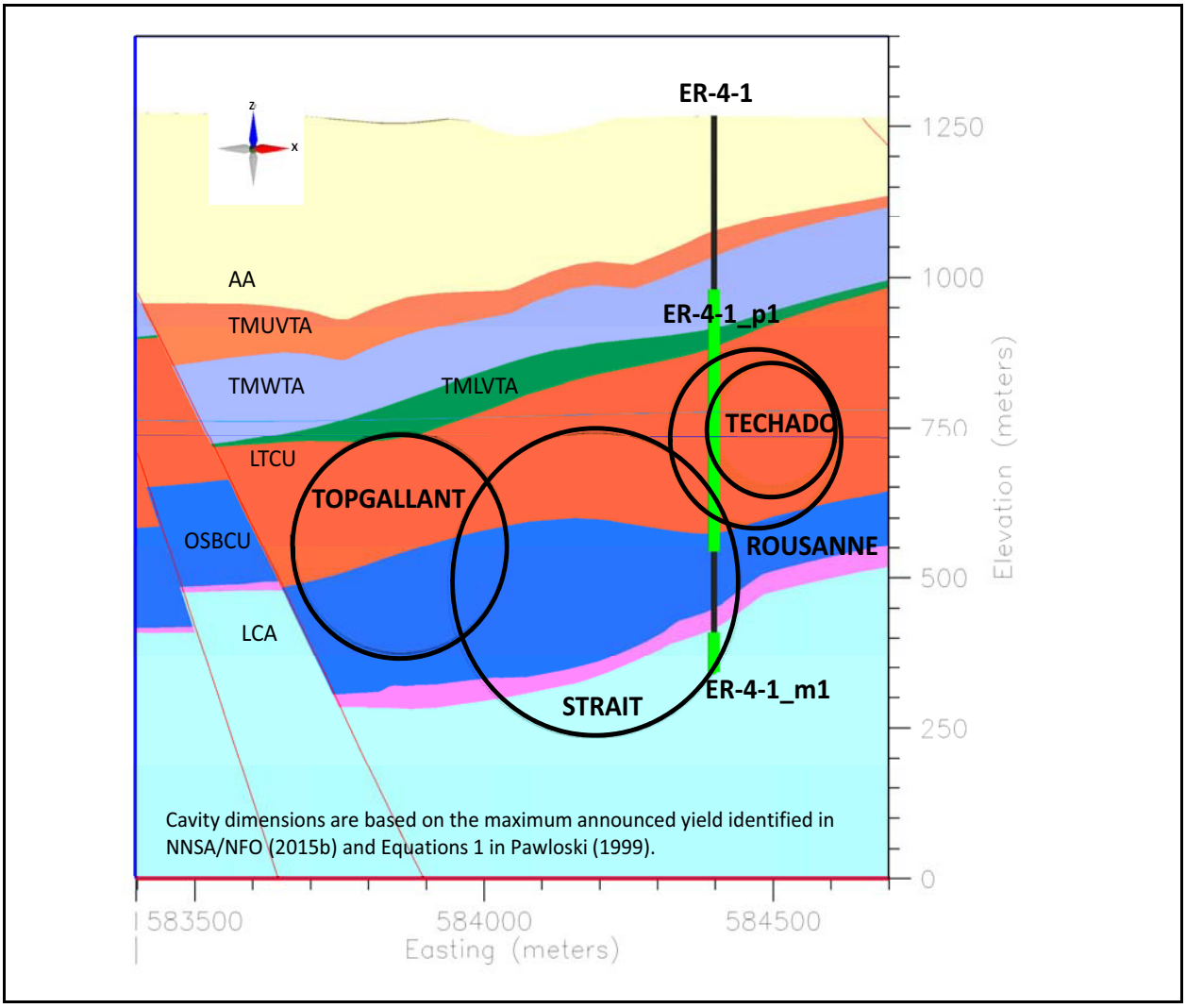

Figure 2-7
Perspective View of STRAIT, ROUSANNE, TECHADO, and TOPGALLANT Detonations ($3R_c$) and Well ER-4-1
Note: Plane cut through ER-4-1 is shown.

2.2.5 Permeability Estimates

Based on the drilling data, transmissivity was solved iteratively using the Cooper-Jacob equation (Cooper and Jacob, 1946):

$$T = 0.183 \frac{Q}{s_W} \log\left(\frac{2.25(Tt)}{r_W^2 S}\right) \qquad (2\text{-}1)$$

where:

T = Transmissivity (L^2/time)

Q = Constant discharge (L^3/time)

t = Time since pumping began

r_w = Radius of pumped well (L)

s_w = Estimated drawdown (L)

S = Storage coefficient (dimensionless)

Water production rates, estimated from visual observations of surface fluid discharge and bromide concentrations, are likely cumulative across all units below the water table. Production observed in higher intervals at earlier times above the current drill bit location were therefore subtracted when assessing the production at depth. Estimates of the cumulative water production versus depth were compared to the hydrostratigraphic column at each well to estimate the water production originating from different HSUs (Table 2-6).

Table 2-6
Permeability Estimates for WTA, TCU, and LCA

Well	Total Thickness (ft)			Production Rate (gpm)			Permeability (m^2)			T (ft^2/day)
	WTA	TCU	LCA	WTA	TCU	LCA	WTA	TCU	LCA	LCA
ER-2-2	>Water Table	1,080	420	N/A	20	73	N/A	7E-16	9E-15	9
ER-3-3	520	515	210	187	217	79	2E-14	1E-15	2E-14	8
ER-4-1	>Water Table	1,555	215	N/A	4	207	N/A	3E-17	5E-14	37

ft^2/day = Square feet per day
m^2 = Square meter
WTA = Welded-tuff aquifer

The drilling data analysis was not a typical Cooper-Jacob analysis fitting many drawdown points on a semi-log plot of time versus drawdown. The drilling data provide only a single point on the curve, and the Cooper-Jacob equation was solved to roughly estimate transmissivity for this single point. The transmissivity calculations require estimates of elapsed pumping time, water production within an interval, and aquifer storativity. The analysis assumed the pumping time is the elapsed drilling time within the HSU. The specific storage value is assumed to be 1E-06 for the LCA and WTA hydrogeologic units (HGUs), and 1E-05 for the TCU HGU. The dewatered conditions produced during drilling allow an estimate of maximum drawdown during water production. This was done for the LCA, TCU, and WTA HGUs at Wells ER-2-2, ER-3-3, and ER-4-1; permeability estimates for

these HGUs are presented in Table 2-6. The calculated transmissivity values for the LCA are also presented in Table 2-6. The ER-4-1 estimate for transmissivity calculated using drilling data (37 ft^2/day) is quite consistent with the 55- and 56-ft^2/day estimates reported by Jackson (2017) and Navarro (2018), respectively for the analysis of the WDT results (Section 2.5).

2.2.6 Summary

Three model evaluation wells (ER-2-2, ER-3-3, and ER-4-1) were drilled in Yucca Flat near detonations that potentially impacted the LCA. These detonations—CALABASH, WAGTAIL, and STRAIT—are either within approximately $3R_c$ of the saturated LCA (STRAIT) or of a major fault (CALABASH and WAGTAIL). The LCA is estimated to be greater than $3R_c$ below the CALABASH and WAGTAIL WPs, and within $2R_c$ of the STRAIT WP. No significant RN contamination was detected in the LCA at these wells (Table 2-4). A single sample from the LCA at ER-2-2 was reported to have 13.31-pCi/L ^{3}H. This value was qualified as an estimate because laboratory quality control criteria did not meet the acceptance criteria. No ^{3}H was detected in samples collected from the LCA at ER-3-3 or ER-4-1 (Table 2-4).

High ^{3}H was observed in ER-2-2 (23,400,000 and 23,300,000 pCi/L) and ER-4-1 (58,400 and 59,600 pCi/L) samples collected from the TMLVTA and LTCU HSUs, respectively. The elevated ^{3}H was observed adjacent to the CALABASH and STRAIT chimneys, slightly outside the $3R_c$ (based on the announced yield) sphere surrounding the WP (Figures 2-4 and 2-6). Gamma activity was also observed in the LTCU in the ER-4-1 borehole. The gamma and ^{3}H activity at ER-4-1 may likely be attributed to the two more shallow detonations, TECHADO and ROUSANNE, which intersect ER-4-1 within $3R_c$ of these detonations at the locations with elevated ^{3}H and observed gamma activity (Figure 2-7). Although ^{3}H was reported in samples collected while drilling ER-3-3 (0 to 4,558 pCi/L), these results were attributed to analytical noise and not actual ^{3}H detections because most, including the 4,558-pCi/L result, were below the MDC.

The LCA transmissivity was estimated from the drilling data to be 9, 8, and 37 ft^2/day at ER-2-2, ER-3-3, and ER-4-1, respectively (Table 2-6). The ER-4-1 estimate for transmissivity calculated using drilling data (37 ft^2/day) is quite consistent with the 55- and 56-ft^2/day estimates reported by Jackson (2017) and Navarro (2018), respectively, after analysis of the WDT results (Section 2.5). Unfortunately, the LCA at ER-2-2 is inaccessible because the wellbore was plugged (Section 2.2.2), and the ER-3-3 WDT results were not reliable because of poor hole conditions (Navarro, 2018).

Therefore, the transmissivities calculated using drilling data (9 and 8 ft^2/day, respectively) could not be compared to WDT results at ER-2-2 and ER-3-3.

2.3 Sampling Near-field Wells

Near-field wells were sampled to address the *Exchange volume size/shape that extends into the LCA* model evaluation target (Table 2-1). Sampling and analysis of five near-field wells (ER-3-3, ER-4-1, ER-7-1, U-3cn-5, and UE-7nS) that access the LCA near an underground detonation are presented in this section. The locations of these wells are shown on Figure 2-1. Sampling and analysis of an additional near-field well (UE-2ce) that accesses the LCA3 near an underground detonation (NASH) is presented in Section 2.4.

2.3.1 ER-3-3

ER-3-3 was drilled in 2016 and is categorized as a characterization well (DOE/EMNV, 2018). ER-3-3 includes three piezometers accessing the LCA (p1); TMWTA, TMLVTA, and LTCU (p2); and the Timber Mountain upper vitric-tuff aquifer (TMUVTA) (p3). It also includes two screened intervals within the main completion accessing the LCA (m1); and the TMWTA, TMLVTA, and LTCU (m2) (Figure A-2). Groundwater sampling of the main completion (ER-3-3_m1) was conducted at the end of WDT (Navarro, 2018). Approximately 9,500 gal of groundwater (~2.8 well volumes) was purged before sampling (Table 2-3). The field water-quality data (bromide, pH, SEC, purge volume) for samples collected over the pumping period (December 1 to December 15, 2016) are presented in Figure 2-8. Bromide is mixed with the drilling fluid as a tracer, and its concentration is an indication of well development. As can be seen from Figure 2-8, the bromide concentrations declined from an initial concentration of approximately 1.7 mg/L to about 0.2 mg/L, indicating removal of drilling fluids. A high pH (~10) remained throughout the pumping period, which is atypical of the LCA groundwaters in Yucca Flat. This suggests that the sample is not fully representative of the formation water and is likely impacted by the concrete plug used to separate the two main completion intervals.

No RNs were detected with the exception of natural levels of ^{14}C and ^{36}Cl using LLNL's highly sensitive analytical methods (Table 2-4). Tritium was not detected above the 310-pCi/L MDC by the commercial laboratory and the 1.0-pCi/L MDC by LLNL. No ^{137}Cs or ^{90}Sr was detected above the 7.7- and 8.0-pCi/L MDCs for ^{137}Cs and the 0.23- and 0.26-pCi/L MDCs for ^{90}Sr. Although the sample

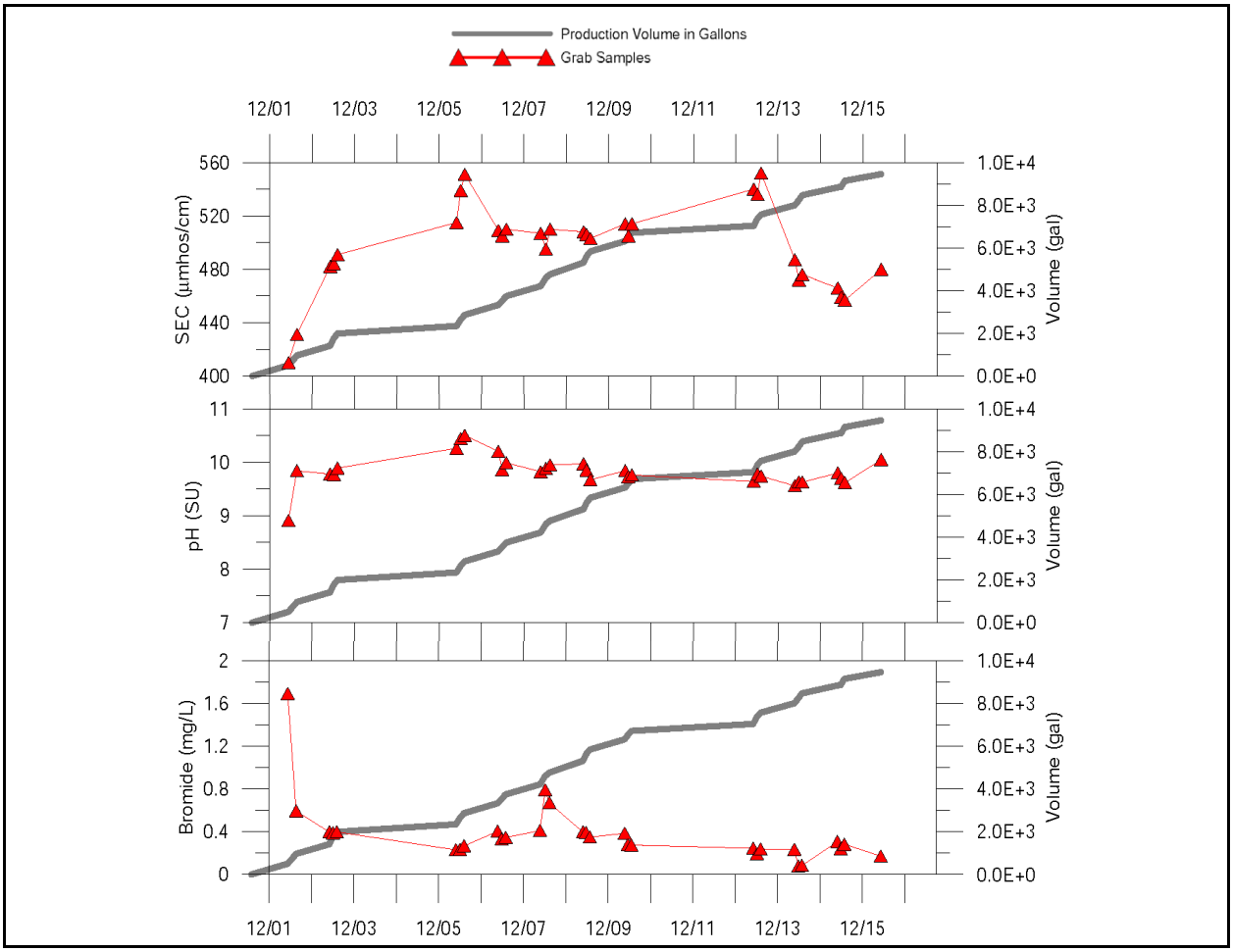

Figure 2-8
Field Water-Quality Measurements during ER-3-3 Pumping
Source: Navarro, 2018

is not considered fully representative of the formation water, the lack of ^{3}H at the low level of detection (1.0 pCi/L) indicates that significant RN transport through the Yucca fault into the LCA does not appear to occur at this location.

2.3.2 ER-4-1

ER-4-1 was drilled in 2016 and is categorized as a characterization well (DOE/EMNV, 2018). ER-4-1 is completed with a piezometer that accesses approximately 512 ft of the LTCU and 95 ft of the OSBCU (Figure A-3). The ER-4-1 main completion (ER-4-1_m1) accesses the LCA between 2,812 to 3,035 ft (857.1 to 925.1 m) bgs (Figure A-3). Groundwater sampling of the main completion (ER-4-1_m1) was conducted at the end of WDT (Navarro, 2018). Approximately 1.7 million gal of groundwater (~1,200 borehole volumes) was purged before sampling. The field water-quality data

associated with the samples are reported in Table 2-3. The low bromide concentration (0.35 mg/L) indicates that drilling fluids were removed before sample collection. The pH (6.8) is relatively consistent with that observed at the other LCA wells, and the turbidity is quite low (0.6) (Table 2-3); therefore, samples are considered to be representative of formation water. No RNs were detected with the exception of natural levels of ^{14}C and ^{36}Cl using LLNL's highly sensitive analytical methods (Table 2-4). Tritium was not detected above the 2.84- and 2.83-pCi/L MDC for the sample and duplicate by the commercial laboratory and the 1.0-pCi/L MDC by LLNL. No ^{137}Cs or ^{90}Sr was detected above the 5.2- and 7.8-pCi/L MDCs for ^{137}Cs and the 0.95- and 0.96-pCi/L MDCs for ^{90}Sr.

Groundwater sampling of the piezometer (ER-4-1_p1) was conducted using a bailer in January 2017 and using a rod pump in March 2018. The ^{3}H concentration was reported as 733 and 648 pCi/L for bailed sample collected at a 623-m (2,044-ft) depth. Approximately 4,150 gal of groundwater was later purged from ER-4-1_p1 using a rod pump. Tritium was reported as 329 and 353 pCi/L for the sample and duplicate. No other RNs were analyzed for these samples. The ^{3}H observed in the piezometer samples is lower than that observed in the depth-discrete bailer samples collected from the open borehole (Section 2.2).

As can be seen from Figure 2-7, the interval accessed by the main completion (ER-4-1_m1) intersects the $3R_c$ extent for STRAIT; and the interval accessed by the piezometer (ER-4-1_p1) intersects the $3R_c$ extent for STRAIT, TECHADO, and ROUSANNE. The absence of detectable levels of ^{3}H in ER-4-1_m1 (LCA) samples and the relatively low levels of ^{3}H in ER-4-1_p1 (LTCU and OSBCU) samples indicate the STRAIT exchange volume is less than $3R_c$ based on the maximum of the assumed yield range (NNSA/NFO, 2015b) and Equation 1 of Pawloski (1999).

2.3.3 ER-7-1

ER-7-1 was drilled in 2003 and is categorized as a characterization well (DOE/EMNV, 2018). The well has a screened interval from 1,852 to 2,500 ft (564 to 762 m) bgs in the LCA (NNSA/NSO, 2004). ER-7-1 was constructed within a cluster of underground nuclear detonations (Figure 2-9). The closest detonation, TORRIDO, is located 200 m north of ER-7-1. TORRIDO was detonated in 1969 at a depth of 514.8 m bgs, with an announced yield of 20 to 200 kt (NNSA/NFO, 2015b). TORRIDO has an estimated R_c of 71 m based on the maximum of the announced yield (200 kt) and Equation 1 in Pawloski (1999), and is therefore located approximately $2.8R_c$ from ER-7-1. The TORRIDO WP was in the OSBCU. At ER-7-1, the LCA was encountered at

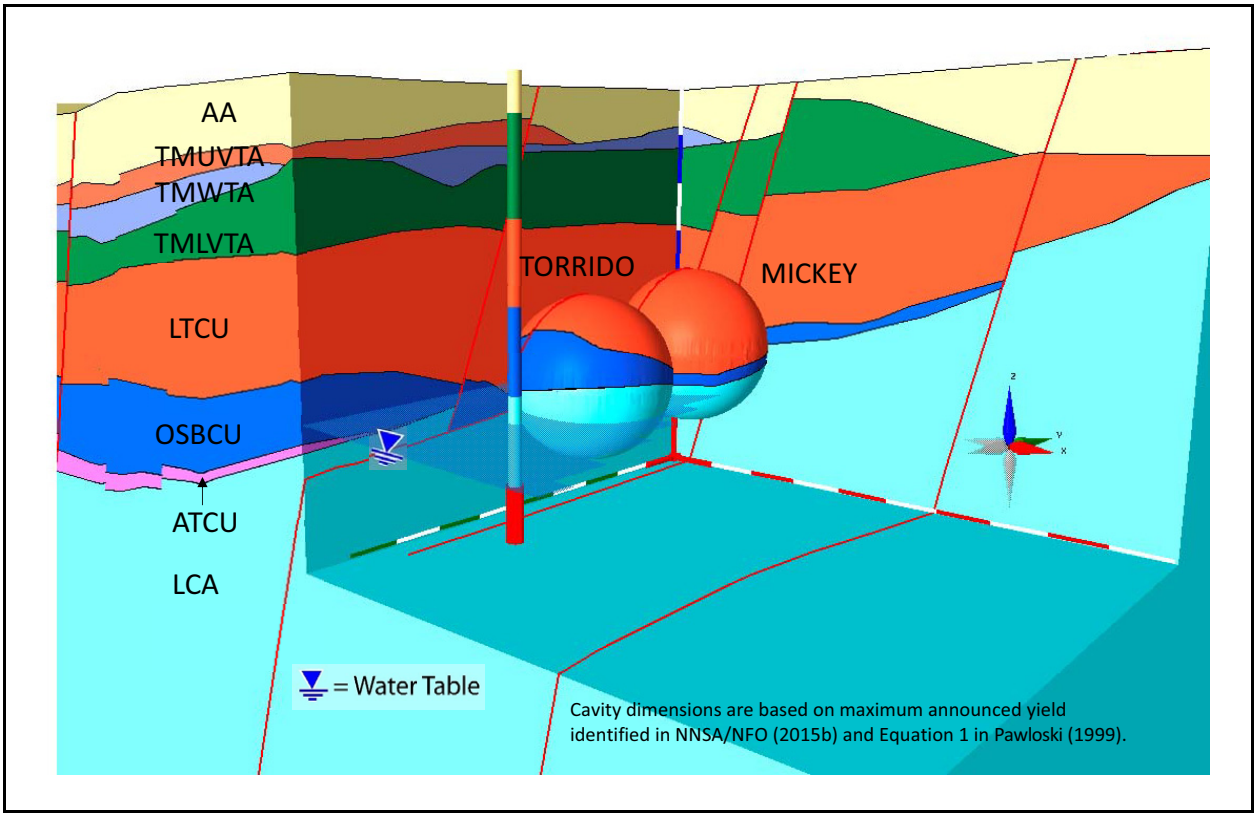

Figure 2-9
Perspective View of TORRIDO and MICKEY ($2R_c$) Detonations and Well ER-7-1
Source: Modified from N-I, 2013

the same depth as the TORRIDO WP, 515 m bgs. The water table is estimated to be at a depth of 573 m bgs at TORRIDO (DOE/NV, 1997). The saturated LCA is therefore likely to be within $1R_c$ of the TORRIDO WP.

The next closest underground detonation is MICKEY (U7m), which is located 500 m north of ER-7-1. MICKEY was detonated in 1967 at a depth of 499.6 m, with an announced yield of 20 to 200 kt (NNSA/NFO, 2015b). MICKEY has an estimated R_c of 72 m based on the maximum of the announced yield (200 kt) and Equation 1 in Pawloski (1999). The MICKEY WP was in the LTCU. The water table is estimated to be at a depth of 566 m bgs at MICKEY (DOE/NV, 1997). The saturated LCA is therefore likely to be within $1R_c$ of the MICKEY WP.

Hourly samples collected during ER-7-1 drilling indicated that ^3H remained at background levels (Shaw, 2003). The lack of ^3H detected during drilling suggests that the TORRIDO exchange volume extent is less than $3R_c$. Little detectable activity in the ER-7-1 groundwater was observed in 2003 (Navarro, 2019a). Tritium was reported as 117.2 ± 4.3 pCi/L, which was considered to be an upper

limit due to possible post-sampling contamination. No other RNs were detected with the exception of natural levels of ^{14}C, ^{36}Cl, and uranium (U) using LLNL's highly sensitive analytical methods. No ^{137}Cs and ^{90}Sr were detected above the 6.9- and 8.7-pCi/L MDCs for ^{137}Cs and the 0.48- and 0.52-pCi/L MDCs for ^{90}Sr.

Groundwater sampling was initiated on June 20, 2014, after purging approximately 24,000 gal of groundwater, which equates to approximately 5.5 well volumes (one well volume is approximately 4,333 gal). No RNs were detected with the exception of natural levels of ^{14}C and ^{36}Cl (Table 2-4). Tritium was not detected above the 2.2-pCi/L and 2.3-pCi/L MDCs by the commercial laboratory and the 1.1-pCi/L MDC by LLNL. No ^{137}Cs or ^{90}Sr was detected above the 6.7- and 7.1-pCi/L MDCs for ^{137}Cs and the 0.52- and 0.59-pCi/L MDCs for ^{90}Sr.

2.3.4 U-3cn-5

U-3cn-5 was drilled in 1965 and 1966 and is categorized as an early detection well (DOE/EMNV, 2018). This well is located 122 m laterally from the BILBY WP and was drilled to a depth of 3,025 ft (922 m) bgs, well below the BILBY cavity in the LCA (Figure 2-10). BILBY (U3cn) was detonated in 1963 at a depth of 713 m, with an announced yield of 249 kt (NNSA/NFO, 2015b). BILBY has a measured R_c of 63.7 m (Zavarin, 2014). The BILBY detonation was emplaced in the OSBCU within about 150 m ($2.2R_c$) of the LCA. A post-shot diagnostic hole, Well U-3cn PS 2, was drilled into the BILBY chimney and cavity (793 m depth) 10 days after the BILBY detonation. Well U-3cn PS 2 has perforations approximately 200 m above the WP and is open to the cavity (Figure 2-10). Water levels in U-3cn-5 completed in the LCA are 15.8 m lower than U-3cn PS 2. Thus, the groundwater gradient is from the tuff to the carbonate.

A groundwater sample was collected from U-3cn-5 on November 13, 2017, after purging about 5,900 gal of groundwater, which equates to approximately 22 well volumes. Tritium was detected at 10.2 pCi/L and 12.3 pCi/L in the sample and duplicate. Consistent with the early detection analytical suite (Table 2-2), no other RNs were analyzed. This is the first time ^{3}H has been detected in U-3cn-5 samples in more than four decades, although sporadic ^{3}H detections have been reported historically in samples collected from this well (Figure 2-11). Lyles (1990) reports results from the LTHMP that range from -12.4 pCi/L (less than the MDC) to 966 pCi/L for pumped samples collected between 1972 and 1981 with no observable trends (Figure 2-11). The MDCs for these analyses are estimated based on the reported error (Lyles, 1990). Most of the earliest ^{3}H results are low (<10 pCi/L)

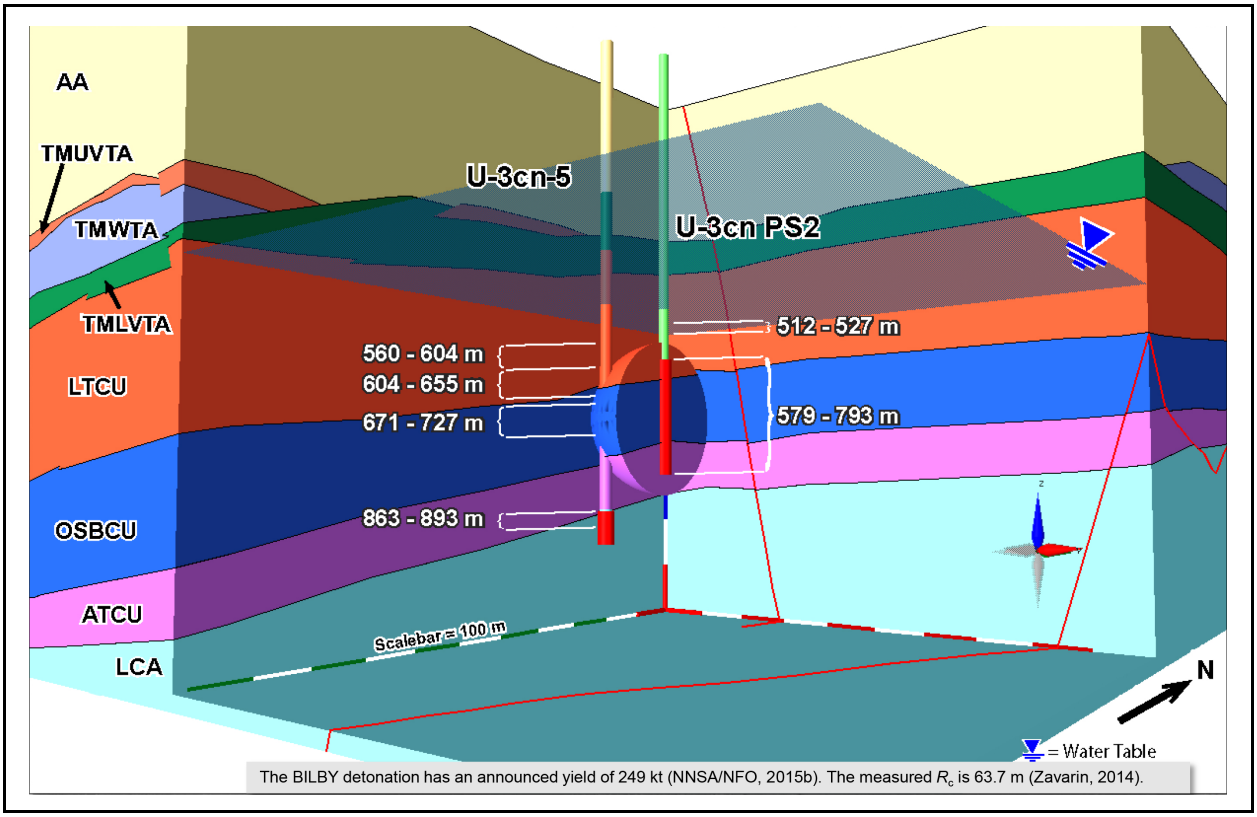

Figure 2-10
Perspective View of BILBY Detonation ($2R_c$) and Wells U-3cn 5 and U-3cn PS 2
Source: Modified from N-I, 2013

compared to the typical MDCs (10 to 43 pCi/L) reported in the later samples. Similarly, values reported as detections are often similar to the MDCs reported within the same time period (Figure 2-11). Because many of the results are near, or below, the estimated MDCs, there is uncertainty regarding the actual presence of ^{3}H in these samples.

Hydraulic tests were conducted in U-3cn PS 2 and U-3cn-5 between 1964 and 1973; these tests are summarized in Tompson et al. (2008). Between 1964 and 1966, a series of pumping tests was conducted in U-3cn PS 2, extracting water from two intervals (Figure 2-10). One is located in a 214-m interval at the bottom of the hole, crossing the cavity; and the other is in a 15-m, packed-off interval just below the water table at 512-m depth (Figure 2-10). ^{3}H activities near the cavity were between 2E+08 and 3E+08 pCi/L, and ^{3}H activities from the chimney region above the cavity were between 1E+06 and 1E+08 pCi/L. The ^{3}H decreased from 4E+07 to 8E+06 pCi/L in samples collected between 1977 and 2007 from the upper interval near the water table at Well U-3cn PS 2. The presence of ^{14}C, ^{36}Cl, ^{90}Sr, ^{99}Tc, ^{106}Ru, ^{129}I, ^{137}Cs, ^{234}U, ^{235}U, ^{238}U, and $^{239+240}Pu$ was observed in

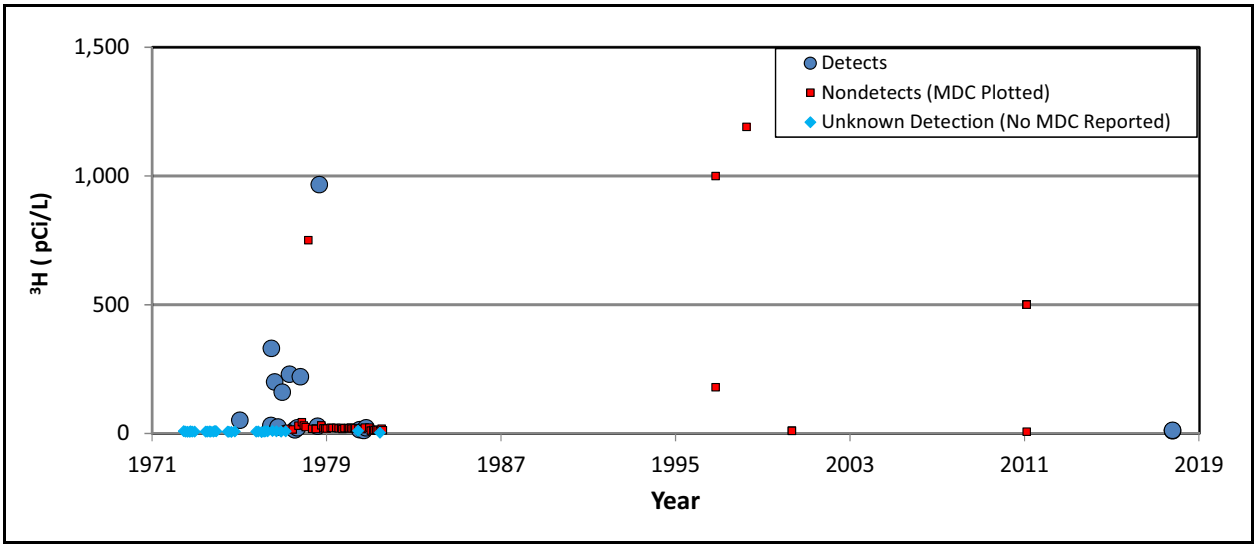

Figure 2-11
U-3cn-5 ^{3}H Results (1961 to 2018)

these samples; none exceeded the MCL (Navarro, 2019a). These U-3cn PS 2 results indicate initial ^{3}H contamination (2E+08 and 3E+08 pCi/L) within a lateral distance of 2.5R_c of the BILBY WP, which is located approximately 150 m (2.2R_c) above the LCA.

Hydraulic testing at U-3cn-5 was performed between 1965 and 1973, extracting water from several distinct intervals located at, above, and below the general cavity elevation (Figure 2-10). Table 2-7 summarizes the testing dates, the volume of water swabbed, and the range of ^{3}H activities for each tested interval. On February 1, 1966, U-3cn-5 was cased to a depth of 863 m and cemented at 837 to 863 m, isolating the LCA from the tuff units above. The ^{3}H activities were highest in the 671- to 727-m interval, which included the WP depth of 718 m (1.9R_c from the BILBY WP) (Table 2-7). These results are consistent with those observed at U-3cn PS 2, where the ^{3}H activities ranged from 1E+06 to 3E+08 pCi/L. The ^{3}H activity is significantly less in the LCA interval (863 to 893 m). Tritium was detected only in the first three samples collected while pumping the 863- to 922-m interval; all subsequent samples were below the 1.5E+03-pCi/L MDC. This suggests that the first three samples, with elevated ^{3}H, may have represented fluid that moved down the well from the shallow intervals in the tuffs.

In 1997, 1.16E+05 gal of water was purged from U-3cn-5, and ^{3}H was reported as less than 1,790 pCi/L. No other RNs were detected above their MDCs (IT, 1997).

Table 2-7
U-3cn-5 Hydraulic Testing Information

Interval (m)	Dates	Volume Swabbed (gal)	^{3}H Results (pCi/L)
560 – 604	01/03/1966 – 01/05/1966	6,656	1.6E+06 – 8.5E+06
604 – 655	01/01/1966 – 01/02/1966	7,461	1.6E+06 – 3.2E+06
671 – 727	12/19/1965 – 12/22/1965	7,446	<1.3E+03 – 1.3E+08
863 – 893	02/01/1966 – 02/04/1966	2,000	<1.3E+03 – 9.4E+04
863 – 922	11/21/1966 – 11/23/1966	Pumped [a]	<1.3E+03 – 1.1E+04
863 – 922	03/06/1967 – 09/22/1969	Pumped [b]	<1.5E+03

Source: Tompson et al., 2008

[a] Pumped volume not reported.
[b] Pumped continuously at about 60 gpm.

Zavarin (2012) reports results for a sample collected from U-3cn-5 in March 2011, and no RNs were detected above background levels using high-resolution analysis of ^{3}H, ^{14}C, ^{36}Cl, ^{99}Tc, ^{129}I, and U isotopes (Zavarin, 2012). No ^{3}H was detected above the 6.5-pCi/L MDC. These results indicate that the groundwater at this location is effectively isolated from the highly contaminated groundwater in the overlying tuff that constitutes the BILBY near-field.

2.3.5 UE-7nS

UE-7nS was drilled in 1976 and is categorized as a source/plume well (DOE/EMNV, 2018). The casing of this well is slotted from 1,995 to 2,199 ft (608.1 to 670.3 m) bgs in the LCA. UE-7nS is located 137 m southeast of the BOURBON detonation (Figure 2-12). BOURBON (U7nS) was detonated in 1967 at a depth of 560 m, with an announced yield of 20 to 200 kt (NNSA/NFO, 2015b). BOURBON has an estimated R_c of 69 m based on the maximum of the announced yield (200 kt) and the equation reported in Boardman (1970). The BOURBON WP was in the unsaturated LCA. The water level was reported as 1968.38 ft (600 m) bgs in July 2018 (USGS, 2019). Thus, the bottom of the BOURBON cavity is likely located in the saturated LCA. A fault was identified nearby at a depth of 594 m, very close to the water table (Buddemeier and Isherwood, 1985).

A sample was collected from UE-7nS on June 10, 2015, using a bailer at a depth of 2,018 ft bgs. Field measurements at the time of sampling are presented in Table 2-3. Tritium activities were reported by the commercial laboratories as 45.16 pCi/L. The value was reported with a “J” qualifier, indicating

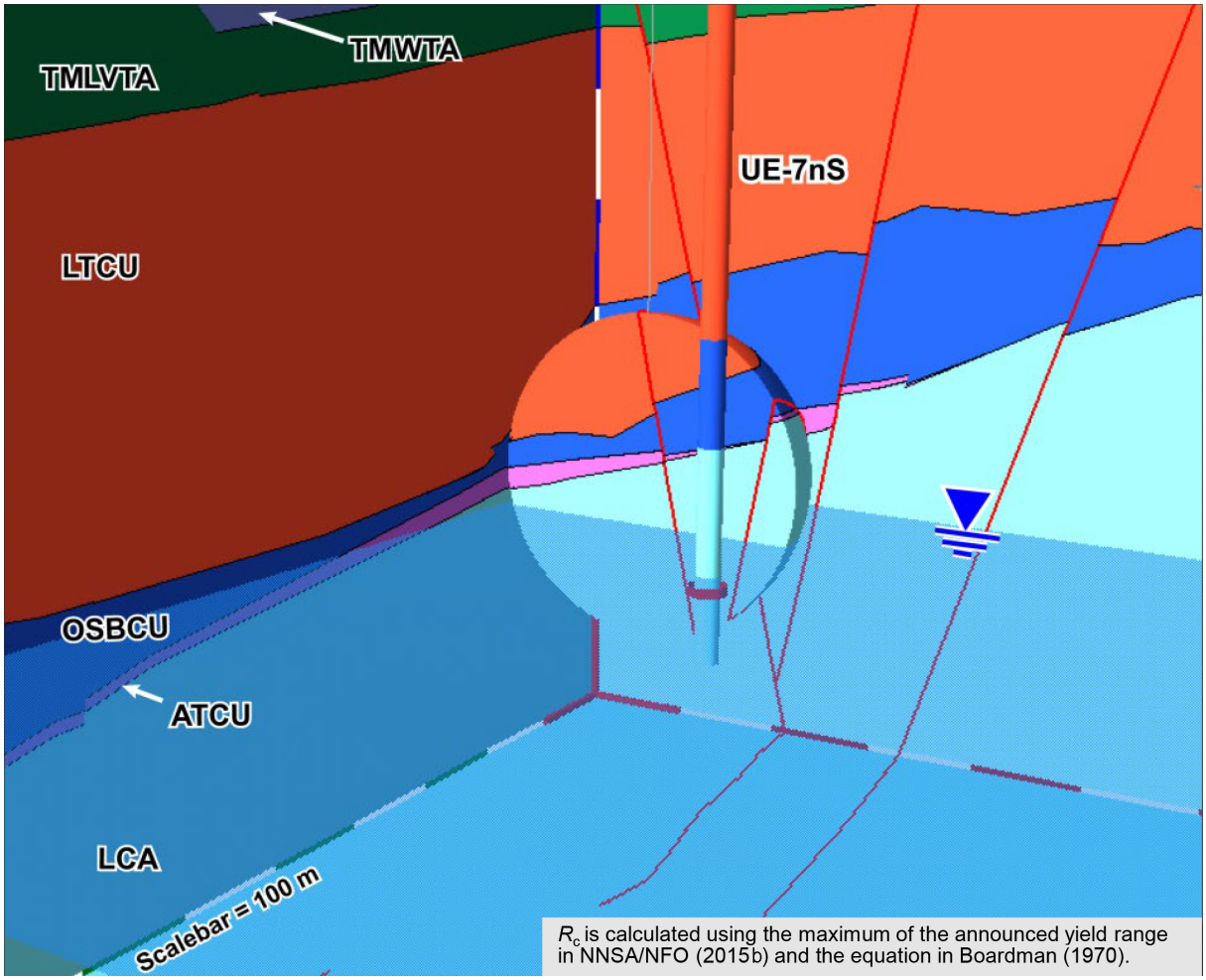

Figure 2-12
Perspective View of BOURBON Detonation ($2R_c$) and Nearby Observations Wells
Source: Modified from N-I, 2013

that the result is an estimation (the laboratory control sample recovery exceeded the control limits). LLNL reported a ^{3}H activity of 53.3 pCi/L. The rod pump could not be used to pump samples because the well was not able to sustain sufficient production to deliver groundwater to the surface. This resulted from excessive drawdown condition. Only ^{3}H was measured for these bailed samples.

Groundwater has been sampled at this well periodically for a variety of RNs (Navarro, 2019a). Intermittent pumping and groundwater sampling took place at UE-7nS from 1976 through 1987. A gradual increase in ^{3}H activity was observed over this time period (Figure 2-13). The maximum ^{3}H activity observed in these samples was 4,640 pCi/L, which was observed in 1984. This equates to 23 percent of the 20,000-pCi/L MCL for ^{3}H. After 1987, sampling was performed using a wireline bailer, and a steady decrease in ^{3}H activity was observed (Figure 2-13). Only limited analyses of other

RNs are available. Samples collected by LLNL in 2001 and 2004 were analyzed for ^{3}H, ^{14}C, ^{36}Cl, and ^{129}I. Although samples were collected from the same depth, 2,025 ft (617 m), a decrease in ^{3}H (4,600 to 132 pCi/L), ^{36}Cl (1.4E-03 to 2.4E-04 pCi/L), and ^{129}I (6.1E-04 to 4.1E-05 pCi/L) was observed over this time period. The ^{14}C activity in these samples are essentially the same (Figure 2-13). Samples collected in 2000, 2005, 2008, 2011, and 2015 were analyzed for ^{90}Sr, which was not detected with MDCs ranging from 0.2 (2005) to 1.15 (2008) pCi/L. The MCL for ^{90}Sr is 8 pCi/L. Samples collected in 1983, 1993, and periodically between 2002 and 2015 were analyzed for ^{137}Cs. All but the 1983 sample were nondetects with respect to ^{137}Cs; ^{137}Cs in 1983 was reported as 0.04 pCi/L. Detection limits in the later samples ranged from 0.25 to 8.3 pCi/L (Navarro, 2019a). The MCL for ^{137}Cs is 200 pCi/L.

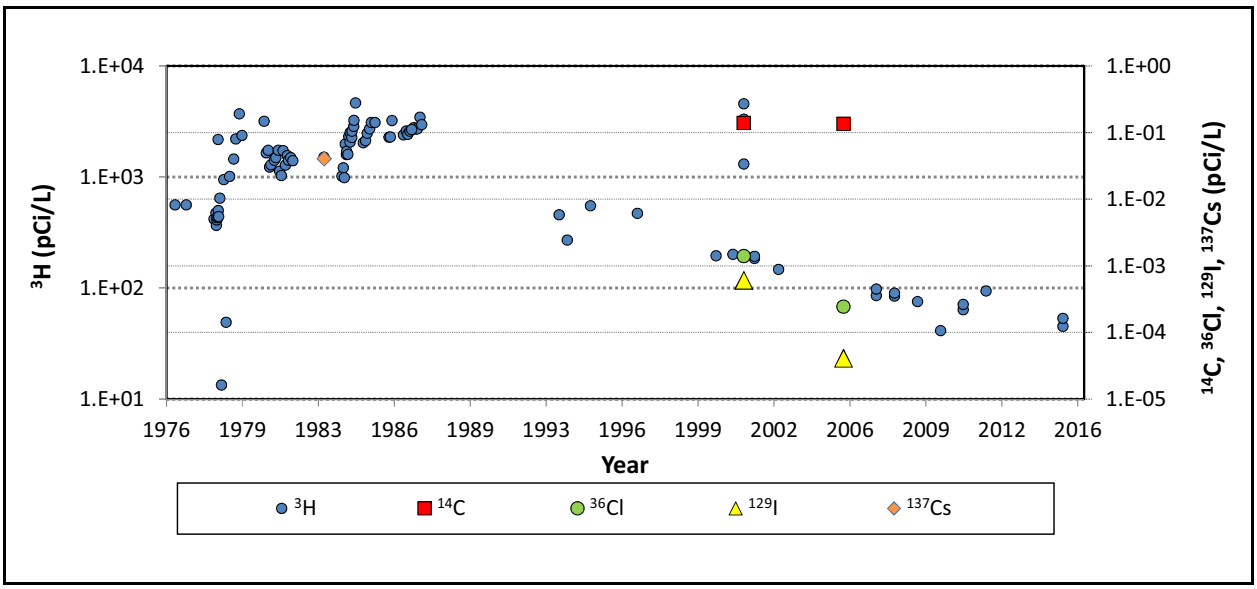

Figure 2-13
RN Activities Relative to MCLs at Well UE-7nS

2.3.6 Summary

Sampling of five near-field wells (ER-3-3, ER-4-1, ER-7-1, U-3cn-5, and UE-7nS) demonstrates a lack of significant contamination in the LCA in the vicinity of underground nuclear detonations near the saturated LCA or near a major fault. No ^{3}H above the 1-pCi/L MDC was observed in three of these wells (ER-3-3, ER-4-1, ER-7-1) and low ^{3}H (10.2 to 53 pCi/L) was observed in the other two (U-3cn-5 and UE-7nS). Four of these wells (ER-4-1, ER-7-1, U-3cn-5, UE-7nS) sampled the LCA near a detonation with a WP within $3R_c$ of the saturated LCA. The low ^{3}H concentrations at these locations suggest that the exchange volume extent is less than $3R_c$ below the WP for these

detonations. There is also no evidence from UE-7nS that the exchange volume for RNs that partition into the gas phase (^{14}C) or that have volatile precursors (^{137}Cs and ^{90}Sr) is more extensive than that of ^{3}H in the vicinity of an LCA-hosted detonation in the UZ.

2.4 Sampling NASH Test Cavity at Satellite Well UE-2ce

Sampling the NASH test cavity at satellite Well UE-2ce was performed to address the following model evaluation targets (DOE/EMNV, 2017d):

- *Extent of RN contamination in the LCA*
- *^{90}Sr mobility in the LCA*
- *^{137}Cs mobility in the LCA*

UE-2ce was drilled in 1977 to a depth of 502.9 m and is categorized as a source/plume well (DOE/EMNV, 2018). Well UE-2ce is located 183 m south of the NASH WP and has a main completion interval in the LCA3 (420 to 495 m bgs). Well UE-2ce is the only LCA/LCA3 location with a history of detectable ^{90}Sr and ^{137}Cs activities. This is also the only LCA/LCA3 location where ^{3}H exists above the 20,000-pCi/L MCL. These factors make UE-2ce a desirable location to evaluate the mobility of ^{90}Sr and ^{137}Cs in a carbonate aquifer.

NASH (U2ce) was a 39-kt (announced yield) test detonated on January 19, 1967 (NNSA/NFO, 2015b). Chimney collapse occurred shortly after detonation (Buddemeier and Isherwood, 1985). The NASH WP (364 m bgs) was above the water table in the LCA3 (DOE/NV, 1997). The tuff-carbonate contact is located at 340 m bgs (Figure 2-14). The R_c formed by the NASH detonation is 95.47 ft (29.10 m) (Zavarin, 2014).

Time series samples were collected from UE-2ce_m1 from December 14 to 16, 2016 (Table 2-3). The ^{3}H activity increased from 120,000 to 143,000 pCi/L over the pumping period (Table 2-4). Although the ^{3}H activity greatly exceeded the 20,000-pCi/L MCL, ^{90}Sr was not detected above its MDC (0.86 to 0.96 pCi/L), and ^{137}Cs was detected at very low levels (0.28 to 2.2 pCi/L). The ^{137}Cs measurements required a specialized analytical procedure by LANL to be able to detect the ^{137}Cs (Table 2-4). Figure 2-15 shows plots of the four RNs detected in the time-series samples. The RN concentration relative to its MCL is shown. As can be seen from Figure 2-15, only ^{3}H exceeds its MCL. The plot also shows an increasing trend with respect to the purge volume for ^{3}H (~17 percent)

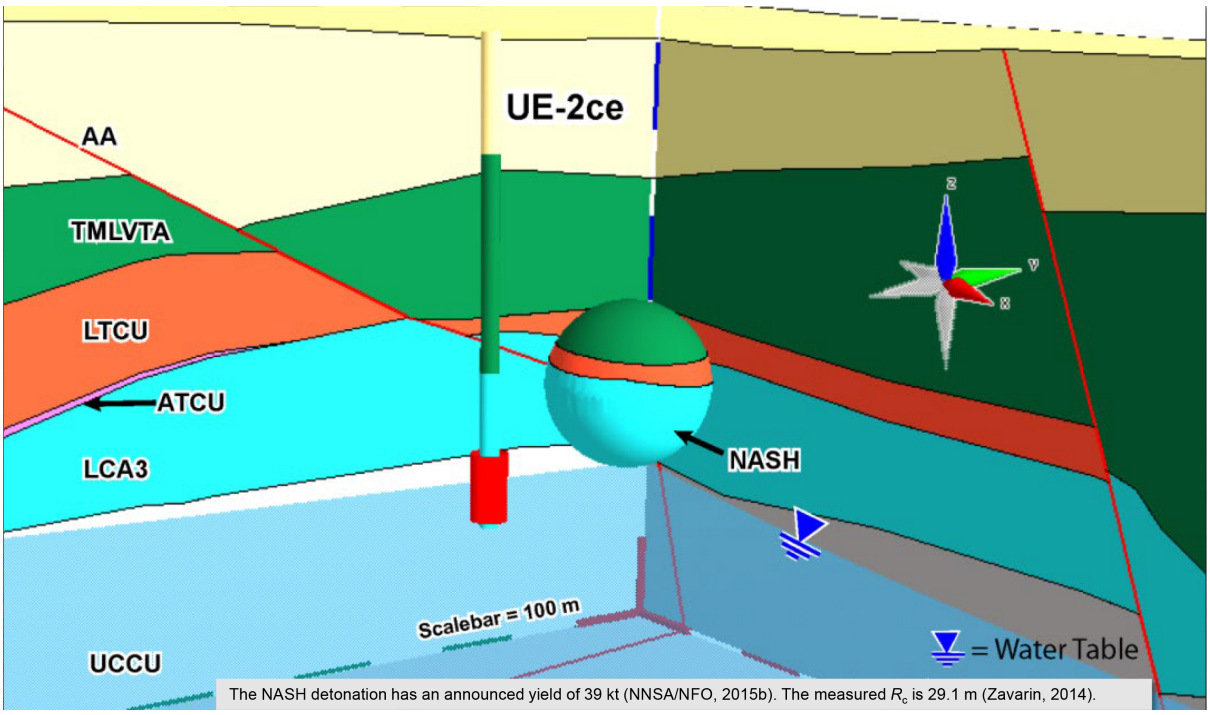

Figure 2-14
Perspective View of NASH Detonation ($2R_c$) and Well UE-2ce
Source: Modified from N-I, 2013

and ^{14}C (~4 percent), and a decrease in ^{137}Cs (~150 percent). No trend in the ^{129}I activity was observed (Figure 2-15).

2.4.1 Historical Sampling

UE-2ce has been extensively sampled over its history in support of RN migration experiments. Pumping at UE-2ce began in 1977 and continued until the pump failed in 1984, after pumping approximately 42,000 m^3 (Buddemeier and Isherwood, 1985). Samples were collected intermittently during this time period, and ^3H activities increased from 1.6E+04 pCi/L in 1977 to 6.5E+07 pCi/L in 1978 and reduced to 1.7E+07 pCi/L by 1984 when pumping ended. Bailed samples were collected on a few occasions before a new pump was installed in 2008. The ^3H activities were 2 orders of magnitude lower in the bailed samples (1.5E+05 pCi/L in 1993 to 9.3E+04 pCi/L in 2005) than the earlier pumped samples (Figure 2-16). The ^3H activities in 2008 samples increased over the first three days of pumping (1.2E+05 to 2.7E+05 pCi/L) but stabilized (2.4E+05 to 2.7E+05 pCi/L) in subsequent samples (Zavarin, 2010a). Other RNs have been detected in the historical samples, including ^{137}Cs, ^{155}Eu, ^{85}Kr, ^{22}Na, ^{90}Sr, ^{14}C, ^{36}Cl, and ^{129}I (Zavarin, 2010a; Navarro, 2019a).

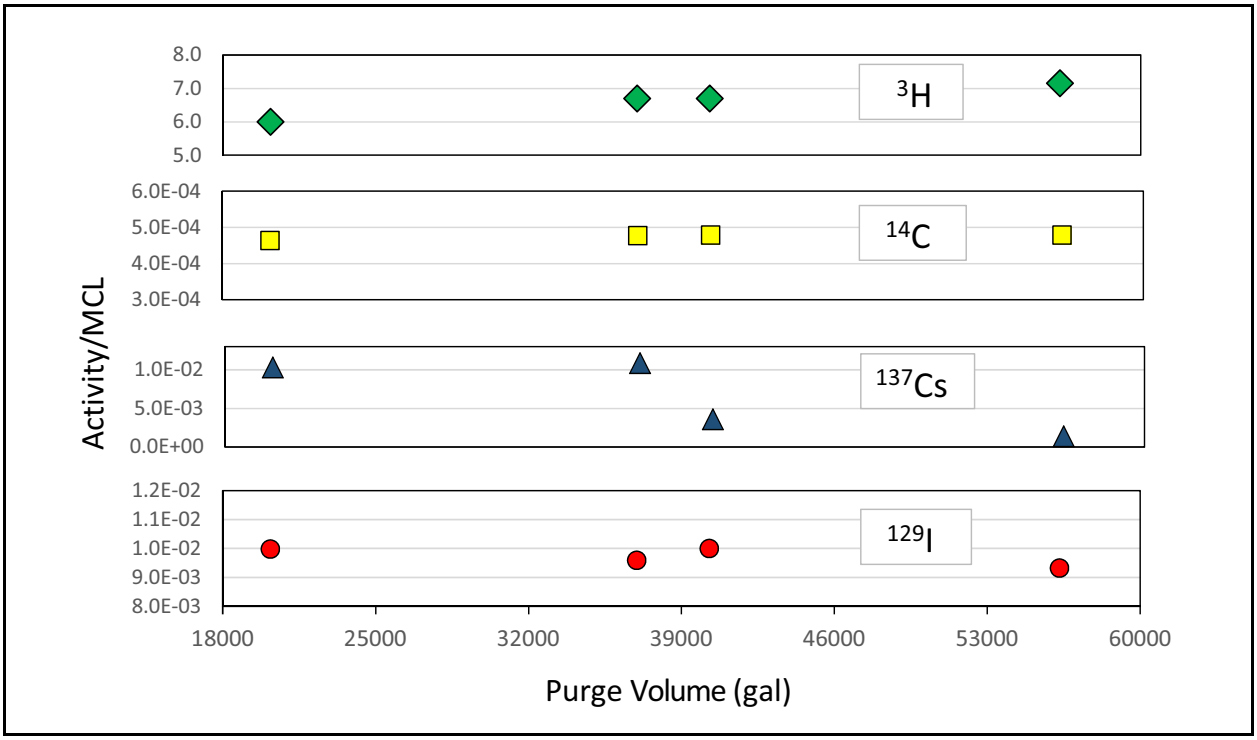

Figure 2-15
Activity Relative to MCL for UE-2ce Samples

Figure 2-16 presents the ^{90}Sr and ^{137}Cs results. The greatest reported concentration of ^{90}Sr was 5.6 pCi/L in 1977, and the greatest reported concentration of ^{137}Cs was 2.1 pCi/L, which was in the most recent samples. Neither RN exceeded its MCL throughout the sampling period (Figure 2-16).

Figure 2-17 compares the relative concentrations of ^{90}Sr and ^{137}Cs to ^{3}H for groundwater samples and for the inventory reported by Finnegan et al. (2016). The ^{3}H, ^{90}Sr, and ^{137}Cs inventory is decay corrected to the sample collection date; an increase over time is observed because of more rapid decay of ^{3}H relative to ^{90}Sr and ^{137}Cs. The concentration of ^{90}Sr and ^{137}Cs relative to ^{3}H in UE-2ce groundwater samples is quite low, 1E-09 to 1E-05 (Figure 2-17). Of greater significance is the low concentration of ^{90}Sr and ^{137}Cs relative to ^{3}H in the groundwater samples when compared to the relative inventory reported by Finnegan et al. (2016). Figure 2-17 shows that ^{90}Sr and ^{137}Cs relative to ^{3}H in groundwater is more than 3 orders of magnitude lower than for the Finnegan et al. (2016) inventory. This indicates processes exist either within the NASH exchange volume and/or along the groundwater flow path that reduce the mobility of ^{90}Sr and ^{137}Cs compared to ^{3}H.

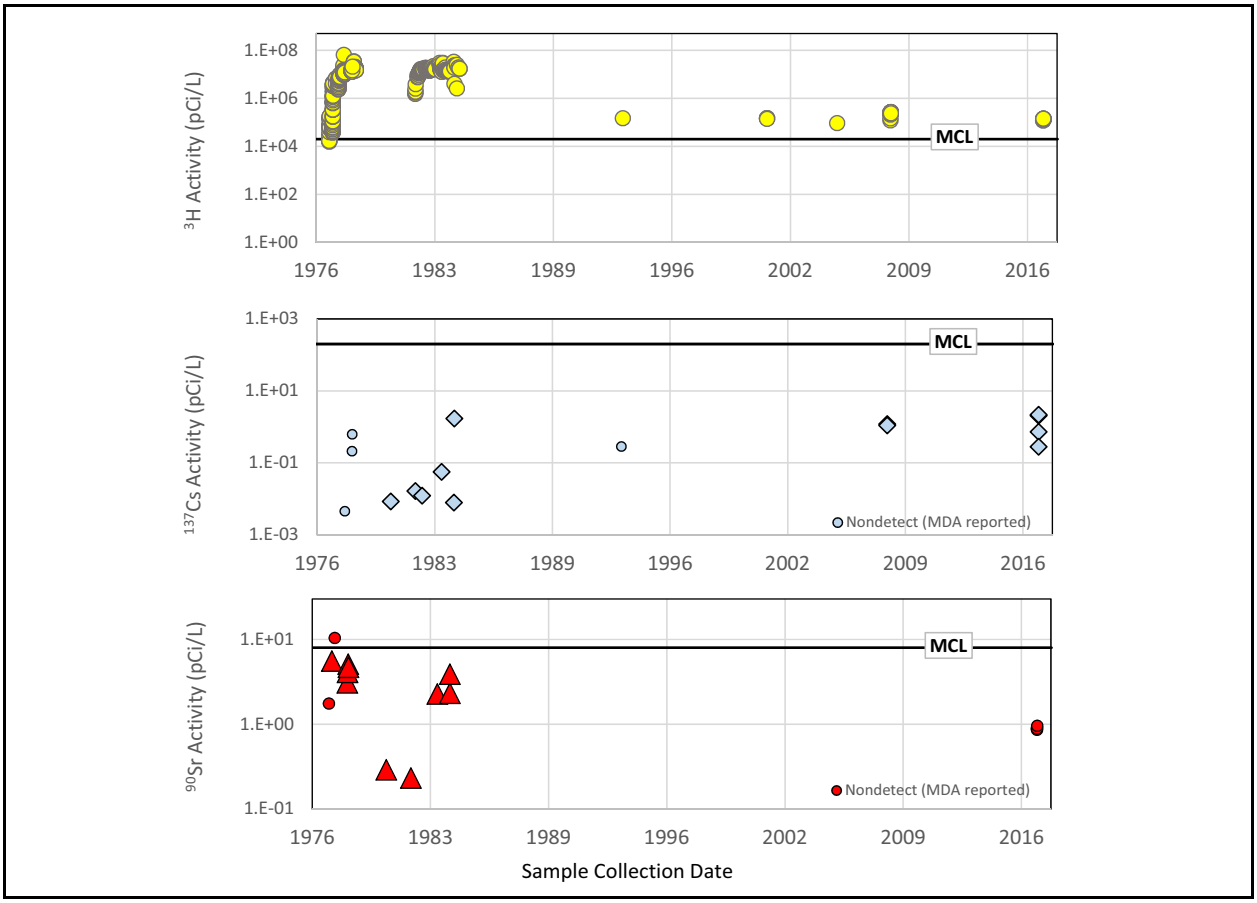

Figure 2-16
Plot of UE-2ce ^{3}H, ^{90}Sr, and ^{137}Cs Activities (1976 to 2016)

Note: Samples collected in 1993, 2001, and 2005 were bailed. All other samples were collected using a pump.

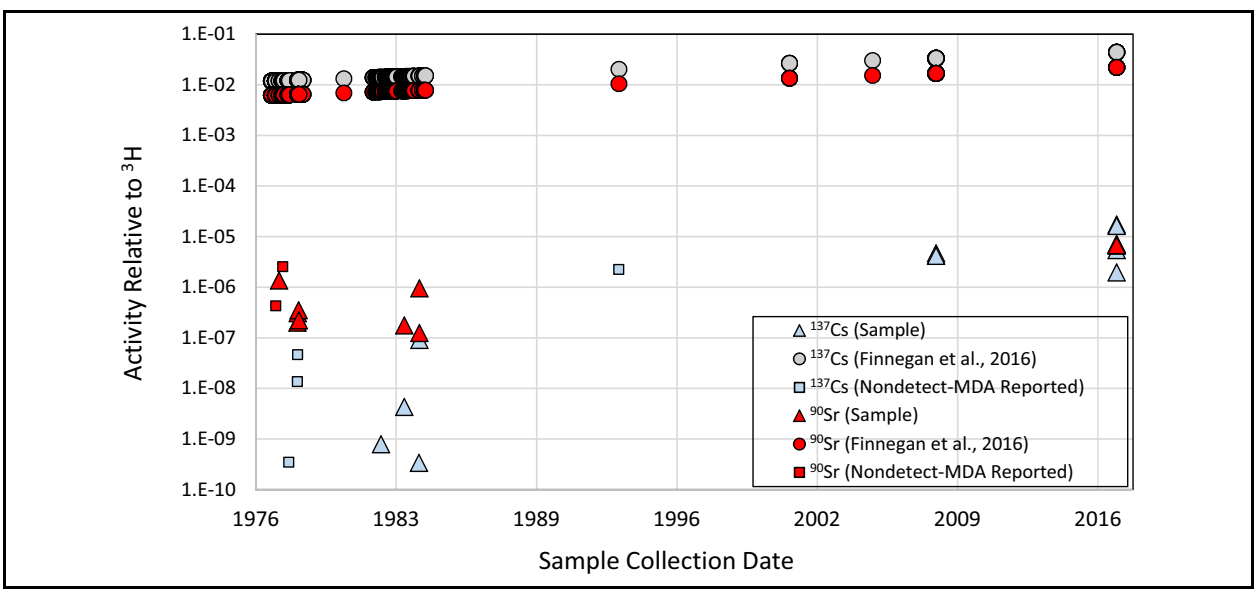

Figure 2-17
Activity Relative to ^{3}H for UE-2ce Samples (1976 to 2016)

2.4.2 Summary

Satellite Well UE-2ce, located 183 m south of the NASH WP (6.3R_c), is the only location within Yucca Flat where an RN has exceeded its MCL in a carbonate aquifer (LCA/lower carbonate aquifer-thrust plate [LCA3]). NASH, detonated within the LCA3, is within ~2.6R_c of the water table. Samples collected from UE-2ce since 1977 have reached ^{3}H activities up to 6.5E+07 pCi/L, with the current ^{3}H activity reported as 1.4E+05 pCi/L. A lower ^{3}H activity in bailed samples as well as an increasing trend with respect to purge volume indicates that pumping pulls the contamination toward the well. Although the ^{3}H activity in the most recent samples greatly exceeded the 20,000-pCi/L MCL, ^{90}Sr was not detected above its MDC (0.86 to 0.96 pCi/L), and ^{137}Cs was detected at very low levels (0.28 to 2.2 pCi/L). No RN other than ^{3}H has exceeded its MCL in UE-2ce groundwater. The ^{90}Sr and ^{137}Cs relative to ^{3}H in groundwater is more than 3 orders of magnitude lower than for the Finnegan et al. (2016) inventory. This indicates processes exist either within the NASH exchange volume and/or along the groundwater flow path that reduce the mobility of ^{90}Sr and ^{137}Cs compared to ^{3}H.

2.5 Performing WDT in the ER-4-1 LCA

Data and analysis from the WDT in the LCA at ER-4-1 addresses several model evaluation targets:

- *Basin flux through testing area*,
- *LCA hydraulic properties*
- *Permeability a*nisotropy

This section summarizes the analysis presented in *Yucca Flat Well Development and Testing Analyses for Wells ER-3-3 and ER-4-1, Nevada National Security Site, Nye County, Nevada* (Navarro, 2018), and the reader is referred to this document for details. Navarro (2018) includes a memorandum (Jackson, 2017) that presents drawdown estimates for the ER-4-1 WDT observation wells and transmissivity estimates for the LCA at ER-4-1. The analyses provided below are primarily summarized from Jackson (2017).

The WDT at ER-4-1 began on January 13 and ended on February 17, 2017. A network of 22 observation locations, 4 background wells, and 1 pumping well was monitored continuously (Table 2-8; Figure 2-18). Of the 22 observation locations, 1 (WW-A) was screened in the AA; 3 (TW-7, ER-3-3 p2, and ER-3-3 p3) were screened in the VAs; 3 (ER-2-1 m, ER-4-1 p1, and

Table 2-8
Estimated Drawdowns in ER-4-1 WDT Observation Locations

Well Name	Estimated Maximum Drawdown (ft)	RMS Error (ft) [a]	Signal-to-Noise Ratio [b]	Drawdown Detection [c]
ER-2-1 main (shallow)	<0.03	0.013	2	Not Detected
ER-2-2 o2	<0.02	0.007	3	Not Detected
ER-3-1-2 (shallow)	<0.02	0.006	3	Not Detected
ER-3-3 p1 [d]	Not Analyzed	Not Analyzed	Not Analyzed	Not Analyzed
ER-3-3 p2 [d]	Not Analyzed	Not Analyzed	Not Analyzed	Not Analyzed
ER-3-3 p3 [d]	Not Analyzed	Not Analyzed	Not Analyzed	Not Analyzed
ER-4-1 p1 [e]	Not Analyzed	Not Analyzed	Not Analyzed	Not Analyzed
ER-5-3-2	<0.02	0.008	3	Not Detected
ER-6-1-2 main	0.06	0.002	30	Detected
ER-6-2	<0.02	0.004	5	Not Detected
ER-7-1	0.06	0.003	20	Detected
TW-7	<0.01	0.004	3	Not Detected
TW-D	<0.02	0.004	5	Not Detected
U-3cn 5	0.13	0.006	22	Detected
UE-1h	<0.01	0.004	3	Not Detected
UE-1q (2600 ft)	<0.01	0.002	5	Not Detected
UE-1r WW	<0.02	0.006	3	Not Detected
UE-4t 2 (1564-1754 ft) [f]	Not Analyzed	Not Analyzed	Not Analyzed	Not Analyzed
UE-7nS	0.08	0.002	40	Detected
UE-10j (2232-2297 ft)	0.04	0.002	20	Detected
WW-2 (3422 ft)	0.02	0.002	10	Detected
WW-A (1870 ft)	<0.01	0.002	5	Not Detected

Source: Jackson, 2017

[a] Root mean square (RMS) error between measured and synthetic water levels in water-level model.
[b] Ratio of estimated maximum drawdown (signal) to RMS error (noise).
[c] Drawdown is not detected where the signal-to-noise ratio is ≤5, indicating drawdown cannot be reliably differentiated from the noise in the dataset. Drawdown is detected definitively where the signal-to-noise ratio is ≥10 and correlation between environmental fluctuations and pumping signals is unlikely.
[d] Water levels have a two-month data gap (November–January) before well development and aquifer testing, which precluded drawdown estimates in these wells.
[e] Water levels not used in drawdown analysis because levels were recovering after well construction and are not representative of hydrologic conditions in the aquifer system.
[f] Water levels not used in drawdown analysis because data show an anomalous rising trend during WDT that is not representative of hydrologic conditions in the aquifer system.

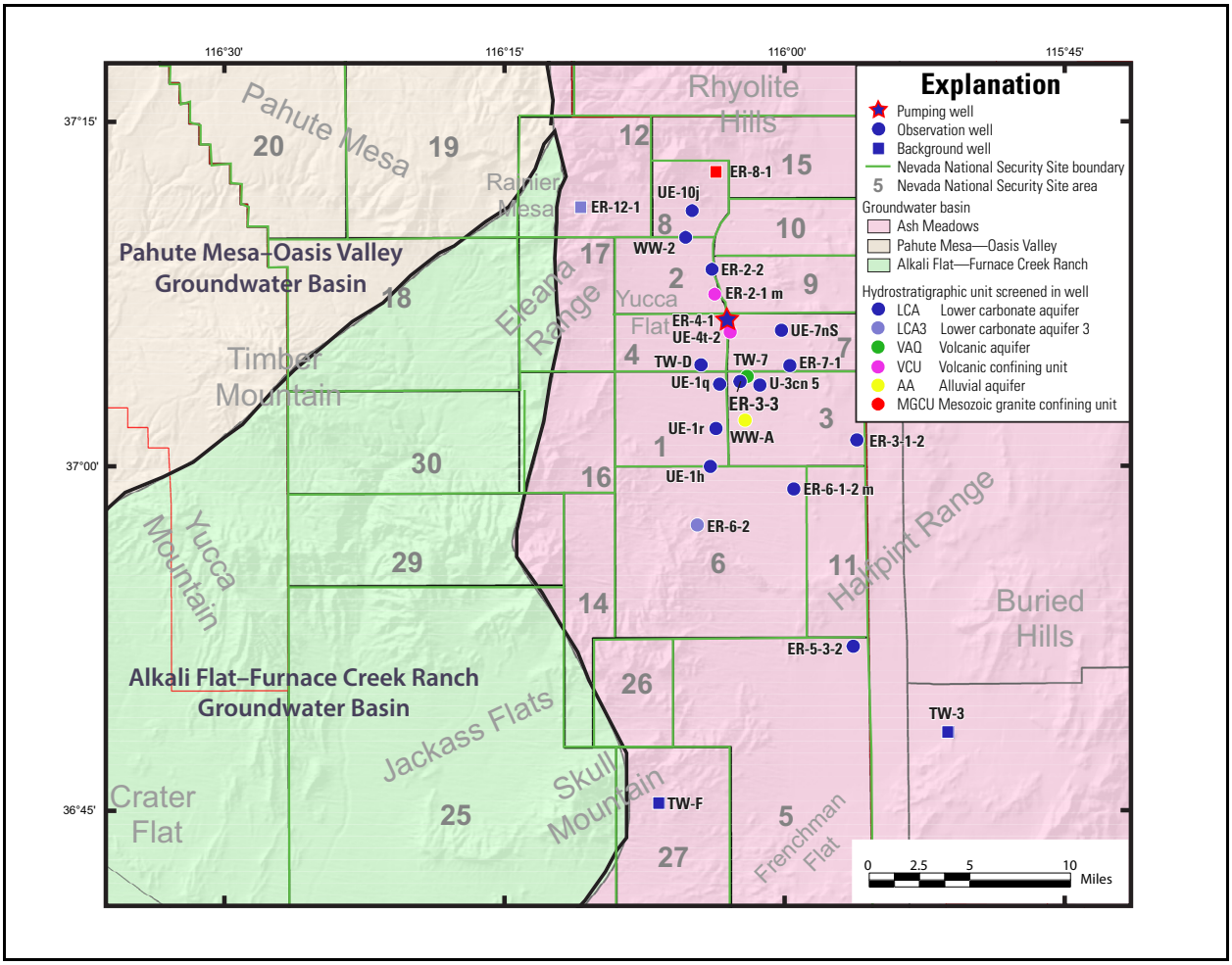

Figure 2-18
Pumping and Observation Wells for ER-4-1 WDT
Source: Jackson, 2017

UE-4t 2) were screened in the volcanic confining unit (VCU); and 15 were in the LCA. (Some wells have multiple observation locations.) Background wells are assumed to be unaffected by the WDT and are used to monitor background water-level changes used in water-level modeling for drawdown estimates.

Step-rate tests over a period of 15 days (17 to 90 gpm) followed by a 10-day constant-rate test (70 to 71 gpm) were performed at ER-4-1. About 1.7 million gal of groundwater was withdrawn from the LCA in Well ER-4-1_m1. (Samples were collected from ER-4-1 at the end of the constant-rate test on February 17, 2017. These samples are described in Section 2.3.2.)

Drawdowns were estimated at 17 observation locations using water-level models as described by Halford et al. (2016). Water levels in five observation wells were not used in the drawdown analysis either because the measurements were determined to be nonrepresentative of hydrologic conditions in the aquifer system or because insufficient data were available before performing the WDT (Table 2-8). Water-level models were used to remove the effects of environmental water-level fluctuations (e.g., barometric pressure, earth tides). Drawdown was detected in 6 of the 17 monitoring locations (Table 2-8), all of them completed in LCA. No drawdown was detected in the monitoring locations located in the volcanic and alluvial units. Figure 2-18 shows that drawdown was detected at wells to the north and southeast, and no drawdown was detected south or southwest of ER-4-1 in the LCA monitoring wells.

Drawdowns in the pumping of Well ER-4-1 m1 were interpreted using the Cooper-Jacob method (Cooper and Jacob, 1946). The period of analysis for estimating transmissivity spans the 10-day constant-rate aquifer test from February 7 to 17, 2017. Jackson (2017) estimated an early-time (~6 hours, ~25,000 gal pumped) transmissivity of 250 ft^2/day, which is representative of LCA transmissivity near ER-4-1; and a late-time (~240 hours, ~1,000,000 gal pumped) transmissivity of 56 ft^2/day, which is representative of LCA transmissivity farther from borehole ER-4-1. An independent analysis (Navarro, 2018) reported values of 296 ft^2/day for early times and a value of 55 ft^2/day for later times, which are consistent with the values from Jackson (2017). The early-time values are likely impacted by near wellbore conditions, and the later time values can be expected to better represent the transmissivity on a larger scale.

2.5.1 Summary

No hydraulic communication was detected between the LCA and AA/VA in the vicinity of ER-4-1. No drawdown was detected in the four monitoring locations located in the AA/VA. In the LCA, as shown in Figure 2-18 and Table 2-8, drawdown was detected at wells to the north and southeast, and no drawdown was detected south or southwest of ER-4-1 LCA monitoring wells. The pattern of drawdown from the ER-4-1 WDT indicates that the Topgallant fault is a barrier to flow in the area investigated, while the Yucca fault allowed hydraulic communication between the central and the eastern areas. The hydraulic conductivities estimated from the WDT are consistent with the previous estimates for the area (N-I, 2013).

2.6 Formalizing the ER-6-1-2 MWAT Reanalysis

An informal reanalysis of the ER-6-1-2 MWAT resulted in considerably lower flux values than those reported for the N-I (2013) base case model (Halford, 2009, 2012, and 2016). The flux through the high-transmissivity eastern corridor of Yucca Flat between Wells ER-7-1 and ER-6-1-2 was estimated to be an order of magnitude lower than the value of 189.6 kilograms per second (kg/s) calculated to flow through the same part of the LCA in the N-I (2013) base case model. Preliminary simulations using the reduced flux values led to CB forecasts of significantly less extent as presented in the document describing the responses to the external peer review (Navarro, 2016b). Formal reanalysis, including documentation, of the ER-6-1-2 MWAT was therefore identified as a required model evaluation activity (Navarro, 2016b). This section summarizes the reanalysis performed and published by the U.S. Geological Survey (USGS) that is documented in detail in Jackson and Halford (2019). Using these transient data in conjunction with steady-state water-level estimates, groundwater flow through Yucca Flat was estimated using a regional, three-dimensional (3-D) groundwater-flow model, referred to as the Death Valley version 3 (DV3) model (Halford and Jackson, 2019).

2.6.1 ER-6-1-2 MWAT

The ER-6-1-2 MWAT took place from February 5 to July 23, 2004, and included well development and step-drawdown testing, a nine-day constant-rate test, and a 90-day constant-rate test (SNJV, 2005). Withdrawals totaled about 75 million gal. Horizontal distances between pumping and observation wells ranged from 0 to 33 miles (mi) (Figure 2-19). Continuous water-level data were available in eight observation wells. Drawdowns in these wells were estimated using water-level models to remove water-level fluctuations resulting from barometric pressure and tidal forces from the measured data (Jackson and Halford, 2019). Drawdowns were detected in six observation wells and were not detected in two observation wells (Table 2-9).

Depth-to-water (DTW) measurements were used to evaluate drawdowns in five observation wells, where discrete measurements were made at approximate weekly to quarterly intervals (Table 2-9). To account for water-level fluctuations resulting from measurement error, barometric pressure, and tidal forces, error bars of $\pm$ 0.2 ft were added; visual inspection of recent (2017) continuous water-level data in these observation wells and other wells in Yucca Flat indicate that barometric pressure and tidal forces cause water levels to fluctuate $\pm$ 0.2 ft. Drawdowns of more than 1 ft were detected in two wells (Table 2-9). Environmental water-level fluctuations (predominantly barometric pressure and

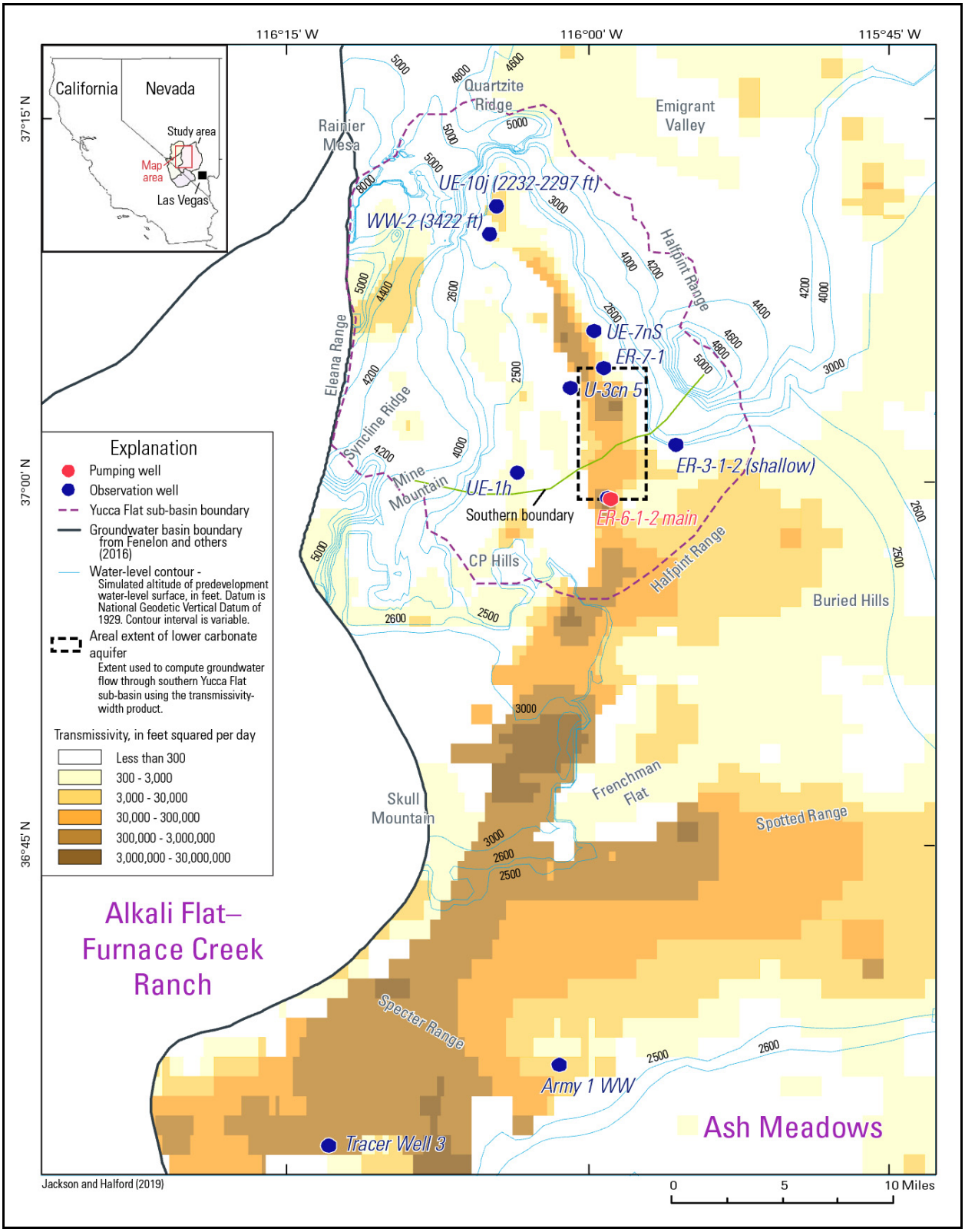

Figure 2-19
Pumping and Observation Wells, Simulated Water-Level Contours, and Transmissivity and Physiographic Features

Table 2-9
Estimated Drawdowns in Observation Wells from ER-6-1-2 MWAT

USGS Well Name	Drawdown Analysis Period	Estimated Maximum Drawdown (ft)	RMS Error (ft) [a]	Signal-to-Noise Ratio [b]	Drawdown Detection [c]
Continuous Water Levels					
ER-3-1-2 (shallow)	03/18/2004 – 11/03/2004	0.33	0.01	25	Detected
ER-6-1 main (lower zone)	03/18/2004 – 11/03/2004	2.11	0.08	26	Detected
ER-6-1 main (upper zone)	03/18/2004 – 11/03/2004	2.25	0.05	44	Detected
ER-6-1-1	03/18/2004 – 11/03/2004	2.41	0.04	56	Detected
ER-6-1-2 piezometer	03/18/2004 – 11/03/2004	<0.05	0.05	1	Not detected
ER-7-1	03/18/2004 – 11/03/2004	1.75	0.06	28	Detected
Tracer Well 3 (AD-6) [d]	03/15/2003 – 12/15/2005	0.08	0.01	7	Detected
UE-1h	03/18/2004 – 11/03/2004	<0.04	0.01	3	Not detected
DTW Measurements					
Army 1 WW (MV-1) [d]	11/01/2003 – 12/01/2004	<0.3 ± 0.2	--	--	Censored
U-3cn 5	11/01/2003 – 12/01/2004	2.3 ± 0.2	--	--	Detected
UE-7nS	11/01/2003 – 12/01/2004	1.2 ± 0.2	--	--	Detected
UE-10j (2232-2297 ft)	11/01/2003 – 12/01/2004	<0.4 ± 0.2	--	--	Censored
WW-2 (3422 ft)	11/01/2003 – 12/01/2004	<0.7 ± 0.2	--	--	Censored

Source: Jackson and Halford, 2019

[a] RMS error between measured and synthetic water levels in water-level model.
[b] Ratio of estimated maximum drawdown (signal) to RMS error (noise).
[c] For continuous measurements, drawdown is detected where the signal-to-noise ratio is ≥5 and correlation between environmental fluctuations and pumping signals is unlikely. For observation wells with DTW measurements, drawdown is detected if measurements show visibly discernible water-level declines during ER-6-1-2 main pumping, whereas drawdown is censored if measurements do not show visibly discernible water-level declines during ER-6-1-2 main pumping because any potential drawdown was masked by barometric pressure and tidal forces. Error bars account for + 0.2 ft water-level fluctuations from barometric pressure, tides, and measurement error.
[d] Water levels affected by pumping in Wells Army 1 WW and ER-6-1-2 main.

-- = Not available

tides) masked drawdowns in two wells (UE-10j [2232-2297 ft] and WW-2 [3422 ft]); and water levels in Army 1 WW were affected by pumping from Army 1 WW and ER-6-1-2 main. Numerical results indicate that a maximum drawdown of less than 0.04 ft in Army 1 WW was induced from pumping during the ER-6-1-2 MWAT.

Estimated drawdowns in observation wells were used to evaluate hydraulic connections within Yucca Flat. Water levels in Well UE-1h were unaffected by pumping during the MWAT, indicating that

pumping did not propagate into western Yucca Flat. Simulated drawdowns of less than 0.5 ft occurred in Wells UE-10j (2232-2297 ft) and WW-2 (3422 ft), showing that pumping propagated more than 14 mi to northern Yucca Flat. The high-transmissivity corridor in Yucca Flat sub-basin is thought to be hydraulically connected to the Ash Meadows discharge area because pumping in ER-6-1-2 main induced drawdowns downgradient in Wells Army 1 WW and Tracer Well 3.

2.6.2 Boundary Flow Estimation

Groundwater flow from southern Yucca Flat was estimated using the DV3 model (Halford and Jackson, 2019). Groundwater flow from Yucca Flat was estimated by simultaneously calibrating to steady-state and transient conditions. Recharge, hydraulic conductivity, specific yield, and specific storage coefficient distributions were estimated by simultaneously calibrating multiple, 3-D, numerical groundwater-flow models of the study area. Multiple models were used to differentiate, and better interpret, effects of predevelopment flow, groundwater development, and aquifer tests on the groundwater system. The groundwater-flow models shared a common domain, grid, and hydrogeologic framework. Model domains extended laterally to no-flow boundaries at the outer boundaries of the four groundwater basins (Figure 2-19). The hydrogeologic framework has 10 HGUs that were defined primarily based on rock type and depth below the water table. Hydraulic conductivity, specific yield, and specific storage coefficient distributions were identical in each model (Halford and Jackson, 2019). Hydraulic properties and recharge rates were distributed with pilot points (RamaRao et al., 1995).

Groundwater flow estimates from southern Yucca Flat were informed primarily by two models: DV3-ER612 and DV3-SS. The DV3-ER612 model simulated pumping during the ER-6-1-2 main MWAT and was calibrated to drawdowns in the 13 observation wells with an RMS error of 0.02 ft. Transmissivity of the carbonate rocks beneath Yucca Flat was estimated primarily by the DV3-ER612 model. The DV3-SS model simulated predevelopment flow. Water-level altitudes in wells, head differences between paired wells, and transmissivity estimates from other aquifer tests directly affected calibration in the Yucca Flat sub-basin. Simulated and measured water levels agreed with RMS errors of 20 and 50 ft in the carbonate rocks beneath Yucca Flat and the study area, respectively. Recharge and groundwater-flow estimates from the DV3-SS model were constrained by discharge measurements at regional springs.

Groundwater flow through the testing area in southern Yucca Flat was estimated for a rectangular box extending between Wells ER-7-1 and ER-6-1-2 main because all flow through nuclear testing areas passes through this volume. The southern extent of the box between Wells ER-7-1 and ER-6-1-2 main was delineated using the simulated water table from the DV3-SS model, steady-state flow paths, a simulated transmissivity map, and estimated drawdowns at observation wells (Figure 2-19; Jackson and Halford, 2019).

Simulated flow from Yucca Flat was sampled from the DV3-SS model with the direct approach using Zone Budget–a groundwater utility (Harbaugh, 1990). Groundwater flow through the transmissive corridor downgradient of underground nuclear testing areas ranged between 560 and 1,200 acre feet per year (acre-ft/yr). The DV3-SS model simulated 560 acre-ft/yr flowing through the transmissive corridor midway between Wells ER-7-1 and ER-6-1-2 main. Simulated head difference between the Wells ER-7-1 and ER-6-1-2 main was 2.4 ft, or 93 percent of the measured head difference. Contributing areas extend from Rainier Mesa to the west, the Halfpint Range to the east, and north of Quartzite Ridge (Figure 2-20).

2.6.3 Yucca Flat Basin Flow Uncertainty Analysis

Two approaches for characterizing the DV3 flow uncertainty were applied. The first approach is the Null Space Monte Carlo (NSMC) method employed in the parameter estimation software PEST code. This approach was successfully applied in the N-I (2013) modeling to characterize flow model uncertainty. The second approach is the Pareto-based hypothesis testing. This second approach may be more successful than the NSMC approach for strongly ill-posed problems in which a covariance matrix of parameter variability cannot be obtained. Each approach and results are described in this section.

The goal of the NSMC and Pareto analyses is to estimate the range of plausible flow through the eastern LCA located within the Yucca Flat basin as identified by the DV3 model. The flow is defined as the flow from the LCA in eastern Yucca Flat to the LCA in northern Frenchman Flat as illustrated in Figure 2-20. The calibrated flow value is 76,000 cubic feet (ft^3/day) (640 acre-ft/yr, or 22 kg/s). The calibrated flow values used in the uncertainty analysis were taken from a near final version of the DV3 model and slightly differ from the flows documented by Halford and Jackson (2019).

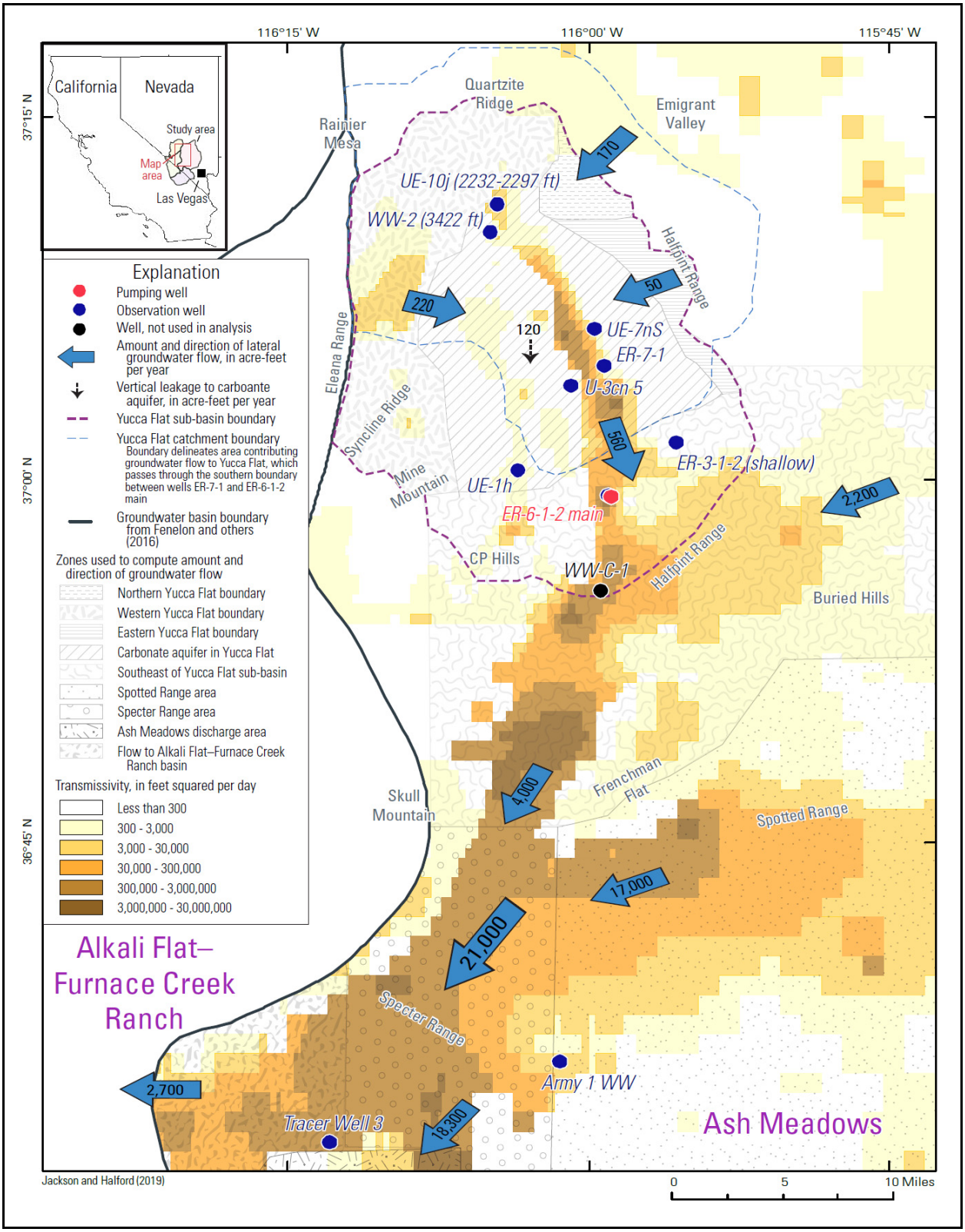

Figure 2-20
Simulated Transmissivity and Groundwater Flow Estimates

2.6.3.1 NSMC Analysis

The NSMC procedure provided with the PEST software allows generation of different parameter fields that maintain model calibration. The calibrated models allow exploration of the impact of parameter uncertainty by generating multiple models that meet reality constraints implicit in the observations used to calibrate the model (Doherty, 2010).

The model solution null space is composed of individual parameters or combinations of parameters that have no influence on model calibration. Choice of different values for these combinations of parameters can be used along with parameters that are sensitive to the calibration data to produce different sets of parameters that will also calibrate the model (Doherty et al., 2010). The calibrated models can then be used to generate a possible range of model parameters and outputs that maintain the model in calibration. The NSMC algorithm in the PEST software calculates the difference between each sampled parameter set and the calibration parameters. The difference is then projected onto the calibration null space, and the projected difference is added to the calibration parameter set. If the relationship between model parameters and model outputs is linear, and the transition between null and solution spaces is distinct, each new parameter set will calibrate the model to the same degree as the original (Doherty et al., 2010). However, this relationship may not be linear, and the NSMC parameter sets require some degree of recalibration to meet the objective function calibration goal. The NSMC method deteriorates with increasing model nonlinearity and with an increasing degree of ill-posedness of the inverse problem (Doherty et al., 2010).

The various DV3 models all used identical parameterizations. Only the water withdrawal rates are different among the models. Two approaches may be used to define parameter uncertainty used for sampling model parameters before null space adjustment. The first approach can be used for any parameterization approach, and uses the parameter uncertainties defined by the permissible ranges allowed during the model calibration or by the calibrated model's parameter covariance matrix. The second approach can be used with a pilot point parameterization approach and parameter uncertainty is defined in the spatial correlation defined in statistical structures (Doherty et al., 2010). For the DV3 models, these structures are the variograms, developed using expert knowledge, used to interpolate the pilot point values onto the model cells. Both approaches were applied to the NSMC analysis of the DV3 models, but only the second approach produced calibrated models. The average objective function from the NSMC was unacceptably high for the model using the first parameter sampling approach and the models could not be used to assess model uncertainty. In contrast, the average

objective function using the second parameter sampling approach was 4E+12 before null space projection and 5E+07 after null space projection (Figure 2-21), indicating the NSMC models were generally calibrated. The calibrated DV3 models achieved an objective function of 1E+07. No attempts were made to recalibrate the NSMC models because the intent here was to obtain estimates of the range of uncertainty, which was judged not to warrant the additional computational effort required by long model run times for the transient models combined with a large number of adjustable parameters. Figure 2-22 presents the observation objective function versus the flow through eastern Yucca Flat. The resulting flow through eastern Yucca Flat ranged from a factor of 0.7 to 1.7 times the calibrated flow rate.

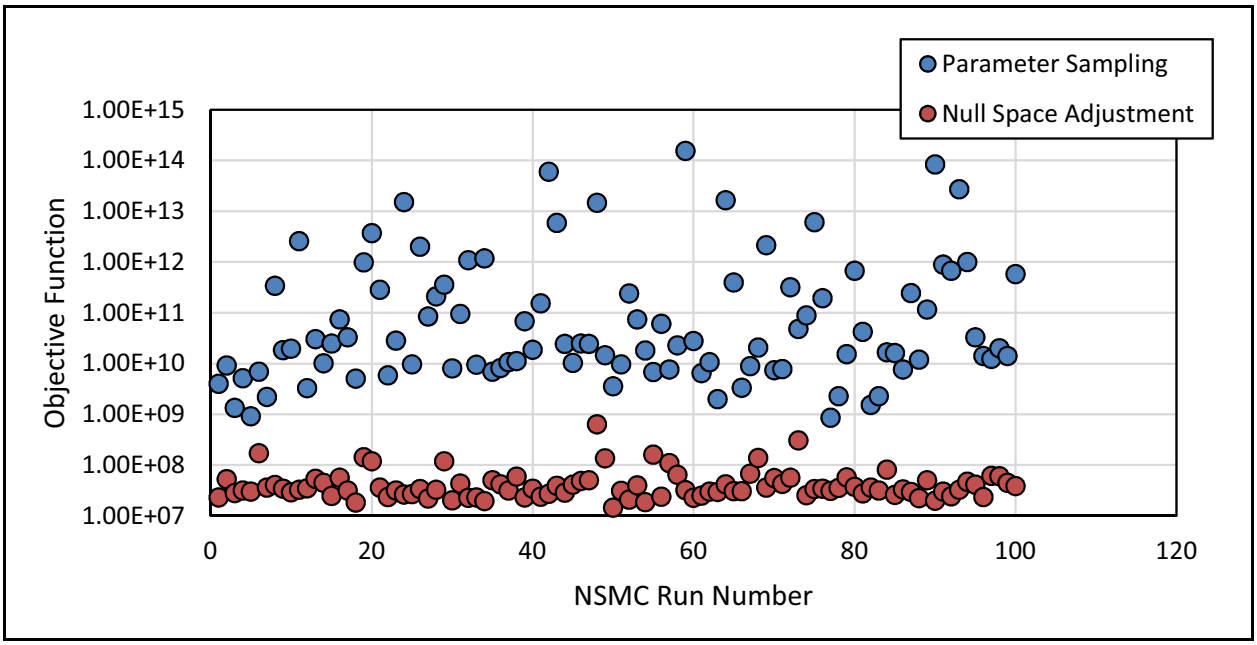

Figure 2-21
NSMC Model Objective Function Values before and after Null Space Adjustment

2.6.3.2 Pareto-Based Hypothesis Testing Description

The Pareto-based hypothesis testing borrows from optimization theory, and two competing objectives are simultaneously optimized. The "Pareto front" defines an optimal tradeoff between two competing objectives whereby neither objective can be better met without simultaneously degrading the other (Doherty et al., 2010). The objectives are the model calibration objective function defined by observations and the objective function defined by the model's ability to simulate a hypothesized event or condition. Two hypothesized conditions were evaluated with the DV3 Pareto analysis. The first condition is a fivefold increase in flow through the saturated LCA in eastern Yucca Flat, and the

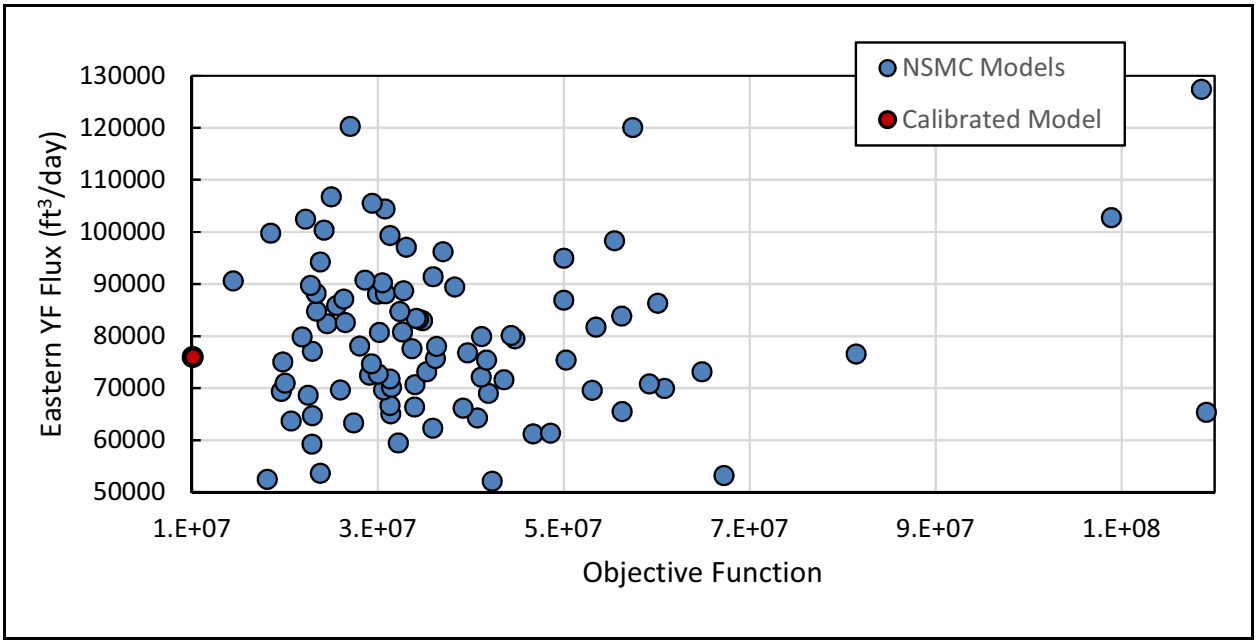

Figure 2-22
DV3 Model Objective Function versus Eastern Yucca Flat Flow from the NSMC Analysis

second condition is a fivefold decrease in the flow. As PEST traverses the Pareto front, it assesses the credibility of the hypothesized event value by the ability of the model to be calibrated using the hypothesized condition.

The Pareto mode of PEST performs a sequence of optimizations that incrementally increase the weight of the hypothesized condition, which is used in the model calibration as an observation. The point where the calibration objective function crosses the threshold of being "calibrated" likely represents the upper limit of the hypothesized condition. For the DV3 model uncertainty assessment, the Pareto analysis was performed using 10 incremental increases in the observation weight of the hypothesized condition and 2 optimization iterations for each weight increment, which likely are the minimum number that can provide useful results. Ideally, 2 to 3 times as many weight increments and optimization iterations would be used to produce a more distinct Pareto front. An expert judgment was made that the significant increase in the effort required to conduct a refined analysis would not result in proportionate improvement in the uncertainty estimation.

Figure 2-23A presents the Pareto front for a 5-times flow increase in terms of the calibration (e.g., steady-state heads) and hypothesized condition objective function values. Figure 2-23B presents the same Pareto front in terms of the objective function relative to the initial objective

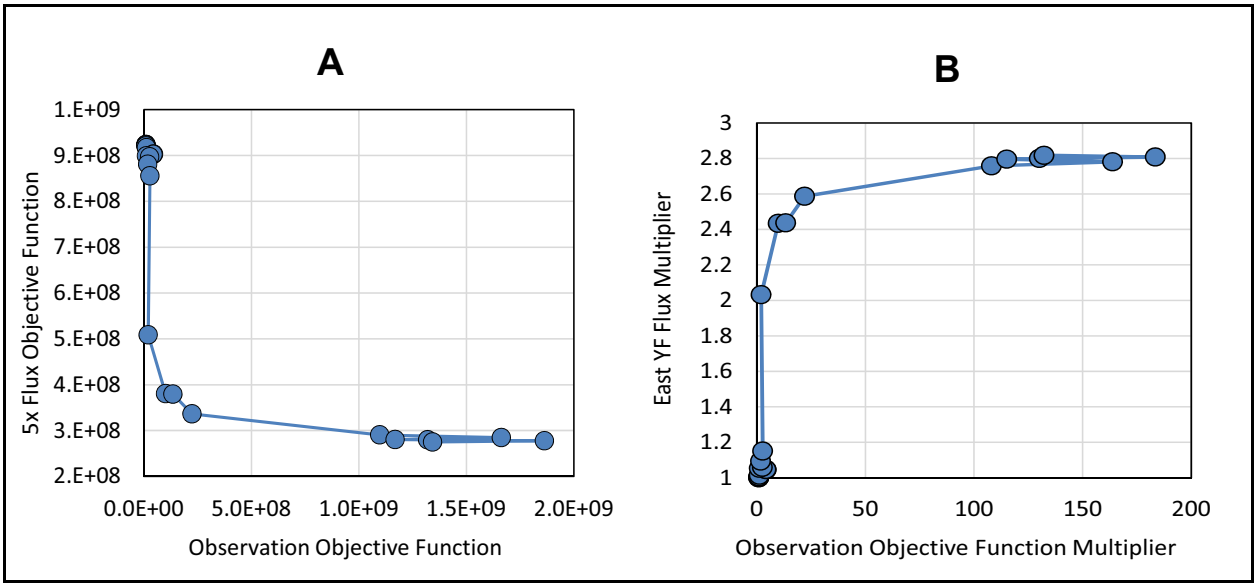

Figure 2-23
Pareto Front as (A) Objective Functions and as (B) Multipliers of Base Case Objective Function and Eastern Yucca Flat Flow for a 5-Times Flow Increase

function from the calibrated model and the flow as a multiple of the initial value from the calibrated model.

A number of notable aspects of the Pareto front are illustrated in Figure 2-23A and B, including the following:

- For a moderate change in the calibration objective function (e.g., a twofold increase), the flow in eastern Yucca Flat can be doubled.
- The value of the eastern Yucca Flat flow cannot be increased beyond approximately 3 times the initial value. As the weight adjustment increments approached the maximum value, the eastern Yucca Flat flow oscillated between about 2.5 to 2.8 times the initial value. As flow values approach 3 times the initial value, the observation objective function rises to more than 100 times the initial value.
- The observation objective function oscillates between 1 to 4 times the initial model objective function for 1 to 1.2 times increase in flow. As flow values surpass 2.4 times the initial value, the observation objective function rises steeply. A more monotonic type relationship between flow increase and observation objective function would be obtained, if more incremental weight increases and optimization iterations were used.

Figure 2-24A presents the Pareto front for a factor of 5-flow decrease in terms of calibration and hypothesized condition objective function values. Figure 2-24B presents the same Pareto front in terms of calibration objective function relative to the initial objective function and the flow as a

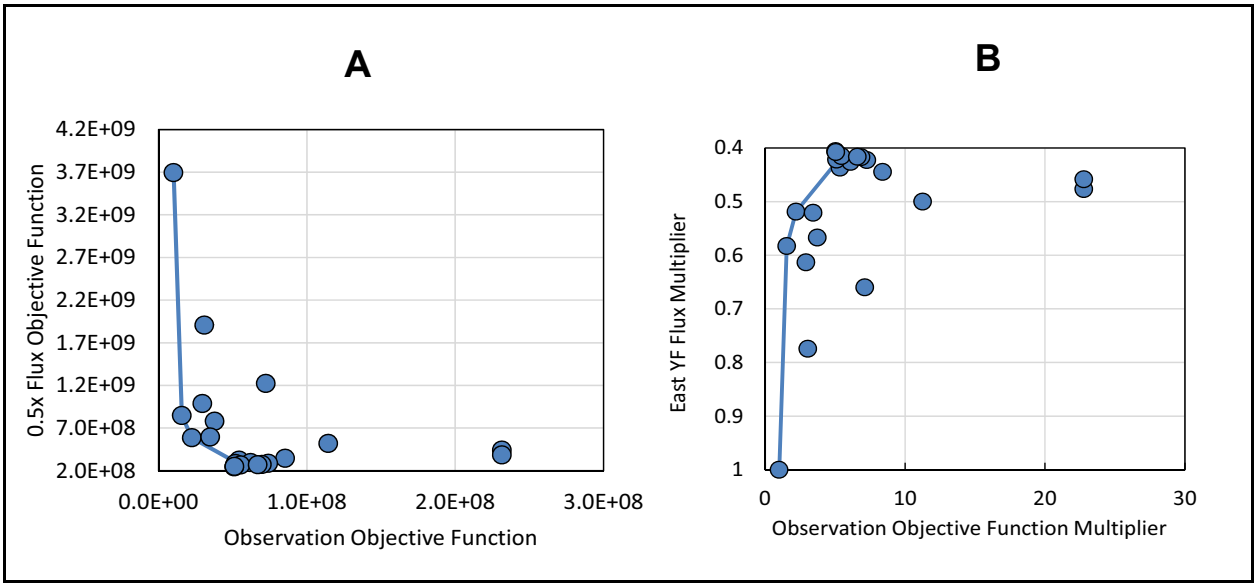

Figure 2-24
Pareto Front as (A) Objective Functions and as (B) Multipliers of Base Case Objective Function and Eastern Yucca Flat Flow for a 5-Times Flow Decrease

multiple of the initial value. A number of notable aspects of the Pareto front are illustrated in Figure 2-24A and B, including the following:

- Similar to the Pareto front for a flow increase, a moderate change in the observation objective function (e.g., twofold increase) produces a factor of 2 change, but in the direction of a decreasing flow.

- The value of the eastern Yucca Flat flow cannot be decreased beyond approximately 0.4 times the calibrated model value. As the weight adjustment increments approached the maximum value, the eastern Yucca Flat flow oscillated between about 0.5 to 0.4 times the initial value, but a 20-times increase in objective function was encountered before arriving at the minimum flow values.

- If sufficient weight increments and optimization iterations are used in the PEST Pareto analysis and the model's behavior is linear, the PEST Pareto optimizations would produce a monotonic relationship between a decreasing hypothesized event objective function and increasing calibration objective function. However, the results obtained from the DV3 model Pareto analysis for decreasing flux did not produce an ideal monotonic relationship between the two competing objective functions due to the limited number of optimization iterations used in the analysis. The Pareto front should be interpreted as the locus of points nearest the axes in Figure 2-24.

2.6.3.3 Comparison of Selected NSMC and Pareto Analyses Models to the Calibrated Model

The choice of the threshold objective function level at which the model is deemed to be "calibrated" is often subjective, but can be estimated by comparison of observations to model values and understanding the model sensitivities.

Three models were compared from the NSMC and Pareto analyses that have a large increase or decrease in the eastern Yucca Flat flow and have objective function values that are similar in magnitude with the calibrated DV3 model. The following aspects of the Pareto and NSMC analyses models were compared to the original model to ensure that the estimated upper and lower bounds of eastern Yucca Flat flow were derived from models with realistic parameters:

1. Overall objective function value
2. RMS error for the steady-state water levels and basin recharges
3. Well hydrographs from the ER-6-1-2 MWAT observation wells
4. Steady-state model recharge
5. LCA flows within the Yucca Flat sub-basin area of the Ash Meadows hydrologic basin
6. Estimated predevelopment water budgets

Table 2-10 presents the objective function value, RMS error for the steady-state water levels, and RMS error for the steady-state basin flow produced by the compared NSMC/Pareto analyses models used for assessing flow uncertainty. The RMS errors in these models are increased by approximately a factor of 2 and are similar to the increase in the overall objective function.

Table 2-10
Summary of the RMS Errors for the Pareto and NSMC Models with Large Flow Changes in Eastern Yucca Flat Simulated by the Calibrated and NSCM/Pareto Analyses Uncertainty Models

Case	Overall Objective Function	Eastern Yucca Flat Flux (ft^3/day)	RMS Error Steady-State Water Levels (ft)	RMS Error Basin Flux (acre-ft/yr)
Calibrated Model	1.015E+07	75,976	61	29
Pareto Iteration 11	2.045E+07	154,316	115	52
NSMC Realization 42	2.702E+07	120,321	119	49
Pareto Iteration 6	2.243E+07	39,427	107	85

Figures 2-25 and 2-26 present drawdowns in response to the ER-6-1-2 pumping simulated by the selected flow uncertainty models. The drawdowns simulated by the uncertainty models were similar to the calibrated model, but the drawdowns simulated by NSMC realization 42 and Pareto analysis iteration 6 were slightly higher near the pumped well and slightly lower in the distal wells.

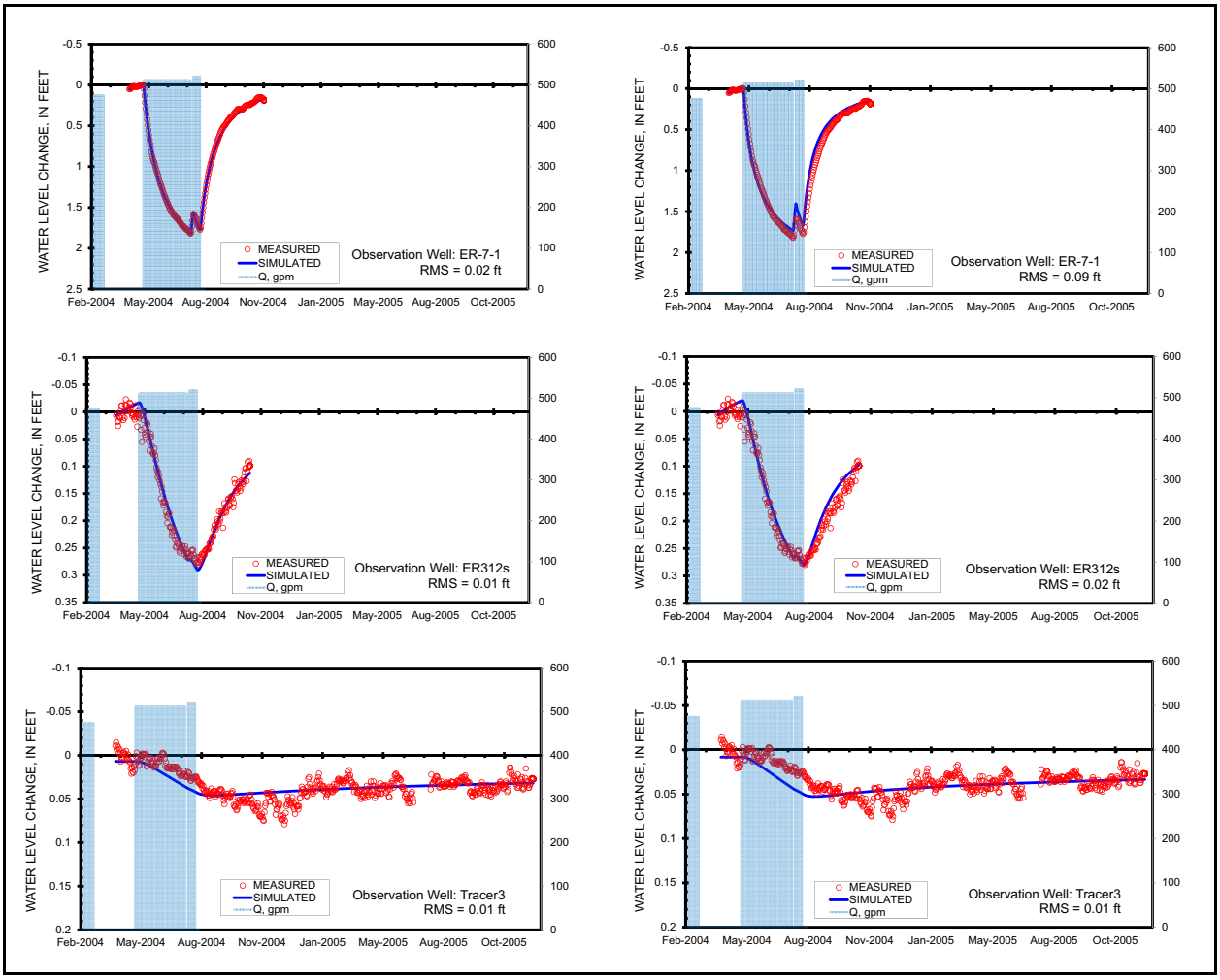

Figure 2-25
Selected Drawdowns from the ER-6-1-2 MWAT for the Calibrated Model (1st column) and Flow Increase Pareto Iteration 11 (2nd column)

Table 2-11 presents flows within the LCA in the vicinity of Yucca Flat, and Figure 2-27 presents the flows in the Ash Meadows groundwater basin simulated by the selected uncertainty models. PEST increased the flow in eastern Yucca Flat by increasing the flow into northern Yucca Flat and by decreasing the flow from western Yucca Flat to Frenchman Flat. The lower flow through the eastern LCA simulated by the Pareto iteration 6 was accomplished by decreasing the northern flow into Yucca Flat. The recharge to the four basins within DV3 model domain were similar among the

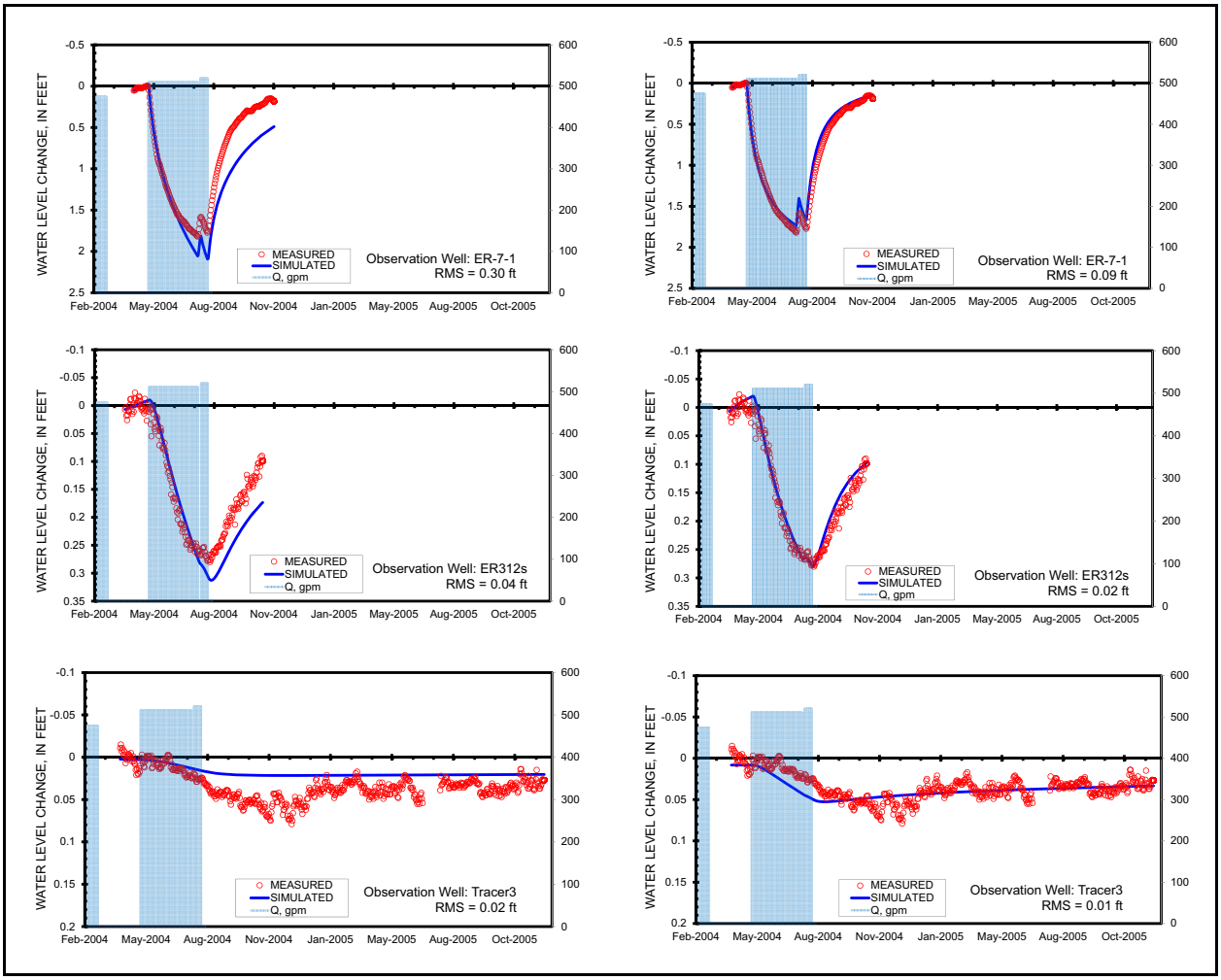

Figure 2-26
Selected Drawdowns from the ER-6-1-2 MWAT NSMC Realization 42 (1st column) and Flow Decrease Pareto Iteration 6 (2nd column)

calibrated and NSMC/Pareto analyses uncertainty models (Table 2-12), as was the flow within the basins (Figures 2-28 through 2-31). One apparent difference between the calibrated model and the Pareto iteration 6 model was a near zero discharge occurring in the Lower Amargosa River zone instead of the expected 1,000 acre-ft/yr discharge (Figure 2-31).

Table 2-11
Lateral Flow into and out of the Eastern LCA in Yucca Flat Simulated by the Calibrated and NSCM/Pareto Analyses Uncertainty Models

Case	Northern Yucca Flat Influx (acre-ft/yr)	Western Yucca Flat to Eastern Yucca Flat (acre-ft/yr)	Eastern Yucca Flat to Northern Frenchman Flat (acre-ft/yr)	Western Yucca Flat to Western Frenchman Flat (acre-ft/yr)
Calibrated Model	220	10	640	90
Flux Increase Pareto Iteration 11	760	10	1,290	10
NSMC Realization 42	460	10	1,010	15
Flux Decrease Pareto Iteration 6	39	4	331	82

2.6.3.4 DV3 Model Analysis of Flow Uncertainty Summary and Conclusions

NSMC and Pareto analyses were used to estimate the range of plausible flow through the eastern LCA located within the Yucca Flat sub-basin calculated by the DV3 model.

The NSMC analysis used several methods to estimate the parameter uncertainty before null space adjustment. Using the posterior covariance matrix obtained from the model calibration to estimate parameter uncertainty resulted in a very poor degree of model calibration, which is likely due to a nonlinear relation between model parameters and model outputs. Sampling the parameters using uncertainty estimated from the variograms used to interpolate the pilot point values onto the model grid generally produced calibrated models, and the resulting flow ranged from a factor of 0.7 to 1.7 times the flow obtained from the calibrated model.

The Pareto analysis determined that the flow through the eastern LCA cannot be increased beyond approximately 2 times or decreased beyond approximately 0.4 times the calibrated model value if the model is to remain calibrated. As the flow approached 3 times the calibrated value, the calibration objective function increased to more than 100 times the calibrated model. The flow stabilized at 0.4 times the calibrated value after 6 of the 10 weight adjustment increments and could not be decreased further. Constraining an acceptable calibration to be a twofold increase or less of the calibrated model value allowed an approximately twofold increase or twofold decrease in the flow within eastern Yucca Flat.

Three models from the NSMC and Pareto analyses with a large increase or decrease in the eastern Yucca Flat flow and similar objective function values to the calibrated model were compared and

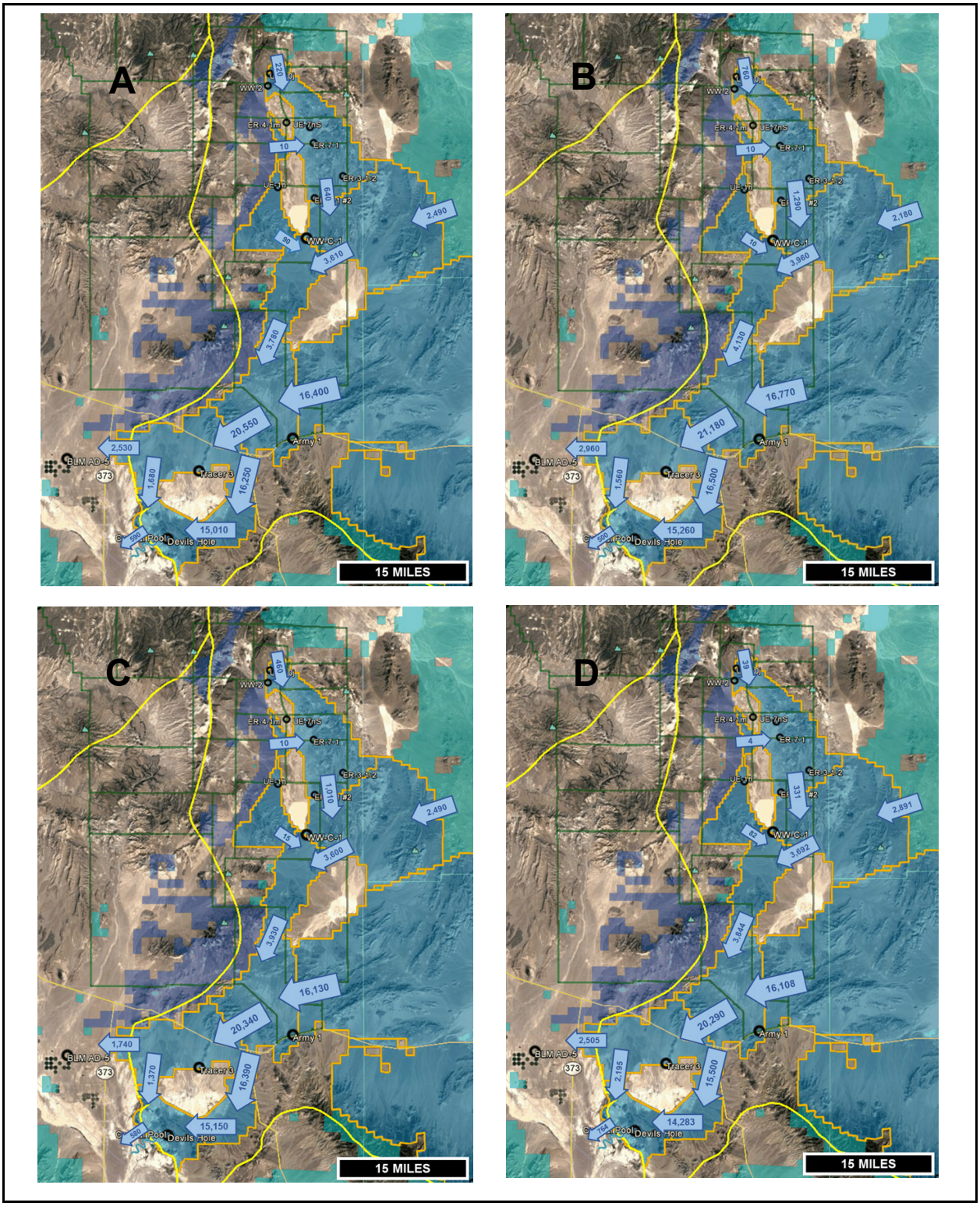

Figure 2-27
LCA Flow near Yucca Flat from the NSMC/Pareto Analyses Uncertainty Models (A = Calibrated model, B = Flow increase Pareto iteration 11, C = NSMC realization 42, D = Flow increase Pareto iteration 6)

Table 2-12
Recharge to the DV3 Model Domain Basins Simulated by the Calibrated and NSMC/Pareto Analyses Uncertainty Models

Case	Recharge to Ash Meadows (acre-ft/yr)	Recharge to Pahute Mesa/Oasis Valley (acre-ft/yr)	Recharge to Alkali Flats Furnace Creek Ranch (acre-ft/yr)	Recharge to Pahrump Valley (acre-ft/yr)
Expected	21,100	6,000	4,800	22,100
Calibrated Model	21,450	6,130	4,820	22,310
Flux Increase Pareto Iteration 11	22,700	6,230	4,910	22,700
NSMC Realization 42	21,480	6,130	4,830	22,330
Flux Decrease Pareto Iteration 6	20,820	5,950	4,860	22,100

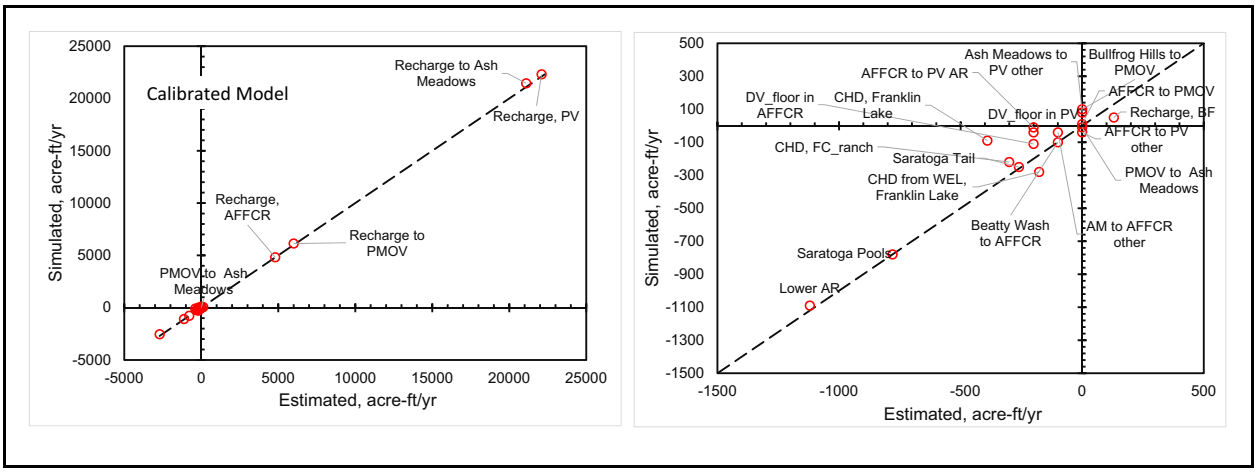

Figure 2-28
Expected and Simulated Water Budgets for the Calibrated Model

Note: AFFCR = Alkali Flat-Furnace Creek Ranch, AM = Ash Meadows, AR = Amargosa River, BF = Bullfrog Hills, CHD = Constant head discharge, DV = Death Valley, FC = Furnace Creek, PMOV = Pahute Mesa Oasis Valley, PV = Pahrump Valley, WEL = Wells.

were found to have similar behavior with respect to observations as the calibrated model. The uncertainty of the flow through the eastern LCA in Yucca Flat is likely a factor of 2 increase or decrease relative to the calibrated value.

2.6.4 Summary

Reanalysis of the ER-6-1-2 MWAT data led to an estimate of 20 kg/s for the basin flux through the testing area in the southern Yucca Flat. Uncertainty analysis using the NSMC and Pareto Front techniques led to an uncertainty estimate of a factor of 2 in this basin flux value.

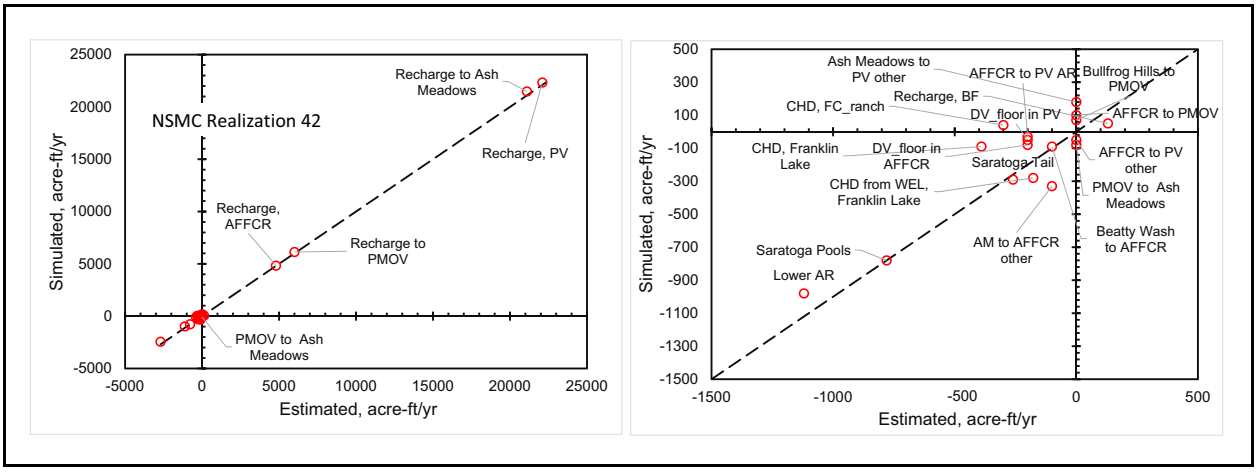

Figure 2-29
Estimated and Simulated Water Budgets for NSMC Realization 42 Model

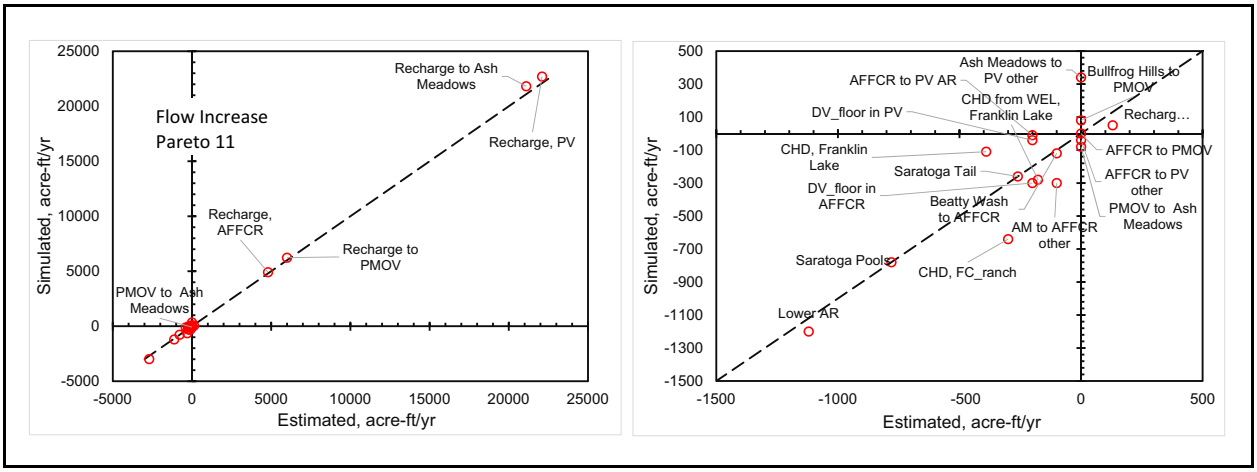

Figure 2-30
Estimated and Simulated Water Budgets for the Pareto Analysis Flow Increase Iteration 11 Model

2.7 Evaluating ER-4-1 and Other Yucca Flat Groundwater Geochemistry

This analysis relies principally on scatterplots of chemical or isotopic pairs to infer the upgradient areas from which Well ER-4-1 groundwater was derived, and downgradient areas toward which it flows. It is based on groundwater geochemical and isotopic data from the LCA documented in Appendix A of Stoller-Navarro Joint Venture (SNJV) (2006a) and newly acquired groundwater data from model evaluation Wells ER-3-3 and ER-4-1 (Table 2-13). Sampling locations are shown in Figure 2-32. ER-3-3 and ER-4-1 were sampled in December 2016 and February 2017, respectively; sampling information is presented in Table 2-3 and described in Sections 2.3.1 and 2.3.2. Average concentrations of groundwater chemical and isotopic data from these wells are presented in

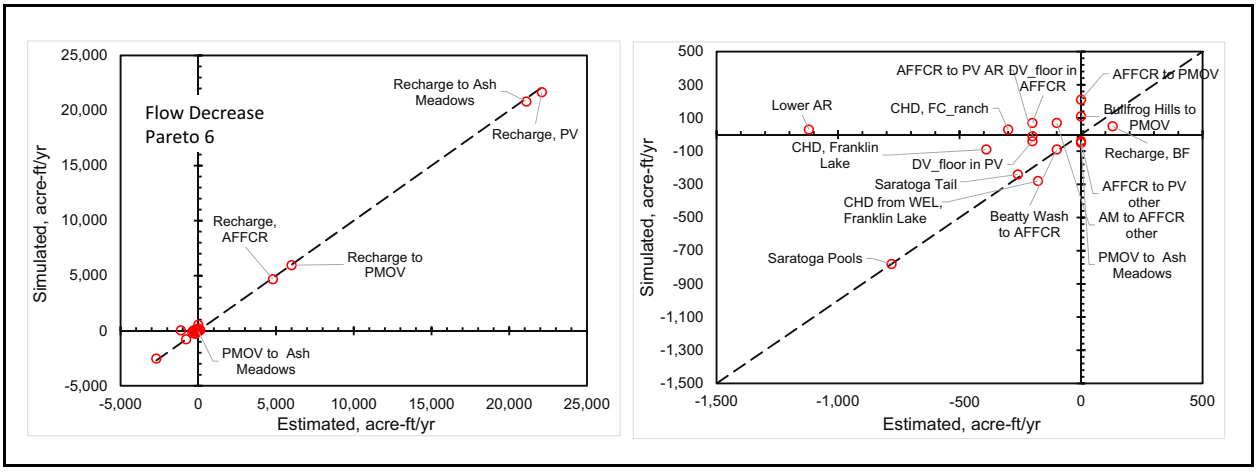

Figure 2-31
Expected and Simulated Water Budgets for the Pareto Analysis Flow Decrease Iteration 6 Model

Table 2-13. Unfortunately, ER-3-3 groundwater samples are considered unreliable given the small volumes of groundwater that could be pumped from the well and the unnaturally high pH (10.1) that suggests the influence of the concrete plug used to separate the two main completion intervals. Interpretations of the ER-3-3 data with regard to flow directions and mixing should therefore be made cautiously, with the limitations of the data in mind. Groundwater data for all other LCA wells used in this analysis are listed in Appendix A of SNJV (2006a) and in Table 2-13.

This analysis displays geochemical and isotopic data from the LCA, and also considers interpretations from SNJV (2006a) in which mixing with groundwater draining from the saturated tuff and alluvial aquifers was inferred to have occurred in order to explain water chemistry trends. Maps of hydraulic heads (Figure 2-33) are used to infer overall groundwater flow directions, and then groundwater geochemical and isotopic data are used to confirm or refute possible flow directions based on similarities and differences in the groundwater geochemical and isotopic data from different well pairs. Similarities in groundwater geochemical and isotopic data between well pairs indicates that they have a common source and lie along a flow path. However, it is important to consider as many geochemical or isotopic data pairs as possible because many wells are similar with respect to one or a few chemical or isotopic species, but wells that lie along a common flow path are likely to have similar values for all chemical or isotopic constituents, or have them vary in a way that is explainable with simple reaction pathways. And, of course, the wells inferred to lie along a flow path must be compatible with the interpreted hydraulic gradients, while allowing for the possibility

Table 2-13
LCA Groundwater Compositions Used for Flow Path Analysis

Location	pH (SU)	Temp (°C)	HCO_3 (mg/L)	Cl (mg/L)	SO_4 (mg/L)	Ca (mg/L)	Na (mg/L)	Mg (mg/L)	K (mg/L)	SiO_2 (mg/L)	Sr (ppb)	$\delta^{18}O$ (‰)	$\delta^{2}H$ (‰)	$\delta^{13}C$ (‰)	^{14}C (pmc)	$^{36}Cl/Cl$ (Ratio)
ER-3-1	6.7	41	584	42	67	91	139	34	18.3	35	917	-14.1	-109	-2.3	1	1.31E-13
ER-3-3	10.1	19.4	222	8.8	54	25.5	100	5.3	13.5	106	124	-13.7	-107	-1.0	8.3	--
ER-4-1	6.8	32.1	621	25.1	52	84	70	42	13	50	402	-13.77	-104.7	-2.15	4.19	--
ER-6-1-2	7.7	39.9	244	11	34.3	33	44	13	7.5	33	213	-14.1	-106	-6.2	2.4	4.33E-13
ER-6-2	7.6	34.9	373	19	58	58	63	20	10.8	31	337	-14.1	-106	-4.3	--	2.00E-13
ER-7-1	7.7	49.4	241	11	34.1	34	47	14	7	33	230	-14.00	-106	-6.3	5.3	3.77E-13
ER-12-1	7.7	25	221	17	343	94	37	64	3.6	20	199	-12.5	-94	-9.6	11	7.80E-13
ER-12-2	8.2	35.2	300	6.8	27.3	5.5	114	1.8	3.1	22	323	-13.7	-101.1	-5.5	2	6.90E-13
ER-12-3	8.0	30.6	120	6.0	26	17.4	29.8	8.0	2.8	25.3	138	-14.5	-106	-5.7	3.0	5.39E-13
ER-12-4	7.9	26	84.5	8.9	13	8.65	29.5	8.65	3.98	15.8	51.8	-13.8	-101.2	-7.05	6.9	5.70E-13
TW-D	7.9	23.9	238	7.3	30	12	84	5.0	8.3	44	112	-14.2	-108	-5.5	3	--
U-3cn-5	7.3	45	263	32	36	32	56	19	9	56	227	-14.1	-104	-6.8	3	4.08E-13
UE-1h	8.2	25.3	270	43.4	3	13	101	9	24	11	177	-13.8	-104.5	-11.2	18	1.61E-13
UE-1r	7.8	--	251	7.0	13	20	--	9.4	--	--	--	--	--	--	--	--
UE-1q	7.9	27.7	197	11	24	24	39	14	7	51	140	-14.5	-108	-5.5	8	7.90E-13
UE-2ce	7.9	32.9	405	17	11	53	40	25	21	47	188	-12.9	-100	-5.3	--	--
UE-7nS	7.6	34.7	167	27	0.8	20	58	3.5	4.6	21	89	-14.0	-106	-2.0	--	--
UE-10j-1	6.4	32.7	552	23.9	79	107	68	45	13	41	470	-13.6	-104	-3.6	7	2.41E-13
UE-10j-2	6.7	32.3	403	16	67	68	43	30	8.3	36	320	-13.2	-102	-5.7	11	3.91E-13
UE-10j-3	7.1	32.1	322	12.8	59	60	37	27	7.3	32	270	-12.8	-100	-7.7	13	4.45E-13
WW-2	7.4	34.6	202	7.4	20	30	28	15	6.6	56	79	-13.5	-103	-11.2	10	--
WW-C	7.0	34.7	544	36	66	67	127	30	15.0	35	704	-14	-107	-4.0	0.6	1.76E-13

Note: Results include those from Appendix A of SNJV (2006a) and newly acquired groundwater data from model evaluation Wells ER-3-3 (December 2016) and ER-4-1 (February 2017) (Table 2-3).

-- = Not available

Ca = Calcium
HCO_3 = Bicarbonate
K = Potassium
Mg = Magnesium
Na = Sodium
pmc = Percent modern carbon
SiO_2 = Silicon dioxide
SO_4 = Sulfate
°C = Degree Celsius
ppb = Parts per billion

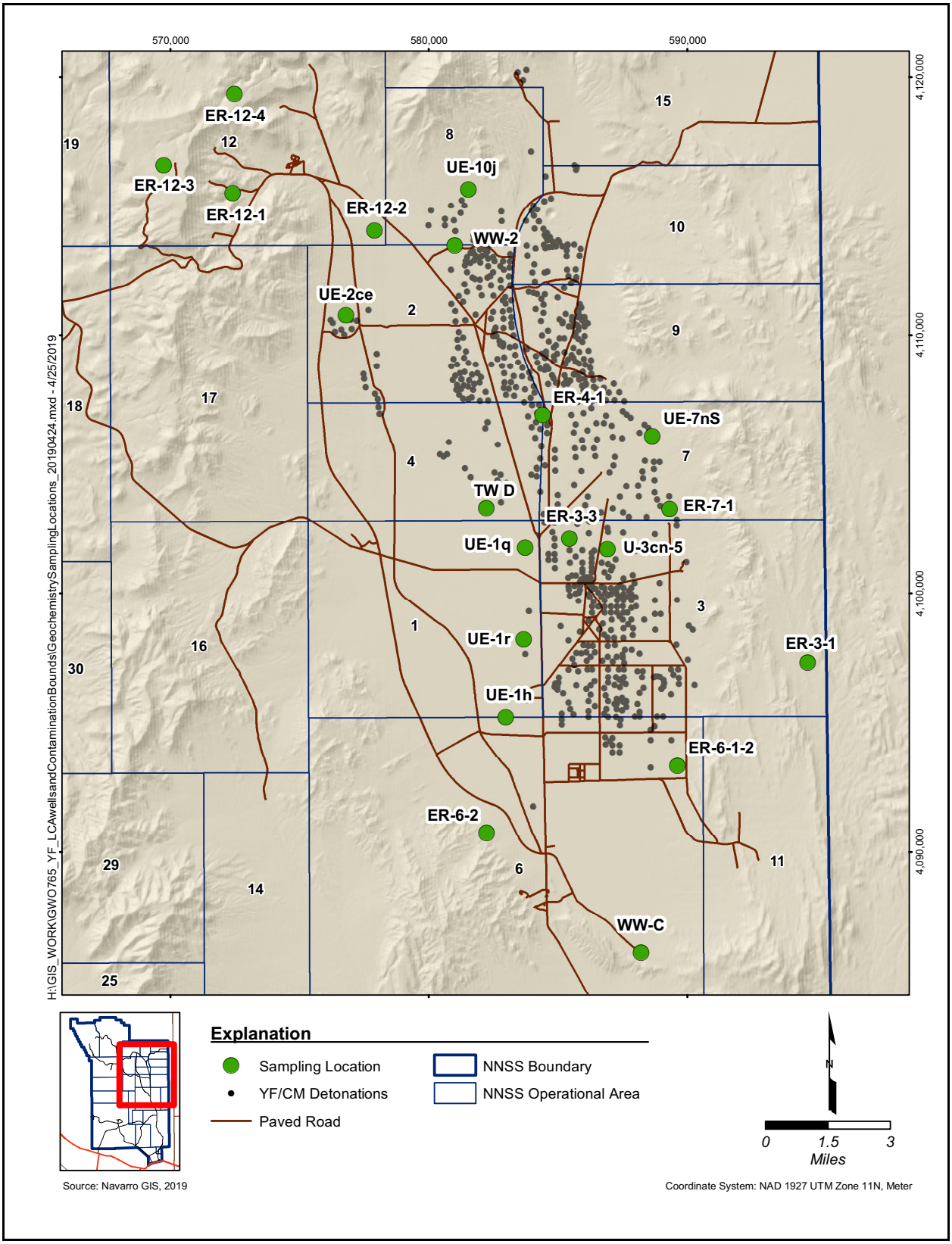

Figure 2-32
Geochemistry Sampling Locations

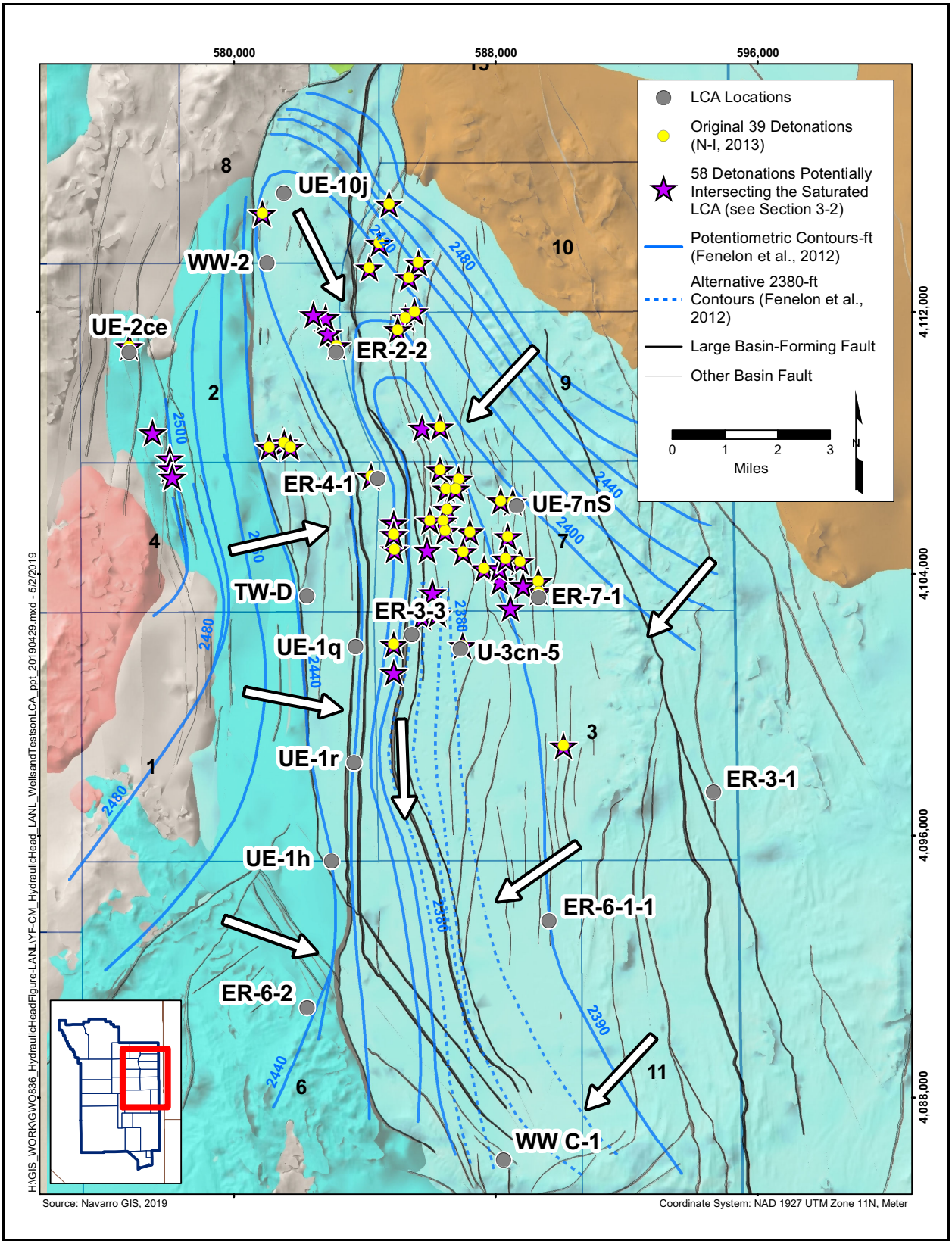

Figure 2-33
Potentiometric Contours and Inferred Flow Paths

that flow directions may not be exactly aligned with the inferred hydraulic gradients due to permeability anisotropy.

2.7.1 Predevelopment Hydraulic Heads in the LCA

A map of predevelopment hydraulic heads and interpreted contours in the LCA, presented in Fenelon et al. (2012), was used to select wells that could lie along a flow path. Flow directions on the map were drawn assuming that the LCA is isotropic and that flow is perpendicular to the contours as drawn (Figure 2-33). The map indicates that flow converges from the perimeter of the basin toward a potentiometric trough in the center of the basin that roughly coincides with the two strands of the Yucca fault and extends from the southern end of the basin as far north as approximately U-3cn-5. Although the exact position of the trough is uncertain, as indicated by the dashed lines, the trough is estimated to be present somewhere between Wells UE-1q and U-3cn-5 and extend to the southern end of the basin. Wells within the trough include ER-3-3 and WW-C. Based on this interpretation, groundwater from the northern, western, and eastern parts of the basin would all merge and potentially mix in the trough, so that WW-C groundwater could resemble any of the upgradient members to varying degrees, based on the relative inflow to that trough from that portion of the basin. Given the presence of the hydraulic trough in the center of the basin, groundwater from west of the trough (e.g., TW-D, UE-1q, UE-1r, UE-1h, ER-6-2) and groundwater from east of the trough (e.g., UE-7nS, ER-7-1, U-3cn-5, ER-6-1-1, and ER-3-1) would never be groundwater sources for, or mix with, groundwater of the other region except within the trough.

Groundwater flow paths at a large angle to the hydraulic gradient are investigated because of the strong north–south trend of the major structure features and given sparse head data that form the basis for the contours. The possibility that the hydraulic trough does not hydraulically separate the western and eastern parts of the basin is also investigated by allowing for the possibility that wells in eastern Yucca Flat are downgradient from Well ER-4-1, which is located west of the hydraulic trough.

2.7.2 Potential Sources of ER-4-1 Groundwater

Based on hydraulic gradients shown in Figure 2-33, potential upgradient LCA or LCA3 wells contributing groundwater to the LCA at ER-4-1 are UE-10j, ER-12-1, ER-12-2, ER-12-3, ER-12-4, WW-2, UE-2ce, and possibly TW-D and UE-1q. Well UE-10j had LCA groundwater completions from three zones, with zone 1 being the deepest and zone 3 being the shallowest. Groundwater from

UE-10j zone 1 (UE-10j-1) was inferred in SNJV (2006a) to be representative of deep regional groundwater inflow into Yucca Flat basin, whereas the two shallower zones (UE-10j-2 and UE-10j-3) represent regional underflow mixed to varying degrees with local paleo-recharge along the northern margin of the basin. Groundwater sampled from the shallowest zone (UE-10j-3) was estimated to contain more than 90 percent local recharge (SNJV, 2006a).

2.7.2.1 Alkalinity versus pH

Alkalinity and pH from Well ER-4-1 are most similar to values measured from the deep interval of UE-10j (UE-10j-1) (Figure 2-34). The two shallower zones from UE-10j (UE-10j-2 and UE-10j-3) indicate that their local recharge component has lower alkalinity and higher pH than the deep groundwater sample from UE-10j-1. Groundwater from the LCA3 in the Rainier Mesa area (ER-12-1, ER-12-2, ER-12-3) and from the upper tuff confining unit (UCCU) (ER-12-2) have much higher pH and lower alkalinity, as do Wells TW-D and UE-1q, which were interpreted in SNJV (2006a) to be composed of groundwater draining from the VAs near a major fault. Groundwater from WW-2 is strikingly distinct from UE-10j-1 and ER-4-1, despite being located between them, and could include a large component of VA groundwater (SNJV, 2006a). Groundwater from UE-2ce is very distinct from ER-4-1 groundwater, primarily due to its higher pH.

2.7.2.2 Calcium versus Sodium

The calcium and sodium concentrations for ER-4-1 groundwater display a striking similarity to concentrations measured at UE-10j-1 (Figure 2-35). The trend in cation concentrations for UE-10j-1, UE-10j-2, and UE-10j-3 indicates that the local recharge component present in the shallower portions of the well is dilute with respect to both calcium and sodium. With the exception of groundwater from Well ER-12-1, the groundwater from the other potential source area wells is quite distinct from ER-4-1, and the other potential source area wells are not obvious sources for the groundwater at ER-4-1.

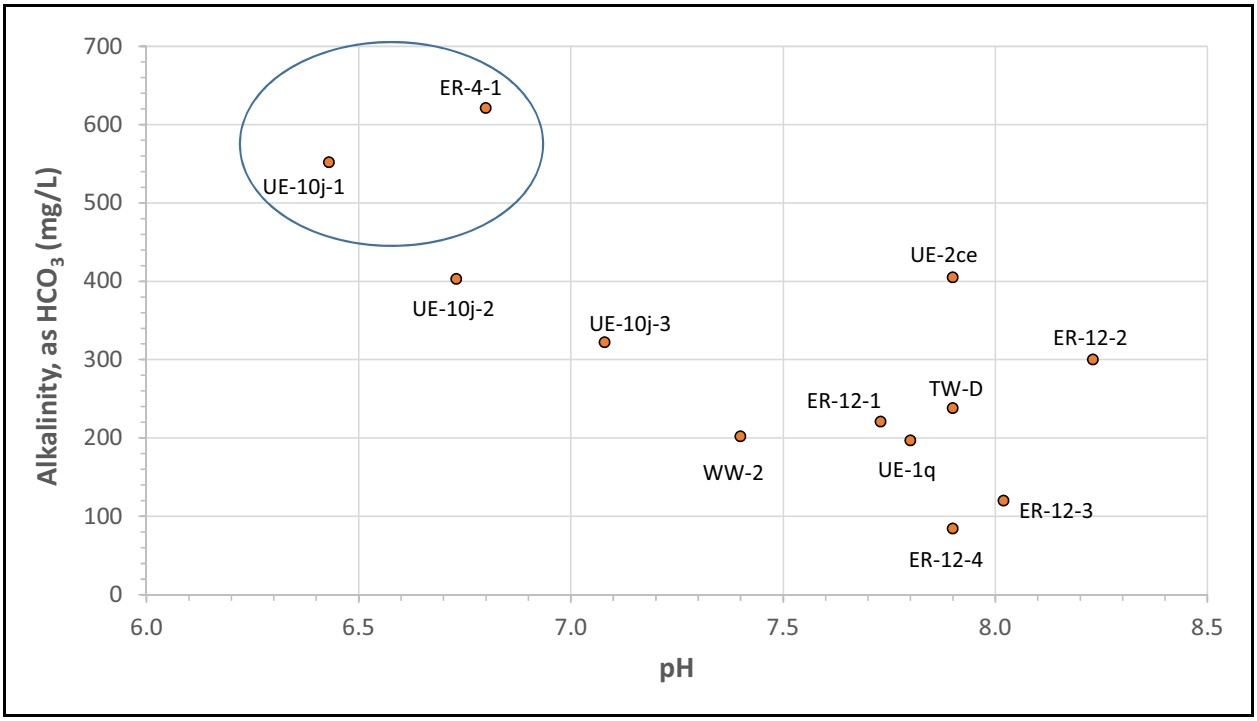

Figure 2-34
Alkalinity versus pH for Potential ER-4-1 Groundwater Source Area Wells

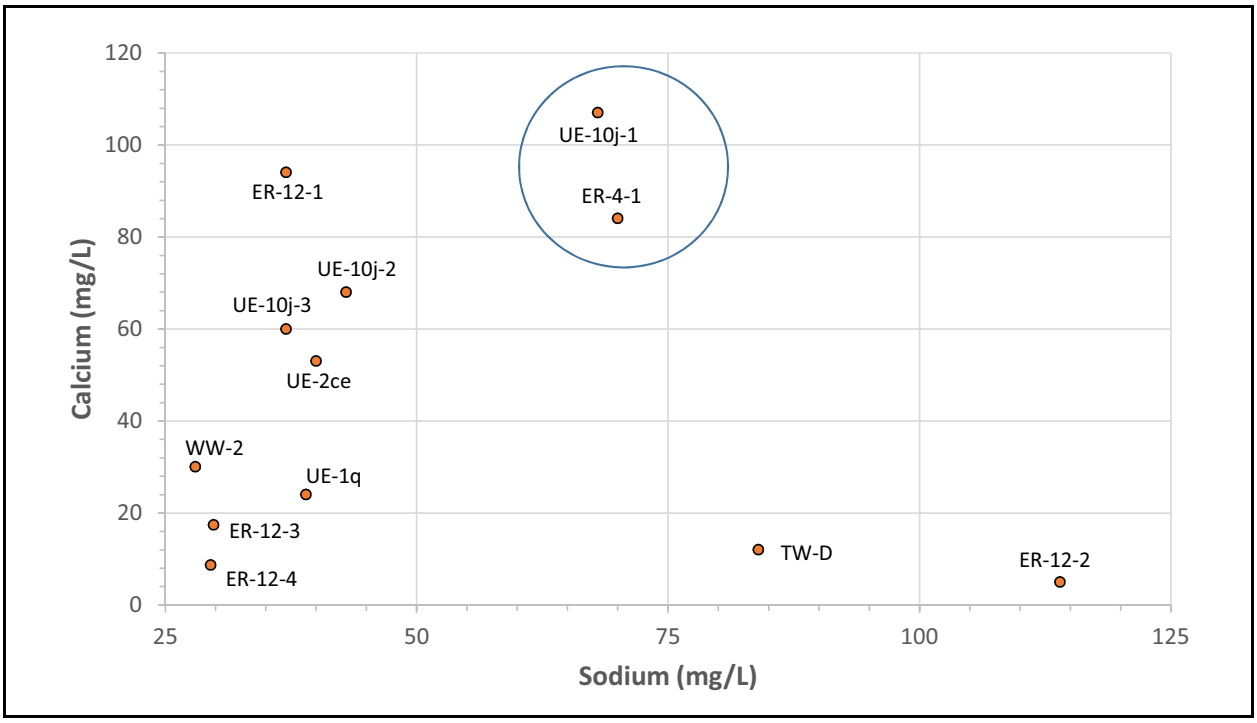

Figure 2-35
Calcium versus Sodium for Potential ER-4-1 Groundwater Source Area Wells

2.7.2.3 Sulfate versus Chloride

Although sulfate and chloride concentrations from ER-4-1 and UE-10j-1 are similar, they are not particularly distinct from those of other potential upgradient source areas of ER-4-1 groundwater with the exception of ER-12-1, which has much higher sulfate (Figure 2-36). Wells ER-4-1 and UE-10j-1 are primarily differentiated from the other samples by their higher Cl concentrations.

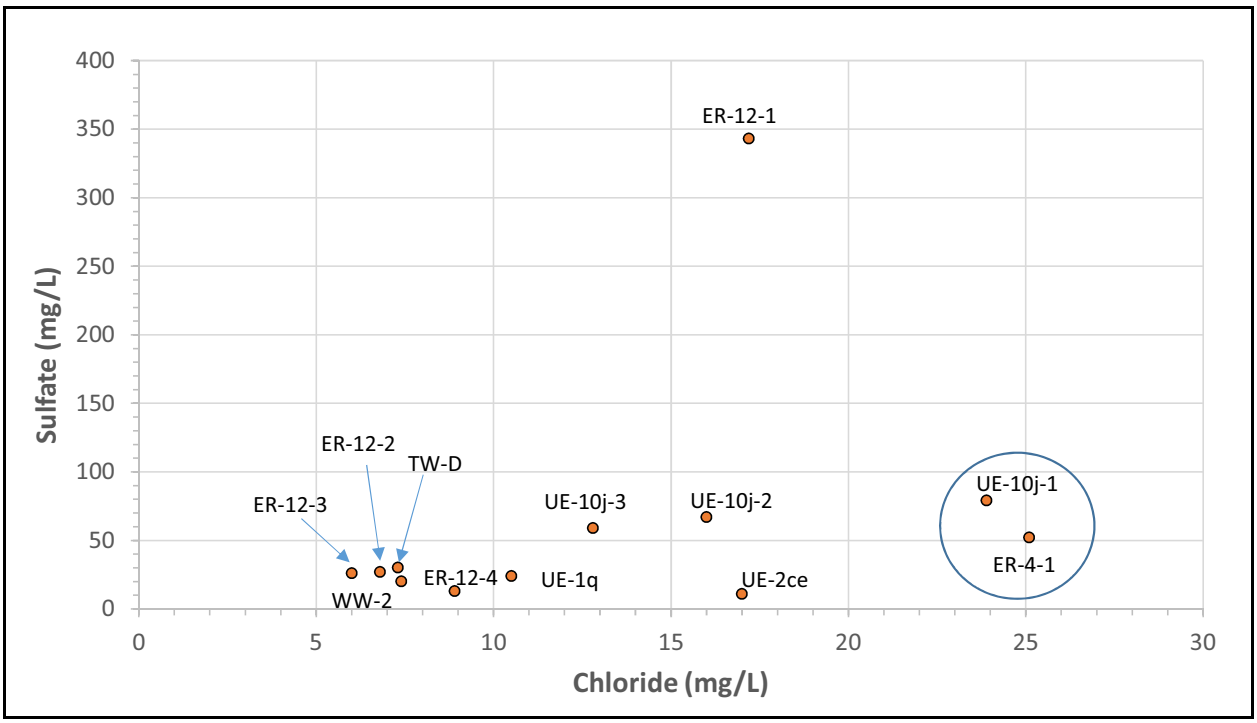

Figure 2-36
Sulfate versus Chloride for Potential ER-4-1 Groundwater Source Area Wells

2.7.2.4 Magnesium versus Potassium

Magnesium and potassium from ER-4-1 and UE-10j-1 show strong similarities to each other and larger differences relative to data from the other wells (Figure 2-37). The groundwater at ER-4-1 is distinct from groundwater at Wells UE-1q and TW-D in western Yucca Flat, suggesting groundwater at ER-4-1 does not originate from the western part of the basin.

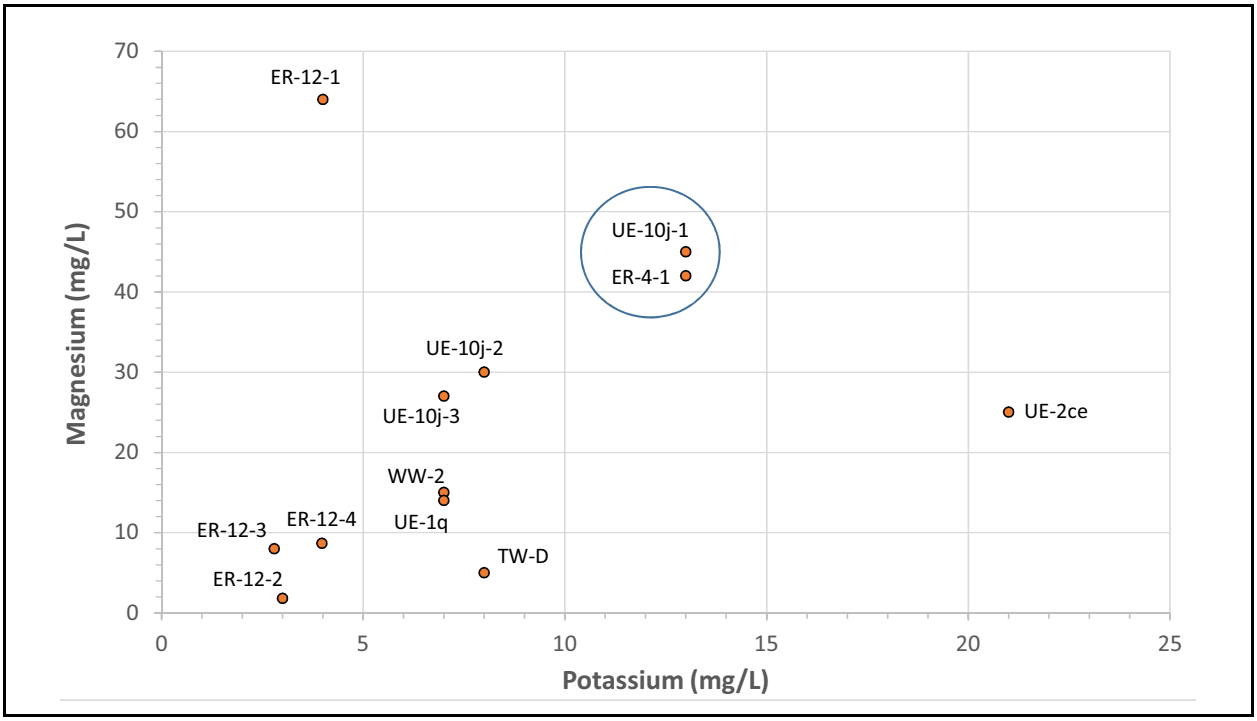

Figure 2-37
Magnesium versus Potassium for Potential ER-4-1 Groundwater Source Area Wells

2.7.2.5 δ^2H versus $\delta^{18}O$

The stable isotopes deuterium (^2H) and oxygen-18 (^{18}O) travel as part of the water molecule and are not subject to water/rock interactions at normal aquifer temperatures, making them potentially useful groundwater tracers. However, it is known that they have varied over time in response to major climatic changes (e.g., Merlivat and Jouzel, 1979; White and Chuma, 1987; Claassen, 1986; Winograd et al., 1992 and 2006); seasonal and long-term differences in the paths of storm tracks (Benson and Klieforth, 1989); and the effects of differences in condensation temperatures (Ingraham et al., 1991; Moscati and Schofield, 2012).

The δ^2H versus $\delta^{18}O$ data from the LCA and LCA3 in and near Yucca Flat are shown in Figure 2-38 relative to the global meteoric water line (GMWL) of Craig (1961). With the exception of data from ER-12-3 and ER-12-4, isotopic data from most wells plot below the present-day GMWL, indicating a possible pluvial origin for the groundwater (White and Chuma, 1987; Merlivat and Jouzel, 1979). There is again a strong similarity between ER-4-1 groundwater and groundwater from UE-10j-1, with most other samples being sufficiently different to eliminate them as possible sources of ER-4-1 groundwater. (Note: LLNL reported two very distinct values for the δ^2H of ER-4-1 groundwater: -105

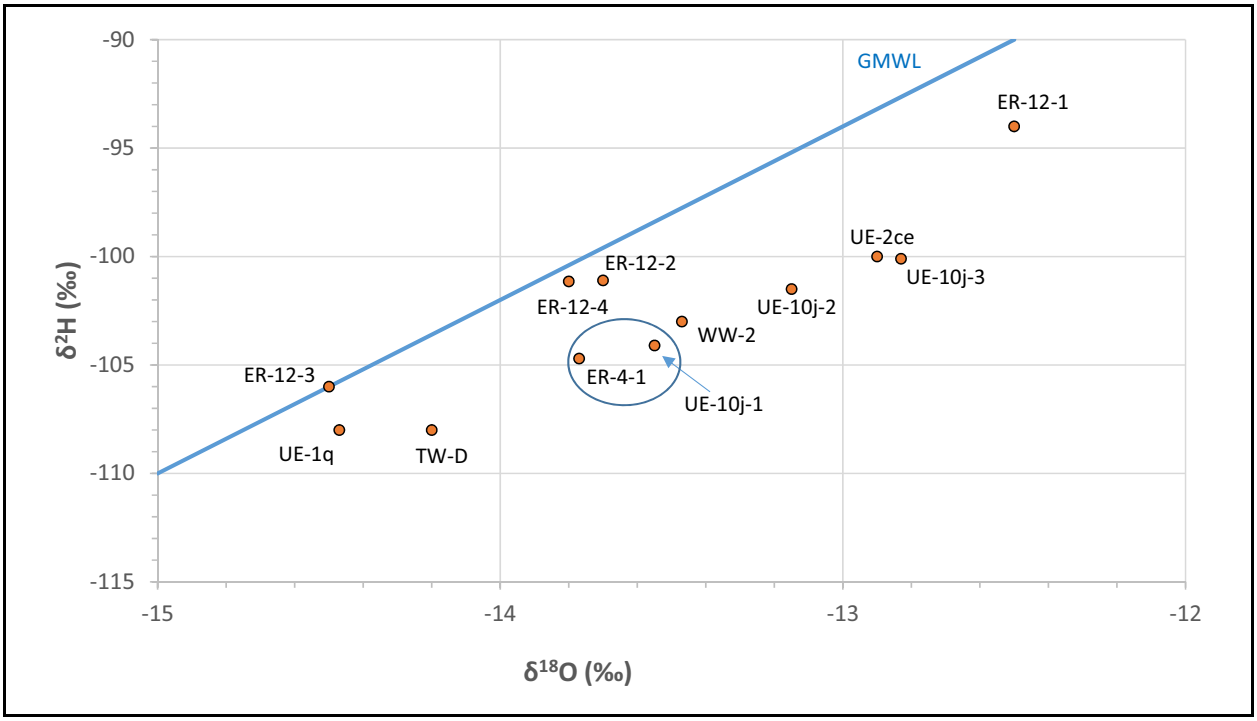

Figure 2-38
δ^2H versus δ^{18}O for Potential ER-4-1 Groundwater Source Area Wells

and -95 per mil. The first value was chosen because it, like all other geochemical and isotopic species, closely matches the δ^2H of UE-10j-1 groundwater, whereas the second value of δ^2H has rarely been measured in Yucca Flat LCA groundwater and would put the ER-4-1 sample well above the GMWL.)

2.7.2.6 Carbon Isotopes

Carbon isotope data from ER-4-1 and potential upgradient source wells are shown in Figures 2-39 and 2-40. The plot of δ^{13}C versus alkalinity (Figure 2-39) shows that groundwater from ER-4-1 is higher in alkalinity and heavier in δ^{13}C relative to groundwater at UE-10j-1. This is consistent with the groundwater having acquired additional isotopically heavy marine carbonate as it flowed between UE-10j-1 and ER-4-1. Figure 2-40 shows the same increase in δ^{13}C values and a decrease in ^{14}C activity as groundwater flows between Wells UE-10j-1 and ER-4-1. Part of the decrease in ^{14}C activity between these wells occurs because of water-rock interaction, and part of it occurs because of radioactive decay during ^{14}C transport between the wells. The decrease in ^{14}C that occurs between the wells due to water/rock interaction must be identified before ^{14}C can be used as a basis for estimating travel time and groundwater velocity between the wells.

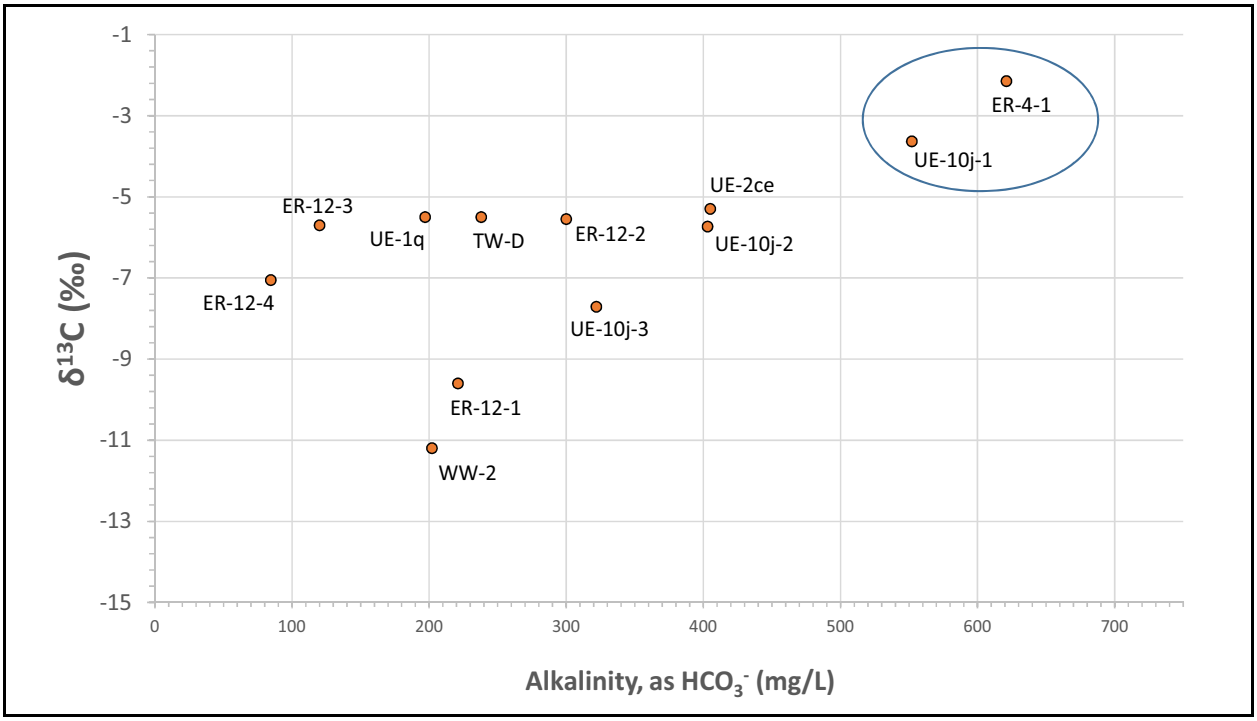

Figure 2-39
$\delta^{13}C$ versus Alkalinity for Potential ER-4-1 Groundwater Source Area Wells

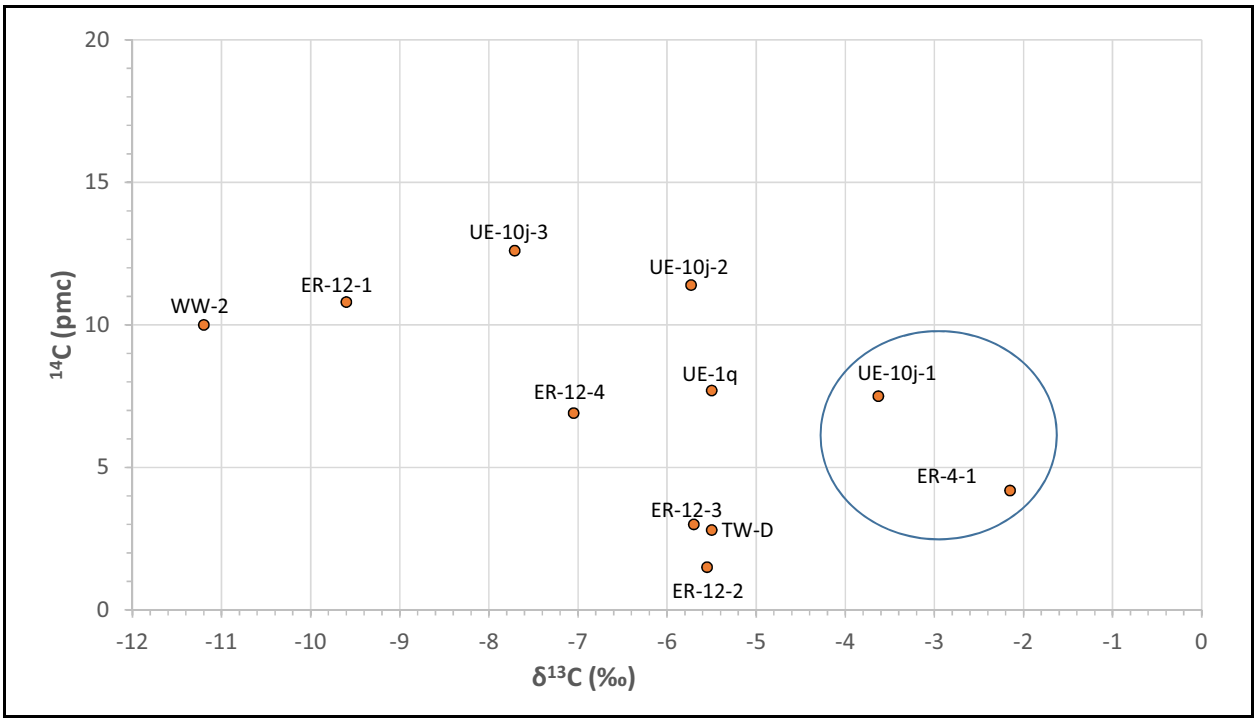

Figure 2-40
Carbon Isotopes for Potential ER-4-1 Groundwater Source Area Wells

2.7.2.7 Summary Investigation of Source Area for ER-4-1 Groundwater

Groundwater from Well ER-4-1 resembles groundwater from UE-10j-1 in every respect, whereas all other upgradient groundwater samples have one or more significant differences with ER-4-1 groundwater, indicating they are not the source of ER-4-1 groundwater. Groundwater from UE-10j-1 was assumed in SNJV (2006a) to be deep regional underflow in the LCA, undiluted by local recharge or drainage from the shallow volcanic rocks. A similar interpretation is proposed for ER-4-1 groundwater. Therefore, either groundwater from the deep interval of UE-10j (i.e., UE-10j-1) is the source of ER-4-1 groundwater, or ER-4-1 groundwater flows from an area that has yet to be sampled. If UE-10j-1 groundwater is indeed the source of ER-4-1 groundwater, carbon isotope data indicate that water/rock interactions with the carbonate rock matrix altered both the $\delta^{13}C$ and ^{14}C activities of LCA groundwater as it flowed between UE-10j-1 and ER-4-1. These water/rock interactions have to be quantified and accounted for when determining transit times and groundwater velocities between UE-10j-1 and ER-4-1 from ^{14}C.

2.7.3 Downgradient Flow Paths from ER-4-1

In this section, the same geochemical and isotopic species used to identify the upgradient source of ER-4-1 groundwater are used to identify the possible downgradient flow paths of the ER-4-1 LCA groundwater. All LCA groundwater sampling locations, both upgradient and downgradient of ER-4-1, are used for this purpose. Wells south and east of Well ER-4-1 investigated as potential downgradient destinations of ER-4-1 groundwater are TW-D, UE-1q, UE-1h, UE-1r WW, UE-7nS, ER-7-1, U-3cn-5, ER-6-1-2, WW-C, and ER-6-2.

2.7.3.1 Alkalinity versus pH

Figure 2-41 shows the plot of alkalinity versus pH for groundwater from Well ER-4-1 and other wells tapping the LCA. WW-C is the only downgradient well with alkalinity and pH values similar to Well ER-4-1. Wells UE-10j-1 and ER-3-1 also have similar alkalinity and pH values, but as discussed earlier, Well UE-10j-1 is upgradient of ER-4-1, and Well ER-3-1 lies east of Yucca Flat basin (and upgradient of WW-C), but off any possible flow path from ER-4-1. Wells in eastern Yucca Flat (e.g., UE-7nS, ER-7-1, U-3cn-5 and ER-6-1-2) have much higher pH and much lower alkalinity than ER-4-1. Similarly, wells south of ER-4-1 (e.g., UE-1q, UE-1r WW, UE-1h) also have much lower alkalinity and higher pH than groundwater at Well ER-4-1. Because no simple chemical reactions can

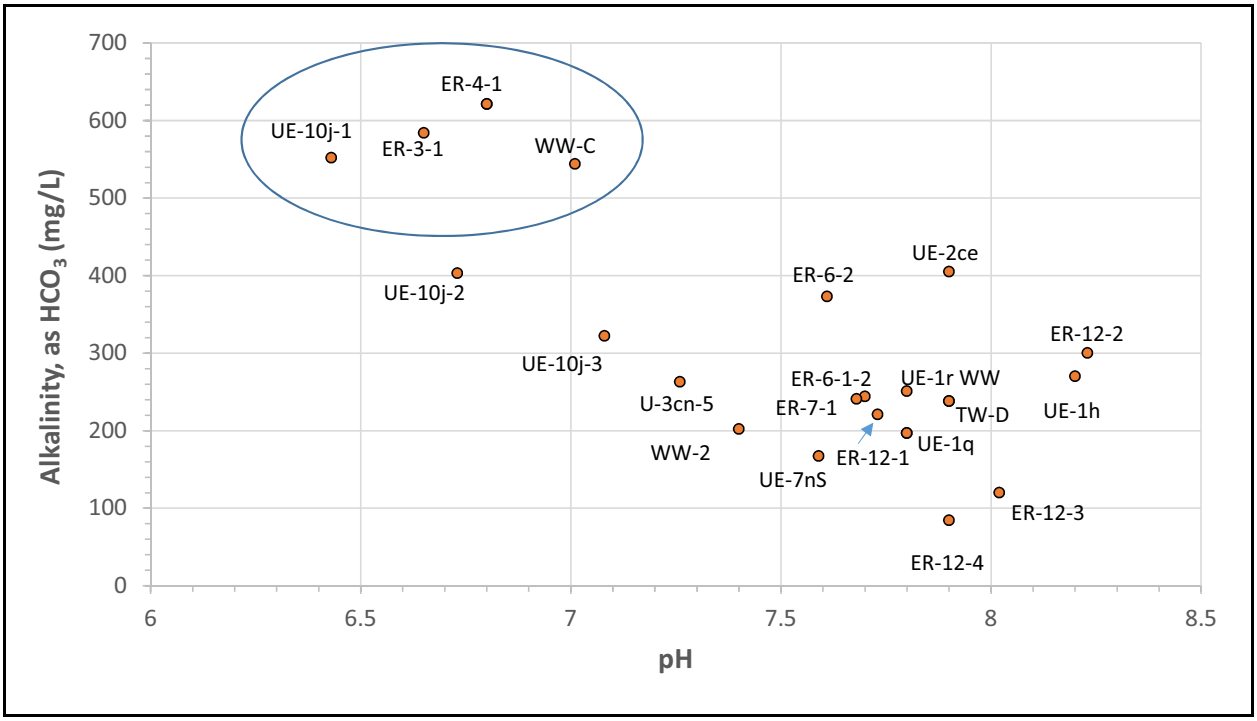

Figure 2-41
Alkalinity versus pH for ER-4-1 and Other LCA and LCA3 Wells

explain the simultaneous decrease in alkalinity and increase in pH, groundwater like that found at ER-4-1 does not appear to be present either south or east of ER-4-1. If present in these areas, groundwater flow from ER-4-1 is volumetrically insignificant relative to flow from other areas. Based on alkalinity and pH alone, ER-4-1 groundwater could be present at WW-C at the southern end of Yucca Flat; however, another possible source of WW-C groundwater is upgradient groundwater from ER-3-1 east of Yucca Flat. Of interest is the fact that Wells ER-7-1 and ER-6-1 are nearly identical in terms of their alkalinity and pH, indicating they could lie along a common flow path.

2.7.3.2 Calcium versus Sodium

Calcium versus sodium for Well ER-4-1 and other LCA or LCA3 wells are shown in Figure 2-42. The plot shows that groundwater from WW-C is more similar to groundwater from ER-3-1 than to groundwater from UE-10j-1 or ER-4-1, principally due to the higher sodium concentrations at both ER-3-1 and WW-C. The smaller calcium and sodium concentrations at WW-C relative to ER-3-1 indicates that additional presence of a more dilute groundwater component at WW-C in addition to ER-3-1 groundwater, perhaps indicating the presence of groundwater from eastern Yucca Flat (ER-6-1-2) or groundwater from west of WW-C (ER-6-2). Mixing models developed for WW-C in

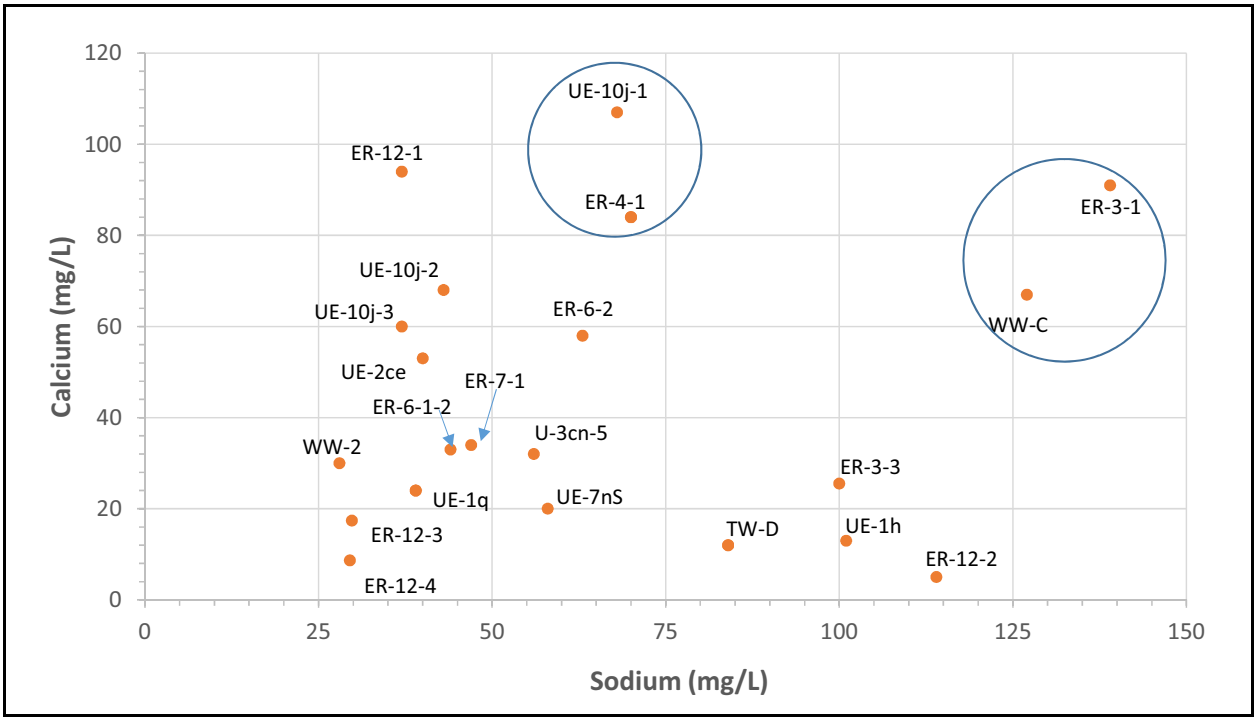

Figure 2-42
Calcium versus Sodium for ER-4-1 and Other LCA and LCA3 Wells

SNJV (2006a) indeed show that models can be found in which each of these wells contributes to groundwater at WW-C. On the basis of this plot, groundwater from ER-4-1 does not appear to be a major component in groundwater at WW-C or at wells in eastern Yucca Flat such as ER-6-1-2 unless it has undergone substantial dilution by groundwater with far less calcium and sodium. On the other hand, groundwater from ER-7-1 and ER-6-1-2 are nearly identical in terms of their calcium and sodium concentrations, suggesting these wells lie along a common flow path. Groundwater from ER-3-3 has much higher sodium concentrations than other samples from eastern Yucca Flat (UE-7nS, U-3cn-5, ER-6-1-2, and ER-7-1), suggesting a different origin for the ER-3-3 groundwater. It also does not resemble groundwater from ER-4-1 in either its Na^{+} or Ca^{2+} composition, although it is similar to nearby upgradient Well TW-D.

2.7.3.3 Magnesium versus Potassium

Magnesium versus potassium for Well ER-4-1 and other LCA or LCA3 wells is presented in Figure 2-43. Groundwater from UE-10j-1 and ER-4-1 have much higher magnesium and potassium concentrations compared with groundwater east (U-3cn-5, UE-7nS, ER-7-1, ER-6-1-2) or south (UE-1q, TW-D) of ER-4-1, indicating ER-4-1 groundwater is not present at these potential

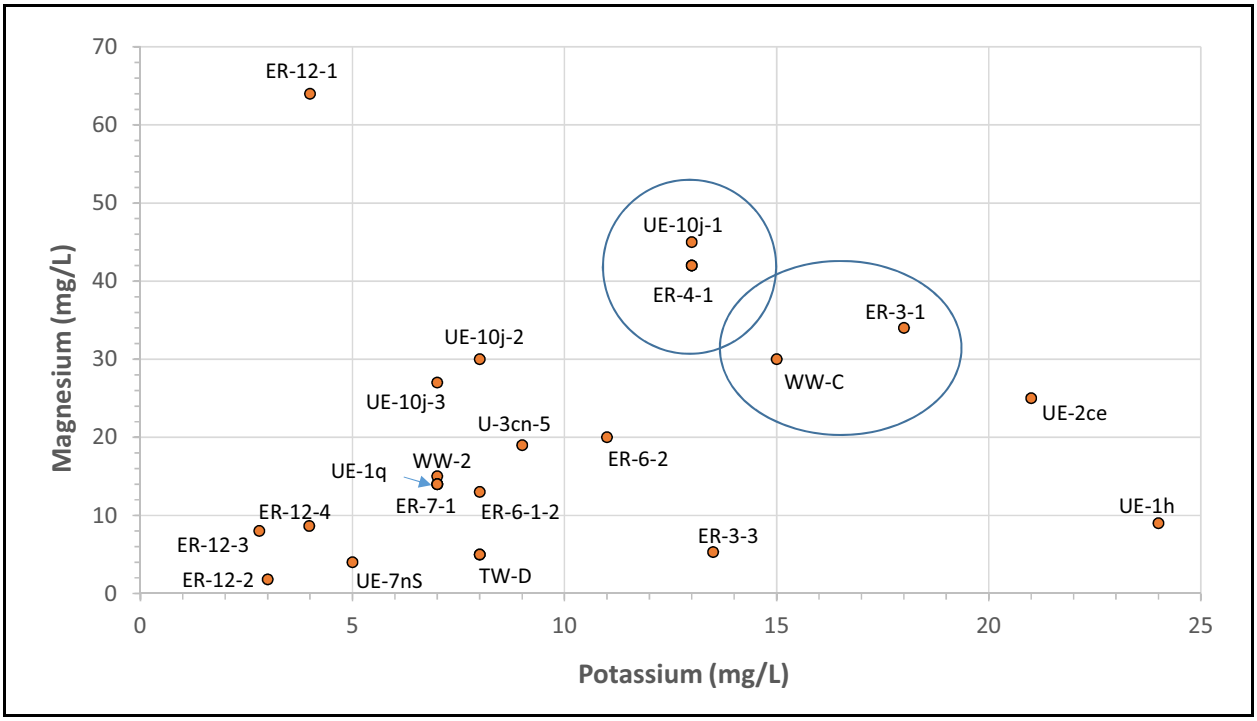

Figure 2-43
Magnesium versus Potassium for ER-4-1 and Other LCA and LCA3 Wells

downgradient wells unless it has undergone substantial dilution by mixing with other groundwater. Groundwater from WW-C plots close to groundwater from ER-4-1 and UE-10j-1 on this plot, but shows a closer affinity with groundwater from east of Yucca Flat at ER-3-1. As with other geochemical and isotopic species, the magnesium and potassium data suggest that groundwater similar to that at ER-3-1 has mixed with smaller amounts of more dilute groundwater, perhaps from ER-6-2 or ER-6-1-2, to produce the groundwater at WW-C. Again, groundwater samples from ER-7-1 and ER-6-1-2 plot close to each other on Figure 2-43, consistent with other geochemical variables examined thus far. Groundwater from ER-3-3 has much higher potassium concentrations than other samples from eastern Yucca Flat (UE-7nS, U-3cn-5, ER-6-1-2, and ER-7-1), again suggesting a different origin for the ER-3-3 groundwater. It also does not resemble groundwater from ER-4-1 in its magnesium composition.

2.7.3.4 Sulfate versus Chloride

Figure 2-44 shows that Wells UE-10j-1 and ER-4-1 have much higher sulfate and moderately more chloride than most wells in eastern Yucca Flat (ER-7-1, ER-6-1-2) or south of ER-4-1 (UE-1q or UE-1r WW). Wells U-3cn-5 and UE-7nS in eastern Yucca Flat and UE-1h south of ER-4-1 have

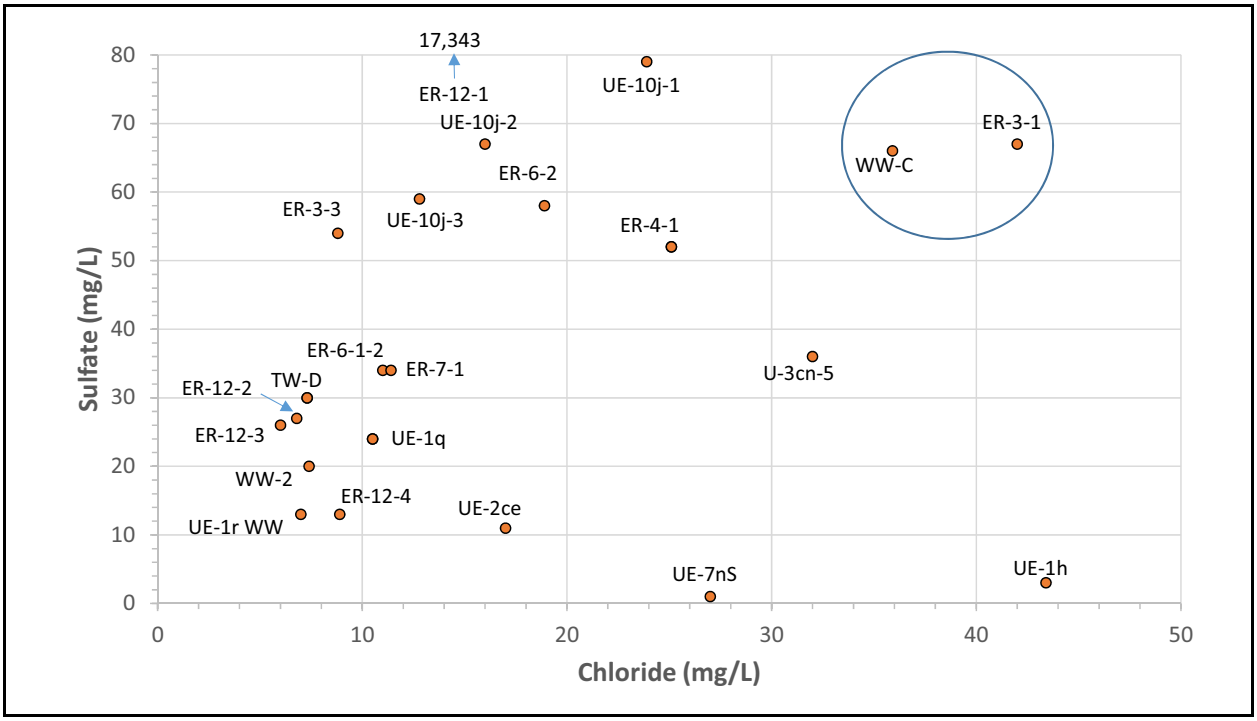

Figure 2-44
Sulfate versus Chloride for ER-4-1 and Other LCA and LCA3 Wells

higher chloride than Well ER-4-1 but much lower sulfate. Both U-3cn-5 and UE-7nS are about $2R_c$ to $3R_c$ from nuclear detonations where reducing conditions may exist immediately after the detonation, so this may explain the relatively low sulfate relative to the chloride concentrations for these wells. In this plot, groundwater from Well WW-C plots roughly intermediate between ER-4-1 and ER-3-1, with only a slightly greater similarity with ER-3-1. Samples from ER-7-1 and ER-6-1-2 plot nearly on top of each other, consistent with a common origin for these groundwater samples. Well ER-3-3 has much higher sulfate than groundwater at ER-7-1 and ER-6-1-2, perhaps due to the use of cement to separate the main completion zones at ER-3-3.

2.7.3.5 δ^2H versus $\delta^{18}O$

Figure 2-45 shows the scatterplot of δ^2H versus $\delta^{18}O$ for Well ER-4-1 and other LCA or LCA3 wells. In terms of δ^2H and $\delta^{18}O$, ER-4-1 is similar to other groundwater from eastern Yucca Flat and to UE-1h, although somewhat isotopically heavier than groundwater from Wells UE-1q and TW-D. Groundwater from WW-C again shows an affinity with groundwater from ER-3-1, although based on δ^2H and $\delta^{18}O$ alone, one cannot rule out the presence of other groundwater sources for WW-C, including groundwater from ER-4-1. The main significance of this plot is that δ^2H and $\delta^{18}O$ do not

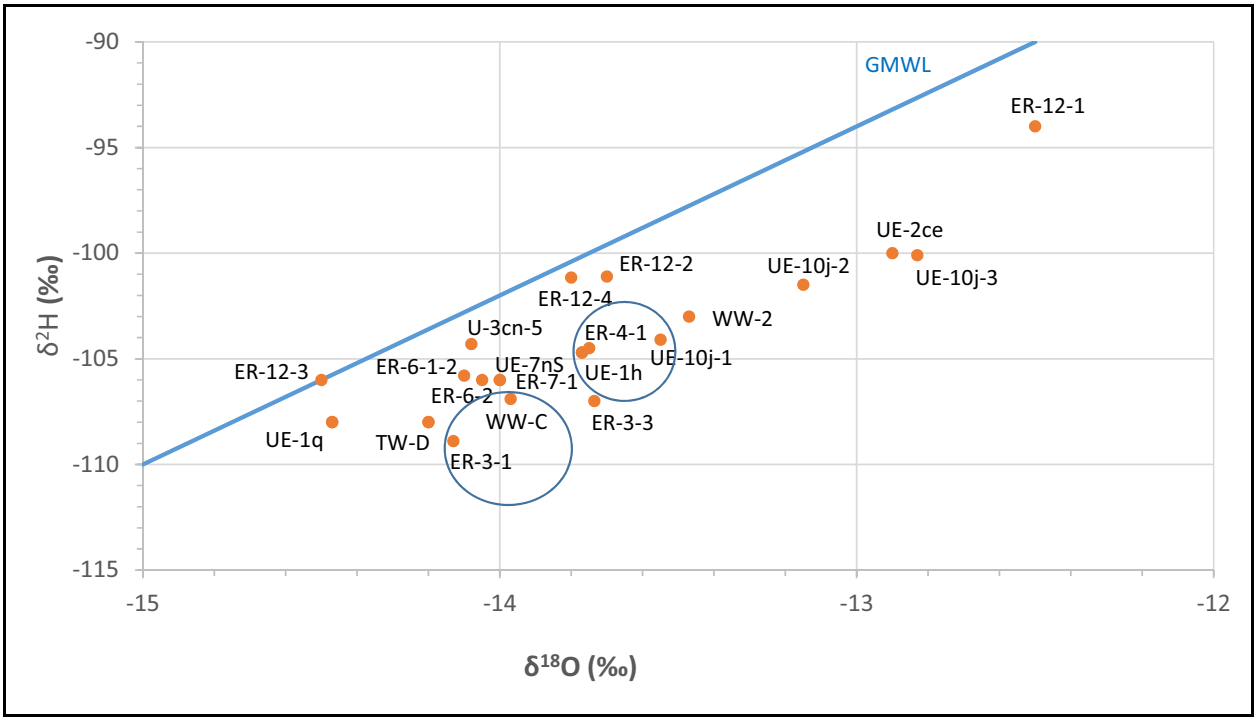

Figure 2-45
δ^2H versus δ^{18}O for ER-4-1 and Other LCA and LCA3 Wells

rule out the possibility that WW-C groundwater is derived mostly from the area of Well ER-3-1. Again, ER-7-1 and ER-6-1-2 groundwater closely resemble each other in terms of their δ^2H and δ^{18}O compositions.

2.7.3.6 Carbon Isotopes

The plot of δ^{13}C versus alkalinity shows that Wells ER-3-1, ER-4-1, UE-10j-1 and WW-C all have higher alkalinity and heavier δ^{13}C than other LCA or LCA3 groundwater in Yucca Flat. Of these four wells (Figure 2-46), WW-C is most similar in alkalinity and δ^{13}C composition to UE-10j-1. The lighter δ^{13}C compositions and lower alkalinity of WW-C groundwater relative to ER-3-1 would again require that ER-3-1 groundwater mix with more chemically dilute and isotopically lighter groundwater in order for it to be a dominant component of WW-C groundwater. These plots suggest that Wells ER-6-1-2 and ER-6-2 could provide the dilute isotopically light groundwater at WW-C. A similar conclusion could be reached from a plot of ^{14}C activity versus δ^{13}C (Figure 2-47), where WW-C is observed to have lighter δ^{13}C and lower ^{14}C activity than ER-3-1 groundwater. Wells ER-7-1 and ER-6-1-2 have nearly identical δ^{13}C values and alkalinity (Figure 2-46), but ^{14}C activities

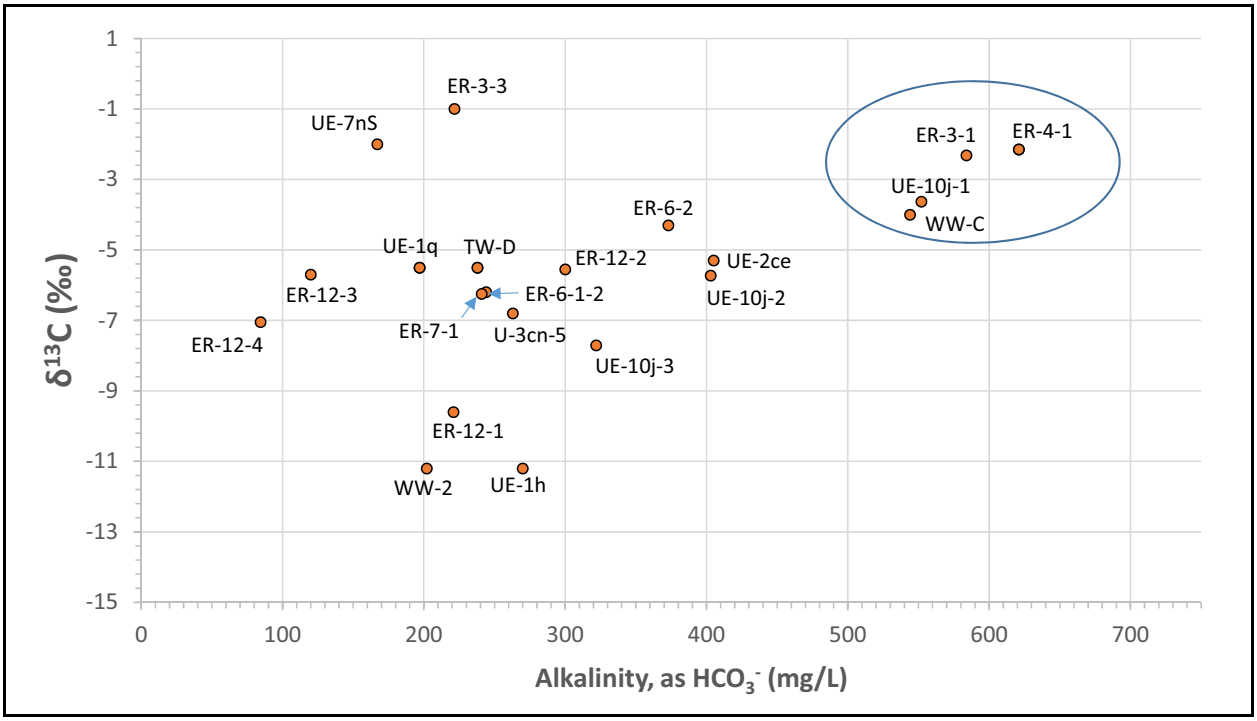

Figure 2-46
δ^{13}C versus Alkalinity for ER-4-1 and Other LCA and LCA3 Wells

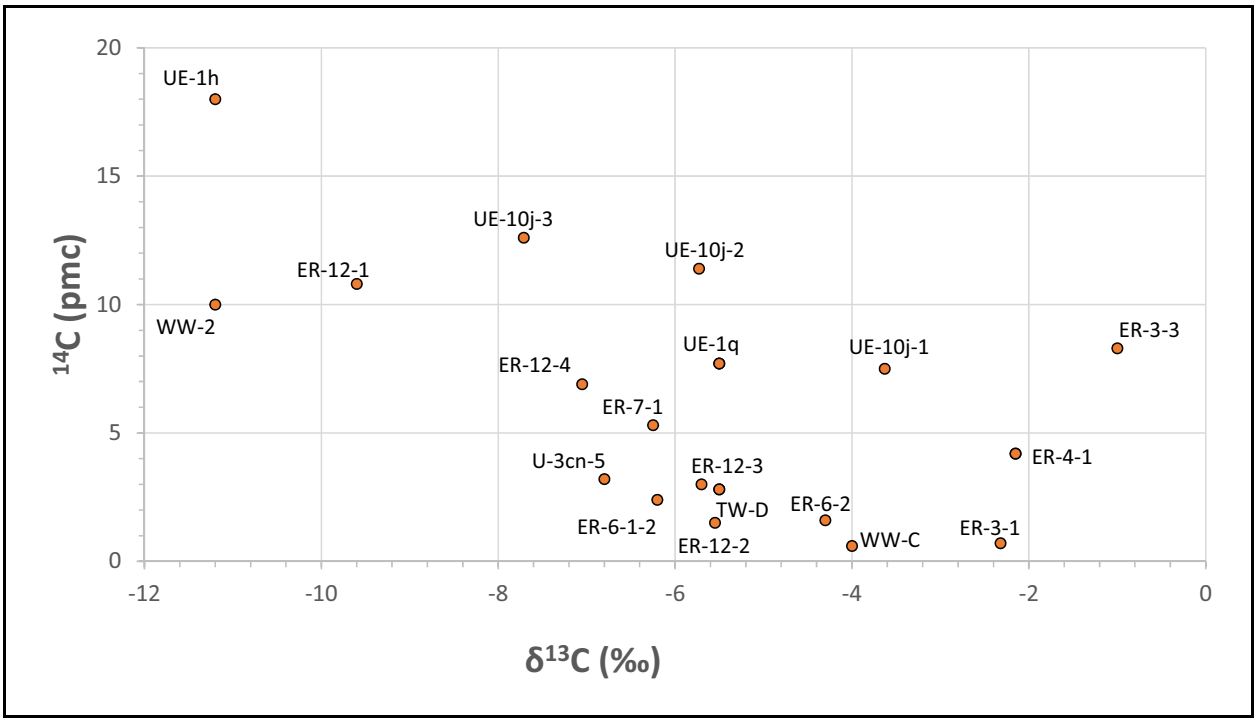

Figure 2-47
Carbon Isotopes for ER-4-1 and Other LCA and LCA3 Wells

are substantially lower at ER-6-1-2 (Figure 2-47), possibly reflecting radioactive decay of ^{14}C as groundwater flowed southward from ER-7-1 (SNJV, 2006a).

2.7.3.7 Estimating Effective Transport Porosity between ER-7-1 and ER-6-1-2 Based on ^{14}C

The strong similarity in geochemical and isotopic compositions of groundwater at ER-7-1 and ER-6-1-2 presented in Section 2.7 supports the existence of a north–south flow path between these wells, as indicated by both the DV3 model and the LCA CAU model. This conclusion is consistent with the results of an in-depth geochemical analysis (SNJV, 2006a) in which mixing and reaction models indicated that ER-6-1-2 groundwater was essentially unmodified, upgradient ER-7-1 groundwater. The estimated ^{14}C transport velocity between the wells was about 2 meters per year (m/yr).

The effective transport porosity between ER-7-1 and ER-6-1-2 can be estimated from the following relationship:

$$v = q/\varphi \qquad (2\text{-}2)$$

where

v = Groundwater velocity estimated from ^{14}C (2 m/yr)

φ = Effective transport porosity

q = Groundwater flux (m/yr)

The flux (q) can be calculated from Darcy's Law using the estimated flow (Q) of 560 acre-ft/yr (2.2E-02 m^3/s) moving through the roughly 5-km-wide high-transmissivity corridor connecting ER-7-1 and ER-6-1-2 (Figure 2-19). Assuming flow occurs through the entire thickness (b) of the LCA of nearly 5,000 m as represented in the Yucca Flat HFM (BN, 2006), the Darcy flux (q) can be estimated as follows:

$$q = Q/A = Q/(b*w) = 8.74E\text{-}10\ m/s\ or\ 0.028\ m/yr \qquad (2\text{-}3)$$

Equation (2-2) can be rearranged to solve for $\varphi = 0.014$, which is within the range of matrix porosity values for the LCA given in the transport data document (SNJV, 2007). Given that the estimated fracture porosity of the LCA is orders of magnitude lower, the value of $\varphi = 0.014$ indicates that some

matrix porosity is involved in ^{14}C migration, probably through matrix diffusion. For comparison, if a flowing thickness of 500 m is assumed, as in the DV3 model, the calculated transport porosity is 0.140, which is well beyond the measured range of LCA matrix porosities.

As an additional check, the measured steady-state hydraulic gradient *(dH/dL)* of 8.31E-05 m/m between ER-7-1 and ER-6-1-2 can be used with Darcy's Law to estimate the effective hydraulic conductivity (*K*) between the wells:

$$q = -K\,(dH/dL) \qquad (2\text{-}4)$$

Inverting Equation (2-4) to solve for *K* yields *K* = 6.03E-03 meters per second (m/s) or, equivalently, a permeability *k* = 1.1E-12 m^2. For comparison, SNJV (2005) analyzed the drawdown response at ER-7-1 in response to the ER-6-1-2 MWAT and calculated an estimated *K* = 4 feet per day (ft/day) or an equivalent *k* of 1.4E-12 m^2, in good agreement with the *k* value estimated from Equation (2-4). Conversely, the use of an effective flow LCA thickness of 500-m yield a *k* of 1.1E-11 m^2, 1 order of magnitude higher than the value estimated from an analytical fit to the ER-7-1 drawdown response. The conclusion of this analysis is that the use of the full thickness of the LCA as represented in the HFM provides a better estimate of both the effective transport porosity and the analytically determined value of *k* than the assumption of a much thinner, actively flowing LCA.

The area between ER-6-1-2 and ER-7-1 contains many relatively short faults (Figure 2-33). Both the drawdown response at ER-7-1 from the ER-6-1-2 MWAT and ^{14}C migration between ER-7-1 and ER-6-1-2 probably took place at least partially along the faults in this area. Although the transport porosity of 0.014 estimated from ^{14}C migration cannot be attributed solely to migration in either country rock or in faults, the estimated transport porosity of 0.014 suggests that matrix diffusion is an important process even in this relatively permeable, highly faulted part of Yucca Flat. Therefore, matrix diffusion is also likely to be important elsewhere in Yucca Flat as well.

2.7.4 Summary

Groundwater in the LCA at ER-4-1 does not appear to move southward along the Carpetbag or Topgallant faults toward UE-1q, UE-1h, or UE-1r WW based on the pronounced difference in geochemical and isotopic compositions between these wells and ER-4-1. Likewise, groundwater from ER-4-1 does not appear to be a component in the groundwater in eastern Yucca Flat (e.g., ER-7-1, U-3cn-5, or ER-6-1-2), which is consistent with the interpretation of hydraulic heads

presented in Fenelon et al. (2012), which proposed a potentiometric trough between ER-4-1 and these wells through which ER-4-1 groundwater flows southward toward WW-C. A number of mixing scenarios that explain the composition of WW-C groundwater are possible, including the presence of UE-10j-1 and ER-4-1 groundwater. However, the preferred model to explain the composition of WW-C groundwater is that groundwater from east of Yucca Flat, represented by LCA groundwater from ER-3-1, flows southwestward toward WW-C, where it mixes with a smaller amount of groundwater flowing south through the high-transmissivity eastern corridor of Yucca Flat (as represented by ER-7-1 and ER-6-1-2 groundwater, and groundwater flowing eastward from the vicinity of ER-6-2 (as represented by ER-6-2 groundwater). The final composition of WW-C groundwater is explained by the relative groundwater flow rates from these different areas. If groundwater from UE-10j-1 and ER-4-1 is present at WW-C, it does so by flowing south in the potentiometric trough west of U-3cn-5, roughly in the vicinity of ER-3-3. The present data from ER-3-3 do not indicate a resemblance with ER-4-1 groundwater that would suggest they lie along a common flow path. However, the measured pH of 10.1 for the ER-3-3 sample indicates that the sample is unlikely to be representative of conditions in the formation.

The effective transport porosity estimated using ^{14}C migration velocities in the highly faulted high-transmissivity corridor between ER-7-1 and ER-6-1-2 leads to a value of 0.014, which is consistent with a conceptualization of fracture flow in the presence of diffusion into the surrounding rock matrix. Use of 5-km-flow thickness for the LCA leads to a permeability estimate of 1.1E-12 m^2, which is in good agreement with the value of 1.4E-12 m^2, obtained from the ER-6-1-2 MWAT data, and indicates that the value of 5 km for the LCA thickness is consistent with the data.

2.8 Investigating LCA Surface Elevations

As noted in N-I (2013), the CB in the LCA is dominated by deeply buried detonations in the northern half of the basin with exchange volumes that are assumed to intersect the saturated LCA. The most significant contaminant inputs into the LCA are derived from exchange volume contaminant inventories emplaced directly into the LCA proper (N-I, 2013). The uncertainty in the number and location of detonations where the exchange volumes intersect the saturated LCA depends on both the size of each exchange volume and the modeled surface elevation of the LCA at each detonation location. The nominal surface that defined the top of the LCA in the flow and transport LCA model (N-I, 2013) was identified from an interpolation made across a series of elevation measurements or

other surrogate elevation indicators. This section introduces a way to investigate uncertainty in this surface as may be inferred from the available measurements and indicators to address the uncertainty in the *Exchange* v*olume size/shape that extends into the LCA* model evaluation target (DOE/EMNV, 2017d).

The LCA surface as modeled in the YF/CM HFM has uncertainty associated with it, especially in areas where the elevation could not be constrained because there were no nearby boreholes. Discrepancies were noted between the LCA surface elevation observed during model evaluation drilling (ER-2-2, ER-3-3, and ER-4-1) and the LCA surface elevations represented in the HFM (BN, 2006). The HFM predicted the top of LCA to be 160 m too shallow in ER-2-2, 124 m too deep in ER-3-3, and 35 m too shallow in ER-4-1 (DOE/EMNV, 2017a, b, and c).

The BN (2006) HFM was developed based on "measured" data augmented by non-measured data generated using expert judgment. Two categories of measured data were used to define the LCA and LCA3 surface:

1. LCA and/or LCA3 surface elevations within YF/CM boreholes as reported in the UGTA Stratigraphy and Lithology Database (Navarro, 2019b) (i.e., "full penetrations"), shown as black dots in Figure 2-48

2. Outcrop data from geologic mapping, shown as blue dots in Figure 2-48

An additional category of measured data that was not specifically used in the development of the HFM but that influenced the non-measured input is the measured total depth of wells that did not penetrate to the top of the LCA (i.e., "partial penetrations"). This category of measured data is shown as red dots in Figure 2-48.

Non-measured data used to define the LCA surface included insights gained from the following:

1. Gravity inversion data (Phelps et al., 1999)

2. Interpretive cross sections, maps of unit extents, and surface geology developed based on expert judgment generally derived from data compiled for the UGTA regional geologic model (IT, 1996)

The CADD/CAP (DOE/EMNV, 2017d) stated that this uncertainty would be addressed based on existing gravity inversion data (Phelps et al., 1999) and on proximity of detonation locations to

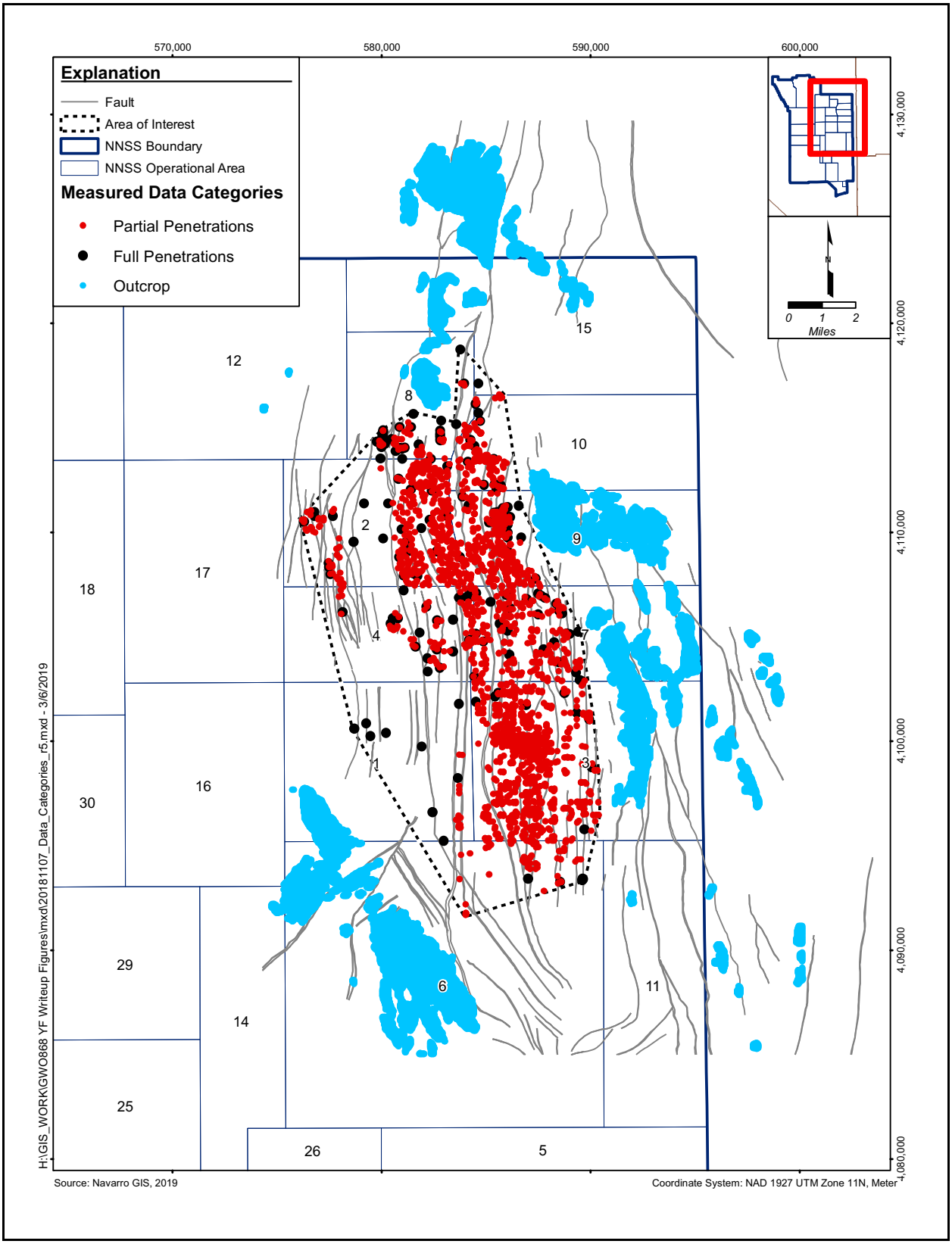

Figure 2-48
Measured Data Used for Estimating LCA/LCA3 Surface Uncertainty

control points provided by boreholes completed in the LCA. However, the gravity inversion data were judged to be insufficient for this purpose because (a) gravity inversion generated a single surface, thus not providing a statistical basis for evaluating LCA surface uncertainty; (b) gravity information was already taken into account in a qualitative manner when constructing the HFM; and (c) gravity inversion creates undulations in the surface in response to heterogeneities but not sharp changes representing faulting.

A statistical technique called "cross-validation" was identified as appropriate for use in estimating uncertainty in the top of the LCA. Hastie et al. (2008) state that cross-validation is "probably the simplest and most widely used method for estimating prediction error." Cross-validation involves predicting the location of the desired surface at each point after randomly or systematically removing one or more elements from a population. As described below, the cross-validation technique is used to explore the uncertainty in the LCA surface by systematically withholding a subset of data points (10 percent) from the interpolation process (i.e., the gridding algorithm used to create the LCA surface). This process is repeated a number of times (100), each time withholding a different subset of data (a different 10 percent), yielding 100 LCA surface realizations.

The cross-validation technique was applied by generating a 3-D LCA surface based on a subset of the available measured and/or nonmeasured data after removing a given percentage of the data. This surface was then compared to the surface obtained using the full dataset. The surfaces were created using the least tension method and incorporating faults from the HFM using EarthVision version 9.1 (Dynamic Graphics, 2015). Initial investigations incorporated retaining random samples of 10, 50, 90, and 100 percent of the measured and non-measured data. A lower RMS error, calculated by comparing against the surface generated using the full dataset, was observed when a larger portion of the measured data and a smaller portion of the nonmeasured data were used. Additional cross-validation iterations incorporated samples using measured datasets including partial penetrations and eliminated the use of the non-measured information. The partial penetration information was incorporated as "greater than" information whereby the depth to LCA must be "greater than" the total depth of the drill holes that do not penetrate the top of the LCA surface. The results of each set of iterations were assessed, leading to variations in methodology and the selected datasets. It was noted that due to the sparseness of the available drillhole LCA contact data, removal of any of this measured data created areas in the coverage with unrealistically high variability in the estimated surfaces.

The final method selected was to include all of the measured drillhole LCA contact data and outcrop data while randomly sampling 90 percent of measured partial penetration data within a given fault block, which were defined using faults represented in the HFM. Because of uncertainty in fault effects, only full and partial penetration data from within each fault block were used to characterize the uncertainty of the LCA surface within the same fault block. Using this approach, 100 random statistical samples were created, retaining 90 percent of the measured partial penetration data and leading to 100 realizations of the surface representing the top of the LCA. The model evaluation wells (ER-2-2, ER-3-3, ER-4-1) were included in these constructions as measured LCA contact data.

The 100 surfaces were queried at all detonation locations and statistical variations described for each location. At detonation locations coincident with a borehole that reaches the LCA (where the elevation of the LCA is known), the statistical values were replaced with the measured known value. Also, at partially penetrating emplacement hole locations, if the statistical surfaces were above the total depth of the partially penetrating emplacement hole, those statistical values were replaced with the measured known total depth of the partially penetrating emplacement hole.

Figure 2-49 shows the total surface variability of the 100 surfaces at each detonation location. The patterns indicate the significance of some fault blocks being well constrained (small values of total variability shown in dark blue) by measured data points while other fault blocks being not as well constrained (large values of total variability shown in purple, reds through yellows). Variability ranges from 0 to about 360 m, with the distribution of variability shown in Figure 2-50. Fifty-five percent of the detonation locations have less than 20 m of vertical variability represented in the 100 statistical surfaces. Fewer than 4 percent of the detonation locations have more than 200 m of variability.

2.8.1 Summary

In order to estimate the uncertainty in the top of the LCA (as defined in the YF/CM HFM [BN, 2006]), 100 LCA surfaces were generated using the least tension method within EarthVision (Dynamic Graphics, 2015) for interpolation of available drillhole (including the model evaluation wells), outcrop, and partial penetration data. Each surface was developed using all known LCA surface elevations from drillholes, and from outcrop data and 90 percent of the partial penetration data within a given fault block. The partial penetration data for each surface were randomly sampled, thus resulting in variability in the 100 surfaces. This method (cross-validation method), whereby

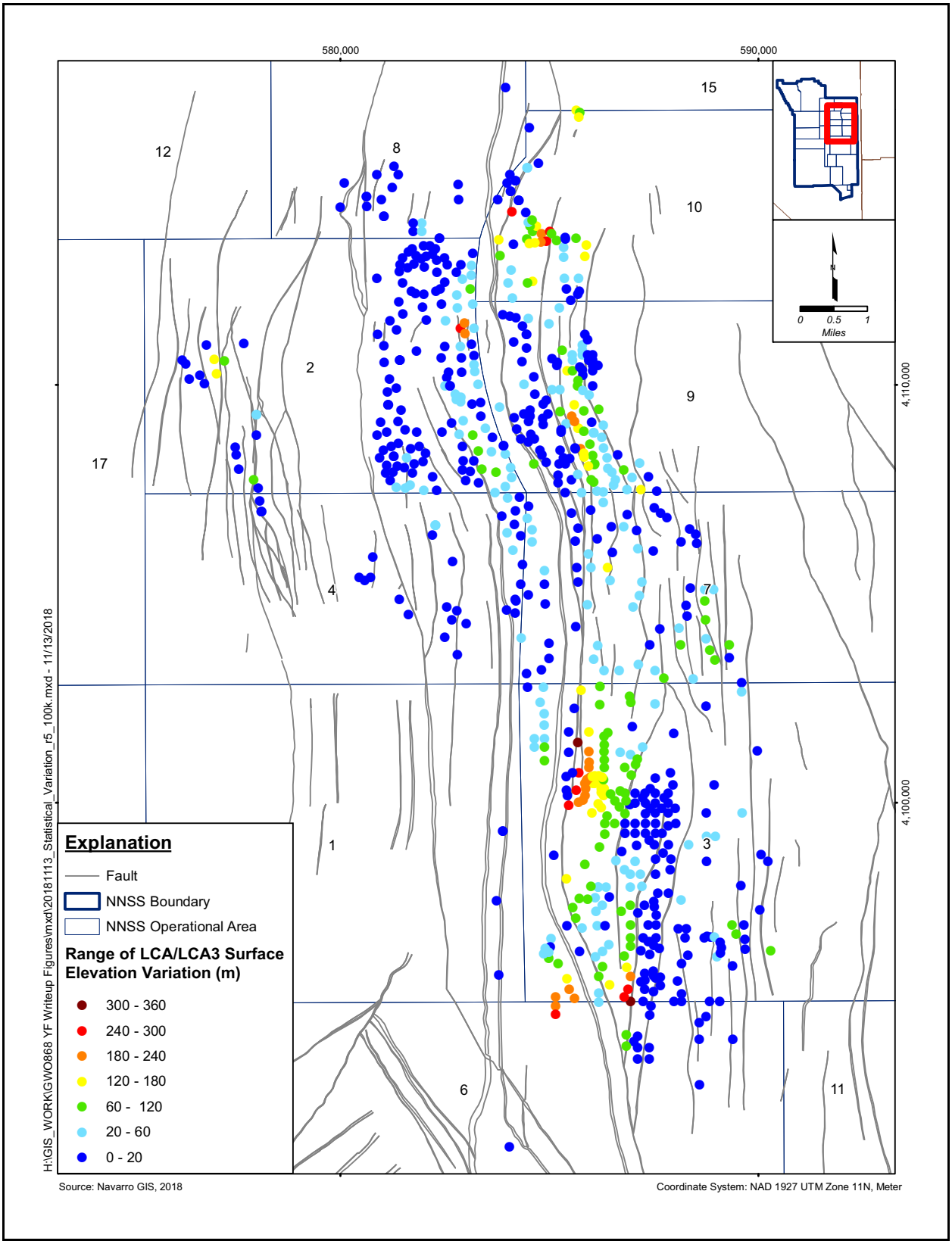

Figure 2-49
Total Surface Variability of 100 LCA/LCA3 Surfaces at Each Detonation Location

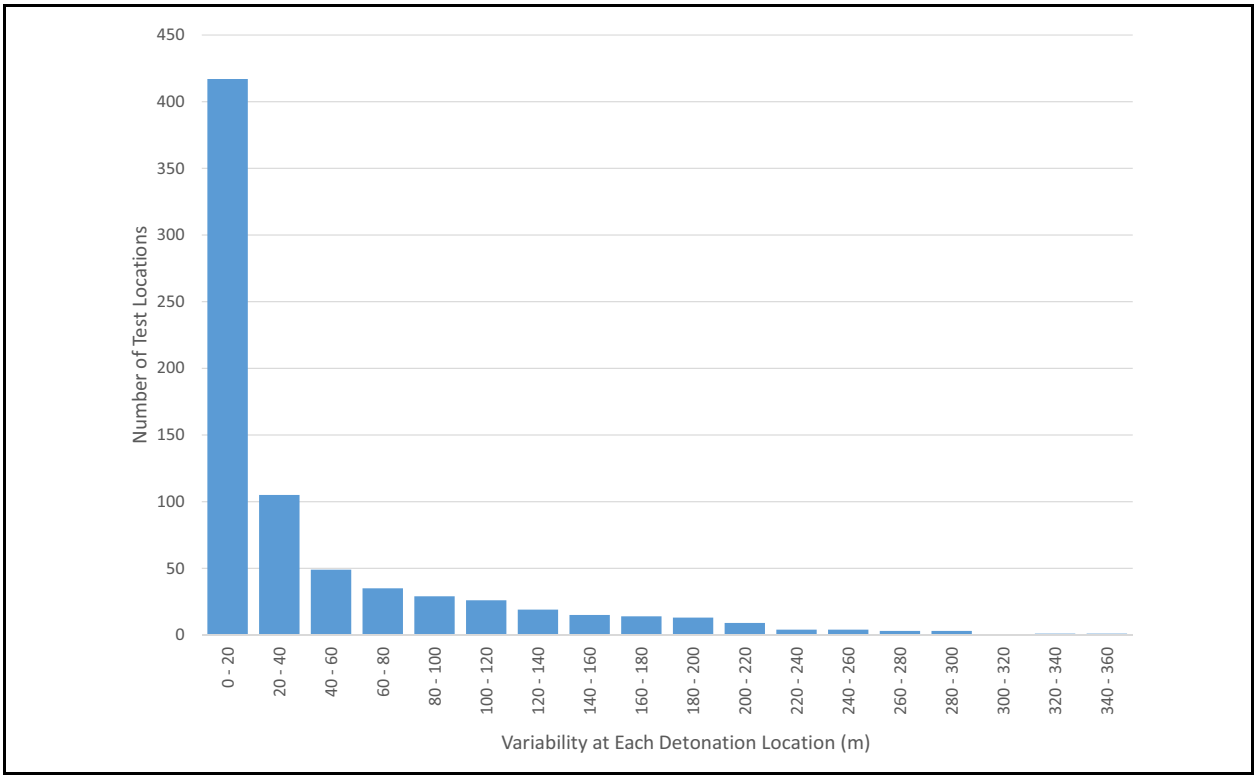

Figure 2-50
Histogram Showing Variability in Top of LCA/LCA3 at Each Detonation Location

locations of the surface are predicted after randomly or systematically removing a percentage of data from a population, is considered one of the simplest and most widely used method for estimating prediction error (Hastie et al., 2008). The variability over these surfaces at detonation locations ranges from 0 to about 360 m, with 50 percent of the detonation locations having less than 20 m of vertical variability. Fewer than 4 percent of the detonation locations have more than 200 m of variability.

2.9 Reviewing Historical Data for Detonations near or within the LCA

2.9.1 Exchange Volume Size and Shape

Historical literature from the weapons testing program was reviewed in attempt to reduce the uncertainty associated with the exchange volume size and shape. The exchange volume, as it pertains to the Yucca Flat flow and transport model, is the volume of rock that encompasses the immediate extent of radioactive contamination after an underground nuclear detonation. The exchange volume is conceptualized as a spherical region centered around the detonation, and its size is defined as a multiplier of the R_c. The R_c is either measured (Zavarin, 2014), in the case that the yield is specified in

NNSA/NFO (2015b); or estimated based on maximum announced yield and the equations in Pawloski (1999) or Boardman (1970) for detonations where the WPs are in carbonate rock.

Detonations that intersect the saturated LCA with a $3R_c$ exchange volume were represented in the base case and the majority of the alternative models (N-I, 2013). This resulted in a total of 39 detonations included in those flow and transport models. An alternative model, included in the N-I (2013) CB ensemble, assumed a $2R_c$ exchange volume radius; the number of detonations with exchange volumes that intersect the saturated LCA decreased to 12.

Factors that impact the size and shape of the exchange volume include the following:

- Phenomenology effects (cavity collapse, test heat, pressure, steam, gas/liquid, depth of burial)
- RN properties (gaseous precursors, volatility, glass partitioning)
- Proximity to saturated and unsaturated conditions
- Rock type (alluvium, tuff, carbonate, granitic)
- Heterogeneities (permeable layers, planes of weakness, fractures/faults)
- Carbon dioxide (CO_2), water (H_2O), and clay content in rock

Understanding the phenomenology of an underground detonation is therefore an important part of this activity.

2.9.1.1 Phenomenology

Four stages of the underground detonation and the associated impacts (Tompson et al., 2011) are summarized below:

- **Detonation.** Pressure force generates a compressive, radially expanding shock wave; and shock energy melts, heats, and physically alters surrounding rock.

- **Cavity formation.** Vaporization and compression of the geologic media (including water) will generate and expand an open, approximately spherical cavity volume centered at the WP. The shock wave and cavity expansion will serve to crush, fracture, compress, or otherwise alter intact rock that extends beyond the cavity wall; and high gas pressures will maintain an open cavity volume. Cavity gases are usually contained because of shock rebound stress, although there are some exceptions (i.e., prompt injection).

- **Cavity collapse and chimney formation.** Cavity gases condense, and the rock overlying the cavity collapses into the cavity and creates a rubblized column or chimney that may extend to the ground surface, where a crater is formed. Krypton-90 (^{90}Kr) and xenon-137 (^{137}Xe) decay to ^{90}Sr and ^{137}Cs. Additional RN redistribution occurs.

- **Final configuration.** Materials are physically altered. A melt-glass zone exists at the cavity bottom. Rubblized rock is found in the cavity to chimney, and altered rock surrounds the cavity wall. Groundwater returns, and residual high temperatures in the rock dissipate with time.

The following typical concepts define the altered zones resulting from the detonation (Figure 2-51):

- **Cavity.** Idealized sphere of radius $1R_c$ representing the maximum extent of the detonation cavity. The conceptualized cavity at HST time zero is composed of the melt-glass puddle that coalesces at the bottom and the in-fallen, rubblized chimney.

- **Melt glass.** A zone at the bottom of the cavity where vaporized and melted material accumulates due to gravity. For detonations in carbonate rock, the nature of the melt glass is uncertain but likely distinct from the typical melt glass produced by tests detonated in silicate rocks (Carle et al., 2008).

- **Chimney.** An idealized cylinder of rubble that falls into the collapsed cavity void, with a radius set to the R_c.

- **Crush zone.** A zone within $1.3R_c$ that is more intensely fractured or "pulverized" (Borg [1973] and Borg et al. [1976]). The material in this zone has failed mechanically and permanently lost porosity due to the compressional shock wave.

- **Altered matrix to $2R_c$.** Matrix permeability is assumed enhanced to $2R_c$ as a result of microfracturing (OTA, 1989).

- **Altered fractures to $3R_c$.** Fracture permeability and in situ rock porosity is enhanced between $1R_c$ and $3R_c$, and the fracture permeability is increased closer to the WP (Boardman and Skrove, 1966; OTA, 1989). The International Atomic Energy Agency (IAEA) (1998a) states that rock permeability is observed to increase significantly during drillback exercises between $2R_c$ and $2.5R_c$.

The exchange volume as discussed in Section 2.9.1 encompasses the cavity, crush, altered matrix, and altered fracture zones, and portion of the chimney contained within these zones (Figure 2-51).

Outside $3R_c$, the existing cracks are opened and strength is reduced, but only temporarily. The open cracks close immediately after the shock wave passes. Because the cracks close and no new cracks are formed the rock properties are not changed. Fracture systems surrounding cavities are influenced in large measure by preexisting heterogeneities such as bedding, jointing, and faults (Borg et al., 1976).

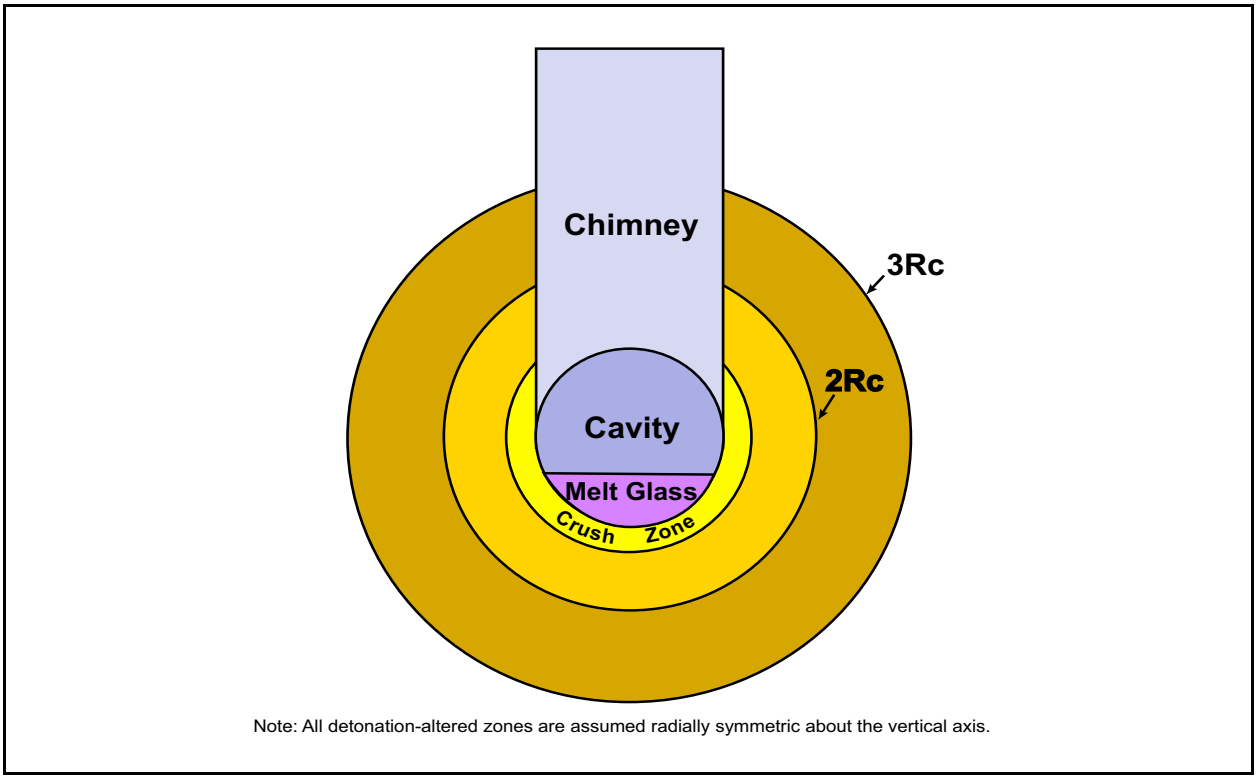

Figure 2-51
Schematic Diagram for Geometry of Detonation-Altered Zones
Source: Modified from Tompson et al., 2011

After an underground nuclear detonation, RNs generally partition into one or more melt glass, water, gas, or rubble phases distributed in and about the cavity and altered zones. Their physical partitioning and spatial distribution are governed by thermodynamic properties of the individual RNs or their precursors, detonation-related phenomenological effects, and other conditions in the rock media where the detonation took place. Specifically, melt glass, water, gas, and rubble fractions have the following characteristics:

- *Melt-glass* fractions typically include between 95 and 100 percent of the actinides and significant amounts of all other RNs (with the exception of ^{3}H, ^{14}C, and ^{85}Kr).
- *Water* fractions, initially, contain large fractions of the ^{3}H inventory and smaller amounts of ^{14}C, ^{36}Cl, ^{39}Ar, ^{85}Kr, and ^{129}I that show up in condensed steam.
- *Gas* fractions include significant fractions of noncondensable species such as ^{14}C, ^{39}Ar, and ^{85}Kr remaining after steam condensation.
- *Rubble* fractions include other condensable species that are segregated from the water fraction by sorption to mineral surfaces.

These concepts are discussed more thoroughly in IAEA (1998a, 1998b, 1998c); in the 2008 LLNL Yucca Flat HST reports (Carle et al., 2008; McNab, 2008; Pawloski et al., 2008; and Tompson et al., 2008); and in Rose et al. (2011) and Tompson et al. (2011).

2.9.1.2 Literature Review

The majority of the available literature regarding testing phenomenology and the resulting near-field contaminant extent was previously considered when developing HST models for UGTA Activity CAUs (e.g., Pawloski et al., 2001; Carle et al., 2007; Tompson et al., 2008; Carle et al., 2008; Tompson et al., 2011). The exchange volume represented in the HST models for the CHESHIRE detonation in Pahute Mesa (Pawloski et al., 2001) and CAMBRIC detonation in Frenchman Flat for Phase II (Carle et al., 2007) were about $1.5R_c$. At CAMBRIC, most contamination was within $1.5R_c$, and only low-level contamination was observed out to $3R_c$. Migration of ^{137}Cs and ^{3}H into the chimney was observed (Tompson et al., 1999; Carle et al., 2007); no ^{3}H was detected in groundwater below the CAMBRIC cavity (Hoffman et al., 1977).

While not a perfect surrogate for deep Yucca Flat detonations, a significant amount of information is available for the RAINIER detonation (post-test drilling and tunneling data). RN data from reentry shafts and holes help constrain the exchange volume extent to between $1.5R_c$ and $3R_c$ (Tompson et al., 2011). RNs with volatile precursors preferentially redistribute into high-permeability unsaturated layers and the chimney.

Gamma logs collected from post-shot drill holes are used to assess the distribution of RNs around a cavity and chimney (Borg et al., 1976). Although RNs such as ^{3}H and ^{90}Sr cannot be detected by gamma logs, the assumption is that the extent of these RNs coincides with the volatile gamma emitters such as ^{137}Cs. Gamma-log data from approximately 70 detonations in Yucca Flat were shown by Borg et al. (1976) to indicate an outer limit of RN extent (above the WP) on the order of $2R_c$ to $3.5R_c$ and a lower limit (below the WP) on the order of $1.3R_c$ to $2.3R_c$. These data also suggest that the exchange volume multipliers decrease with the size of the cavity.

Crow (1976) states that indirect evidence indicates that many cavities formed in the alluvium and tuff are aspherical. Because the confining pressure is least in a vertical upward direction, it is probable that the upper portion of the cavity is larger than the lower hemisphere.

Only limited data are available regarding the exchange volume shape. Although a spherical volume is represented by the HST model, asymmetry in the shape has been reported. Boardman et al. (1964) stated that fractures can be expected to extend about $2R_c$ to $3R_c$ laterally and to less than $1.5R_c$ below the cavity. These results were based on three detonations (GNOME, RAINIER, and HARDHAT) in rock salt, tuff, and granite, respectively (Boardman et al., 1964). RNs with volatile precursors preferentially redistribute into high-permeability unsaturated layers and chimney. One detonation in Rainier Mesa, LOGAN, was observed to have a "skull" shaped cavity with RNs distributed asymmetrically to $2.85R_c$ (Hu and Zavarin, 2007). Factors that might inhibit exchange volume extent below the WP include the following:

- Decreasing permeability with depth
- Anisotropy in permeability
- Increased mineral alteration (e.g., clay, zeolite) with depth
- Presence of clay layers
- Plugging of fractures along volcanic/carbonate interface
- Changes in lithologies, especially when harder, stronger rock occurs at depth

Post-shot drilling has not been consistently deep enough to quantify the extent to which these factors impact the exchange volume size and shape below the WP.

Nimz and Thompson (1992) summarized all known cases where RNs were detected outside the immediate vicinity of the nuclear detonation cavity at the NNSS. Eight of the 10 locations identified are in Yucca Flat. Yucca Flat detonations identified as the source of the RNs are as follows:

- AGILE
- AVENS-ANDORRE
- BILBY
- BOURBON
- COMMODORE
- LATIR
- NASH
- SANDREEF

Historical RN results for BILBY, BOURBON, and NASH are presented in Sections 2.3.4, 2.3.5, and 2.4.1, respectively. These detonations have associated near-field wells that have been historically sampled. High levels of ^{3}H (up to 3E+08 pCi/L) were detected in groundwater in the BILBY chimney and laterally in the nearby well (U-3cn-5) at distances of up to ~$3R_c$. The BOURBON cavity likely intercepts the saturated LCA. These results are not inconsistent with a $3R_c$ exchange volume. RNs,

attributed to groundwater migration, were measured in groundwater at UE-7nS located 137 m (2.6R_c) from the BOURBON WP. Similarly, RNs detected at UE-2ce are indicative of groundwater migration from the NASH detonation and not a maximum exchange volume radius.

The presence of ^{3}H in wells near the AGILE and COMMODORE detonations was thought to result from groundwater movement. Elevated ^{3}H (~10E+07 pCi/L), encountered in the U-3kz (ALEMAN) emplacement hole, was attributed to SANDREEF, which was detonated 340 m (5.6R_c) away about eight years earlier. In addition, ^{3}H activity (~3E+06 to 1E+07 pCi/L), also attributed to the SANDREEF detonation, was observed in UE-3e-4 (1990–1993) located approximately 4.5R_c from SANDREEF. The ^{3}H presence is thought to result from fracture injection and/or groundwater migration within a highly pressurized hydrologic zone at depth. RNs, observed in the UZ at two additional locations, UE-4g-2 (associated with LATIR) and U-9 ITS U-29 (associated with AVENS-ANDORRE), were attributed to prompt injection. It is not known whether the detections resulting from prompt injection represent a significant source term (Nimz and Thompson, 1992).

At INGOT, late-time gaseous transport, rather than prompt injection, is thought to be more likely responsible for migration and distribution of RNs outside the cavity (Smith et al., 1996). A post-shot hole was drilled 10 m from the INGOT cavity edge (U-2gg PSE 3A), and gamma activity (e.g., ^{137}Cs) was confined to the interval between 500 and 550 m (the INGOT WP slant depth is 526 m). No refractory RNs were detected (Smith et al., 1996). An appreciable enrichment of ^{137}Cs relative to ^{90}Sr was observed when compared to the inventory (Finnegan et al., 2016). The extreme ratio of ^{137}Cs/^{90}Sr for the INGOT samples relative to the RN inventory likely represents preferential decay of ^{90}Kr ($t_{1/2}$ = 32.3 seconds) relative to ^{137}Xe ($t_{1/2}$ = 229.2 seconds) during the time required for the gaseous phase to travel through the fracture before deposition.

Carle et al. (2008) provided a comprehensive review of the four detonations that had WPs within carbonate rock (BOURBON, HANDCAR, KANKAKEE, and NASH). The carbonate detonations decompose carbonate rock, release CO_2 gas, and disperse volatile RNs. The CO_2 release is thought to enlarge the exchange volume in the UZ to 5R_c for ^{14}C, ^{137}Cs, and ^{90}Sr.

Current exchange volume conceptualizations used in the Yucca Flat flow and transport model (N-I, 2013) are consistent with the collective physical and radiochemical observations made over decades. Use of maximum yield for detonations may be “conservative” with respect to delineation of initial spatial extent of contamination (maximum exchange volume). An exchange volume range of 1R_c to

$1.5R_c$ reflects a minimum exchange volume size, within which fractured, crushed, or compressed zones exist (depending on rock strength) and a range of $1.5R_c$ to $3R_c$, corresponds to the volume within which fractures are extended and connected by the detonation. The exchange volume size uncertainty (e.g., $1.5R_c$ to $3R_c$) effectively samples the maximum exchange volume for a yield range.

2.9.2 Literature Review of Matrix Sorption Data for Cs and Sr in the LCA

Sutton (2009) reviewed distribution coefficients (K_ds) for RNs, including ^{90}Sr and ^{137}Cs, for carbonate minerals. K_d is the ratio of the RN concentration adsorbed on the solid phase to that in the groundwater. Log K_d distributions for ^{90}Sr and ^{137}Cs on calcite, aragonite, limestone, and dolomite, based on data reported by Sutton (2009), are presented in Figure 2-52. Log K_d distributions are assumed to be normal, with means and standard deviations given in Sutton (2009, Table 2). K_ds reported in the literature are included regardless of particle size, solution composition, or pH. The ranges for K_d values reported by Sutton (2009) are 0.03 to 6.4 milliliters per gram (mL/g) for Sr and 0.03 to 2.4 mL/g for Cs. Yucca Flat specific data using synthetic LCA groundwater reported by Hu et al. (2008b) are shown in Figure 2-52 as black lines at an arbitrary probability of 0.05.

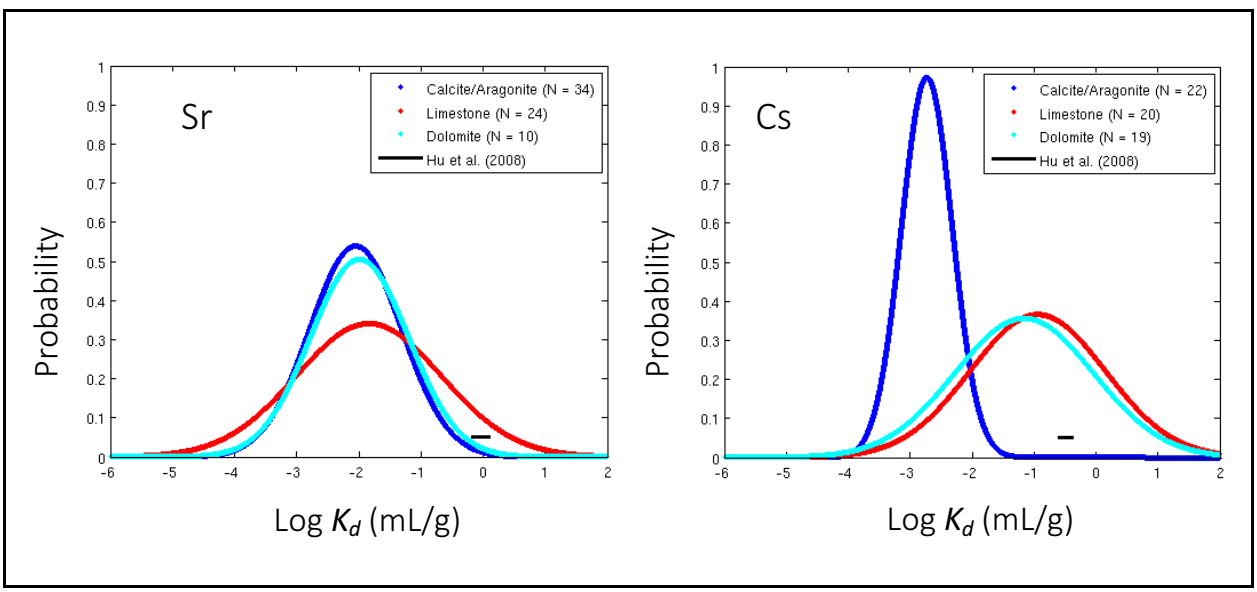

Figure 2-52
K_d Distributions for ^{90}Sr and ^{137}Cs in Carbonate Mineral

Studies performed using site-specific rock are presented in Borg et al. (1976), Hu et al. (2008b), and Zavarin et al. (2008). Borg et al. (1976) used LCA rock from Yucca Flat, although the

specific location is unknown, and simulated well water. The rock was crushed and sieved to >4,000-micrometer (µm) size. The Sr K_d was reported as 0.19 mL/g, and the Cs K_d was reported as 13.5 mL/g. Hu et al. (2008b) measured K_ds for Cs and Sr in LCA rock from ER-6-1 (833 m bgs) and synthetic LCA water. The LCA rock was crushed and sieved to a 75- to 500-µm size range. Sr K_ds ranged from 0.5 to 1.4 mL/g, and Cs K_ds ranged from 0.2 to 0.7 mL/g. Zavarin et al. (2008) also used LCA rock from ER-6-1 (833 m bgs) and synthetic LCA water. Several different particle sizes were evaluated (<75 µm, 75 to 500 µm, and 50 to 2,000 µm). The Sr K_d was 500 mL/g and the Cs K_d was 0.25 mL/g. The Sr K_d was significantly larger than other values reported for carbonate rocks, including the results of Hu et al. (2008b). Zavarin et al. (2008) noted that the recrystallization effects (Zavarin et al., 2005b) may have impacted their measured Sr K_d. Sr^{2+} can substitute for Ca^{2+} in calcite as a result of calcite recrystallization. The impact of recrystallization on Cs K_ds is likely to be lower due to the unfavorable substitution of Cs^{+} for Ca^{2+} in calcite. The K_d values reported in Hu et al. (2008b) are therefore considered more representative than those of Zavarin et al. (2008). Retardation from aluminosilicate fracture linings is not included in these analyses and may increase retardation. A comparison of Cs and Sr breakthrough from fractured cores using both natural fractures and induced fractures showed evidence of sorption in the natural fractures, pointing to fracture-lining minerals in the natural fracture as the likely sorption surface (Zavarin et al., 2007).

Estimates of native LCA rock surface areas (Zavarin et al., 2005a) suggest that the measured K_d are 2 or more orders of magnitude higher than what would be observed in the field. Sample crushing increases the rock's surface area, and therefore the potential for Sr and Cs sorption. André et al. (2009) found that crushed granite surface area is 8 to 70 times greater than the native rock. The native LCA rock surface area is estimated to be approximately 10 times lower than the 75- to 500-µm crushed rock fraction. The surface area reduction of the native rock would lead to K_ds that are also reduced by 1 order of magnitude relative to experimental conditions.

The site-specific values of Hu et al. (2008b), after applying the reduction factor to account for lower surface area of native rock relative to crushed rock, are considered the most representative K_ds for Sr and Cs in LCA rock in Yucca Flat. These values are also relatively consistent with K_ds reported in the literature (Figure 2-52). It is therefore recommended that the following triangular distribution is used to represent LCA K_ds:

- **Sr:** 0.05 (minimum), 0.095 (mode), and 0.14 (maximum) mL/g
- **Cs:** 0.02 (minimum), 0.045 (mode), and 0.07 (maximum) mL/g

These values are quite low and will likely lead to minimal impact on RN transport.

2.9.3 Near-field ^{90}Sr and ^{137}Cs

The ^{90}Sr and ^{137}Cs activities relative to ^{3}H in UE-2ce groundwater were previously shown to be 3 orders of magnitude lower than expected based on the Finnegan (2016) inventory (Section 2.4). Given the low K_ds for these RNs in the LCA (Section 2.9.2), additional processes impacting the ^{90}Sr and ^{137}Cs activities in the near-field environment are necessary to result in this large reduction in ^{90}Sr and ^{137}Cs concentrations in the carbonate environment. The ^{90}Sr and ^{137}Cs activities in other near-field environments, within the NNSS, will therefore be compared to those at UE-2ce.

The wells included in the evaluation along with information regarding their proximity to the detonation, detonation details, and well information are presented in Table 2-14. As shown in Table 2-14, several wells sample the cavity chimney environment. Several detonations have more than one sampling well, providing data at different depth intervals relative to the detonation WP. Many were drilled at a slant to access the cavity from outside the collapse crater. While a few near-field wells access the LCA or LCA3 (UE-2ce, UE-7nS, U-3cn-5), the majority access the overlying volcanic or alluvial units (Table 2-14).

There have been significant differences in sampling and analytical protocols over the years. Samples collected using downhole submersible pumps are more likely to be representative of the bulk fluid composition in the near-field environment. Several of the wells, particularly those that have been converted from post-shot reentry holes, consist of a small-diameter (7.3-centimeter [cm]), carbon-steel piezometer tube. In most cases, these wells have been sampled using only wireline bailers. Given that the standing fluid in these piezometers does not circulate freely with the sampled formation and that thorough purging could not be accomplished, samples collected from these wells tend to be of lower quality than those from pumped wells. Importantly, the presence of particulate material (colloids and larger particles) will typically result in higher than expected ^{90}Sr and ^{137}Cs concentrations in groundwater, particularly in argillic and zeolitized rock. This is due to the high affinity of these RNs to clay and zeolite minerals. High particle concentrations in sampled water may result from incomplete well development and/or particle resuspension during pumping. Thus, the ^{90}Sr and ^{137}Cs results must be examined in the context of other sample-specific and well-specific groundwater parameters.

Table 2-14
Wells Sampling Vicinity of an Underground Nuclear Detonation

Detonation	Date [a]	HSU [b]	Yield Range (kt) [a]	Well	HSU [b]	Sampling Location with Respect to Detonation Cavity, Chimney, or WP [c]
Yucca Flat/Climax Mine						
ALEMAN	09/11/1986	TMLVTA	<20	UE-3e-4	LTCU (p1,p2) TMLVTA (p3)	58 m north
BASEBALL	01/15/1981	LTCU	20-150	U-7ba PS 1AS	LTCU	Cavity/Chimney region
BILBY	09/13/1963	OSBCU	249	U-3cn-5	LCA	129 m southeast
				U-3cn PS 2	OSBCU	Cavity/Chimney region
BOURBON	01/20/1967	LCA	20-200	UE-7nS	LCA	137 m southeast
DALHART	10/13/1988	LTCU	<150	U-4u PS 2A	LTCU	Chimney region
GASCON	11/14/1986	LTCU	20-150	U-4t PS 3A	LTCU	~54 m from cavity wall
				UE-4t 1	LTCU	~170 m south
INGOT	03/09/1989	TMWTA	20-150	U-2gg PSE 3A	TMLVTA	65 m beneath cavity
NASH	01/19/1967	LCA3	39	UE-2ce	LCA3	183 m from WP
Western and Central Pahute Mesa						
ALMENDRO	06/06/1973	BFCU	200-1,000	U-19v PS 1D	BFCU	Cavity/Chimney region
BENHAM	12/19/1968	CHZCM	1,500	ER-20-5-1	TSA, CHZCM	280 m southwest
				ER-20-5-3	CHLFA5, CHZCM	
BULLION	06/13/1990	CHZCM	20-150	ER-20-6-1	CHLFA3, CHZCM	166 m southwest
				ER-20-6-2	CHLFA3, CHZCM	207 m southwest
				ER-20-6-3	CHLFA3, CHZCM	296 m southwest
CAMEMBERT	06/26/1975	BFCU	200-1,000	U-19q PS 1d	BFCU	Chimney region
CHANCELLOR	09/01/1983	PLFA	143	U-19ad PS 1A	PLFA, CHVTA	Cavity
CHESHIRE	02/14/1976	CHLFA4	200-500	U-20n PS 1DD-H	CHLFA4	Cavity
				UE-20n 1	CHLFA4	~300 m from cavity
Frenchman Flat						
CAMBRIC	05/14/1965	AA	0.75	RNM-1	AA	Cavity
				RNM-2S	AA	91 m from cavity

[a] NNSA/NFO, 2015b
[b] N-I, 2013; NNSA/NFO, 2014; DOE/EMNV, 2018; Navarro, 2019b
[c] Hu et al., 2008a

BFCU = Bullfrog confining unit
CHLFA = Calico Hills lava-flow aquifer
CHLFA3 = Calico Hills lava-flow aquifer 3
CHLFA4 = Calico Hills lava-flow aquifer 4
CHLFA5 = Calico Hills lava-flow aquifer 5
CHVTA = Calico Hills vitric-tuff aquifer
CHZCM = Calico Hills zeolitic composite unit
PLFA = Paintbrush lava-flow aquifer
TSA = Topopah Spring aquifer

Table 2-15
Near-field ^{3}H, ^{90}Sr, and ^{137}Cs Concentrations (pCi/L)
(Page 1 of 2)

Well	Sampling Period	Sampling Method	^{3}H			^{90}Sr			^{137}Cs		
			Min.	Max.	n [a]	Min.	Max.	n [a]	Min.	Max.	n [a]
Yucca Flat/Climax Mine											
UE-3e-4	1990–2009	Pump/Pressure Tube	2.2E+03	1.0E+07	73 (70)	--	--	0	<0.28	<0.47	2
U-7ba PS 1AS	1995	Bailer	5.5E+06	4.3E+07	5 (5)	--	--	0	65	1.3E+05	5 (4)
U-3cn-5	1965–2017	Pump	<6.5	9.5E+07	121 (4) [b]	4.6E-04	5.9E-01	4	<0.001	<101	7
U-3cn PS 2	1964–2007	Pump	2.2E+06	2.7E+08	69 (69)	0.06	2.4	5	0.8	U 10.6	15
UE-7nS	1977–2015	Pump/Bailer	13.4	4.6E+03	132	<0.14	<1.1	6	0.04	<7.6	17
U-4u PS 2A	1992–2008	Bailer before 1997 Pump after 1997	1.5E+07	5.8E+07	26 (26)	3.1	3.1	1	2.0	603	8 (1)
U-4t PS 3A	1993–2008	Bailer	6.0E+02	6.7E+04	6 (2)	--	--	0	<0.34	<0.34	1
UE-4t 1	1990–2008	Pressure Tube	<8.4	1.7E+03	9	--	--	0	--	--	0
U-2gg PSE 3A	1994–2015	Bailer	3.5E+03	7.5E+03	5	--	--	0	0.90	2.7	2
UE-2ce	1977–2016	Pump	1.6E+04	6.5E+07	434 (428)	0.08	2.3	14	<0.005	<6.8	22
Western and Central Pahute Mesa											
U-19ad PS 1A	2004–2008	Pump	1.1E+07	2.2E+07	10 (10)	1.8E+03	1.8E+03	2 (2)	1.2E+04	2.9E+04	6 (6)
U-19v PS 1D	1965–2009	Bailer	2.0E+05	2.4E+08	32 (32)	--	--	0	<0.25	2.7	5
U-19q PS1d	1998–2003	Pump	1.1E+07	2.4E+07	10 (10)	<0.75	<0.75	1	7.9	12	3
U-20n PS 1DD-H	1976–2005	Pump	2.7E+07	1.9E+09	80 (80)	0.8	266	9 (7)	0.1	3.8E+03	39 (22)
UE-20n 1	1987–2012	Pump	3.8E+05	3.6E+08	103 (103)	--	--	0	0.003	3.2	18
ER-20-5-1	1996–2015	Pump	2.5E+07	7.2E+07	22 (22)	<0.55	UJ 1.4	4	<6.7	16.3	11
ER-20-5-3	1996–2015	Pump	6.5E+04	2.9E+05	31 (31)	<0.46	4.3	5	0.05	U 13.9	11
ER-20-6-1	1996–2017	Pump	<270	1.7E+06	12 (4)	2.2	2.2	1	1.4	39.8	5
ER-20-6-2	1996–2017	Pump	U 340	9.4E+05	10 (6)	<0.57	<0.57	1	1.4	13.2	3
ER-20-6-3	1996–2017	Pump	<183	4.0E+03	9	4.2	4.2	1	<8.1	UJ 16.2	3

Table 2-15
Near-field ^{3}H, ^{90}Sr, and ^{137}Cs Concentrations (pCi/L)
(Page 2 of 2)

Well	Sampling Period	Sampling Method	^{3}H			^{90}Sr			^{137}Cs		
			Min.	Max.	n [a]	Min.	Max.	n [a]	Min.	Max.	n [a]
Frenchman Flat											
RNM-1	1974–2014	Pump	1.1E+02	5.3E+09	114 (13)	1.77	4E+03	19 (15)	0.62	1.5E+03	32 (4)
RNM-2S	1975–2019	Pump	2.2E+01	3.0E+06	1,015 (770)	0.02	2.6	7	0.001	<6.6	15

[a] Value in parenthesis is the number of samples that exceeded the MCL.
[a] See Section 2.3.4 for a discussion of the elevated ^{3}H results.

U = Compound was analyzed for, but was not detected ("Non-detect").
UJ = Compound was non-detect, but result is biased low.

Table 2-15 presents the ^{3}H, ^{90}Sr and ^{137}Cs activities reported for samples collected from these locations. The RNs historically analyzed in a particular sampling event were dependent on the sampling objectives. While ^{3}H was usually included in the analysis, other RNs such as ^{90}Sr and ^{137}Cs were only inconsistently analyzed. In fact, no ^{90}Sr data are available for several wells, and no ^{137}Cs data are available for one well (Table 2-15). Table 2-15 identifies the minimum and maximum ^{3}H, ^{90}Sr and ^{137}Cs activities, number of samples (n), and time period sampled. The number of samples that exceeded the MCL is also presented. While the majority of the samples exceeded the ^{3}H MCL, the ^{90}Sr and ^{137}Cs exceedances were primarily limited to a few locations that access the detonation cavity and chimney (RNM-1, U-19ad PS 1A, U-7ba PS 1AS, and U-20n PS 1DD-H). In some cases, these high activities were likely an artifact of the poor water quality, as described in the following text. Reduced ^{90}Sr and ^{137}Cs activities relative to ^{3}H in the detonation cavity primarily results from their partitioning into the melt glass and sorption onto rock.

Some samples from the RNM-1 cavity and chimney had elevated ^{90}Sr and ^{137}Cs activities. In fact, the maximum ^{90}Sr concentration was greater than samples collected from other near-field wells (Table 2-15). The ^{137}Cs activity in one sample from the RNM-1 cavity (1.5E+03 pCi/L) and one from the chimney (360 pCi/L) exceeded the MCL (200 pCi/L). The ^{137}Cs activity for subsequent samples were below the MCL. The maximum ^{3}H activity in these samples was 3.7E+09 pCi/L (5 orders of magnitude above the MCL).

The high ^{90}Sr and ^{137}Cs concentrations observed at U-19ad PS 1A are unique (Table 2-15). This well was thoroughly developed, and sampling was conducted using a submersible pump. RN concentrations are some of the highest measured at the NNSS (Zavarin, 2010b; Navarro, 2019a). Colloid concentrations in these samples were reported to be 4E+10 particles per milliliter (mL) (Abdel-Fattah et al., 2005), which is equivalent to 30 mg/L. These colloid concentrations are higher than average which may, in part, explain the unusually high ^{90}Sr and ^{137}Cs concentrations observed at this location.

Samples collected from U-7ba PS 1AS were bailed from an undeveloped post-shot hole. The particulate concentrations ranged from 53,000 to 110,000 mg/L (Thompson et al., 1995). Degueldre et al. (1996) suggested that colloid loads in deep, low ionic strength groundwater from crystalline rock will likely not exceed 0.1 mg/L under ambient hydrogeochemical conditions and may only reach 10 mg/L during transient hydrothermal or tectonic events. The median colloid concentrations in

NNSS groundwater from recent sampling (0.5 mg/L) is consistent with the low values proposed by Degueldre et al. (1996). Based on the median colloid concentration reported for NNSS groundwater, colloid concentrations in groundwater transported downgradient from the nuclear detonation cavities is anticipated to be at least 4 to 5 orders of magnitude lower than the colloid concentrations measured in these samples. This will also reduce the ^{90}Sr and ^{137}Cs concentrations to below their MCLs.

While all U-4u PS 2A samples exceeded the ^{3}H MCL, only a single sample exceeded the ^{137}Cs MCL. The ^{137}Cs MCL exceedance was observed in a bailed sample collected in 1993 that was reported to be a thick brown sludge with black particles (Thompson et al., 1995). The sample was centrifuged to separate the bulk of the suspended material; the supernate was then filtered through 45-nanometer-pore-size filters before the liquid scintillation counting. The ^{3}H content was similar to that in 1992. Grab samples (~150 mL total) were combined with the pressure tube sample (~2,100 mL), and then dried and counted for ^{137}Cs (Thompson et al., 1995). The high ^{137}Cs observed in these samples is likely associated with the particulates and is not representative of the groundwater in this environment. No ^{137}Cs MCL exceedances were observed in subsequent samples collected with a pump; ^{90}Sr was not analyzed in the pumped samples.

The ^{90}Sr and ^{137}Cs concentrations at U-20n PS 1DD-H are approximately 1 order of magnitude lower than at U-19ad PS 1A, which correlates with the lower colloid concentrations observed at this site (Abdel-Fattah et al., 2005). At U-20n PS 1DD-H, approximately 2E+09 particles per mL were reported, which is equivalent to 4 -mg/L colloid concentration. This colloid concentration is higher than median colloid concentrations at the NNSS (0.5 mg/L).

Figure 2-53 presents the probability of ^{3}H, ^{90}Sr, and ^{137}Cs initial activities relative to their MCLs in the cavity for the 39 detonations included in the N-I (2013) model. The probabilities were estimated using the screening approach described in N-I (2013, Appendix C). The screening approach estimates cavity concentrations based on sampled distributions of HSU specific K_ds and melt-glass partitioning factors. The K_d for the HSU associated with WP depth was selected for each detonation. Of the 39 detonations, 3 took place in the LCA/LCA3 and the remaining took place in an overlying volcanic unit. The ^{90}Sr and ^{137}Cs activities are significantly greater in the cavities located in the LCA when compared to tuffaceous units (Figure 2-53) as expected based on the significantly lower K_d and melt-glass partitioning in carbonate rocks.

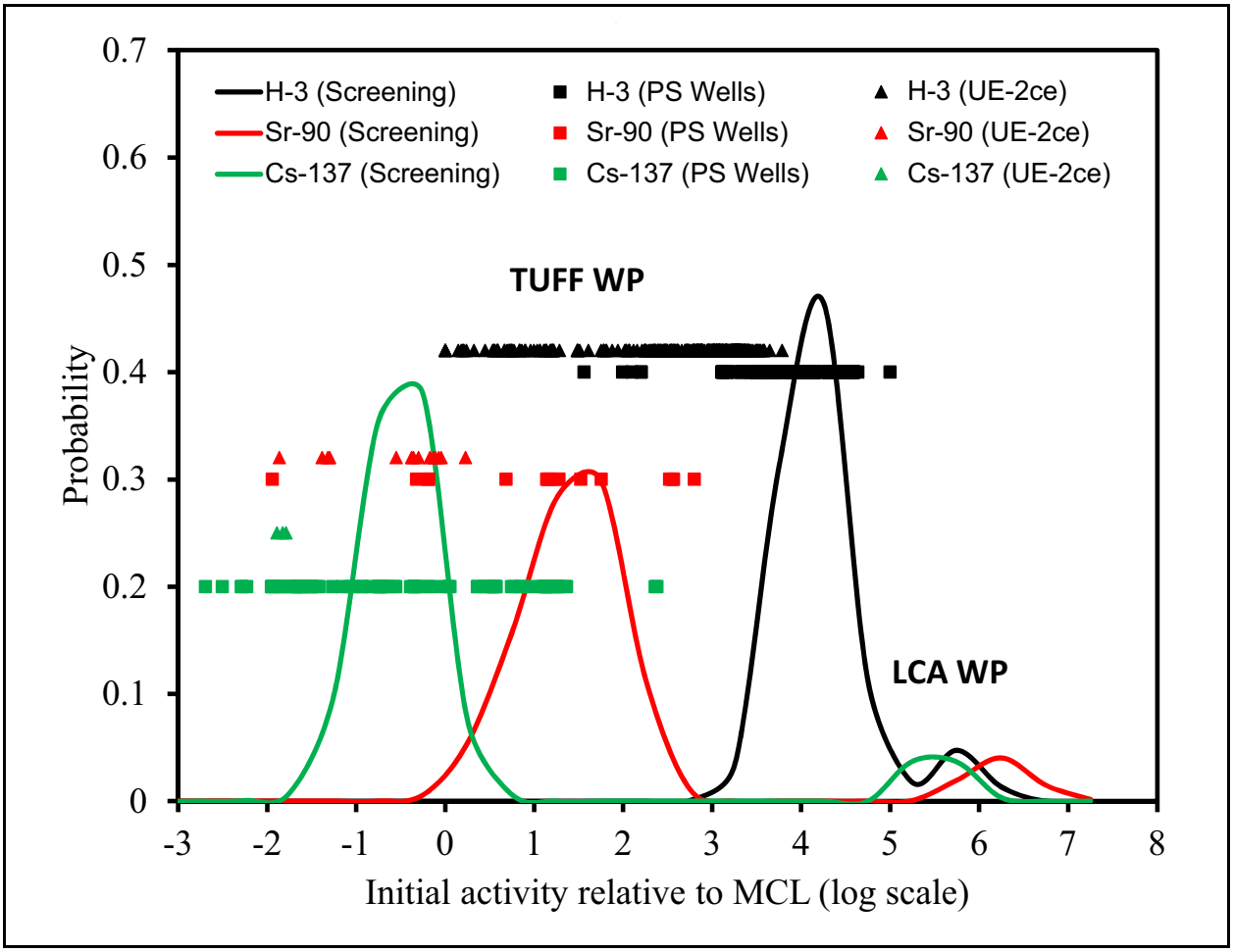

Figure 2-53
Initial ^{3}H, ^{90}Sr, ^{137}Cs Activities Relative to MCL

Figure 2-53 also presents the decay corrected ^{3}H, ^{90}Sr, and ^{137}Cs activities relative to their MCL for the post-shot (PS) well samples with detectable ^{90}Sr and ^{137}Cs, including Well UE-2ce samples (Table 2-15). These values were decay corrected to the detonation date. As previously mentioned, most samples collected away from the cavity chimney environment do not have detectable ^{90}Sr and ^{137}Cs. Figure 2-53 shows that the cavity and chimney sample concentrations are generally consistent with distributions of screening results for detonations with WPs in tuffs, and not for those in the LCA/LCA3. The ^{90}Sr and ^{137}Cs activities for UE-2ce samples are clearly shown to be greatly reduced when compared to those anticipated for carbonate rocks based on the screening approach. In some cases, elevated ^{137}Cs was observed (Figure 2-53). These elevated activities were primarily attributed to the high particulate concentrations observed in samples from these locations as previously described.

Table 2-16
Wells Drilled to the Saturated LCA

Detonation Name	Hole Name	Depth (m)			
		WP [a]	Total [b]	Saturated LCA [a]	Cement [b]
FOREST	U-7a	387	823	813	760
MIZZEN	U-7ah	637	978	863	663
SANDREEF	U-7aq	701	1,103	1,082	742
STRAKE	U-7ae	518	870	817	689
TAJIQUE	U-7aa	332	587	571	579 [c]
TOPGALLANT	U-4e	713	1,022	999	729

[a] N-I (2013)
[b] Zavarin (2019)
[c] Well was cased to a depth of 580 m, and the annulus and bottom of the hole (within the casing) were filled with cement.

2.9.4 Wells Drilled to the Saturated LCA

While investigating the LCA surface elevations (Section 2.8), six emplacement holes were identified that were drilled into the saturated LCA (Table 2-16). Although the WPs for these emplacement holes are well above the saturated LCA, the total depths for the wells were found to be much deeper (Table 2-16). These holes were therefore investigated to ensure that they did not provide a direct pathway from the nuclear detonation to the LCA.

Hole histories, summarized in Zavarin (2019), were examined to determine whether cement was used to plug the holes before the detonation of the nuclear device. With the exception of the TAJIQUE detonation, cement was filled to a depth above the saturated LCA (Table 2-16). The cement plug for the TAJIQUE detonation was approximately 8 m below the saturated LCA depth. This emplacement hole was cased to 580 m and the annulus filled with cement, thus sealing the hole from access to the saturated LCA. In addition, 240 m of coarse backfill was added above the cement at U-7aa (Zavarin, 2019). The hole histories therefore provided sufficient evidence that the holes were filled with cement before detonation and/or plugged to a depth above the casing (annulus filled with cement), thus eliminating direct access to the LCA.

2.9.5 Containment Scientist Interviews

Containment scientists at LANL (Kwicklis and Birdsell, 2016) and LLNL (Zavarin, 2017) were interviewed to help address the *Exchange volume size/shape that extends into the LCA* model evaluation target. Understanding the steps taken to ensure isolation of detonations from the LCA was thought to provide insight regarding the detonations identified to have exchange volumes that potentially intersect the saturated LCA. This section summarizes the information gained by these interviews.

In the early years of the underground nuclear testing programs, concerns over WP proximity to carbonate rock were limited in scope. Characterization practices were improved after the BANEBERRY detonation (December 18, 1970). Radioactivity released as a result of the BANEBERRY detonation resulted in exposure to personnel, which prompted action to strengthen technical and administrative procedures to substantially reduce the probability of a similar future occurrence. These actions included more extensive geologic and geophysical investigations and a more vigorous analytical program to better understand the behavior of nuclear detonations in the various environments. After BANEBERRY, the practice was to avoid the LCA due to generation of large amounts of noncondensable gases (CO_2) that could compromise containment and avoid shock-wave reflection that could disrupt the "containment cage."

Where possible, containment scientists generally sought to place the device so the WP was at least $3R_c$ from the LCA surface estimated from the USGS gravity map, plus 100-m uncertainty. In certain areas, such as Area 10, these criteria could not be met.

The containment scientists recognized clay-rich paleocolluvium (ATCU) as indicator of proximity of LCA, though ATCU varied considerably in thickness (a few feet to hundreds of feet). Two-dimensional (2-D) hydrodynamic calculations performed by LLNL indicated that cavity growth downward would be inhibited by the presence of a hard surface such as the LCA. LLNL calculations also indicated that LCA could fracture, although LANL calculations indicated little LCA fracturing. LANL scientists noted that where nonwelded tuffs were underlain by welded tuffs, cavity dimensions indicated by post-shot drilling would be asymmetrical (R_c smaller in welded tuffs). The Yucca fault was not considered an issue by LANL; smaller faults were more a concern.

2.9.6 Summary

Historical data were evaluated to address the following model evaluation targets

- *Exchange volume size/shape that extends into the LCA*
- *^{90}Sr mobility in the LCA*
- *^{137}Cs mobility in the LCA*

Available literature regarding testing phenomenology and near-field contaminant extent were reevaluated in attempt to reduce the uncertainty associated with the R_c multiplier used to estimate the exchange volume size. Most of these data had been previously considered when developing HST models for UGTA Activity CAUs. Limited data suggest that the exchange volume radius may be less below the cavity when compared to the lateral extent (Borg et al., 1976; Boardman et al., 1964; Crow, 1976).

The concentrations of ^{3}H, ^{90}Sr, and ^{137}Cs in wells in the vicinity of an underground nuclear detonation were evaluated. It was shown that, in general, the ^{90}Sr and ^{137}Cs concentrations in wells sampling the cavity and chimney in volcanic rock and alluvium are consistent with the initial activities estimated using the screening approach described in N-I (2013, Section C.4.0). The ^{90}Sr and ^{137}Cs activities for UE-2ce samples are greatly reduced when compared to those anticipated for carbonate rocks based on the screening approach.

Values for ^{90}Sr and ^{137}Cs K_ds for carbonate minerals were evaluated. Site-specific values, after applying a reduction factor to account for lower surface area of native rock relative to crushed rock, are considered the most representative.

Hole histories were examined for six emplacement holes that were drilled into the saturated LCA. The holes were filled with cement before detonation and/or plugged to a depth above the casing (annulus filled with cement), thus eliminating direct access to the LCA.

Containment scientists were interviewed regarding the placement of detonations near the LCA and the steps they took to evaluate the potential for contamination of the LCA. Where possible, containment scientists generally sought to place the device so the WP was at least $3R_c$ from the LCA surface estimated from the USGS gravity map, plus 100-m uncertainty. The location of faults was also a consideration when placing the device.

3.0 MODEL EVALUATION TARGETS AND RESULTS

The CADD/CAP (DOE/EMNV, 2017d) identified eight model evaluation targets associated with key model uncertainties that potentially impact the forecasted extent of contaminant transport within the YF/CM CAU (Table 1-1). Data collection/data analysis activities performed to address these targets are described in Section 2.0. This section applies results of these activities to address the model evaluation targets. In some cases, additional data analysis was required to address a given target. For these cases, the supplementary analyses are also presented in this section. A summary of the model evaluation targets and their resolutions is also provided.

3.1 Basin Flux through Testing Area

The YF/CM LCA is an advection-dominated system where the fluid flux exerts a primary influence on the contaminant transport times and distances. Thus, the uncertainty in basin flux estimates strongly controls the uncertainty in the CB estimates. This was recognized in the CADD/CAP (DOE/EMNV, 2017d). Historical estimates of the basin flux through the LCA in Yucca Flat cover a wide range of values (e.g., 40 acre-ft/yr given in Winograd and Thordarson [1975], 7,500 acre-ft/yr in N-I [2013] to 10,000 acre-ft/yr given by SNJV [2007]). An informal reanalysis of the ER-6-1-2 MWAT had resulted in significantly lower flux values (Halford, 2009, 2012, and 2016). Hence, as discussed in Section 2.6.2, a formalized reanalysis of the ER-6-1-2 was conducted by calibrating two models: DV3-ER612 and DV3-SS. The most probable estimate resulting from this reanalysis of groundwater flow moving past underground nuclear testing areas in Yucca Flat sub-basin is less than 600 acre-ft/yr (~23 kg/s) (Figure 2-20). A value of 512 acre-ft/yr (20 kg/s) is used as a target for calibrating the Yucca Flat LCA flow model, as discussed in Section 4.2.4. Areas contributing groundwater flow to Yucca Flat extend from Rainier Mesa to the west, the Halfpint Range to the east, and north of Quartzite Ridge. Uncertainty analysis conducted on a version of the DV3 model using the NSMC and the Pareto front methods is presented in Section 2.6.3. This analysis led to an estimate of a factor of 2 uncertainty in the flux through the LCA in Yucca Flat.

3.1.1 Conclusions

A value of 20 kg/s for the basin flux through the testing area in the eastern Yucca Flat was selected for use as a calibration target in the revised LCA model. The flux value was estimated to have a factor of 2 uncertainty.

3.2 Exchange Volume Size and Shape That Extends into the Saturated LCA

CBs described in N-I (2013) are dominated by deeply buried detonations in the northern half of the basin with exchange volumes assumed to intersect the saturated LCA at $2R_c$ (12 detonations) or $3R_c$ (39 detonations). The uncertainty in the number and location of detonations where the exchange volume intersects the saturated LCA depends both on the size of the exchange volume and the modeled surface elevation of the LCA at each detonation location. The exchange volume size and shape were evaluated by several data collection activities (Sections 2.1, 2.2, 2.3, and 2.9). Investigation of LCA surface elevations is described in Section 2.8.

3.2.1 Exchange Volume Size and Shape

The size and shape of the exchange volume were evaluated by four model evaluation activities: sampling LCA completions for RNs (Section 2.1); drilling evidence from ER-2-2, ER-3-3, and ER-4-1 (Section 2.2); sampling near-field wells (Section 2.3); and review of historical data for detonations near or within the LCA (Section 2.9). The primary goal of these activities was to determine whether sufficient evidence exists to support reducing the exchange volume extent below the detonation cavity to less than $3R_c$. While limited studies indicated that the exchange volume radius is smaller below the cavity (Boardman et al., 1964; Borg et al., 1976; Crow, 1976), this is based on too few data to provide a sound basis for revising the current conceptualization that the exchange volume is a spherical region centered around the detonation. The evidence provided by the new well and historical data evaluations indicates that the exchange volume size uncertainty (e.g., $1.5R_c$ to $3R_c$) effectively samples the maximum exchange volume extent for Yucca Flat and that the approach used in N-I (2013) is reasonable. Consistent with N-I (2013) the uncertainty in the exchange volume size will be based on a triangular distribution symmetric about the mean of the minimum and maximum R_c multipliers presented in Table 3-1. The exchange volumes for more volatile RNs are larger than those for refractory RNs, and gas-phase redistribution in unsaturated settings will produce the largest exchange volumes for gaseous RNs such as $^{14}CO_2$.

Table 3-1
Exchange Volume Size (Defined by R_c Mulitplier)

Type	RN	R_c Multiplier
Refractory	^{63}Ni, ^{235}U, ^{237}Np, ^{238}U, ^{238}Pu, ^{239}Pu, and ^{240}Pu	1 to 1.5
Volatile/Gaseous	^{3}H, ^{14}C, ^{36}Cl, ^{41}Ca, ^{90}Sr, ^{99}Tc, ^{129}I, ^{135}Cs and ^{137}Cs	1.5 to 3

Ni = Nickel
Np = Neptunium

3.2.2 LCA Surface Uncertainty

The statistical technique "cross-validation" was used to estimate the uncertainty in the saturated LCA surface (Section 2.8). Using this approach, 100 LCA surfaces were generated using all available full penetration and outcrop data and randomly removing a portion (10 percent) of the available partial penetration data in each realization. Full penetration data are LCA elevations known from boreholes that intercept the LCA, and partial penetration data are elevations known to be above the LCA from wells that did not intercept the LCA. At detonation locations coincident with a borehole that reaches the LCA (where the elevation of the LCA is known), the statistical surfaces were replaced with the measured known value. Also, at partially penetrating emplacement hole locations, if the statistical surfaces were above the total depth of the partially penetrating emplacement hole, the statistical values were replaced with the measured known total depth of the partially penetrating emplacement hole.

3.2.3 Exchange Volume Intersecting the Saturated LCA

Using the exchange volume size and shape (Section 3.2.1) and the LCA surface uncertainty (Section 3.2.2), detonations that could be potential contaminant sources to the LCA were identified and the potential impact on transport from each of these detonations was estimated.

3.2.3.1 Identification of Detonations Intersecting the Saturated LCA

Using the 100 statistical LCA surfaces and the water table (DOE/NV, 1997), and assuming the largest possible exchange volume (i.e., $3R_c$), the WPs of 54 detonations within Yucca Flat were determined to be within $3R_c$ of saturated LCA for at least one realization. The NASH detonation was not found to be within $3R_c$ of the saturated LCA because of the deep (527 m bgs) water table depth reported in DOE/NV (1997). Carle et al. (2008) indicate that a chimney and vadose drainage process occurred at

NASH that resulted in a water table at about 440 m bgs. Applying this water table to the analysis resulted in the inclusion of NASH as a detonation within $3R_c$ of the saturated LCA3. Three more detonations (BLENTON, CALABASH, and MIDLAND) were added to this list to ensure that all the sources from the N-I (2013) LCA model were included in the LCA flow and transport model. Therefore, a total of 58 detonations were included as RN sources in the LCA flow and transport model. These 58 detonations are compared to the 39 previously identified (N-I, 2013) within $3R_c$ of saturated LCA in Table 3-2.

Each LCA surface realization lead to different sets of intersected contaminated exchange volumes. A given detonation and exchange volume may be (1) wholly isolated above the LCA in one realization (and, thus, not a source), (2) bisected by the LCA surface in another (and, thus, rendered as a partial source), or (3) possibly emplaced below the surface entirely in a third (within the LCA, as a whole source). In each case, different portions of the exchange volume contaminant inventory for that detonation become eligible for transport in the LCA model—zero in the first case, a fraction in the second, and all of it in the third. Thus, the contaminant inventories that became incorporated into the LCA model differed from one realization to another.

3.2.3.2 Estimating the Potential Impact on Transport from Identified Detonations

Before transport calculations were performed (see Section 4.7), the potential contribution of each of the 58 detonations (Table 3-2) to the CB was estimated by calculating a "relative volume" for each detonation. Using the R_c multiplier for ^{3}H in Table 3-1 ($1.5R_c$ to $3R_c$), 100 exchange volume multiplier samples were obtained using a triangular distribution symmetric about the mean of the minimum and maximum (the R_c multiplier for ^{3}H was used because N-I (2013) concluded that ^{3}H dominates the extent of contaminant migration in the LCA). For each sampled R_c multiplier, an exchange volume was calculated, resulting in 100 sampled exchange volumes per detonation. At each detonation location, the water table was compared to each of the 100 LCA/LCA3 top surface elevations, resulting in 100 samples of the top surface of the saturated LCA/LCA3. The 100 sampled exchange volumes were compared with each of the 100 sampled saturated LCA/LCA3 elevations, resulting in 10,000 possible intersections of the exchange volume with the saturated LCA/LCA3 surface (i.e., 10,000 volume fractions intersecting the saturated LCA/LCA3) at each of the 58 detonation locations. The "relative volume" for each detonation was then calculated as the total volume that intersects the saturated LCA/LCA3 summed over all 10,000 realizations normalized to the total

Table 3-2
Detonations within $3R_c$ of the Saturated LCA Based on the HFM and Statistically Derived Surfaces

Detonation	Type [a]	N-I (2013)	Current	Detonation	Type [a]	N-I (2013)	Current
ARTESIA	Partial	X	X	KLICKITAT	Partial	X	X
ATRISCO	Partial	X	X	KLOSTER	Partial	--	X
AUK	Partial	--	X	LAMPBLACK	Partial	X	X
BASEBALL	Partial	X	X	LAREDO	Full	X	X
BILBY	Partial	X	X	MICKEY	Partial	X	X
BLENTON	Partial	X	--	MIDLAND	Partial	X	--
BORREGO	Partial	X	X	MIERA	Partial	X	X
BOURBON	Full	X	X	MUNDO	Partial	X	X
BULKHEAD	Partial	X	X	NASH [b]	Full	X	--
BYE	Full	X	X	OBAR	Partial	X	X
CALABASH	Partial	X	--	PALISADE-2	Partial	--	X
CAN-RED	Full	X	X	PALISADE-3	Partial	--	X
CORDUROY	Full	X	X	PALIZA	Partial	--	X
CORNICE-GREEN	Partial	X	X	PIRANHA	Partial	--	X
CORNICE-YELLOW	Partial	X	X	POTRILLO	Partial	X	X
COTTAGE	Full	X	X	ROQUEFORT	Partial	--	X
COULOMMIERS	Partial	--	X	SHAPER	Partial	X	X
CREWLINE	Partial	--	X	SHUFFLE	Full	X	X
CUP	Partial	X	X	STODDARD	Partial	--	X
EDAM	Partial	X	X	STRAIT	Full	X	X
ESCABOSA	Partial	--	X	TAHOKA	Partial	X	X
GORBEA	Partial	--	X	TAN	Partial	--	X
GRAPE A	Partial	X	X	TANYA	Full	X	X
GRAPE B	Partial	X	X	TERRINE-WHITE	Partial	--	X
HAREBELL	Partial	--	X	TERRINE-YELLOW	Partial	X	X
HERMOSA	Partial	X	X	TEXARKANA	Partial	--	X
KANKAKEE	Full	X	X	THISTLE	Partial	X	X
KEELSON	Partial	--	X	TIJERAS	Partial	--	X
KINIBITO	Partial	--	X	TORRIDO	Partial	X	X

[a] Full penetrations intersect the LCA or LCA3, and therefore no uncertainty in its location exists.
[b] NASH not identified because of the deep SZ (527 m bgs) reported in DOE/NV (1997).

X = Included
-- = Not included

volume of the detonation with the greatest volume (TORRIDO). The $3R_c$ exchange volumes for the 58 detonations are presented in Figure 3-1, colored by relative volume. The detonations with low relative volumes (purple) are estimated to have a much smaller contribution to the CB than detonations with higher relative volumes.

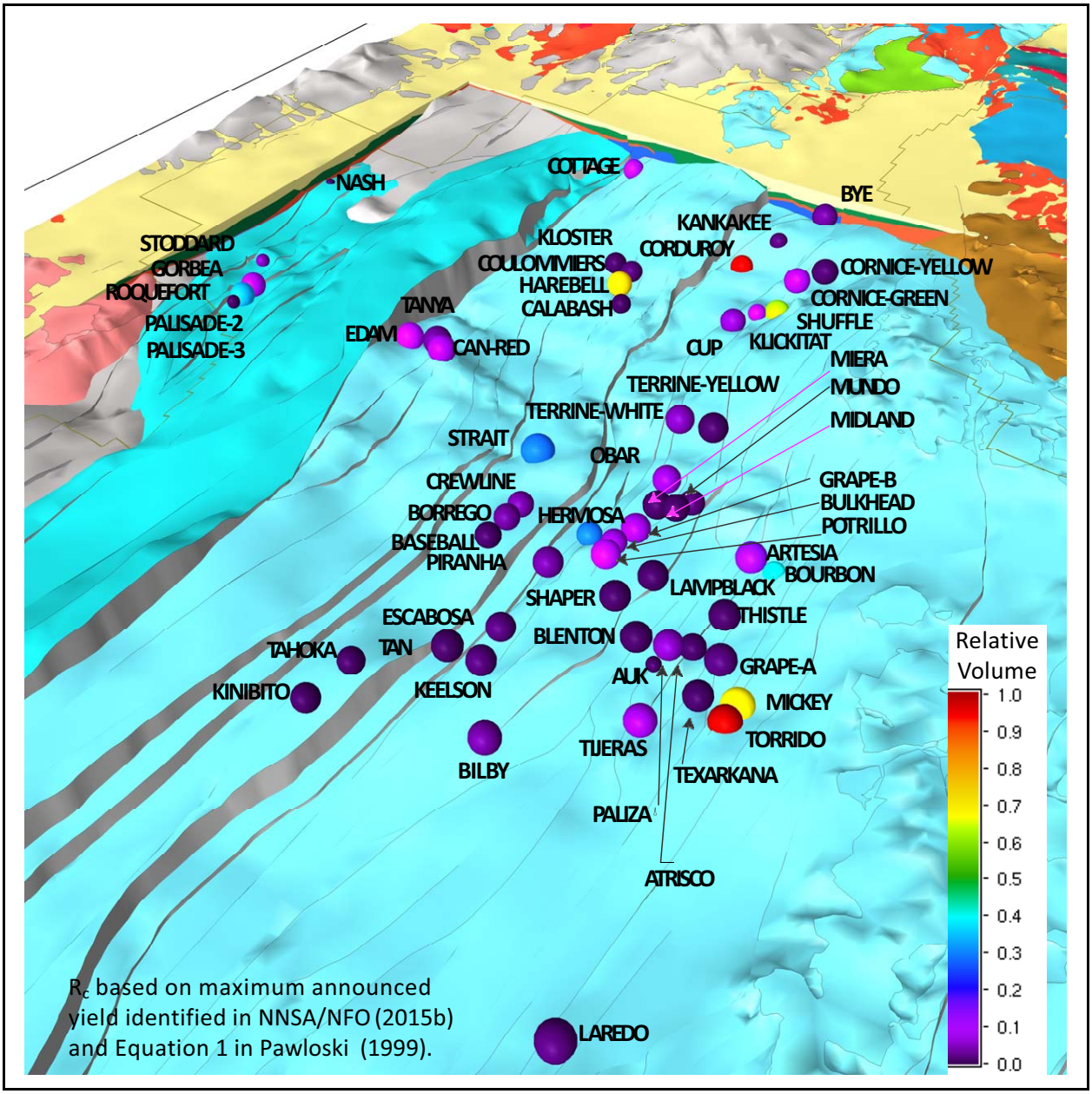

Figure 3-1
Location of Detonations Potentially within $3R_c$ of the Saturated LCA/LCA3

Note: Relative volume is the total volume that intersects the saturated LCA/LCA3 summed over all 10,000 realizations normalized to the total volume of the detonation with the greatest volume (TORRIDO).

3.2.4 Conclusions

There are insufficient data to provide a sound basis for revising the current conceptualization that the exchange volume is a spherical region centered around the detonation. The uncertainty in the exchange volume size was described by assigning a triangular distribution to the exchange volume radius multiplier symmetric about the mean of the range given in Table 3-1. The uncertainty in the saturated LCA surface was addressed by generating 100 LCA surfaces using the cross-validation technique based on all available data. Fifty-eight detonations were determined to have $3R_c$ exchange volumes that may intersect the saturated LCA/LCA3. Although the NASH detonation was not originally found to be within $3R_c$ of the saturated LCA3, applying a water table that accounted for chimney and vadose drainage processes resulted in its inclusion.

3.3 Extent of RN Contamination in the LCA

The extent of contamination was evaluated by four model evaluation activities: sampling LCA completions for RNs (Section 2.1); interpreting drilling evidence from ER-2-2, ER-3-3, and ER-4-1 (Section 2.2); sampling near-field wells (Section 2.3); and sampling NASH test cavity at satellite Well UE-2ce (Section 2.4). Fifteen LCA completions were sampled between 2016 and 2018 (Table 2-4). No test-derived RNs were detected in 10 of the 15 LCA completions despite the close proximity to detonation cavities and/or faults for several locations. Detection of ^{3}H at concentrations below 100 pCi/L (0.5 percent MCL) occurred in samples collected from 4 of the 15 wells: ER-2-2 (13.31 pCi/L), UE-7nS (53 pCi/L), U-3cn-5 (10.2 and 12.3 pCi/L), and WW C-1 (12.2 and 13.5 pCi/L). Groundwater in 1 of the 15 wells, UE-2ce, has ^{3}H above its MCL (increasing from 120,000 to 143,000 pCi/L over the sampling period). No other test-related RNs were observed above their MCL in the groundwater collected from any of the wells sampling LCA completions.

3.3.1 Conclusions

In summary, except near NASH in northwest Yucca Flat, no LCA/LCA3 groundwater has been identified with RN concentrations that exceed SDWA standards (CFR, 2018). Locations sampled include those near deep TCU-hosted SZ detonations (BILBY and STRAIT), deep TCU-hosted SZ detonations near faults (CALABASH and WAGTAIL), deep TCU-hosted UZ detonations (MICKEY/TORRIDO), and a deep UZ LCA-hosted detonation (BOURBON). Most known

contamination is still confined to volcanic units and alluvium, indicating that the TCU is an effective barrier to RN migration to LCA.

3.4 LCA Hydraulic Properties

The distribution of hydraulic properties of the LCA within Yucca Flat strongly influences rates and directions of groundwater flow, and along with the distribution of LCA source terms, determines the extent and location of the CB. In the LCA, the matrix hydraulic conductivity is insignificant relative to the bulk rock hydraulic properties, indicating that bulk hydraulic conductivity is determined by the extent of fracturing and faulting. The LCA model includes both faults that are explicitly represented in the model, and country rock that includes smaller unrecognized faults as well as fractures. Hydraulic property analyses presented in SNJV (2004) and summarized in N-I (2013) indicated that pumping scale hydraulic conductivities are approximately log-normally distributed with a median log K = 0.0 (or K = 1 m/d) and 5th- and 95th-percentile values of approximately log K = -2.25 (K = 5.6E-03 m/d) and log K = 2.25 (1.77E+02 m/d). Although there are additional data for slug tests and laboratory measurements, these are considered to provide less representative information because they test much smaller volumes of the aquifer than the pumping-scale values.

Faults are conceptualized as containing an internal architecture that can consist of a relatively narrow (centimeters to decimeters wide), low-permeability gouge or brecciated zone along the slip plane; and a wider (meters to tens of meters) damage zone of increased fracturing that grades back into the average fracturing typical of the country rock with increasing distance from the slip surface. The fractures in the damage zone are sub-parallel to the fault plane. Thus, the potential for anisotropy in fault hydraulic properties is created by the fault gouge, which inhibits cross-fault flow; and a zone of higher fracture density in the damage zone, which promotes fault-parallel flow. This conceptualization led to the development of zoned faults in the N-I (2013) LCA model. The N-I (2013) LCA flow model also included three broad zones in Yucca Flat—west, central, and east—within which country rock hydraulic conductivity was assumed to be constant. The hydraulic conductivity in the eastern zone defined in the N-I (2013) model was strongly informed by hydraulic responses in the 2004 ER-6-1-2 MWAT (SNJV, 2004), and was estimated to be significantly higher than in the central or western zones, which did not show responses to the ER-6-1-2 MWAT. The absence of cross-hole test responses to the ER-6-1-2 MWAT in the central zone, which includes the rock between the eastern strand of the Yucca fault and the Topgallant fault, prompted the drilling of

three new wells in this zone: ER-2-2, ER-3-3, and ER-4-1. Unfortunately, as described in Section 2.2.2, borehole instabilities and high uphole ^3H concentrations at Well ER-2-2 led to the isolation of the LCA with a cement plug soon after the LCA was reached, before aquifer testing or groundwater sampling in the LCA could be done. Borehole instability also led to the sloughing of weaker rocks around the well screen in the LCA at Well ER-3-3, which complicated the assessment of aquifer properties at the well and limited opportunities to get representative groundwater samples from the LCA at Well ER-3-3. Transmissivity estimates (Section 2.2.5) made from LCA water production at Wells ER-2-2 and ER-3-3 during drilling (before borehole collapse), in combination with the results of water production and aquifer testing at Well ER-4-1, confirmed the result of the N-I (2013) model calibration that the hydraulic conductivity of the LCA in the central zone was far less than in the eastern zone, despite the central zone being defined by the major basin-forming faults. The LCA hydraulic properties target was also informed more directly by the ER-4-1 WDT (Section 2.5), which pumped about 1.7 million gal of groundwater at a rate of approximately 70 gpm over 10 days and produced identifiable water level responses at wells as far north as UE-10j and as far south as ER-6-1-2. Early and late-time transmissivity values of 250 and 56 ft^2/day were interpreted directly from the drawdown data at the pumping Well ER-4-1. A valuable outcome of this WDT was the cross-hole drawdown observations for calibration of the LCA flow model that informed model hydraulic properties in previously uncharacterized parts of the basin.

As part of the development of the DV3 model, historical single-well pumping data from the LCA were reexamined using consistent interpretative techniques to eliminate multiple interpretations of the same pumping events that created the impression that LCA transmissivity data were far more numerous than they actually are (Halford and Jackson, 2019). These transmissivity data were then used in the DV3 model as observations to condition the hydraulic property field using a pilot point approach to introduce spatial variability in transmissivity estimates. As described in Section 4.2.3.1, the revised LCA CAU model uses a similar pilot point approach to accommodate heterogeneity in the hydraulic properties of the country rock and does away with the simple three-zone approach used in the N-I (2013) model. Unlike the DV3 model, however, the revised LCA CAU model allows for the full thickness of the LCA as represented in the Bechtel Nevada (BN) (2006) HFM to participate in the flow and transport model, rather than limit the active LCA thickness to the upper 500 m below the water table as in the DV3 model. The reason that the revised LCA CAU model includes the full thickness of the LCA as represented in the HFM is that the available transmissivity versus depth data—which includes data reinterpreted by Halford and Jackson (2019), as well as data not

reinterpreted but presented in the YF/CM hydrologic data document (HDD) (SNJV, 2006b)—do not show any evidence that transmissivity systematically decreases with depth (Figure 3-2). These data are summarized in Table 3-3. In fact, the deepest intervals tested show that significant transmissivity persists down to at least 1 mi (5,280 ft) bgs. LCA thickness of 5 km is consistent with the porosity estimates derived from the geochemistry data as discussed in Section 2.7.3.7

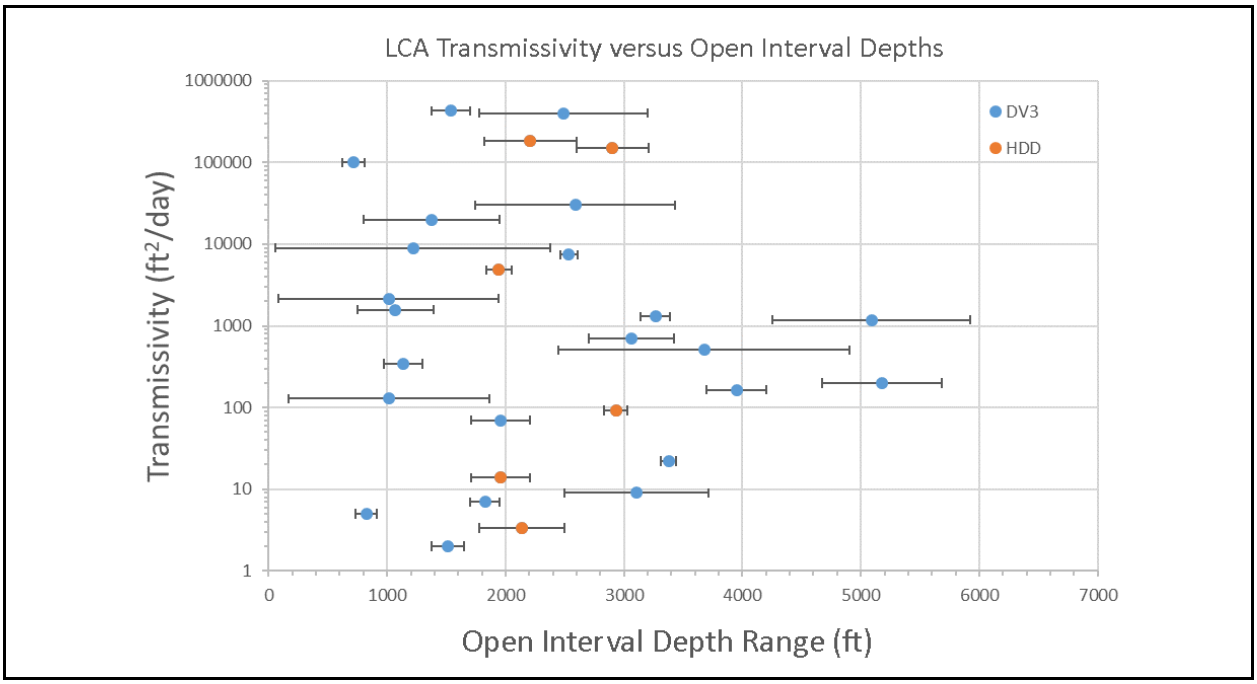

Figure 3-2
Transmissivity Plotted against the Open Interval Depth Range for LCA Detonations in Yucca Flat and Vicinity

Note: Data in blue are estimates recalculated by Halford and Jackson (2019). Data in orange are for tests that were not re-interpreted by Halford and Jackson (2019) but were included in the HDD (SNJV, 2006c).

Table 3-3
Transmissivity Data
(Page 1 of 2)

Well	Depth Top Open (ft)	Depth Bottom Open (ft)	Midpoint Depth (ft)	Screen Length (ft)	LogK (ft/day)	T (ft²/day)
DV3 (Jackson and Halford, 2019)						
Tracer Well 3 ATSSH-1	620	807	714	187	2.7	100,000
TW-4	751	1,390	1,071	639	0.4	1,570
TW-10	975	1,301	1,138	326	0.02	343
Army 1 WW	800	1,946	1,373	1,146	1.2	20,000

Table 3-3
Transmissivity Data
(Page 2 of 2)

Well	Depth Top Open (ft)	Depth Bottom Open (ft)	Midpoint Depth (ft)	Screen Length (ft)	LogK (ft/day)	T (ft^2/day)
TW-5	735	916	826	181	-1.6	5
TW-F (3400')	3,142	3,392	3,267	250	0.7	1,300
TW-3	165	1,860	1,013	1,695	-1.1	129
UE-25 p1	4,256	5,923	5,090	1,667	-0.1	1,180
ER-5-3-2	4,674	5,683	5,179	1,009	-0.7	200
WW-C	1,373	1,701	1,537	328	3.1	427,000
ER-6-2	1,746	3,430	2,588	1,684	1.3	30,000
ER-6-1-2	1,775	3,200	2,488	1,425	2.4	400,000
UE1q (2600')	2,459	2,606	2,533	147	1.7	7,400
UE-16dWW	81	1,944	1,013	1,863	0.1	2,150
TW-D	1,700	1,950	1,825	250	-1.6	7
UE-7nS	1,707	2,205	1,956	498	-0.9	70
UE-2ce	1,378	1,650	1,514	272	-2.1	2
TW-1 (3700-4206')	3,700	4,206	3,953	506	-0.5	164
WW-2 (3422')	2,700	3,422	3,061	722	-0.01	700
ER-12-1	3,309	3,442	3,376	133	-0.8	22
UE-10j (2380')	55	2,380	1,218	2,325	0.6	9,000
ER-12-3 main	2,447	4,908	3,678	2,461	-0.7	504
ER-12-4 main	2,501	3,715	3,108	1,214	-2.1	9
YF/CM HDD (SNJV, 2006b)						
U-3cn-5	2,832	3,030	2,931	198	-0.3	92
ER-7-1	1,775	2,500	2,138	725	-2.3	3
ER-6-1-1	1,835	2,052	1,944	217	1.3	4,820
UE-7nS	1,707	2,205	1,956	498	-1.6	14
ER-6-1 main lower	2,600	3,206	2,903	606	2.4	151,000
ER-6-1 main upper	1,819	2,599	2,209	780	2.4	183,000

These same data were converted to estimates of hydraulic conductivity (ft/day) using the well-screen length and plotted against screen length (Figure 3-3). The data suggest that while there is no relation between hydraulic conductivity and screen length, the variability in the data is larger for short screen lengths that can either hit or miss conductive zones, but that variability decreases with increasing

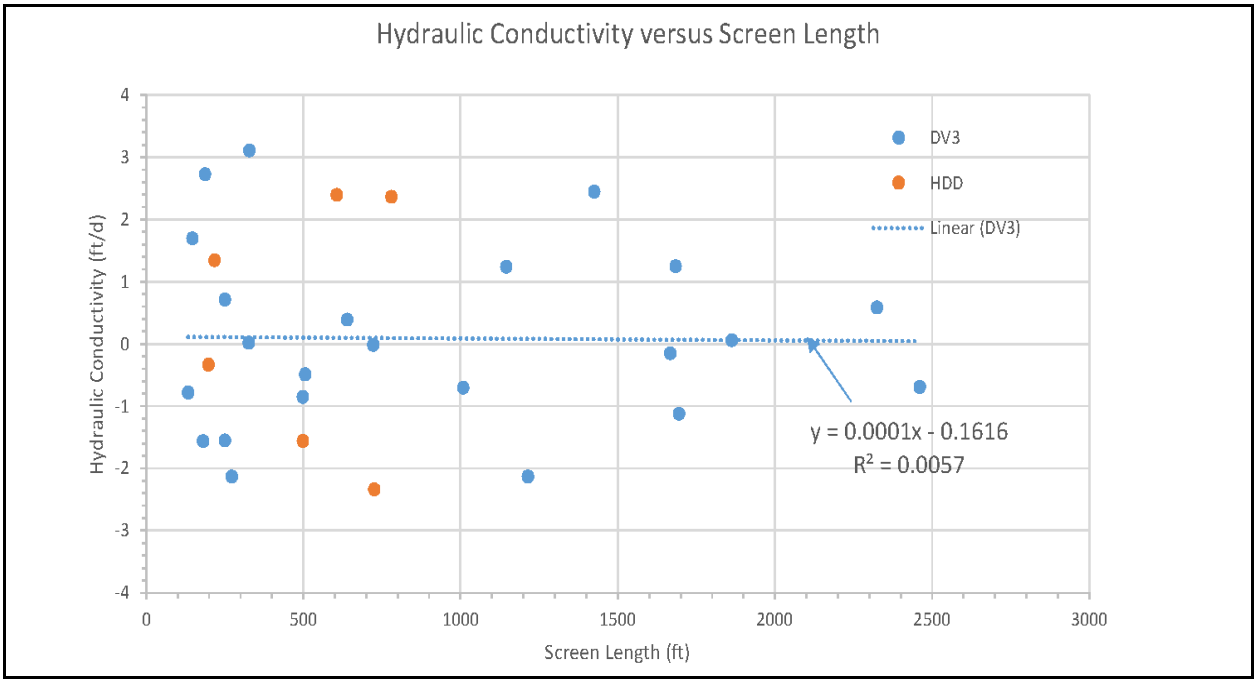

Figure 3-3
Hydraulic Conductivity Plotted against Well Screen Length for LCA Detonations in Yucca Flat and Vicinity

Note: Data in blue are based on transmissivity estimates recalculated by Halford and Jackson (2019). Data in orange are for tests that were not reinterpreted by Jackson and Halford (2019), but were included in the HDD (SNJV, 2006b).

screen lengths as thicker intervals sample larger, more representative aquifer volumes. As well, it appears that the large screen length data approach the mean value of 1 ft/day.

3.4.1 Conclusions

In summary, the LCA hydraulic properties target was successfully addressed through the use of the ER-4-1 WDT cross-hole drawdown observations that informed model parameters in previously uncharacterized parts of the basin (Section 2.5). The basin flux estimates obtained from the DV3 model calibrated using ER-6-1-2 MWAT data and associated uncertainty analysis (Section 2.6) provided additional constraints on hydraulic properties. Data presented in this section were used as observations to condition the hydraulic property field using pilot points in the revised LCA CAU model calibration (see Section 4.2.3).

3.5 ^{90}Sr and ^{137}Cs Mobility in the LCA

As shown in Figures 3-4 and 3-5, ^{90}Sr and ^{137}Cs were significant contributors to the modeled extent of contamination in the LCA in the N-I (2013) LCA base case model. Including matrix sorption as an alternative model (N-I, 2013) reduced this extent. Figure 3-4 compares the N-I (2013) base case model's CB to the CB that resulted when matrix sorption of Sr, Cs, C, and Ni on carbonate rock is taken into account. Figure 3-5 presents the exceedance volume for each RN for the base case and for the alternative model with matrix sorption (N-I, 2013). The exceedance volume is the total volume of model nodes that have a 5 percent or greater probability of exceeding the MCL when considering all RNs at any time up to 1,000 years. For the N-I (2013) base case model, ^{90}Sr has a greater exceedance volume than ^{3}H (Figure 3-5). Even when matrix sorption is included in the model, ^{90}Sr and ^{137}Cs significantly contribute to the exceedance volume (Figure 3-5).

The K_d distributions for Cs and Sr that were applied in the N-I (2013) alternative matrix sorption model are presented in Table 3-4. Table 3-4 also reports the MCL and the Yucca Flat inventory for ^{3}H, ^{90}Sr, and ^{137}Cs (Finnegan et al., 2016). The inventory associated with detonations located more than 328 ft (100 m) above the water table and those that were detonated below that level are presented (Table 3-4). (The water table used for this determination is reported in DOE/NV [1997].) As can be seen from Table 3-4, the inventory relative to the MCL is greater for ^{90}Sr (~12,000 to 58,000) and ^{137}Cs (~900 to 2,900) than ^{3}H (~200 to 500). Given the relatively similar half-lives (Table 3-4), it is not unexpected that these RNs would dominate the CB if processes that decrease their mobility are not taken into account.

To address this, a path forward was identified to account for matrix sorption and revision to the source term model as described in this section. First, K_d distributions were developed to represent ^{90}Sr and ^{137}Cs sorption in the LCA. Second, a new source term distribution model has been developed that takes into account ^{90}Sr and ^{137}Cs sorption on infallen rock in the cavity. These model refinements are expected to result in model results that are more consistent with observed RN concentrations in LCA wells within Yucca Flat compared with the base case model documented in N-I (2013).

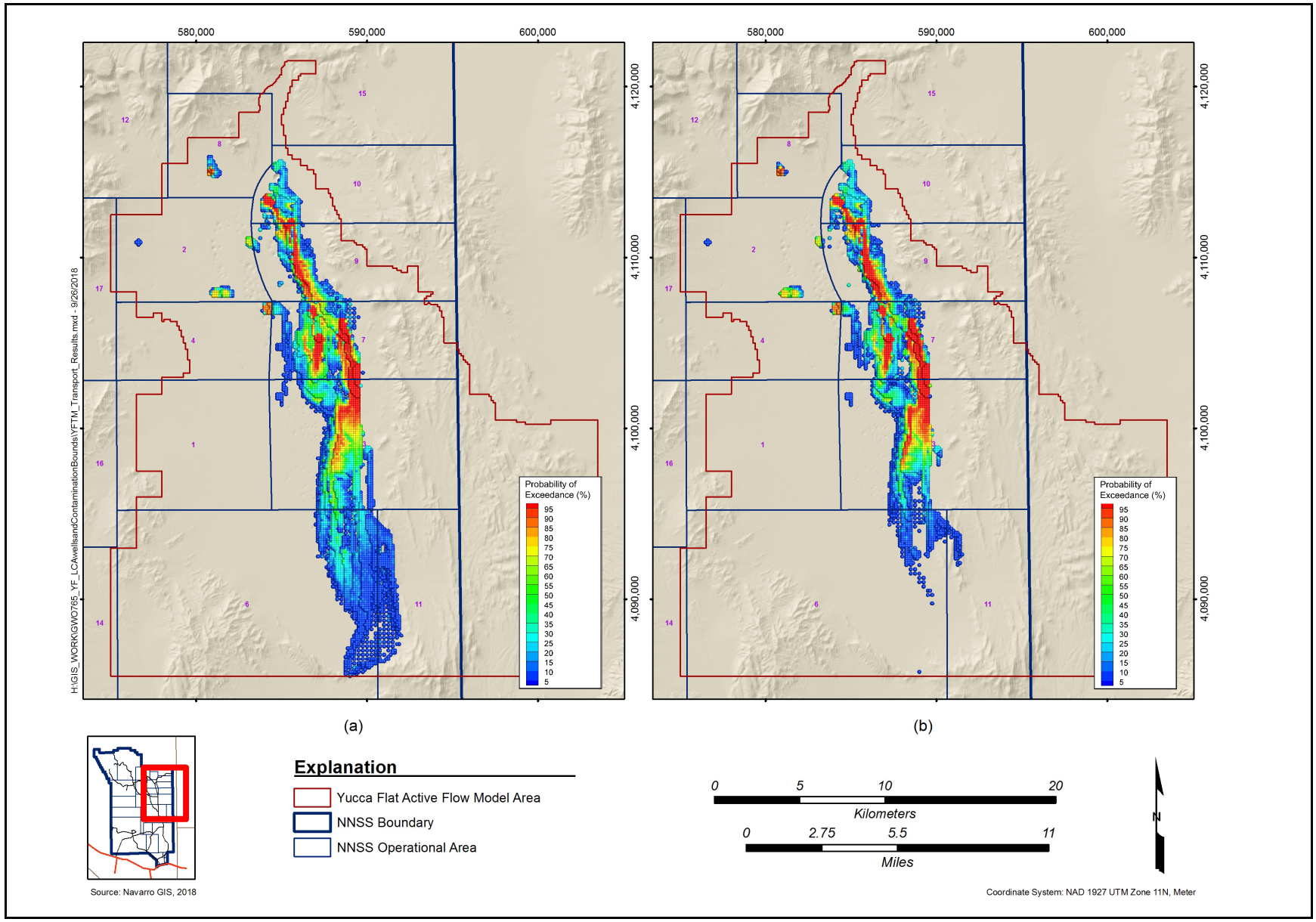

Figure 3-4
Time-Cumulative Probability of MCL Exceedance for LCA Sources: (a) Base Case and (b) Alternative Matrix Sorption for Sr, Cs, C, and Ni
Source: Modified from N-I, 2013

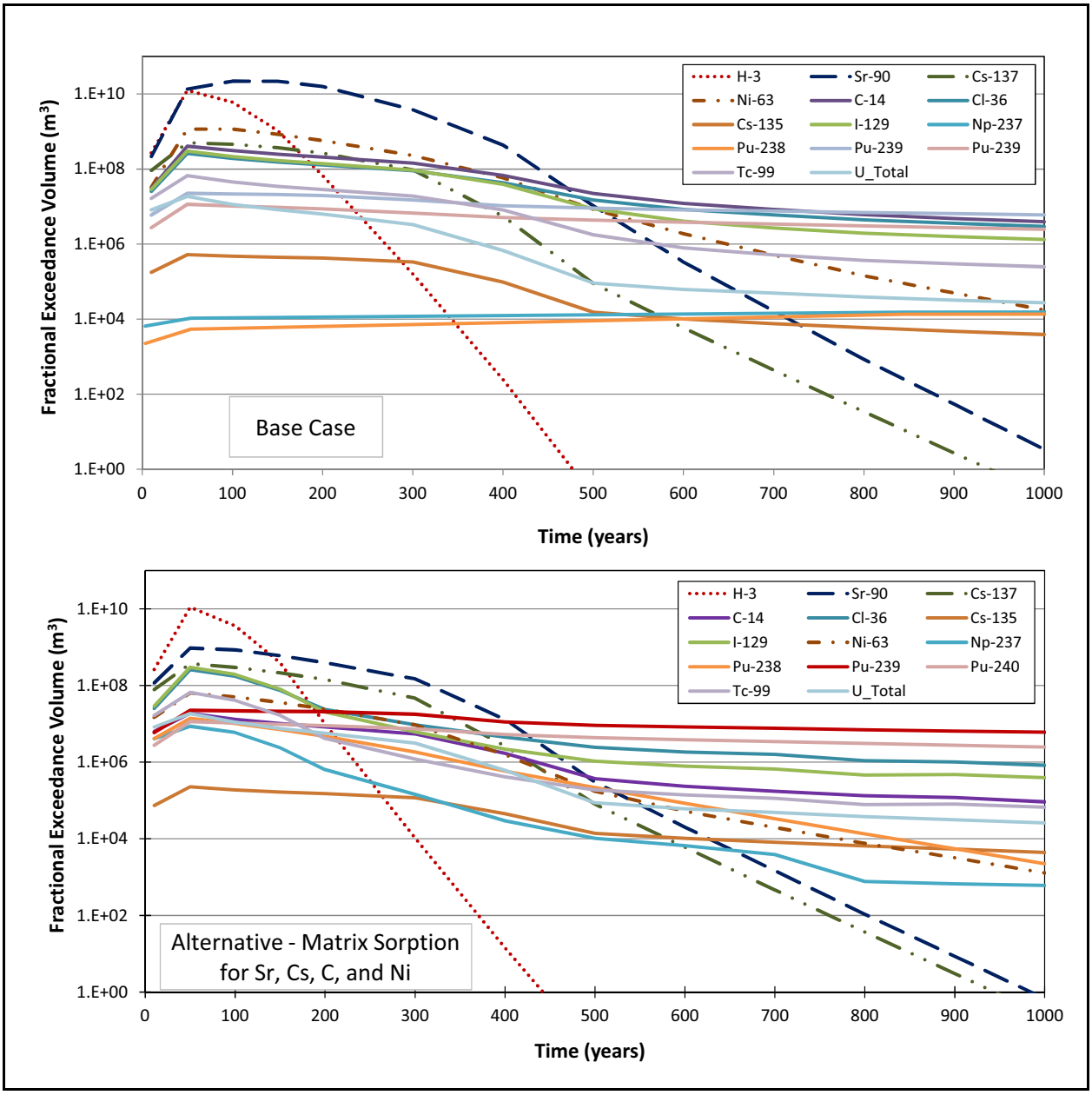

Figure 3-5
Fractional Exceedance Volume for LCA Sources Base Case and Alternative with Matrix Sorption for Sr, Cs, C, and Ni
Source: Modified from N-I, 2013

Table 3-4
LCA Transport Model K_d Distributions (mL/g)

RN	MCL (pCi/L) [a]	Half-Life (years) [b]	Inventory (Ci) [b]		Glass Partitioning (%) [c]		LCA K_d Distribution (mL/g) [c, d]		
			Above Water Table	Below Water Table	Carbonate [e]	Silicic Rock	Lower Bound	Upper Bound	Mode
^{3}H	20,000	12.32	4.77E+06	1.07E+07	0	0	0	0	0
^{90}Sr	8	28.78	9.26E+04	4.62E+05	5	40-80	5	16	10.5
^{137}Cs	200	30.07	1.84E+05	5.86E+05	5	25-40	0.2	6.8	3.5

[a] EPA (2002)
[b] Decay corrected to September 30, 2012 (Finnegan et al., 2016).
[c] N-I (2013)
[d] Triangular distribution used for the N-I (2013) alternative matrix sorption model.
[e] For carbonate, "glass" consists of calcite, dolomite, and their decomposition products instead of silicate glass.

3.5.1 LCA Matrix Sorption of ^{90}Sr and ^{137}Cs

The literature review described in Section 2.9.2 resulted in the recommendation of the following triangular distribution to represent K_ds for the LCA and LCA3:

- **Sr:** 0.05 (minimum), 0.095 (mode), and 0.14 (maximum) mL/g
- **Cs:** 0.02 (minimum), 0.045 (mode), and 0.07 (maximum) mL/g

These values are quite low and are expected to lead to minimal impact on RN transport.

3.5.2 Source Term Distribution Model

As shown in Section 2.4, the measured concentrations of ^{90}Sr and ^{137}Cs relative to ^{3}H are more than 3 orders of magnitude lower in UE-2ce groundwater samples than for the RN inventory reported in Finnegan et al. (2016). Sorption to the LCA material accounts for some of this reduction, but impact of additional processes on ^{90}Sr and ^{137}Cs concentrations in the near-field environment must be considered. Although NASH was detonated in the LCA3, ^{90}Sr and ^{137}Cs activities in UE-2ce groundwater were found to be more consistent with cavities filled with volcanic rocks than with carbonate rocks (Section 2.9.3). To address these observations in the near-field environment, detonation phenomenology was taken into account.

Section 2.9.1.1 describes the phenomenology of an underground detonation including the final stages when the rocks above the detonation cavity collapse into the cavity, creating a rubblized chimney. The

gaseous ^{90}Kr and ^{137}Xe decay to ^{90}Sr and ^{137}Cs. In the final configuration, a melt-glass zone exists at the cavity bottom; rubblized rock is found in the cavity to chimney; and crushed and altered rock surrounds the cavity wall. The exchange volume encompasses the cavity, crush and altered rock zones, and portion of the chimney contained within these zones (Figure 2-51).

A revised source term conceptual model was therefore developed that assumes equilibrium sorption between all rocks in the exchange volume, including rocks that collapsed into the cavity. The ^{90}Sr and ^{137}Cs adsorb on to the infallen chimney rubble within the cavity. HSU-specific K_ds are assigned to the infallen rubble to account for RN sorption. The rubble within the cavity and the altered zone outside the cavity are distinguished using different porosity values. Aqueous RNs then migrate into the exchange volume via fractures. This model assumes that (1) early injection of gas phase RNs to the exchange volume is negligible compared to later transport of the RN mass in aqueous phase; and (2) the solution within the exchange volume is well mixed and fully equilibrated with the rocks within the exchange volume.

3.5.3 Conclusions

Site-specific K_d values will be used to represent sorption of Sr and Cs in LCA rock in Yucca Flat. These values are quite low and are expected to lead to minimal impact on RN transport. A revised source term distribution model for Sr and Cs is selected that accounts for sorption of Sr and Cs on the tuffs in the cavity from the collapsed chimney, resulting in lower initial concentrations of these RNs.

3.6 Fault Transport Properties

The transport properties of faults can have an important impact on the location and extent of contaminant transport, and hence on the extent of the CBs. The CADD/CAP (DOE/EMNV, 2017d) identified three model evaluation activities as potentially helping to contribute to uncertainty reduction in fault transport properties: (1) sampling LCA completions for RNs (Section 2.1); (2) interpreting drilling evidence from ER-2-2, ER-3-3, and ER-4-1 (Section 2.2); and (3) sampling near-field wells (Section 2.3). The rationale for selecting these activities as potentially contributing to uncertainty reduction in fault transport property uncertainty is that identification of a contaminant plume moving within a fault zone in the LCA would allow the parameters in a transport model to be calibrated using the observed contaminant concentrations in the plume. However, the absence of a contaminant plume in the LCA at any of the LCA/LCA3 completions except near NASH at UE-2ce

(which is unfaulted) eliminates the opportunity to calibrate fault transport parameters based on field measurements, especially in view of the associated uncertainty in source term inputs to the LCA (Section 2.9.1). Although unable to reduce uncertainty in fault transport parameters in the LCA, the three model evaluation activities did demonstrate that faults through the TCU near the BOURBON, CALABASH, TORRIDO, and WAGTAIL detonations were not important pathways for RN migration to the LCA; and that no major new fracture pathways extending to the LCA were created in the TCU below the WPs of these detonations.

Of the two sets of fault transport parameter distributions examined in the N-I (2013) report, the case that was labeled "alternative fault transport porosity" had larger fracture porosities and smaller fracture spacing in the damage zone than the case that had been labeled in N-I (2013) as the "base case." The alternative fault transport porosity case represented a physically more realistic conception of the damage zone with a higher fracture density (smaller fracture spacing) than the adjacent country rock. The alternative case resulted in less extensive transport, primarily because the alternative parameter set slowed advective transport and promoted more matrix diffusion in the damage zone. The calculation of these parameters is described in Section 6.3.6.1 of N-I (2013) and in Section 4.7.3 of this report.

Although it does not directly distinguish between the two alternative fault transport parameter sets, the analysis of effective transport porosity using ^{14}C migration velocities presented in Section 2.7.3 in the highly faulted high-transmissivity corridor between ER-7-1 and ER-6-1-2 indicates that fault properties do allow for significant matrix diffusion in this heavily faulted zone, consistent with the fault transport parameters of the alternative fault transport porosity case. As shown in Section 4.0, this is an especially critical region because it is through this corridor that RNs from the testing area are expected to move, so the effective transport properties there directly impact the extent of the CB.

3.6.1 Conclusions

The absence of a contaminant plume in the LCA at any of the LCA/LCA3 completions (except near NASH at UE-2ce, where LCA is unfaulted) eliminated the possibility of calibrating fault transport parameters to field measurements. The models presented in this report use distributions for fracture spacing, aperture, and porosity from the case that was labeled in N-I (2013) as the "alternative fault transport porosity case." The rationale for adopting this non-conservative approach is that it

represents a more realistic conceptualization of fault damage zones as having higher fracture density (smaller fracture spacing) than the adjacent country rock.

3.7 Permeability Anisotropy

The permeability anisotropy model evaluation target was evaluated by two activities: performing WDT in the ER-4-1 LCA (Section 2.5), and evaluating ER-4-1 and other Yucca Flat groundwater geochemistry (Section 2.7). The intent of this target is to reduce uncertainty in flow direction in the central part of the basin, which can be in a direction different than the hydraulic gradient due to anisotropy in permeability. Groundwater geochemistry was used to evaluate whether flow directions are aligned with the gradient or at a large angle to it (Section 2.7). This approach provides a qualitative and perhaps quantitative indication of whether anisotropy is strong enough to affect anticipated transport directions.

The steady-state, predevelopment hydraulic head contours for Yucca Flat developed by Fenelon et al. (2012) shown in Figure 2-33 indicate convergent groundwater flow from the perimeter of the basin toward a potentiometric trough aligned roughly with the Yucca fault. It is important to recognize, however, that the contours are based on relatively sparse data and are therefore highly interpretive. The groundwater geochemistry indicates that ER-4-1 groundwater is derived principally from the area of UE-10j-1, rather than from groundwater in western Yucca Flat, as represented by either UE-2ce or TW-D groundwater. The similarity of groundwater from Wells UE-10j-1 and ER-4-1 (Section 2.7) is also consistent with the response of UE-10j-1 to the ER-4-1 WDT (Section 2.5). A flow path between UE-10j-1 and ER-4-1 would imply more north–south flow than indicated by the hydraulic contours shown on Figure 2-33. A possible cause of north–south flow between UE-10j-1 and ER-4-1 flow could be the Yucca fault, which could intercept groundwater and redirect it southward toward ER-4-1.

Based on pronounced differences in their geochemical compositions, groundwater from the vicinity of ER-4-1 does not appear to flow south along the Topgallant fault toward Wells UE-1q, UE-1r, or UE-1h, consistent with the absence of a response at these wells to the ER-4-1 WDT. Thus, the Topgallant fault does not appear to be especially permeable either along or across its strike. Although groundwater from the vicinity of Well ER-4-1 cannot be traced southward, neither can it be traced downgradient into eastern Yucca Flat. This could be either because there is a groundwater trough roughly coincident with the Yucca fault, as drawn on Figure 2-33, which redirects groundwater flow

southward through the vicinity of ER-3-3; or because the groundwater flowing east from ER-4-1 is diluted and mixed with groundwater of a different composition moving southward at greater rates in the high-transmissivity eastern corridor.

Groundwater at Wells ER-7-1 and ER-6-1-2 is nearly identical in its geochemical and isotopic composition, except for lower ^{14}C activities at ER-6-1-2, implying that groundwater movements between ER-7-1 and ER-6-1-2 is more north–south than suggested by the hydraulic gradient shown in Figure 2-33. This would be consistent with the north–south alignment of faults in the area. The predominantly north–south flow inferred from the groundwater geochemistry is consistent with the north–south flow directions in the high-transmissivity eastern corridor simulated with both the DV3 and LCA CAU models.

Groundwater in the southernmost part of the basin at WW-C is similar to groundwater from east of Yucca Flat at ER-3-1, mixed with a smaller amount of groundwater moving southward from the vicinity of ER-6-1-2. This is consistent with a large groundwater flux entering Yucca Flat south of the Half-Pint range in the southeastern part of the basin where the HFM (BN, 2006) indicates the lower clastic confining unit (LCCU) is structurally lower, allowing a greater saturated thickness of LCA. The groundwater at WW-C appears slightly more dilute than the groundwater at ER-3-1, indicating that it also could contain a smaller volume of groundwater from the vicinity of ER-6-1-1 or from the southwestern part of the basin near ER-6-2. Thus, on the basis of its geochemical and isotopic composition, it appears that groundwater converges toward WW-C, as shown on Figure 2-33. However, this apparent convergence of groundwater flow based on geochemistry could be due, in part, to the fact that approximately 2.5 billion gal of water was pumped from WW-C and WW C-1 between 1970 and 2008, which would have drawn groundwater from all directions toward the pumping wells.

3.7.1 Conclusions

The ER-4-1 WDT results indicate permeability anisotropy due to the Yucca fault is mild, and the Topgallant fault may be a barrier to flow. Flow directions inferred from geochemistry are similar to flow directions inferred from hydraulic gradients, indicating that anisotropy is not a significant factor in determining flow directions. One possible exception is that the flow in high-transmissivity corridor in eastern Yucca Flat between Wells ER-7-1 and ER-6-1-2 could be more north–south than suggested

by the water table contours (Fenelon et al., 2012), probably due to the north–south alignment of faults in the area. This is indicated by the almost identical groundwater compositions at these wells.

Calibration of the Yucca Flat LCA flow model (discussed in Section 4.0) is also an important means of identifying anisotropy in country rock and fault conductivities. This discussion is deferred until Section 4.2.

3.8 Summary

Data collection described in Table 2-1 has been conducted, and the data analyzed and interpreted. All model evaluation targets identified in the CADD/CAP have been addressed.

Table 3-5 summarizes the model evaluation targets and their resolution. The following summarizes the primary model improvements resulting from model evaluation activities:

1. A value of 20 kg/s for the basin flux through the testing area in eastern Yucca Flat was selected for use as a calibration target in model revision. The flux value was estimated to have a factor of two uncertainty.

2. The uncertainty in the exchange volume size was described by assigning a triangular distribution to the exchange radius multiplier. The uncertainty in the saturated LCA surface was addressed by generating 100 LCA surfaces using the cross-validation technique. Fifty-eight detonations were included as source terms.

3. A revised source term distribution model for Sr and Cs was selected that accounts for sorption of Sr and Cs on the tuffs in the cavity from the collapsed chimney, resulting in lower initial concentrations of these RNs.

4. Distributions for fracture spacing, aperture and porosity from the case that was labeled in N-I (2013) as the “alternative fault transport porosity case” were selected because they represent a more realistic conceptualization of fault damage zones as having higher fracture density (smaller fracture spacing) than the adjacent country rock.

Table 3-5
Model Evaluation Target Summary and Resolution
(Page 1 of 2)

Model Evaluation Target	Discussion	Resolution
Basin flux through testing area	Overall volumetric flow rates through the testing area were shown in Navarro (2016b) to have a dominant effect on the southern extent of the CB.	• Formalized the ER-6-1-2 MWAT analysis to characterize groundwater flux through the testing area. • Established uncertainty limits (roughly a factor of 2 higher or lower) on the basin flux estimates through the testing area using the DV3 model. • Used basin fluxes and flux through the testing area to constrain the LCA flow model.
Exchange volume size/shape that extends into the LCA	The CB in the LCA is dominated by deeply buried detonations in the northern half of the basin with exchange volumes that are assumed to intersect the saturated LCA at $2R_c$ (12 detonations) or $3R_c$ (39 detonations) (N-I, 2013). The uncertainty in number and location of tests where the exchange volume intersects the saturated LCA depends both on the size of the exchange volume and the modeled surface elevation of the LCA.	• Distributions that represent uncertainty of LCA surfaces at each detonation were developed. • Identified detonations that intersect ($3R_c$) the saturated LCA when considering uncertainty of LCA surfaces. • Performed transport calculations using the LCA flow model that samples exchange volume triangular distribution and 100 saturated LCA surfaces. • These adjustments better represent the LCA source term.
Extent of RN contamination in the LCA	Evaluation of the present extent of RN contamination in the saturated LCA can be used to bound the present-day CBs.	• Collected samples from LCA completions including near-field wells. • Evaluated the extent of contamination with respect to fault location and proximity to detonations. • Performed transport calculations using the revised base case model, and compared forecasted CB extent at 50 years and 50th percentile to observed RN activities. • Transport results were more consistent with contaminant observations, increasing confidence in the revised models.
LCA hydraulic properties	The flow system, and hence the CB uncertainty, is strongly influenced by groundwater flow and transport properties of fault zones and the country rock.	• Hydraulic transmissivity was estimated by formalizing ER-6-1-2 MWAT reanalysis; analyzing WDT in ER-4-1 LCA; and analyzing drilling evidence from ER-2-2, ER-3-3, and ER-4-1, along with the results of the LCA flow model. • Confidence in the LCA flow model has been increased by obtaining consistent results.
^{90}Sr mobility in the LCA	^{90}Sr was shown to be a significant contributor to the modeled extent of contamination in the LCA, and including matrix sorption in the model for ^{90}Sr significantly reduced this extent (N-I, 2013, Section 6.0 and Figure 6-84).	• New K_d distribution was developed to incorporate fractured LCA matrix retardation. • Implemented alternative source term distribution that takes into account sorption on collapsed chimney material. • Performed transport calculations using the LCA flow model and source term distribution. • These adjustments better match observed ^{90}Sr concentrations, and reduce the role of ^{90}Sr in CB and exceedance volumes.

Table 3-5
Model Evaluation Target Summary and Resolution
(Page 2 of 2)

Model Evaluation Target	Discussion	Resolution
^{137}Cs mobility in the LCA	^{137}Cs was shown to be a significant contributor to the modeled extent of contamination in the LCA, and including matrix sorption in the model for ^{137}Cs significantly reduced this extent (N-I, 2013, Section 6.0 and Figure 6-84).	• New K_d distribution was developed to incorporate fractured LCA matrix retardation. • Implemented alternative source term distribution that takes into account sorption on collapsed chimney material • Performed transport calculations using the LCA flow model and source term distribution • These adjustments better match observed ^{37}Cs concentrations, and reduce the role of ^{37}Cs in CB and exceedance volumes.
Fault transport properties	Faults exert controlling influence on the groundwater flow system in the LCA. Fault damage zone transport properties such as fracture aperture, spacing, and porosity have considerable uncertainty associated with them.	• Used information obtained from sampling LCA completions and analyzing WDT in ER-4-1 LCA. • Current model with more realistic fault widths reduces the influence of alternative fault transport properties on CBs. • Allowed for heterogeneity in both fault and country rock transport parameters in model revisions.
Permeability anisotropy	Predominantly north–south faults with low-permeability fault cores and damage zones with higher fracture densities parallel to the slip plane create a higher permeability in the north–south direction compared with an east–west direction (N-I, 2013).	• Obtained permeability anisotropy estimates by analyzing WDT in ER-4-1 LCA, and evaluating geochemistry at ER-4-1 and other Yucca Flat wells, along with particle tracks from the LCA flow model. • Confidence in the LCA flow model has been increased by obtaining consistent results.

Note: R_c calculated based on the maximum of the yield range reported in NNSA/NFO (2015b) and Equation 1 in Pawloski (1999).

4.0 MODEL REFINEMENTS

The N-I (2013) base case flow and transport model for YF/CM was refined and recalibrated to incorporate the results of the model evaluation data collection activities with the overall goal of producing more realistic models as documented in the CADD/CAP (DOE/EMNV, 2017d). These model refinements, along with associated uncertainty analysis, are described in this section. The overly conservative nature of the N-I (2013) flow and transport model was primarily due to overestimating total flow and groundwater velocity through the Yucca Flat LCA and overestimating source term concentrations of ^{90}Sr and ^{137}Cs. Both of these issues were identified as targets for model evaluation (Sections 3.1 and 3.5). Data collection and analysis activities (Sections 2.1, 2.4, 2.6, and 2.9) were conducted to reduce uncertainties in both these targets. At the time of the N-I (2013) model development, there was a large uncertainty in boundary flux values. Reanalysis of the ER-6-1-2 MWAT (Jackson and Halford, 2019), as part of the model evaluation data collection/data analysis activities (Section 2.6), has resulted in considerably lower flow estimates than those estimated for the N-I (2013) model. Overestimating the source term concentrations of ^{90}Sr and ^{137}Cs was due to neglecting sorption within the exchange volume when allocating the radiological source term (RST) between the three CAU scale models, when in-fallen tuffaceous materials are likely present in the cavity and chimney; Section 3.5 addressed these. To address the overly conservative nature of the N-I (2013) flow and transport modeling, the LCA flow model was recalibrated using realistic constraints on the flow through the Yucca Flat sub-basin, and the allocation of the RST to the LCA model was recalculated considering sorption within the exchange volume. The refined and recalibrated LCA groundwater flow and transport model for YF/CM, referred to as the “LCA flow model” or “LCA model” in this report, supersedes the N-I (2013) model. The “LCA flow model” refers to the base case as well as three alternative models described later in this section. “Base case,” unless otherwise qualified as the N-I (2013) base case, is used synonymously with “LCA flow model base case.”

This section presents hydrogeologic background information, and the technical basis for the LCA model recalibration and resulting forecast of the extent of contamination. The organization and content of this section is as follows:

- Section 4.1,"Introduction," presents the overall modeling approach and the significant assumptions made during the recalibration of the LCA flow model.
- Section 4.2, "Base Case Model Recalibration," presents the LCA flow model calibration and hydrogeologic data from model evaluation activities that were used to calibrate the model. The model described in this section constitutes the base case.
- Section 4.3, "LCA Flow Model Uncertainty Analysis," presents the results of the calibration of two alternative conceptual models that may lead to more extensive transport. It also presents the results of global uncertainty analysis using the NSMC method.
- Section 4.4, "Evaluation of Transient Pumping in Wells WW-C and WW C-1 on Transport," presents an evaluation of transient pumping from WW-C and WW C-1 on particle breakthrough near the model's southern boundary from particles originating from the 58 detonations with exchange volumes potentially within $3R_c$ of the saturated LCA.
- Section 4.5, "LCA Flow Modeling Summary and Conclusions," presents a summary of the major results of the LCA flow model refinement.
- Section 4.6, "LCA Model HST," presents the HST and how the RST is allocated to the LCA model. Many of the Yucca Flat detonations have exchange volumes that span across the UZ, SZ AA/VA, and saturated LCA. The fraction of the RST that resides in the LCA model must be calculated considering the uncertainty in the extent of the exchange volume and initial distribution of RNs within the exchange volume.
- Section 4.7, "Contaminant Boundary Forecasts," presents the evaluation of contaminant transport from underground nuclear detonations using the calibrated base case and three alternative flow fields. This section also presents a comparison of the extents contamination forecasted by the model with present time observations.
- Section 4.8, "Transport Modeling Summary and Conclusions," presents a summary of the major results of the transport modeling.

4.1 Introduction

The LCA is a regionally extensive aquifer that extends through several hydrographic basins in southern Nevada. The LCA has been the focus of a considerable characterization effort over the last several decades because of its significance as a water resource in southern Nevada and eastern California. This characterization has included regional evaluation of the potentiometric surface and

general flow directions and rates, evaluation of the areas and amounts of regionally significant recharge and discharge rates, evaluation of regional geochemistry and regional temperature profiles as indicators of the regional flow paths, and modeling of the groundwater basins in the Death Valley region. This regional information has been supplemented by additional characterization at the scale of the YF/CM CAU as part of the FFACO (1996, as amended) corrective actions for the YF/CM CAU. The most recent data for the YF/CM CAU are from the model evaluation activities (Section 2.0). These and earlier data were used to refine the N-I (2013) LCA flow model.

The approach taken to develop and recalibrate the LCA flow model is similar to the approach taken to develop and calibrate the N-I (2013) LCA flow model. The same HFM, computation grid, and the boundary types are used, with the exception that the spatial parameterization of the model domain uses the pilot point method for assigning country rock hydraulic conductivity and specific storage. The pilot point method estimates parameters at discrete locations (pilot points) throughout the model domain and interpolates the pilot point values onto the model mesh (RamaRao et al., 1995). Pilot points allow for spatial heterogeneity in rock properties and calibration to transmissivity observations that would not be possible in a model using large zones to assign rock properties (e.g., the N-I [2013] model). As with the N-I (2013) modeling, the LCA flow system is separate from the overlying SZ AA/VA system, and the boundary between the LCA and the overlying saturated HSUs is treated as a recharge boundary to the LCA.

The Yucca Flat LCA flow model conceptualization is unchanged from the N-I (2013) modeling. Water sources that produce flow through the Yucca Flat sub-basin are from precipitation and underflow. Pre-development LCA head contours interpreted by Fenelon et al. (2012) indicate gradients are from the perimeter of the basin toward a hydraulic trough near or east of the Yucca fault. Flow directions drawn aligned with the estimated gradient suggest convergent groundwater flow toward WW C-1. The flow is controlled by major structural features including faults and heterogeneities in country rock hydraulic properties. The trough is the result of a highly transmissive north–south corridor in the Yucca Flat sub-basin located east of the Yucca fault and is hydraulically connected with the Ash Meadows discharge area (Jackson and Halford, 2019). The corridor is several miles wide, and the aquifer is highly anisotropic, with enhanced flow parallel to the corridor as a result of the high degree of open faults and fractures along the axis of the corridor (Fenelon et al., 2012).

4.2 Base Case Model Recalibration

The purpose of the YF/CM LCA flow model recalibration is to reconcile model results with measured states of the aquifer system. This is accomplished with reality constrained adjustment of boundary fluxes, prescribed heads, and hydraulic properties for the country rock and faults within a hydrostratigraphic framework in order to match the specified calibration targets. Targets included observed steady-state water levels, aquifer drawdown and recovery resulting from aquifer testing, measured transmissivity at tested wells, and basin flow estimated from a regional model. The LCA flow model was used to develop particle trajectories from RN source locations. The particle trajectories were then used to conduct transport simulations forecasting RN migration for a period of 1,000 years. This section describes the flow model calibration approach and the calibration results for the base case.

4.2.1 Calibration Approach

The Yucca Flat LCA hydraulic properties are estimated by simultaneously calibrating three 3-D groundwater models using identical parameterization. The three models include a steady-state model of pre-development flow conditions, a transient stress response model of the ER-6-1-2 MWAT pumping, and a transient stress response model of the ER-4-1 WDT pumping. The steady-state model provides initial conditions for the transient stress response models. All three models share the same underflow and recharge boundary conditions, hydraulic conductivity, and specific storage values. The temporal separation of the ER-6-1-2 MWAT and ER-4-1 WDT pumping (e.g., 13 years) allows for independent simulation of these two events.

The Yucca Flat LCA model is a highly parameterized groundwater model and has more parameters than can be estimated uniquely on the basis of the calibration dataset. The model calibrations present an ill-posed inverse problem and will not have unique parameter estimation solutions without implementing regularization. The model calibrations are performed with the parameter estimation software PEST (Doherty, 2018). The PEST software obtains a unique calibration from the fundamentally non-unique inverse problem by using regularized inversion and Tikhonov regularization. The PEST software suite also includes a variety of utilities for model pre-processing, post-processing, and understanding model uncertainty.

Tikhonov regularization supplements the information content of a calibration dataset with expert knowledge that compensates for a deficit of information in the calibration dataset (Doherty, 2018). The regularization approach taken for the LCA model calibration augments the measurement objective function with a regularization objective function that penalizes for parameter inhomogeneity. Tikhonov regularization observations were specified with equations derived from the geostatistical structures used to interpolate pilot point values onto the model mesh for hydraulic conductivity and specific storage. This information defines preferred differences between pilot points and penalizes large differences between pilot point values. Initial pilot point and fault parameter values are the average hydraulic conductivity from pump test data and provide a fall-back position if the pilot points parameters are insensitive to the observation data.

As PEST proceeds through the inversion process, PEST relaxes the Tikhonov regularization constraints in order to achieve fits with heterogeneous parameters. The relaxation takes place through reduction of the regularization weight factor (Doherty, 2018). If there is strong evidence for the existence of parameter heterogeneity in the observation data, PEST will estimate the heterogeneous parameters. The initial regularization objective function is always zero when starting with homogeneous pilot point values, which facilitates making homogeneity the preferred condition.

Although the revised model calibration approach is similar to the N-I (2013) approach, a number of notable departures from the previous approach were used:

- Total basin flux was reduced, as described in Section 3.1.
- Model calibration using pilot points for country rock hydraulic conductivity and specific storage allow for spatial heterogeneity.
- Faults are 1 model cell wide and use east–west to north–south anisotropy in place of a low-permeability core.
- Faults with lengths of less than 3 km are not defined with specific zones (Section 4.2.3.2). However, pilot points may introduce heterogeneity representing these smaller faults if there is strong evidence for them in the observation data.
- Calibration includes ER-4-1 WDT responses, transmissivity observations, and a transmissivity-width product flow target in eastern Yucca Flat as defined by the DV3 model.

4.2.2 Model Area and Mesh

The model was constructed with the LANL finite element heat-mass (FEHM) groundwater flow and transport modeling code, Version 3.23 (Zyvoloski et al., 1997b). The flexibility of finite elements allows for the resolution of the grid to vary spatially to capture source areas and complex structures, such as faults with higher resolution than other areas where coarser discretization is sufficient.

The lateral model boundaries were selected so as to include all areas that can potentially capture and transport RN contamination within the carbonate aquifers emanating from the underground nuclear detonation sites within Yucca Flat. The LCA numerical model is based on the HFM constructed for the YF/CM area in BN (2006). The model domain includes only those regions within the study area where the LCA, upper carbonate aquifer (UCA), LCA3, and confining units separating these units are present. The LCA pinches out in the east, north, and northwest, forming the eastern, northern, and northwestern boundaries of the LCA model. The top of the LCA is above the water table in the eastern portions of the model area, and the top of the LCA3 is above the water table in the western portions of the model area, which provides the model's upper boundary in these areas.

The areal extent of the LCA flow and transport model is presented in Figure 4-1 along with faults included in the model domain and the areal extent of the Yucca Flat hydrographic sub-basin. The model extends from -5,500 m above mean sea level (amsl) at the base to +1,500 m amsl at the top. The model spans approximately 36 km in the north–south direction and 28.5 km in the east–west direction. The LCA model domain does not extend to the entire Yucca Flat sub-basin area in the north and extends beyond Yucca Flat sub-basin in the model's southwest and southeast corners. The model volume was discretized into a finite element mesh with 2,917,285 elements by 537,503 nodes. Mesh refinement was performed in the vicinity of faults, with the finest resolution being about 125 m. The model domain is unchanged from the N-I (2013) model.

4.2.3 Model Parameters

Model parameterization used a combined zonation-pilot point approach. Hydraulic conductivity and specific storage within the country rock are distributed using pilot points (RamaRao et al., 1995), and fault properties are assigned using discrete zones.

A total of 230 hydrogeologic properties and boundary conditions were specified as model input parameters for the model calibration. Of the 230 parameters, 197 were allowed to independently

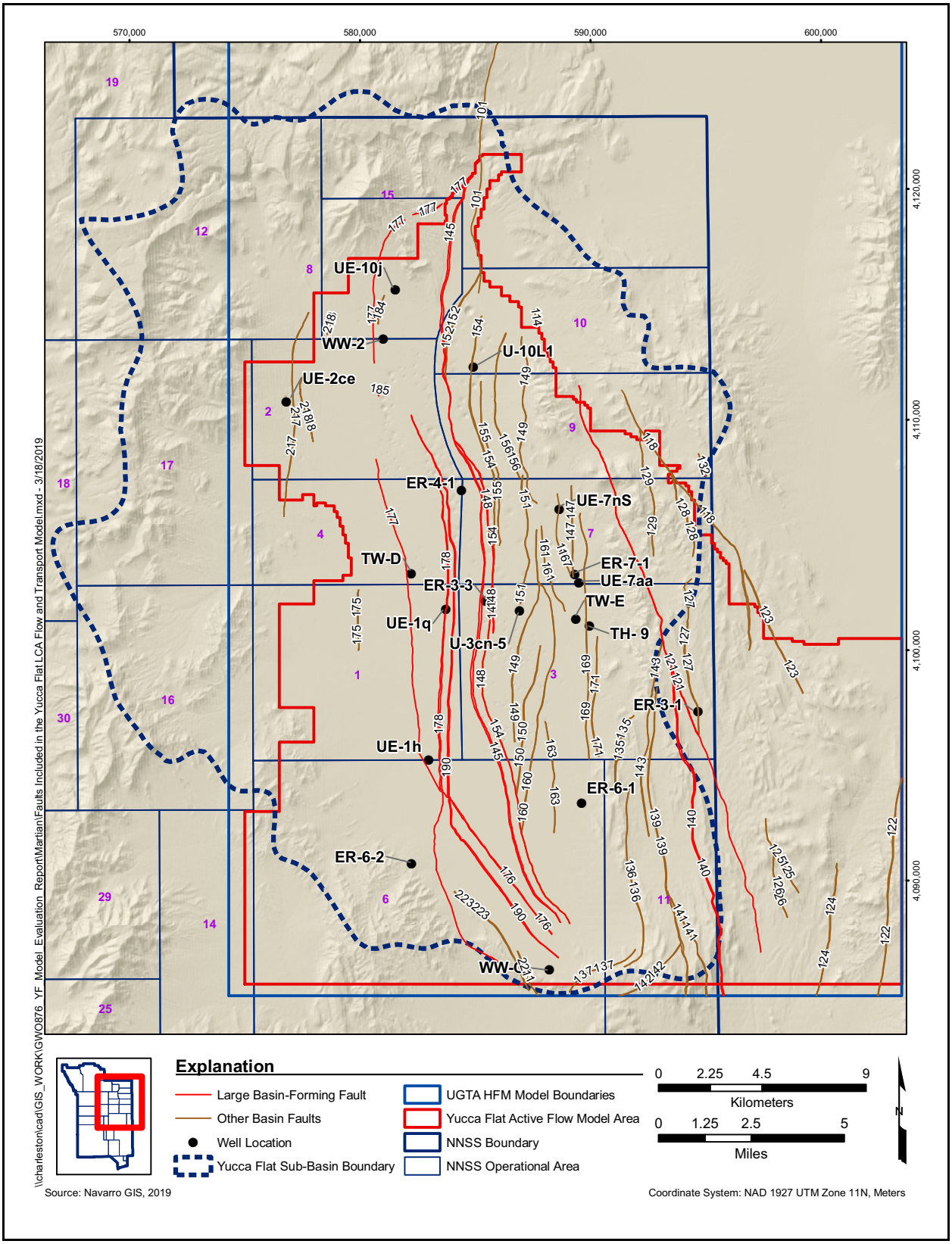

Figure 4-1
Areal Extent and Faults Included in the LCA Flow Model

adjust during the calibration process (33 parameters are tied to other parameters; see Section 4.2.3.2). The model parameters comprise the following:

- 159 country rock hydrogeologic property pilot points
- 12 hydraulic conductivity values for fault and country rock zones
- 12 hydraulic conductivity anisotropy values for fault and country rock zones
- 9 underflow or vertical recharge values on model boundaries
- 3 specified head values at 3 pilot points on the southern boundary
- 2 specific storage values for fault and country rock zones

4.2.3.1 Pilot Points

A uniform grid of pilot points was used with additional pilot points assigned in areas of interest (i.e., the ER-4-1 and ER-6-1-2 MWAT stress response areas). The hydraulic conductivity pilot point grid spacing is 3 km, and specific storage grid spacing is 6 km. Pilot point spacing in the vicinity of the stress responses areas is less than the 3- and 6-km uniform spacing (Figure 4-2). The pilot point values are kriged to the mesh nodes using isotropic, exponential variograms with ranges of 3.5 and 20 km for hydraulic conductivity and specific storage, respectively. Variogram ranges were selected using expert judgment to provide continuous property interpolation onto the model grid from pilot point locations and to allow heterogeneity in areas where data density is sufficient to inform the pilot point parameters. The available Yucca Flat hydrologic data are insufficient for discerning spatial trends and correlation lengths. Interpolated pilot point values for hydraulic conductivity and specific storage provide lateral heterogeneity, but are kept uniform with depth. Hydraulic conductivity within fault zones are superimposed over the interpolated hydraulic conductivity field. The revised LCA model uses the full ~5-km thickness of LCA as defined by the HFM.

4.2.3.2 Faults

Fault zones normally consist of a fault core and damage zone. The core experiences most of the fault displacement and is the fault slip zone. In major faults, the core may be a couple of meters thick and is composed of breccias that are crushed and altered into a soft material. The damage zone is considerably thicker than the core and is characterized by the presence of fractures. The damage zone is the main conduit for water along the fault axis and may have a permeability as much as 10,000 higher than the core or country rock (Gudmundsson, 2011). The presence of faults and high-permeability damage zones likely contribute to the hydraulic trough inferred to exist in eastern Yucca Flat (Section 4.1). Faults within Yucca Flat are conceptualized to behave as barriers to

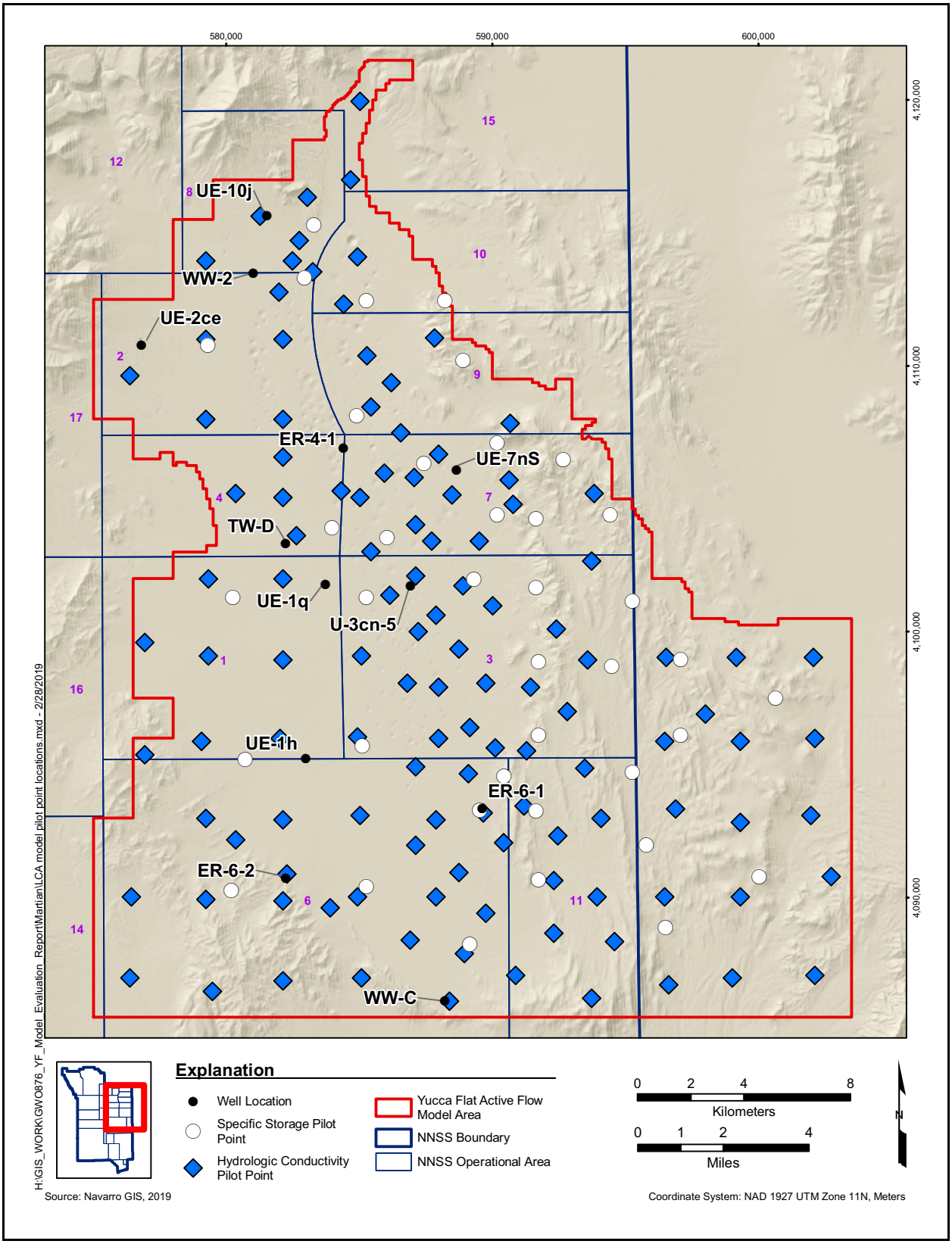

Figure 4-2
LCA Flow Model Pilot Point Locations

cross-flow due to the presence of the fine-grained material in a fault core and conduits along axis due to open fractures within a damage zone on either side of the fault core. The fault damage zone is conceptualized to be hydraulically homogeneous at the scale of the LCA model and be best represented with zones of piecewise constancy.

The N-I (2013) model included only the main surface faults in the model. A total of 107 faults are included in the N-I (2013) model with trace lengths that very from approximately 0.1 km to the entire north–south distance of the Yucca Flat sub-basin. These faults are modeled as single fault planes that extend to the base of the model unless the faults terminate against other faults. The main basin-forming faults dip to the east- and west-dipping faults in the model typically terminate against east-dipping faults. Only faults with traces greater than 3 km in length are included in the LCA flow model refinement for several reasons:

- The pilot point approach captures small scale heterogeneities that could not be captured with the very large N-I (2013) model country rock zones.
- Faults may extend to the base of the 5-km-deep model, and faults with trace lengths less than 3-km trace would have extreme depth-to-length ratios.
- Recalibrations of the N-I (2013) model for the external peer review comment response document (Navarro, 2016b) found the model could be calibrated equally well with or without faults of less than 3 km in length.
- Excluding faults of less than 3 km in length reduces dimensionality and lessens the ill-posedness of the inverse problem.

In order to further reduce the problem dimensionality, it was decided to allow only the large basin-forming faults (Yucca, Topgallant, Carpetbag, YF_121, and YF_140) to vary independently. The hydrogeologic properties of the lesser faults were allowed to vary, but in unison (i.e., the property values were tied). These smaller faults were broken into two groups: faults east of the Yucca fault and faults west of the Yucca fault. All faults are simulated as narrow features parameterized as being 1 cell wide, and the calibrated east–west anisotropy controls cross-flow. Figure 4-1 illustrates the faults included in the LCA model and the Yucca Flat sub-basin.

4.2.3.3 Boundary Conditions

The Yucca Flat sub-basin is an approximately 200-square-mile (mi^2) portion of the 4,200-mi^2 area that drains to Ash Meadows. Groundwater flow through the Yucca Flat sub-basin is derived from

local recharge in the Yucca Flat sub-basin and from lateral inflow from the surrounding sub-basins. Groundwater flow may enter northern Yucca Flat from Emigrant Valley but is limited by low-permeability rocks that surround the northern Yucca Flat LCA. The Yucca Flat sub-basin is bounded by the UCCU of the Eleana Range to the west, the mesozoic granite confining unit (MGCU) to the north, and the LCCU of the Halfpint Range to the northeast (Jackson and Halford, 2019).

4.2.3.3.1 Estimated Boundary Flows

Precipitation-derived recharge within the Yucca Flat sub-basin from highlands in the west and northeast was estimated by Winograd and Thordarson (1975) to be 250 acre-ft/yr and vertical leakage rates through the TCU to the LCA to be between 25 and 65 acre-ft/yr. Lateral inflow in northern Yucca Flat from Emigrant Valley is estimated at a rate of less than 40 acre-ft/yr (Winograd and Thordarson, 1975). Lateral groundwater underflow from the Halfpint Range in the southeast has been estimated at flow rates ranging from less than 100 acre-ft/yr to as much as 300 acre-ft/yr (Winograd and Thordarson, 1975; and Harrill et al., 1988). Harrill et al. (1988) estimated the total lateral and vertical leakage rate into the LCA to be 700 acre-ft/yr. Fenelon et al. (2016) performed a regional water-budget analysis of the Pahute Mesa-Oasis Valley flow system and the surrounding basins, and found that recharge amounts to the Yucca Flat hydrographic area to be between 700 and 1,500 acre-ft/yr.

Jackson and Halford (2019) estimated groundwater flow through the underground nuclear testing areas in Yucca Flat by calibrating the DV3 model to results from the ER-6-1-2 MWAT (Section 2.6). The DV3 model simulated 560 acre-ft/yr flowing through the roughly 5-km-wide transmissive corridor midway between Wells ER-7-1 and ER-6-1.

4.2.3.3.2 LCA Model Boundary Condition Assignments

The LCA model applies lateral flow boundary conditions along the western, eastern, and northern boundaries. Constant head boundary conditions are applied along the model's southern boundary, where flow is conceptualized to exit the model domain. The LCA model domain does not extend to the entire Yucca Flat sub-basin area in the north and extends beyond Yucca Flat sub-basin in the model's southwest and southeast corners. Total flow through the model domain will be greater than the total Yucca Flat sub-basin flow estimated by the DV3 model within the Yucca Flat sub-basin because of inflow occurring in the model's southwest and southeast corners (Figure 4-1).

The DV3 model (Jackson and Halford, 2019) predicts most of the western lateral flow to the LCA occurs in the northern half of the LCA model domain. Precipitation derived recharge occurring in the western Yucca Flat highlands (e.g., east of the Eleana Range drainage divide) must be specified as part the western lateral flow boundary condition. The N-I (2013) model allowed only lateral recharge on the model's southwest boundary. To bring the LCA model into better agreement with the DV3 model, additional flux boundaries were assigned to a central–west and northwest region of the LCA model. The lateral flux values used in the LCA flow model were taken from a near final version of the DV3 model, and slightly differ from the flows documented by Halford and Jackson (2019) and summarized in Section 2.6.

The LCA model range of permissible boundary flow values were approximately a factor of 2 increase or decrease of the DV3 model, which was from an uncertainty analysis performed on the DV3 model (Section 2.6.3). The east lateral inflow was allowed to increase only by a factor of 1.5 due to the very large value of the inflow compared to the other inflows. The west lateral inflows were each allowed to vary by a factor of 2 increase over the DV3 model's total western value. This was done to give PEST the freedom to place most of the western boundary flow estimated from the DV3 at any western lateral boundary location. If all western lateral boundaries had reached the upper limit, the permissible values would have been adjusted. Figure 4-3 illustrates lateral boundary locations, permissible calibration ranges, and the DV3 model predicted flows. The permissible ranges of the LCA model boundary flows illustrated in Figure 4-3 were derived from a nearly final draft version of the DV3 model. The boundary flow values from the DV3 model illustrated in Figure 4-3 were taken from the final version of the DV3 model and differ from the draft version.

4.2.3.4 Optimization "Super Parameters"

The PEST software defines "super parameters" through singular value decomposition of the sensitivity (Jacobian) matrix, which links model parameters to model outputs used in the calibration process. Super parameters are the coefficients by which orthogonal combinations of parameters are multiplied to form the overall estimated parameter set (Doherty, 2018). In most highly parameterized groundwater models, the number of super parameters is much smaller than the total number of model parameters because there need to be only as many super parameters as there are dimensions in the solution space (Doherty, 2018). These so-called "super parameters" can be estimated in lieu of actual model parameters, thereby greatly reducing the computational burden of the parameter optimization.

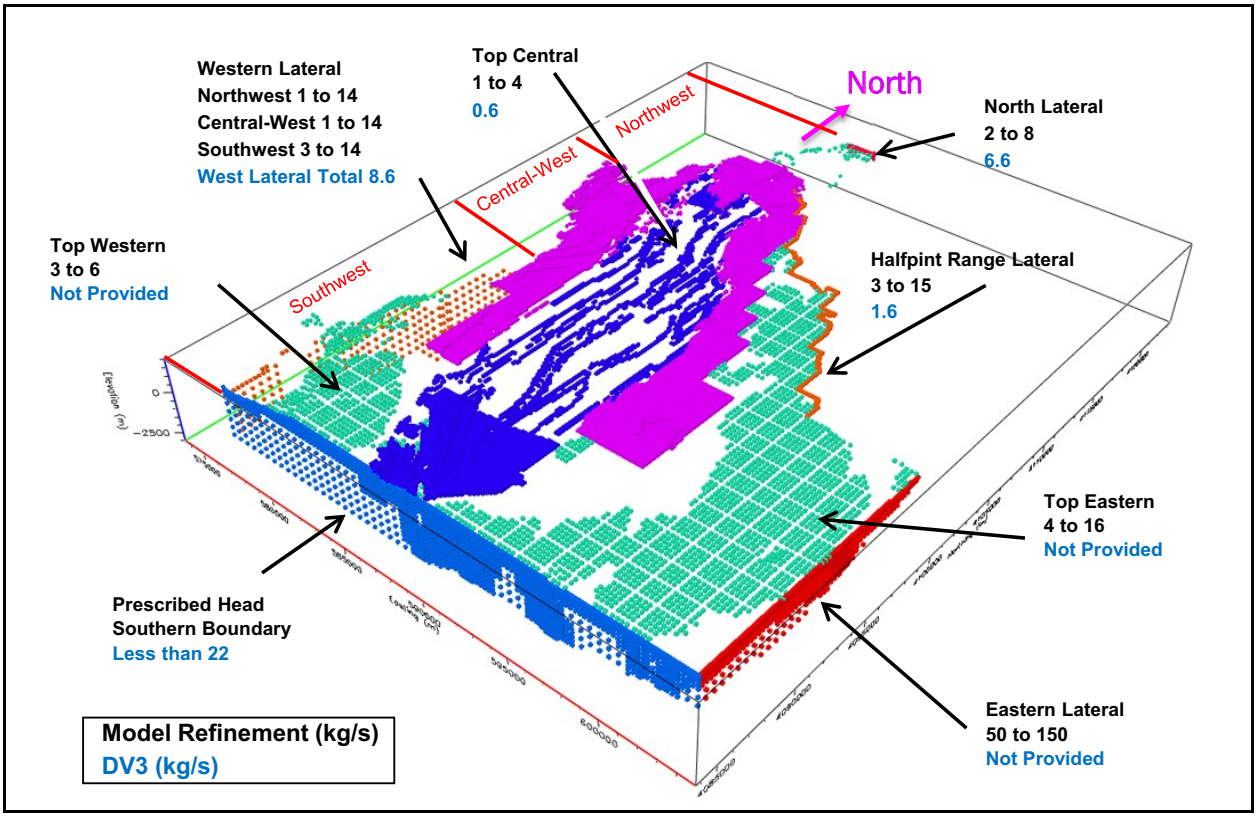

Figure 4-3
LCA Model Domain Boundary Locations, Permissible Ranges, and DV3 Predicted Flows

The dimension of solution space is unknown until the parameter estimation is complete and must be estimated before parameter estimation. The PEST software estimates optimal solution space dimension assuming linearity and recommended using 78 super parameters for the LCA model. There is no penalty for using too many super parameters, but there is possible loss of model information for using too few super parameters; thus, the model was calibrated using 90 super parameters.

4.2.4 Observations Used for Model Calibration

Hydraulic conductivity distributions, specific storage distributions, boundary inflows, and anisotropy factors were estimated by minimizing a weighted composite sum-of-squares objective function. The objective function was informed by steady-state heads, aquifer stress responses, transmissivity measurements, and basin flux of groundwater through the underground nuclear testing area. Groundwater levels, drawdowns, and transmissivities were measured at 17 wells within the Yucca Flat LCA. This section describes the observation data used in the model calibration and formulation

of the objective function. The observation dataset is largely unchanged from the N-I (2013) model calibration with exception of the additional data gathered during model evaluation activities. Most notable of the additional data are the aquifer stress responses from the ER-4-1 WDT pumping and groundwater flow through the testing area estimated from reanalysis of the ER-6-1-2 MWAT.

4.2.4.1 Steady-State Water Levels and Gradients

Hydraulic head is the most available hydrogeologic measurement used to constrain the LCA flow model. Fenelon et al. (2012) developed maps of the hydraulic head distributions in the major aquifer systems within Yucca Flat from a detailed evaluation and assessment of available water-level measurements. Although the Yucca Flat groundwater system is not in true steady-state, Fenelon et al. (2012) concluded transient responses have only a minimal influence on the general pre-development flow directions in the aquifers. Hydraulic heads in Yucca Flat LCA wells that are considered to be representative of pre-development conditions were identified, and these hydraulic heads were used as water-level observations in the steady-state model calibration.

Many of the observation wells that penetrate the LCA in the study are open over a large vertical extent that includes the lower portion of the TCUs. As a result, interpreting the water-level data from these wells is uncertain because water levels may be influenced by the overlying HSU. While the LCA is generally more transmissive than the overlying confining units and hence water levels in wells penetrating the LCA should be representative of the LCA, it is not uncommon for the upper portion of the LCA to be characterized by an argillic paleosol that has a very low permeability (Drellack et al., 2012). As a result, water levels in wells with screens extending into the overlying HSUs may be elevated compared to the water levels from wells with screens solely located with the LCA. As was done in the N-I (2013) modeling, water levels from wells open to the overlying HSUs have not been used in the calibration of the LCA flow field. They include observations in Wells UE-10 ITS 3, UE-10 ITS 5, and UE-10bf in northern Yucca Flat.

East of the Yucca fault, the steady-state heads have an approximately 9-m north-to-south head drop. Heads in western Yucca Flat are higher by approximately 10 m than heads in eastern Yucca Flat, and heads are higher in the southwest than northwest, suggesting some northward flow is possible in western Yucca Flat. The steady-state heads have generally been interpreted as indicating that groundwater from both the east and west sides of the basin flow toward a north–south-oriented potentiometric trough in the center of the basin, where the major faults are located, and follow

primarily north–south direction along the trough before eventually exiting Yucca Flat into the CP and Frenchman Flat basins before eventually discharging in springs at Ash Meadows or Death Valley (Fenelon et al., 2012).

A total of 17 steady-state heads along with gradients from 6 well pairs were used as observations in the steady-state model calibration. Only wells located in eastern Yucca Flat and aligned with the general north–south gradient were used as gradient observations. Adding steady-state water-level gradients to the objective function placed additional emphasis on the observation information that is most informative to transport because the gradient drives the rate of RN migration away from the source areas. Furthermore, including gradients allows the model to maintain realistic flows if the absolute value of water levels cannot be matched but gradients can be matched. The steady-state water-level data and gradient well pairs are presented in Figure 4-4. The blue arrows in Figure 4-4 illustrate the location of each gradient well pair.

4.2.4.2 ER-6-1-2 MWAT Pumping Responses

The ER-6-1-2 MWAT took place from February 5 to July 23, 2004, and included well development and step-drawdown testing, a 9-day constant-rate test, and a 90-day constant-rate test (SNJV, 2005). Withdrawals totaled about 75 million gal. As part of model evaluation data collection activities (Section 2.6), Halford and Jackson (2019) performed reanalysis of ER-6-2-1 MWAT to estimate groundwater flow through the Yucca Flat sub-basin. Water-level drawdowns in 13 observation wells were estimated (Table 2-9). Halford and Jackson (2019) used water-level models to estimate drawdowns in eight wells with continuous water-level data.

Drawdowns were detected in six of eight observation wells within the LCA of Yucca Flat. Drawdowns were detected in eastern Yucca Flat but were not detected in western Yucca Flat. The response in ER-7-1, which is aligned with ER-6-1-2 along the longitudinal axis of the faults, was prompt and substantial. The response at ER-3-1, which is closest to the pumped well but located transverse to the fault direction, was delayed and smaller compared to other wells in the eastern Yucca Flat. The drawdowns at UE-7nS and U-3cn-5 are of similar magnitude as those at ER-7-1. Well UE-1h did not show any response to pumpage at ER-6-1-2, possibly because several major faults with substantial offsets act as hydraulic barriers separating Wells UE-1h and ER-6-1-2.

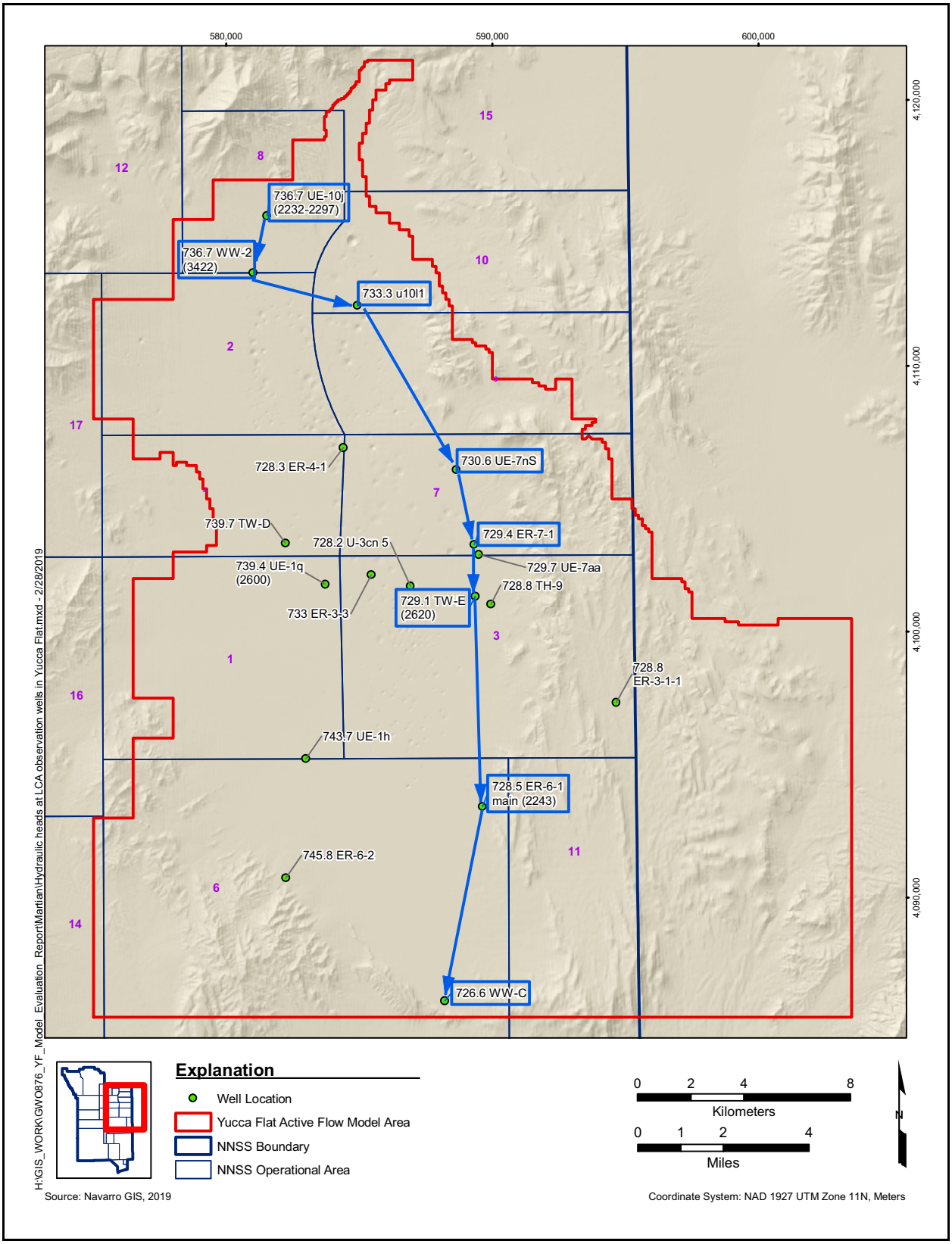

Figure 4-4
Hydraulic Heads at LCA Observation Wells in Yucca Flat

The estimated drawdowns or absence of pumping stress responses were used as observations in the LCA model calibration. The water-level models provide a total of 360 observations at 8 wells within the LCA model domain. Figure 2-19 illustrates the locations of observation wells that were evaluated for possible responses to the ER-6-1-2 MWAT, and Figure 4-5 illustrates drawdowns used for the LCA model calibration.

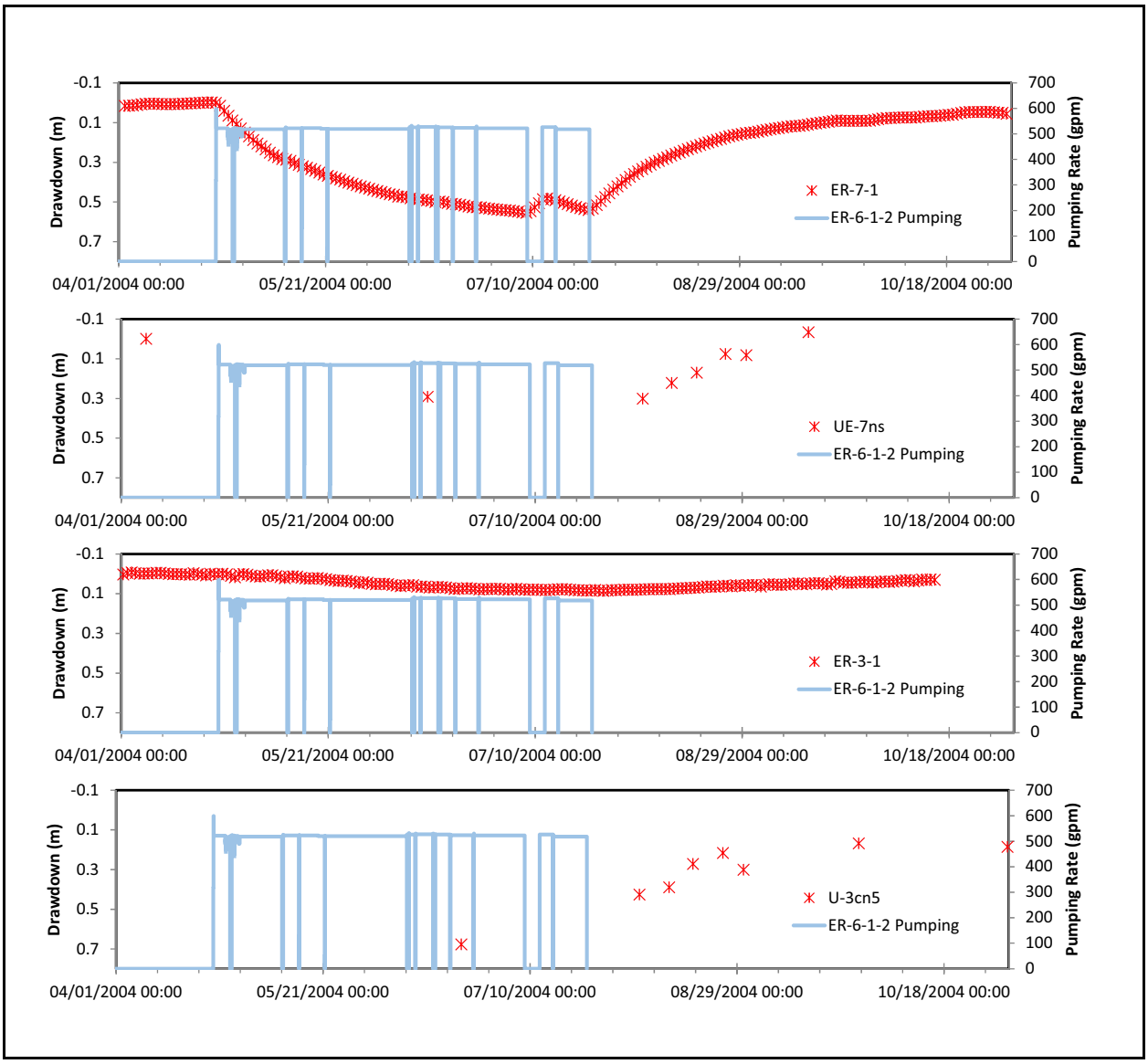

Figure 4-5
ER-6-1-2 MWAT Estimated Drawdowns for Wells ER-7-1, UE-7nS, ER-3-1-2, and U-3cn-5

4.2.4.3 ER-4-1 WDT Pumping Responses

The WDT at ER-4-1 began on January 13 and ended on February 17, 2017. A network of 17 pumping, observation, and background wells were monitored continuously (Figure 2-18). Observation wells were monitored for potential drawdowns related to the ER-4-1 m1 WDT. Similar to the ER-6-1-2 MWAT reanalysis, Jackson (2017) used water-level models to estimate drawdowns in the monitored wells. Drawdown was detected in 6 of the 17 wells. Drawdowns were detected at wells to the north and southeast, and no drawdowns were detected south or southwest of ER-4-1 (Section 2.5, Table 2-8). These results suggest that the Topgallant fault may be a barrier to drawdown propagation and that the Yucca fault may function as a leaky barrier.

As was done with the ER-6-1-2 MWAT responses, the estimated drawdowns or non-responses were used as observations in the LCA model calibration. The water-level models provide a total of 1,000 observations at 12 wells within the LCA model domain. Figure 4-6 illustrates the locations of observation wells that were evaluated for possible responses to the ER-4-1 WDT, and Figure 4-7 illustrates drawdowns used for model calibration.

4.2.4.4 Transmissivity Measurements

The pilot point model parameterization method allows including transmissivity observation data in the LCA model calibration. Transmissivity has been estimated from aquifer tests in 11 wells located within the Yucca Flat LCA and was used as observations in the model calibration. Observation weights considered volume of water extracted during aquifer testing and magnitude of the estimated transmissivity value. The conversion of transmissivity to hydraulic conductivity simply uses well screen length.

Discerning spatial trends in LCA transmissivity is difficult because there are few estimated transmissivity values, and nearby estimated values can be vastly different. For example, Wells WW-C and WW C-1 are spatially separated by less than 100 ft and may be considered a single location within the spatial discretization of the LCA model. In terms of well construction, both wells are open to the LCA over an interval of approximately 350 ft. However, the response to pumping in these wells was very different. At WW C-1, a short (4-hour) pump test conducted at a pumping rate of 293 gpm produced a 56.9-ft drawdown. In contrast a 1.3-hour pump test conducted at a pumping rate of 459 gpm in WW-C produced only 0.6 ft of drawdown. The differences in transmissivity at nearby

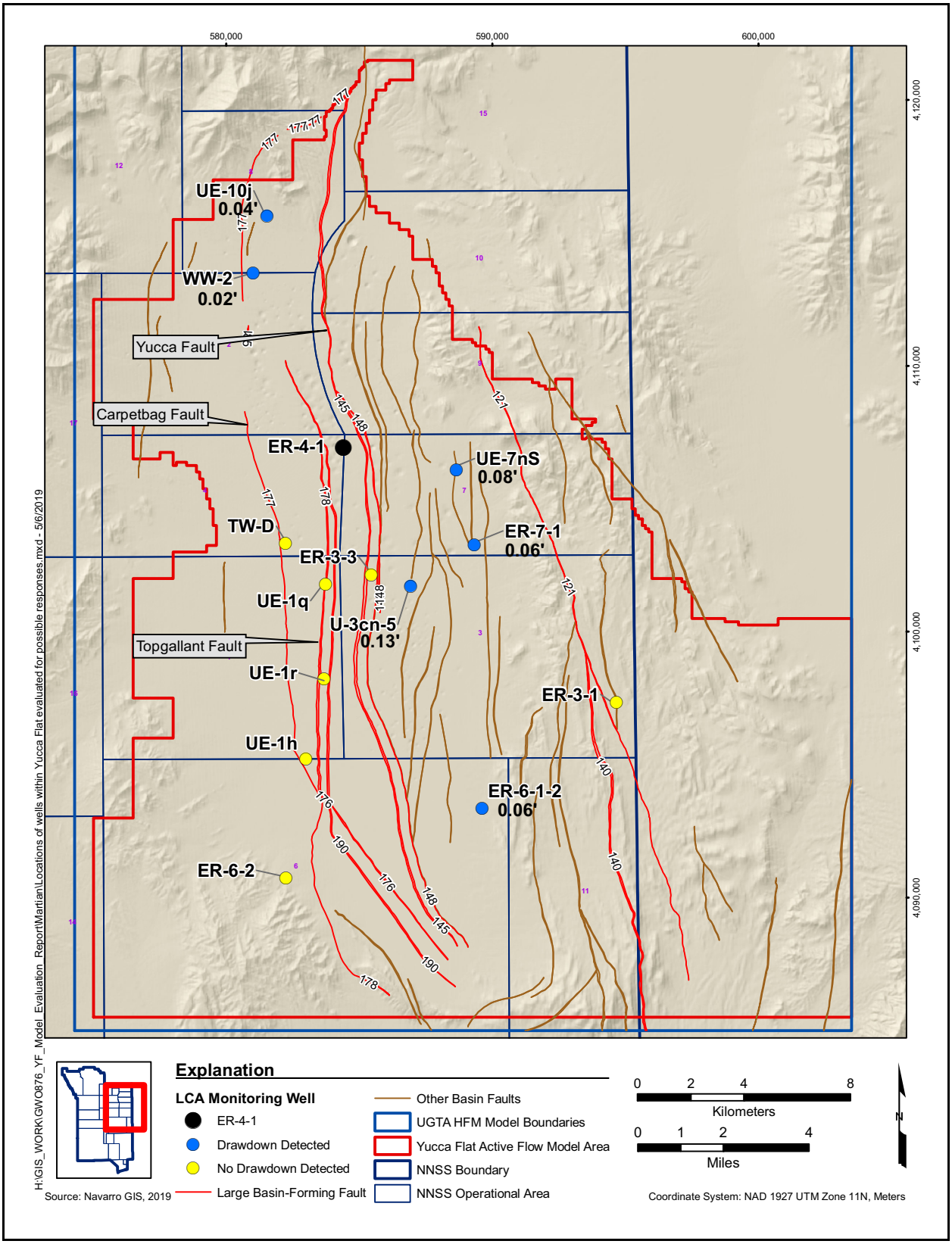

Figure 4-6
Locations of Wells within Yucca Flat Evaluated for Possible Responses to the ER-4-1 WDT Pumping

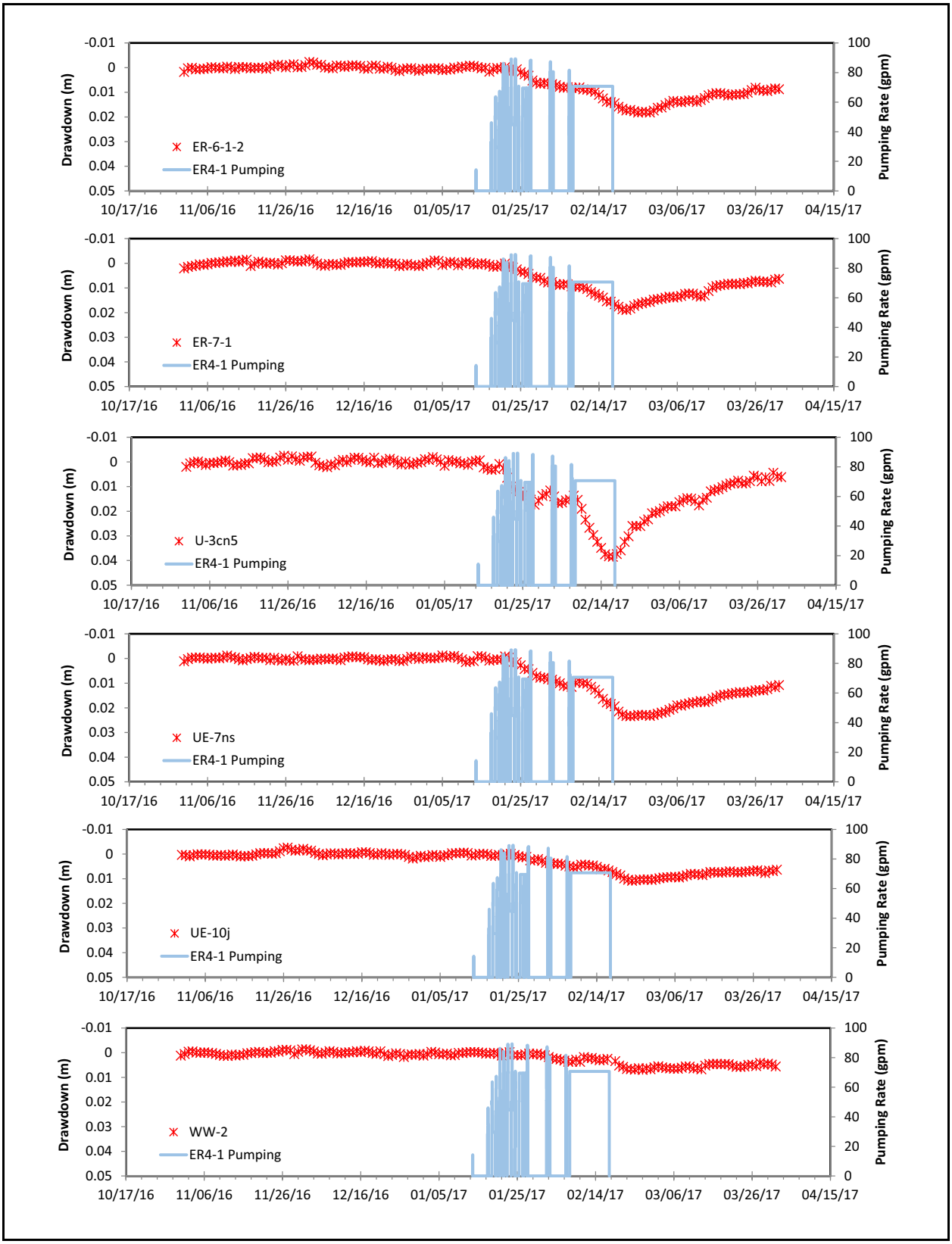

Figure 4-7
ER-4-1-2 WDT Estimated Drawdowns for Wells ER-6-1-2, ER-7-1, U-3cn-5, UE-7nS, and WW-2

wells likely reflect local variation in the formation, with larger values reflecting more fractured or faulted material and the lower values representing the country-rock.

Nonetheless, the highest transitivity measurements most often coincide with the potentiometric trough near or east of the Yucca fault hypothesized by Fenelon et al. (2012). Transmissivity is highest in southeastern Yucca Flat. Wells WW-C and ER-6-1 have the highest estimated transmissivity values, and estimated values exceed 400,000 ft^2/day (Jackson and Halford, 2019). Estimated transmissivities tend to be lower in the western Yucca Flat. Estimated transmissivities in Wells TW-D and UE-2ce are less than 10 ft^2/day (Jackson and Halford, 2019). Figure 4-8 illustrates the transmissivity observation locations and values with symbol size scaled by the logarithm of transmissivity.

The LCA transmissivity data are considered to be less certain compared to other types of observations used in the LCA model calibration. The increased uncertainty is due to the unknown aquifer thickness contributing to production during aquifer tests and because transmissivity measurements can be very different between wells within close proximity of one another.

4.2.4.5 Transmissivity Width Product Flux

Groundwater flow was estimated between Wells ER-7-1 and ER-6-1-2 main as part of formalizing the ER-6-1-2 MWAT reanalysis (Section 2.6). The majority of flow through the nuclear testing areas likely passes through a corridor of transmissive carbonate rocks between Wells ER-7-1 and ER-6-1-2, and the total groundwater flow is likely less than 600 acre-ft/yr. A 20 kg/s (~500 acre-ft/year) flow observation between Wells ER-6-1-2 and ER-7-1 was used as a observation in the LCA model calibration. The simulated flow observation was implemented as the flow rate passing through a west–east line of 7.6-km length midway between Wells ER-6-1-2 and ER-7-1.

4.2.4.6 Objective Function Formulation

The LCA model objective function included the following observations groups: (1) steady-state heads, (2) steady-state gradients aligned along the general flow direction, (3) drawdown responses to the ER-4-1 WDT and ER-6-1-2 MWAT pumping, (4) the groundwater flow rate in eastern Yucca Flat estimated by the DV3 model, and (5) transmissivity measurements.

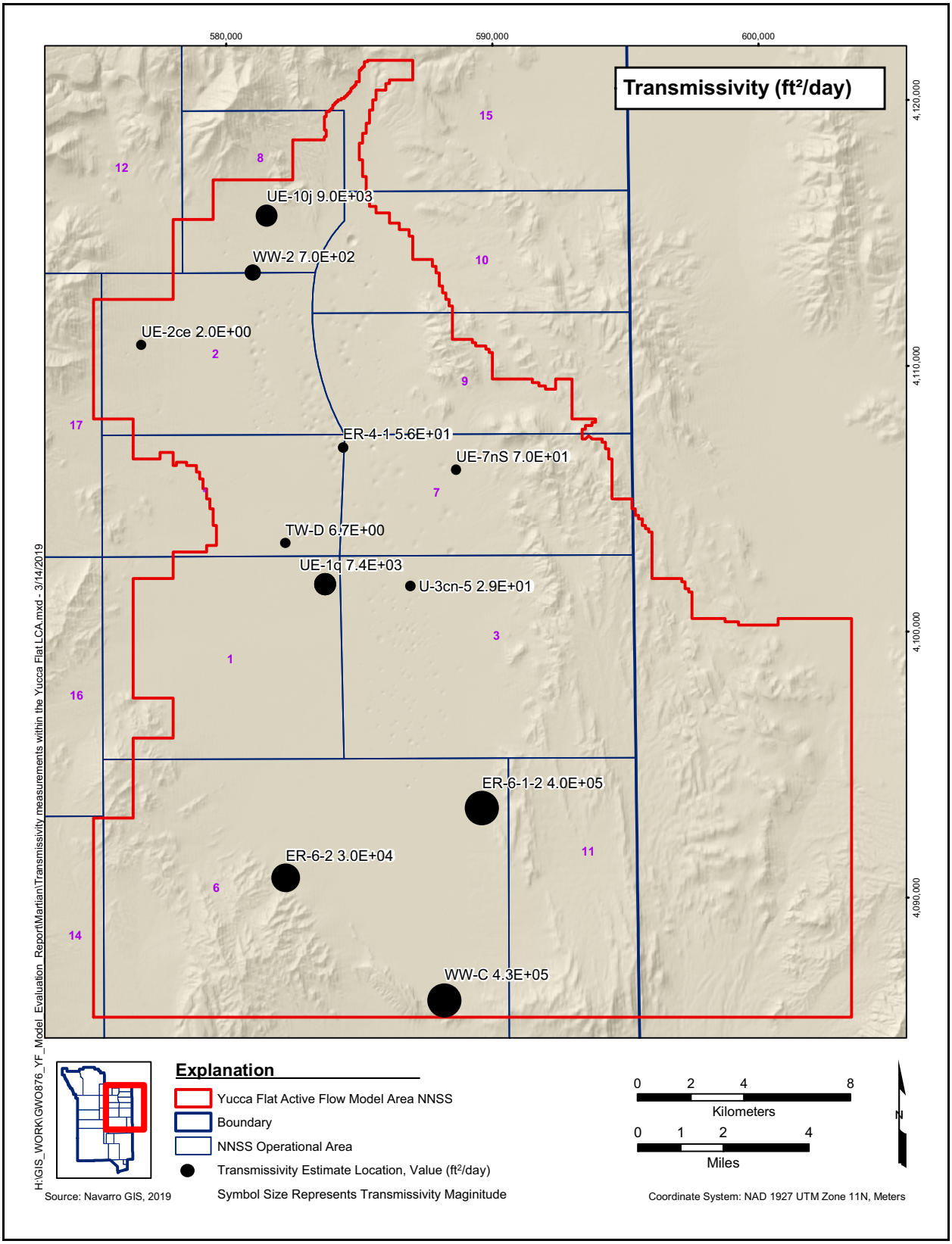

Figure 4-8
Transmissivity Measurements within the Yucca Flat LCA

The calibration observation weights were selected such that each observation group is visible in the objective function. More emphasis was placed on the most certain and informative observations to transport. The objective function observation weights consider the following: the number and magnitude of observations, uncertainty, and value of information provided to transport calculations. Most emphasis was placed on the steady-state heads, gradients, and the flow rate through eastern Yucca Flat. The second-most emphasis was placed on the ER-4-1 MWAT responses. Both of these observation groups are considered highly reliable and informative to the CAU model, with the steady-state heads and gradient being the most informative because the gradient drives the rate of RN migration away from the source areas. The flux through the high-permeability corridor in eastern Yucca Flat estimated from DV3 model flow between Wells ER-7-1 and ER-6-1 is also considered highly reliable and informative to the CAU model.

Although the ER-6-1-2 MWAT responses are informative to the CAU model because of the large area of the LCA that experienced drawdown, the drawdowns simulated by the model are less reliable because the drawdown was observed to occur beyond the model's southern boundary while the model has a steady-state prescribed head at the southern boundary, which does not allow accurate simulation of the LCA response to pumping. Transmissivity values simulated by the model are also less reliable because aquifer thickness seen by the pump testing is uncertain and transmissivity measurements have considerable variability in nearby locations. The LCA thickness greatly exceeds the well screen thicknesses at the pumped wells, and the total model transmissivity at each well location can be considerably higher than the observations.

Several model calibrations were attempted during the LCA model refinement work, and the weights were adjusted iteratively to ensure observations remained visible in the objective function. The adjustment of weights largely consisted of moderately increasing the weights for the observations that did not have good agreement with the model. Observation weights were not adjusted during any single calibration attempt. The Yucca Flat LCA model is highly parameterized, and the calibration objective function likely has many local minima. Increasing the weights for model observations that did not achieve good agreement during preliminary calibration attempts forced PEST to further explore parameter solution space and find a better global minimum.

4.2.5 Calibration Results

The PEST model run cycle consisted of three FEHM simulations. The first was a steady-state FEHM run that provided the initial conditions for the subsequent transient pumping simulations of the ER-6-1-2 MWAT and ER-4-1 WDT. PEST was invoked to optimize parameters that minimize the objective function. These three model runs were performed for each PEST iteration, and all adjustable hydrogeologic parameters remained the same for steady-state and transient model runs.

4.2.5.1 Agreement with Observations

Agreement with observation data was evaluated with scatter plots, maps of residuals (simulated minus measured), water-level profiles, hydrographs, and hydraulic-property distributions. Good agreement was achieved with most observations. Table 4-1 lists each observation group's contributions to the objective function and the RMS error.

Table 4-1
Observation Group Contribution to the Measurement Objective Function and RMS Error for the Base Case

Observation Group	Objective Function	RMS Error	RMS Error Units
Steady-State Heads	2.7E+02	1.2E+00	m
ER-6-1-2 MWAT	8.9E+01	4.6E-02	m
ER-4-1 WDT	1.7E+02	1.5E-03	m
Steady-State Gradient	7.0E+00	6.9E-05	m/m
Transmissivity	8.5E+01	8.7E-01	Log10 m^2/day
DV3 Flow between ER-7-1 and ER-6-1	1.6E-01	N/A	N/A
Total	620.9	N/A	N/A

The relative contributions of each observation group to the overall objective function mostly reflect the relative observation group weights. Although the observation of groundwater flow in eastern Yucca Flat contributes a small amount to the final objective function, the uncalibrated initial contribution was comparable to the initial steady-state head observation weight contribution. The small contribution to the final objective function is because the model was able to nearly identically match the observation value.

4.2.5.1.1 Steady-State Head and Gradient

The calibrated LCA potentiometric surface with residuals defined as the model value less the measured value is presented in Figure 4-9. A scatter plot of the simulated versus observed heads at the 17 observation wells is presented in Figure 4-10. The water level in Well ER-4-1 is anomalously low compared to the surrounding wells. The predicted water level was 739.5 m before drilling, and the observed water was 728.4 m (DOE/EMNV, 2017c). The observed water level is also lower than the approximately 731-m potentiometric surface estimated by Fenelon et al. (2012). There is a cold trough in the center of the basin coinciding with the Yucca, Topgallant, and Carpetbag faults (Reiner, 2007; N-I, 2013). The groundwater temperatures in the center of the basin are 10 to 30 degrees Celsius colder than the temperatures on the east and west of basin. Elevated water column temperatures affect the water levels by decreasing the density of the column of water in the well and, thus for a given bottom hole pressure, the water level in the well with the higher temperature will be greater than the water level in the well with the lower temperature. Well ER-4-1 is located in the center of the cold trough, and temperature effects may explain the anomalously low water level in this well. There are insufficient data to correct the water level measured in this well, Hence, the water level in Well ER-4-1 was considered less certain than the other steady-state heads, and the observation weight was reduced compared to the other steady-state head weights. The coefficient of determination (R^2) value is 0.95 and 0.99 including and excluding the water level from Well ER-4-1, respectively.

The well pairs selected as gradient observations include only wells located within the high-transmissivity corridor in eastern Yucca Flat and aligned with the general north–south gradient. The agreement between simulated and observed steady-state heads is very good; hence, the agreement between simulated and observed gradients is also very good. The north–south hydraulic gradient in eastern Yucca Flat between Wells WW-2 and WW-C is 4E-04, and the average RMS error for the gradient observations was 7E-05. Figure 4-11 illustrates the simulated and observed steady-state water-level profiles in western and eastern Yucca Flat.

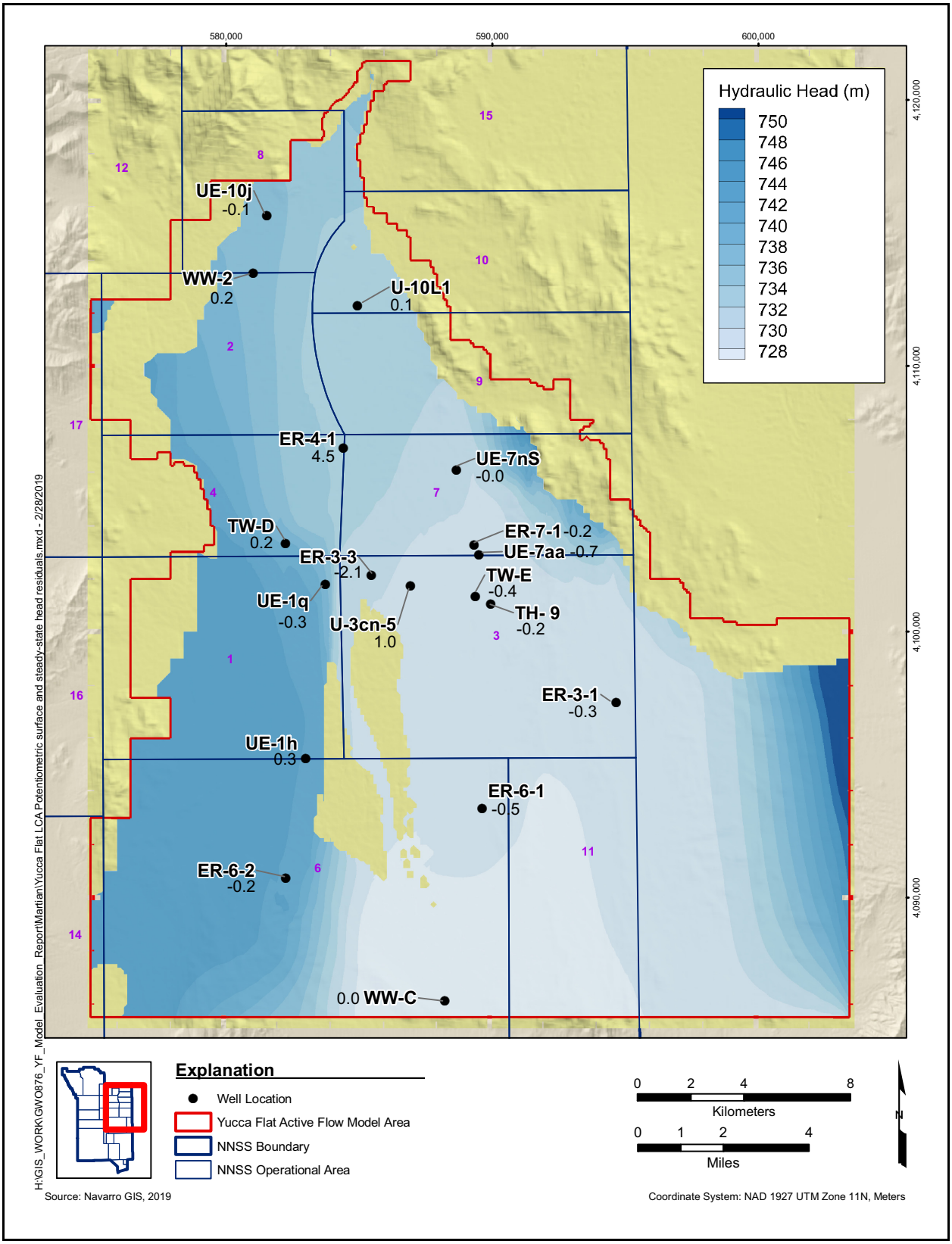

Figure 4-9
Yucca Flat LCA Potentiometric Surface and Steady-State Head Residuals for the Base Case Flow Field

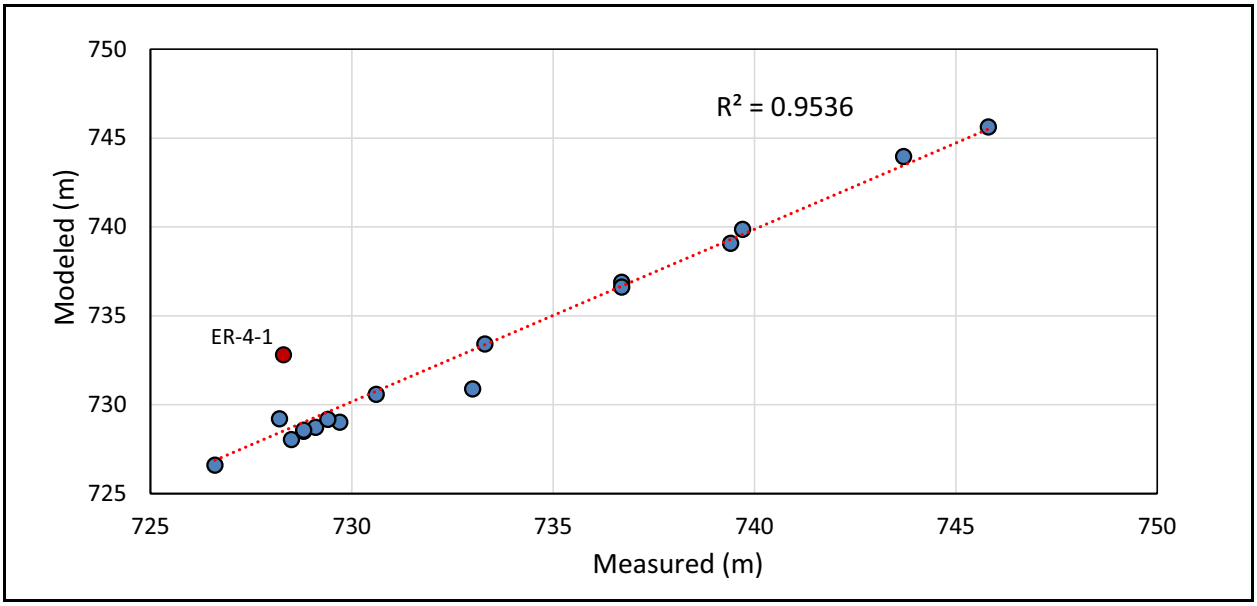

Figure 4-10
Modeled versus Measured Steady-State Heads for the Base Case Flow Field

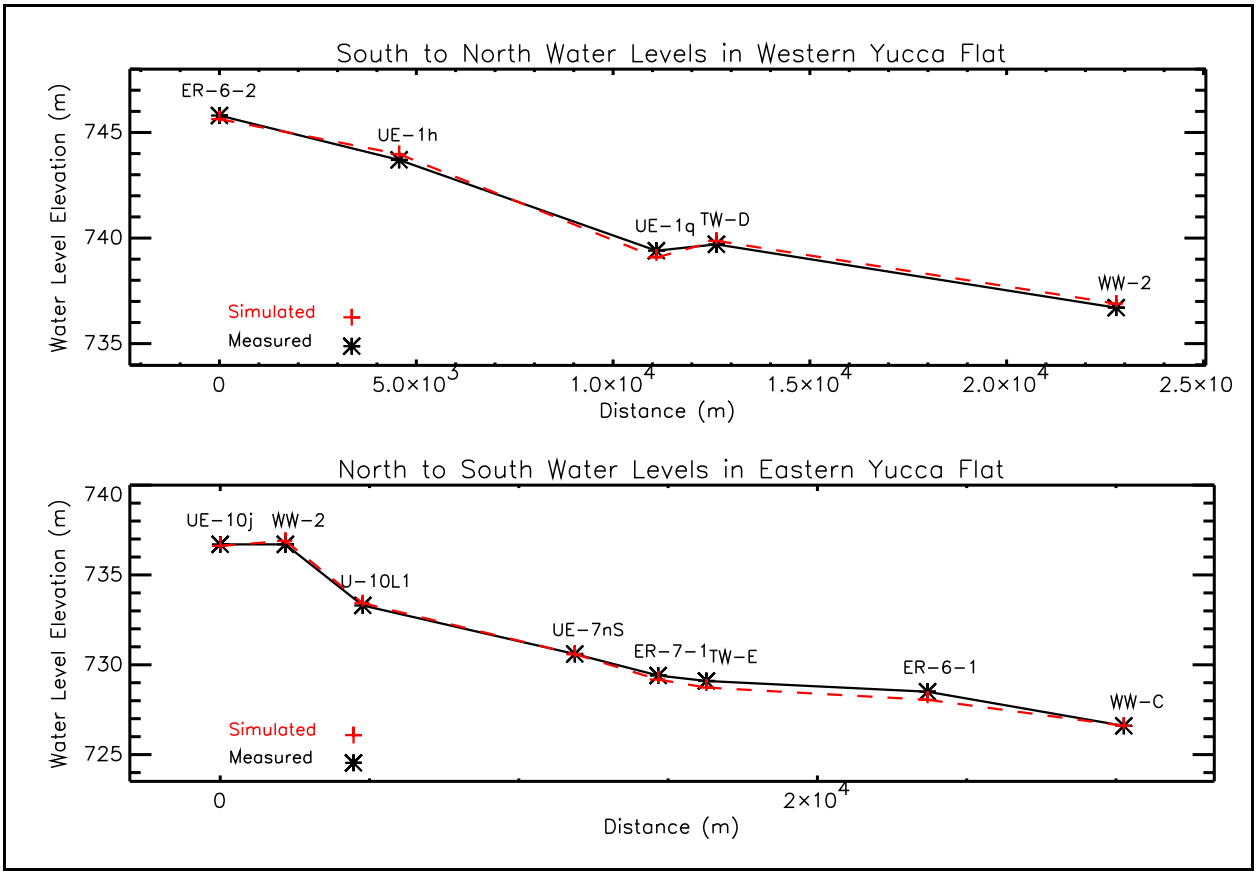

Figure 4-11
Western and Eastern Yucca Flat Water-Level Profiles for the Base Case Flow Field

4.2.5.1.2 ER-6-1-2 MWAT and ER-4-1 WDT Responses

The observed and simulated drawdowns for the wells that responded to the ER-6-2-1 MWAT and ER-4-1 WDT are presented in Figures 4-12 and 4-13, respectively. Good agreement with the observations was achieved with the drawdowns for both pumping tests. Although not presented in Figures 4-12 and 4-13, the simulated drawdowns at wells that did not respond to the pumping stress were negligible, and good agreement was achieved with both responding and non-responding wells. The model was able to replicate the apparent hydraulic isolation of the LCA in western Yucca Flat seen in the ER-6-1-2 MWAT and ER-4-1 WDT responses by introducing a strong east–west to north–south anisotropy of Topgallant fault, thereby making the fault a barrier to cross-flow.

Figures 4-14 and 4-15 present the scatter plots of modeled versus measured drawdowns for the ER-4-1 WDT and ER-6-1-2 MWAT pumping, respectively. The R^2 value is 0.95 and 0.96 for the ER-4-1 and ER-6-1-2 responses, respectively.

4.2.5.1.3 Transmissivity

The calibrated LCA model's transmissivity field is presented in Figure 4-16 along with the estimated values. Generally, simulated transmissivity at estimation locations was within 2 orders of magnitude of estimations. The RMS error of the log transmissivity was 1.9 ft^2/day. The large RMS error for the transmissivity observation group compared to other observation groups reflects the low weights assigned to transmissivity estimations and high uncertainty. The uncertainty is high because the well screens represent only a small fraction of the entire LCA thickness, and the aquifer thickness contributing to the pump test is unknown. Typically, well screen thickness is 100 m or less, yet the LCA model thickness is approximately 5 km in the deepest areas. The most significant hydrologic features are a high-transmissivity corridor in eastern Yucca Flat and a barrier behavior of the Topgallant fault, which hydraulically isolates western Yucca Flat from the ER-4-1 WDT and ER-6-1-2 MWAT pumping.

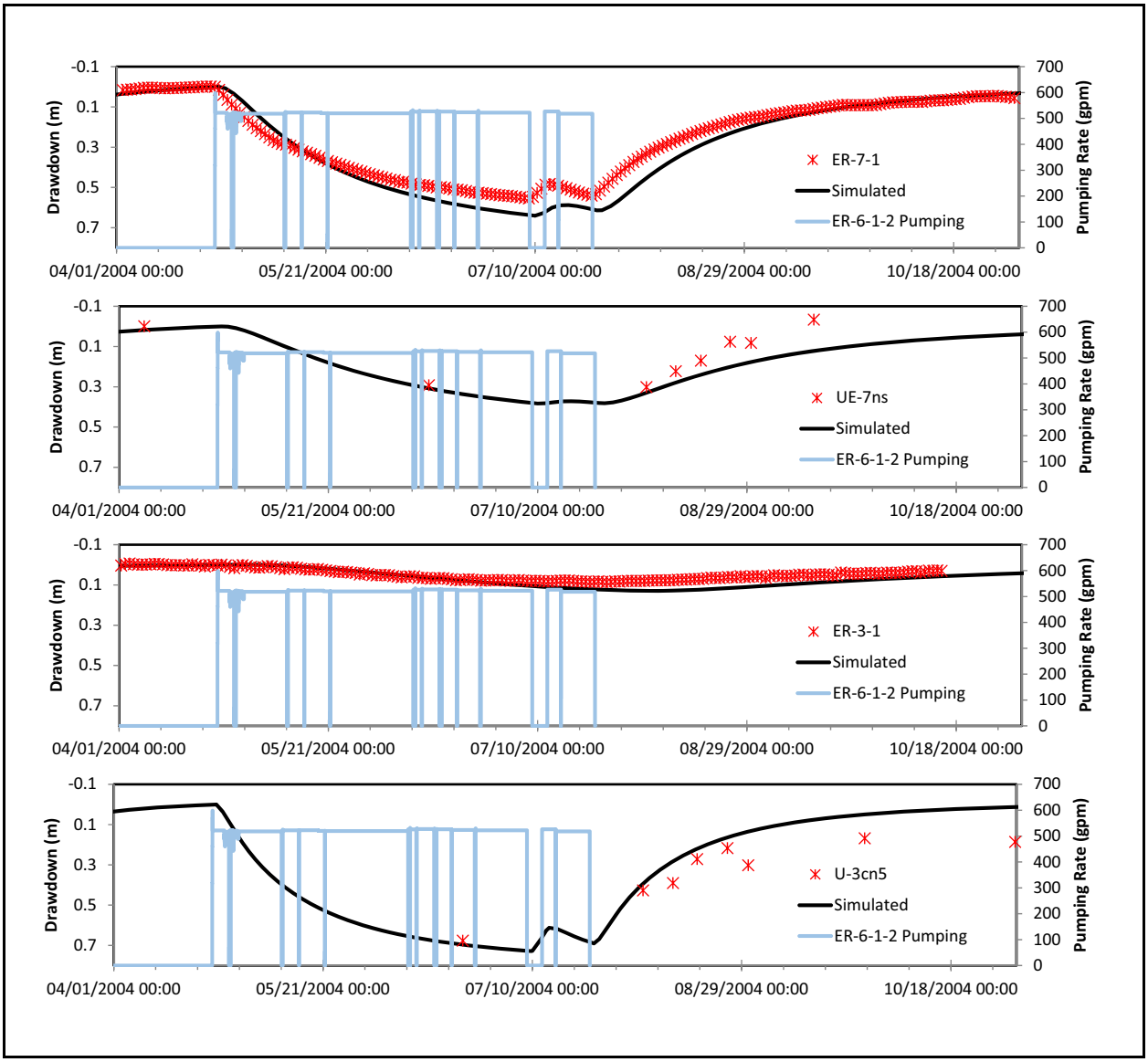

Figure 4-12
Simulated and Observed Drawdown Hydrographs at the Responding ER-6-1-2 MWAT Wells for the Base Case Flow Field

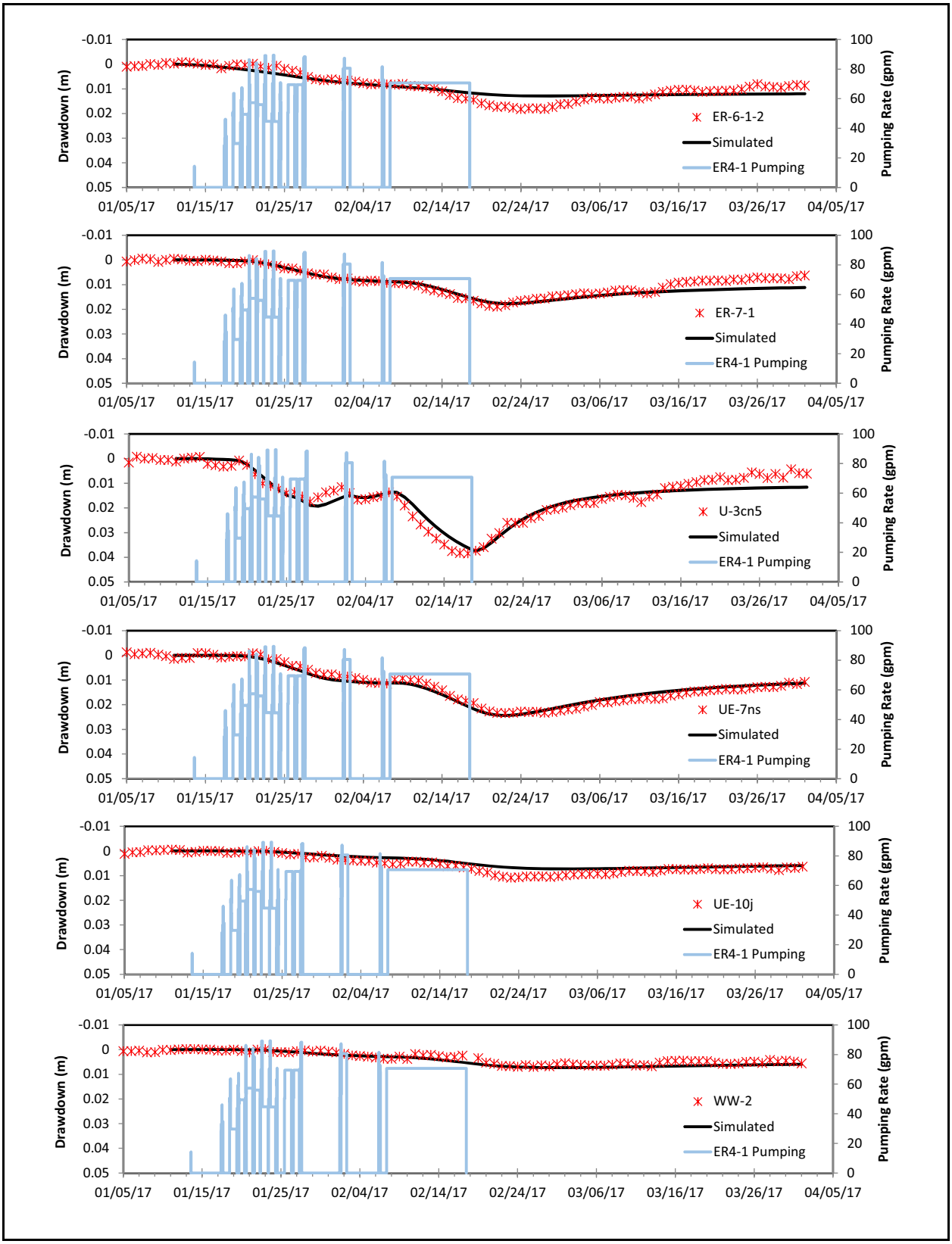

Figure 4-13
Simulated and Observed Drawdown Hydrographs at the Responding ER-4-1 WDT Wells for the Base Case Flow Field

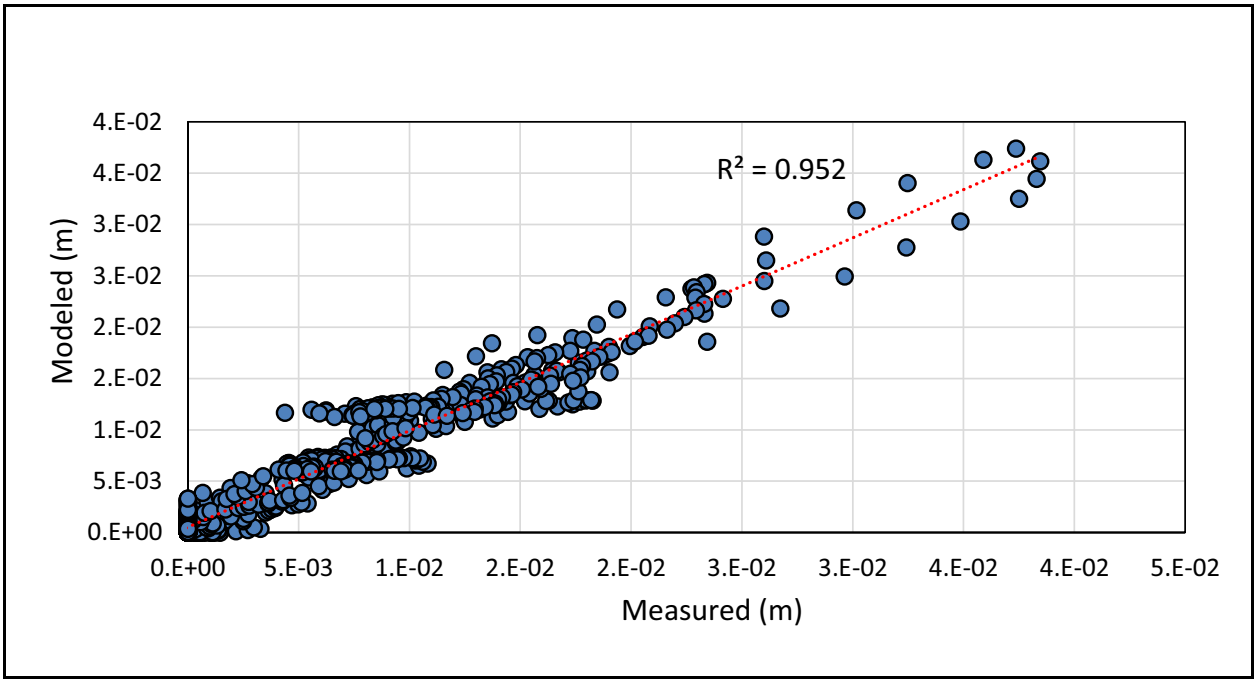

Figure 4-14
Modeled versus Measured ER-4-1 WDT Drawdowns for the Base Case Flow Field

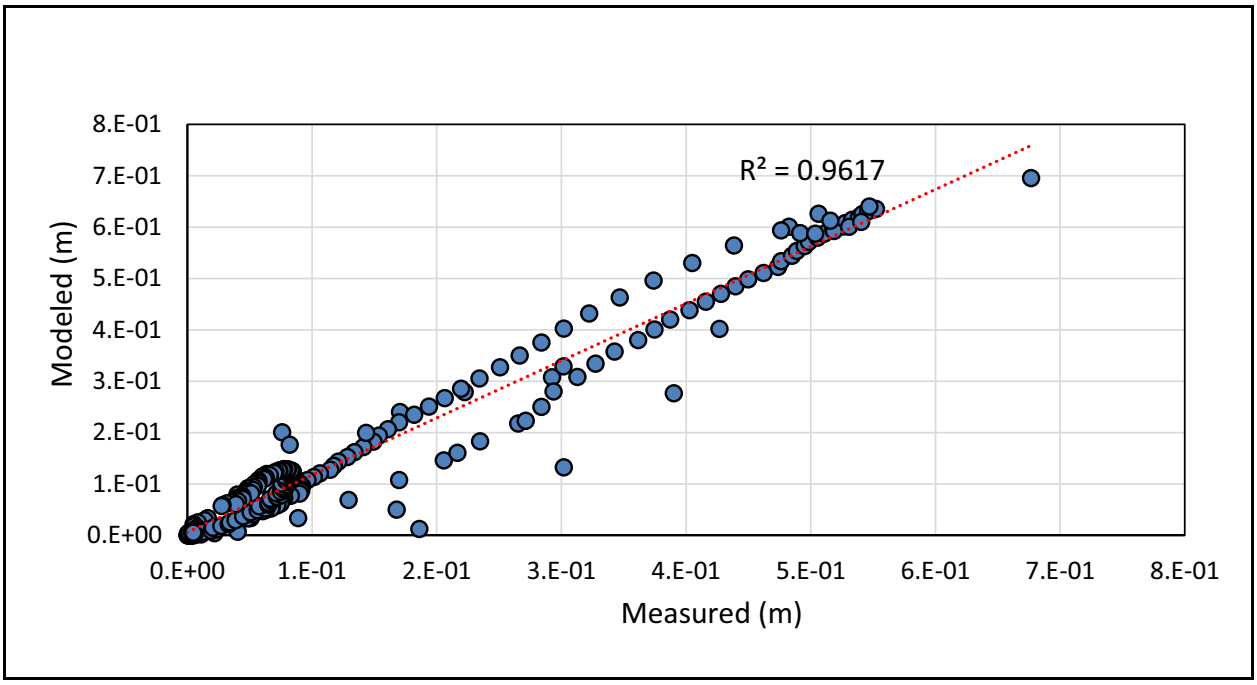

Figure 4-15
Modeled versus Measured ER-6-1-2 MWAT Drawdowns for the Base Case Flow Field

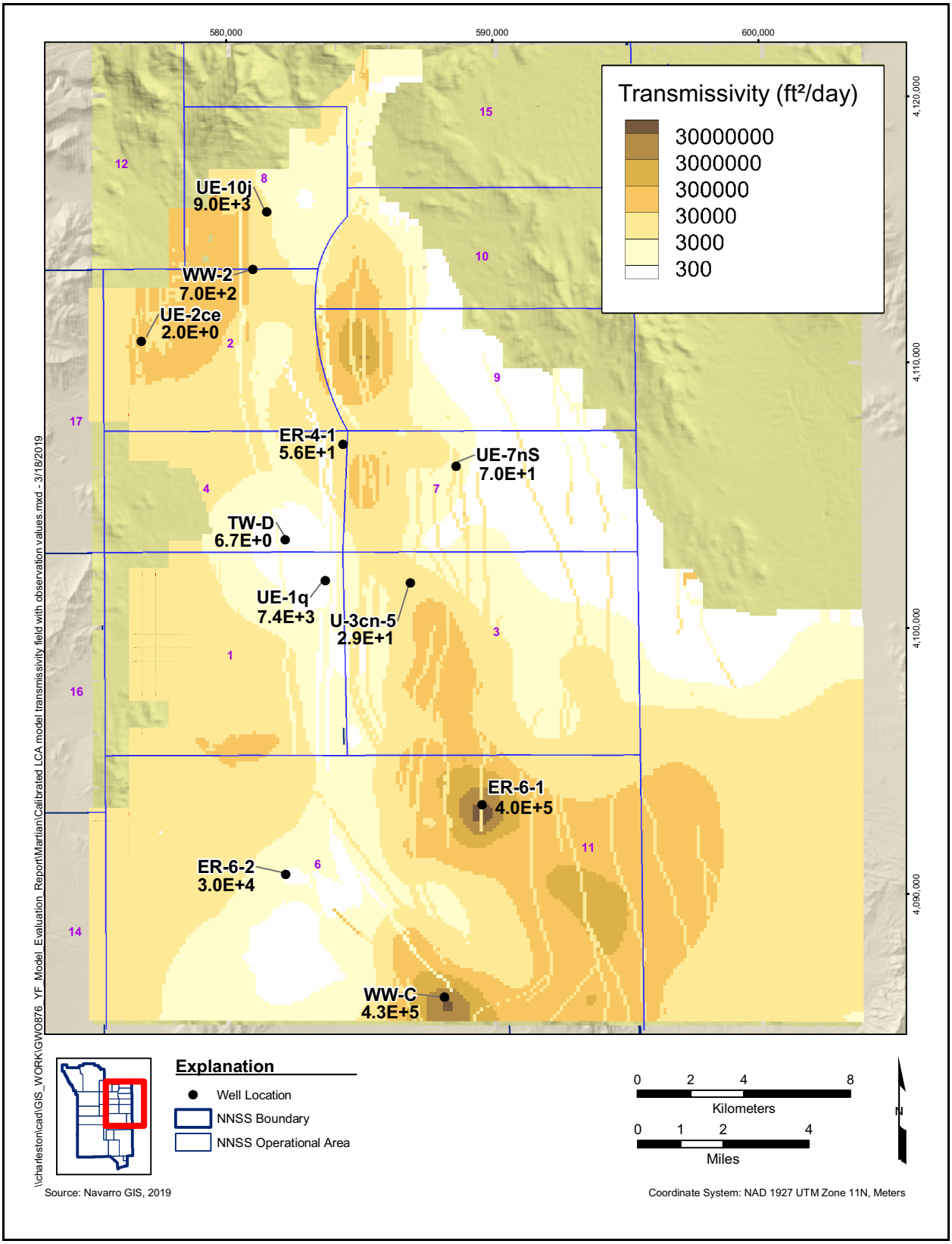

Figure 4-16
Calibrated LCA Model Transmissivity Field with Observation Values for the Base Case Flow Field

4.2.5.2 Calibrated Model Parameters

The LCA model calibration parameters are hydraulic conductivity, anisotropy, specific storage for the faults and country rock, and boundary fluxes. Country rock hydraulic properties were calibrated using pilot points. Fault hydraulic properties were calibrated with zonation, and the fault hydrologic barrier effect to cross-flow was calibrated with an east–west to north–south fault anisotropy factor.

As discussed in Section 4.2.1, the LCA model calibration is an ill-posed inverse problem and will not have a unique parameter estimation solution. Because the calibration problem is non-unique, some model parameters will not be completely identifiable. Associated with the singular value decomposition performed by the PEST software to calculate super parameters, a parameter identifiability index can be calculated, which identifies the parameters that can be estimated during the inverse modeling process. Identifiability ranges between 0 and 1, with parameters having an identifiability index of 1 being fully identifiable and parameters having an identifiability index of 0 being totally unidentifiable.

The parameter identifiability index for each Yucca Flat LCA flow model parameter is presented in Figure 4-17A. A total of 12 parameters have an identifiability greater than 0.8 and are highly identifiable. Figure 4-17B presents the model parameters that have an identifiability greater than 0.5, and a total of 28 parameters have an identifiability index greater than 0.5. The following parameters and their identifiability values are notable: (1) Topgallant fault (190_topgalla) is highly identifiable as behaving as hydraulic barrier (i.e., low permeability and strong east–west to north–south anisotropy); (2) country rock is highly identifiable as having a strong east–west to north–south anisotropy (lcahaniso); (3) the lateral flux (cwflux) is highly identifiable as being larger in the model's northern half of the western boundary; and (4) fault permeability in eastern Yucca Flat (114_yf_91bn1) is highly identifiable. The permeability of the Yucca fault was not among the highly identifiable parameters; the identifiability index was 0.24 and 0.02 for the western and eastern branches, respectively, implying that a large range of values could calibrate the model equally well. The low identifiability for the Yucca fault is noteworthy, because the permeability of the Yucca fault was the most highly correlated model parameter to particle breakthrough near the model's southern boundary in the N-I (2013) NSMC analysis.

Figure 4-18 presents the identifiability index for country rock hydraulic conductivity and specific storage pilot points. Within the region of the ER-4-1 WDT and ER-6-1-2 MWAT pumping-test

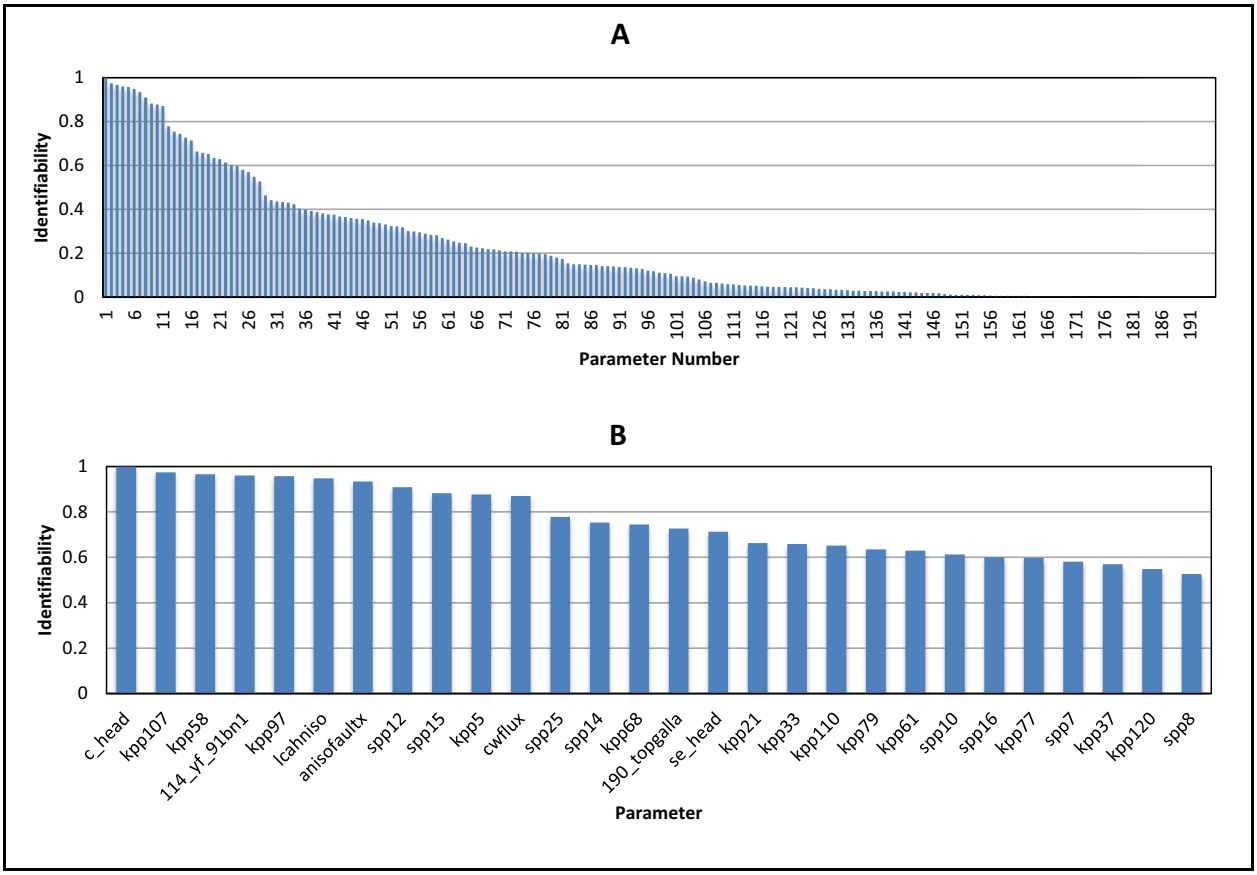

Figure 4-17
Identifiability Index for Independent Parameters: (A) All Parameters and (B) Parameters with Identifiability Index Greater than or Equal to 0.5 for the Base Case Flow Field

influence, the identifiability of pilot points is the highest. The identifiability of pilot points in the area of the ER-4-1 WDT response is higher than those within the area of the ER-6-1-2 MWAT pumping response, because the area of ER-6-1-2 responses overlaps the ER-4-1 area of response, and both pump tests inform the model parameters. Outside these regions, the pilot points have lower identifiability, with the exception of the locations of steady-state water level and transmissivity observations (e.g., WW-C, ER-6-2, UE-2ce, and UE-10j well locations).

The distribution of pilot point LCA hydraulic conductivity is presented in Figure 4-19. The median value is 0.84 ft/day, which is similar to the geometric mean of 3 ft/day from the Yucca Flat hydrologic data summary (SNJV, 2006b) for LCA hydraulic conductivity data and to the distribution of hydraulic conductivity for Yucca Flat plotted in Figure 3-3. The calibrated fault permeability and anisotropy values are presented in Table 4-2. The fault permeability is similar to the median pilot point permeability. Although the faults have a similar permeability to country rock, faults provide hydraulic

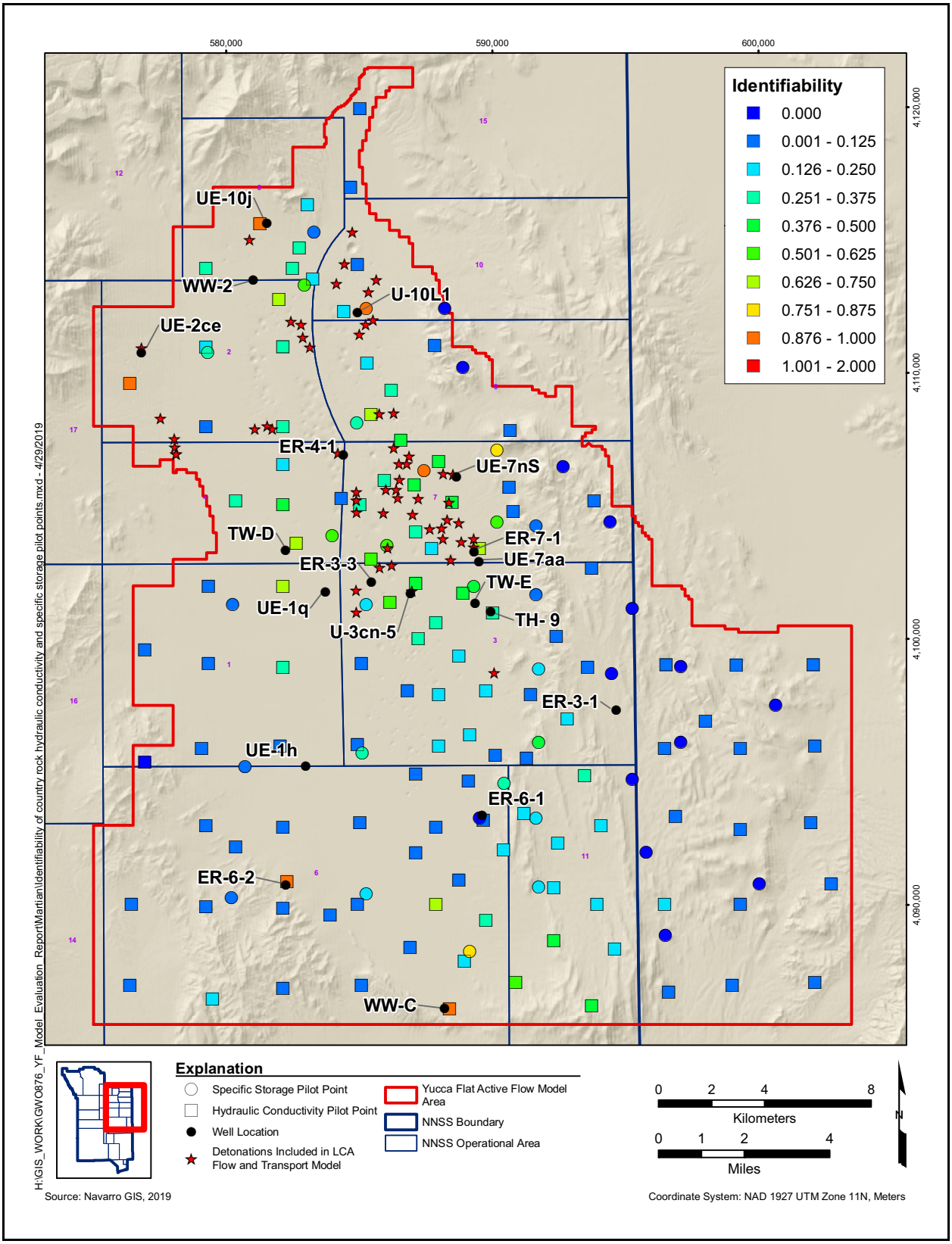

Figure 4-18
Identifiability of Country Rock Hydraulic Conductivity and Specific Storage Pilot Points for the Base Case Flow Field

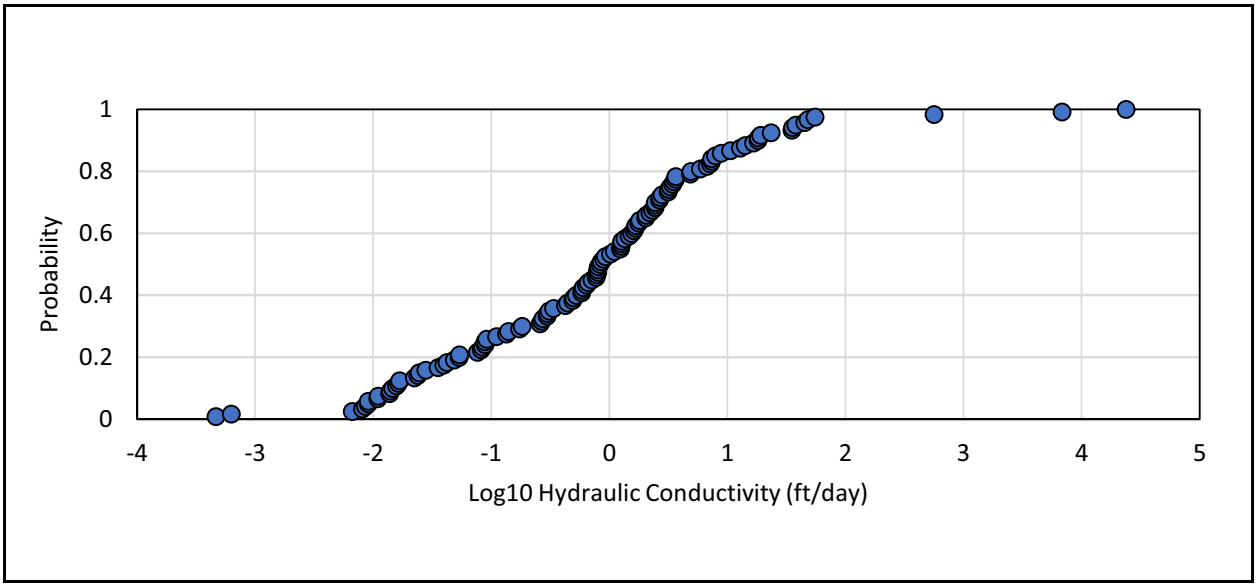

Figure 4-19
Cumulative Distribution Function of Calibrated Country Rock Pilot Point Hydraulic Conductivity for the Base Case Flow Field

Table 4-2
Calibrated Fault Permeability and Anisotropy for the Base Case Flow Field

Fault	Model Parameter	Permeability (m^2)	Hydraulic Conductivity (ft/day)	East–West to North–South Anisotropy
Tied Eastern	114_yf_91bn1	7.16E-13	6.50	1.00
Tied Western	175_yf_26egh	4.81E-13	4.37	1.00
Yucca Fault Western Branch	145_yf1	1.35E-13	1.22	1.00
Yucca Fault Eastern Branch	148_yf2	1.31E-13	1.19	1.00
Carpetbag Fault Eastern Branch	176_yf_50b	2.05E-13	1.87	1.00
Carpetbag Fault Western Branch	177_carpetba	5.46E-14	0.50	5.12E-01
Topgallant Fault Western Branch	178_topgalla	1E-14	0.09	1.19E-03
Topgallant Fault Eastern Branch	190_topgalla	1E-14	0.09	1.36E-02
Fault 121	121_hp40	4.16E-13	3.78	1.00
Fault 140	140_hp50_yf1	5.92E-13	5.38	1.00
Country Rock Pilot Point Geometric Average	KPP [a]	8.54E-13	0.72	1.55E-01

[a] KPP refers to country pilot point model parameters. There are 120 parameters (kpp1–kpp120).

connections through regions of very low hydraulic conductivity and also a behave as barriers to cross-flow in regions of very high hydraulic conductivity. The model calibration produced moderate to strong east–west to north–south anisotropy in Topgallant and Carpetbag faults, and in the country rock. The calibrated anisotropy values are consistent with the large-scale extensional faulting that has occurred in the Yucca Flat area. The major basin-forming faults generally strike in a northerly direction (e.g., Yucca, Topgallant, and Carpetbag faults). Flow properties are probably most enhanced in a direction parallel to the strike of the fault. Horizontal flow perpendicular to the strike of the fault is probably least enhanced due to the presence of the fault core material and the tendency for fractures to form parallel to the strike of the fault (Prothro et al., 2009). The conceptual model characterizes both the LCA country rock and fault zones to be fractured rock. However, the LCA fault zones are characterized as more highly fractured than the LCA country rock.

The primary hydrologic feature identified by the ER-6-1-2 MWAT reanalysis (Section 2.6) within Yucca Flat is a high-transmissivity corridor that is hydraulically connected with the Ash Meadows discharge area, which corresponds with a potentiometric trough (Sections 4.1 and 4.2.4.1). Simulated transmissivity in the high-transmissivity corridor, extending from Yucca Flat to Ash Meadows, exceeds 300,000 ft^2/day (Jackson and Halford, 2019). This feature is also present in the Yucca Flat LCA model, but the corridor is wider and hydraulic conductivity is lower than the DV3 model. During model calibration, the width of the corridor was constrained by delayed or absent responses in wells located west and east of the corridor (e.g., ER-3-1 and UE-1h) and prompt response in wells aligned with the corridor (e.g., ER-7-1 and Tracer Well 3).

Figure 4-20 compares the calibrated LCA and DV3 model transmissivity fields. The more diffuse corridor simulated by the LCA model is because the LCA model includes anisotropy and discrete fault zones, which are aligned with the corridor. These features are absent in the DV3 model. Both a high north–south to east–west anisotropy and faults allow increased drawdown in a north–south direction with a less narrow high-permeability corridor. Both models also contain higher transmissivity in the northwest of the sub-basin. The higher transmissivity in the northwest of the model results from the model needing to accommodate increased flow due to recharge without significantly increased heads. The northwest model area has a higher land surface area and increased precipitation compared to lower areas.

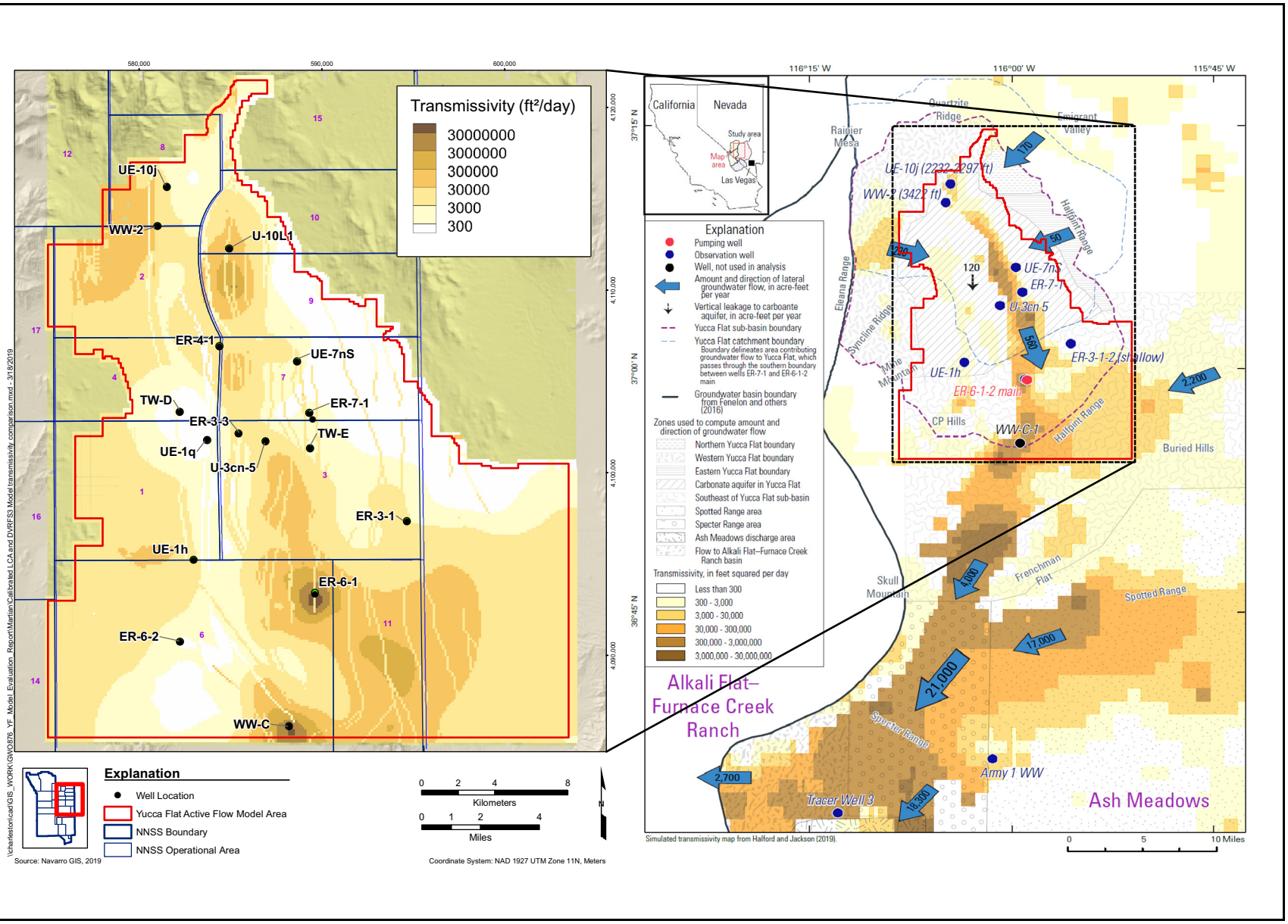

Figure 4-20
Calibrated LCA and DV3 Model Transmissivity Comparison for the Base Case Flow Field

Halford and Jackson (2019) estimated groundwater flow through the Yucca Flat sub-basin using the DV3 model. The areas contributing groundwater flow to Yucca Flat extend from Rainier Mesa to the west, the Halfpint Range to the east, and north of Quartzite Ridge (Jackson and Halford, 2019). The amount of groundwater flow in the Yucca Flat sub-basin and moving past underground nuclear testing areas was estimated to be 22 kg/s (560 acre-ft/yr). Table 4-3 presents the calibrated LCA model boundary flux values. The total flow through the Yucca Flat LCA model domain is 184 kg/s (4,700 acre-ft/yr), but the total flow through the Yucca Flat sub-basin area is approximately 25 kg/s (640 acre-ft/yr). The large difference between the total flow through the LCA model and Yucca Flat sub-basin estimated by Halford and Jackson (2019) is because the LCA model domain extends beyond Yucca Flat sub-basin in the model's southwest and southeast corners. A very large inflow occurs through the LCA model's southeast corner as well as in the same general area within the DV3 model. A similar condition exists on the LCA model's southwest corner, but the inflow is much smaller. The inflows in the LCA model's southeast and southwest corners do not flow through the underground testing area or the Yucca Flat sub-basin, and are excluded from the flow estimated by the DV3 model.

Table 4-3
Calibrated LCA Model Boundary Fluxes for the Base Case

Boundary	Calibrated LCA Model Flux (kg/s)	DV3 (kg/s)	DV3 (acre-ft/yr)
Southwest lateral[a]	3	Not provided	Not provided
Central–west lateral	14	Not provided	Not provided
Northwest lateral	1	Not provided	Not provided
West lateral total	18	8.6	220
North lateral	2	6.6	170
Halfpint range lateral	3	1.6	40
Eastern lateral[a]	150	Not provided	Not provided
Top central	1	0.6	15
Top western[a]	6	Not provided	Not provided
Top eastern	4	Not provided	Not provided
Top western[a] + top eastern	10	4.5	115
Total through Yucca Flat basin[a]	184 (25[a])	22	560

[a] Flux does not flow through the Yucca Flat testing area in the base case.

All LCA model boundary inflows reached either the lower or upper bound of permissible ranges specified during LCA model calibration. The PEST software will adjust the model parameters to values that optimize the agreement with observations, and it was not unexpected that the flux parameter end members optimized the LCA model instead of the central values. This is because the LCA model domain does not extend to an entire basin that would have zero flux boundaries, and the model is uninformed by data from areas outside the model domain. The DV3 model must provide this external information through setting the permissible range of flux values at each LCA model boundary area. The end members of the LCA model flux parameters were determined from an uncertainty analysis of the DV3 model (Section 2.6.3). The result of the optimized flux values being at the end members was that the LCA model substituted flow from the northwest for flow from the north. However, all flow originating from the north and northwest flow through the central testing area in eastern Yucca Flat before exiting in the south. The flux through the eastern Yucca Flat high-transmissivity area is slightly larger than the DV3 model, and transport from the main testing area in eastern Yucca Flat should not be underestimated.

4.2.5.3 Calibrated Model Flow Paths

Particle tracking and Darcy velocities were used to evaluate flow paths through the model domain. Figure 4-21 illustrates the resulting particle flow paths and time histories for particles placed on the LCA model's uppermost perimeter using the average matrix porosity of the LCA (0.024). As expected, groundwater flow in the eastern half of the basin is primarily southward. In the west, the flow is primarily eastward toward the major faults in the center of the basin, with some northerly flow component in the northwest areas. The northward flow results from the northwest lateral and vertical inflow needing to move around the northern end of the Topgallant fault, which acts as a flow barrier in the LCA model. Nearly all groundwater entering the northern half of the basin passes through the high-transmissivity eastern corridor before converging near WW-C at the model's southern boundary.

The Darcy velocity vectors at 0 m amsl are presented in Figure 4-22. Because the volcanic tuffs in the south–central model area extend slightly below 0 m amsl, velocity vectors are not present in two areas. Vertical flow rates in the LCA are relatively small compared to lateral flow rates, and therefore the velocity at a particular location is quite similar at any depth. Excluding the high Darcy velocities from the southeast because of the large underflow, velocities are highest in the high-transmissivity

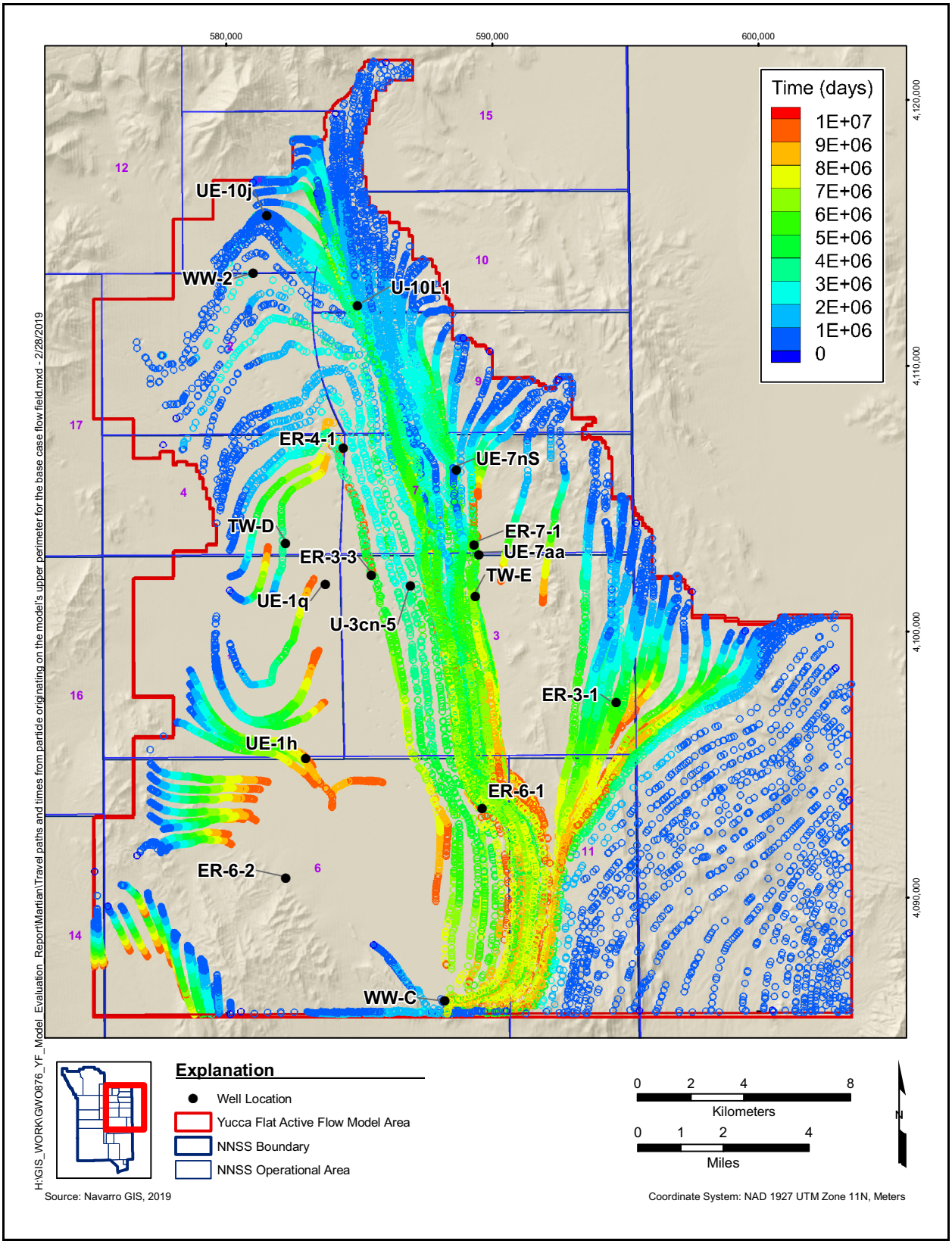

Figure 4-21
Travel Paths and Times from Particle Originating on the Model's Upper Perimeter for the Base Case Flow Field

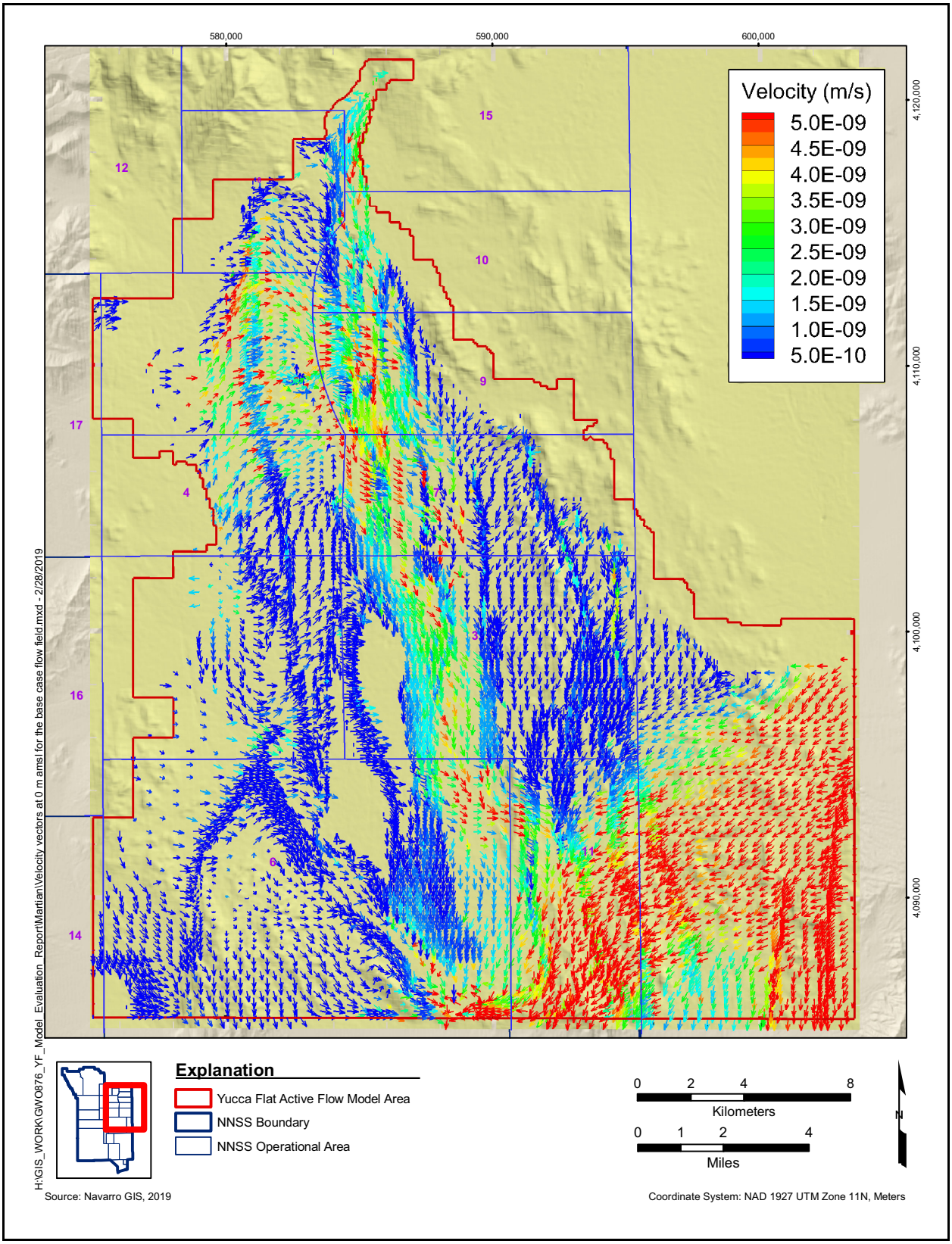

Figure 4-22
Velocity Vectors at 0 m amsl for the Base Case Flow Field

corridor in eastern Yucca Flat. Using a total porosity of 0.024, the calculations result in very slow water velocities with a range of 0.7 to 7 m/yr. However, this is a low estimate of transport velocity because not all matrix porosity is accessed by solutes during transport.

The potential RN migration pathways were evaluated with particle-tracking simulations. Source particles were released at the 58 detonation locations that may create contamination within the LCA immediately after detonation from any of the LCA surfaces considered in Section 2.8. A total of 500 particles were released within the exchange volume sphere segment intersecting the saturated LCA at each of the 58 locations. The simulation was conducted assuming that particles do not diffuse and that the medium porosity is uniformly 0.0045. This effective porosity value was chosen to reflect the central tendency of the LCA fracture porosity summarized in the Yucca Flat transport data summary report (SNJV, 2007).

The particle breakthrough crossing a hypothetical east–west fence at northing 4,090,000 m (4.5 km north of the LCA model's southern boundary) at 1,000 years provides an integrated transport metric for evaluating transport velocity and comparing different models. The particle paths and time histories after 1,000 years of travel time are presented in Figure 4-23. The cumulative particle breakthrough from the calibrated LCA model is presented in Figure 4-24. The breakthrough is reflective of advective-only transport without considering the effects of radioactive decay, matrix diffusion, and sorption. The initial breakthrough begins after approximately 900 years, and the total particle breakthrough is approximately 1 percent of the total number of particles released at the 58 $3R_c$ source locations.

4.3 LCA Flow Model Uncertainty Analysis

4.3.1 Introduction

Modeling flow and transport in complex environmental systems requires quantification of uncertainty in model response due to uncertainty in model input. The Yucca Flat model evaluation plan (Navarro, 2016a) states that the MER will contain model refinements and an assessment of model uncertainties. Unexpected and more extensive RN transport due to model uncertainty is the primary concern for the LCA model refinement. Therefore, the goal of the uncertainty analysis is to identify and include models that are likely to lead to more extensive transport than the base case and still have permissible fits to the calibration data.

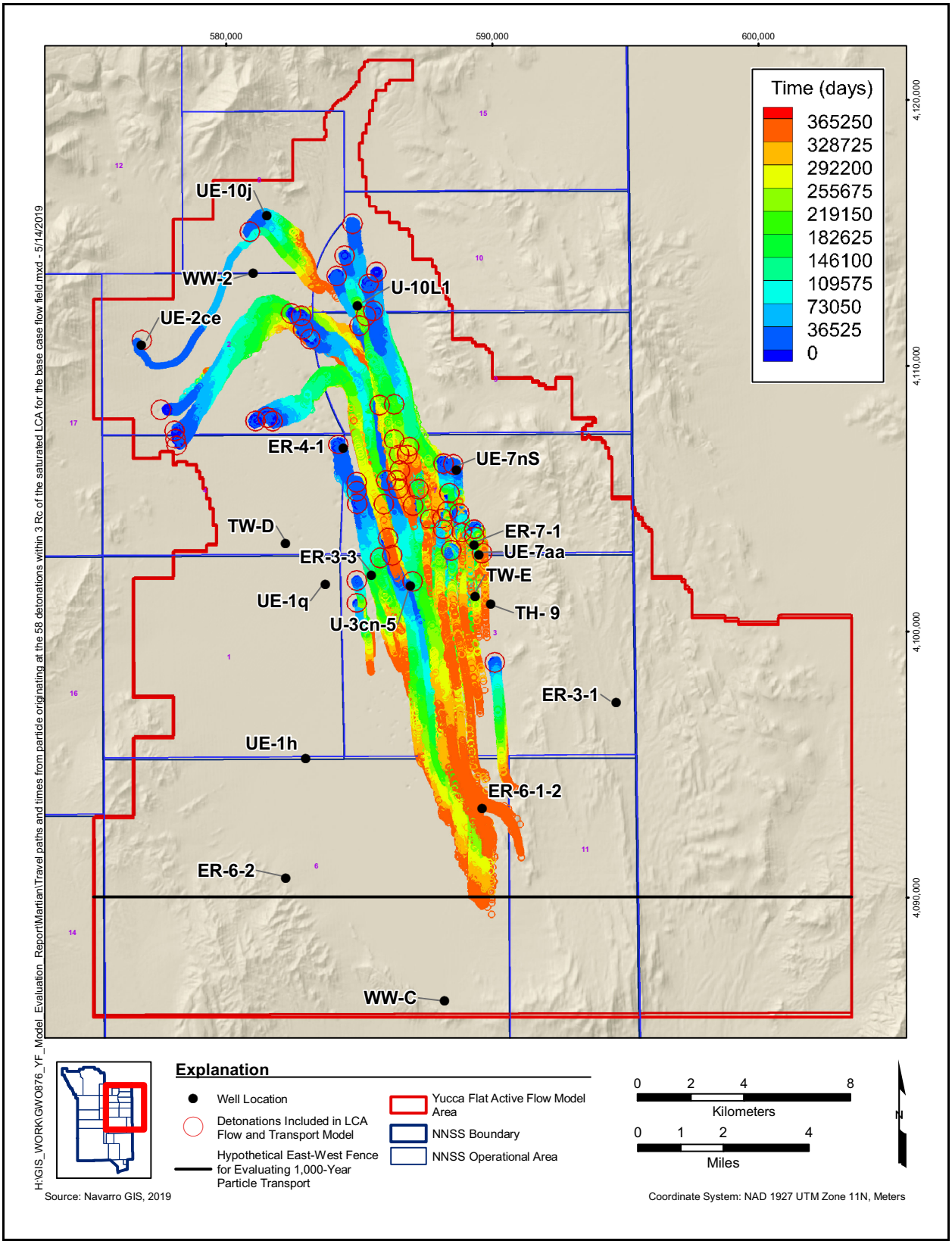

Figure 4-23
Travel Paths and Times from Particle Originating at the 58 Detonations Included in LCA Flow and Transport Model for the Base Case Flow Field

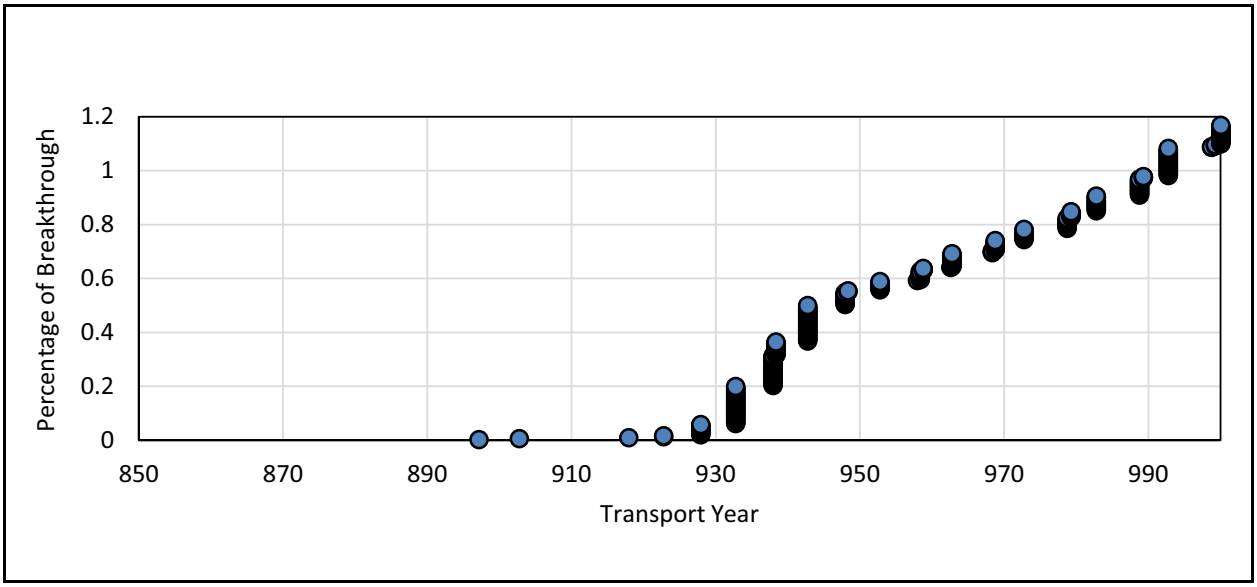

Figure 4-24
Cumulative Particle Breakthrough near the LCA Model's Southern Boundary for the Base Case

For the LCA flow model, two categories of uncertainty analyses were performed:

- **Identification of Alternative Conceptual Models with More Extensive Transport.** Because of the uncertainty in flux through the Yucca Flat testing areas and because fault properties may lead to more extensive transport, two alternative models were constructed to bound the transport that may result from these uncertainties. The first model uses an upper-bound flow rate calibration target (40-kg/s Basin Flux), and the second model considers a high-permeability Yucca fault (High-K Yucca Fault).

- **Global Parameter Uncertainty.** PEST, like most gradient-based parameter estimation software packages, may find a calibrated parameter set that minimizes the observation objective function only in the vicinity of local minima. This result is strongly influenced by the initial parameter values. Therefore, it is necessary to examine the parameters and associated groundwater flow fields associated with optimizations that result from different initial parameterizations. The PEST's NSMC method was used to perform the global parameter uncertainty analysis.

Out of the NSMC models, a model with acceptable calibration (see Section 4.3.3) and more southerly particle tracks compared to the other three models was also selected as an alternative model (NSMC run #28) to bound the transport forecasts. Thus, the base case and three alternative models were selected for transport CB calculations.

4.3.2 Alternative Flow Models with Extensive Transport

Two alternative flow models with more extensive transport than the base case were constructed, and model parameters were fully optimized. The goal of the alternative model calibrations was to generate flow fields that would be expected to lead to greater transport distances and different transport pathways than the base case, and that also achieve a similar quality of calibration as the base case. The two alternative conceptual models are (1) upper limit estimate of the basin flux through the nuclear testing area of 40 kg/s (i.e., 40-kg/s Basin Flux), and (2) high transmissivity within the Yucca fault (i.e., High-K Yucca Fault). The two alternative conceptual models and calibration results are described in this section.

4.3.2.1 40-kg/s Basin Flux

An uncertainty analysis was performed on the DV3 model (Section 2.6.3) and determined that the uncertainty in the groundwater flow rate through the eastern Yucca Flat nuclear testing area is approximately a factor of 2. Consequently, an alternate flow field was generated by recalibrating the LCA flow model with a twofold increase (20 kg/s to 40 kg/s) in the groundwater flow rate target between Wells ER-7-1 and ER-6-1 (Section 4.2.4.5).

The model calibration achieved an objective function value of 652, which is similar to the base case objective function of 621. Figures 4-25 through 4-27 present the potentiometric surface, transmissivity field, and particle tracks from particles originating from the 58 detonations within $3R_c$ of the saturated LCA, respectively. Nearly all western recharge is routed northward around the Topgallant fault into the high-transmissivity corridor, providing the additional water needed to match the higher groundwater flow target between Wells ER-7-1 and ER-6-1, which was accomplished by decreasing the transmissivity within the model's southwest corner (Figure 4-26). As expected, the increased flow through the eastern Yucca Flat testing area increased transport velocities from the 58 detonations within $3R_c$ of the saturated LCA compared to the base case (Figure 4-27). The particle breakthrough fraction near the model's southern boundary within 1,000 years is 21 percent, and first breakthrough occurs after approximately 400 years.

4.3.2.2 High-K Yucca Fault

As discussed in Section 4.2.5.2, the identifiability of the Yucca fault permeability is low, implying a wide range of values could calibrate the model equally well. Furthermore, the permeability of the

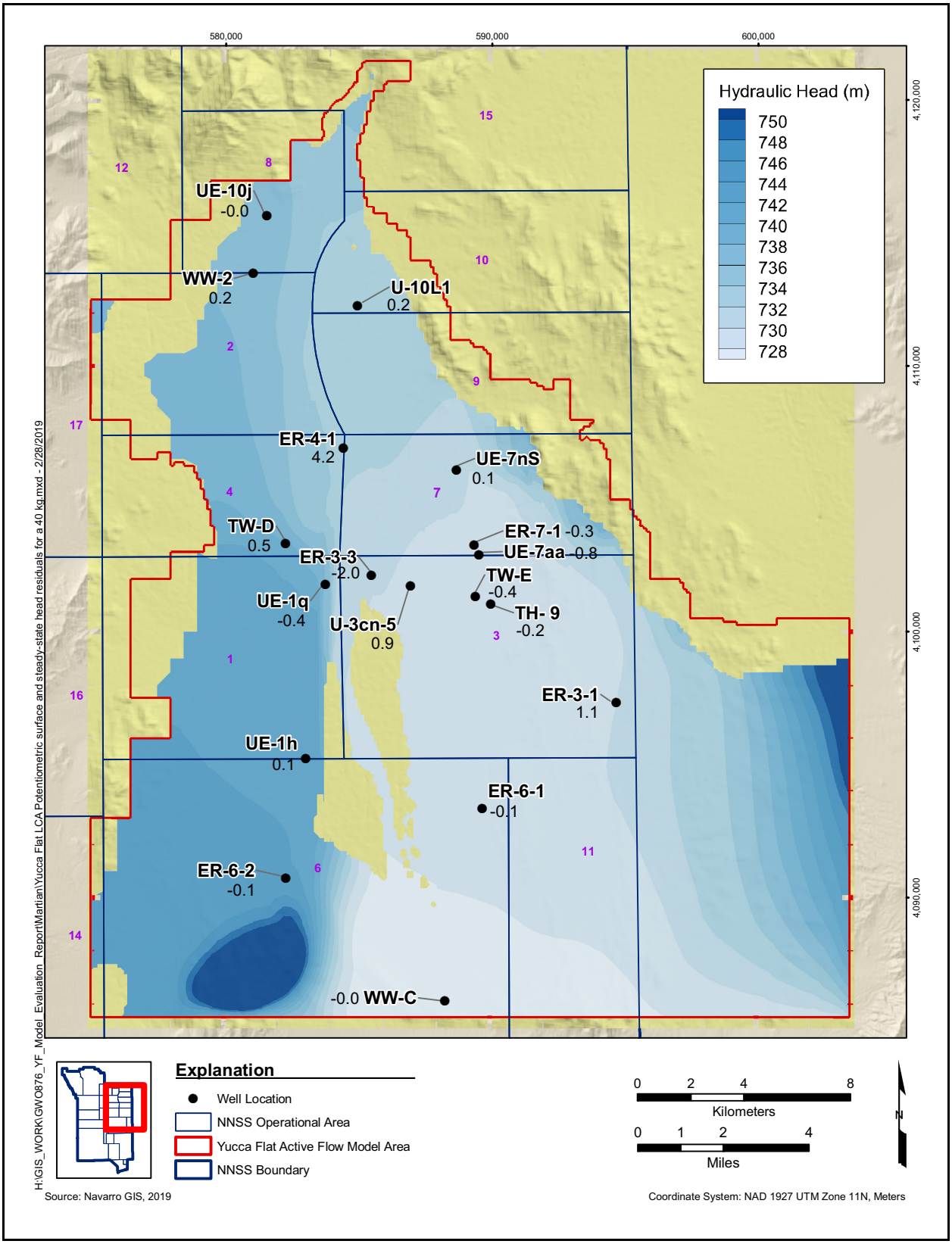

Figure 4-25
Yucca Flat LCA Potentiometric Surface and Steady-State Head Residuals for a 40-kg/s Transmissivity-Width Flux Flow Field

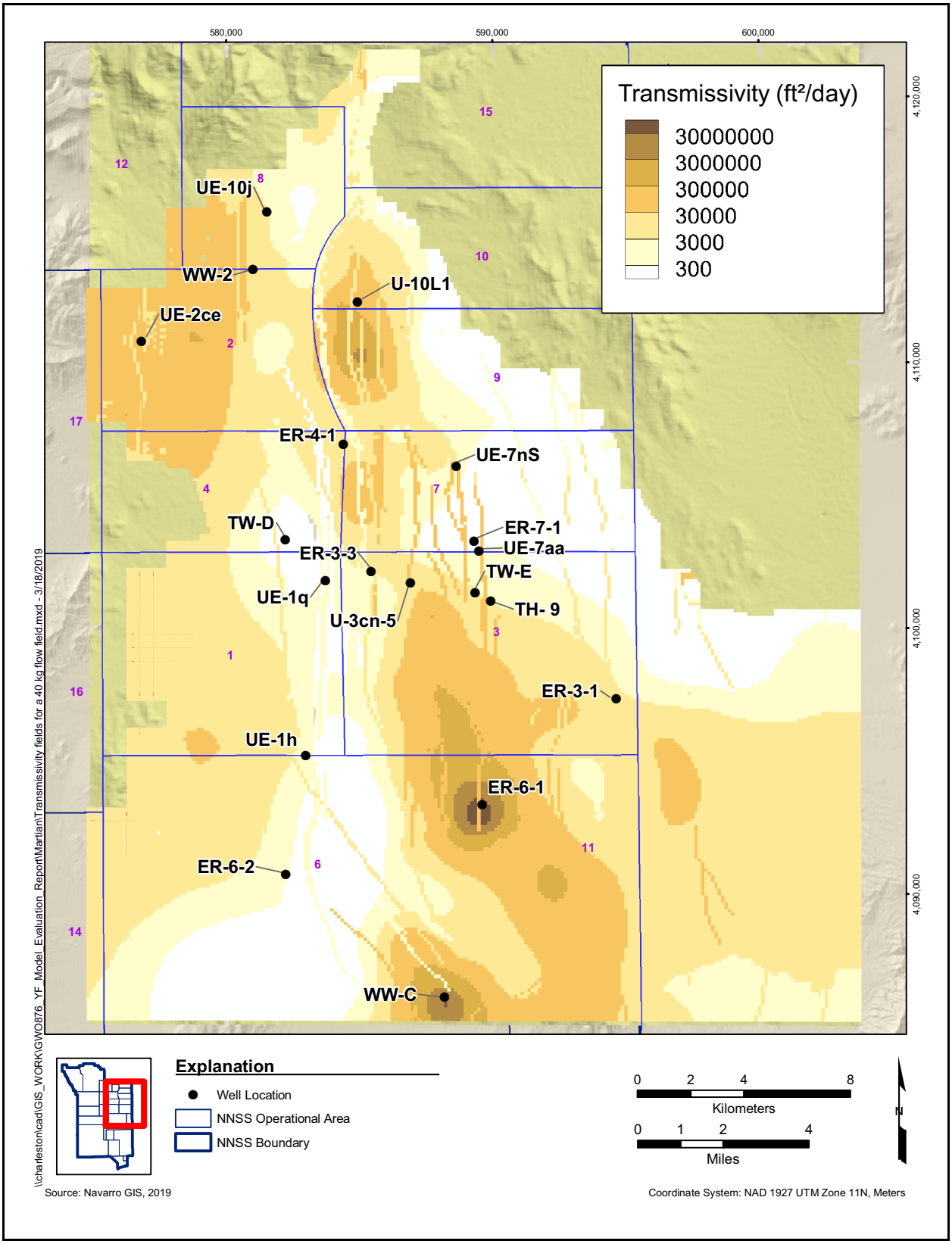

Figure 4-26
Transmissivity Fields for a 40-kg/s Transmissivity-Width Flux Flow Field

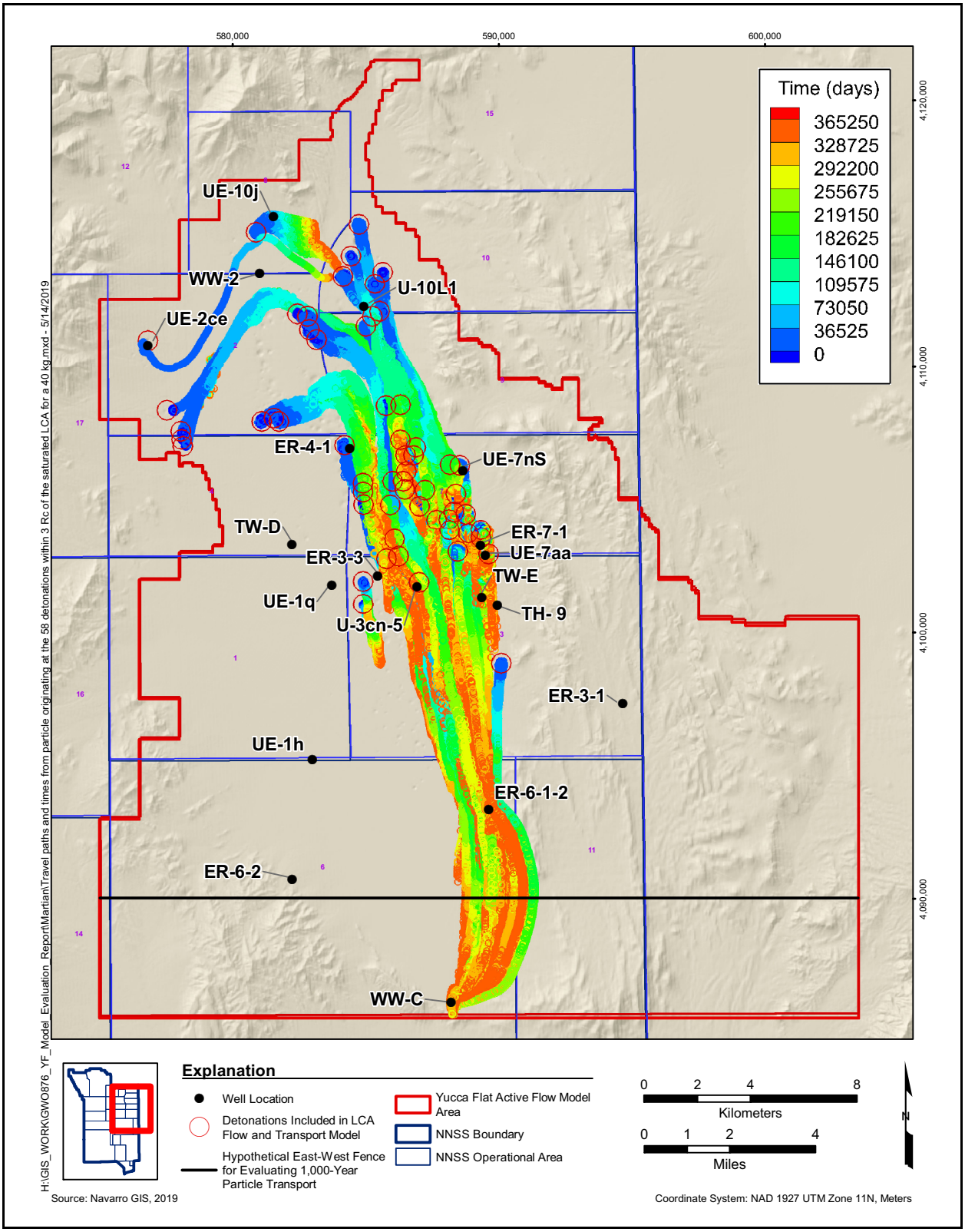

Figure 4-27
Travel Paths and Times from Particle Originating at the 58 Detonations Included in LCA Flow and Transport Model for a 40-kg/s Transmissivity-Width Flux Flow Field

Yucca fault was the most highly correlated model parameter to particle breakthrough near the model's southern boundary in the N-I (2013) modeling. In order to address the likelihood that the Yucca fault may have a higher transmissivity and transport velocity than the base case, the High-K Yucca Fault model was created. Permeability of the two Yucca fault strands was specified at 5E-12 m^2, and other parameters were allowed to adjust around this fixed value. The optimized Yucca fault permeability from the base case calibration was 1E-13 m^2. A model calibration was attempted using a specified high-permeability of 8.77E-11 m^2, which was the highest measured value in a fault within the ER-6-1-2 borehole from the ER-6-1-2 MWAT analysis (SNJV, 2006c), but the model could not be satisfactorily calibrated to the steady-state heads and gradient in eastern Yucca Flat.

The LCA model calibration with a high transmissivity specified for the Yucca fault achieved an objective function value of 600, which is slightly better than the base case objective function of 621. Figures 4-28 through 4-30 present the potentiometric surface, transmissivity field, and particle tracks from particles originating form the 58 detonations within $3R_c$ of the saturated LCA. The transmissivity and flow field are similar to the base case, except the transmissivity and groundwater velocity in the Yucca fault are much higher. The trace of the Yucca fault passes through the main testing area in Yucca Flat, and the increased flow through the Yucca fault increased the amount of particle breakthrough compared to the base case (Figure 4-30). The particle breakthrough fraction near the model's southern boundary within 1,000 years was 11 percent, and first breakthrough occurs after approximately 300 years. Although not apparent in the plan view presented in Figure 4-30, groundwater flow channelization occurs in the Yucca fault, and deeper particle transport occurs in the Yucca fault compared to the base case.

4.3.3 Global Uncertainty Analysis

This section explores the effects of parametric uncertainties on the LCA flow model. As discussed in Section 4.2.3, the LCA model contains 197 independent parameters, including pilot points for country rock hydraulic conductivity and specific storage, fault permeability and specific storage, and boundary fluxes. The dimension of the solution space is given by the number of parameters that are significantly informed by the observations, and the solution space for the LCA model base case was found to be 42. The calibration null space is the parameters or combinations of parameters that have no influence on model calibration, and the dimension of the null space is the number of independent parameters less the dimensions of the solution space (Doherty et al., 2010). Because the LCA model's

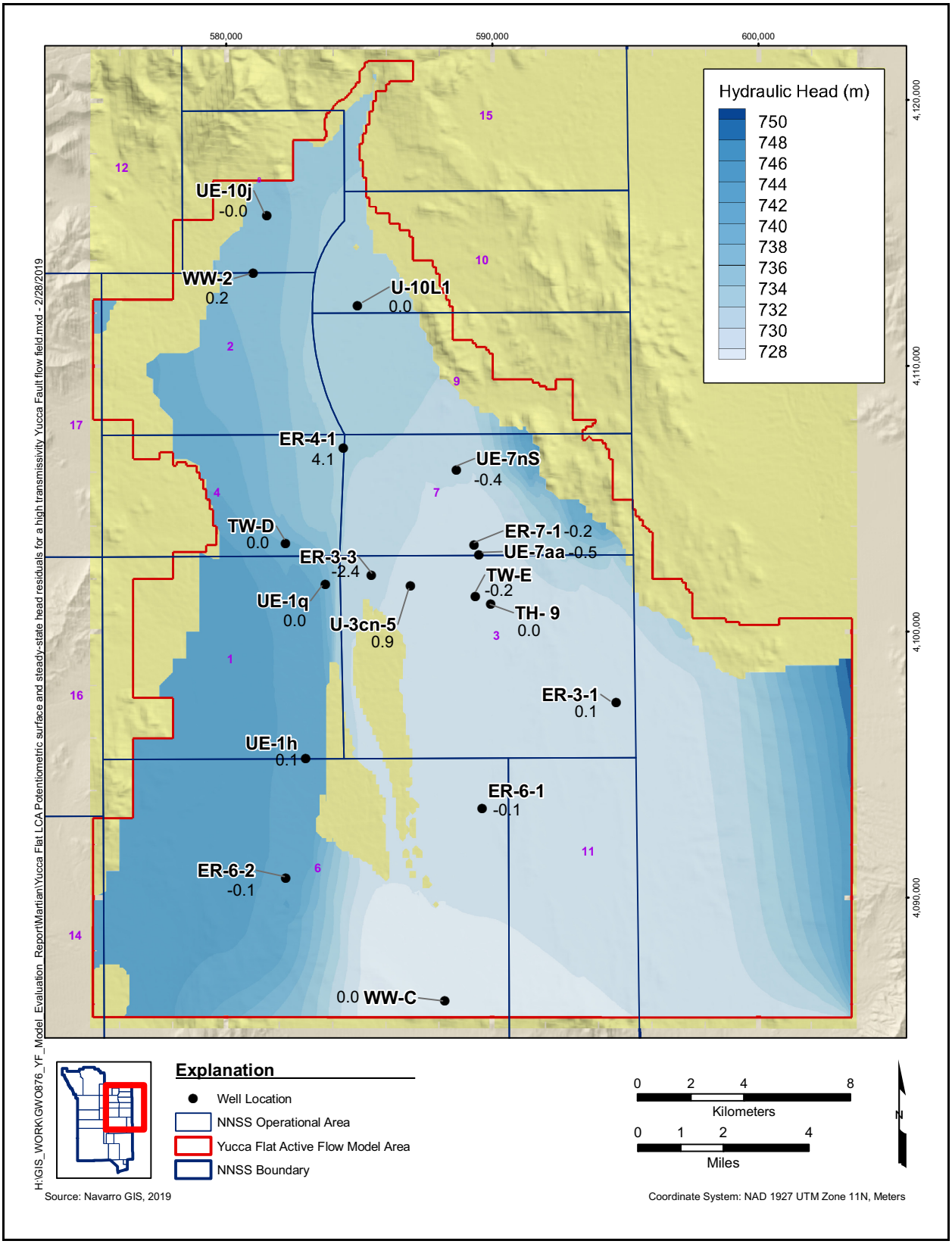

Figure 4-28
Yucca Flat LCA Potentiometric Surface and Steady-State Head Residuals for a High-K Yucca Fault Flow Field

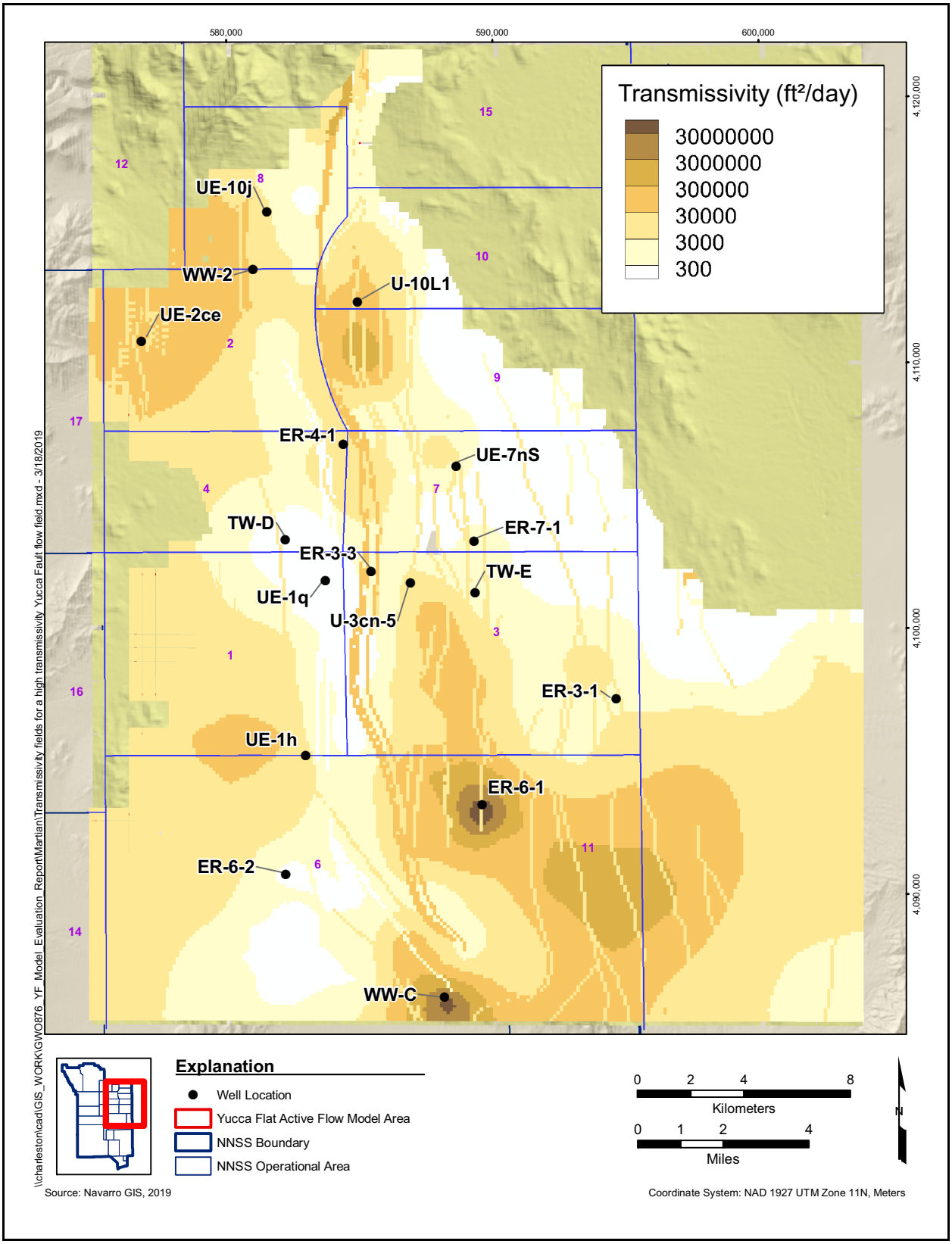

Figure 4-29
Transmissivity Fields for a High-K Yucca Fault Flow Field

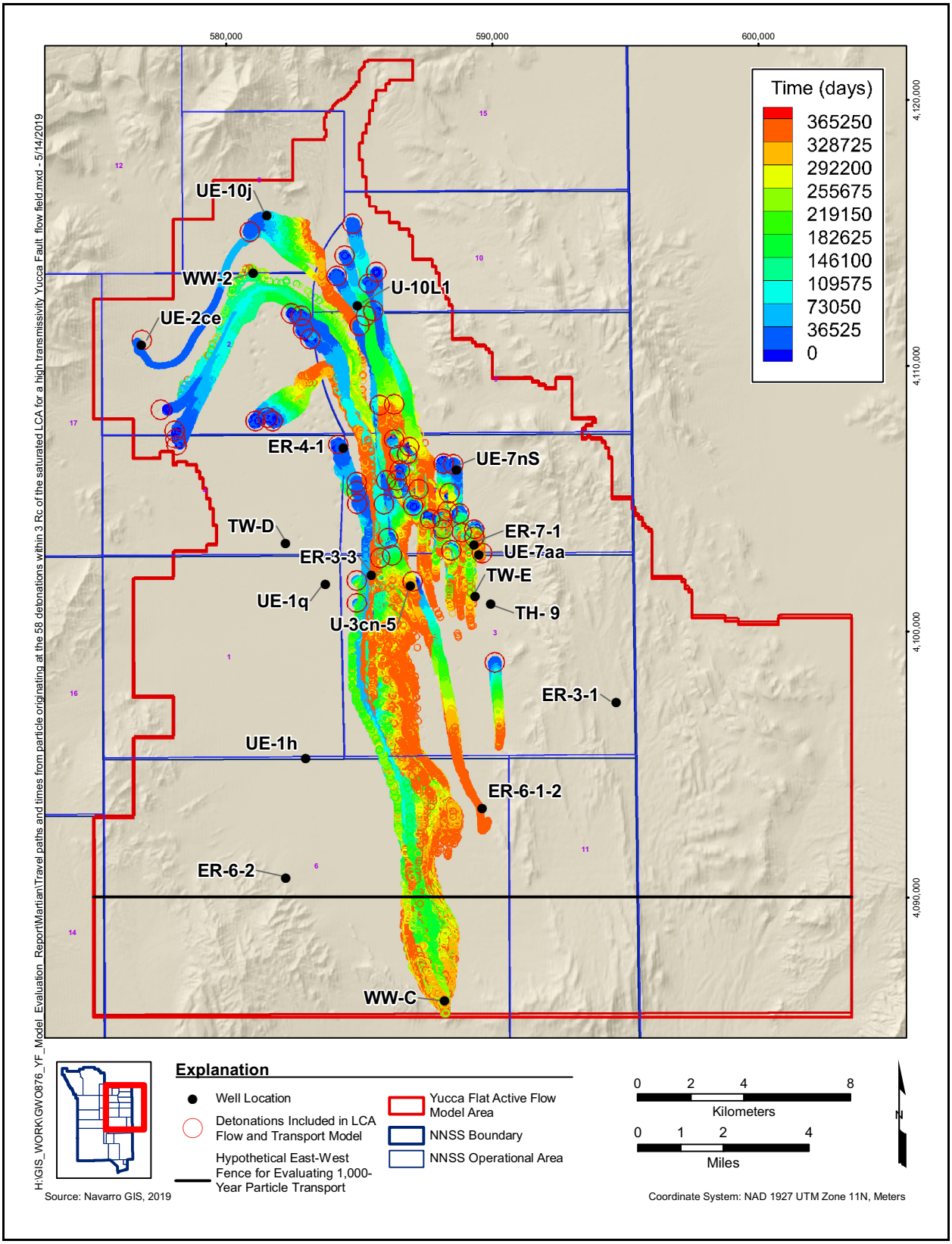

Figure 4-30
Travel Paths and Times from Particle Originating at from the 58 Detonations Included in LCA Flow and Transport Model for a High-K Yucca Fault Flow Field

null space comprises a large fraction of the parameter space, there can be many alternative calibration sets with alternative flow fields that have fits to the calibration data that are similar to the base case model. Furthermore, highly parameterized models, such as the Yucca Flat LCA flow model, typically have a non-convex objective function space, and PEST may identify a local minima instead of a global minima. Therefore, a global uncertainty analysis was performed that examines many optimized parameter sets which are determined from many different initial parameter sets.

PEST's NSMC method was applied to the base case calibrated flow model to generate 100 alternative flow fields using different initial parameterizations. PEST's NSMC method uses a special technique to sample all parameters by using information regarding the parameter and null spaces of the Jacobian matrix and to efficiently create many alternative models that provide as reasonable a solution as the base case calibration. The NSMC method functions optimally when the relationship between model parameters and model outputs is linear, and the transition between null and solution spaces is distinct. When these conditions are satisfied, the method can converge within as few as one iteration. The NSMC method deteriorates with increasing model nonlinearity and with an increasing degree of ill-posedness of the inverse problem (Doherty et al., 2010).

The NSMC method was applied to the calibrated base case, but the NSMC approach did not produce models with comparable fits to observations as the base case, and recalibration was needed for each NSMC model. The poor performance of the NSMC method for the LCA model is the outcome of nonlinearity and a strong degree of ill-posedness of the LCA model. The very large range of permissible pilot point hydraulic conductivity (e.g., 8 orders of magnitude) contributed to the poor performance of the NSMC method. Calibration for each of the 100 NSMC models required almost as much computational effort as calibrating the original base case model.

The PEST software considers a parameter optimization complete when the objective function cannot be lowered further, and PEST uses several criteria to determine whether the optimization is complete, all of which are set by the user. During the model calibration, PEST performs successive parameter optimization iterations that consist of calculating of the Jacobian matrix and testing of parameter upgrades. Two criteria were used to determine whether LCA model calibration was complete: (1) three optimization iterations in which the relative change in the objective function is less than 0.005, or (2) three successive iterations in which the objective function does not become lower.

As discussed in Section 2.6.3, the choice of the threshold objective function level at which the model is deemed to be "calibrated" is often subjective, but it can estimated by comparison of observations to model values and understanding the model sensitivities. For example, agreement with steady-state heads in confining units is not as critical as in aquifers because flow rates in confining units are low and contribute less to the overall water budget. Achieving an objective function of 10 times the base case (6,200) was selected as the maximum acceptable value for the NSMC model calibrations. Generally, models achieving an objective function of approximately 6,000 had fair agreement with the observation trends but did not always accurately reproduce the observed conditions. For example, drawdowns resulting from the ER-4-1 WDT or ER-6-1-2 MWAT pumping were simulated at the same locations as the observations, but the magnitude and timing of drawdown could be a factor of 2 different.

Figures 4-31 through 4-33 present the simulated drawdowns in response to the ER-6-1-2 MWAT and ER-4-1-2 WDT pumping, and the steady-state head profile, respectively, for NSMC model 99. Model 99 is the NSMC model with the largest objective function that was considered acceptable (i.e., 5,420, or ~9 times the base case value).

Of the 100 NSMC models considered, 27 models reached the PEST termination criteria; 41 models were estimated to have complete optimizations as indicated by an oscillating or increasing objective function at the time the calibrations were terminated; and 12 models had steadily decreasing objective functions but had achieved an objection function of less than 10 times the base case. Five models of the 27 that reached the PEST termination criteria had objective functions that were greater than 10 times the base case value and were not considered further. The remaining 20 models had steadily decreasing objective functions that were higher than 10 times the base case. A total of 75 of the NSMC models had achieved an acceptable calibration and the objective function values for these 75 calibrations are presented in Figure 4-34. The flow fields from these 75 calibrated models were used to assess alternative flow paths and estimate the maximum extent of southern transport in the LCA through simulations of particle transport.

Hydrogeologic parameters and boundary conditions vary in each of the 75 NSMC alternative flow fields. For example, flow through the Yucca Flat sub-basin ranges between 9 and 39 kg/s as shown in the bar chart of basin flows (Figure 4-35A), and has an central tendency of approximately 22 kg/s as

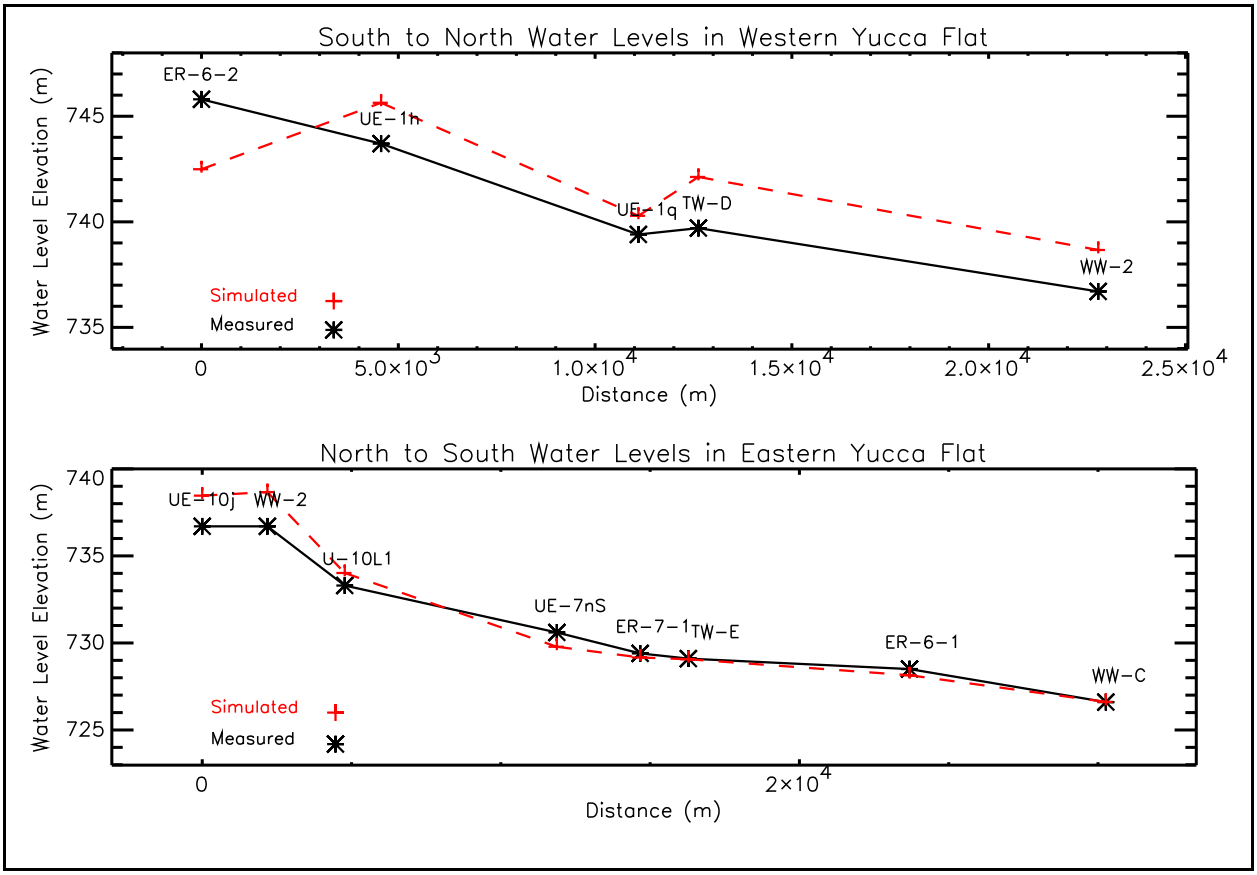

Figure 4-31
Western and Eastern Yucca Flat Water-Level Profiles for NSMC Model 99

shown in the histogram of basin flows (Figure 4-35B). The calibrated value of flow for the base case is 25 kg/s and may be considered an average case. It is notable that none of the 75 models with an acceptable calibration simulated a flux through the testing area greater than that of the 40-kg/s Basin Flux model (Section 4.3.2.1).

For the base case flow field, the mean fault hydraulic conductivity is similar to the mean country rock hydraulic conductivity. Although hydraulic conductivity is similar, faults influence the flow field by allowing flow and transport through regions of low country rock hydraulic conductivity and by acting as barriers to cross-flow in regions of high country rock hydraulic conductivity. Figure 4-36 presents the mean fault and pilot point hydraulic conductivity for each of the NSMC models. The mean fault and country rock hydraulic conductivity vary over 2 orders of magnitude and can be very different, which has profound influence the flow field. For example, the base case, NSMC model 3, and NSMC model 41 all achieved a similarly low objective function but have different fault behavior. Figure 4-37 illustrates the transmissivity field for NSMC models 3 and 41. The faults in NSMC model 3 are

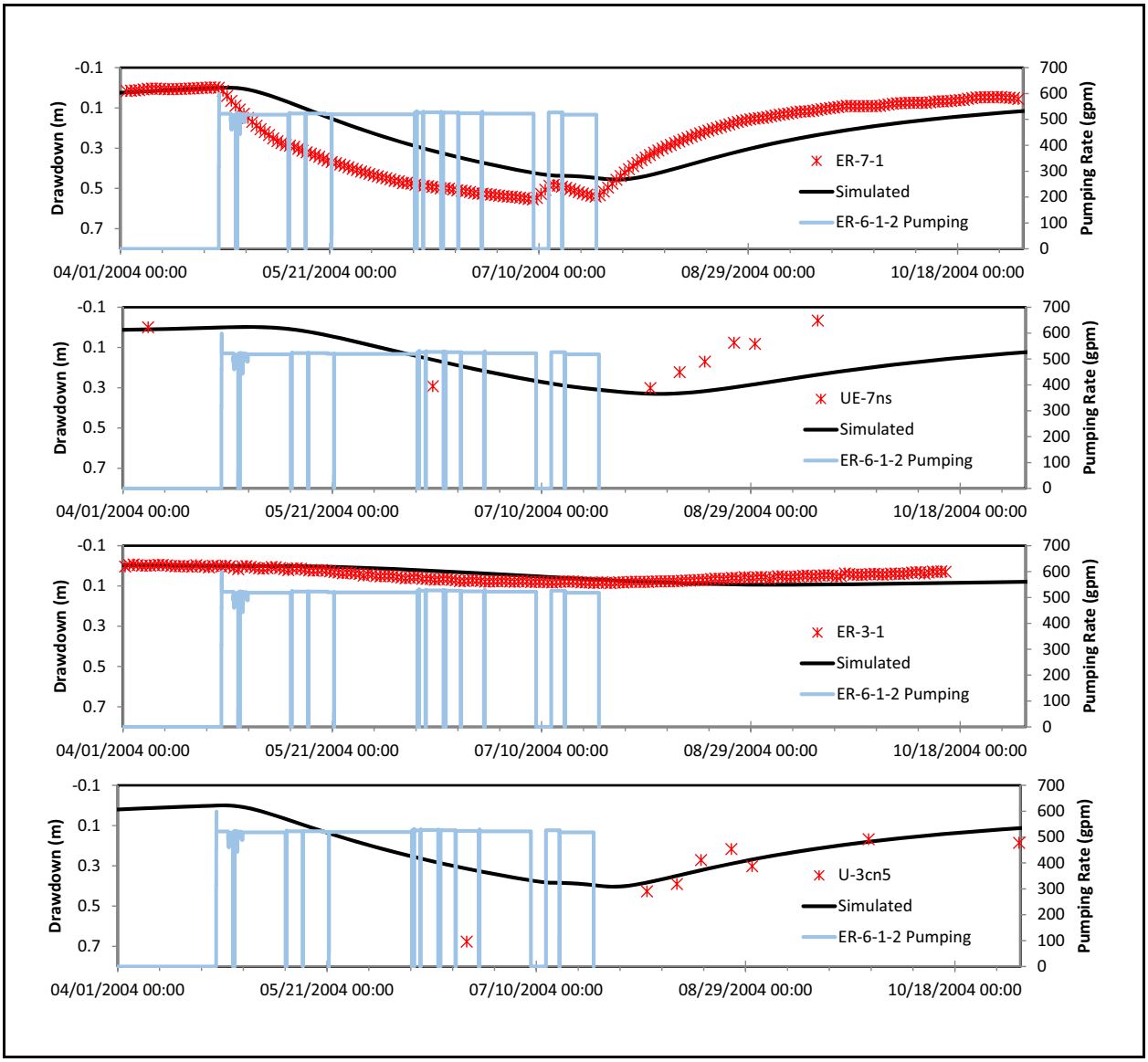

Figure 4-32
Simulated and Observed Drawdown Hydrographs at the Responding ER-6-1-2 MWAT Wells for NSMC Model 99

conduits in lower hydraulic conductivity country rock, but faults in NSMC model 41 have a lower hydraulic conductivity compared to the country rock hydraulic conductivity and are flow barriers. Faults acting as conduits will result in faster groundwater flow within the fault zones and potentially increased transport. The NSMC models illustrate that many alternative combinations of fault and country rock hydraulic conductivity can transmit a similar amounts of water through the system.

The similar mean pilot point and fault hydraulic conductivity obtained during the calibration of the base case and alternative models is because of the regularization approach used in the PEST

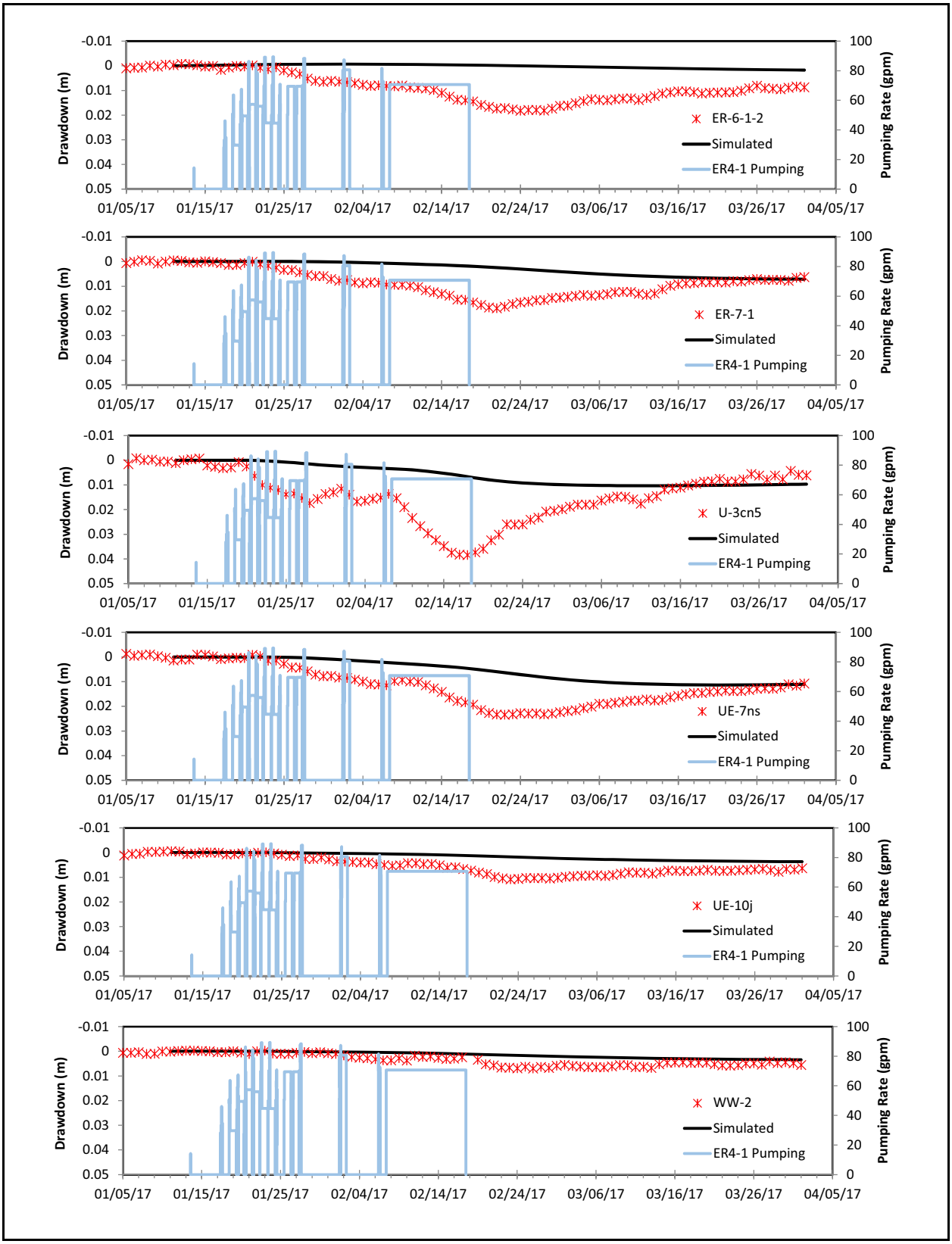

Figure 4-33
Simulated and Observed Drawdown Hydrographs at the Responding ER-4-1 WDT Wells for NSMC Model 99

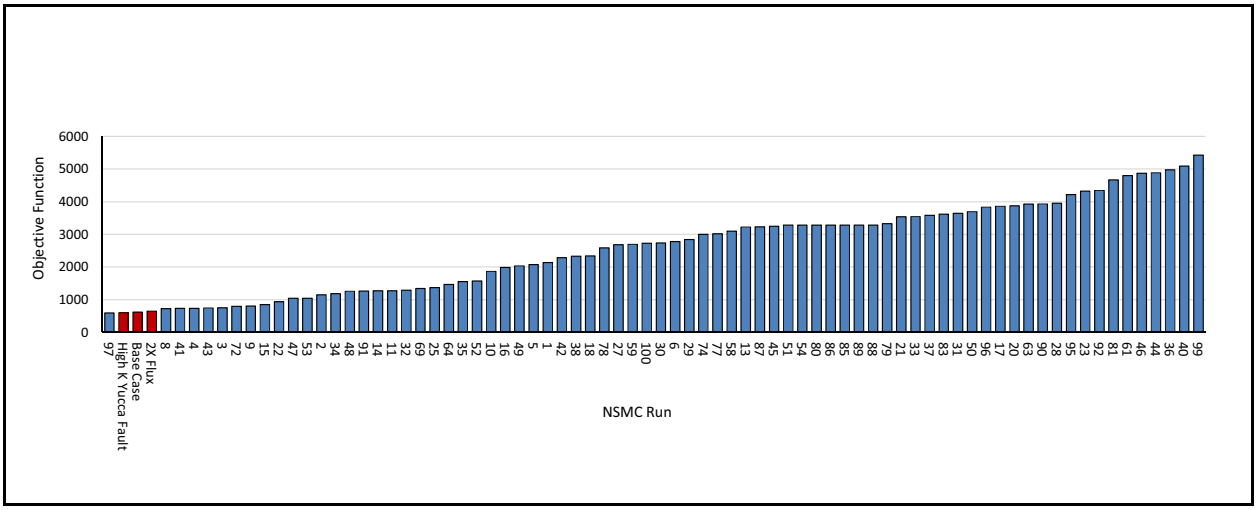

Figure 4-34
Calibrated Objective Functions (Sorted) for the NSMC Models

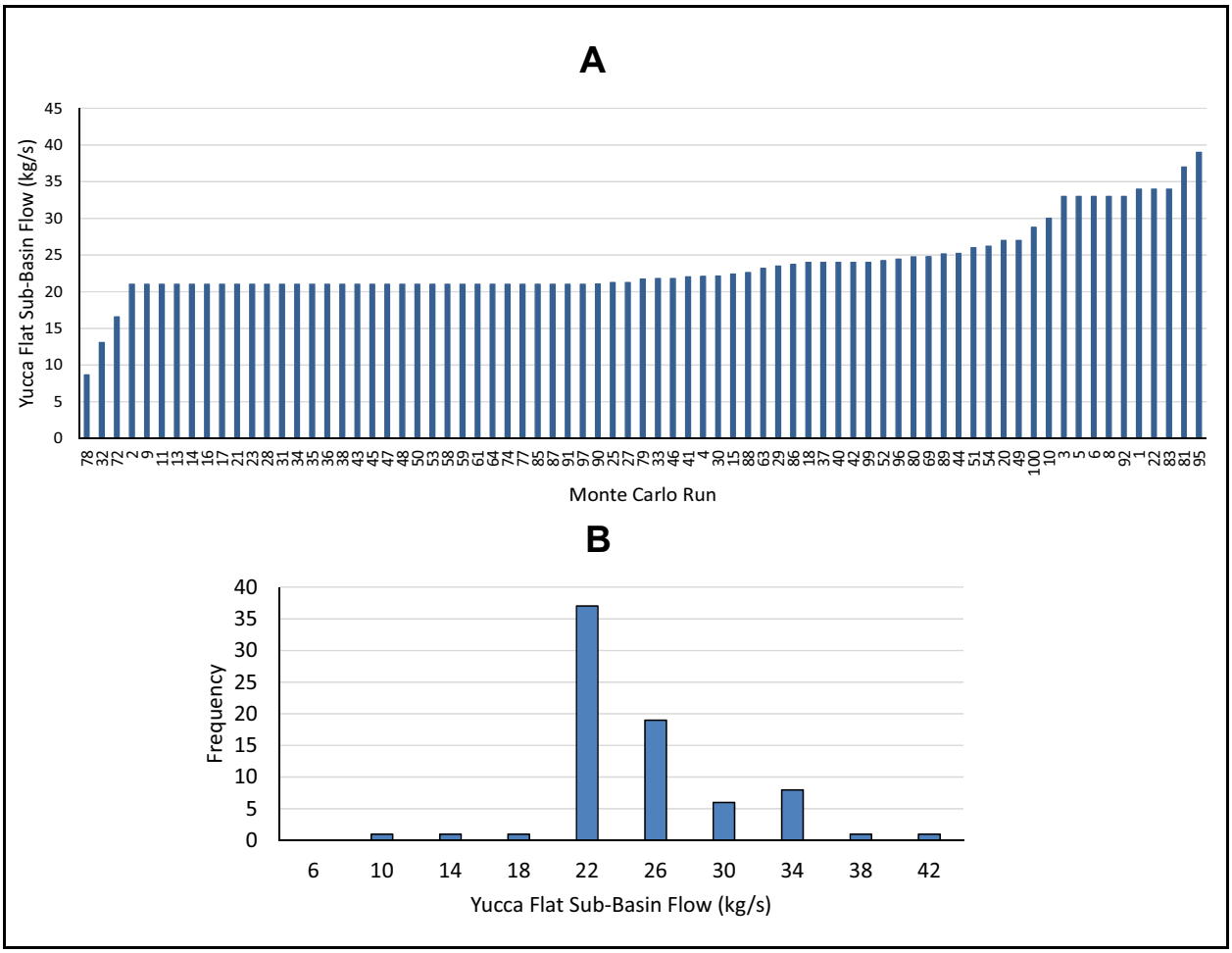

Figure 4-35
Flow through the Yucca Flat Sub-Basin for the NSMC Models

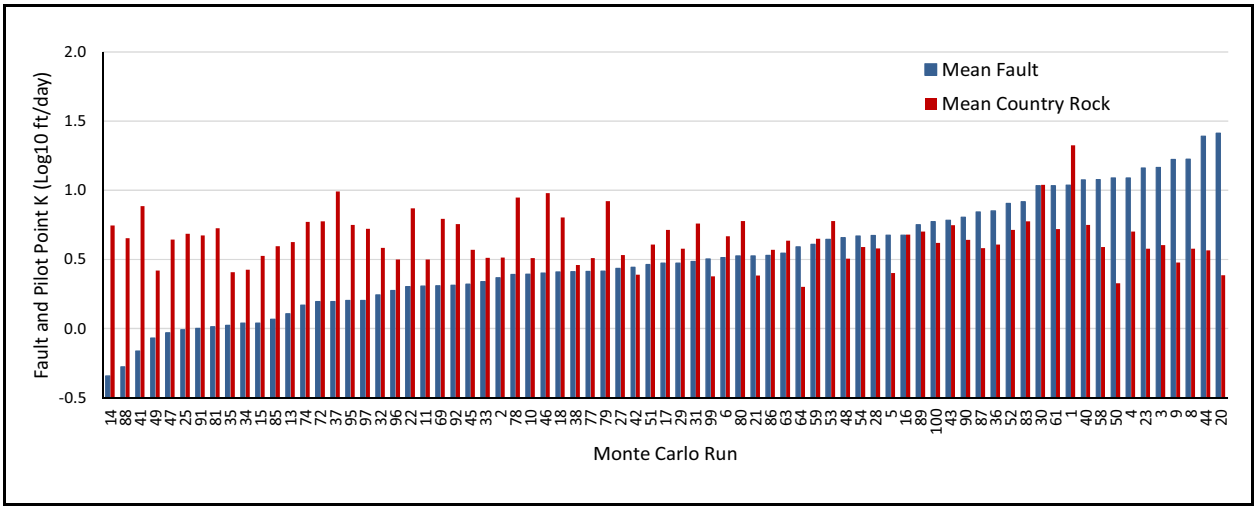

Figure 4-36
Mean Fault and Country Rock Hydraulic Conductivity for the NSMC Models

parameter optimizations. Regularization penalizes the objective function for parameter inhomogeneity and will allow heterogeneity only if supported by improving the agreement with observations. The NSMC analysis did not include regularization because regularization promotes adherence to a default parameter condition and the goal of the NSMC analysis is the opposite of this. The goal of the NSMC analysis is to generate stochastic initial parameterizations that influence the optimization outcome important to decision-making—in this case, particle transport—by allowing parameters that have no influence on the simulated observations to vary over permissible ranges. Implementing regularization within the NSMC model calibrations would have generated many models similar in nature to the base case model.

Histograms for the Topgallant and Yucca fault hydraulic conductivity and anisotropy are presented in Figure 4-38. Hydraulic isolation of western Yucca Flat from eastern Yucca Flat, as was evident by the absence of drawdowns in western Yucca Flat wells during the ER-4-1 WDT and ER-6-1-2 MWAT pumping, required a barrier behavior for Topgallant fault in all NSMC models (i.e., low hydraulic conductivity and strong east–west to north–south anisotropy). Strong to moderate east–west to north–south anisotropy for country rock was also needed to calibrate most of the NSMC models, as illustrated by the central tendency illustrated in Figure 4-39. Many of the NSMC models with acceptable calibrations allowed a higher Yucca fault hydraulic conductivity than was considered in the High-K Yucca Fault model. However, these NSMC models had a much higher objective function than the High-K Yucca Fault model. The goal of the alternative model calibrations was to produce models with a similar quality of calibration as the base case.

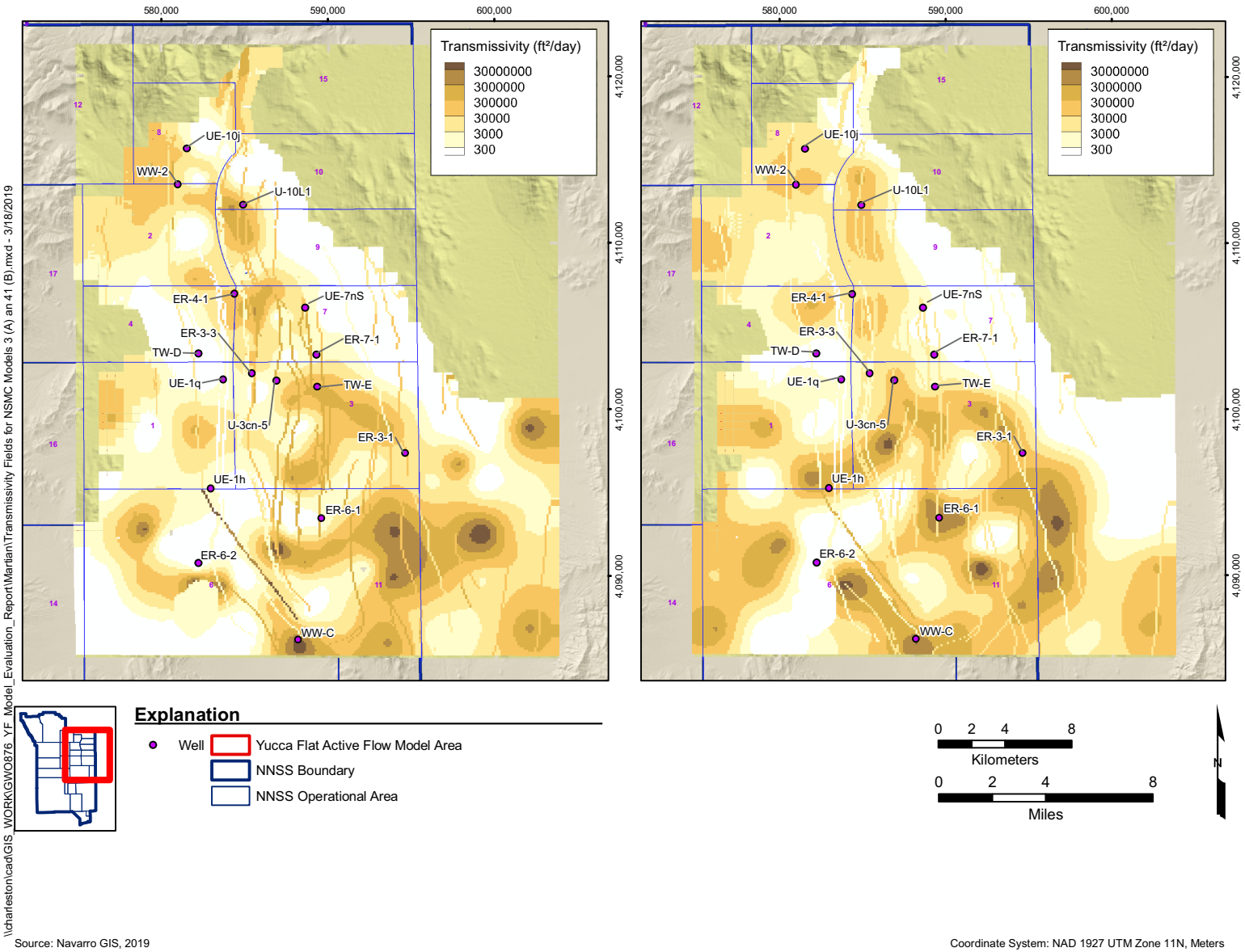

Figure 4-37
Transmissivity Fields for NSMC Models 3 (left) and 41 (right)

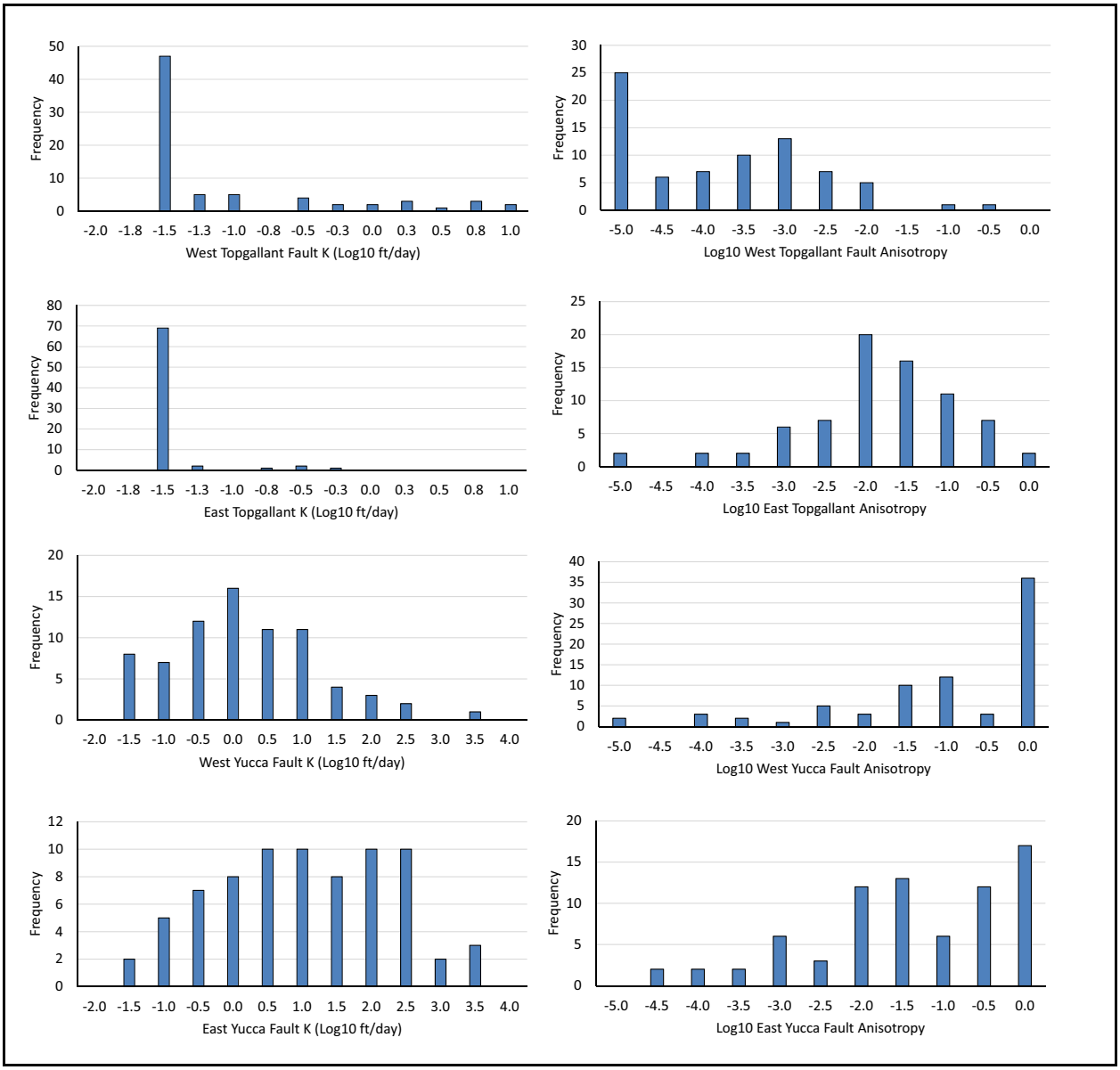

Figure 4-38
Topgallant and Yucca Fault Hydraulic Conductivity and Anisotropy Histograms for the NSMC Models

Particle-tracking simulations were conducted to estimate the potential for contaminant migration for each of the alternative NSMC models discussed above. As was done for the base case model (Section 4.2.5.3), source particles were released at the 58 detonation locations potentially within $3R_c$ of the saturated LCA. The goal was to assess the potential variations in flow paths and Darcy velocities relative to the base case and other NSMC models. The results were used to select the flow field with the maximum potential for transport for full probabilistic transport calculations, as discussed in Section 4.7.

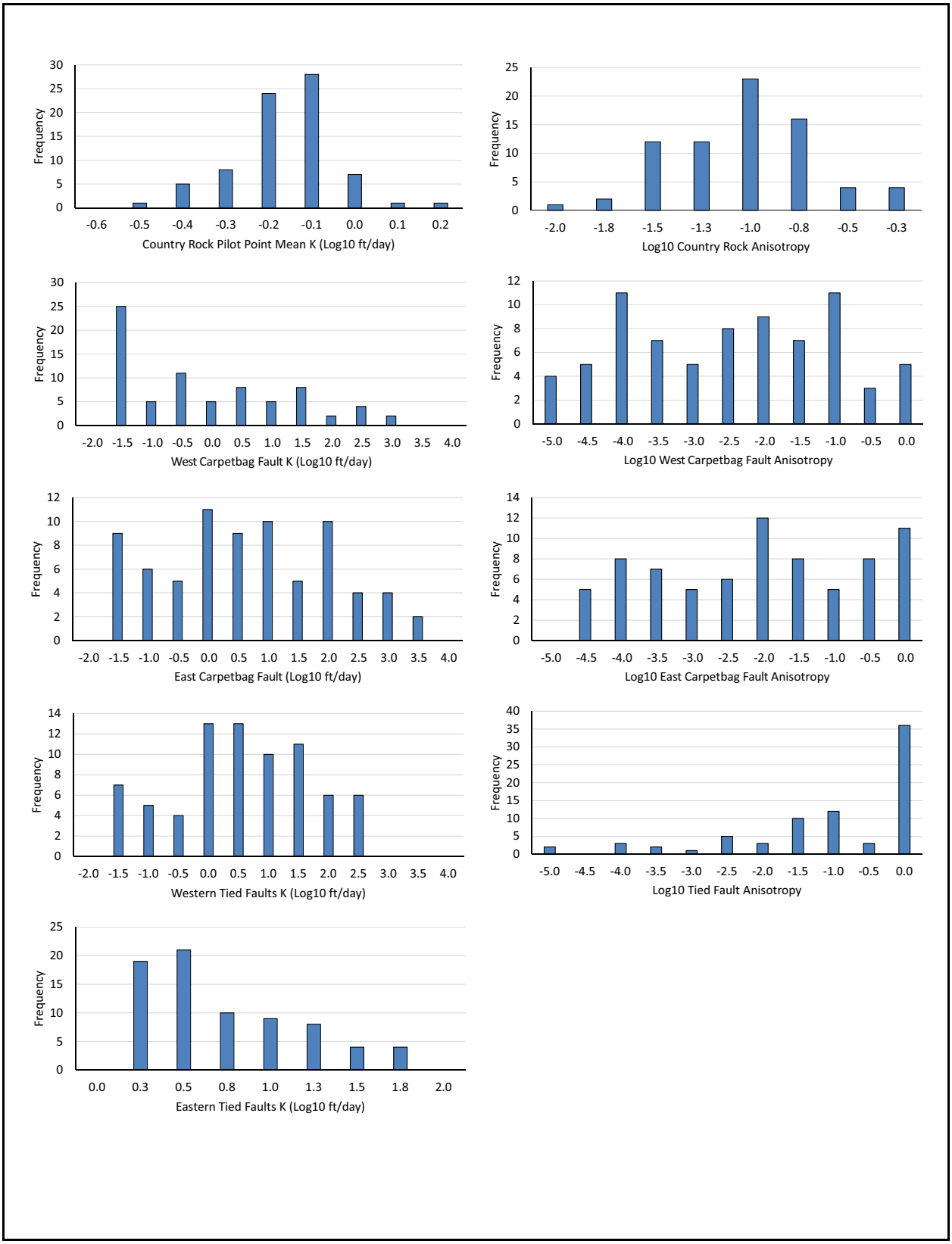

Figure 4-39
Country Rock, Carpetbag, and Tied Fault Hydraulic Conductivity and Anisotropy Histograms for the NSMC Models

The number of particles reaching a southern reference location (northing 4,090,000 m) within 1,000 years was used as a transport metric to compare the NSMC flow fields and is presented in Figure 4-40. The percentage of particles passing the reference location varies between 0 and 27 percent and has a median value of 4 percent. Only one of the NSMC flow fields has more particle breakthrough than the 40-kg/s Basin Flux model presented in Section 4.3.2.1. It is clear from the shape of the cumulative distribution that the NSMC runs represent a wide range of flow conditions. The vast majority of NSMC flow fields have much slower transport compared the N-I (2013) NSMC models.

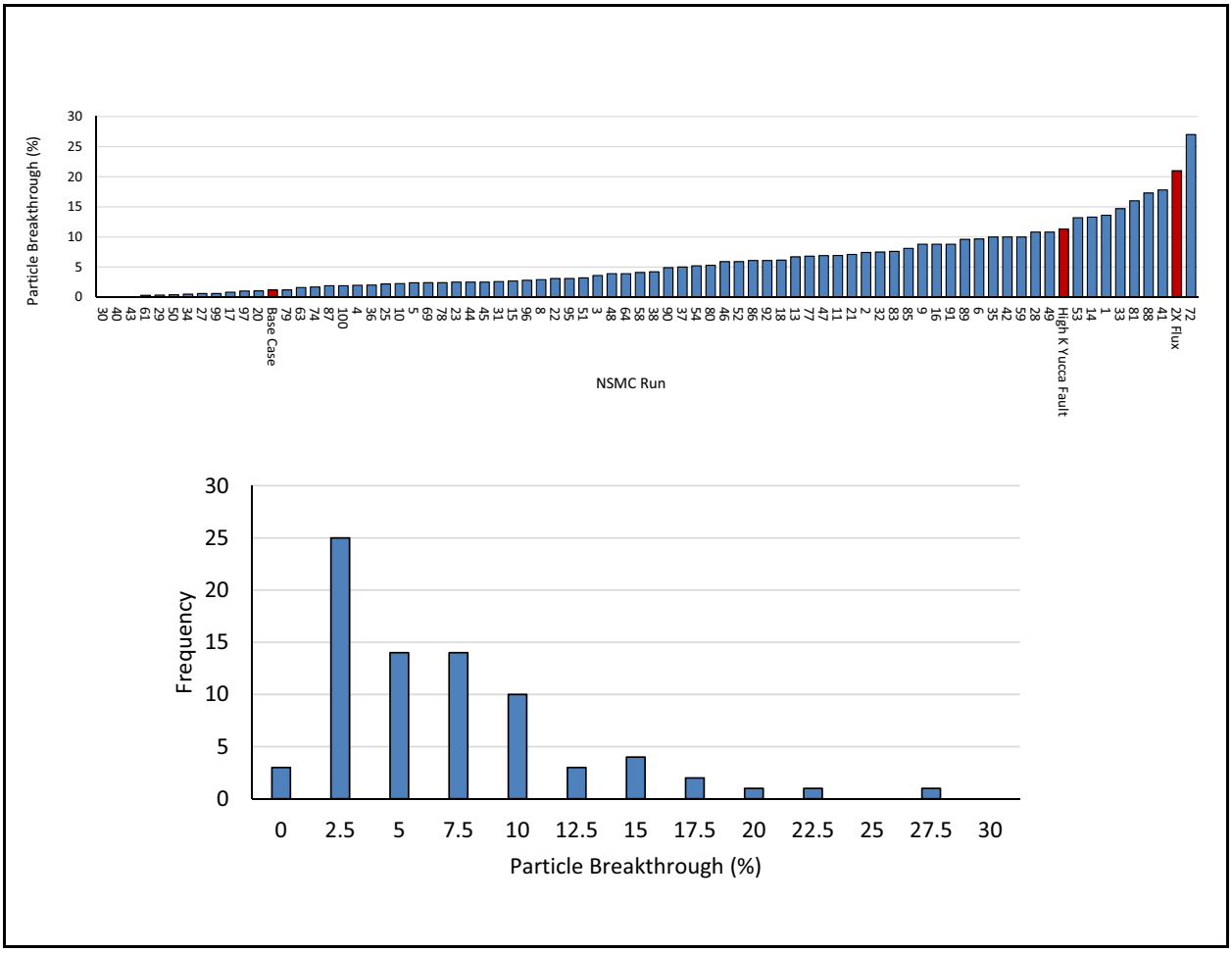

Figure 4-40
Distribution and Histogram for Percentage of Particles Reaching the Northing Location of 4,090,000 m within 1,000 Years from 58 Detonations Potentially within 3R_c of the Saturated LCA

As can been seen in Figure 4-36, faults can have much higher permeability than average country rock permeability, and a larger proportion of groundwater can flow through faults compared to the surrounding country rock. Deep particle transport occurs in faults under these conditions due to flow channelization within the narrow fault zones. Inflow to the LCA model includes vertical recharge and lateral underflow. The majority of the lateral under flow within the model's northern half is shallow and enters near the model's upper surface. The combination of vertical gradients created as shallow inflow enters the higher section of faults, and high fault permeability promotes deep circulation. There is no data to support or refute the very deep groundwater circulation in faults (several kilometers bgs) simulated by some of the NSMC models. The deepest wells within Yucca Flat are limited to approximately 1 km bgs.

Figure 4-41 presents a perspective view (viewed from the west) of the particle tracks for NSMC models 3 and 41. Deep particle transport occurs in NSMC model 3 compared to NSMC model 41. The transmissivity fields for these models were discussed earlier in this section and are illustrated in Figure 4-41. Similar deep particle transport behavior was seen for the High-K Yucca Fault model compared to the base case model.

Tritium dominates the other RNs within the HST in terms of initial radioactivity and also in the extent of contaminant migration that is above SDWA standard (CFR, 2018) (see Section 4.7). However, due to the short half-life (12.3 years) of ^{3}H, the maximum extent of contamination decreases significantly during the next few hundred years. Particle travel distances do not include the effects of radioactive decay, diffusion, and dispersion. Because of the short half-life of ^{3}H, particle travel distances at 200 years are a more useful estimate of the CB extent than 1,000-year particle transport distances when comparing NSMC flow fields. Tritium dominates the extent of contaminant migration, but radioactive decay will reduce the ^{3}H contribution to the volume of water exceeding the MCL below other RNs after approximately 200 years (see Figure 4-71).

Figure 4-42 presents the 1,000-year time-cumulative CB (see Section 4.7) for the base case, the 40-kg/s Basin Flux case, and the High-K Yucca Fault case, along with polygons identifying the maximum particle transport extents within 200 years predicted by all LCA flow models included in the uncertainty analysis (base case, alternative transport, and NSMC). The black polygon illustrates the particle transport extent of the base case, the 40-kg/s Basin Flux case, and the High-K Yucca Fault case; and the blue polygon illustrates the additional transport extent predicted by the 75 NSMC

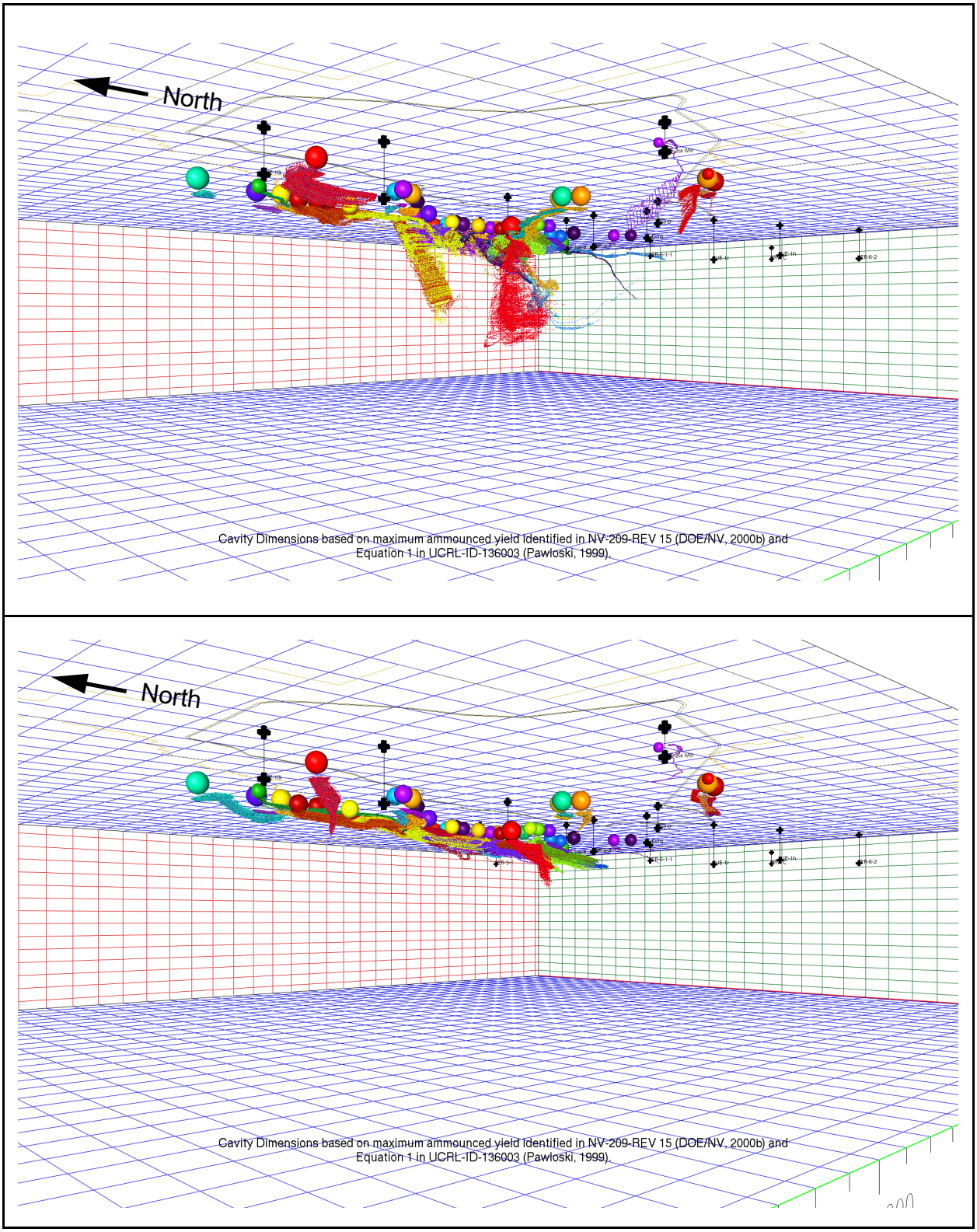

Figure 4-41
Perspective View of Particle Paths for NSMC Models 3 (top) and 41 (bottom) Flow Fields

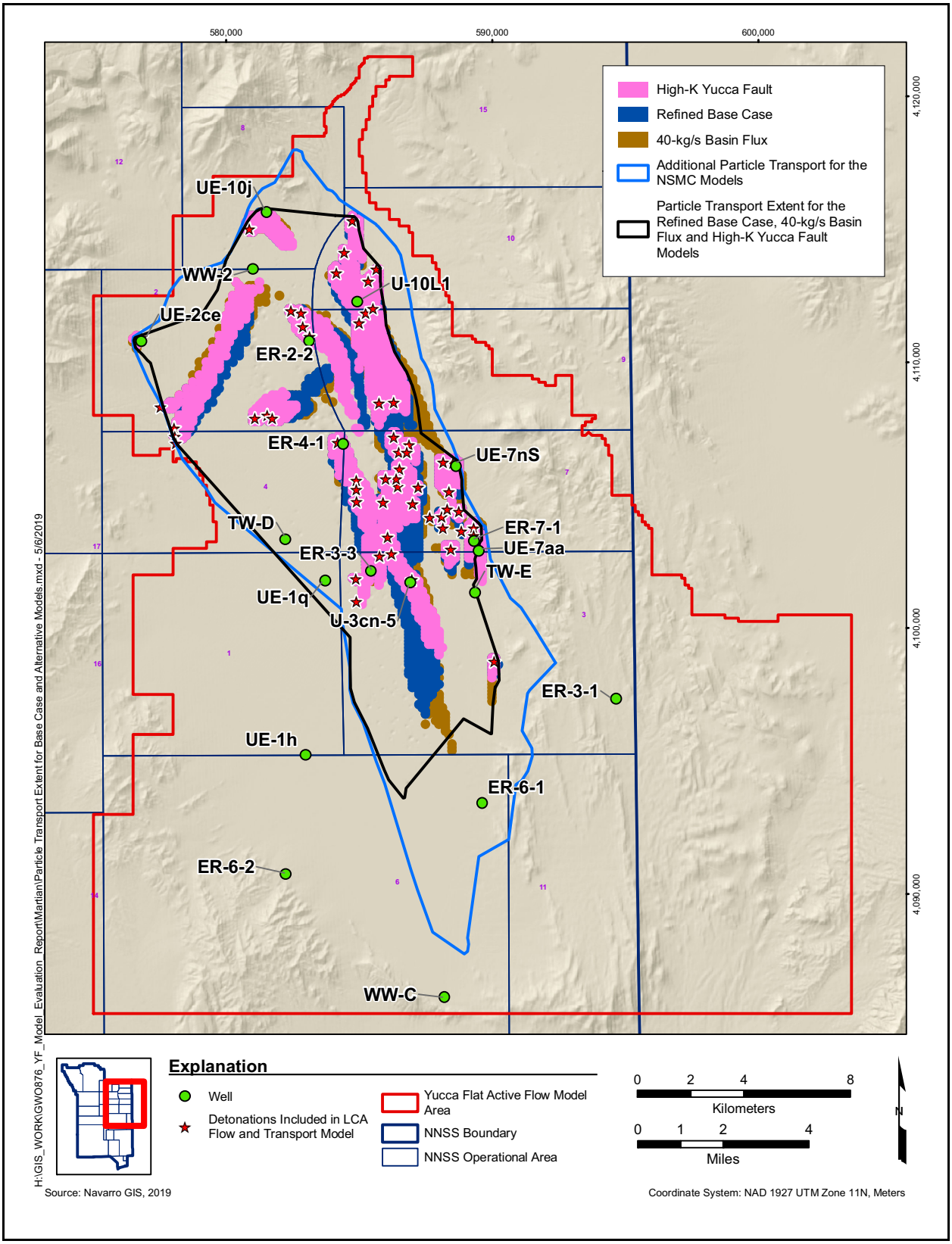

Figure 4-42
1,000-Year Time-Cumulative Probability of Exceedance of MCLs with NSMC 200-Year Particle Transport Extent

models with an acceptable calibration. The 200-year particle tracks approximate the extent of MCL exceedance predicted by the probabilistic transport models, which indicates that none of the NSMC models would predict MCL exceedance beyond approximately the midpoint between the ER-6-1 well cluster and WW-C.

In order to demonstrate the flow path variability among the NSMC models, 200-year particle tracks superimposed over the transmissivity are plotted in Figure 4-43 for 10 of the NSMC models. Eight of the models were selected because they have an acceptable calibration and particle tracks that extend beyond the bounding polygon for the base, 40-kg/s Basin Flux, and High-K Yucca Fault cases shown in Figure 4-42. Two of the NSMC models (NSMC models 41 and 74) have faults with lower permeability compared to the average country rock permeability and have less southerly particle tracks. The important model parameters for these 10 NSMC models are provided in Tables 4-4 and 4-5. A common aspect of the NSMC model with more southerly particle tracks compared to other NSMC models is that these models have a high permeability for the Yucca fault or the tied eastern fault group.

The source detonations contributing to the southerly particle tracks for each of the selected models are listed in Table 4-6. As can be seen in this table, the largest number of detonations contributing to the more extensive particle tracks for a single model is five, and is associated with NSMC model 28. A summary of the source detonations and explanation of the particle tracks seen from each of the sources listed in Table 4-6 includes the following:

- **NSMC models 3 and 8.** The LAREDO detonation is the southernmost detonation that may have a direct source to the LCA. The detonation is located in eastern Yucca Flat very near a fault that is within the tied eastern fault parameter group (Section 4.2.3.2). Both models have similar parameters and the permeability of the tied eastern fault group that is higher than the surrounding country rock on a large scale, resulting in higher particle velocity in faults.

- **NSMC model 4.** The TERRINE YELLOW detonation is located in northeast Yucca Flat very near a fault that is within the tied eastern fault parameter group. The fault and high country rock hydraulic conductivity in the local area near the detonation provide a hydraulic connection to the Yucca fault. Similar to NSMC models 3 and 8, high fault permeability increases transport south from this detonation compared to other NSMC models.

- **NSMC model 11.** The BASEBALL and BORREGO detonations are located in central Yucca Flat within a local area of high country rock permeability that is hydraulically connected to the Yucca fault. The PIRAHNA detonation is located very near the Yucca fault. The high permeability in the country rock surrounding these detonations along with a high Yucca fault

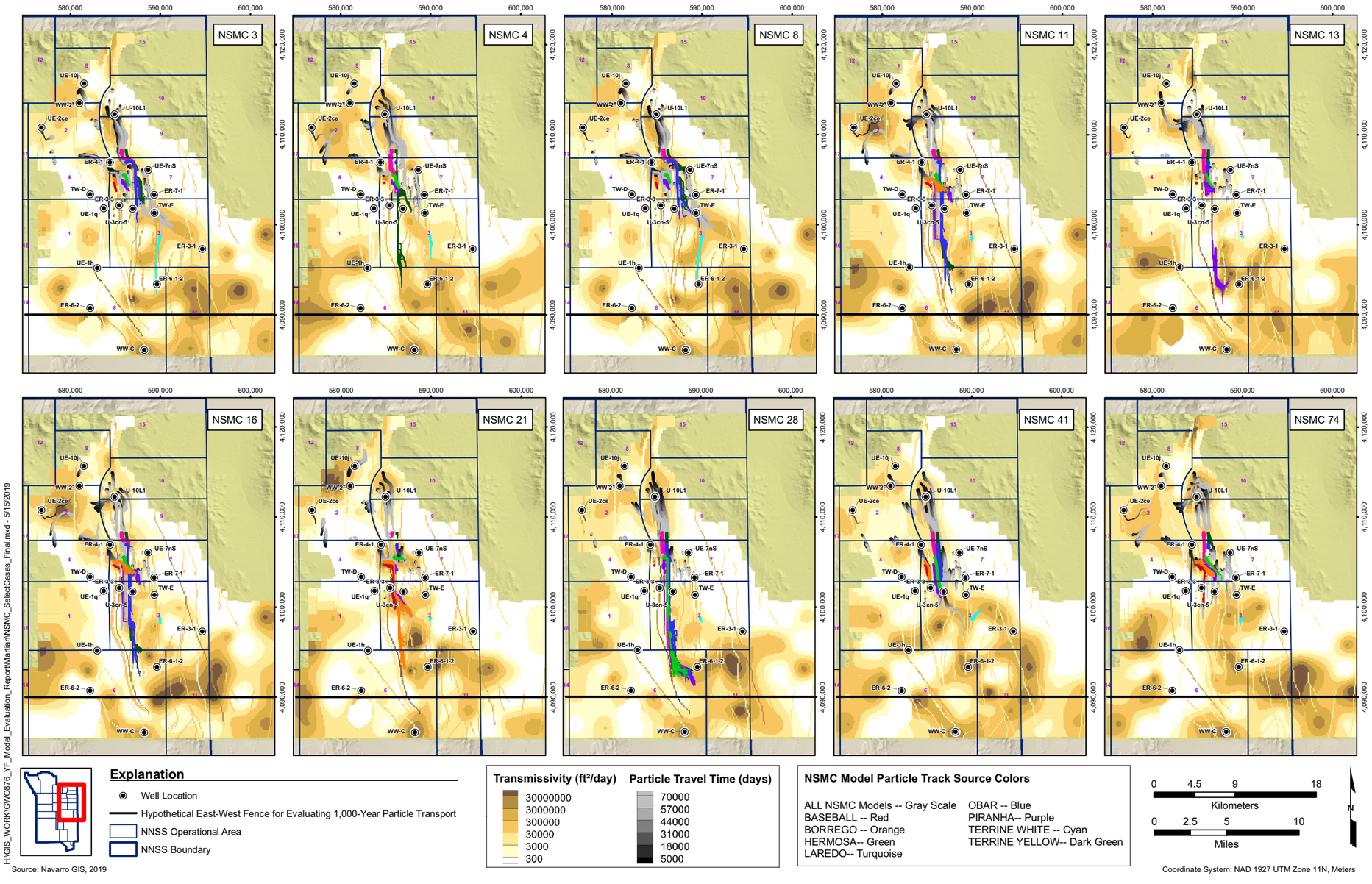

Figure 4-43
Particle Tracks and Transmissivity Field for Selected NSMC Models

Table 4-4
Hydraulic Conductivity Parameters for Select NSMC Models

NSMC Model	West Yucca Fault	East Yucca Fault	West Carpet bag Fault	East Carpetbag Fault	West Topgallant Fault	East Topgallant Fault	Western Tied Faults	Eastern Tied Faults	Pilot Point Geometric Mean
	Log10 Hydraulic Conductivity (ft/day)								
3	-0.60	1.29	-0.08	3.44	-1.56	-1.56	0.32	1.50	0.22
4	-1.51	1.69	0.39	-0.08	-1.56	-1.56	0.81	1.30	0.15
8	-0.60	1.22	0.08	3.44	-1.56	-1.56	0.31	1.58	0.24
11	-0.32	2.44	1.47	-0.36	-1.56	-1.56	0.54	0.23	0.30
13	-1.06	3.44	-1.56	1.85	-0.72	-1.56	-0.15	0.14	0.20
16	0.81	2.93	-0.78	0.07	-1.56	-1.56	-0.71	1.15	0.17
21	0.02	3.44	-1.46	0.71	-1.56	-1.56	-0.62	0.88	0.42
28	-0.88	3.44	-1.56	2.57	-1.56	-1.56	1.26	0.50	0.24
41	0.06	-1.17	-1.56	2.13	-1.56	-1.56	-1.26	0.19	0.05
74	-1.07	0.59	0.58	1.75	-1.56	-1.56	-0.16	0.29	0.11

Table 4-5
Basin Flux and Anisotropy Parameters for Select NSMC Models

NSMC Model	Yucca Flat Basin Flux (kg/s)	West Yucca Fault	East Yucca Fault	West Carpetbag Fault	East Carpetbag Fault	West Topgallant Fault	East Topgallant Fault	Tied Faults	Country Rock Geometric Mean
		Fault Log10 East–West to North–South Anisotropy							
3	33	-4.22	-2.42	-1.40	-2.20	-2.84	-1.45	0.00	-1.03
4	22	0.00	-2.78	-1.57	-1.19	-5.00	-1.05	0.00	-1.25
8	33	-4.17	-2.45	-1.38	-2.20	-2.81	-1.38	0.00	-0.97
11	21	-2.65	-1.81	-4.56	-3.24	-1.16	-2.01	0.00	-0.98
13	21	0.00	0.00	-2.80	-2.46	-5.00	-2.29	0.00	-1.16
16	21	-4.11	-2.22	-1.76	-4.60	-3.72	-1.97	0.00	-1.23
21	21	0.00	0.00	-4.48	-4.20	-3.43	-1.58	0.00	-0.95
28	21	0.00	-1.74	-0.41	-0.09	-2.41	-2.42	0.00	-1.56
41	22	-0.11	-1.83	-3.37	-2.09	-3.46	-1.99	0.00	-1.02
74	21	0.00	-1.34	-2.25	-2.25	-2.59	-1.89	0.00	-1.24

Table 4-6
Detonations in NSMC Models with Greater Particle Transport

Sources Responsible for 200-Year Particle Tracks with Southern Extent Greater than Base Case, 40-kg/s Basin Flux, and High-K Yucca Fault Case	NSMC Particle Tracks with Greater Southern Extent							
	NSMC Model Number							
	3	4	8	11	13	16	21	28
BASEBALL	No	No	No	**Yes**	No	No	No	No
BORREGO	No	No	No	**Yes**	No	No	**Yes**	No
HERMOSA	No	No	No	No	No	No	No	**Yes**
LAREDO	**Yes**	No	**Yes**	No	No	No	No	No
OBAR	No	No	No	No	No	**Yes**	No	**Yes**
PIRANHA	No	No	No	**Yes**	**Yes**	No	No	**Yes**
TERRINE- WHITE	No	No	No	No	No	No	No	**Yes**
TERRINE-YELLOW	No	**Yes**	No	No	No	**Yes**	No	**Yes**

permeability increases the southern extent of particle tracks. It is important to note the fault transmissivity traces illustrated in Figure 4-43 reflect the hydraulic conductivity at the model's surface multiplied by the model depth. The Yucca fault dips eastward, and the particle tracks within the Yucca fault at depth are more eastward than the surface fault trace.

- **NSMC model 13.** Similar to NSMC model 11, the very close proximity of the PIRANHA source to the Yucca fault and a very high permeability of the Yucca fault increases the southern extent of particle tracks. The behavior of particle movement in NSMC model 13 differs from NSMC model 11 because the country rock permeability near BORREGO and BASEBALL is less as hydraulically connected to the Yucca fault. The Yucca fault provides the primary hydraulic connection between north and south Yucca Flat because the country rock permeability near the boundary between of Areas 3 and 7 is very low. A similar behavior of the Yucca fault is seen in NSMC models 21 and 28.

- **NSMC model 16.** The TERRINE YELLOW and OBAR detonations are located in northeast Yucca Flat near faults that are within the tied eastern fault parameter group. The fault and high country rock hydraulic conductivity near the detonations provide a hydraulic connection to the Yucca fault. The behavior of particle movement in NSMC model 16 differs from NSMC model 4 because the country rock permeability surrounding OBAR is high compared to the same area in NSMC 11. The high permeability for the tied eastern fault group and the Yucca fault increases particle migration southward.

- **NSMC model 21.** The BORREGO detonation is located in central Yucca Flat within an area of high country rock permeability that is hydraulically connected to the Yucca fault. NSMC models 11 and 21 have very similar parameters. The Yucca fault has a very high permeability in both models and a large amount of northern recharge flows into the fault northwest of the BORREGO and BASEBALL detonations. The behavior of particle movement from the BORREGO and BASEBALL detonations in NSMC model 21 differs from NSMC model 11 because the permeability of the Yucca fault is one order of magnitude higher in NSMC model 21. The slightly more northern location of BORREGO allows more northwest recharge entering the Yucca fault to flow past BORREGO compared to BASEBALL.

- **NSMC model 28.** The HERMOSA, OBAR, PIRANHA, TERRINE WHITE, and TERRINE YELLOW detonations are located in country rock with higher-than-average country rock permeability and are in close proximity to the Yucca fault. The strong hydraulic connection to the Yucca fault increases particle migration southward. The Yucca fault permeability for NSMC model 28 (2,770 ft/day) is among the highest of the NSMC models.

- **NSMC models 41 and 74.** Flow in these NSMC models is more spread out and occurs in both country rock and faults, which results in lower particle velocities from detonations near faults, and particle tracks are less southerly compared to the other NSMC models presented in Figure 4-43.

The long, narrow particle paths seen in many of the NSMC flow fields illustrated in Figure 4-43 are due to particles traveling within high-permeability faults. Because the source locations for the

particles are identical from run to run, the differences in the extent of migration from individual detonations is mostly attributed to variability in fault and country rock permeability among the NSMC realizations. Although boundary flow values vary among the NSMC models, the variability in flow is small compared to variability in permeability. Differences in permeability within local areas of country rock surrounding detonations allow these detonations to be more or less hydraulically connected the high-permeability faults and account for the different particle tracks seen in NSMC models with similar fault permeabilities.

A total of 13 NSMC flow fields have 200-year particle tracks that extend beyond the southern extent of particle tracks from the base case and extensive transport alternative models (Figure 4-42). However, none of the NSMC flow fields predict particle tracks will reach LCA model's southern boundary within 200 years. NSMC model 28 (Figure 4-44) was identified as having significant particle transport at 200 years from the largest number of detonations and was selected for running full probabilistic transport simulations (see Section 4.7.4). Figure 4-45 presents the transmissivity field for NSMC model 28. Faults have a higher permeability than the surrounding country rock, especially the eastern splay of the Yucca fault. As with the High-K Yucca Fault model and NSMC model 3 discussed earlier in this section, this realization is influenced by vertical hydraulic gradients and high Yucca fault permeability that cause particles to descend significantly deeper in the LCA than in the basecase (Figure 4-44). The permeability of the eastern splay of the Yucca fault is 2 of orders of magnitude higher than the other faults in the NSMC model 28, making Yucca fault the dominant flow channel.

4.3.4 LCA Flow Model Uncertainty Analysis Conclusions

Based on the LCA flow model uncertainty analyses presented in this section, the following is concluded:

- The upper bound for groundwater flow through the Yucca Flat sub-basin (Figure 4-1) is approximately a twofold increase over the value estimated by Halford and Jackson (2019), which leads to significantly increased transport distance from RN source areas compared to the base case.

- Similar to the upper-bound (two-times) groundwater flow case, the High-K Yucca Fault case increased travel distances, but the increase is only along the fault trace, and total particle breakthrough near the model's southern boundary is less than for the upper-bound (two-times) groundwater flow model.

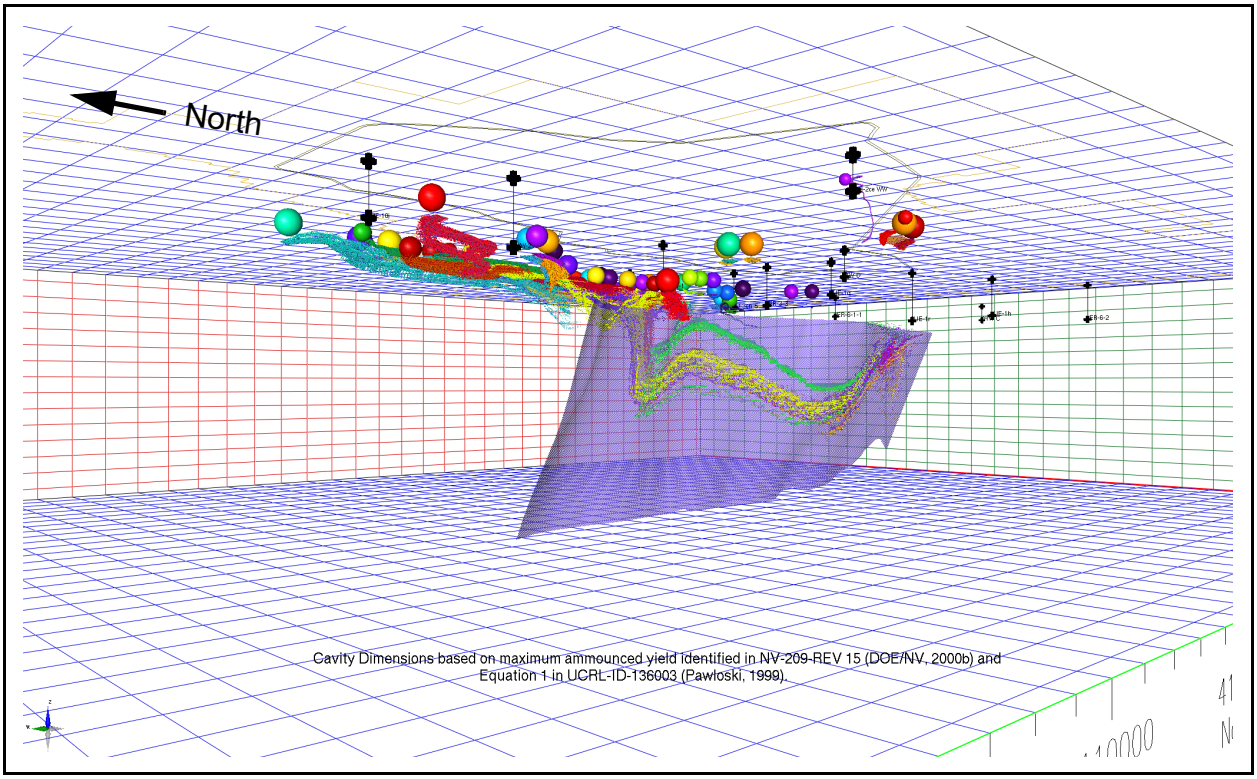

Figure 4-44
Perspective View of Particle Paths for NSMC Model 28 Flow Field along with the Eastern Splay of Yucca Fault (purple surface)

- The NSMC models illustrate that many alternative combinations of fault and country rock hydraulic conductivity can transmit similar amounts of water through the system and have adequate agreement with calibration observations within the LCA (i.e., water levels, pumping test drawdowns and estimates of transmissivity).

- The NSMC flow fields provide an adequate representation of the flow system variability and provide confidence that the extent of contaminant transport is adequately represented by the base case and alternative models run through probabilistic transport.

- The particle tracks produced by the NSMC flow fields show local variability, but southerly transport is confined to the Yucca fault and eastern Yucca Flat, and no transport pathways reach the Yucca Flat sub-basin's southern boundary within 200 years (Figure 4-42). Transport velocity is much reduced from the N-I (2013) models.

- The NSMC models with more southerly particle tracks compared to other NSMC models have a high permeability for the Yucca fault or the tied eastern fault group. Furthermore, the permeability of faults is generally higher than the surrounding country rock on a large scale (e.g., Yucca Flat Basin scale), resulting in higher particle velocity in faults.

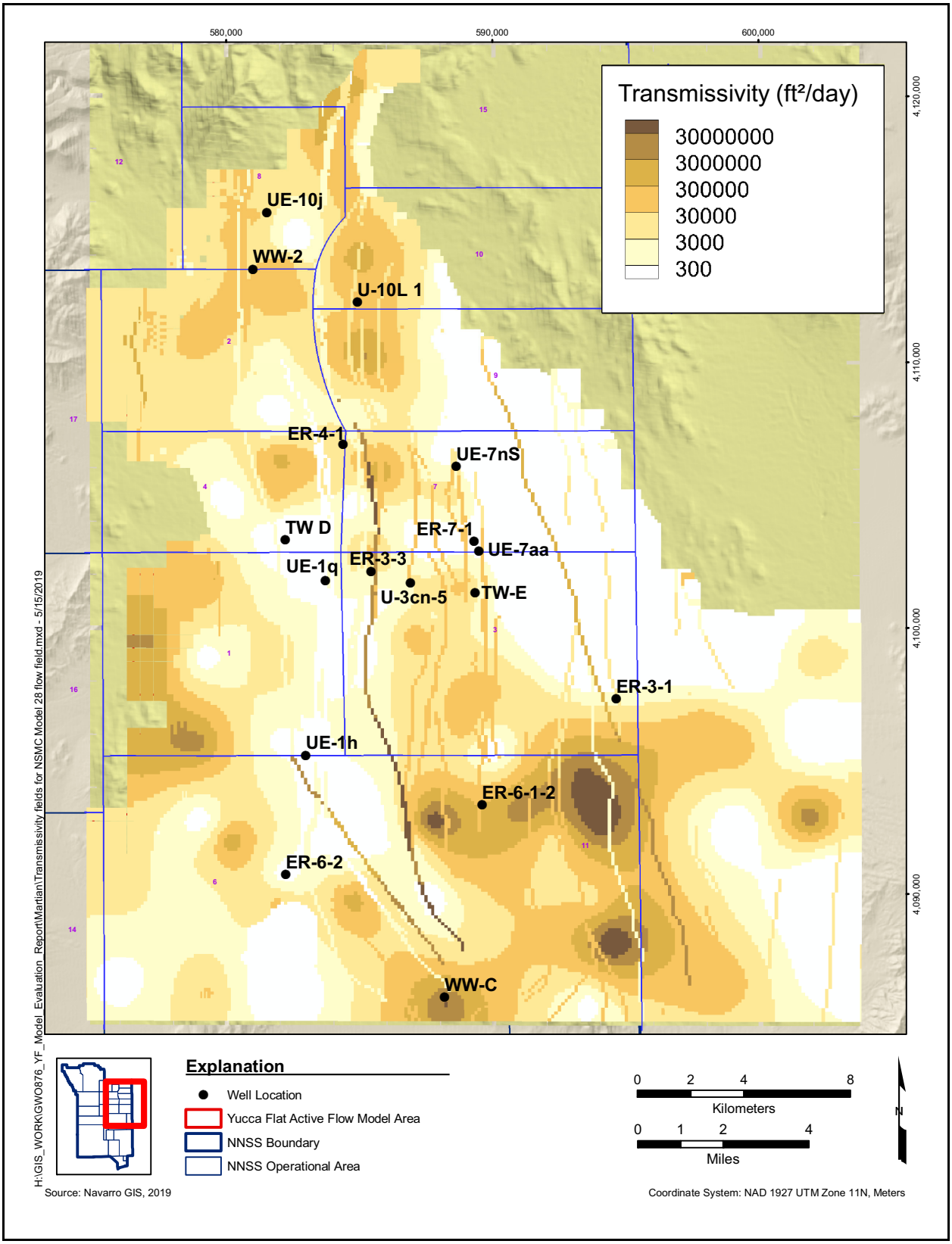

Figure 4-45
Transmissivity Fields for NSMC Model 28 Flow Field

- An extensive effort was made using the NSMC method to find alternative flow fields that result in either more extensive or different transport pathways than the base and the two alternative flow model calibrations. No significantly different flow fields were found.

The CADD/CAPP (DOE/EMNV, 2017d) states three models with alternative fault conceptualizations and increased transport compared to the N-I (2013) base case LCA model will be explored further, using the more realistic basin groundwater flux constraints. The three models are (1) models containing faults without low-permeability cores, (2) models containing only faults with trace lengths greater than 3 km, and (3) models with only the largest basin-forming faults. The base case and uncertainty models (i.e., the two more extensive transport and 75 NSMC models) meet the commitment of the model evaluation and the CADD/CAPP reports for the following reasons:

- All refined LCA flow models contain only faults with traces greater than 3 km, and fault anisotropy is used in place of a low-permeability core.
- Increased particle transport occurs in models with fewer faults compared to the base case because higher fault permeability results from using fewer faults in the model calibration. The High-K Yucca Fault model and NSMC model 28 represent the extreme case of using fewer faults in the model calibration because the Yucca fault has a very large permeability compared to other faults and the trace of the Yucca fault passes through the center of the testing area to the model's southern boundary.

4.4 Evaluation of Transient Pumping in Wells WW-C and WW C-1 on Transport

Tritium has been observed in WW C-1 and WW-C since the early 1960s (Section 2.1.3). The PER Committee postulated that the pumping in WW C-1 and WW-C may have captured ^{3}H from upgradient underground nuclear testing and is the cause for low levels of ^{3}H that have been observed in these wells. While the LCA flow and transport model is intended for probabilist simulations to forecast 95 percent 1,000-year CB, and not intended for simulating very low levels of detection (i.e., 12 pCi/L) at a specific location. the model was used to assess the level of influence the pumping at WW-C and WW C-1 might have on the overall contaminant transport forecasts,

The transient WW-C and WW C-1 pumping was simulated using the LCA flow models (base case, 40-kg/s Basin Flux, and High-K Yucca Fault) and the effect of pumping was evaluated on particle breakthrough near the model's southern boundary from particles originating from the 58 detonations with exchange volumes within $3R_c$ of the saturated LCA.

Water has been pumped from LCA water supply wells for potable or industrial use and to support nuclear testing activities. The majority of total water production occurred in WW-C and WW C-1 located in southern Yucca Flat near the LCA model's southern boundary. Well WW-C was used from September 1961 to July 1995, with an average annual production of 39.6 million gal. Well WW C-1 is located in close proximity to WW-C. The well started production in June 1962 and was regularly used until July 2013. Average annual production was 24.7 million gal for the years of 1962 through 2008. The estimated withdrawal rates from Wells WW-C and WW C-1 and are presented in Figure 4-46.

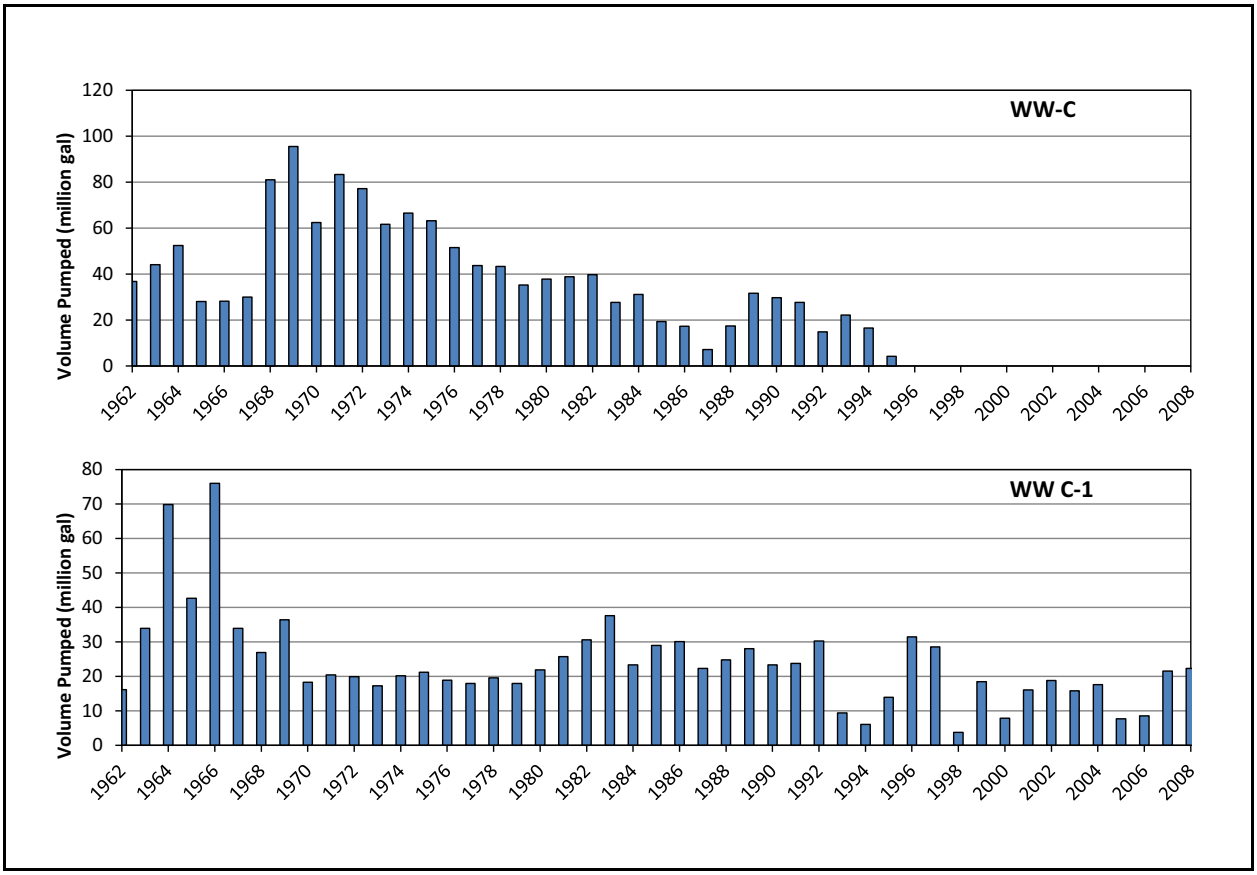

Figure 4-46
Production History for WW-C and WW C-1 Pumping Wells

The effects of including transient pumping in Wells WW-C and WW C-1 are as follows: the percentage of particles moving south of Northing 4,090,000 m near the model's southern boundary increased from 1.2 to 1.4 percent for the base case, 21 to 24 percent for the case with a twofold increase in groundwater flow between Wells ER-7-1 and ER-6-1, and 11 to 12 percent for the High-K

Yucca Fault case. Figure 4-47 illustrates the 1,000-year particle distribution for the three flow fields. Changes in the spatial distribution of the particles at 1,000 years cannot be visually discerned from plots of particle positions resulting from the steady-state flow fields illustrated in Figures 4-23, 4-27, and 4-30.

Pumping in Wells WW-C and WW C-1 was found to have small effects on particle breakthrough near the model's southern boundary because of the following: (1) drawdown is small compared to the steady-state gradient; (2) water levels quickly recover to pre-pumping levels upon cessation of pumping; and (3) the approximately 50-year pumping period is short compared to the first particle arrival time at the southern boundary (e.g., 900 years for the base case and 300 years for High-K Yucca Fault flow fields). The LCA transmissivity at Well WW-C is the highest estimated value within the Yucca Flat. Simulated transmissivity in the LCA and DV3 models near WW-C exceed 1 million ft^2/day (Figure 4-20). Although the WW-C and WW C-1 wells are located near the model's southern boundary, which has a specified head boundary condition, the simulated head at the time of peak pumping is still higher than the specified head boundary nearest to WW-C, and no water pumped from WW-C and WW -C-1 was withdrawn from the southern boundary. This finding is consistent with Fenelon et al. (2012), in that historical pumping in the LCA would affect water levels east of Carpetbag fault, but maximum responses are small (no more than several feet), and most of the response would dissipate quickly once the pumping ceases.

4.5 LCA Flow Modeling Summary and Conclusions

The goal of the LCA flow model refinement was to produce more realistic flow and transport models compared to the N-I (2013) model that also reproduce the observations within the LCA (i.e., steady-state and transient water levels and estimated basin flows). The overly conservative nature of the N-I (2013) transport model was primarily due to overestimating total groundwater flow and velocity through the Yucca Flat testing area and source term concentrations for ^{90}Sr and ^{137}Cs. Considerably lower groundwater flow values than those reported for the base case (N-I, 2013) model have resulted from reanalysis of the ER-6-1-2 MWAT as part of the model evaluation data collection/data analysis activities and were used in calibrating the LCA flow models. Although data collection activities have reduced model uncertainty, particularly in the total basin flow, uncertainties still persist in all aspects of the LCA flow model. Therefore, it is not possible to conclusively identify a representative flow field during model refinement. However, a more realistic base case along with

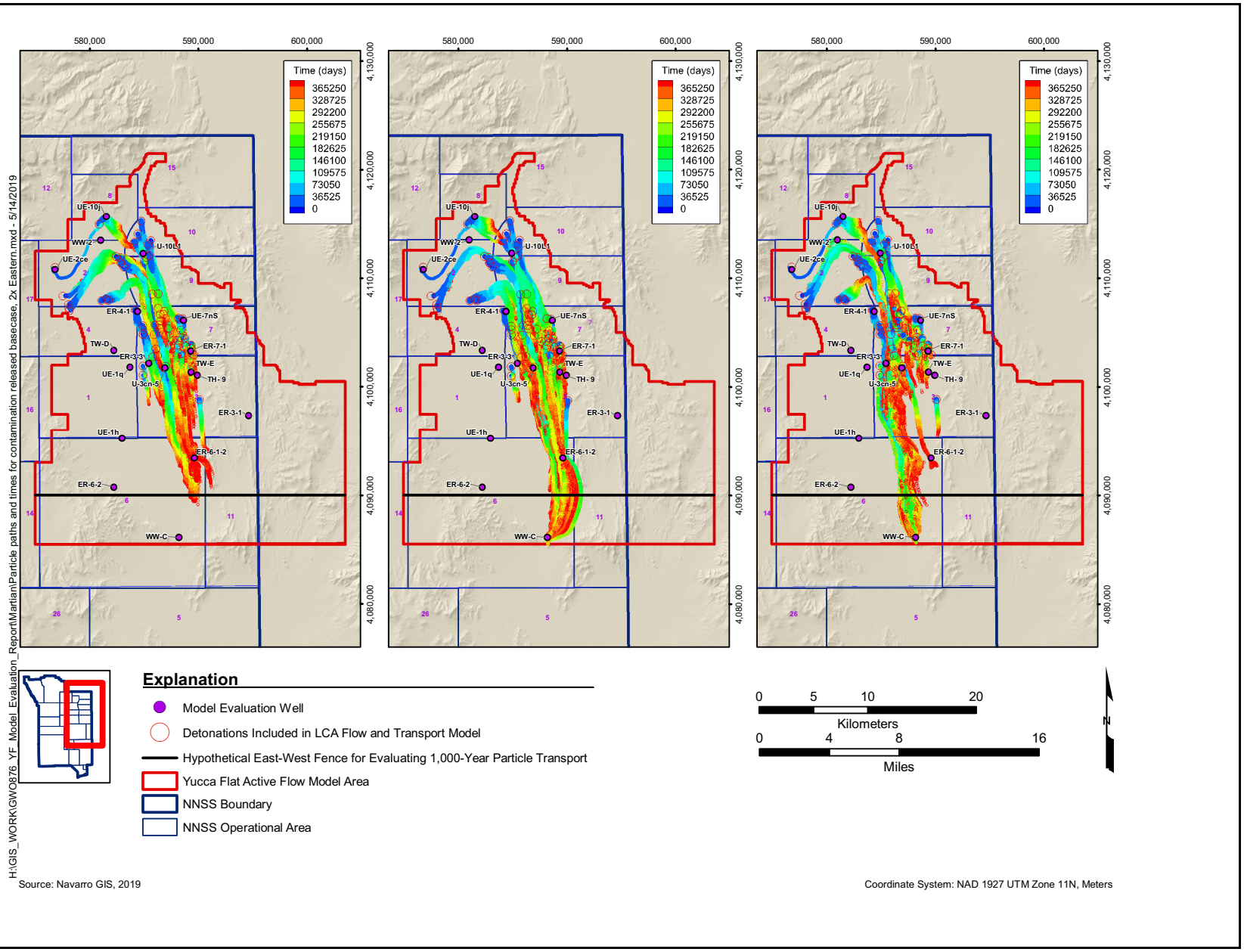

Figure 4-47
Particle Paths and Times for Contamination Released at Each Detonation Included in the LCA Flow and Transport Model for the Base Case (left), 2 Times Eastern Yucca Flat Flow Rate (center), and High-K Yucca Fault (right)

three alternative flow fields that lead to greater transport have been developed that are expected to realistically bound RN transport.

Calibrations of alternative models resulting from conceptualization of more extensive transport conditions and a global uncertainty analysis using the NSMC approach identified the range in possible flow fields given the LCA observations, and the constraints provided by uncertainty in the ranges of hydraulic properties. Uncertainty exists in how faults influence the flow field. Model calibrations with similarly low objective function could have very different fault behavior. Faults can behave as flow conduits in lower hydraulic conductivity country rock or as leaky flow barriers in higher hydraulic conductivity country rock. Faults acting as conduits will result in faster groundwater flow within the fault zones and potentially increased transport. Deep particle transport occurs in faults under these conditions due to flow channelization within the narrow fault zones and vertical gradients created as shallow recharge enters the higher section of faults. The LCA flow model uncertainty analyses illustrate that many alternative combinations of fault and country rock hydraulic conductivity can transmit similar amounts of water through the system.

Based on the above summary, it is concluded that the LCA flow models developed and calibrated in this section are a reasonable representation of the range of possible flow conditions that could potentially affect the extent of contaminant transport in Yucca Flat. The key findings that support this conclusion are summarized as follows:

- Model refinement has produced a set of models that have Yucca Flat basin flow values consistent with the DV3 model and significantly reduced particle travel compared to the N-I (2013) models.
- The model refinement used the pilot point model parameterization approach that facilitates generation of more realistic transmissivity fields compared to the N-I (2013) that are consistent with the observed hydrogeologic conditions in Yucca Flat.
- Many alternative combinations of fault and country rock hydraulic conductivity can transmit similar amounts of water through the system and have adequate agreement with observations within the LCA (i.e., water levels, pumping test drawdowns, basin flow, and measurements of transmissivity).
- Topgallant fault is highly identifiable as being a hydraulic barrier between eastern and western Yucca Flat (i.e., low hydraulic conductivity and strong east–west to north–south anisotropy). Hydraulic isolation of western Yucca from eastern Yucca Flat was evident by the

absence of drawdowns in western Yucca Flat wells during the ER-4-1 WDT and ER-6-1-2 MWAT pumping.

- The model calibration produced moderate to strong east–west to north–south anisotropy in faults and the country rock that is highly identifiable. The calibrated anisotropy values are consistent with the large-scale extensional faulting that has occurred in the Yucca Flat area. The major basin-forming faults generally strike in a northerly direction (e.g., Yucca, Topgallant, and Carpetbag faults), thereby creating higher north–south permeability.

- Most groundwater entering in the northern half of the basin passes through a high-transmissivity corridor in eastern Yucca Flat before exiting in the south.

- Flow in eastern Yucca Flat is generally southward through the high-transmissivity corridor. Flow in western Yucca Flat is generally eastward/southeastward in the southwest and is generally northeastward in the northwest.

- The particle tracks produced by the NSMC flow fields show local flow path variability, but no travel pathways reach the Yucca Flat sub-basin boundary within 200 years. Contaminant migration likely occurs in eastern Yucca Flat, with most of the contamination remaining north of the ER-6-1 well cluster.

- Pumping of WW-C and WW C-1 has a negligible effect on particle breakthrough near the model's southern boundary.

4.6 LCA Model HST

This section presents the revised HST for the LCA transport model. The revisions include considering sorption in the calculation of source term initial concentrations and considering depth to LCA in the HST parametric uncertainty. The RST is the total residual RN inventory in water, glass, other phases, or mineralogic forms resulting from one or more underground nuclear detonations, which may or may not be readily available to groundwater. In groundwater transport modeling, the HST defines the boundary condition for the contaminant releases to the environment, and estimating the HST is crucial for assessing the potential groundwater contamination. The framework for the development of the HST conceptual model for Yucca Flat is described in SNJV (2009), and the implementation of the HST conceptual model for the Phase I transport calculations is described in N-I (2013).

The overly conservative nature of the N-I (2013) flow and transport modeling was in part due to overestimating the source term concentrations of ^{90}Sr and ^{137}Cs. The approach taken to calculate the HST for the refined LCA model is similar to the approach taken to calculate the N-I (2013) HST, with the exception that the overly conservative nature of the N-I (2013) HST was corrected by considering

RN sorption onto the in-fallen cavity/chimney rubble in the calculation of the initial source area concentration (Section 3.5.2). An additional departure from the N-I (2013) HST is that the contact depth of the LCA is recognized as being uncertain.

4.6.1 HST Allocation to the LCA Model

The total RST inventory in the YF/CM CAU comprises about 39 percent of the total RN activity in 2012 of all detonations in the UGTA CAUs. The unclassified inventory of the RST for the NNSS presented in Finnegan et al. (2016) provides an estimate of radioactivity remaining underground after the nuclear testing. This inventory is referred to as the "Finnegan inventory" in this section. The Finnegan inventory is decay corrected to September 30, 2012. Initial RN concentrations distributed around each detonation point in the exchange volume comprise the model HST and are calculated considering the RN inventory, melt-glass partitioning factors, exchange volume size, glass dissolution amounts, depth to the LCA, and sorption to in-fallen rubble within the cavity.

Three models were developed in N-I (2013) to address the unique hydrogeologic conditions contributing to RN migration at Yucca Flat: (1) the UZ, (2) the saturated zone within the alluvium and Tertiary volcanics (SZ AA/VA), and (3) the Paleozoic carbonate aquifer known as the LCA. The HST must be allocated between the models for detonations with source volumes that span two or more models. Revision of the N-I (2013) HST requires recalculating the initial exchange volume concentration within the three models to determine the inventory fraction initially within the LCA model. As discussed in Section 2.9, sorption within the UZ and SZ AA/VA models can significantly reduce exchange volume initial RN concentrations and the fraction of inventory within the LCA HST.

A stochastic approach (Monte Carlo) was used for simulating transport to explore the range of parametric uncertainty. For each realization, the uncertain HST parameter values were sampled from parameter distributions. Uncertain parameters were assumed to be mutually independent. They are also assumed to be independent for each detonation, with the exception of depth of the LCA (which was taken to be consistent across the 58 detonations), and sampling of the distributions was performed using the Latin hypercube method. The assumptions associated with the HST calculation and parameter distributions are as follows:

- **Consideration of melt-glass partitioning uncertainty.** The Rainier Mesa HST (Tompson et al., 2011) reviewed partitioning of RNs into the melt glass from the original IAEA work (IAEA, 1998a), the RAINIER site, and the CHANCELLOR site. These data provided a basis

for estimating ranges of partitioning behavior for the Finnegan et al. (2016) RNs. The RST associated with the melt glass is excluded from the HST because the melt-glass dissolution is minimal within transport simulation time frame (N-I, 2013). Table 4-7 presents melt-glass partitioning distributions.

Table 4-7
Parametric Uncertainty Distribution for Melt-Glass Partitioning Factors

Data	0 to 50% Melt-Glass Fraction	30 to 70% Melt-Glass Fraction	40 to 80% Melt-Glass Fraction	20 to 70% Melt-Glass Fraction	25 to 40% Melt-Glass Fraction	70 to 90% Melt-Glass Fraction	95 to 100% Melt-Glass Fraction
Distribution	Triangular	Triangular	Triangular	Triangular	Triangular	Triangular	Triangular
Low	0	30	40	20	25	70	95
High	50	70	80	70	40	90	100
Mode	25	50	60	45	32.5	80	97.5
RNs	^{36}Cl,^{129}I	^{41}Ca	^{90}Sr, ^{99}Tc	^{135}Cs	^{137}Cs	^{235}U,^{238}U	^{63}Ni, ^{237}Np, ^{238}Pu, ^{239}Pu, ^{240}Pu

- **RN-specific exchange volume radii.** The exchange volume radii are based on observations of RN distributions from the Rainier Mesa RAINIER and central Pahute Mesa CHANCELLOR detonations (Tompson et al., 2011), and from numerical modeling performed for the Yucca Flat HST (Carle et al., 2008). The exchange volume is dependent on the RN's group of being refractory, volatile, or gaseous. Volatile and gaseous RNs have exchange volumes with radii ranging from 1.5 to $3R_c$ within the saturated zone and include ^{3}H, ^{14}C, ^{36}Cl, ^{41}Ca, ^{90}Sr, ^{99}Tc, ^{129}I, ^{135}Cs, and ^{137}Cs. Refractory RNs have exchange volumes radii ranging from 1 to $1.5R_c$ and include ^{63}Ni, ^{235}U, ^{238}U, ^{237}Np, ^{238}Pu, ^{239}Pu, and ^{240}Pu. The exchange volume radii are sampled using triangular distributions as described in Section 3.2.1.

- **Estimation of RST uncertainty.** The uncertainty in the RST for each RN is based on the qualitative uncertainty estimates provided in Finnegan et al. (2016). The uncertainty was reported to be ±300 percent for ^{3}H, ± a factor of 10 for activation products, ±30 percent for fission products, and ±20 percent for residual fuel and tracer RNs. The uncertainty is parameterized with log triangular distributions symmetric about the mean with the ranges identified in Finnegan et al. (2016) representing the minimum and maximum extent of the distributions. Table 4-8 presents the Finnegan RST parametric uncertainty distributions.

- **Initial exchange volume concentration considers sorption.** Sorption processes will greatly reduce aqueous RN concentrations within the exchange volume's cavity/chimney for many RNs. The revised conceptual model for the initial RN concentrations in the exchange volume is presented in Section 3.5.2. The initial concentration calculation assumes equilibrium between the fracture and matrix porosity within the cavity/chimney and within the exchange volume fractures outside the cavity. The exchange volume fracture porosity is assumed to be 0.001 beyond the cavity for all rock types except alluvium, and the cavity/chimney porosity is a sampled random variable with a triangular distribution (min = 0.3, mode = 0.4, max = 0.5),

Table 4-8
Parametric Uncertainty Distributions for the Finnegan RST

Data	Fission Products Log RST Multiplier	Unspent Nuclear Fuel Log RST Multiplier	Nuclear Fuel Activation Products Log RST Multiplier	^{3}H Log RST Multiplier	Activation Products Log RST Multiplier
Distribution	Triangular	Triangular	Triangular	Triangular	Triangular
Low	-0.1139	-0.07918	-0.1761	-0.4772	-1
High	0.1139	0.07918	0.1761	0.4772	1
Mean/Mode	0	0	0	0	0
RN	^{90}Sr, ^{99}Tc, ^{129}I, ^{135}Cs, ^{137}Cs	^{235}U,^{238}U	^{237}Np, ^{238}Pu, ^{239}Pu, ^{240}Pu	^{3}H	^{14}C, ^{36}Cl, ^{41}Ca, ^{63}Ni

representative of the range of values used in HST modeling performed by LLNL (Carle et al., 2007; Tompson et al., 2008 and 2011). The alluvium is assumed to be porous media in the entire exchange volume, and the porosity is 0.34 (N-I, 2013). The HSU K_d values are assumed to be a lognormal-distributed random variable, and the distribution mean values and standard deviation values are the values used in the RN screening from N-I (2013, Appendix C). Table 4-9 presents the K_ds assigned by rock HSU. The cavity/chimney K_d is the thickness weighted average K_d based on the thicknesses of the HSUs between the exchange volume top and WP.

Table 4-9
Parametric Uncertainty Distributions for HSU-Specific K_ds
(Page 1 of 2)

HSU	Ca	Cs	Sr	Ni	Sm	Eu	Am	Np	Pu	U
Log10 K_d Mean (mL/g)										
AA	2.39	4.09	2.07	2.84	3.68	3.30	3.59	0.57	2.39	0.20
ATCU	2.73	3.52	2.39	3.58	4.01	3.62	4.31	0.95	3.09	0.77
LCA	-0.21	0.0 [a]	-2.18	-0.29	4.34	3.78	3.94	1.20	2.23	-1.94
LTCU	3.30	3.88	3.12	2.79	3.27	2.88	3.53	0.23	2.32	0.07
MGCU	0.84	4.05	0.61	2.87	3.17	2.95	3.60	0.13	2.48	0.11
OSBCU	3.17	3.86	2.98	3.00	3.28	2.95	3.71	0.24	2.50	0.13
TMLVTA	2.32	3.54	2.07	2.81	3.26	2.87	3.54	0.19	2.32	-0.04
TMUVTA	2.64	3.70	2.41	3.01	4.08	3.56	3.99	1.00	2.66	0.18
TMWTA	2.13	3.50	1.88	2.66	3.18	2.77	3.41	0.11	2.19	-0.15
TSA	2.44	3.63	2.26	1.97	2.11	1.85	2.66	-0.88	1.46	-0.97
TUBA [b]	2.44	3.63	2.26	1.97	2.11	1.85	2.66	-0.88	1.46	-0.97
UTCU	3.35	3.83	3.18	2.23	2.36	2.10	2.92	-0.62	1.72	-0.71

Table 4-9
Parametric Uncertainty Distributions for HSU-Specific K_ds
(Page 2 of 2)

HSU	Ca	Cs	Sr	Ni	Sm	Eu	Am	Np	Pu	U
Log10 K_d Standard Deviation (mL/g)										
AA	0.28	0.35	0.29	0.39	0.36	0.34	0.19	0.26	0.31	0.24
ATCU	0.25	0.29	0.29	0.32	0.33	0.44	0.28	0.19	0.36	0.24
LCA	0.41	0.0 [a]	0.33	0.39	0.39	0.36	0.06	0.35	0.40	0.35
LTCU	0.37	0.28	0.34	0.32	0.32	0.42	0.27	0.19	0.35	0.24
MGCU	0.30	0.33	0.23	0.41	0.52	0.55	0.29	0.21	0.38	0.28
OSBCU	0.35	0.29	0.33	0.32	0.40	0.50	0.29	0.18	0.37	0.25
TMLVTA	0.27	0.32	0.29	0.32	0.33	0.43	0.28	0.19	0.36	0.24
TMUVTA	0.29	0.31	0.31	0.32	0.31	0.32	0.17	0.30	0.31	0.24
TMWTA	0.26	0.33	0.29	0.32	0.31	0.41	0.27	0.20	0.36	0.24
TSA	0.35	0.32	0.33	0.32	0.52	0.56	0.30	0.21	0.38	0.28
TUBA [b]	0.35	0.32	0.33	0.32	0.52	0.56	0.30	0.21	0.38	0.28
UTCU	0.39	0.28	0.35	0.32	0.52	0.56	0.30	0.21	0.38	0.28

Source: Values from the screening analysis presented in N-I (2013).

[a] LCA Cs K_d is zero.
[b] TUBA uses the TSA K_d value.

TUBA = Tub Spring aquifer
UTCU = Upper tuff confining unit
Am = Americium
Eu = Europium
Sm = Samarium

- **LCA contact depth.** The LCA contact depth was investigated as contributing to the exchange volume size/shape that extends into the LCA model (Section 2.8). As part of the investigation, 100 unique surfaces were generated using a cross-validation approach for including the LCA depth in the HST parametric uncertainty. Depth to LCA uncertainty was included in the HST calculation by randomly sampling an LCA surface that was used consistently across the 58 selected detonations for each of the 100 HSTs which were generated for transport calculations.

The N-I (2013) modeling screened the RNs that are relevant to forecasting the Yucca Flat CB. Initial RN concentrations in exchange volumes were calculated considering uncertainties in inventory, partitioning, exchange volume size, glass dissolution, and matrix sorption. The 95th-percentile concentration at one-tenth of the MCL was used as the screening criteria to determine which RNs should be retained for analysis. The retained RNs are ^{3}H, ^{14}C, ^{36}Cl, ^{41}Ca, ^{63}Ni, ^{90}Sr, ^{99}Tc, ^{129}I, ^{135}Cs, ^{137}Cs, ^{235}U, ^{238}U, ^{237}Np, ^{238}Pu, ^{239}Pu, and ^{240}Pu.

Figure 4-48 presents the cumulative distribution for initial concentrations from the 100 realizations of the 58 detonations within $3R_c$ of the saturated LCA. Initial concentrations are generally consistent with the screening concentrations calculated in N-I (2013). Tritium has the highest initial concentrations and may be higher than 1E+06 times the MCL. At the 50 percent confidence interval ^{3}H, ^{14}C, ^{36}Cl, ^{90}Sr, ^{99}Tc, and ^{129}I exceed the threshold concentration of 1 MCL. Increasing the confidence interval to 95 percent, ^{137}Cs, ^{238}U, and ^{239}Pu are added to the list of RNs exceeding the threshold.

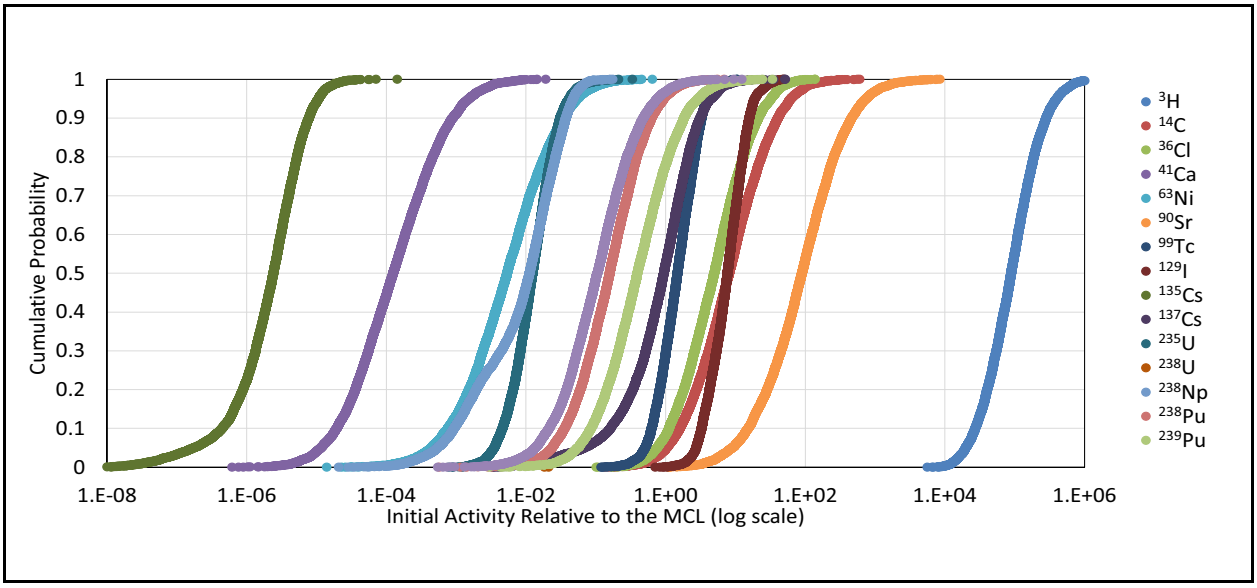

Figure 4-48
Cumulative Distribution Function for RN Initial Concentrations within the Exchange Volume

4.6.2 NASH Source Term

Satellite Well UE-2ce, located 183 m south of the NASH WP, is the only known location within Yucca Flat where an RN has been found to exceed its MCL in a carbonate aquifer (Table 2-4). However, the HST allocation to the LCA model discussed in Section 4.6.1 would mostly exclude the NASH source because the NASH WP is located within the UZ and only a few realizations place a small part of the exchange volume below the water table.

An alternative source term for the NASH detonation is generated using the Yucca Flat carbonate test HST modeling performed by Carle et al. (2008). This carbonate HST modeling attributed ^{3}H flux to the water table from perched water drainage into the NASH cavity/chimney. Carle et al. (2008)

provide the transient mass flux to the water table for a non-decaying species. The flux rate is used to scale a decaying source terms for ^{3}H and other RNs. Uncertainty in the source term is introduced using the RST uncertainty from Finnegan et al. (2016) as an HST multiplier.

The cavity at NASH intersects the tuff above the WP and includes a significant fraction of tuff in the cavity/chimney rubble. The revised RST allocation to the LCA model assumes equilibrium sorption within the exchange volume and considers the cavity/chimney K_d an uncertain parameter. The source terms for sorbing RNs were also scaled from Carle et al. (2008) ^{3}H breakthrough by assuming that transport through the saturated zone is identical to ^{3}H, but sorption occurs within the exchange volume. Initial concentrations within the exchange volume were from the revised RST. The model includes three assumption: (1) the perched water drainage to the water table is primarily from within the cavity/chimney system that is within $3R_c$ of the WP; (2) the volume of water flowing through the source area from precipitation derived recharge is insignificant compared to the volume of water from perched water drainage; and (3) RN sorption occurs only within the tuffaceous cavity/chimney rubble. The observations of ^{3}H, ^{90}Sr, and ^{137}Cs in Well UE-2ce are generally consistent with the scaled NASH source term. The ratio of ^{90}Sr and ^{137}Cs relative to ^{3}H is 10E-09 to 10E-05 at Well UE-2ce (Section 2.4).

4.7 Contaminant Boundary Forecasts

This section presents the evaluation of contaminant transport from underground nuclear detonations using the calibrated LCA flow model and three alternative flow fields. As described below, the transport models require the following information:

- Calibrated flow models (Sections 4.2.5, 4.3.2.1, 4.3.2.2, and 4.3.3)
- Maximum exchange volume size (Section 3.2.1)
- Highest saturated LCA elevation (Section 3.2.2)
- HST allocation to the LCA (Sections 4.6.1 and 4.6.2)
- Transport parameter distributions (Section 4.7.3)

This section also presents a comparison of the extents of contamination forecast by the model with present-day observations.

4.7.1 Transport Conceptual Model

The LCA contaminant transport conceptual model is unchanged from what is described in detail in N-I (2013). Contaminant transport is conceptualized as occurring in a dual-porosity system, in which solutes interact between fracture and matrix water through the matrix diffusion coefficient (D_m). Transport process include radioactive decay of the species, advection and dispersion in porous and fractured media, diffusion from fracture water into matrix water, and sorption onto immobile minerals. All sorption reactions are assumed to occur under equilibrium conditions and are characterized either with a matrix (K_d) for the matrix or with a retardation factor (R_f) for sorption on the linings of the fractures. Decay chains and their daughter products are not explicitly included in the radioactive decay process. Colloid-facilitated transport is not considered.

4.7.2 Numerical Model Approach

As described in N-I (2013), two numerical codes are used to simulate flow and transport processes in the LCA at Yucca Flat: FEHM (Zyvoloski et al., 1997a) and PLUMECALC (Robinson et al., 2011). FEHM uses a particle-tracking algorithm called "sptr" to determine flow paths and particle trajectories from the velocity field of the flow model. This particle-tracking algorithm defines the temporal and spatial distribution of advective-dispersive particle trajectories along the forecast travel paths derived from the velocity fields developed in FEHM. PLUMECALC is a convolution-based transport code that uses the particle-track information generated by FEHM to calculate the mobile resident solute concentration (i.e., volume-averaged concentrations of RNs dissolved in mobile fluid) by superposition of solute flux over the particles.

PLUMECALC requires the following inputs:

- Particle trajectories and transport times (i.e., particle tracks) from each source location, developed from each flow model
- Source contaminant mass flux distributions for each modeled RN as a function of time at each source location
- Transport parameter distributions

Particle tracks were created using each of the LCA flow models (i.e., the base case [Section 4.2.5], High-K Yucca Fault [Section 4.3.2.2], 40-kg/s Basin Flux [Section 4.3.2.1], and NSMC model 28 [Section 4.3.3]). Each LCA source (i.e., each of the 58 detonations identified in Section 3.2.3.1;

Table 3-2) was simulated with 10,000 particles in FEHM-sptr in order to create the particle information for input to PLUMECALC. The initial particle locations were randomly distributed within a region defined by an inverted spherical cap, as shown in Figure 4-49 for the BOURBON detonation, for example. The dimensions of the inverted spherical cap were unique to each source location. Assuming an exchange volume with a radius of $3R_c$ for the purpose of particle placement (the largest R_c multiplier listed in Table 3-1) centered at the WP, the height of the spherical cap was determined using the highest saturated LCA elevation at each detonation location (Section 3.2.2). This produced the largest possible distribution of particles (i.e., the largest spherical cap). For a few sources, the initial particle locations were adjusted to ensure all particles were placed within the LCA model grid. This adjustment varied from source to source, but was between a minimum of 25 m and a maximum of 250 m (for comparison, the width of the smallest model cells in the LCA grid is 125 m). For example, the active LCA nodes of the LCA model grid are discontinuous just under the location of the NASH WP. Therefore, the initial particle locations for NASH were moved west 178.9 m and south 80.3 m (for a total offset of 196 m; for comparison, nodal spacing in this region of the grid is 125 m) in order to ensure placement in an area with nodal continuity in the LCA.

A stochastic (i.e., Monte Carlo) approach was used for simulating transport for 1,000 years to explore the range of parametric uncertainty. In this Monte Carlo approach, for a given calibrated groundwater flow field and particle trajectories that are calculated for the given advective flow field with a given dispersivity, 400 transport realizations are performed, with each realization sampling the uncertain transport parameter values from parameter distributions (see Section 4.7.3), and the uncertain source mass flux from source mass flux distributions for each RN. The RNs modeled are ^{3}H, ^{14}C, ^{36}Cl, ^{41}Ca, ^{63}Ni, ^{90}Sr, ^{99}Tc, ^{129}I, ^{135}Cs, ^{137}Cs, ^{235}U, ^{238}U, ^{237}Np, ^{238}Pu, ^{239}Pu, and ^{240}Pu (Section 4.6.1). For all detonations except NASH, the source contaminant mass flux was determined by applying the portion of the inventory contained in the saturated LCA at the day of the detonation as presented in Section 4.6.1. The source contaminant mass flux from NASH was generated using the Yucca Flat carbonate test HST modeling performed by Carle et al. (2008) as described in Section 4.6.2. The source contaminant mass flux for each detonation was divided equally amongst the 10,000 particles starting at that source.

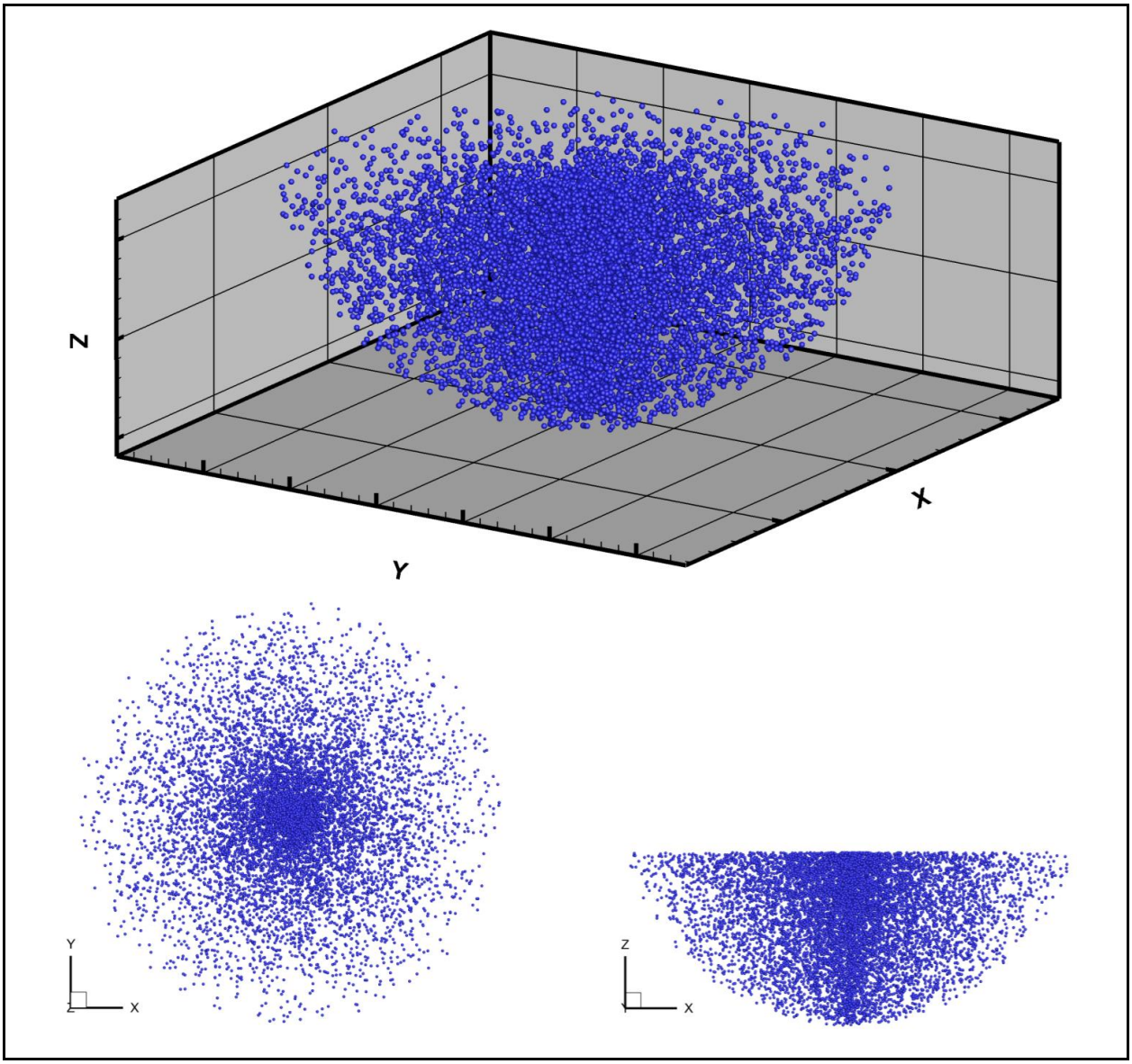

Figure 4-49
Initial Particle Locations for the BOURBON Detonation

4.7.3 Transport Parameters

This section presents the parameter distributions used for the transport modeling. Transport parameters include fracture properties (fracture porosity, fracture conductivity, and fracture spacing or fracture aperture); matrix porosity; matrix diffusion (D_m); dispersivity; fracture retardation (R_f); and matrix sorption. In this work, fracture porosity and fracture conductivity are sampled as independent parameters; fracture spacing is assumed; and fracture aperture is calculated from

Equation (4-1) (see Section 4.7.3.2). Note that Darcy velocity obtained from the flow model is used for calculating the advective transport.

The distributions for the fracture parameters, matrix porosity, and matrix diffusion parameters were the same as those used for the alternative LCA parameterization given in Table 6-1 of N-I (2013).

The distributions for matrix K_d were the same as those used for the alternative LCA parameterization given in Table 6-3 of N-I (2013) for U only. Sorption was not modeled for ^{14}C and ^{63}Ni. Site-specific ^{90}Sr and ^{137}Cs K_d distributions were developed and used to account for retardation in the LCA matrix (this was a model evaluation target; see Section 3.5.1). The model evaluation transport runs used a revised (decreased) K_d distribution for Pu that was developed in response to a comment by the external peer review panel that the values used for Pu retardation may be too high (see Section 2.5.1 and Table 2-10 of Navarro, 2016b).

The distributions for fracture retardation were the same as those used for the alternative LCA parameterization given in Table 6-2 of N-I (2013), except that a minimum value of zero was used for Pu. This revised distribution for Pu was developed in response to the external peer review panel comment (see Section 2.5.1 and Table 2-10 of Navarro, 2016b).

The distributions for the source data and the methods used to develop model distributions for the fracture parameters, matrix porosity, and matrix diffusion parameters are tabulated in Table 4-10. The fracture retardation and matrix sorption distributions are tabulated in Tables 4-11 and 4-12, respectively. As was done in N-I (2013), the uncertainty in LCA transport parameters is treated stochastically by conducting Latin hypercube sampling over the range of uncertain inputs.

4.7.3.1 Fracture Porosity

The fracture porosity distributions for the model evaluation transport runs are the same as those used for the alternative LCA parameterization given in Table 6-1 of N-I (2013) and is described in Section 6.3.6.1 of N-I (2013). Statistics defining the distributions are shown in Table 4-10. The lower two-thirds of the full distribution is sampled for the country rock, and the upper third of the full distribution is sampled for the faults. The fracture porosity distributions are illustrated in Figure 4-50.

Table 4-10
Source Data Distributions and Methodology for Developing Fracture Parameters, Matrix Porosity, and Tortuosity Distributions
(Page 1 of 2)

Parameter [a]	Mean [b]	Standard Deviation [b]	Lower Bound [c]	Most Likely [d]	Upper Bound [c]	Distribution Type	Comments	Source
Fracture Porosity (unitless), ϕ_f (PLUMECALC Input Parameter)								
CR	N/A	N/A	2E-04	N/A	2E-02	Log Uniform	Sampled lower 2/3 of full distribution	SNJV (2007) and Section 6.3.6.1 of N-I (2013)
FZ	N/A	N/A	2E-04	N/A	2E-02	Log Uniform	Sampled upper 1/3 of full distribution	SNJV (2007) and Section 6.3.6.1 of N-I (2013)
Log Hydraulic Conductivity (m/day), *K* (Used in Calculation of Hydraulic Fracture Aperture)								
CR	0.16	1.34	N/A	N/A	N/A	Lognormal	Sampled lower 2/3 of full distribution	SNJV (2006b), and Sections 6.3.1.2 and 6.3.6.1 of N-I (2013)
FZ	0.16	1.34	N/A	N/A	N/A	Lognormal	Sampled upper 2/3 of full distribution	SNJV (2006b), and Sections 6.3.1.2 and 6.3.6.1 of N-I (2013)
Fracture Aperture Multiplier (unitless) (Used in Calculation of Tracer Fracture Aperture)								
CR	N/A	N/A	2	5	10	Triangular	Derived from assessment of hydraulic and tracer apertures	Sections 6.3.1.2 and 6.3.6.1 of N-I (2013)
FZ	N/A	N/A	5	10	20	Triangular	Derived from assessment of hydraulic and tracer apertures	Sections 6.3.1.2 and 6.3.6.1 of N-I (2013)
Tracer Fracture Aperture (m), *b* (PLUMECALC Input Parameter)								
CR	N/A	N/A	N/A	N/A	N/A	N/A	Hydraulic aperture calculated using Equation (4-1) with sampled hydraulic conductivity and assumed fracture spacing of 3 m; tracer aperture used in model calculated from hydraulic aperture and sampled fracture aperture multiplier	Section 6.3.6.1 of N-I (2013)
FZ	N/A	N/A	N/A	N/A	N/A	N/A	Hydraulic aperture calculated using Equation (4-1) with sampled hydraulic conductivity and assumed fracture spacing of 0.5 m; tracer aperture used in model calculated from hydraulic aperture and sampled fracture aperture multiplier	Section 6.3.6.1 of N-I (2013)

Table 4-10
Source Data Distributions and Methodology for Developing Fracture Parameters, Matrix Porosity, and Tortuosity Distributions
(Page 2 of 2)

Parameter [a]	Mean [b]	Standard Deviation [b]	Lower Bound [c]	Most Likely [d]	Upper Bound [c]	Distribution Type	Comments	Source
Total Matrix Porosity (unitless), ϕ_m (PLUMECALC Input Parameter)								
CR	0.0263	0.0163	N/A	N/A	N/A	Normal	Calculated as the sampled porosity data multiplied by a sampled matrix porosity reduction factor	SNJV (2007) and Section 6.3.6.2 of N-I (2013)
FZ	0.0263	0.0163	N/A	N/A	N/A	Normal	From porosity data	SNJV (2007) and Section 6.3.6.2 of N-I (2013)
Matrix Porosity Reduction Factor (unitless) (Used to Calculate Total Matrix Porosity in the Country Rock)								
CR	N/A	N/A	0.2	N/A	0.8	Uniform	Developed from results of flowing feature analysis presented in Appendix J of N-I (2013)	Section 6.3.6.2 and Appendix J of N-I (2013)
Tortuosity (unitless), τ (Used to Calculate Matrix Diffusion Coefficient)								
CR & FZ	N/A	N/A	N/A	N/A	N/A	N/A	Correlated with matrix porosity using Equation (4-3)	Sections 6.3.3 and 6.3.6.3 of N-I (2013)
Free-Water Diffusion Coefficient (m^2/s) D_o (Used to Calculate Matrix Diffusion Coefficient)								
CR & FZ	N/A	N/A	N/A	3E-10 & 2.24E-09	N/A	N/A	Value of 3E-10 m^2/s used for RNs with an atomic mass greater than 137, and value of 2.24E-09 m^2/s used for RNs with an atomic mass less than or equal to 137	Sections 6.3.3.2 and 6.3.6.3 of N-I (2013)
Matrix Diffusion Coefficient (m^2/s) (PLUMECALC Input Parameter)								
CR & FZ	N/A	N/A	N/A	N/A	N/A	N/A	Calculated as the matrix tortuosity multiplied by the RN free-water diffusion coefficient using Equation (4-2)	Sections 6.3.3 and 6.3.6.3 of N-I (2013)

[a] CR = Country rock; FZ = Fault zones
[b] Applicable for lognormal and normal distributions only
[c] Applicable for log-uniform and triangular distributions only
[d] Applicable for triangular distributions only

Table 4-11
LCA Transport Model Fracture Retardation Distributions

RN	Fracture Retardation Parameter Distribution				Source
	Lower Bound	Upper Bound	Mode	Shape	
^{90}Sr	1	2.5	1.75	Triangular	Table 12-3 of SNJV (2007) and Table 6-2 of N-I (2013)
$^{135/137}Cs$	1.8	320	160.9	Triangular	Table 12-3 of SNJV (2007) and Table 6-2 of N-I (2013)
^{237}Np	1	10	5.5	Triangular	Table 12-3 of SNJV (2007) and Table 6-2 of N-I (2013)
U	1	1.6	1.3	Triangular	Table 12-3 of SNJV (2007) and Table 6-2 of N-I (2013)
$^{238/239/240}Pu$	0	50	25	Triangular	Table 2-10 of Navarro (2016b)

Note: All other RNs are considered to be non-sorbing on fracture surfaces.

Table 4-12
LCA Transport Model K_d Distributions

RN	K_d Distribution (mL/g)				Source
	Lower Bound	Upper Bound	Mode	Shape	
^{90}Sr	0.05	0.14	0.095	Triangular	Section 3.5.1
$^{135/137}Cs$	0.02	0.07	0.045	Triangular	Section 3.5.1
U	0.03	30	15.015	Triangular	Table 6-3 of N-I (2013)
$^{238/239/240}Pu$	0.76	1096	548.38	Triangular	Table 2-10 of Navarro (2016b)

Note: All other RNs of potential significance are considered to be non-sorbing in the matrix.

4.7.3.2 Fracture Aperture

The fracture aperture distributions for the model evaluation transport runs are the same as those used for the alternative LCA parameterization given in Table 6-1 of N-I (2013). As described in Section 6.3.6.1 of N-I (2013), the hydraulic fracture aperture was calculated from hydraulic conductivity and fracture spacing by the use of the cubic law:

$$b = (12ks)^{1/3} \tag{4-1}$$

where:

b = hydraulic fracture aperture (length [L])

k = permeability (L^2)

s = fracture spacing (L)

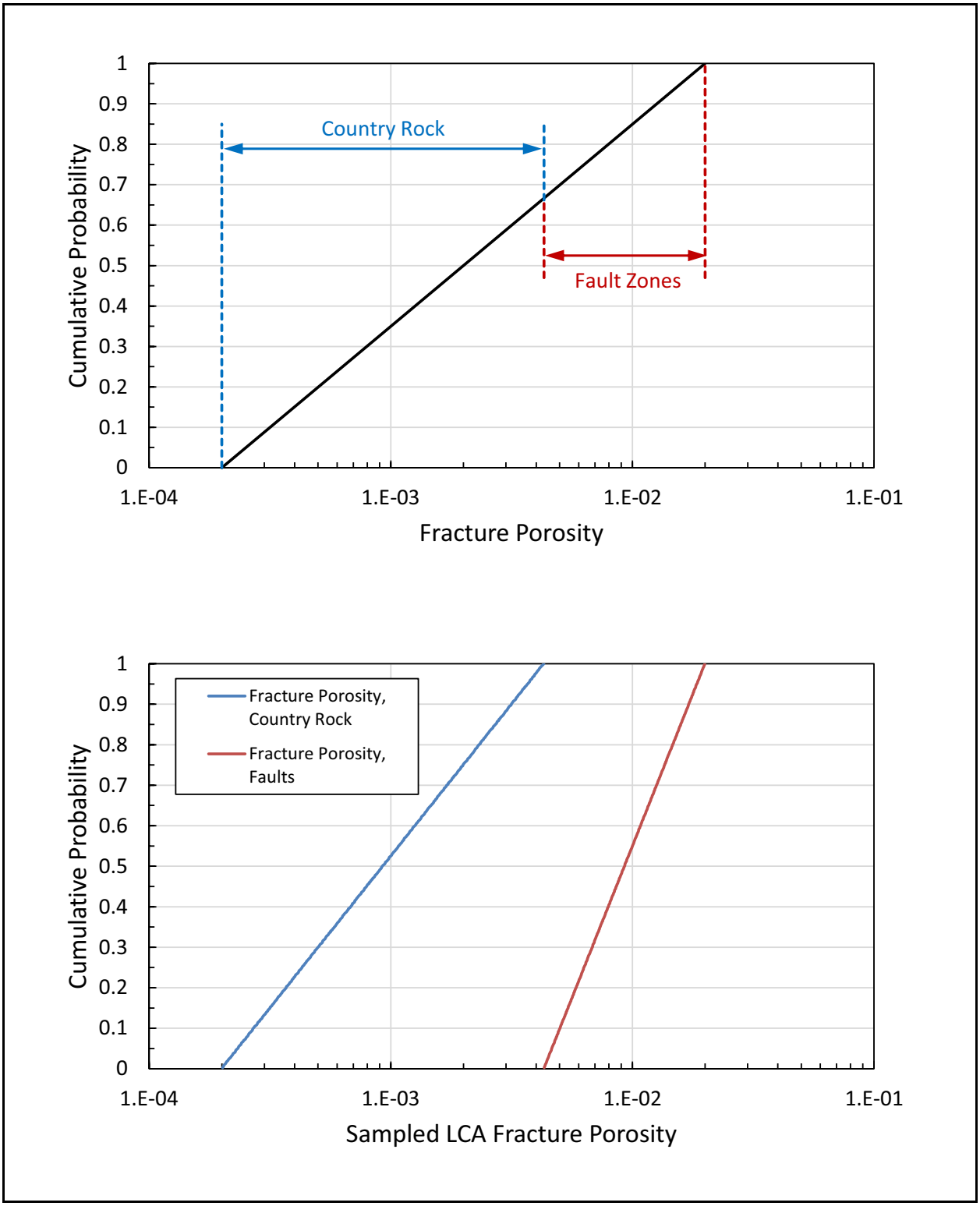

Figure 4-50
Fracture Porosity: (top) Distribution Sampled and (bottom) Distribution of the Model Values for the Country Rock and Fault Zones

Because Equation (4-1) requires permeability, the sampled hydraulic conductivities were converted to permeabilities. The parameter values used for the conversion were a fluid density of 997 kilograms per cubic meter (kg/m^3), a fluid viscosity of 8.91E-04 kilograms per meters per second kg/(m·s), and a gravitational acceleration of 9.81 meters per square second (m/s^2).

For the country rock, a fracture spacing of 3 m was assumed. For the fault zones, a fracture spacing of 0.5 m was assumed.

The hydraulic fracture aperture was calculated using Equation (4-1) with sampled hydraulic conductivity. The tracer fracture aperture that was input to PLUMECALC was calculated from the hydraulic fracture aperture and sampled fracture aperture multiplier.

The hydraulic conductivity distributions for the model evaluation transport runs are the same as those used for the alternative LCA parameterization given in Table 6-1 of N-I (2013). Statistics defining the distributions are shown in Table 4-10. The lower two-thirds of the full distribution is sampled for the country rock, and the upper 2/3 of the full distribution is sampled for the faults. The hydraulic conductivity distributions are illustrated in Figure 4-51. The fracture aperture multiplier distributions for the model evaluation transport runs are the same as those used for the alternative LCA parameterization given in Table 6-1 of N-I (2013). Statistics defining the distributions are shown in Table 4-10. The calculated fracture aperture distributions (input to PLUMECALC) are illustrated in Figure 4-52.

4.7.3.3 Matrix Porosity

The matrix porosity distributions for the model evaluation transport runs are the same as those used for the alternative LCA parameterization given in Table 6-1 of N-I (2013) and is described in Section 6.3.6.2 of N-I (2013). For the country rock, the matrix porosity is calculated from the sampled matrix porosity multiplied by a sampled matrix porosity reduction factor. Statistics defining the LCA total matrix porosity distributions and matrix porosity reduction factor distribution are shown in Table 4-10. The sampled LCA matrix porosity distributions are illustrated in Figure 4-53. Because the matrix porosity reduction factor is applied only to the country rock (Table 4-10), the matrix porosity distribution within the fault zone samples larger values compared to the country rock.

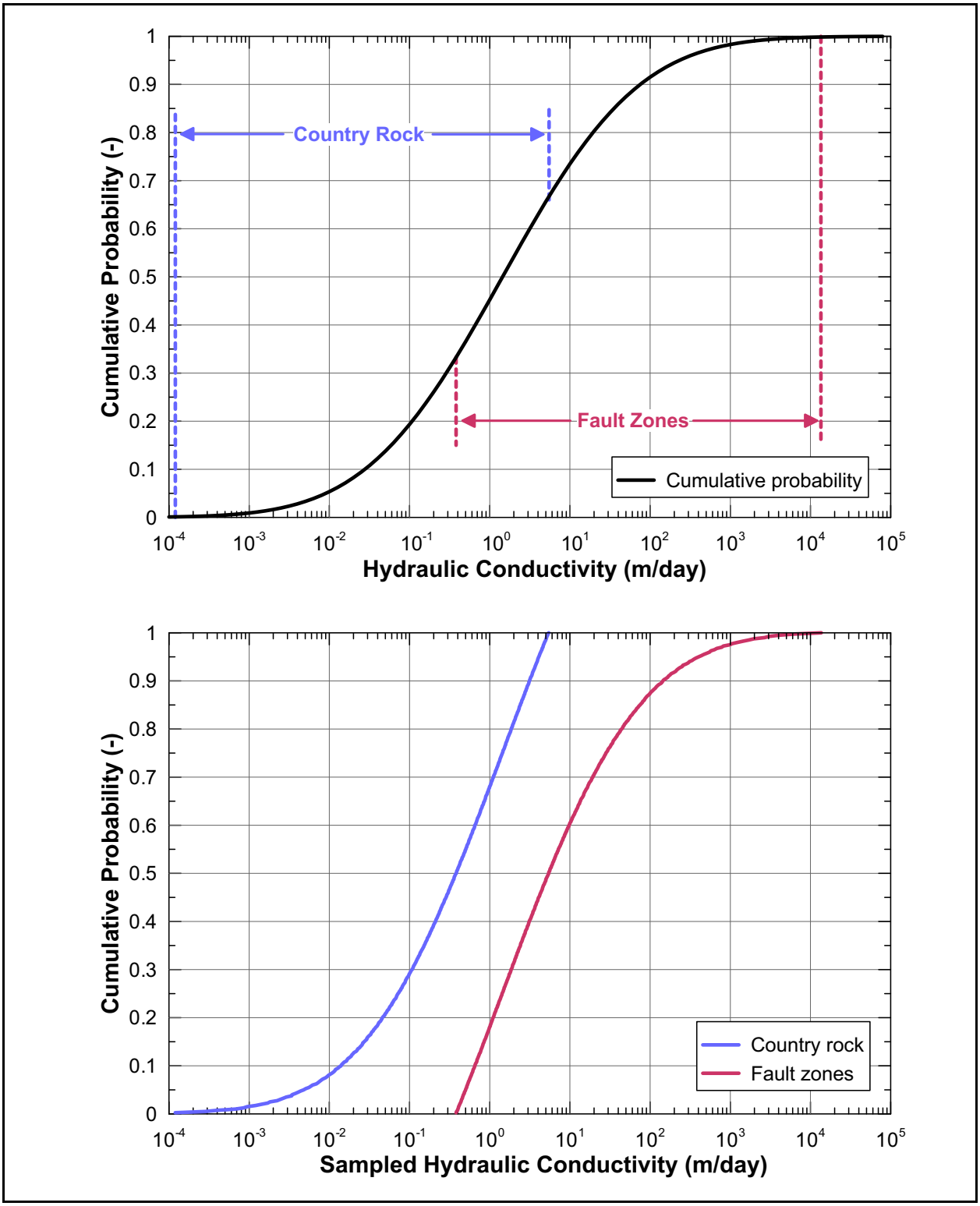

Figure 4-51
Hydraulic Conductivity: (top) Distribution Sampled and (bottom) Distribution of the Sampled Values Used To Calculate Hydraulic Fracture Aperture for the Country Rock and Fault Zones
Source: N-I (2013)

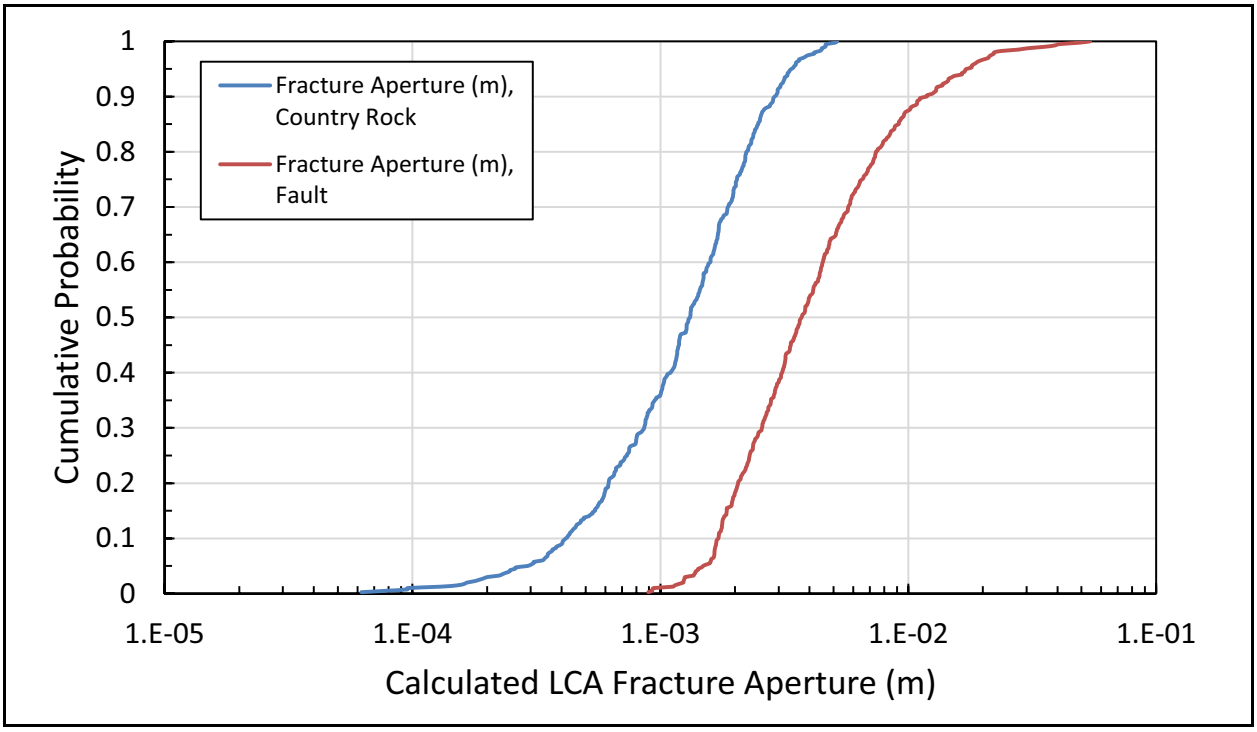

Figure 4-52
Calculated LCA Fracture Aperture

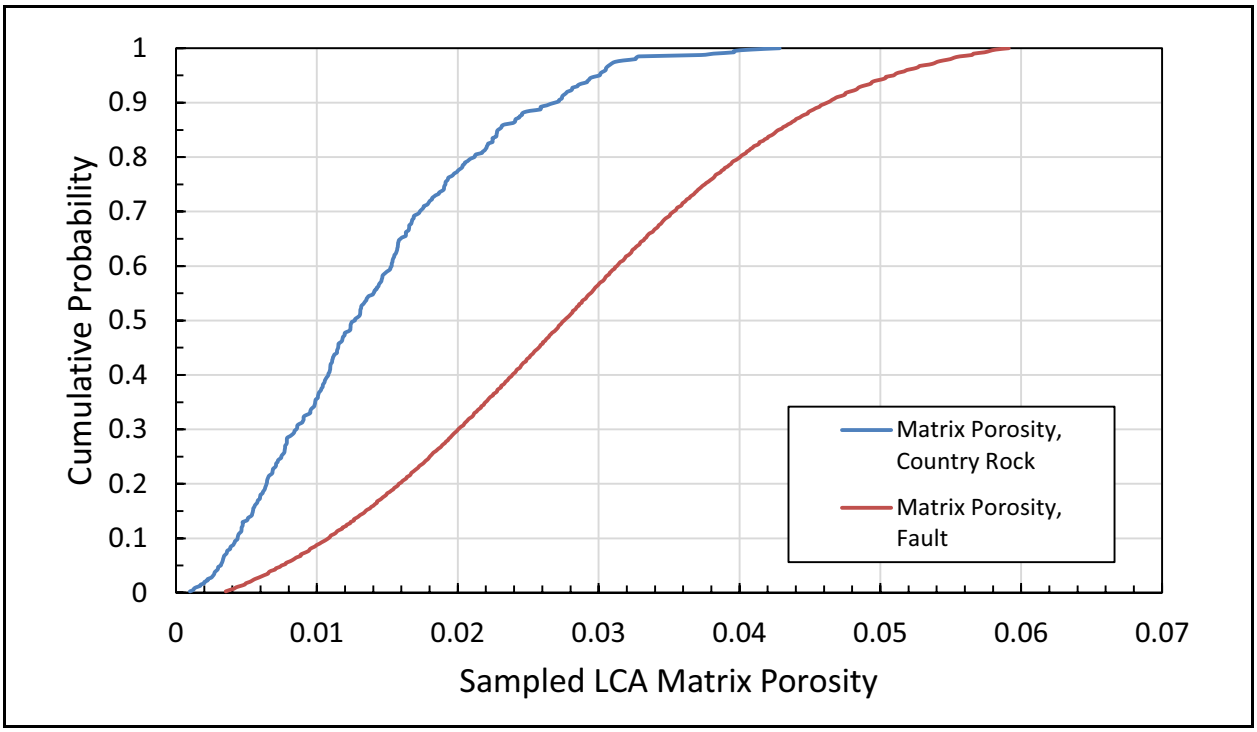

Figure 4-53
Sampled LCA Matrix Porosity

4.7.3.4 Matrix Diffusion Coefficient Parameters (Matrix Tortuosity and Free-Water Diffusion Coefficients)

The matrix diffusion coefficient distributions for the model evaluation transport runs are the same as those used for the alternative LCA parameterization given in Table 6-1 of N-I (2013) and described in Sections 6.3.3 and 6.3.6.3 of N-I (2013). The matrix diffusion coefficient is calculated as the matrix tortuosity multiplied by the RN free-water diffusion coefficient:

$$D_m = \tau D_o \qquad (4\text{-}2)$$

where:

D_m = matrix diffusion coefficient (L^2/t)

τ = matrix tortuosity (unitless)

D_o = solute free-water diffusion coefficient (L^2/t)

As noted in Table 6-1 and Section 6.3.3.2 of N-I (2013), RNs with an atomic mass greater than 137 were assigned a free-water diffusion coefficient of 3.0E-10 m^2/s (the D_o for ^{137}Cs), and those with an atomic mass less than or equal to 137 were assigned a free-water diffusion coefficient of 2.24E-09 m^2/s (the D_o for ^{3}H). As described in Table 6-1 and Sections 6.3.3.1 and 6.3.6.3 of N-I (2013), the matrix tortuosity was calculated from the sampled matrix porosity using the following correlation:

$$\log \tau = 20.38\,\phi_m - 2.13 \qquad (4\text{-}3)$$

where:

ϕ_m = matrix porosity (unitless)

The calculated matrix tortuosity distribution is illustrated in Figure 4-54. The calculated matrix diffusion coefficient distribution is illustrated in Figure 4-55.

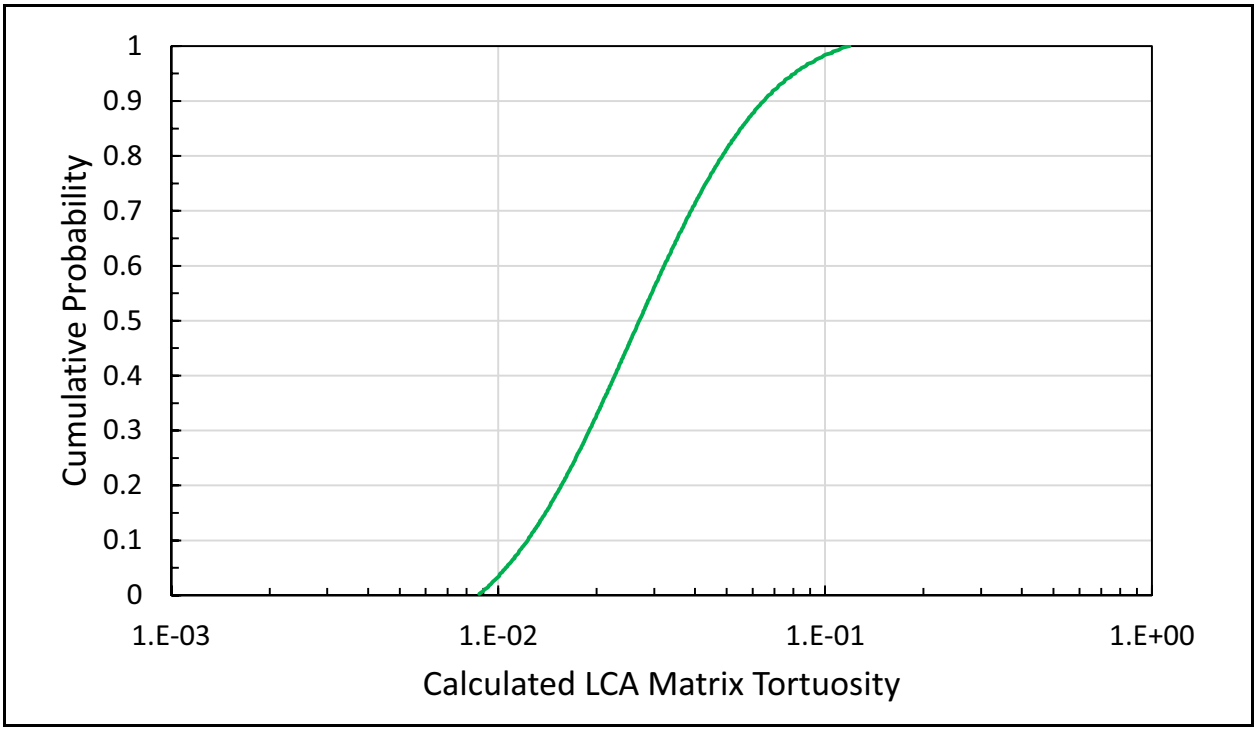

Figure 4-54
Calculated LCA Matrix Tortuosity

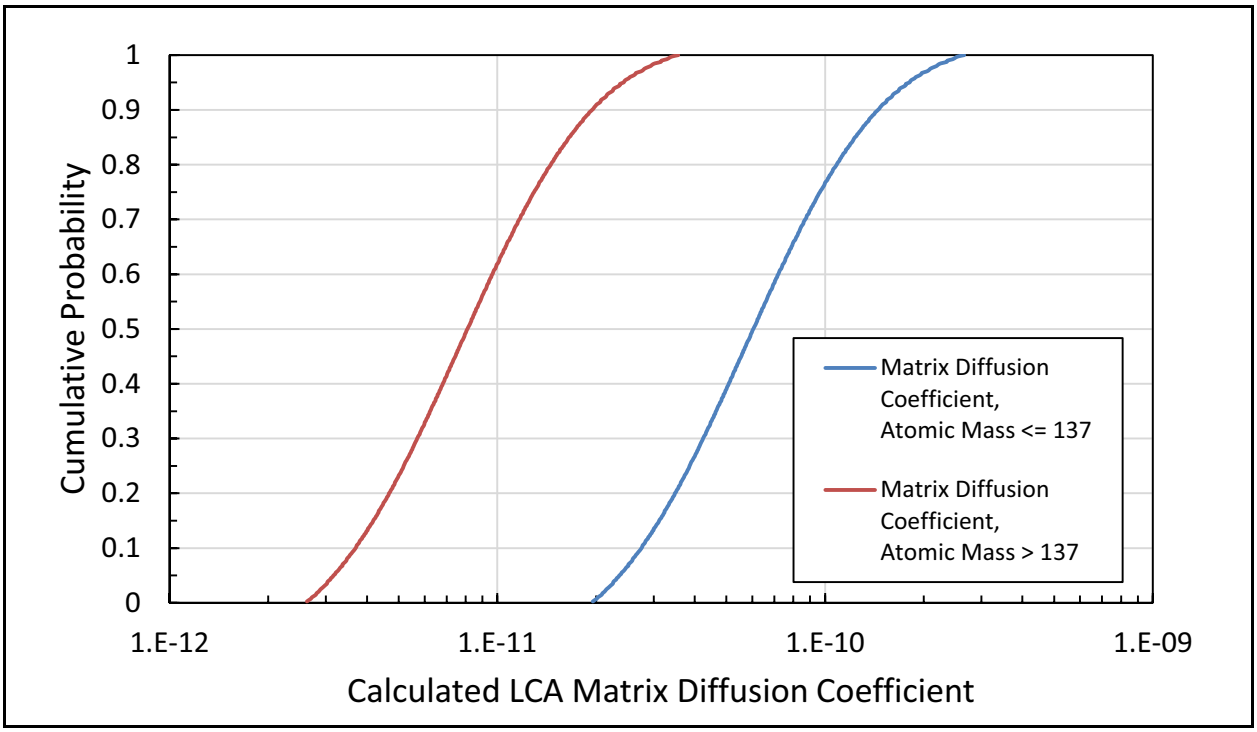

Figure 4-55
Calculated LCA Matrix Diffusion Coefficient

4.7.3.5 Dispersivity

Dispersivity is an input to FEHM-sptr when creating particle tracks (Section 4.7.2). The following dispersivity values were used:

- Longitudinal dispersivity = 20 m
- Horizontal transverse dispersivity = 2 m
- Vertical transverse dispersivity = 0.2 m

The assumed dispersivity values are small, because heterogeneity in country rock hydraulic conductivity and between country rock and fault hydraulic conductivity are expected to play the dominant role in the spreading of the contaminant plume.

4.7.3.6 Fracture Retardation

The distributions for fracture retardation (R_f) were the same as those used for the alternative LCA parameterization given in Table 6-2 of N-I (2013), except that a minimum value of zero was used for Pu. This revised distribution for Pu was developed in response to the external peer review panel comment (see Section 2.5.1 and Table 2-10 of Navarro, 2016b). Statistics defining the fracture retardation distributions are shown in Table 4-11. The fracture retardation distributions are illustrated in Figure 4-56.

4.7.3.7 Matrix Sorption

The distributions for matrix K_d were the same as those used for the alternative LCA parameterization given in Table 6-2 of N-I (2013) for U only. Sorption was not modeled for ^{14}C and ^{63}Ni. Site-specific ^{90}Sr and ^{137}Cs K_d distributions were developed and used to account for retardation in the fractured LCA matrix (Section 3.5.1). The model evaluation transport runs used a revised (decreased) K_d distribution for Pu that was developed in response to the external peer review panel comment (see Section 2.5.1 and Table 2-10 of Navarro, 2016b). Statistics defining the matrix K_d distributions are shown in Table 4-12. The matrix K_d distributions are illustrated in Figure 4-57.

4.7.4 Results

In this section, transport results are presented for the LCA flow model base case, High-K Yucca Fault, 40-kg/s Basin Flux, and NSMC model 28.

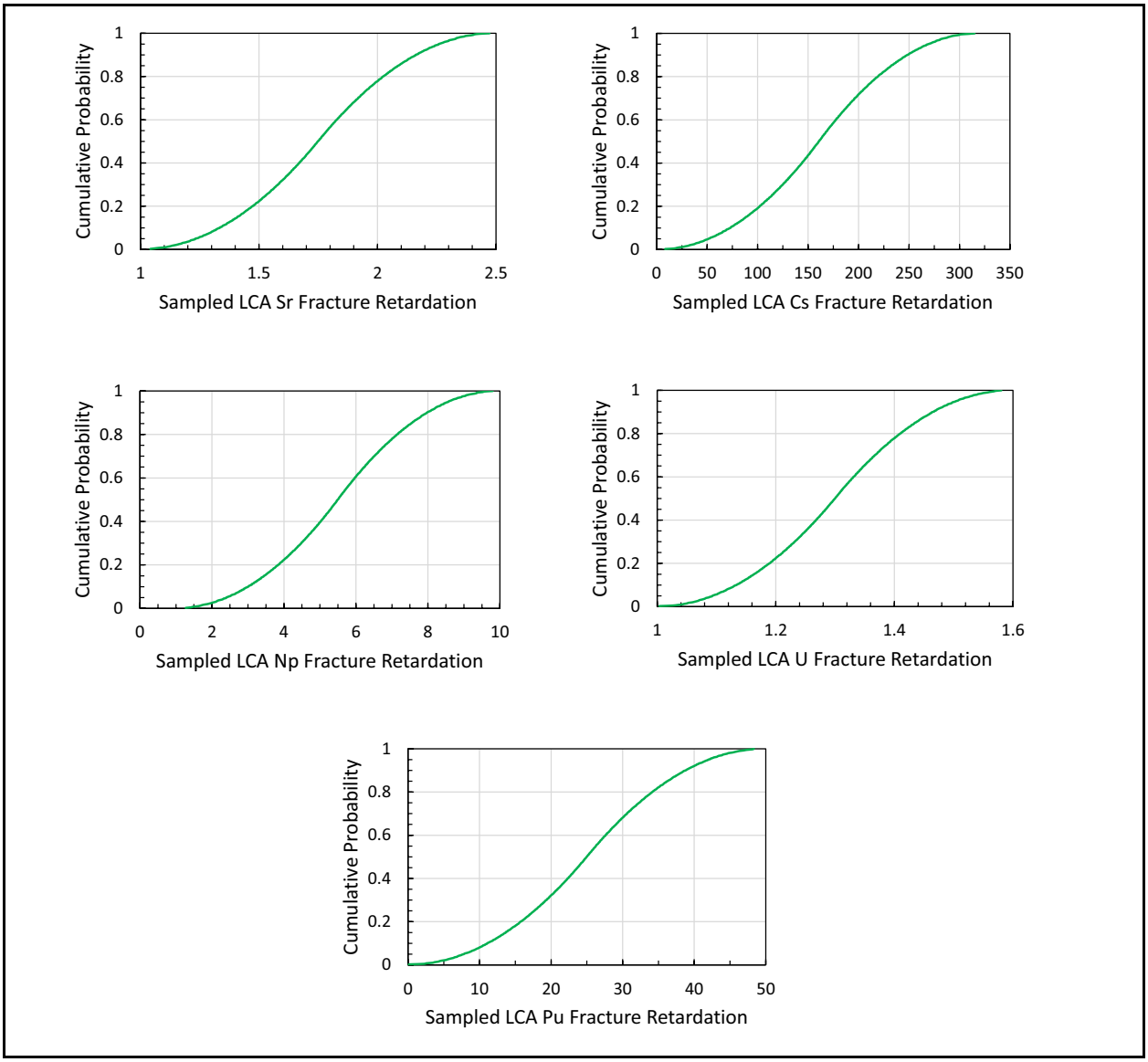

Figure 4-56
Sampled LCA Fracture Retardation Coefficient Distributions

Given (1) the particle trajectories and transport times developed from the LCA flow model, (2) input mass fluxes as a function of time and space, and (3) transport parameter values, PLUMECALC calculates the contaminant concentration in each control-volume cell at specified times from the start of testing in the YF/CM CAU (July 26, 1957). The discrete times chosen for analysis are at 10, 50, 100, 150, 200, 300, 400, 500, 600, 700, 800, 900, and 1,000 years.

The approach taken to identify the extent of contaminant migration is to perform transport simulations for all sources and all significant RNs over a range of uncertain transport parameter and source term values and to evaluate the probability of exceeding the SDWA MCLs (CFR, 2018) for

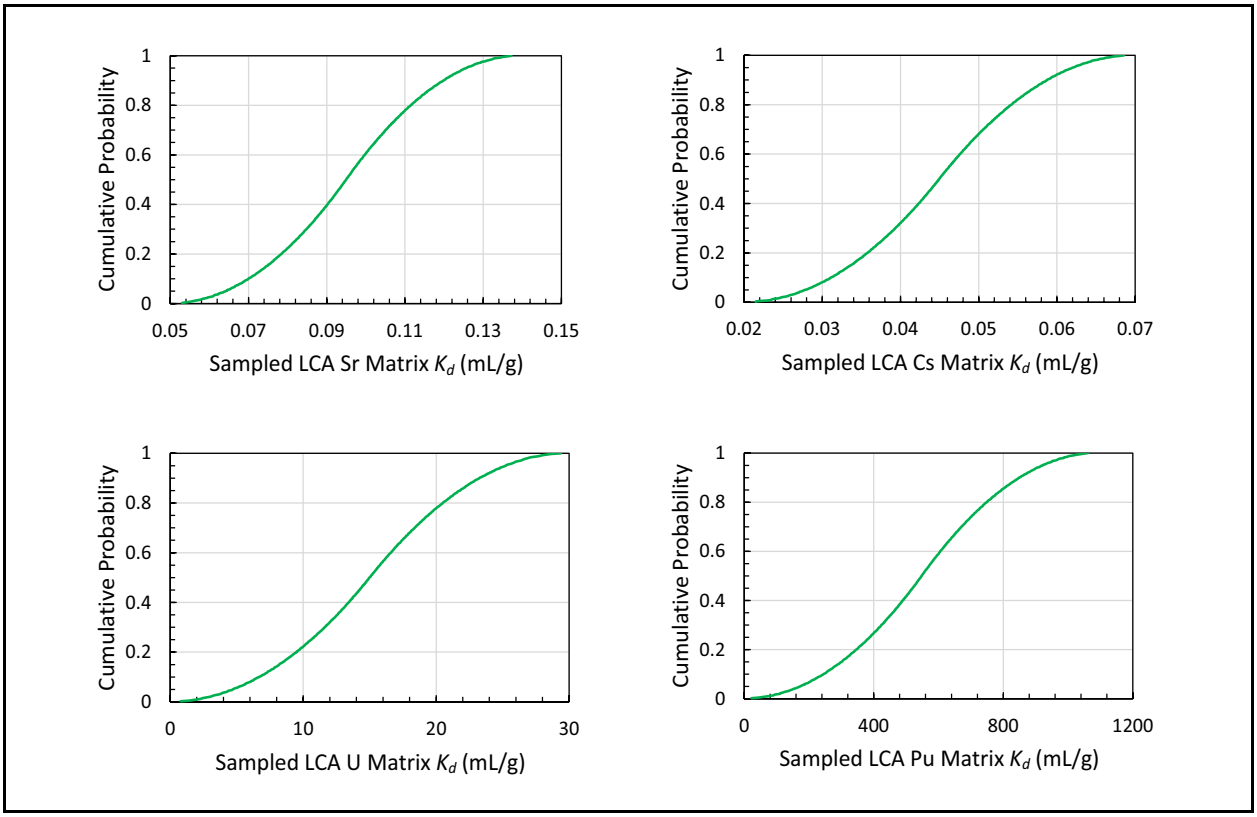

Figure 4-57
Sampled LCA Matrix K_d Distributions

each modeled RN within each grid cell. Probabilities are calculated for the alpha emitters (considering contributions from all modeled alpha emitters); for the beta emitters (considering contributions from all modeled beta emitters); for U; and for any of the three (i.e., the highest probability of exceeding the MCL of any of the alpha emitters, beta emitters, and U).

The exceedance volume is calculated for each category of RN (i.e., alpha emitters, beta emitters, U), as well as for all categories combined. The exceedance volume is defined as the total (summed) volume of all cells with a 5 percent or greater probability of exceeding the SDWA standard (CFR, 2018). If a model cell exceeds the standard, that cell's volume is added to the exceedance volume. The time-cumulative exceedance volume (CEV) is defined as the total volume of all model cells equal to or exceeding the SDWA standard at any time up to 1,000 years for a specific realization.

The average fractional exceedance volume (FEV) is also calculated for each category of RN (i.e., alpha emitters, beta emitters, U), as well as for all categories combined. The FEV is a

time-specific measure, averaged across all 400 realizations, for the contribution of each RN to the exceedance volume.

4.7.4.1 LCA Flow Model Base Case Contaminant Boundary

Figure 4-58 shows the forecasted 1,000-year time-cumulative probability of exceedance of alpha-emitter and beta- and photon-emitter MCLs for the LCA flow model base case. The time-cumulative probability of exceedance uses the probability of exceeding the MCL at each node for each individual modeled time step (10, 50, 100, 150, 200, 300, 400, 500, 600, 700, 800, 900, and 1,000 years) and identifies the maximum probability of MCL exceedance at each node regardless of the time that maximum occurs.

The plumes are colored by the probability of any RN class (i.e., any alpha emitter, beta emitter, or U) exceeding the MCL at that model cell. Only probabilities greater than 5 percent (i.e., the 95th percentile) are displayed. At the scale shown in Figure 4-58, most of the dots have a size similar to the model cell size. However, cell sizes vary throughout the model, thus, the dots are spaced a little further apart in areas with larger model cells. The 2-D CB perimeter is defined by the ground surface area that is obscured in Figure 4-58 by the collection of colored dots.

Figure 4-58 represents a collection of 3-D plumes from multiple source locations. The top of the Yucca Flat LCA model grid (which is a factor in determining vertical placement of the sources in the model) is not flat, and all sources are not located at the same elevation. Therefore, when plumes from multiple sources converge downstream, the plume from a source at a higher elevation will partially obscure the plume from the source at a lower elevation. For this reason, the plumes in Figure 4-58 are displayed such that at each *x*,*y* location, the maximum probability of MCL exceedance at any depth is shown. This was not done for similar figures shown in N-I (2013).

The time-varying forecasted CB for the LCA flow model base case is shown in Figures 4-59 through 4-62 at discrete times. As was done for Figure 4-58, the plumes in Figures 4-59 through 4-62 are displayed such that at each *x*,*y* location, the maximum probability of MCL exceedance at any depth is shown. These figures illustrate the largest extent of MCL exceedance occurs between 100 and 150 years, after which the plume begins to shrink because of radioactive decay of the short-lived RNs.

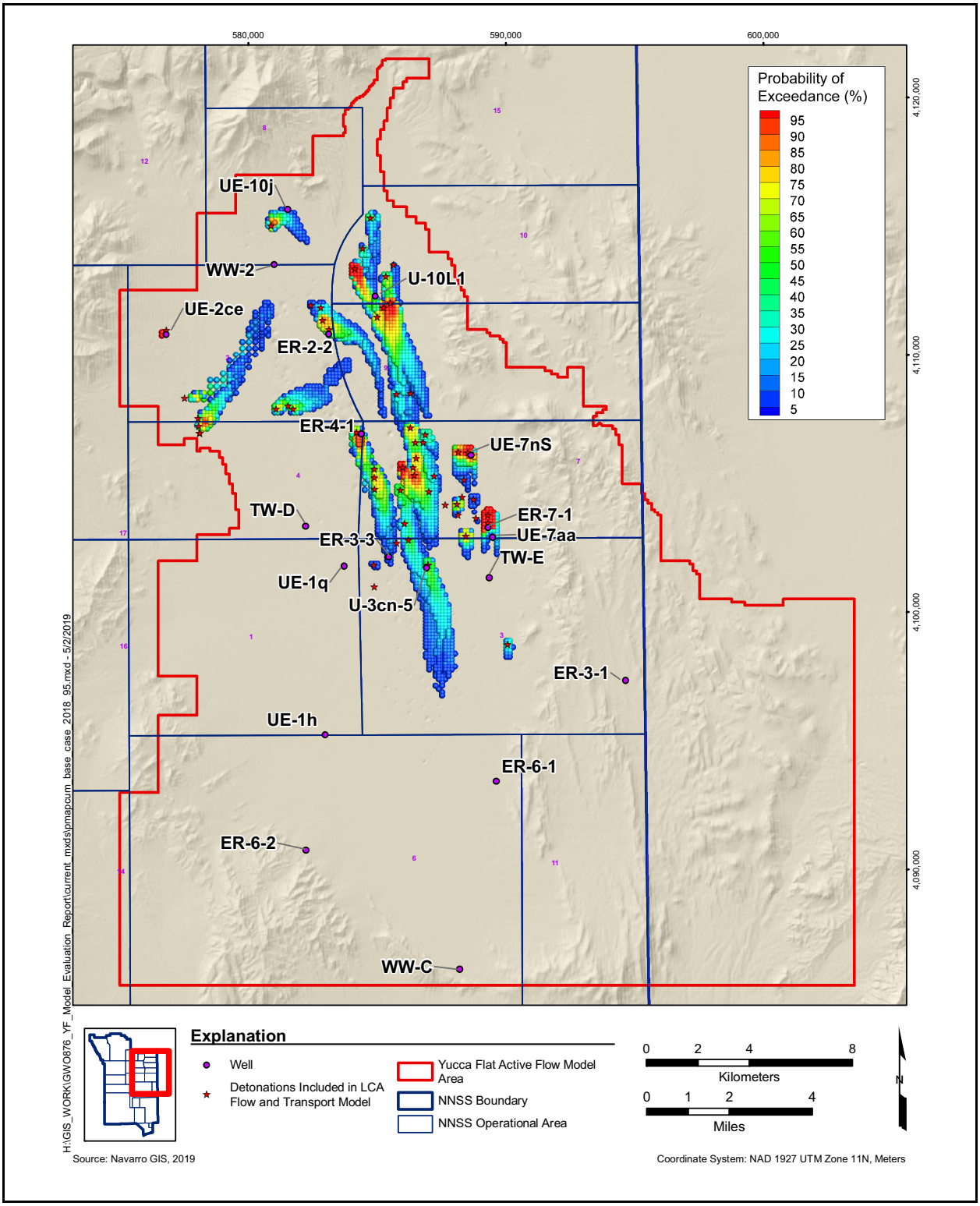

Figure 4-58
1,000-Year Time-Cumulative Probability of Exceedance of MCLs for the LCA Model Flow Base Case

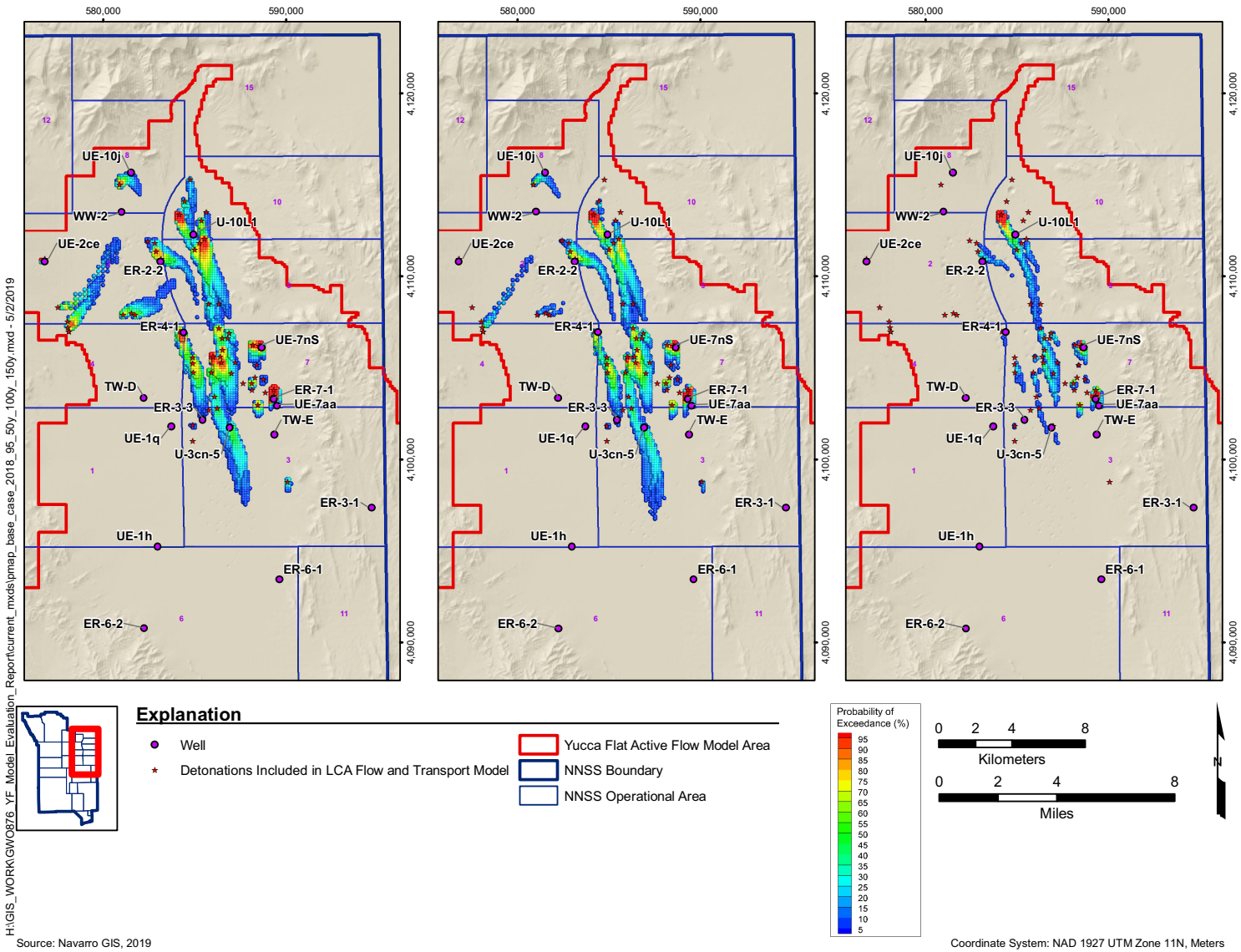

Figure 4-59
Probability of Exceedance of MCLs for the LCA Flow Model Base Case (left) at 50 Years, (center) at 100 Years, and (right) at 150 Years

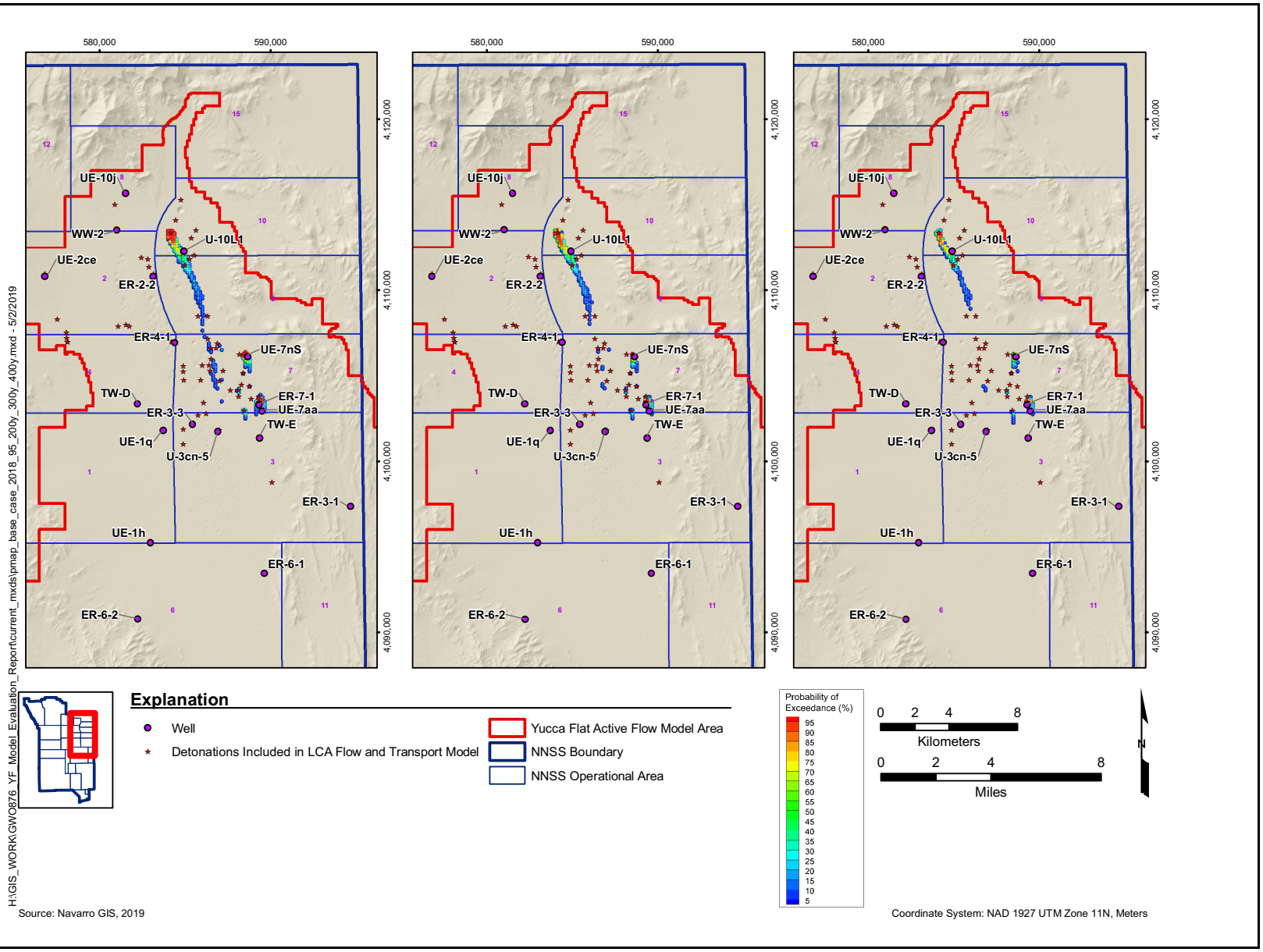

Figure 4-60
Probability of Exceedance of MCLs for the LCA Flow Model Base Case (left) at 200 Years, (center) at 300 Years, and (right) at 400 Years

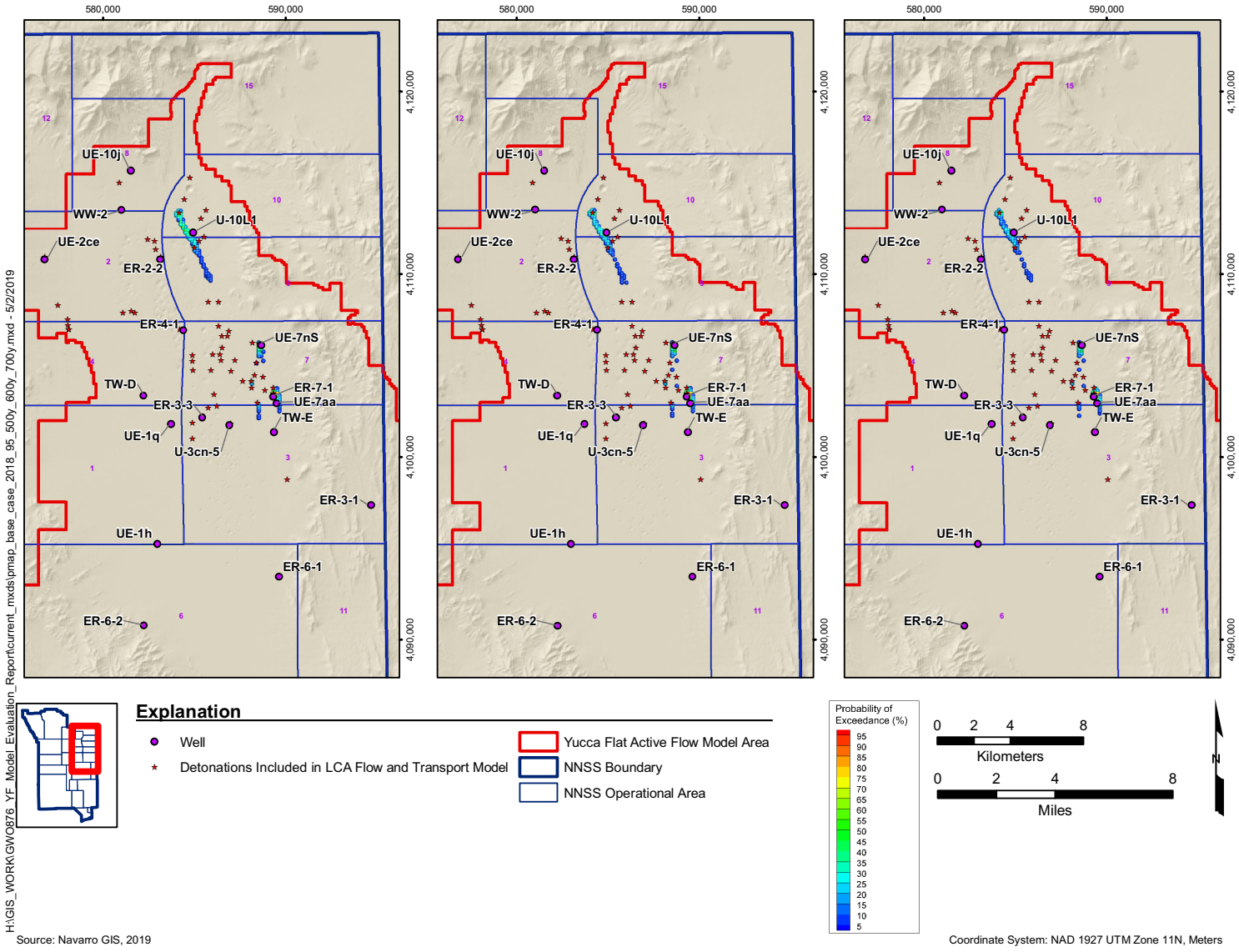

Figure 4-61
Probability of Exceedance of MCLs for the LCA Flow Model Base Case (left) at 500 Years, (center) at 600 Years, and (right) at 700 Years

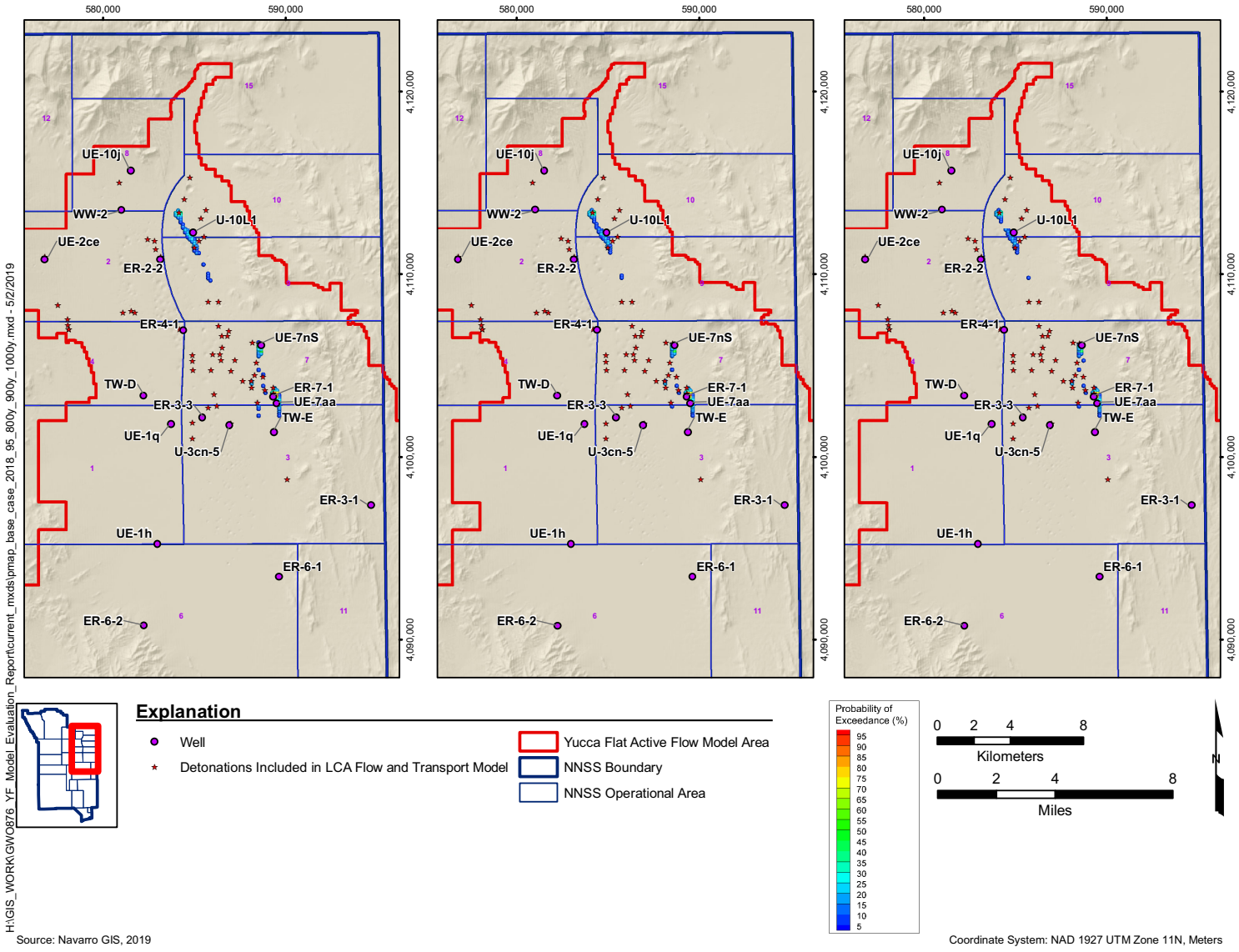

Figure 4-62
Probability of Exceedance of MCLs for the LCA Flow Model Base Case (left) at 800 Years, (center) at 900 Years, and (right) at 1,000 Years

4.7.4.2 Comparison of LCA Flow Model Base Case with 2013 Base Case

Figure 4-63 shows the forecasted 95th-percentile maximum extent of contamination over 1,000 years for both the LCA flow model base case and the 2013 base case. The plumes are colored by probability of exceeding the MCL. When compared to the 2013 base case, the refined model base case shows much less extent of contamination. The maximum extent of the 1,000-year CB of the refined model base case is north of ER-6-1, while the maximum extent of the 1,000-year CB of the 2013 base case touches the southern boundary of the model.

4.7.4.3 Comparison of LCA Flow Model Base Case with Alternative Cases

Figures 4-64 and 4-65 show the forecast 95th-percentile 1,000-year time-cumulative CB for the LCA flow model base case and High-K Yucca Fault (Figure 4-64), and 40-kg/s Basin Flux and NSMC model 28 (Figure 4-65). Although there are some differences in the shapes and directions of plumes, the overall extent of contamination is similar for all four cases.

The forecast 50th-percentile 1,000-year time-cumulative CBs are shown in Figure 4-66 for the base case and High-K Yucca Fault, and in Figure 4-67 for the 40-kg/s Basin Flux and NSMC model 28. Again, the overall extent of contamination is similar for all four cases.

Figures 4-68 and 4-69 show the forecast 5th-percentile 1,000-year time-cumulative CB of the base case and High-K Yucca Fault (Figure 4-68), and the 40-kg/s Basin Flux and NSMC model 28 (Figure 4-69). For all four models, at the 5th percentile, eight detonations are shown to contribute to the CB: BOURBON, CORDUROY, HERMOSA, KLICKITAT, MICKEY, NASH, SHUFFLE, and TORRIDO. In NSMC model 28, two additional detonations contribute to the 5th-percentile 1,000-year time-cumulative CB: ROQUEFORT and STODDARD. This is due to lower velocities in the western part of the domain of NSMC model 28, resulting in higher concentrations near these two sources.

The cumulative distribution functions (CDFs) of cumulative MCL exceedance volumes (CEVs) for the four model evaluation transport cases are shown in Figure 4-70. Also shown in Figure 4-70 is the CDF of the CEV for the 2013 base case from N-I (2013) for comparison. All four model evaluation cases have a CEV that is roughly 1 order of magnitude lower than the 2013 base case. Of the four model evaluation cases, 40-kg/s Basin Flux has the highest distribution of CEVs, indicating that this case has the largest volume of model cells that exceed the SDWA standard (CFR, 2018). The refined

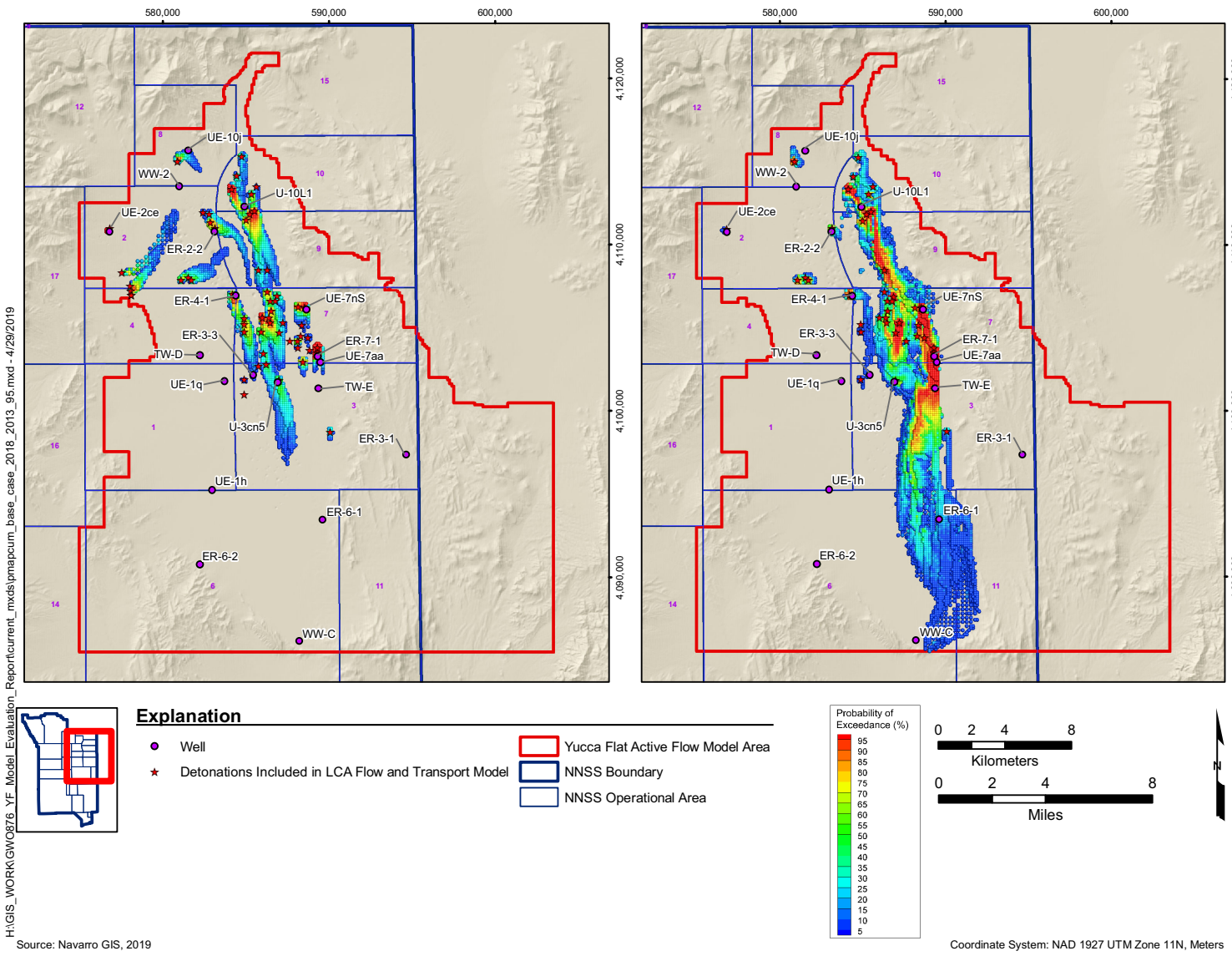

Figure 4-63
1,000-year Time-Cumulative Probability of Exceedance of MCLs for (left) LCA Flow Model Base Case and (right) 2013 Base Case

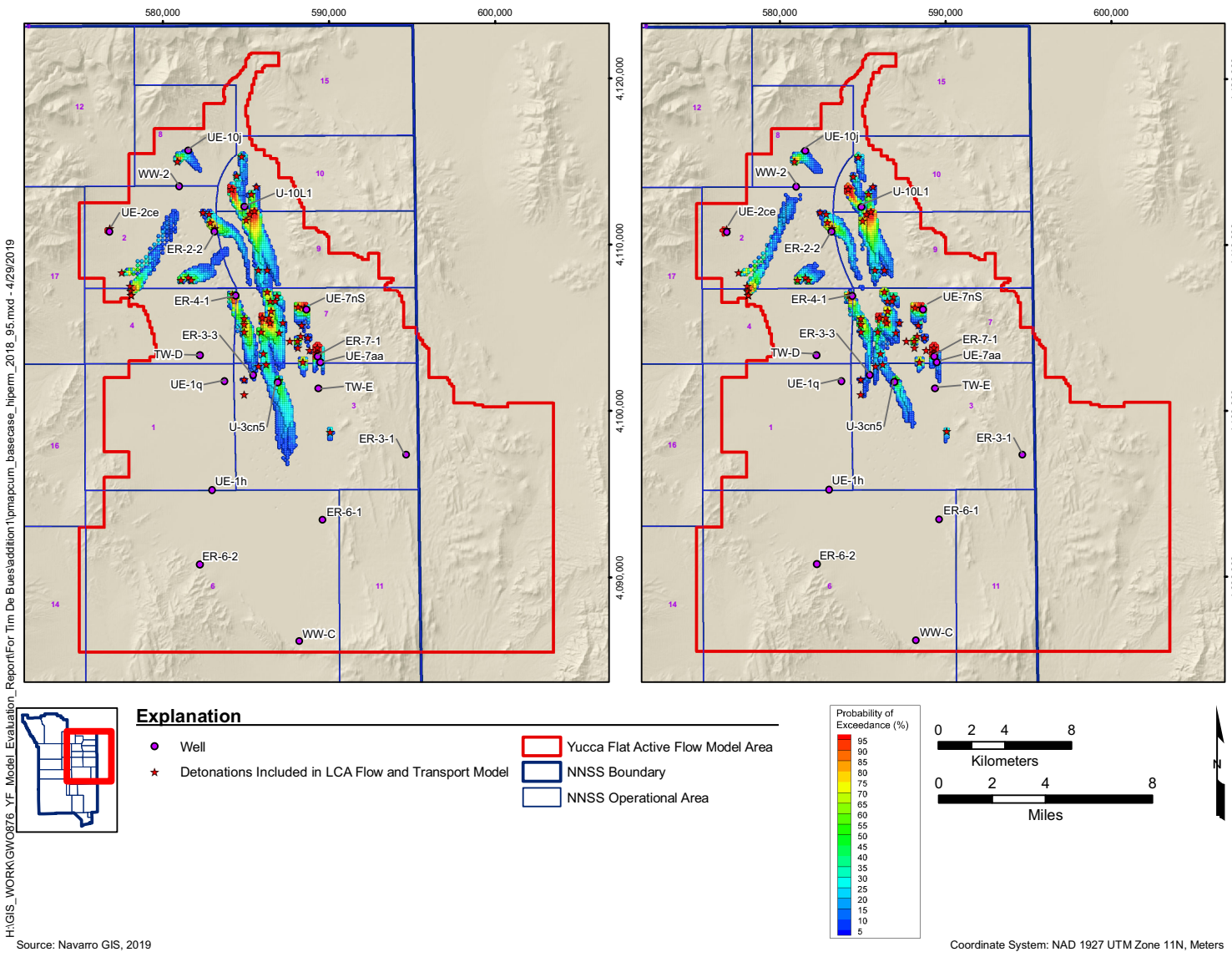

Figure 4-64
95th-Percentile 1,000-year Time-Cumulative Probability of Exceedance of MCLs for (left) LCA Flow Model Base Case and (right) High-K Yucca Fault

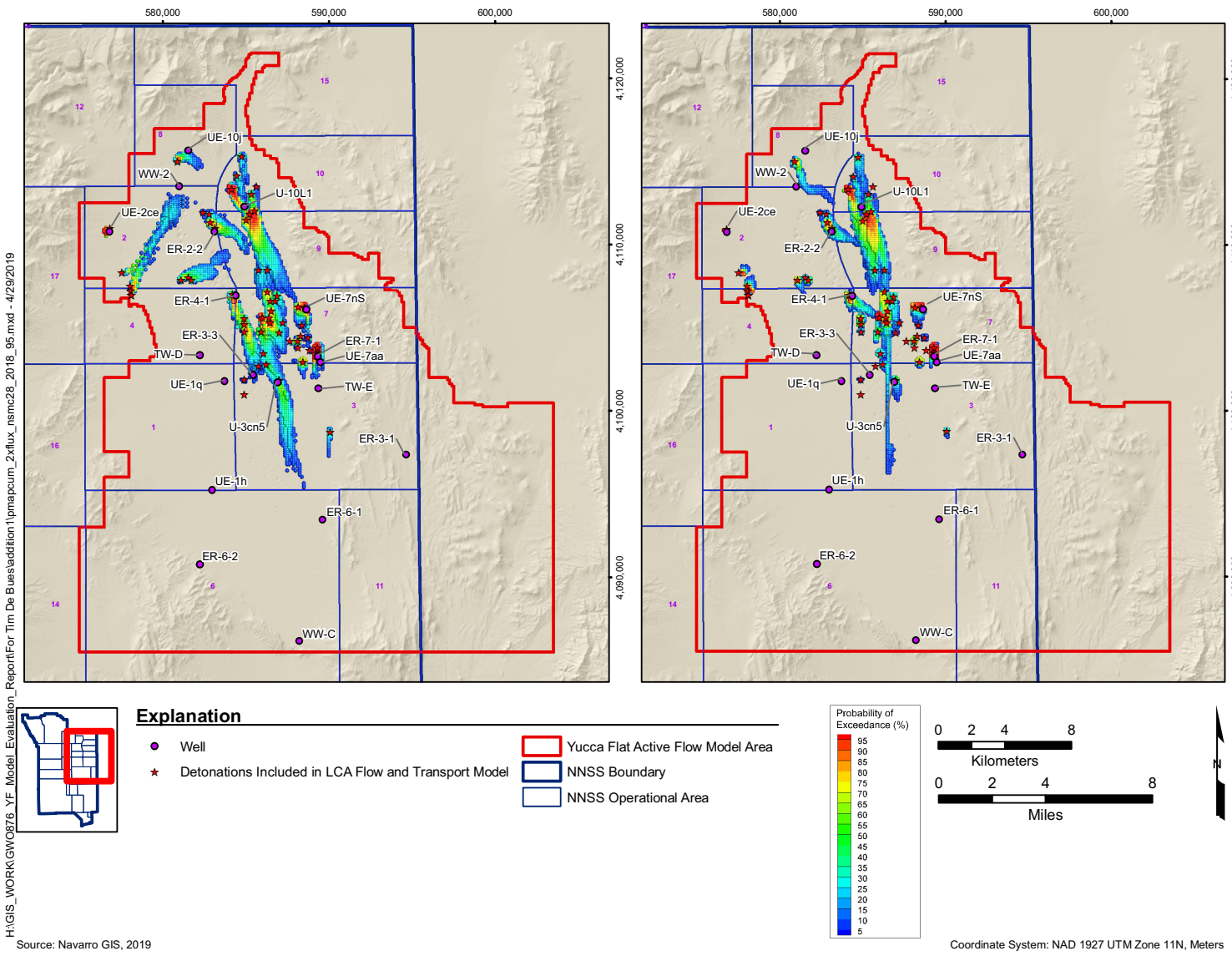

Figure 4-65
95th-Percentile 1,000-year Time-Cumulative Probability of Exceedance of MCLs for (left) Alternative Case with 40-kg/s Basin Flux and (right) NSMC Model 28

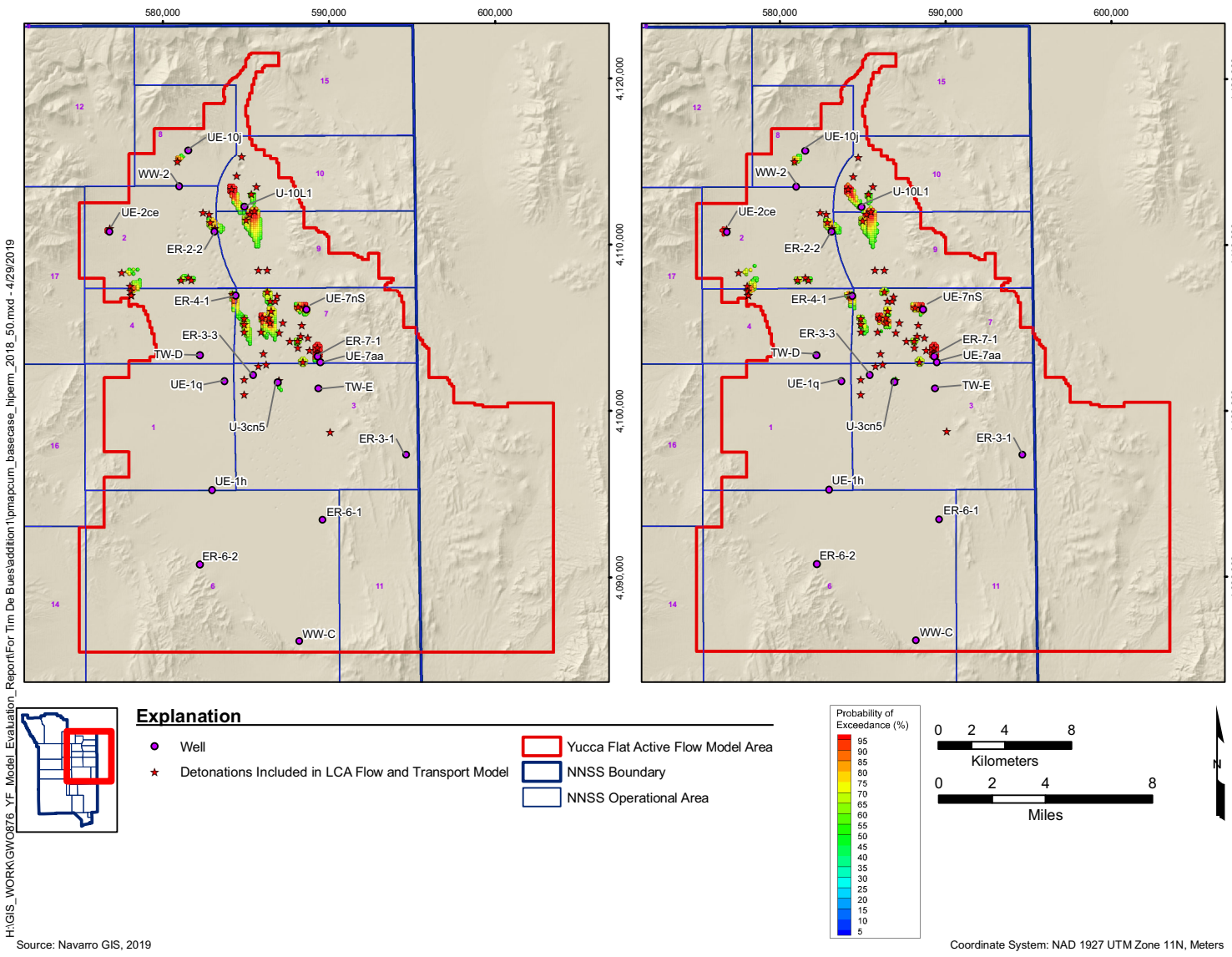

Figure 4-66
50th-Percentile 1,000-year Time-Cumulative Probability of Exceedance of MCLs for (left) LCA Flow Model Base Case and (right) High-K Yucca Fault

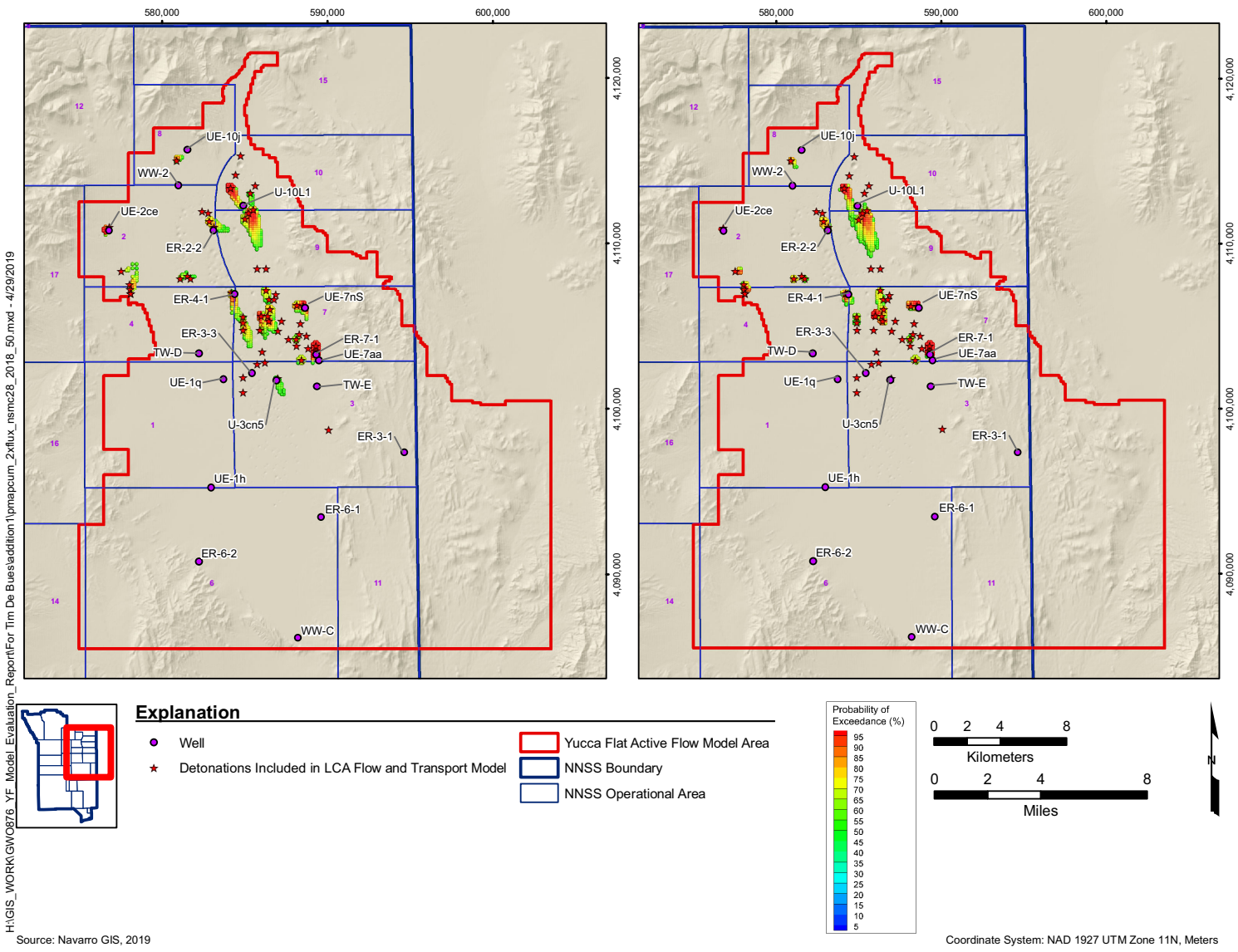

Figure 4-67
50th-Percentile 1,000-year Time-Cumulative Probability of Exceedance of MCLs for (left) 40-kg/s Basin Flux and (right) NSMC Model 28

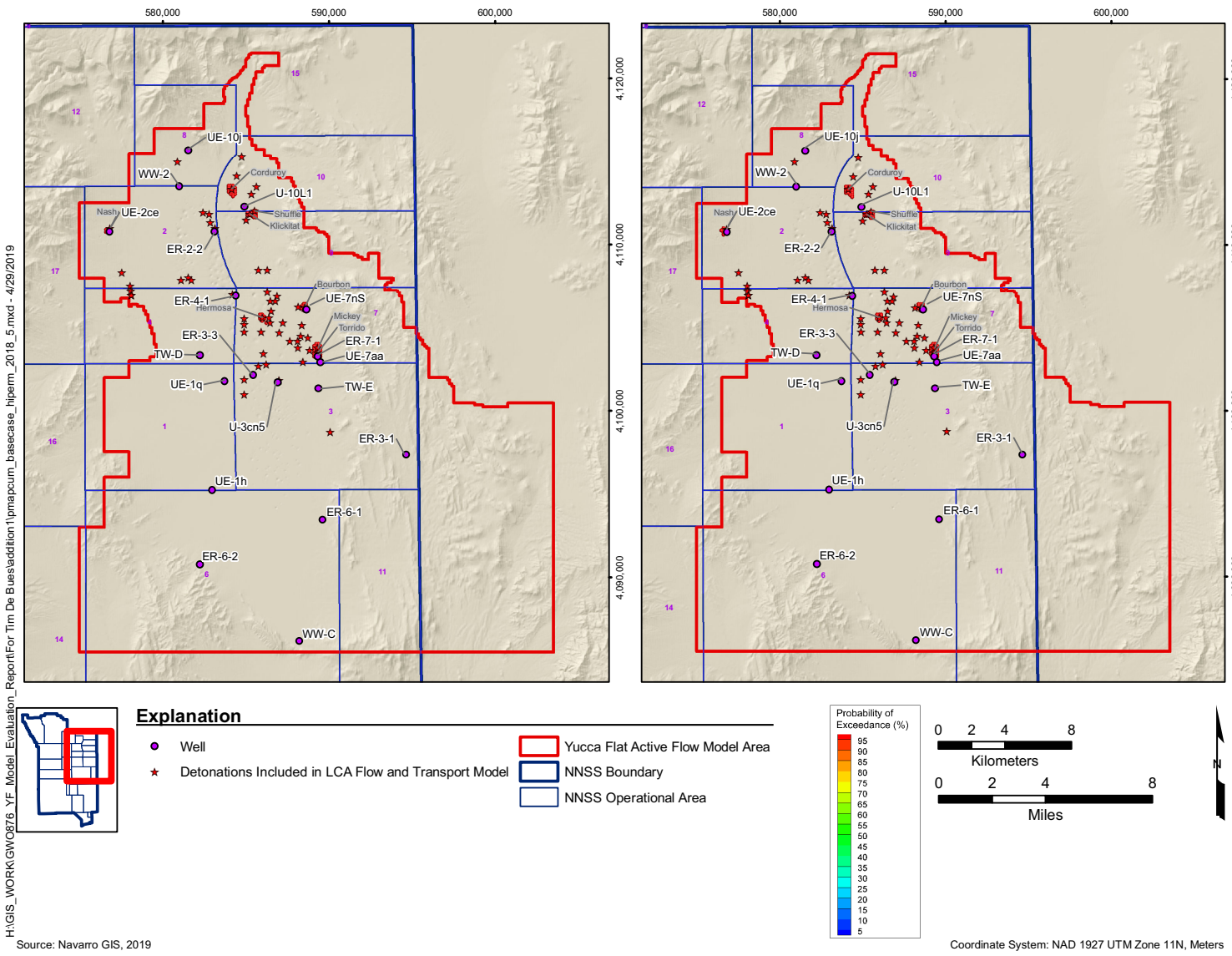

Figure 4-68
5th-Percentile 1,000-year Time-Cumulative Probability of Exceedance of MCLs for (left) LCA Flow Model Base Case and (right) High-K Yucca Fault

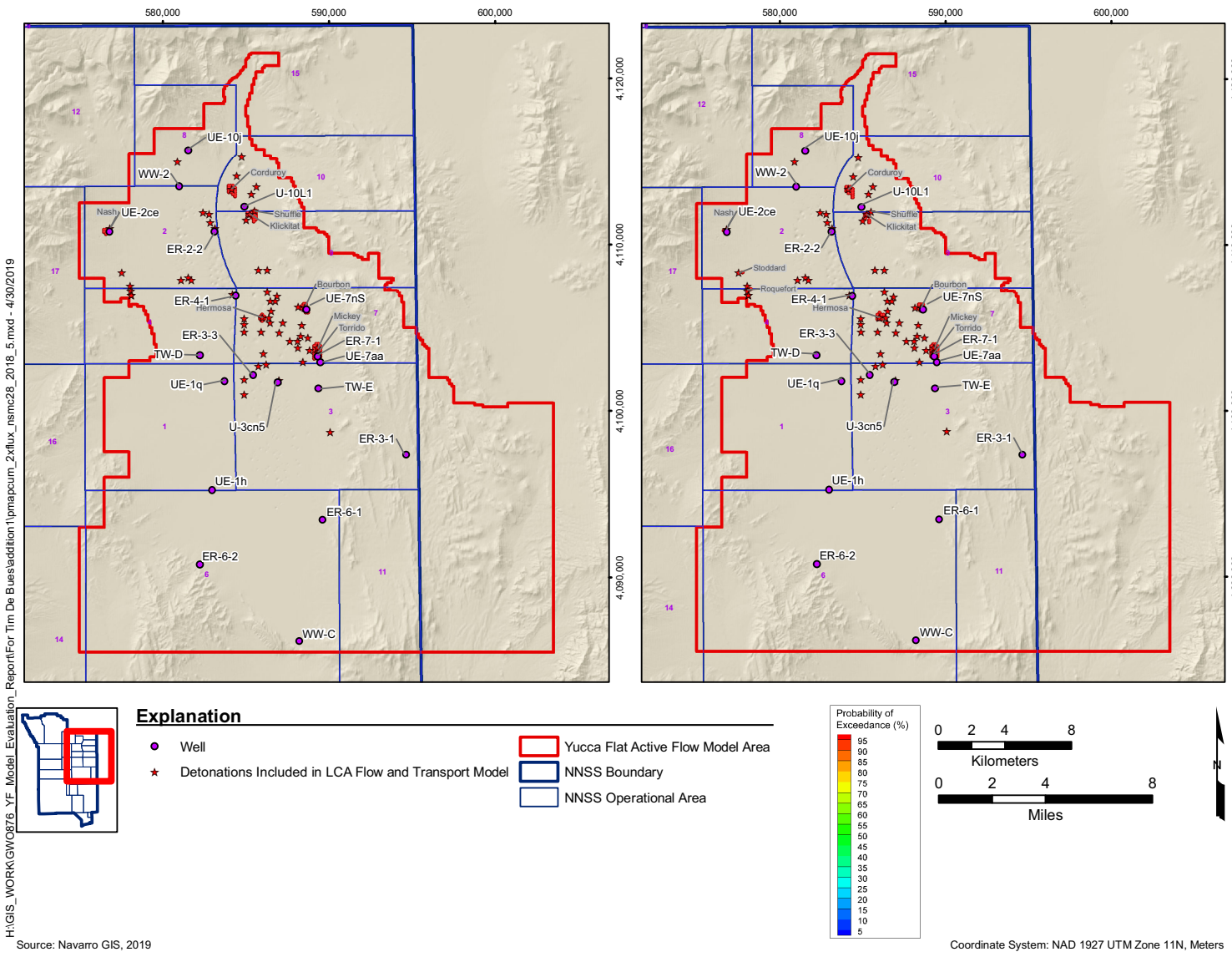

Figure 4-69
5th-Percentile 1,000-year Time-Cumulative Probability of Exceedance of MCLs for (left) 40-kg/s Basin Flux and (right) NSMC Model 28

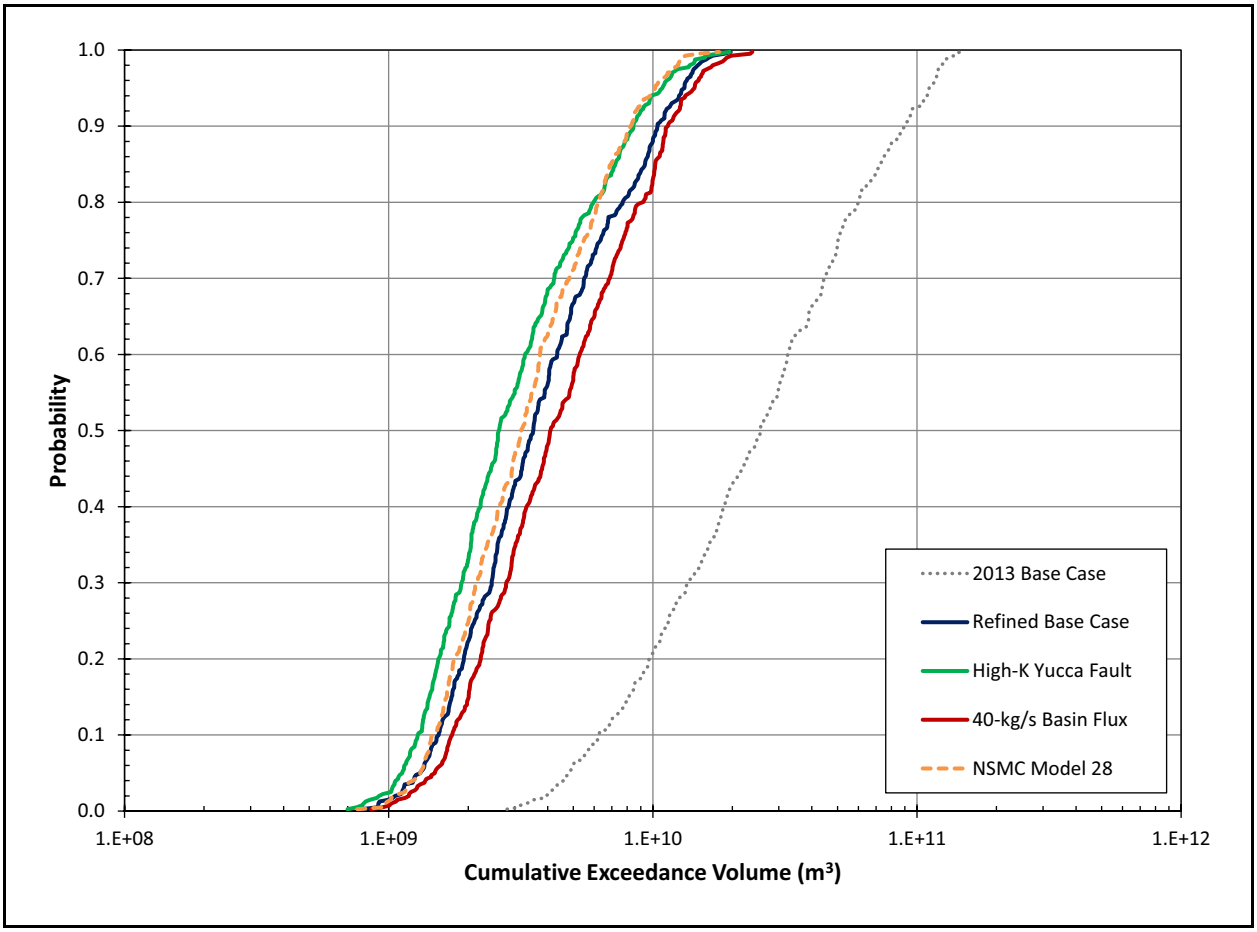

Figure 4-70
Distributions of Cumulative MCL Exceedance Volume for Model Evaluation Transport Runs Compared with 2013 Base Case

base case has the next highest distribution of CEVs. NSMC model 28 and High-K Yucca Fault have the lowest distributions of CEVs. As discussed in Sections 4.3.2.2 and 4.3.3, High-K Yucca Fault and NSMC model 28 are both characterized as having deep channelized flow in the Yucca fault. Given that the fault zones are modeled as more fractured than the country rock, there is greater opportunity for matrix diffusion to occur within the fault zones, resulting in decreased contaminant concentrations. This results in a lower probability of exceeding the SDWA standard (CFR, 2018) within the model cells identified within the Yucca fault, which, in turn, leads to CBs for High-K Yucca Fault and NSMC model 28 that are less extensive than the LCA model base case.

Average fractional exceedance volume (FEV) plots for the four model evaluation cases are shown in Figure 4-71. Similar trends are noted in all four cases. Tritium contributes most to the exceedance

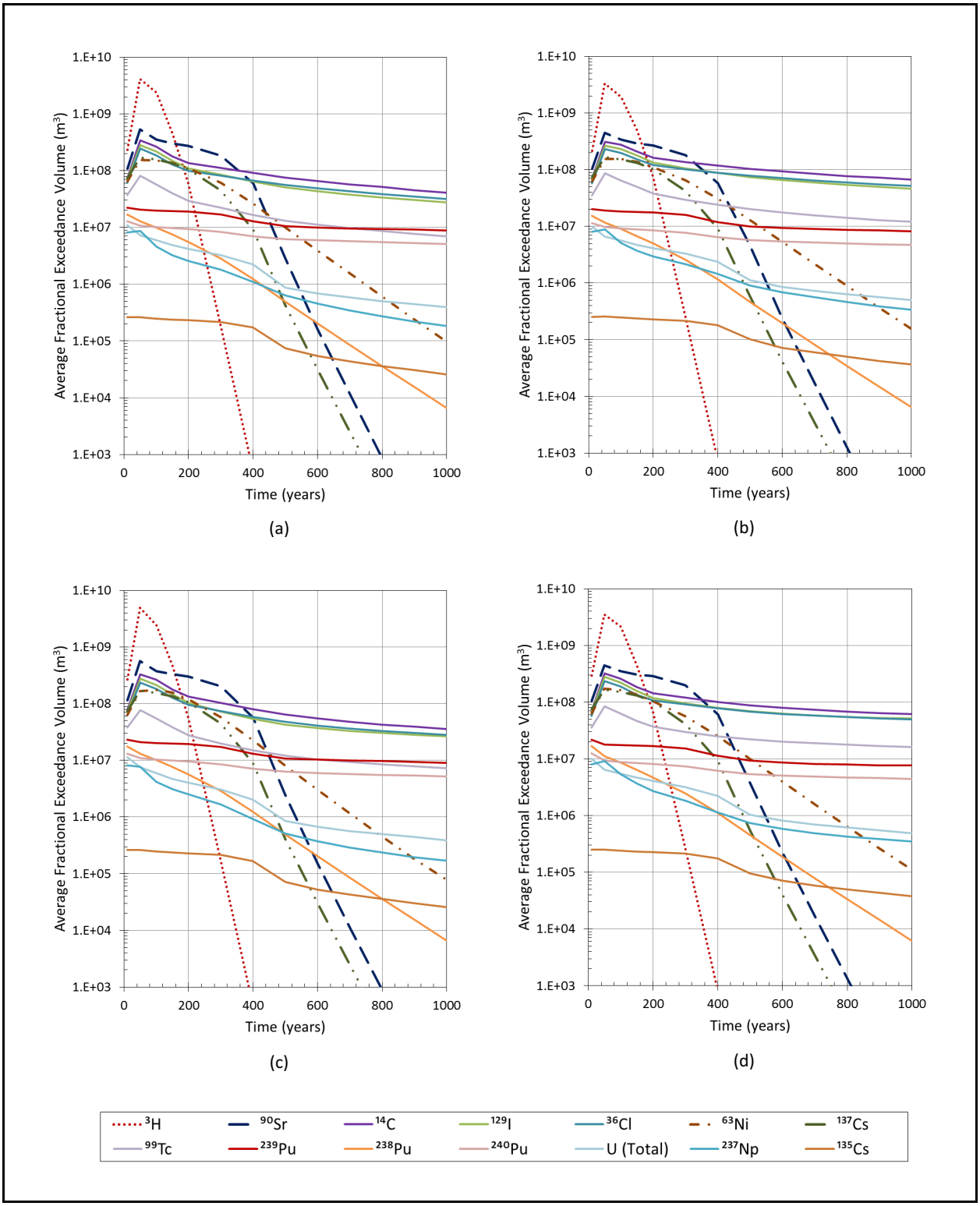

Figure 4-71
Average Fractional Exceedance Volume for (a) LCA Flow Model Base Case, (b) High-K Yucca Fault, (c) 40-kg/s Basin Flux, and (d) NSMC Model 28

volume up to approximately 150 years, followed by ^{90}Sr up to about 400 years, followed by ^{14}C, ^{129}I, and ^{36}Cl out to 1,000 years.

4.7.4.4 Comparison of the Extents of Contamination Forecasted by the Model with Present Time Observations

Measurements indicate (Table 2-4) that ^{3}H has been detected in five LCA locations: ER-2-2, UE-2ce (NASH), UE-7nS (BOURBON), U-3cn-5 (BILBY), and WW C-1. Of these five locations, ^{3}H was observed above the MCL only at UE-2ce (143,000 pCi/L). Observed ^{3}H concentrations are very low (10.2 to 53.3 pCi/L) at ER-2-2, UE-7nS, U-3cn-5, and WW C-1. No ^{3}H has been observed at ER-3-3, ER-4-1, ER-6-1-1, ER-6-2, ER-7-1, UE-1h, UE-1q, UE-10j, WW-2, or TW-D.

Table 4-13 compares ^{3}H observations in Yucca Flat LCA completions with the 50-year, 50th-percentile forecast CBs for the refined base case and three alternative cases, shown in Figures 4-72 and 4-73 (50 years is the output time that is closest to present day). A "Yes" in the table indicates that the transport model forecasts a CB with some probability of exceeding the MCL above 5 percent at the listed observation location, and a "No" in the table indicates that the transport model forecasts a CB with a probability of exceeding the MCL that is 5 percent or less at the listed observation location. Examining Table 4-13 results in the following observations regarding the 50-year, 50th-percentile CB forecasts:

- At UE-2ce, where ^{3}H is observed above the MCL, all transport models except NSMC model 28 have forecast ^{3}H above the MCL. In NSMC model 28 the direction of flow at NASH is initially to the east in NSMC model 28, not to the south toward UE-2ce; therefore, the ^{3}H plume does not intersect UE-2ce.

- At ER-2-2, UE-7nS, and U-3cn-5, where ^{3}H is observed below the MCL, all transport models forecast ^{3}H above the MCL at ER-2-2 and UE-7nS, and all transport models except NSMC model 28 forecast ^{3}H above the MCL at U-3cn-5. Generally, these forecasts are conservative.

- At WW C-1, where ^{3}H is observed below the MCL, none of the transport models forecast ^{3}H above the MCL, which is consistent with this observation.

- At locations where ^{3}H is not observed, the 50-year, 50th-percentile forecast CBs for all four transport models indicate some probability of exceeding the MCL at ER-4-1 and ER-7-1 only. This is inconsistent with observations, indicating that all four models are conservative.

Table 4-13
Comparison of 50-Year, 50th-Percentile CB Forecasts to Present Time Observations

LCA Completion	^{3}H Observed (see Table 2-4)	50-Year, 50th-Percentile CB Forecasts, LCA Flow Model, ^{3}H above MCL at Well Location			
		Base Case	High-K Yucca Fault	40-kg/s Basin Flux	NSMC Model 28
UE-2ce (NASH)	**Yes (>MCL)**	**Yes**	**Yes**	**Yes**	No
ER-2-2	**Yes (<MCL)**	**Yes**	**Yes**	**Yes**	**Yes**
UE-7nS (BOURBON)	**Yes (<MCL)**	**Yes**	**Yes**	**Yes**	**Yes**
U-3cn-5 (BILBY)	**Yes (<MCL)**	**Yes**	**Yes**	**Yes**	No
WW C-1	**Yes (<MCL)**	No	No	No	No
ER-3-3	No	No	No	No	No
ER-4-1	No	**Yes**	**Yes**	**Yes**	**Yes**
ER-6-1-1	No	No	No	No	No
ER-6-2	No	No	No	No	No
ER-7-1	No	**Yes**	**Yes**	**Yes**	**Yes**
UE-1h	No	No	No	No	No
UE-1q	No	No	No	No	No
UE-10j	No	No	No	No	No
WW-2	No	No	No	No	No
TW-D	No	No	No	No	No

4.7.4.5 CB Forecasts

Figure 4-74 shows the 1,000-year time-cumulative 95th-percentile 1,000-year, CBs forecasts for the LCA flow model base case, High-K Yucca Fault, 40-kg/s Basin Flux, and NSMC model 28, with a single color representing each case. Figure 4-75 shows the 50th-percentile 50 years CB forecasts for the same cases. The time-cumulative CBs are all north of Well ER-6-1, and the 50th-percentile CBs show limited extent of contamination at 50 years.

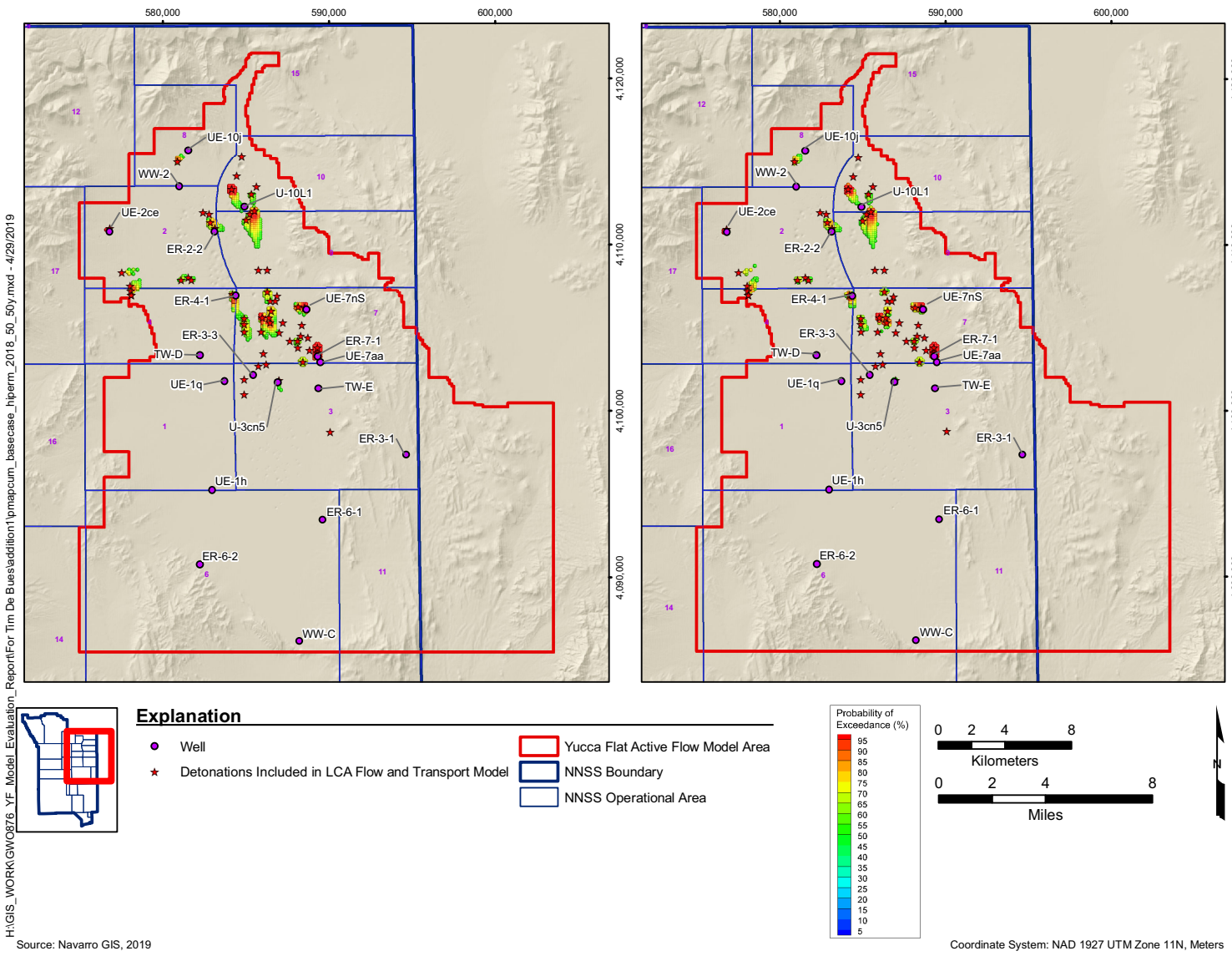

Figure 4-72
50th-Percentile Probability of Exceedance of MCLs at 50 Years for (left) LCA Flow Model Base Case and (right) High-K Yucca Fault

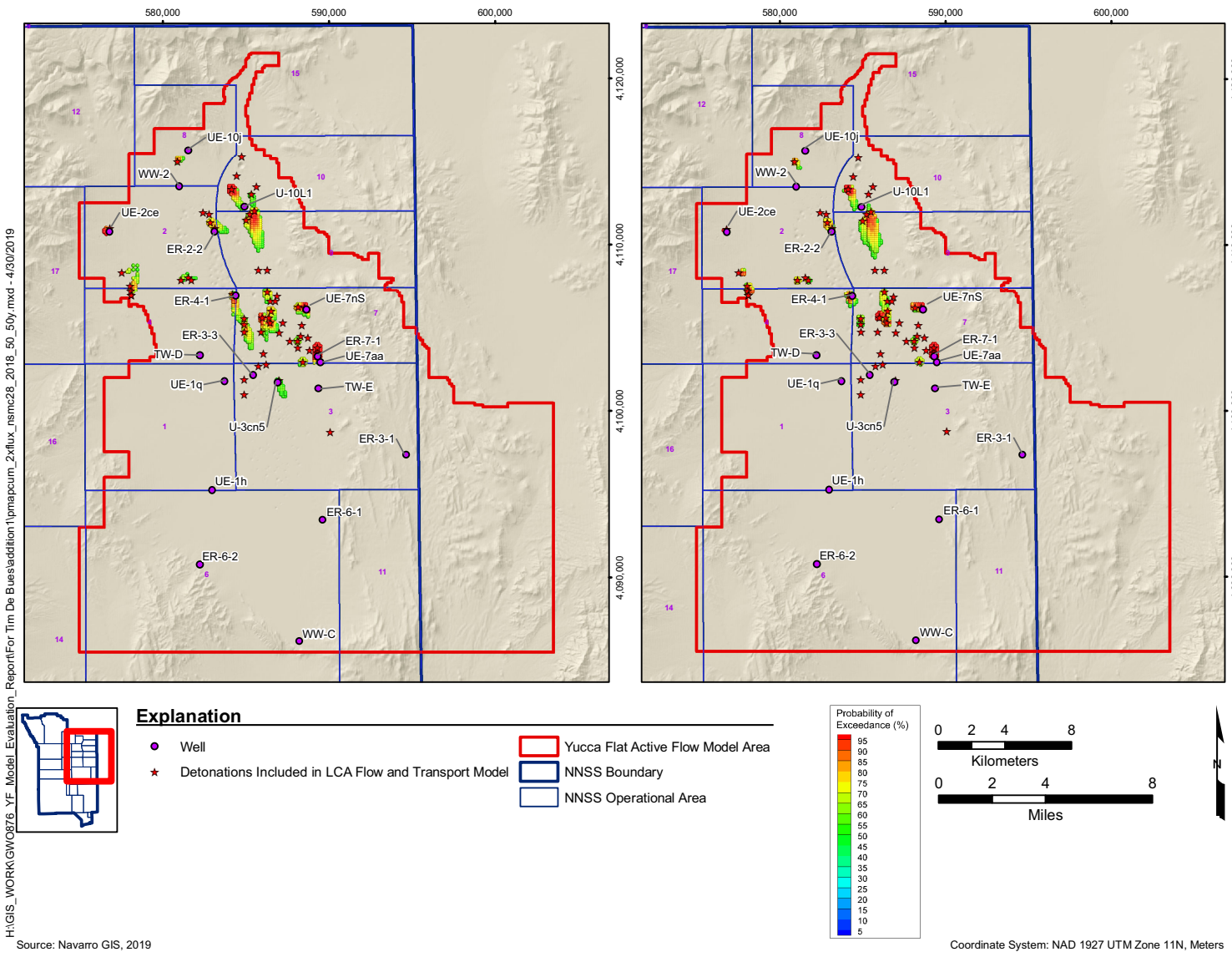

Figure 4-73
50th-Percentile Probability of Exceedance of MCLs at 50 Years for (left) 40-kg/s Basin Flux and (right) NSMC Model 28

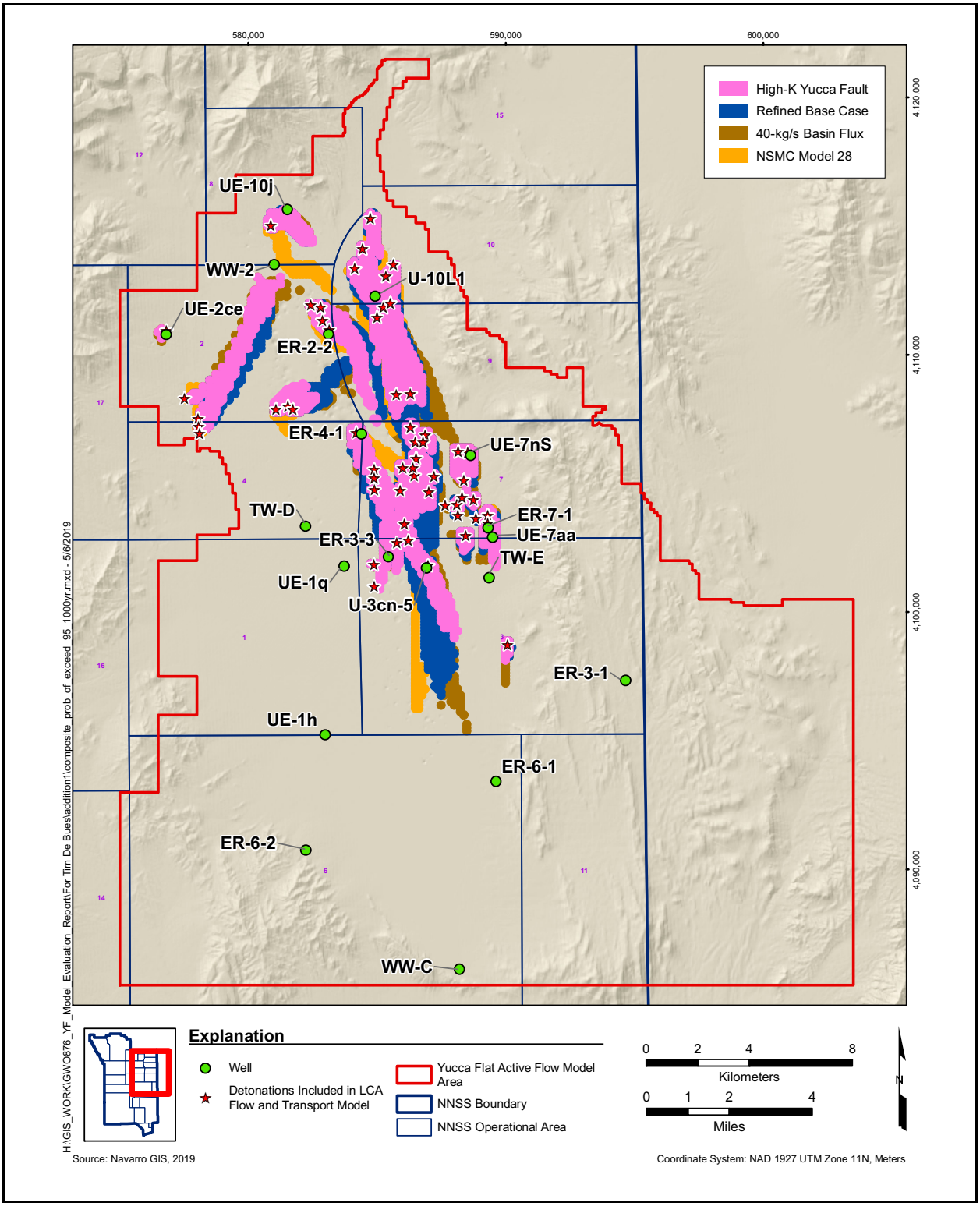

Figure 4-74
1,000-Year Time-Cumulative Probability of Exceedance of MCLs CB Forecasts

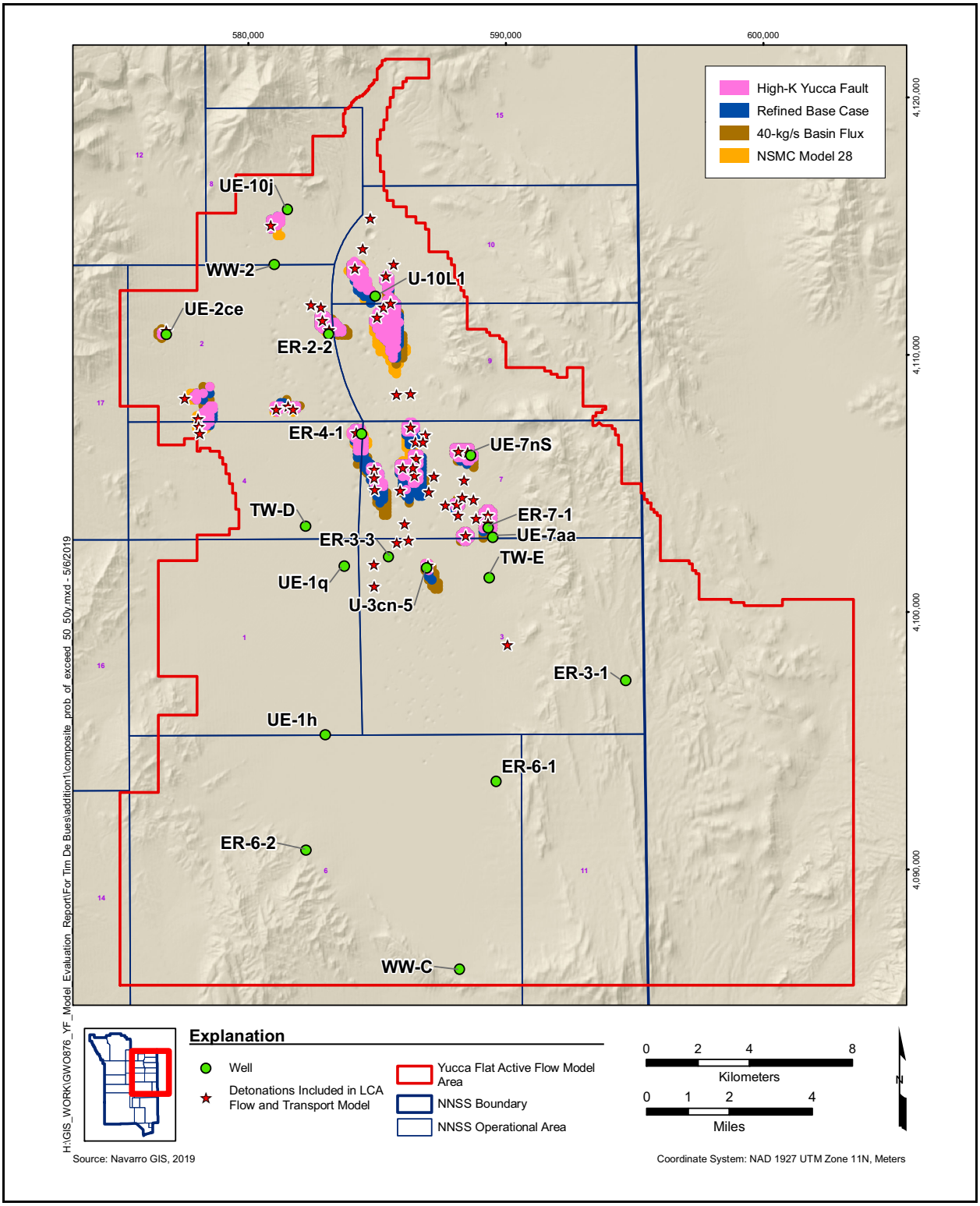

Figure 4-75
50th-Percentile Probability of Exceedance of MCLs CB Forecasts at 50 Years

4.8 Transport Modeling Summary and Conclusions

The following observations can be made from the transport model results:

- Tritium dominates the extent of contaminant migration, but due to the short half-life, the maximum extent of contamination decreases significantly after 150 years.
- Model forecasts predict that once the ^{3}H plume has decayed, the extent of contaminant migration is dominated by ^{90}Sr up to about 400 years, followed by ^{14}C, ^{129}I, and ^{36}Cl out to 1,000 years.
- Less mobile contaminants (including alpha emitters like ^{237}Np or U) are insignificant contributors to the extent of contaminant migration.
- Only eight detonations are shown to consistently contribute to the CBs: BOURBON, CORDUROY, HERMOSA, KLICKITAT, MICKEY, NASH, SHUFFLE, and TORRIDO
- At UE-2ce, where ^{3}H is observed above the MCL, all transport models except NSMC model 28 have forecast ^{3}H above the MCL. In NSMC model 28 the direction of flow at NASH is initially to the east in NSMC model 28, not to the south toward UE-2ce; therefore, the ^{3}H plume does not intersect UE-2ce.
- At ER-2-2, UE-7nS, and U-3cn-5, where ^{3}H is observed below the MCL, all transport models forecast ^{3}H above the MCL at ER-2-2 and UE-7nS, and all transport models except NSMC model 28 forecast ^{3}H above the MCL at U-3cn-5. Generally, these forecasts are conservative. This is probably related to the use of the maximum of the announced yield range to estimate R_c and exchange volume size, which will tend to overestimate the extent of contamination initially in the LCA.
- At locations where ^{3}H is not observed, the 50-year, 50th-percentile forecast CBs for all four transport models indicate some probability of exceeding the MCL at ER-4-1 and ER-7-1 only. This is inconsistent with observations, indicating that all four models are conservative. This is probably related to the use of the maximum of the announced yield range to estimate R_c and exchange volume size, which will tend to overestimate the extent of contamination initially in the LCA.

Transport results from the LCA flow model base case, High-K Yucca Fault, 40-kg/s Basin Flux, and NSMC model 28 all show much less extent of contamination than the N-I (2013) base case. The 1,000-year CBs are north of Well ER-6-1, and the 50-year, 50th-percentile CBs show limited extent of contamination. The CBs forecasted with the refined model remain within the Yucca Flat basin and are more consistent with contaminant observations in the Yucca Flat LCA. The current models indicate that the YF/CM CAU is likely to meet its regulatory boundary objective, which is to verify that RN contamination from the YF/CM CAU is contained within the Yucca Flat basin, thus not impacting the Frenchman Flat LCA or downgradient receptors.

5.0 MODEL EVALUATION TEAM RECOMMENDATIONS

The CADD/CAP stage of the UGTA strategy (FFACO, 1996 as amended) requires an MER (this report) that describes, in addition to the impact of the new data on the flow and transport model, the Model Evaluation Team's recommendations for model refinements, additional data collection, or advancement to the CR stage (DOE/EMNV, 2017d). The focus of data collection and model evaluation during the CADD/CAP (DOE/EMNV, 2017d) was on more realistic representation of flow patterns and flow rates through the LCA in the Yucca Flat basin, along with better representation of the HSTs of deep nuclear tests likely to introduce RNs directly into the LCA because of their depths of burial and the uncertainty in the LCA surface. These goals were achieved through the following:

1. Development of greatly improved estimates of basin flux through the testing area (Section 3.1) and groundwater influxes into Yucca Flat that are consistent with regional water budgets, based on the improved regional flow system model (DV3).

2. Improved LCA source terms inputs (Section 3.5) that recognized the importance of sorption on debris within the cavity/chimney system.

3. Probabilistic approaches to LCA source term inputs that simultaneously considered uncertainty in exchange volume size and LCA surface uncertainty (Section 3.2).

4. Additional hydraulic property estimates (Section 3.4).

5. Additional transient cross-hole water-level response data from the ER-4-1 WDT (Section 2.5).

6. Improved understanding of the present-day extent of contamination (Section 3.3) through repeated sampling of LCA wells, including three new wells drilled in 2016 and 2017 specifically to find contamination in the LCA near large-yield tests close to the LCA surface or nearby faults.

7. Development of a refined flow and transport model (Section 4.0) incorporating the information and insights gained from all the model evaluation activities discussed in Sections 2.0 and 3.0.

A successful comparison between basin-wide flow patterns estimated with particle tracking and flow patterns inferred from geochemical patterns in the groundwater also lent support to the overall validity of the flow and transport model results.

5.1 Model Refinements

This section describes the revised base case and alternative flow and transport models for the LCA in Yucca Flat, and presents rationale for their selection. The alternative models that were run included one in which the flux target in the calibration was doubled relative to the base case (from 20 to 40 kg/s) (i.e., 40-kg/s Basin Flux); one in which the permeability of the Yucca fault was fixed at a high value of 5.E-12 m^2 with other model parameters calibrated (i.e., High-K Yucca Fault); and one NSMC case (model 28) selected because it led to more southerly particle travel than the other two cases. The three alternative models were intended to account for uncertainty in the flux through the eastern corridor, impact of enhanced flow through the Yucca Fault, and local flow field variability resulting form parametric uncertainty as explored by the NSMC analysis. In addition to the two alternative flow models, NSMC analysis was performed to assess the influence of parametric uncertainty on flow and transport pathways and distances. As described in Section 4.3.3, 100 different flow models were considered by choosing parameter sets randomly using the PEST software.

The N-I (2013) LCA base case model was revised to incorporate the results of the model evaluation activities described in the YF/CM CADD/CAP (DOE/EMNV, 2017d). The revised model uses the same computational grid as the N-I (2013) model. Some of the salient features of the revised model are as follows:

1. Use of a groundwater flux constraint in eastern Yucca Flat, based on the reanalysis of the ER-4-1 WDT and ER-6-1-2 MWAT data (Sections 2.5 and 2.6)

2. Use of narrow fault zones with anisotropy representing the effects of the low-permeability fault cores (Section 4.2.3.2)

3. The application of basin flux constraints from the DV3 model onto the boundaries of the LCA model (Section 4.2.3.3)

4. The use of pilot points to allow more heterogeneity in LCA rock properties along with the use of hydraulic conductivity measurements as calibration observations to condition the hydraulic property field (Section 4.2.3.1)

5. Zonation parameterization of only faults with trace lengths greater than 3 km (Section 4.2.3.2)

6. Incorporation of 58 Yucca Flat tests as potential source terms (Section 3.2.3.1), based on the analysis of the uncertainty in the top surface of the LCA and the exchange volume radius

7. A revised HST model for the LCA that includes sorption of RNs such as ^{90}Sr and ^{137}Cs on the tuffaceous rubble in the cavities (Section 4.6)

The LCA flow model was calibrated with adjustable parameters (Section 4.2.3) that consist of permeability values at country rock pilot points and zones, fault permeability values, fault and country rock anisotropy factors, flux values on model boundaries, and specified head values at three pilot points on the southern boundary. The adjustable parameters also included specific storage values. The model objective function was defined (Section 4.2.4) using steady-state head values, a groundwater flux target for the high-transmissivity corridor in the eastern Yucca Flat, steady-state gradient values, transient drawdown values resulting from the ER-6-1-2 and ER-4-1 MWATs, and transmissivity measurements at selected wells. The observation weights used in the objective function calculation were selected to place the most emphasis on the steady-state heads, the transmissivity width-product between Wells ER-7-1 and ER-6-1 in the high-permeability corridor in eastern Yucca Flat, and the ER-4-1 MWAT responses because these observation groups are considered highly reliable and informative to the CAU model. Additionally, a pilot point objective function was constructed from regularization constraint of homogeneity placed on the permeability and specific storage values at pilot points. The calibrated model was found to yield a very good match to all of the observations used in the calibration.

Three alternative models (Section 4.3.2) included all of the same features as the base case model, and their calibration data and weights were also the same as the base case model, except (1) the target flux through the eastern corridor in the high flux alternative was increased from 20 to 40 kg/s to account for the estimated uncertainty in the flux estimate; (2) the permeability of the Yucca fault was fixed at 5.E-12 m^2 in the High-K Yucca Fault alternative, and (3) an example of local flow path variations resulting from parametric uncertainty sampled in NSMC run #28. Together, the base case and three alternatives investigate the potential effects of possible flux uncertainty and transport pathway uncertainty on future contaminant extent.

NSMC analysis was performed to assess the influence of parametric uncertainty on flow and transport pathways and distances on 100 different flow models by choosing parameter sets randomly using the PEST software. Of these, 75 flow models reached an acceptable level of calibration. Particle tracks for these models from the 58 source locations displayed considerable local variability, but conformed to the general flow patterns depicted by the base case and the alternative flow models. Some of the NSMC models displayed 200-year particle travel distances somewhat greater than the

base case and the alternative flow models while remaining well north of the Yucca Flat basin's southern boundary. Transport simulations were conducted on one of these NSMC models: NSMC model 28. The 1,000-year 95th-percentile boundary for NSMC model 28 was found to be consistent with the transport boundary for the base case and the alternative flow models. This was included as an alternative model.

5.2 Additional CADD/CAP Data Collection

The Model Evaluation Team concludes that the datasets used to construct and evaluate the base case and alternative flow and transport models are sufficient. The models are already consistent with a wide variety of experimental and observational data that indicate they are suitable tools for informing regulatory decisions. Hence, no additional data collection is recommended during the CADD/CAP phase.

5.3 Advancement to Closure Stage

The Model Evaluation Team maintains that sufficient confidence now exists in these models that they can be used to support regulatory decisions. These decisions include developing a monitoring well network; identifying use restriction boundaries; and complying with the regulatory boundary objective to verify that RN contamination from the YF/CM CAU is contained within the Yucca Flat basin, thus not impacting the Frenchman Flat LCA or downgradient receptors. The Model Evaluation Team therefore recommends that the YF/CM CAU (CAU 97) move to the closure (CR) stage of the UGTA strategy, where long-term monitoring data are expected to confirm model forecasts.

The basic overall flow patterns and flow rates in the LCA following CADD/CAP are now adequately known. Fifty-eight nuclear detonations likely to contribute RNs to the LCA have been identified and included as possible source terms in the models. The results of model evaluation presented in this report show that base case and three alternative flow and transport models (40-kg/s Basin Flux, High-K Yucca Fault, and NSMC model 28) developed during the CADD/CAP stage are consistent with a wide variety of data collected over several decades, including key data collected or reanalyzed as part of model evaluation.

6.0 PER Committee Recommendations

6.1 Background

The PER Committee consisted of a panel of experts from Desert Research Institute, LLNL, Navarro, NDEP, Nye County, and USGS. The committee met multiple times with the Model Evaluation Team to review various components of the team's analysis of the model evaluation data (i.e., geology, hydraulic testing, evaluation of historical UGT data, water levels, groundwater sampling results, and geochemistry/radiochemistry) and their relevance to the model evaluation targets presented in Table 4-1 in the CADD/CAP (DOE/EMNV, 2017d). Six formal presentations were given by the Model Evaluation Team, followed by comments provided to the team by the PER Committee. These comments included requests for additional information and clarification on data, analysis, and approaches used to address the model evaluation targets and suggestions for additional analysis of data and model results. The Model Evaluation Team responded to all of the PER comments and performed additional modeling and analyses, which the PER Committee subsequently reviewed. As a result of this iterative process, the PER Committee is in agreement with the Model Evaluation Team that the model evaluation targets were satisfactorily addressed to move to the CR stage. Presentations from these meetings, the PER Committee's review comments, and the Model Evaluation Team's responses are archived in the UGTA Technical Data Repository.

The focus of this model evaluation effort on the LCA CAU model and the exclusion of the overlying SZ AA/VA and UZ CAU models resulted from justified conclusions from earlier modeling efforts that RNs originating from detonations in the volcanic rocks and alluvium cannot effectively migrate to the LCA in such a way as to influence the definition and evolution of the 1,000-year CB. The conceptual model for groundwater flow and contaminant transport in the YF/CM CAU is documented in the CADD/CAP (DOE/EMNV, 2017d) and the YF/CM flow and transport model report (N-I, 2013).

6.2 Recommendations

The PER Committee made the following recommendations regarding the path forward for the YF/CM CAU:

1. The 2018 detection of low-level ^{3}H at WW C-1 located at the southern edge of Yucca Flat is viewed as a legitimate observation that is part of a series of observations made since the 1960s. However, there is considerable uncertainty about the source (or sources) of this ^{3}H (Pohlmann, 2018). The PER Committee is concerned about this uncertainty, and about potential implications it might have for the conceptualizations of the HST and mechanisms of groundwater flow and transport as represented in the YF/CM CAU LCA model. The PER Committee recommends that data collection called for in the current sampling plan for WW C-1 (DOE/EMNV, 2018) be supplemented by collection of additional data to better assess the ^{3}H source and suggests that this is a necessary step to support interpretations of future monitoring results (Pohlmann, 2018).

2. As presented to the PER Committee, the results of the NSMC flow simulations confirm that the base case and alternative models are reasonably representative of the wider range of transport outcomes that are produced by incorporating flow system variability, and therefore are appropriate for calculation of the CBs. However, development of an effective monitoring network must address variability and uncertainty in groundwater flow paths, as represented in the NSMC results. Thus, the PER Committee recommends that the NSMC simulations be used as a framework for developing a monitoring well network that accounts for this variability and uncertainty.

3. The PER Committee is satisfied that issues and concerns raised during the PER process were effectively addressed through additional data collection, analysis, and model refinements as documented in this report. The YF/CM CAU LCA "model" should be regarded as the complete understanding of groundwater flow and RN transport in the LCA component of the YF/CM CAU, including relevant uncertainties, as gathered from data, physical, and chemical conceptualizations, numerical modeling, and subsequent interpretations. As such, the model is subject to revision or reinterpretation as new data or information are acquired. As a result, the committee has concluded that the current YF/CM LCA model is suitable for designing a monitoring well network and developing effective institutional controls, and that advancement to the CR stage is recommended.

7.0 REFERENCES

Abdel-Fattah, A., D. Smith, M. Murrell, S. Goldstein, A. Nunn, R. Gritzo, B. Martinez, and P. Reimus. 2005. *Colloid Characteristics and Radionuclide Associations with Colloids in Source-Term Waters at the Nevada Test Site*, LA-UR-05-5312. Los Alamos, NM: Los Alamos National Laboratory.

André, M., M.E. Malmström, and I. Neretnieks. 2009. "Specific Surface Area Determinations on Intact Drillcores and Evaluation of Extrapolation Methods for Rock Matrix Surfaces." In *Journal of Contaminant Hydrology*, Vol. 110(1–2): pp. 1–8.

Andres, C.D., Nevada Division of Environmental Protection, Bureau of Federal Facilities. 2017a. Letter to R.F. Boehlecke (NNSA/NFO) titled "Acceptance of the Flow and Transport Model for Corrective Action Unit (CAU) 97: Yucca Flat/Climax Mine, Corrective Action Decision Document /Corrective Action Plan (CADD/CAP) Studies, *Federal Facility Agreement and Consent Order (FFACO)*," 23 January. Las Vegas, NV.

Andres, C.D., Nevada Division of Environmental Protection, Bureau of Federal Facilities. 2017b. Letter to R.F. Boehlecke (Environmental Management [EM] Nevada Program) titled "RE: Submittal of Final Corrective Action Decision Document/Corrective Action Plan (CADD/CAP) for Corrective Action Unit (CAU) 97: Yucca Flat/Climax Mine, Nevada National Security Site, Nevada, Revision 1, August 2017, *Federal Facility Agreement and Consent Order (FFACO)*," 21 August. Las Vegas, NV.

BN, see Bechtel Nevada.

Bechtel Nevada. 2006. *A Hydrostratigraphic Model and Alternatives for the Groundwater Flow and Contaminant Transport Model of Corrective Action Unit 97: Yucca Flat–Climax Mine, Lincoln and Nye Counties, Nevada*, DOE/NV/11718--1119. Prepared for the U.S. Department of Energy, National Nuclear Security Administration Nevada Site Office. Las Vegas, NV.

Benson, L., and H. Klieforth. 1989. "Stable Isotopes in Precipitation and Ground Water in the Yucca Mountain Region, Southern Nevada: Paleoclimatic Implications." In *Aspects of Climate Variability in the Pacific and the Western Americas*. Geophysical Monograph Vol. 55: pp. 41–59. Washington, DC: American Geophysical Union.

Boardman, C.R. 1970. "Engineering Effects of Underground Nuclear Explosives." In *Proceedings of Symposium on Engineering with Nuclear Explosives*, CONF-700101. pp. 43–67. Las Vegas, NV. 14–16 January.

Boardman, C.R., D.D. Rabb, and R.D. McArthur. 1964. "Responses of Four Rock Mediums to Contained Nuclear Explosions." In *Journal of Geophysical Research*, Vol. 69(16): pp. 3457–3469.

Boardman, C.R., and J. Skrove. 1966. "Distribution in Fracture Permeability of a Granitic Rock Mass following a Contained Nuclear Explosion." In *Journal of Petroleum Technology*, Vol. 18(5): pp. 619–623.

Borg, I.Y. 1973. *Comparison of Shock Effects in Granitic Rock Recovered from the Monique Event, Algeria, and the Piledriver Event, Nevada Test Site,* UCRL-51349. Livermore, CA: Lawrence Livermore Laboratory.

Borg, I., R. Stone, H.B. Levy, and L.D. Ramspott. 1976. *Information Pertinent to the Migration of Radionuclides in Ground Water at the Nevada Test Site, Part 1: Review and Analysis of Existing Information,* UCRL-52078, Pt. 1. Livermore, CA: Lawrence Livermore National Laboratory.

Buddemeier, R.W., and D. Isherwood comps. 1985. *Radionuclide Migration Project 1984 Progress Report*, UCRL-53628. Livermore, CA: Lawrence Livermore National Laboratory.

CFR, see *Code of Federal Regulations.*

Carle, S.F., R.M. Maxwell, G.A. Pawloski, D.E. Shumaker, A.F.B. Tompson, and M. Zavarin. 2007. *Evaluation of the Transient Hydrologic Source Term for the Cambric Underground Nuclear Test at Frenchman Flat, Nevada Test Site*, UCRL-TR-226916. Livermore, CA: Lawrence Livermore National Laboratory.

Carle, S.F., M. Zavarin, Y. Sun, and G.A. Pawloski. 2008. *Evaluation of Hydrologic Source Term Processes for Underground Nuclear Tests in Yucca Flat, Nevada Test Site: Carbonate Tests,* LLNL-TR-403485. Livermore, CA: Lawrence Livermore National Laboratory.

Claassen, H.C. 1973. *Water Quality and Physical Characteristics of Nevada Test Site Water-Supply Wells*, NTS-242; Open-File Report USGS-474-158. Washington, DC: U.S. Geological Survey.

Claassen, H.C., 1986. "Late Wisconsin Paleohydrology of the West-Central Amargosa Desert, Nevada, U.S.A." In *Chemical Geology: Isotope Geoscience Section*, Vol. 58(4): pp. 311–323.

Code of Federal Regulations. 2018. Title 40 CFR Part 141, "National Primary Drinking Water Regulations." Washington, DC: U.S. Government Printing Office.

Colton, R.B. 1965. *Fissures in Playas, Nevada Test Site and Vicinity*, U.S. Geological Survey Technical Letter, NTS-137.

Cooper, H.H., and C.E. Jacob. 1946. "A Generalized Graphical Method for Evaluating Formation Constants and Summarizing Well Field History." In *Eos, Transactions American Geophysical Union*, Vol. 27(4): pp. 526–534.

Craig, H. 1961. "Isotopic Variations in Meteoric Waters." In *Science*, Vol. 133(3465): pp. 1702–1703. Washington, DC: American Association for the Advancement of Science.

Crow, N.B. 1976. *First Observations of Tritium in Ground Water Outside Chimneys of Underground Nuclear Explosions, Yucca Flat, Nevada Test Site*, UCRL-52073. Livermore, CA: Lawrence Livermore Laboratory.

DOE/EMNV, see U.S. Department of Energy Environmental Management Nevada Program.

DOE/NV, see U.S. Department of Energy, Nevada Operations Office.

Dynamic Graphics, see Dynamic Graphics, Inc.

Degueldre, C., R. Grauer, A. Laube, A. Oess, and H. Silby. 1996. "Colloid Properties in Granitic Groundwater Systems. II. Stability and Transport Study." In *Applied Geochemistry*, Vol 11(5): pp. 697–710.

Doherty, J. 2010. *Methodologies and Software for PEST-Based Model Predictive Uncertainty Analysis,* Watermark Numerical Computing webpage at http:\\www.pesthomepage.org\Downloads.php file pest_uncert.zip accessed on 2 January 2018.

Doherty, J. 2018. "Methodologies and Software for PEST-Based Model Predictive Uncertainty Analysis." Brisbane, Australia: Watermark Numerical Computing. Available at http:\\www.pesthomepage.org\Downloads.php?file=pest_uncert.zip. As accessed on 2 January.

Doherty, J., R.J. Hunt, and M.J. Tonkin. 2010. *Approaches to Highly Parameterized Inversion: A Guide to Using PEST for Model-Parameter and Predictive-Uncertainty Analysis,* Scientific Investigations Report 2010-5211. Reston, VA: U.S. Geological Survey.

Doty, G.C., and F.E. Rush. 1985. *Inflow to a Crack in Playa Deposits of Yucca Lake, Nevada Test Site, Nye County, Nevada*, Water-Resources Investigations Report 84-4296. Denver, CO: U.S. Geological Survey.

Drellack, S.L., L.B. Prothro, J.L. Gonzales, J.M. Mercadante, and D.N. Haugstad. 2012. Written communication. Subject: *Low Water Production from Carbonate Aquifers at Rainier Mesa: Implications for the Distribution of Hydraulic Conductivity within the Lower Carbonate Aquifer, Nevada Test Site and Vicinity*. Las Vegas, NV: National Security Technologies, LLC.

Dynamic Graphics, Inc. 2015. *EarthVision 9: Software for 3D Modeling & Visualization*. Alameda, CA.

EPA, see U.S. Environmental Protection Agency.

Elliott, P.E., and M.T. Moreo. 2011. *Groundwater Withdrawals and Associated Well Descriptions for the Nevada National Security Site, Nye County, Nevada*, 1951-2008, Data Series 567. Reston, VA: U.S. Geological Survey.

FFACO, see *Federal Facility Agreement and Consent Order*.

Federal Facility Agreement and Consent Order. 1996 (as amended March 2010). Agreed to by the State of Nevada; U.S. Department of Energy, Environmental Management; U.S. Department of Defense; and U.S. Department of Energy, Legacy Management. Appendix VI, which contains the Underground Test Area Strategy, was last modified June 2014, Revision No. 5.

Fenelon, J.M., D.S. Sweetkind, P.E. Elliott, and R.J. Laczniak. 2012. *Conceptualization of the Predevelopment Groundwater Flow System and Transient Water-Level Responses in Yucca Flat, Nevada National Security Site, Nevada,* Scientific Investigations Report 2012-5196. Carson City, NV: U.S. Geological Survey.

Fenelon, J.M., K.J. Halford, and M.T. Moreo. 2016. *Delineation of the Pahute Mesa–Oasis Valley Groundwater Basin, Nevada,* Scientific Investigations Report 2015–5175. Carson City, NV: U.S. Geological Survey.

Finnegan, D.L., S.M. Bowen, J.L. Thompson, C.M. Miller, P.L. Baca, L.F. Olivas, C.G. Geoffrion, D.K. Smith, W. Goishi, B.K. Esser, J.W. Meadows, N. Namboodiri, and J.F. Wild. 2016. *Nevada National Security Site Radionuclide Inventory, 1951–1992: Accounting for Radionuclide Decay through September 30, 2012,* LA-UR-16-21749. Los Alamos, NM: Los Alamos National Laboratory.

Gudmundsson, A. 2011. *Rock Fractures in Geological Processes*. Cambridge, UK: Cambridge University Press.

Halford, K., U.S. Geological Survey. 2009. Personal communication to A. Tompson (LLNL) regarding specified fluxes to lateral boundaries of the UGTA LCA model for Yucca Flat, 16 January. Carson City, NV.

Halford, K., U.S. Geological Survey. 2012. Personal communication to A. Tompson (LLNL) regarding groundwater flow estimates for the Yucca Flat/Climax Mine CAU, 9 October. Carson City, NV.

Halford, K., U.S. Geological Survey. 2016. Personal communication to J. Fenelon (USGS) regarding response to External Peer Review Team Report, 15 April. Carson City, NV.

Halford, K.J., and T.R. Jackson. 2019. Written communication. Subject: *Characterization and Effects of Pumping in the Death Valley Regional Groundwater Flow System, Nevada and California, with Special Reference to Devils Hole*. Reston, VA: U.S. Geological Survey.

Halford, K., C.A. Garcia, J. Fenelon, and B. Mirus. 2016. *Advanced Methods for Modeling Water-Levels and Estimating Drawdowns with SeriesSEE, an Excel Add-In,* Techniques and Methods Report 4-F4. Reston, VA: U.S. Geological Survey.

Harbaugh, A.W. 1990. *A Computer Program for Calculating Subregional Water Budgets Using Results from the U.S. Geological Survey Modular Three-Dimensional Ground-water Flow Model*, Open-File Report 90-392. Reston, VA: U.S. Geological Survey.

Harrill, J.R., J.S. Gates, and J.M. Thomas. 1988. *Major Groundwater Flow Systems in the Great Basin Region of Nevada, Utah and Adjacent States,* Hydrological Atlas HA-694-C, scale 1:1,000,000. Denver, CO: U.S. Geological Survey.

Hastie, T., R. Tibshirani, and J. Friedman. 2008. *The Elements of Statistical Learning: Data Mining, Inference, and Prediction*, Second Edition. New York, NY: Springer Science+Business Media.

Hoffman, D.C., R. Stone, and W.W. Dudley, Jr. 1977. *Radioactivity in the Underground Environment of the CAMBRIC Nuclear Explosion at the Nevada Test Site*, LA-6877-MS. Los Alamos, NM: Los Alamos National Laboratory.

Hu, Q., and M. Zavarin. 2007. *Evaluation of the Rainier Mesa/Shoshone Mountain CAU HST Transport Parameters Based on Solid and Water Sampling,* UCRL-MI-234814, pp. 62. Livermore, CA: Lawrence Livermore National Laboratory.

Hu, Q.H., T.P. Rose, M. Zavarin, D.K. Smith, J.E. Moran, and P.H. Zhao. 2008a. "Assessing Field-Scale Migration of Radionuclides at the Nevada Test Site: 'Mobile' Species." In *Journal of Environmental Radioactivity*, Vol. 99(10): pp. 1617–1630.

Hu, Q.H., M. Zavarin, and T.P. Rose. 2008b. "Effect of Reducing Groundwater on the Retardation of Redox-Sensitive Radionuclides." In *Geochemical Transactions*, Vol. 9(12): pp. 1–24.

IAEA, see International Atomic Energy Agency.

IT, see IT Corporation.

Ingraham, N.L., B.F. Lyles, R.L. Jacobson, and J.W. Hess. 1991. "Stable Isotopic Study of Precipitation and Spring Discharge in Southern Nevada." In *Journal of Hydrology,* Vol. 125(3–4): pp. 243–258.

International Atomic Energy Agency. 1998a. *The Radiological Situation at the Atolls of Mururoa and Fangataufa, Technical Report, Volume 3: Inventory of Radionuclides Underground at the Atolls,* IAEA-MFTR-3. In "Proceedings of an IAEA Conference, Vienna, 30 June – 3 July." Vienna, Austria.

International Atomic Energy Agency. 1998b. *The Radiological Situation at the Atolls of Mururoa and Fangataufa, Technical Report, Volume 4: Release to the Biosphere of Radionuclides from Underground Nuclear Weapons Tests at the Atolls,* IAEA-MFTR-4. In "Proceedings of an IAEA Conference, Vienna, 30 June – 3 July." Vienna, Austria.

International Atomic Energy Agency. 1998c. *The Radiological Situation at the Atolls of Mururoa and Fangataufa, Technical Report, Volume 6: Dose Due to Radioactive Materials Present in the Environment or Released from the Atolls,* IAEA-MFTR-6. In "Proceedings of an IAEA Conference, Vienna, 30 June – 3 July." Vienna, Austria.

IT Corporation. 1996. *Regional Geologic Model Data Documentation Package (Underground Test Area Subproject Phase I Data Analysis Task, Volume I, Parts 1 and 2),* ITLV/10972--181. Prepared for the U.S. Department of Energy, Nevada Operations Office. Las Vegas, NV.

IT Corporation. 1997. Written communication. Subject: *Environmental Restoration Program Underground Test Area Subproject Data Analysis, Technical Letter, Hydrology of Bilby Site (U-3cn)*. September. Las Vegas, NV.

IT Corporation. 1999. *Value of Information Analysis for Corrective Action Unit 97: Yucca Flat, Nevada Test Site, Nevada,* DOE/NV/13052--079; ITLV/13052--079. Las Vegas, NV.

Jackson, T., U.S. Geological Survey. 2017. Memorandum to D. Galloway (USGS Water Mission Area, Indianapolis, Indiana) titled "AQUIFER TEST PACKAGE—Drawdown estimation and analysis of the *ER-4-1 m1* multiple-well aquifer test of the lower carbonate aquifer, Yucca Flat, Nevada National Security Site," 1 June. Henderson, NV.

Jackson, T., and K. Halford. 2019. Written communication. Subject: *Estimation of Groundwater Flow through Yucca Flat Based on Analysis of a Multiple-Well Aquifer Test at Well ER-6-1-2 Main, Nevada National Security Site*. Reston, VA: U.S. Geological Survey.

Kwicklis, E., Yucca Flat/Climax Mine CAU Lead. 2015. "Recommendations for New Wells in Corrective Action Unit 97: Yucca Flat/Climax Mine, NNSS, following the Yucca Flat Peer Review," LA-UR-15-25932. Technical memo dated 20 March. Los Alamos, NM: Los Alamos National Laboratory.

Kwicklis, E., Yucca Flat/Climax Mine CAU Lead. 2016. "Yucca Flat/Climax Mine Model Evaluation Planning –Expert Elicitation." Technical memo dated 1 September. Los Alamos, NM: Los Alamos National Laboratory.

Kwicklis, E., and K. Birdsell, Los Alamos National Laboratory. 2016. Written communication. Subject: "Interview with LANL Containment Scientists to Learn about Testing Practices in Yucca Flat," 1 November. Los Alamos, NM.

LLNL, see Lawrence Livermore National Laboratory.

Lantz, M.W., comp. 1978. *Environmental Surveillance Report for the Nevada Test Site, July 1976 Through December 1976,* NVO-410-39. Las Vegas: Reynolds Electrical & Engineering Co., Inc.

Lawrence Livermore National Laboratory. 2005. Letter report to B. Wilborn (NNSA/NSO) titled "Isotope Analyses: Environmental Monitoring Well ER-6-2," 5 August. Livermore, CA: Lawrence Livermore National Laboratory, Environmental Radiochemistry Group.

Lyles, B.F. 1990. *Tritium Variations in Groundwater on the Nevada Test Site*, DOE/NV/10384-38; Publication No. 45086. Las Vegas, NV: Desert Research Institute, Water Resources Center.

McNab, W.W. 2008. *Evaluation of Hydrologic Source Term Processes for Underground Nuclear Tests in Yucca Flat, Nevada Test Site: Unsaturated Tests and the Impact of Recharge*, LLNL-TR-403360. Livermore, CA: Lawrence Livermore National Laboratory.

Merlivat, L., and J. Jouzel. 1979. "Global Climatic Interpretation of the Deuterium Oxygen-18 Relationship for Precipitation." In *Journal of Geophysical Research: Oceans,* Vol. 84(C8): pp. 5029–5033.

Moscati, R.J., and K.M. Scofield. 2011. *Meteoric Precipitation at Yucca Mountain, Nevada: Chemical and Stable Isotope Analyses, 2006–09*, Scientific Investigations Report 2011-5140. Reston, VA: U.S. Geological Survey.

Navarro GIS, see Navarro Geographic Information Systems.

N-I, see Navarro-Intera, LLC.

NNSA/NFO, see U.S. Department of Energy, National Nuclear Security Administration Nevada Field Office.

NNSA/NSO, see U.S. Department of Energy, National Nuclear Security Administration Nevada Site Office.

Navarro. 2016a. Written communication. Subject: *Model Evaluation Plan for Corrective Action Unit 97: Yucca Flat/Climax Mine Nevada National Security Site, Nevada*. Las Vegas, NV.

Navarro. 2016b. *Response to External Peer Review Team Report for Corrective Action Unit 97: Yucca Flat/Climax Mine, Nevada National Security Site, Nye County, Nevada,* Rev. 1, N/0002653--031-REV. 1. Las Vegas, NV.

Navarro. 2018. *Yucca Flat Well Development and Testing Analyses for Wells ER-3-3 and ER-4-1, Nevada National Security Site, Nye County, Nevada,* Rev. 0, N/00002653--043. Las Vegas, NV.

Navarro. 2019a. Written communication. Subject: "UGTA Chemistry Database (UCDB)," UGTA Technical Data Repository Database Identification Number UGTA-4-1197. Las Vegas, NV. As accessed on 21 February.

Navarro. 2019b. Written communication. Subject: "UGTA Stratigraphy and Lithology Database," UGTA Technical Data Repository Database Identification Number UGTA-4-134. Las Vegas, NV. As accessed on 5 March.

Navarro Geographic Information Systems. 2018–2019. ESRI ArcGIS Software.

Navarro-Intera, LLC. 2013. *Phase I Flow and Transport Model Document for Corrective Action Unit 97: Yucca Flat/Climax Mine, Nevada National Security Site, Nye County, Nevada*, Rev. 1, N-I/28091--080. Las Vegas, NV.

Navarro-Intera, LLC. 2015. *External Peer Review Team Report for Corrective Action Unit 97: Yucca Flat/Climax Mine, Nevada National Security Site, Nye County, Nevada,* Rev. 0, N-I/28091--091. Las Vegas, NV.

Nimz, G.J., and J.L. Thompson. 1992. *Underground Radionuclide Migration at the Nevada Test Site*, UCRL-ID-111013. Livermore, CA: Lawrence Livermore National Laboratory.

OTA, see U.S. Congress, Office of Technology Assessment.

Pawloski, G.A. 1999. *Development of Phenomenological Models of Underground Nuclear Tests on Pahute Mesa, Nevada Test Site—BENHAM and TYBO*, UCRL-ID-136003. Livermore, CA: Lawrence Livermore National Laboratory.

Pawloski, G.A., A.F.B. Tompson, and S.F. Carle eds. 2001. *Evaluation of the Hydrologic Source Term from Underground Nuclear Tests on Pahute Mesa at the Nevada Test Site: The CHESHIRE Test*, UCRL-ID-147023. Livermore, CA: Lawrence Livermore National Laboratory.

Pawloski, G.A., A.F.B. Tompson, S.F. Carle, R.L. Detwiler, Q. Hu, S. Kollet, R.M. Maxwell, W.W. McNab, S.K. Roberts, D.E. Shumaker, Y. Sun, and M. Zavarin. 2008. *Evaluation of Hydrologic Source Term Processes for Underground Nuclear Tests in Yucca Flat, Nevada Test Site: Introduction and Executive Summary,* LLNL-TR-403428. Livermore, CA: Lawrence Livermore National Laboratory.

Phelps, G.A., V.E. Langenheim, and R.C. Jachens. 1999. *Thickness of Cenozoic Deposits of Yucca Flat Inferred from Gravity Data, Nevada Test Site, Nevada*, Open-File Report 99-310. Menlo Park, CA: U.S. Geological Survey.

Pohlmann, K., Desert Research Institute. 2018. Memorandum to B. Wilborn (DOE/EMNV) titled "Effects of Tritium Detections at WW C-1 on the Decision To Move to Closure of the Yucca Flat/Climax Mine CAU," 26 December. Las Vegas, NV.

Prothro, L.B., S.L. Drellack Jr., D.N. Haugstad, H.E. Huckins-Gang, and M.J. Townsend. 2009. *Observations on Faults and Associated Permeability Structures in Hydrogeologic Units at the Nevada Test Site*, DOE/NV/25946--690. Las Vegas, NV: National Security Technologies, LLC.

RamaRao, B.S., A.M. Lavenue, G. de Marsily, and M.G. Marietta. 1995. "Pilot Point Methodology for Automated Calibration of an Ensemble of Conditionally Simulated Transmissivity Fields 1. Theory and Computational Experiments." In *Water Resources Research*, Vol. 31(3): pp. 475–493.

Reiner, S.R. 2007. *Ground-Water Temperature Data, Nevada Test Site and Vicinity, Nye, Clark, and Lincoln Counties, Nevada, 2000–2006,* Data Series 269. Carson City, NV: U.S. Geological Survey.

Robinson, B.A., Z.V. Dash, and S.L. Painter. 2011. *User's Guide for the PLUMECALC Application with Subgridding,* LA-UR-11-02090. Los Alamos, NM: Los Alamos National Laboratory.

Rose, T. 2003. Memorandum to B. Bangerter (NNSA/NSO) titled *Isotopic Analyses: Environmental Monitoring Well ER-6-1 #2*. Livermore, CA: Lawrence Livermore National Laboratory.

Rose, T.P., Q. Hu, P. Zhao, C.L. Conrado, R. Dickerson, G.F. Eaton, A.B. Kersting, J.E. Moran, G. Nimz, B.A. Powell, E.C. Ramon, F.J. Ryerson, R.W. Williams, P.T. Wooddy, and M. Zavarin. 2011. *Radionuclide Partitioning in an Underground Nuclear Test Cavity*, LLNL-TR-409817. Livermore, CA: Lawrence Livermore National Laboratory.

Russell, C., Desert Research Institute. 2018. Memorandum to B. Wilborn and J. Myers (DOE/EMNV) titled "Observation of Tritium in WW-C and WW-C 1," 21 June. Las Vegas, NV.

Shaw, see Shaw Environmental, Inc.

SNJV, see Stoller-Navarro Joint Venture.

Shaw Environmental, Inc. 2003. Written communication prepared for U.S. Department of Energy. Subject: "Yucca Flat ER-7-1 Well Data Report." May 2003. Las Vegas, NV.

Smith, D.K., B.K. Esser, J.M. Kenneally, R.J. Nagle, J.H. Rego, and J.L. Royval. 1996. *Hydrologic Resources Management Program FY 1995 Progress Report*, UCRL-ID-123486. Livermore, CA: Lawrence Livermore Laboratory.

Stoller-Navarro Joint Venture. 2004. *Phase II Hydrologic Data for the Groundwater Flow and Contaminant Transport Model of Corrective Action Unit 98: Frenchman Flat, Nevada*, Rev. 0, S-N/99205--032. Las Vegas, NV.

Stoller-Navarro Joint Venture. 2005a. *Analysis of Hydraulic Responses from the ER-6-1 Multiple-Well Aquifer Test, Yucca Flat FY 2004 Testing Program, Nevada Test Site, Nye County, Nevada,* Rev. 0, S-N/99205--051. Las Vegas, NV.

Stoller-Navarro Joint Venture. 2006a. *Geochemical and Isotopic Evaluation of Groundwater Movement in Corrective Action Unit 97: Yucca Flat/Climax Mine, Nevada Test Site, Nevada*, Rev. 0, S-N/99205--070. Las Vegas, NV.

Stoller-Navarro Joint Venture. 2006b. *Phase I Hydrologic Data for the Groundwater Flow and Contaminant Transport Model of Corrective Action Unit 97: Yucca Flat/Climax Mine, Nevada Test Site, Nye County, Nevada,* Rev. 0, S-N/99205--077. Las Vegas, NV.

Stoller-Navarro Joint Venture. 2006c. *Well ER-6-1 Tracer Test Analysis: Yucca Flat, Nevada Test Site, Nye County, Nevada*, Rev. 0, S-N/99205--084. Las Vegas, NV.

Stoller Navarro Joint Venture. 2007. *Phase I Contaminant Transport Parameters for the Groundwater Flow and Contaminant Transport Model of Corrective Action Unit 97: Yucca Flat/Climax Mine, Nevada Test Site, Nye County, Nevada*, Rev. 0, S-N/99205--096. Las Vegas, NV.

Stoller-Navarro Joint Venture. 2009. *Unclassified Source Term and Radionuclide Data for Corrective Action Unit 97: Yucca Flat/Climax Mine, Nevada Test Site, Nevada*, Rev. 2, S-N/99205--114. Las Vegas, NV.

Sutton, M. 2009. *Review of Distribution Coefficients for Radionuclides in Carbonate Minerals*, LLNL-SR-415700. Livermore, CA: Lawrence Livermore National Laboratory.

Thompson, J.L., comp. and ed. 1995. *Laboratory and Field Studies Related to the Hydrologic Resources Management Program. October 1, 1993—September 30, 1995*, LA-12917-PR. Los Alamos, NM: Los Alamos National Laboratory

Tompson, A.F.B., C.J. Bruton, and G.A. Pawloski eds. 1999. *Evaluation of the Hydrologic Source Term from the Underground Nuclear Tests in Frenchman Flat and the Nevada Test Site: The CAMBRIC Test,* UCRL-ID-132300. Livermore, CA: Lawrence Livermore National Laboratory.

Tompson, A.F.B., ed., R.M. Maxwell, R.L. Detwiler, Q. Hu, S. Kollet, and S.K. Roberts. 2008. *Evaluation of Hydrologic Source Term Processes for Underground Nuclear Tests in Yucca Flat, Nevada Test Site: Saturated Tests*, LLNL-TR-403429. Livermore, CA: Lawrence Livermore National Laboratory.

Tompson, A.F.B., M. Zavarin, W.W. McNab, S.F. Carle, D.E. Shumaker, C. Lu, Y. Sun, G.A. Pawloski, Q. Hu, and S.K. Roberts. 2011. Written communication. Subject: *Hydrologic* Source Term Processes and Models for Underground Nuclear Tests at Rainier Mesa and *Shoshone Mountain, Nevada National Security Site.* Livermore, CA: Lawrence Livermore National Laboratory.

USGS, see U.S. Geological Survey.

U.S. Congress, Office of Technology Assessment. 1989. *The Containment of Underground Nuclear Explosions,* OTA-ISC-414. Washington, DC: U.S. Government Printing Office.

U.S. Department of Energy Environmental Management Nevada Program. 2017a. *Completion Report for Well ER-2-2 Corrective Action Unit 97: Yucca Flat/Climax Mine*, Rev. 1, DOE/NV--1559-REV. 1. Las Vegas, NV.

U.S. Department of Energy Environmental Management Nevada Program. 2017b. *Completion Report for Well ER-3-3 Corrective Action Unit 97: Yucca Flat/Climax Mine*, Rev. 0, DOE/NV--1569. Las Vegas, NV.

U.S. Department of Energy Environmental Management Nevada Program. 2017c. *Completion Report for Well ER-4-1 Corrective Action Unit 97: Yucca Flat/Climax Mine*, Rev. 0, DOE/NV--1576. Las Vegas, NV.

U.S. Department of Energy Environmental Management Nevada Program. 2017d. *Corrective Action Decision Document/Corrective Action Plan for Corrective Action Unit 97: Yucca Flat/Climax Mine Nevada National Security Site, Nevada,* Rev. 1, DOE/NV--1566-REV. 1. Las Vegas, NV.

U.S. Department of Energy Environmental Management Nevada Program. 2018. *Nevada National Security Site Integrated Groundwater Sampling Plan*, Rev. 1, DOE/NV--1525-REV. 1. Las Vegas, NV.

U.S. Department of Energy, National Nuclear Security Administration Nevada Field Office. 2014. *Nevada National Security Site Integrated Groundwater Sampling Plan*, Rev. 0, DOE/NV--1525. Las Vegas, NV.

U.S. Department of Energy, National Nuclear Security Administration Nevada Field Office. 2015a. *Underground Test Area Activity Quality Assurance Plan Nevada National Security Site, Nevada*, Rev. 2, DOE/NV--1450-Rev. 2. Las Vegas, NV.

U.S. Department of Energy, National Nuclear Security Administration Nevada Field Office. 2015b. *United States Nuclear Tests, July 1945 through September 1992,* DOE/NV--209-REV 16. Las Vegas, NV.

U.S. Department of Energy, National Nuclear Security Administration Nevada Site Office. 2004. *Well Completion Report for Well ER-7-1*, DOE/NV/11718--865. Prepared by Bechtel Nevada. Las Vegas, NV.

U.S. Department of Energy, Nevada Operations Office. 1997. *Shaft and Tunnel Nuclear Detonations at the Nevada Test Site: Development of a Primary Database for the Estimation of Potential Interactions with the Regional Groundwater System,* DOE/NV--464, UC-700. Las Vegas, NV.

U.S. Department of Energy, Nevada Operations Office. 2000a. *Corrective Action Investigation Plan for Corrective Action Unit 97: Yucca Flat/Climax Mine, Nevada Test Site, Nevada*, DOE/NV--659. Las Vegas, NV.

U.S. Department of Energy, Nevada Operations Office. 2000b. *United States Nuclear Tests, July 1945 through September 1992*, DOE/NV--209-REV 15. Las Vegas, NV.

U.S. Environmental Protection Agency. 1996. *Offsite Environmental Monitoring Report, Radiation Monitoring Around United States Nuclear Test Areas, Calendar 1993,* EPA/402/R-96/007. Washington, DC: Office of Radiation and Indoor Air.

U.S. Environmental Protection Agency. 2002. *Radionuclides in Drinking Water: A Small Entity Compliance Guide,* EPA 815-R-02-001. Washington, DC: Office of Ground Water and Drinking Water.

U.S. Geological Survey. 2019. "Groundwater Levels for Nevada." As accessed at http://nwis.waterdata.usgs.gov/nwis/gwlevels on 5 March.

White, A.F., and N.J. Chuma. 1987. "Carbon and Isotopic Mass Balance Models of Oasis Valley–Fortymile Canyon Groundwater Basin, Southern Nevada." In *Water Resources Research*, Vol. 23(4): pp. 571–582. Washington, DC: American Geophysical Union.

Winograd, I.J., and W. Thordarson. 1975. *Hydrogeologic and Hydrochemical Framework, South-Central Great Basin, Nevada-California, with Special Reference to the Nevada Test Site,* Professional Paper 712-C.

Winograd I.J., T.B. Coplen, J.M. Landwehr, A.C. Riggs, K.R. Ludwig, B.J. Szabo, P.T. Kolesar, and K.M. Revesz. 1992. "Continuous 500,000-Year Climate Record from Vein Calcite in Devils Hole, Nevada." In *Science,* Vol. 258(5080): pp. 255–260.

Winograd I.J., J.M. Landwehr, T.B. Coplen, W.D. Sharp, A.C. Riggs, K.R. Ludwig, and P.T. Kolesar. 2006. "Devils Hole, Nevada, $\delta^{18}O$ Record Extended to the Mid-Holocene." In *Quaternary Research,* Vol. 66(2): pp. 202–212.

Zavarin, M., Lawrence Livermore National Laboratory. 2010a. Memorandum to B. Wilborn (NNSA/NSO) titled "Isotopic Analyses: Monitoring Well UE-2ce," 24 August. Livermore, CA.

Zavarin, M., Lawrence Livermore National Laboratory. 2010b. Memorandum to B. Wilborn (NNSA/NSO) titled "Isotopic Analyses: Monitoring Well U-19ad PS#1A (Chancellor)," 5 January. Livermore, CA.

Zavarin, M., Lawrence Livermore National Laboratory. 2012. Memorandum to B. Wilborn (NNSA/NSO) titled "Isotopic Analyses: Environmental Monitoring Well U-3cn #5," 4 October. Livermore, CA.

Zavarin, M. 2014. *Yields and Cavity Radii of Underground Nuclear Tests with Specified Yields Reported in DOE/NV--209-Rev 15 (2000),* LLNL-TR-664664. Livermore, CA: Lawrence Livermore National Laboratory.

Zavarin, M. 2017. *Interview With LLNL Containment Scientists to Learn about Testing Practices in Yucca Flat, Especially Related to Proximity of Deeper Tests to LCA*, LLNL-MI-722138. 7 February. Livermore, CA: Lawrence Livermore National Laboratory.

Zavarin, M., Lawrence Livermore National Laboratory. 2019. Memorandum to I. Farnham (Navarro) titled "RE: Hole History for Yucca Flat wells that intersect the saturated LCA," 20 February. Livermore, CA.

Zavarin, M., M.R. Johnson, S.K. Roberts, R. Pletcher, T.P. Rose, A.B. Kersting, G. Eaton, Q. Hu, E. Ramon, J. Walensky, and P. Zhao. 2005a. *Radionuclide Transport in Tuff and Carbonate Fractures from Yucca Flat, Nevada Test Site*, UCRL-TR-219836. Livermore, CA: Lawrence Livermore National Laboratory.

Zavarin, M., S.K. Roberts, N. Hakem, A.M. Sawvel, and A.B. Kersting. 2005b. "Eu(III), Sm(III), Np(V), Pu(V), and Pu(IV) Sorption to Calcite." In *Radiochimica Acta*, Vol. 93(2): pp. 93–102.

Zavarin, M., S. Roberts, P. Reimus, and M. Johnson. 2007. *Summary of Radionuclide Reactive Transport Experiments in Fractured Tuff and Carbonate Rocks from Yucca Flat, Nevada Test Site*, UCRL-TR-225271. Livermore, CA: Lawrence Livermore National Laboratory.

Zavarin, M., A.B. Kersting, R.E. Lindvall, and T.P. Rose, eds. 2008. *Hydrologic Resources Management Program and Underground Test Area Project FY 2006 Progress Report,* LLNL-TR-404620. Livermore, CA: Lawrence Livermore National Laboratory.

Zyvoloski, G.A., B.A. Robinson, Z.V. Dash, and L.L. Trease. 1997a. *Summary of the Models and Methods for the FEHM Application–A Finite-Element Heat- and Mass-Transfer Code*, LA-13307-MS. Los Alamos, NM: Los Alamos National Laboratory.

Zyvoloski, G.A., B.A. Robinson, Z.V. Dash, and L.L. Trease. 1997b. *User's Manual for the FEHM Application–A Finite-Element Heat- and Mass-Transfer Code,* LA-13306-M. Los Alamos, NM: Los Alamos National Laboratory.

Appendix A

Well Completion Diagrams and Tritium/Water Production Logs for Model Evaluation Wells

A.1.0 Well Completion Diagrams and Tritium/Water Production Logs for Model Evaluation Wells

This appendix presents the well completion diagrams for the model evaluation Wells ER-2-2 (Figure A-1), ER-3-3 (Figure A-2), and ER-4-1 (Figure A-3); as well as water production and ^{3}H logs for the model evaluation Wells ER-2-2 (Figure A-4), ER-3-3 (Figure A-5), and ER-4-1 (Figure A-6). An expanded view of the well-bore section for Well ER-4-1 from the depth of about 1,020 ft to 2,150 ft is presented in Figure A-7.

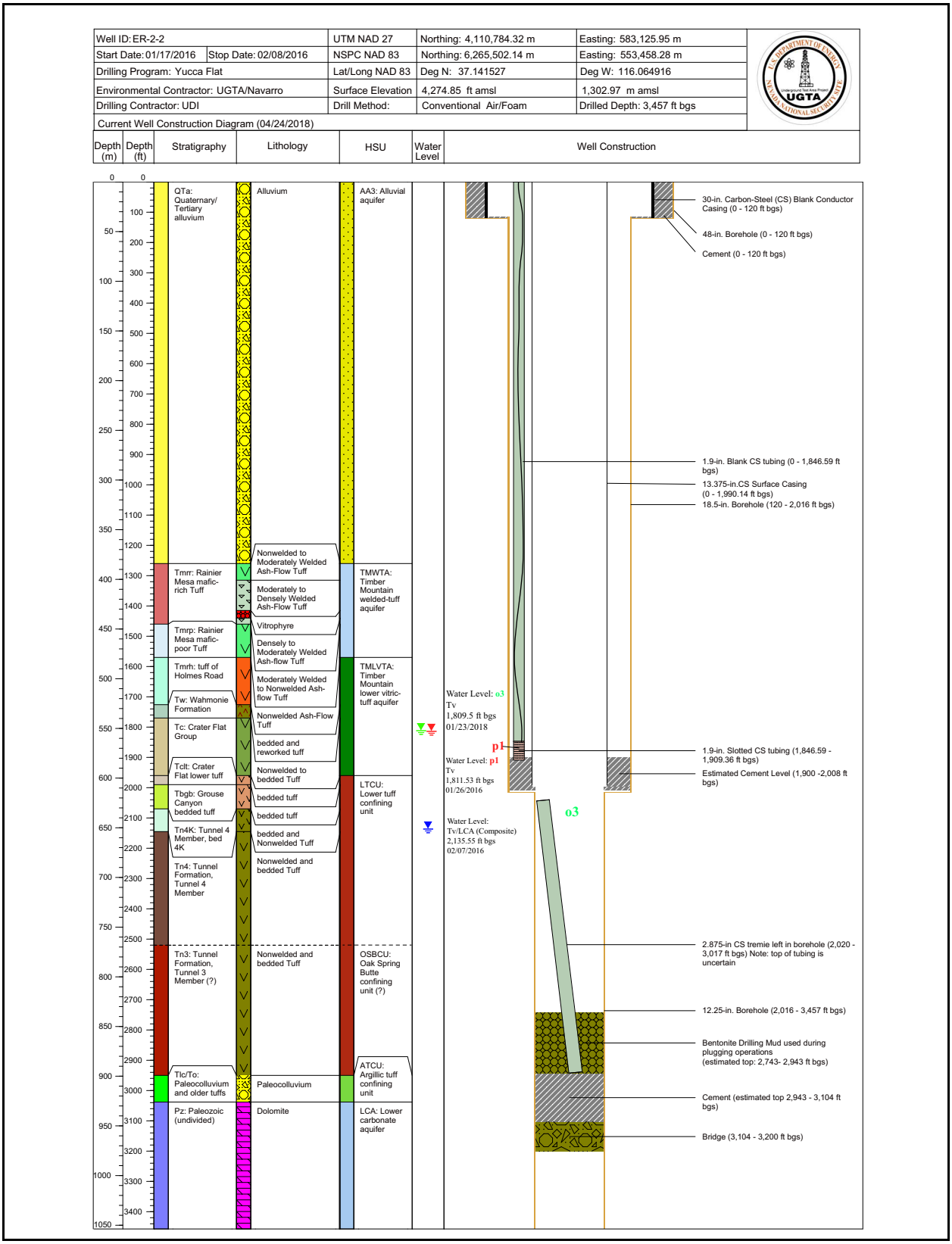

Figure A-1
Well Completion Diagram for ER-2-2

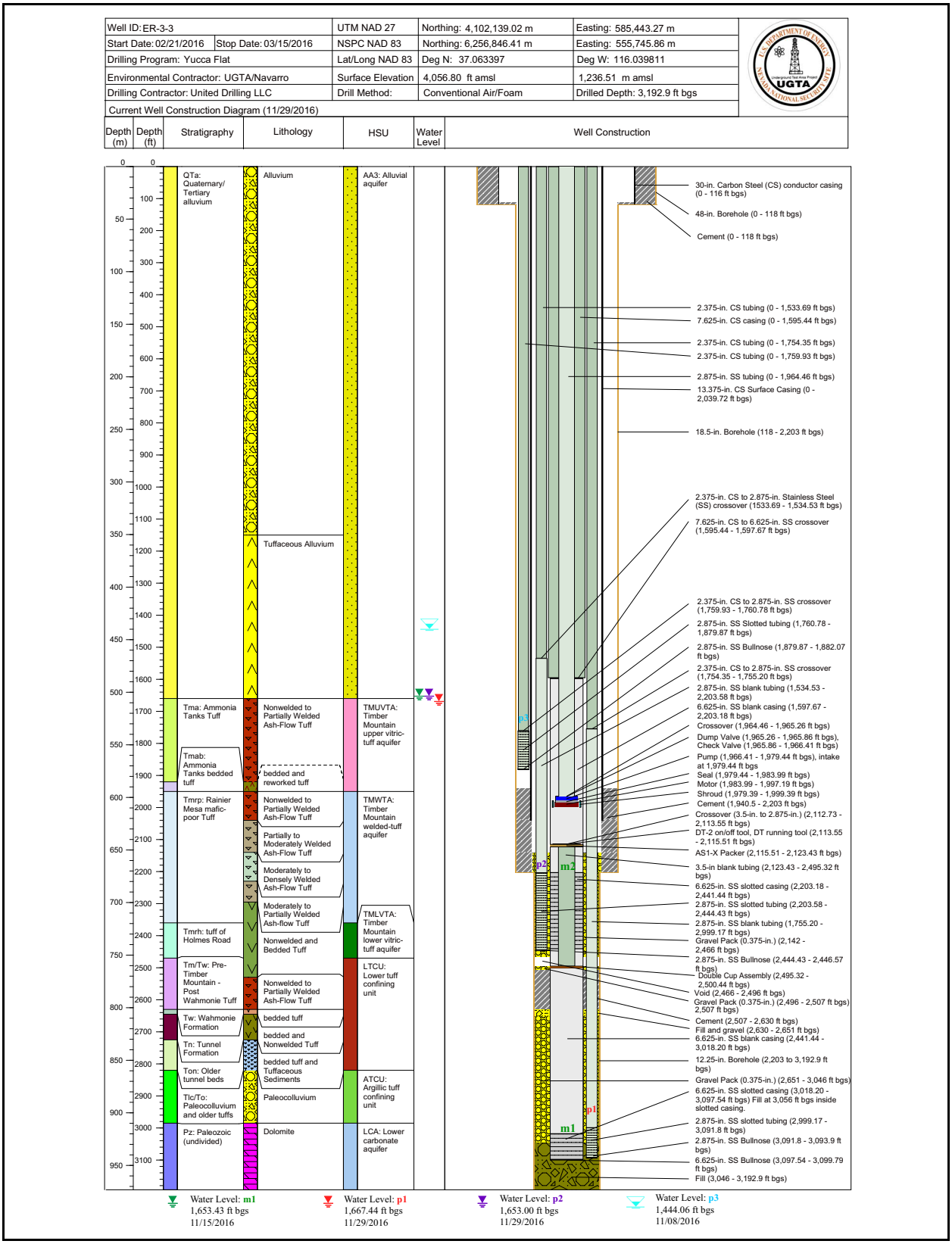

Figure A-2
Well Completion Diagram for ER-3-3

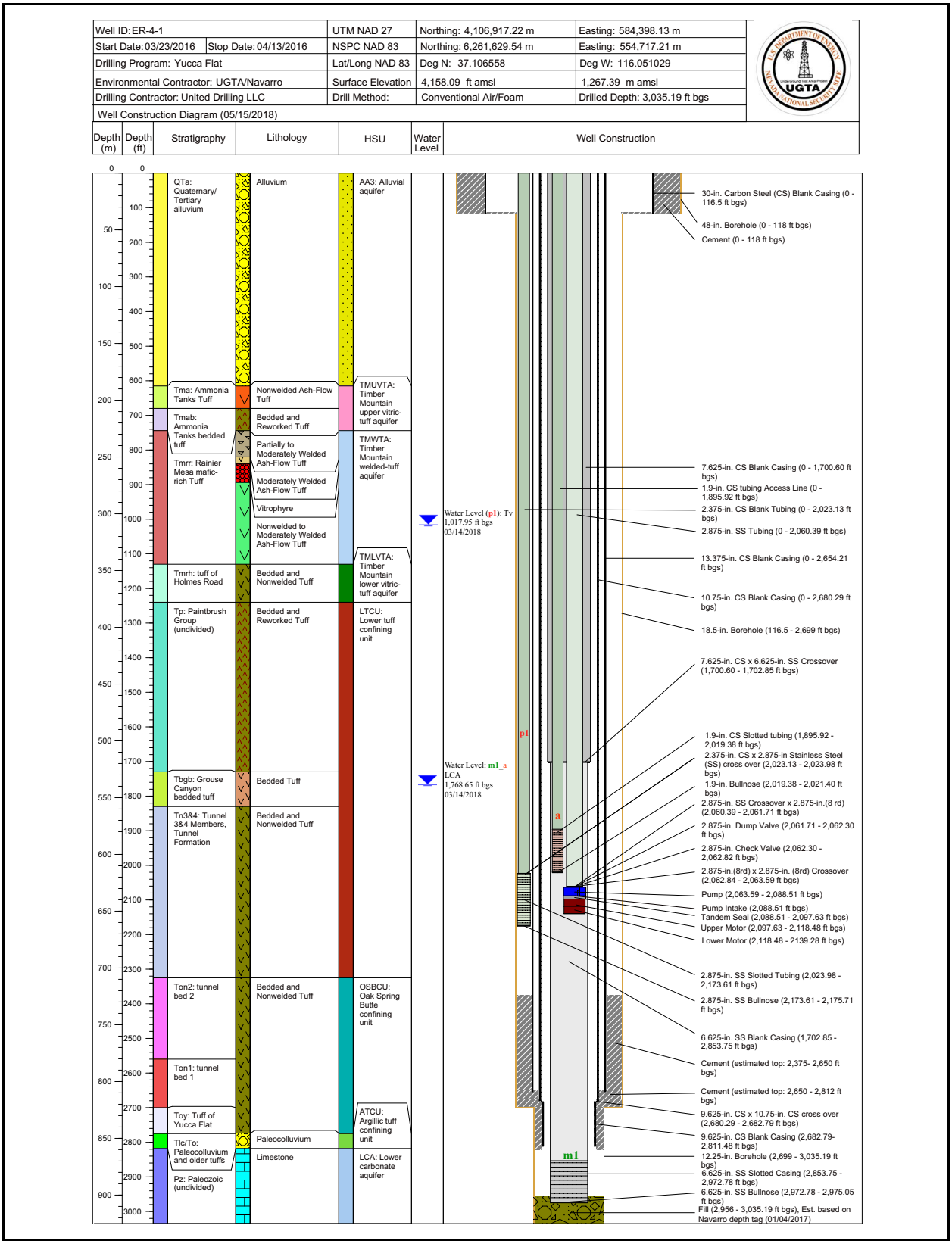

Figure A-3
Well Completion Diagram for ER-4-1

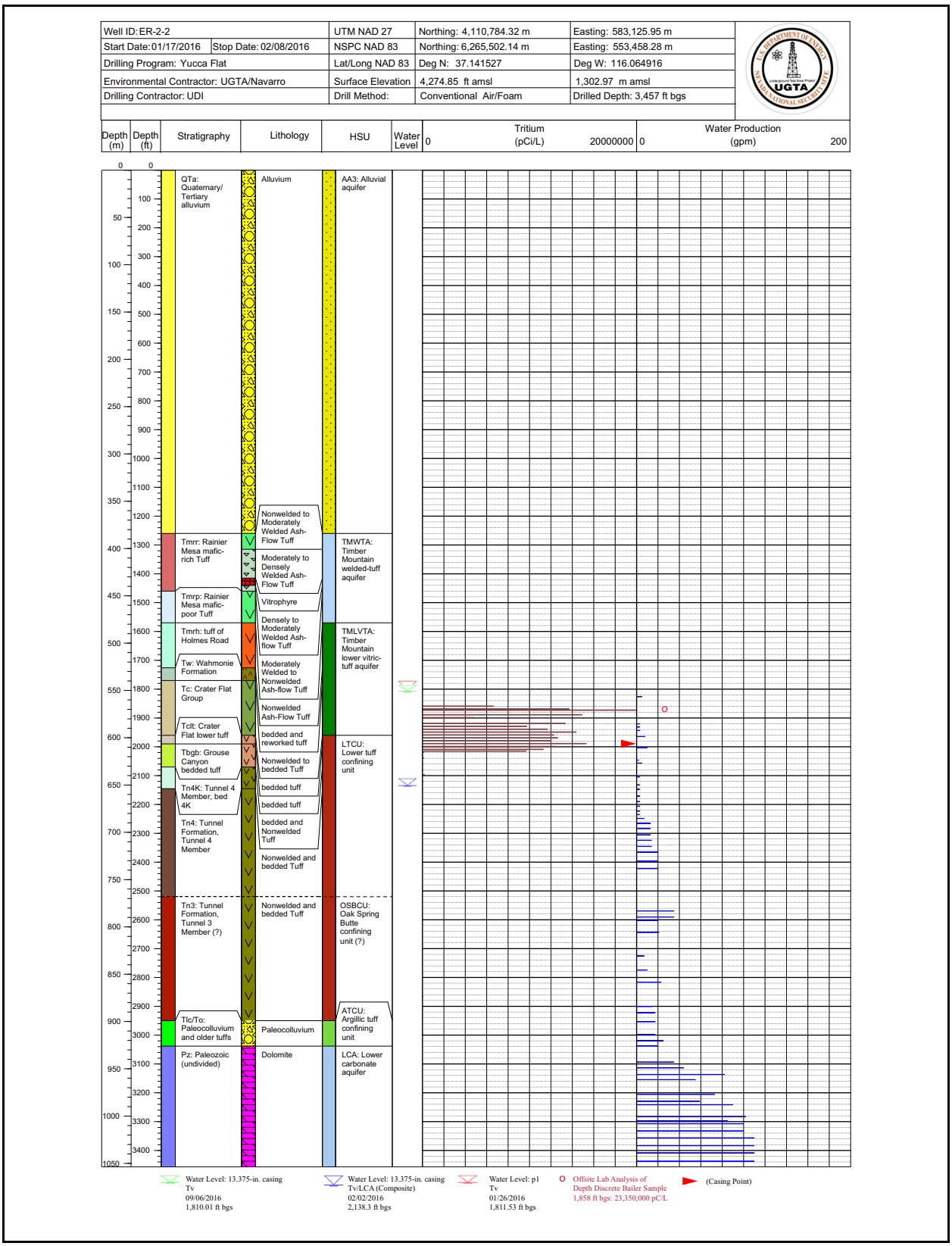

Figure A-4
Water Production and Tritium Log for ER-2-2

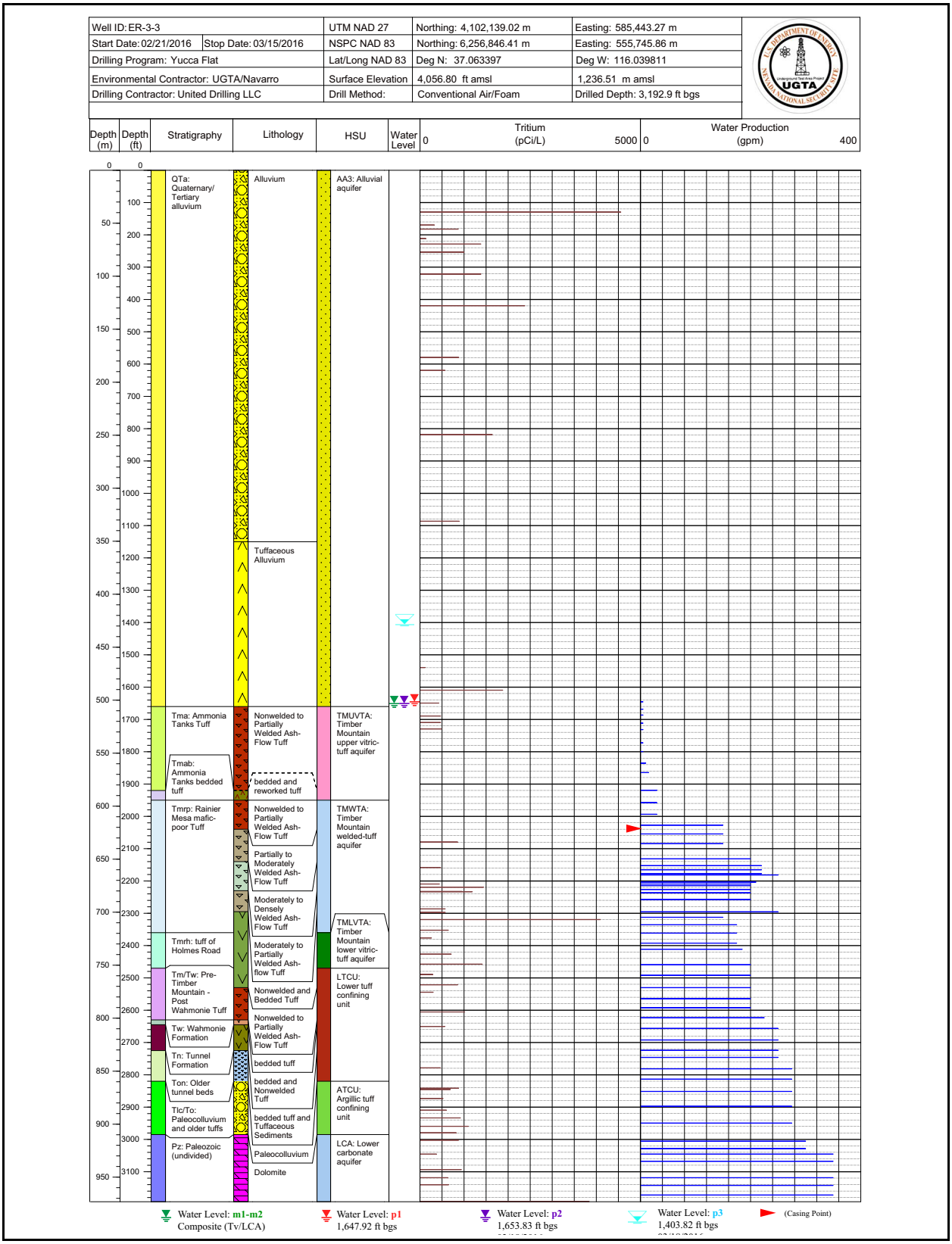

Figure A-5
Water Production and Tritium Log for ER-3-3

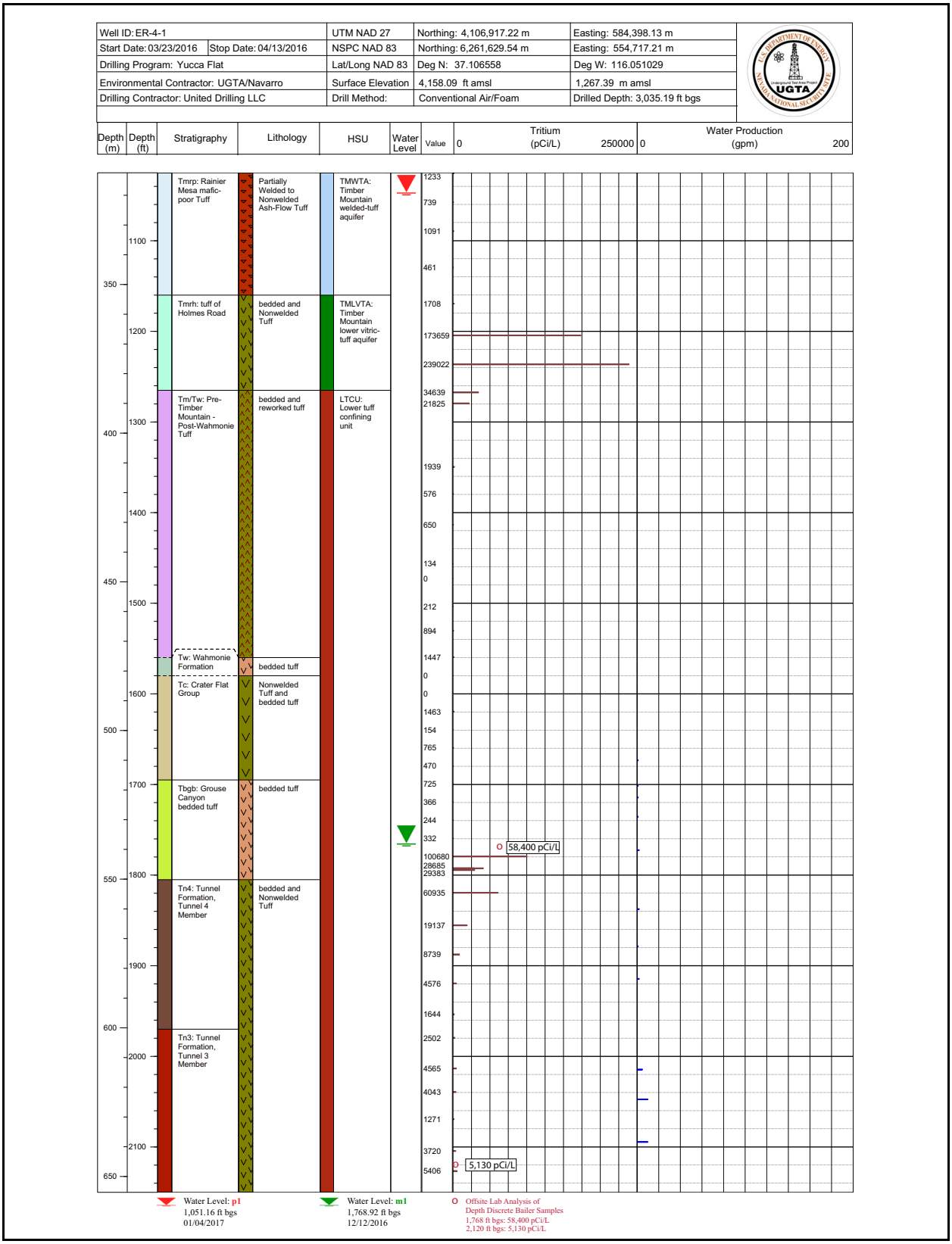

Figure A-6
Water Production and Tritium Log for ER-4-1 (TMWTA, TMLVTA, LTCU)

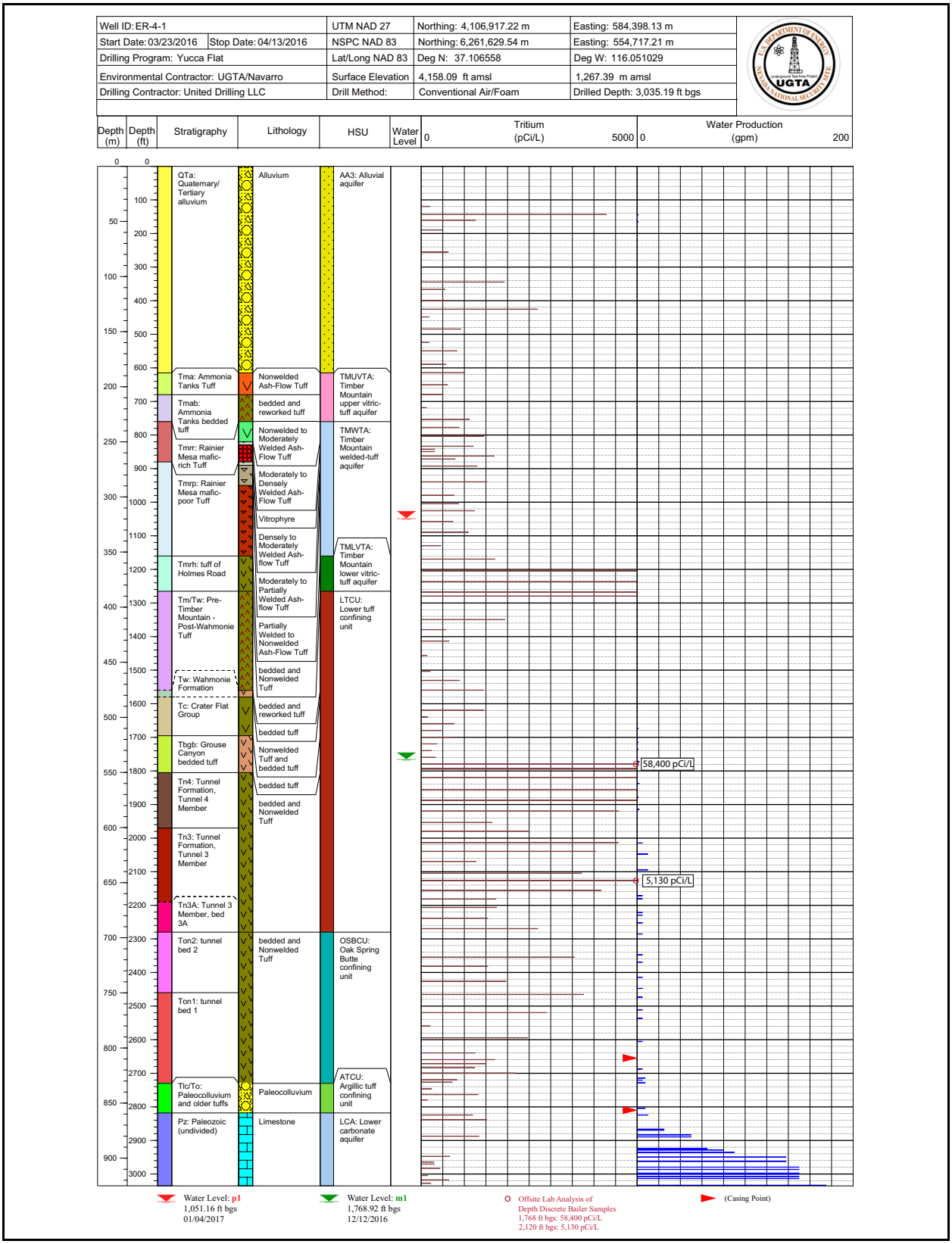

Figure A-7
Water Production and Tritium Log for ER-4-1

Appendix B

Nevada Division of Environmental Protection Comments

(9 Pages)

NEVADA ENVIRONMENTAL MANAGEMENT OPERATIONS ACTIVITY
DOCUMENT REVIEW SHEET

1. Document Title/Number: Model Evaluation Report for Corrective Action Unit 97: Yucca Flat/Climax Mine, Nevada National Security Site, Nye County, Nevada	2. Document Date: May 2019
3. Revision Number: 0	4. Originator/Organization: Navarro
5. Responsible EM Nevada Program Activity Lead: John Myers	6. Date Comments Due: July 8, 2019
7. Review Criteria:	
8. Reviewer/Organization Phone No.: Nevada Division of Environmental Protection	9. Reviewer's Signature:

10. Comment Number/Location		11. Type[a]	12. Comment	13. Comment Response
1.	Page 1-7, Section 1.2, Second Paragraph, First Sentence		"Most of the key LCA…" Please clarify which model uncertainties were addressed that were identified from the sensitivity analysis. How were the rest of the uncertainties identified?	Much of this discussion was deleted and reference to Kwicklis (2016) added. The use of the elicitation to identify and rank model uncertainties in order of importance based on their potential impact on the CB (Kwicklis, 2016) is already presented in Section 1.1. The final paragraph in Section 1.2 now reads as follows: "… As a result, the model evaluation activities described in the CADD/CAP (DOE/EMNV, 2017d) focused on addressing key uncertainties in the LCA models, with uncertainties associated with the UZ and SZ AA/VA models viewed as insignificant from the perspective of defining the CB (Kwicklis, 2016). Therefore, in this MER, emphasis is placed on identifying the subset of the original 747 detonations in the YF/CM CAU that are deep enough to potentially intersect the saturated LCA. It was also intended that model evaluation targets would address model uncertainties that led to conservative assumptions made in the N-I (2013) LCA models that resulted in forecasts of contamination that were far more extensive than current data on groundwater contamination in Yucca Flat would indicate is possible."

[a]Comment Types: M = Mandatory, S = Suggested.
Return Document Review Sheets to Environmental Management Nevada Program Operations Activity, Attn: QAC, M/S NSF 505

NEVADA ENVIRONMENTAL MANAGEMENT OPERATIONS ACTIVITY
DOCUMENT REVIEW SHEET

1. Document Title/Number: Model Evaluation Report for Corrective Action Unit 97: Yucca Flat/Climax Mine, Nevada National Security Site, Nye County, Nevada	2. Document Date: May 2019
3. Revision Number: 0	4. Originator/Organization: Navarro
5. Responsible EM Nevada Program Activity Lead: John Myers	6. Date Comments Due: July 8, 2019
7. Review Criteria:	
8. Reviewer/Organization Phone No.: Nevada Division of Environmental Protection	9. Reviewer's Signature:

10. Comment Number/Location		11. Type[a]	12. Comment	13. Comment Response
2.	Page 2-4, Section 2.1, First Full Paragraph		a. First Sentence: Why was the location for well ER-6-1-2 impractical? Why was well ER-6-1-1 substituted? Please explain in the text. b. Second Sentence: Was there any expected different result from the change in sampling well ER-6-1-1? c. Third Sentence: Why, or how, was it determined well UE-1r does not provide a representative LCA groundwater sample? Is the fourth sentence the reason?	a. Text was revised to read: "Although ER-6-1-2 was the well planned for sampling in the CADD/CAP (DOE/EMNV, 2017d), ER-6-1-1 was sampled instead. ER-6-1-1 and ER-6-1-2 are expected to sample equivalent LCA waters because they are located 167 ft from each other; both sample the LCA and are positioned in rough alignment with the dominant local fracture orientation (SNJV, 2005a). ER-6-1-1 has 300 ft open to the LCA versus the much longer 1,300 ft open in ER-6-1-2; thus, the volume of wellbore open to LCA in ER-6-1-1 is much smaller than that in ER-6-1-2. Sampling was conducted using a low-flow jack pump; hence, it was more practical to purge this well rather than ER-6-1-2 using this pump." b. See response to 2a. above. c. Paragraph was revised to read: "Well UE-1r, also planned for sampling, was not sampled in support of model evaluation because the water sampled from this well is not representative of LCA groundwater. This is because the Timber Mountain welded-tuff aquifer (TMWTA) and Timber Mountain lower vitric-tuff aquifer (TMLVTA) are thought to preferentially provide the majority of the groundwater production at this well. In addition, an obstruction inhibiting access to the LCA was observed."
3.	Page 2-4, Section 2.1.1, First Paragraph, Third Sentence		What additional results are reported in the UGTA Chemistry Database?	Sentence was revised to read: "Results for the remaining analyses listed in Table 2-2 are reported in the UGTA Chemistry Database (Navarro, 2019a)."

[a]Comment Types: M = Mandatory, S = Suggested.
Return Document Review Sheets to Environmental Management Nevada Program Operations Activity, Attn: QAC, M/S NSF 505

NEVADA ENVIRONMENTAL MANAGEMENT OPERATIONS ACTIVITY
DOCUMENT REVIEW SHEET

1. Document Title/Number: Model Evaluation Report for Corrective Action Unit 97: Yucca Flat/Climax Mine, Nevada National Security Site, Nye County, Nevada	2. Document Date: May 2019
3. Revision Number: 0	4. Originator/Organization: Navarro
5. Responsible EM Nevada Program Activity Lead: John Myers	6. Date Comments Due: July 8, 2019
7. Review Criteria:	
8. Reviewer/Organization Phone No.: Nevada Division of Environmental Protection	9. Reviewer's Signature:

	10. Comment Number/Location	11. Type[a]	12. Comment	13. Comment Response
4.	Page 2-10, Section 2.1.2, Fourth Paragraph, First Sentence		The sampling of WW-2 is not discussed in the following paragraph as wells TW-D and UE-1q are.	Fourth sentence was revised to read: "WW-2 was sampled monthly to biannually from 1973 to 2006."
5.	Page 2-11, Section 2.1.2, First Paragraph, Last Two Sentences		Why is it unlikely the ^{3}H will be detected once in a sample but not in subsequent samples from the same well? What defines "mostly" positive values or trends in concentrations?	Sentence was revised to read: "Groundwater contamination is suspected primarily when trends in the ^{3}H concentrations are observed as opposed to sporadic detections that are not repeated in subsequent samples from the same location."
6.	Page 2-11, Section 2.1.2, Second Paragraph, First Sentence		The discussion of well UE-10j seems to be randomly included in this Section as it is not mentioned in any previous paragraph in this Section.	Section 2.1.2 summarizes (or references the section where summarized) the historical results for all LCA completions sampled. UE-10j was not routinely monitored, so it was not described in the previous paragraph. First sentence was revised to read: "UE-10j was previously sampled only in 1993."
7.	Page 2-18, Section 2.2.1, First Paragraph, Fourth Sentence		What determines what "occasion" select discharge samples are also sent to the laboratory?	Sentence was revised to read: "Select discharge samples are also sent to the laboratory if a lower detection limit is desired or to verify an onsite result."
8.	Page 2-21, Section 2.2.3, Second Paragraph, Second Sentence		How is it known that "The majority of the ^{3}H spikes…are likely analytical noise and not actual ^{3}H detections?"	Text was revised to read: "The majority of the ^{3}H spikes shown in Figure A-5, including the 4,558-pCi/L result, are analytical noise and not actual ^{3}H detections because most reported values are near or below the MDC. The MDCs ranged from 1,168 to 10,047 pCi/L, with an average of 1,860 pCi/L. The 4,558-pCi/L result was below the associated 10,047-pCi/L MDC and therefore represents analytical noise instead of an actual detection."
9.	Page 2-26, Section 2.2.6, Second Paragraph, Last Sentence		Why were the ^{3}H sample results attributed to analytical noise and not actual ^{3}H detections?	Added the following at the end of the sentence: "… because most, including the 4,558-pCi/L result, were below the MDC."

[a]Comment Types: M = Mandatory, S = Suggested.
Return Document Review Sheets to Environmental Management Nevada Program Operations Activity, Attn: QAC, M/S NSF 505

NEVADA ENVIRONMENTAL MANAGEMENT OPERATIONS ACTIVITY
DOCUMENT REVIEW SHEET

1. Document Title/Number: Model Evaluation Report for Corrective Action Unit 97: Yucca Flat/Climax Mine, Nevada National Security Site, Nye County, Nevada	2. Document Date: May 2019
3. Revision Number: 0	4. Originator/Organization: Navarro
5. Responsible EM Nevada Program Activity Lead: John Myers	6. Date Comments Due: July 8, 2019
7. Review Criteria:	
8. Reviewer/Organization Phone No.: Nevada Division of Environmental Protection	9. Reviewer's Signature:

10. Comment Number/Location		11. Type[a]	12. Comment	13. Comment Response
10	Page 2-26, Section 2.2.6, Third Paragraph, First Sentence		Why are the estimated LCA transmissivities of 8 and 9 ft^2/day not discussed in this paragraph?	The following sentence was added: "Unfortunately, the LCA at ER-2-2 is inaccessible because the wellbore was plugged (Section 2.2.2), and the ER-3-3 WDT results were not reliable because of poor hole conditions (Navarro, 2018). Therefore, the transmissivities calculated using drilling data (9 and 8 ft^2/day, respectively) could not be compared to WDT results at ER-2-2 and ER-3-3."
11	Page 2-31, Section 2.3.4, Third Paragraph, First Sentence		This sentence seems contradictory to the material presented in the paragraph above it and in this paragraph. Please clarify.	Sentence was revised to read: "This is the first time ^3H has been detected in U-3cn-5 samples in more than four decades, although sporadic ^3H detections have been reported historically in samples collected from this well (Figure 2-11)."
12	Page 2-33, Section 2.3.4, First Partial Paragraph		What is the conclusion of the data presented in this paragraph for the hydraulic test conducted in U-3cn PS 2?	Added the following sentence: "These U-3cn PS 2 results indicate initial ^3H contamination (2E+08 and 3E+08 pCi/L) within a lateral distance of 2.5R_C of the BILBY WP, which is located approximately 150 m (2.2R_c) above the LCA." Note: This is significant because in the next paragraph, it is explained that similar ^3H concentrations were observed in the tuffs at U-3cn-5 but (with the exception of some early samples) not in the samples collected from the LCA. As stated in the final paragraph, these results indicate that the groundwater at this location is effectively isolated from the highly contaminated groundwater in the overlying tuff that constitutes the BILBY near-field.

[a]Comment Types: M = Mandatory, S = Suggested.
Return Document Review Sheets to Environmental Management Nevada Program Operations Activity, Attn: QAC, M/S NSF 505

NEVADA ENVIRONMENTAL MANAGEMENT OPERATIONS ACTIVITY
DOCUMENT REVIEW SHEET

1. Document Title/Number: Model Evaluation Report for Corrective Action Unit 97: Yucca Flat/Climax Mine, Nevada National Security Site, Nye County, Nevada	2. Document Date: May 2019
3. Revision Number: 0	4. Originator/Organization: Navarro
5. Responsible EM Nevada Program Activity Lead: John Myers	6. Date Comments Due: July 8, 2019
7. Review Criteria:	
8. Reviewer/Organization Phone No.: Nevada Division of Environmental Protection	9. Reviewer's Signature:

10. Comment Number/Location		11. Type[a]	12. Comment	13. Comment Response
13	Page 2-33, Section 2.3.4, Second Paragraph, Seventh Sentence		Why does the low volume of groundwater removed from the said interval suggest that the likely source of ^{3}H in the samples is from the more shallow intervals?	The following text seems to only add confusion and was therefore deleted: "The low volume of groundwater removed from this interval suggests that the likely source of ^{3}H in these samples is from the more shallow intervals. Once pumped, the ^{3}H reduced below the MDCs. In fact, …" The next sentence was revised to read: "Tritium was detected only in the first three samples collected while pumping the 863- to 922-m interval; all subsequent samples were below the 1.5E+03-pCi/L MDC."

[a]Comment Types: M = Mandatory, S = Suggested.
Return Document Review Sheets to Environmental Management Nevada Program Operations Activity, Attn: QAC, M/S NSF 505

NEVADA ENVIRONMENTAL MANAGEMENT OPERATIONS ACTIVITY
DOCUMENT REVIEW SHEET

1. Document Title/Number: Model Evaluation Report for Corrective Action Unit 97: Yucca Flat/Climax Mine, Nevada National Security Site, Nye County, Nevada	2. Document Date: May 2019
3. Revision Number: 0	4. Originator/Organization: Navarro
5. Responsible EM Nevada Program Activity Lead: John Myers	6. Date Comments Due: July 8, 2019
7. Review Criteria:	
8. Reviewer/Organization Phone No.: Nevada Division of Environmental Protection	9. Reviewer's Signature:

10. Comment Number/Location		11. Type[a]	12. Comment	13. Comment Response
14	Page 2-87, Section 2.8.1		This sentence/paragraph does not fully explain how the uncertainty was estimated. Please expand the explanation.	Paragraph was revised to read: "In order to estimate the uncertainty in the top of the LCA (as defined in the YF/CM HFM [BN, 2006]), 100 LCA surfaces were generated using the least tension method within EarthVision (Dynamic Graphics, 2015) for interpolation of available drillhole (including the model evaluation wells), outcrop, and partial penetration data. Each surface was developed using all known LCA surface elevations from drillholes, and from outcrop data and 90 percent of the partial penetration data within a given fault block. The partial penetration data for each surface were randomly sampled, thus resulting in variability in the 100 surfaces. This method (cross-validation method), whereby locations of the surface are predicted after randomly or systematically removing a percentage of data from a population, is considered one of the simplest and most widely used method for estimating prediction error (Hastie et al., 2008). The variability over these surfaces at detonation locations ranges from 0 to about 360 m, with 50 percent of the detonation locations having less than 20 m of vertical variability. Fewer than 4 percent of the detonation locations have more than 200 m of variability."
15	Page 3-12, Section 3.4.1		What new information about the LCA hydraulic properties were gathered from the ER-6-1 MWAT re-analysis? Please include this information.	Changed last sentence on page 3-12 to read: "The basin flux estimates obtained from the DV3 model calibrated using ER-6-1-2 MWAT data and associated uncertainty analysis (Section 2.6) provided additional constraints on hydraulic properties. Data presented in this section were used as observations to condition the hydraulic property field using pilot points in the revised LCA CAU model calibration (see Section 4.2.3)."

[a]Comment Types: M = Mandatory, S = Suggested.
Return Document Review Sheets to Environmental Management Nevada Program Operations Activity, Attn: QAC, M/S NSF 505

NEVADA ENVIRONMENTAL MANAGEMENT OPERATIONS ACTIVITY
DOCUMENT REVIEW SHEET

1. Document Title/Number: Model Evaluation Report for Corrective Action Unit 97: Yucca Flat/Climax Mine, Nevada National Security Site, Nye County, Nevada	2. Document Date: May 2019
3. Revision Number: 0	4. Originator/Organization: Navarro
5. Responsible EM Nevada Program Activity Lead: John Myers	6. Date Comments Due: July 8, 2019
7. Review Criteria:	
8. Reviewer/Organization Phone No.: Nevada Division of Environmental Protection	9. Reviewer's Signature:

10. Comment Number/Location		11. Type[a]	12. Comment	13. Comment Response
16	Page 3-21, Section 3.8, Second Paragraph, Second Sentence		What makes these findings "Key Findings?"	Sentence was revised from "Table 3-5 summarizes the results. Key summary findings are as follows:" to "Table 3-5 summarizes the model evaluation targets and their resolution. The following summarizes the primary model improvements resulting from model evaluation activities:"
17	Page 3-22, Table 3-5, **Resolution** for "Extent of RN contamination in the LCA" **Model Evaluation Target**		Please provide a "conclusion" or "result" for the evaluation that was performed as is done for the other targets.	Added the following bullet: "Transport results were more consistent with contaminant observations, increasing confidence in the revised models."
18	Page 4-12, Section 4.2.3.3.2, Second Paragraph, Last Sentence		Please provide a reference for the "final version of the DV3 model."	An ROTC will be completed with the reference for the final version once this USGS document has completed the formal review process and is finalized. In addition, this ROTC will include the final reference for the report *Estimation of Groundwater Flow through Yucca Flat Based on Analysis of a Multiple-Well Aquifer Test at Well ER-6-1-2 Main, Nevada National Security Site.* This report cannot be finalized until the DV3 report is finalized.
19	Page 4-24, Section 4.2.5.1, Second Paragraph, Second Sentence		Please remove the "a" between "…to the initial" and "steady-state head…"	Revised as suggested.

[a]Comment Types: M = Mandatory, S = Suggested.
Return Document Review Sheets to Environmental Management Nevada Program Operations Activity, Attn: QAC, M/S NSF 505

NEVADA ENVIRONMENTAL MANAGEMENT OPERATIONS ACTIVITY
DOCUMENT REVIEW SHEET

1. Document Title/Number: Model Evaluation Report for Corrective Action Unit 97: Yucca Flat/Climax Mine, Nevada National Security Site, Nye County, Nevada	2. Document Date: May 2019
3. Revision Number: 0	4. Originator/Organization: Navarro
5. Responsible EM Nevada Program Activity Lead: John Myers	6. Date Comments Due: July 8, 2019
7. Review Criteria:	
8. Reviewer/Organization Phone No.: Nevada Division of Environmental Protection	9. Reviewer's Signature:

10. Comment Number/Location		11. Type[a]	12. Comment	13. Comment Response
20	Page 4-102, Section 4.7.3.6, Second Sentence		Because it is referenced in this paragraph and others in the document, what was the comment by the external peer review panel that resulted in the revised distribution for Pu?	This external peer review comment was first mentioned in the last sentence of the first paragraph on page 4-92. This sentence was revised to read: "The model evaluation transport runs used a revised (decreased) K_d distribution for Pu that was developed in response to a comment by the external peer review panel that the values used for Pu retardation may be too high (see Section 2.5.1 and Table 2-10 of Navarro, 2016b)." To make it clear that the same peer review comment is referred to in the second paragraph on Page 4-92 and Sections 4.7.3.6 and 4.7.3.7 on Page 102, the following revisions were made: • Sentence on Page 4-92 (second paragraph) was revised to read: "This revised distribution for Pu was developed in response to the external peer review panel comment (see Section 2.5.1 and Table 2-10 of Navarro, 2016b)." • Sentence on Page 4-102 (Section 4.7.3.6) was revised to read: "This revised distribution for Pu was developed in response to the external peer review panel comment (see Section 2.5.1 and Table 2-10 of Navarro, 2016b)." • Sentence on Page 4-102 (Section 4.7.3.7) was revised to read: "The model evaluation transport runs used a revised (decreased) K_d distribution for Pu that was developed in response to the external peer review panel comment (see Section 2.5.1 and Table 2-10 of Navarro, 2016b)."

[a]Comment Types: M = Mandatory, S = Suggested.
Return Document Review Sheets to Environmental Management Nevada Program Operations Activity, Attn: QAC, M/S NSF 505

NEVADA ENVIRONMENTAL MANAGEMENT OPERATIONS ACTIVITY
DOCUMENT REVIEW SHEET

1. Document Title/Number: Model Evaluation Report for Corrective Action Unit 97: Yucca Flat/Climax Mine, Nevada National Security Site, Nye County, Nevada	2. Document Date: May 2019
3. Revision Number: 0	4. Originator/Organization: Navarro
5. Responsible EM Nevada Program Activity Lead: John Myers	6. Date Comments Due: July 8, 2019
7. Review Criteria:	
8. Reviewer/Organization Phone No.: Nevada Division of Environmental Protection	9. Reviewer's Signature:

	10. Comment Number/Location	11. Type[a]	12. Comment	13. Comment Response
21	Page 4-127, Section 4.8, Last Paragraph, Last Sentence		The complete regulatory boundary objective is not proved. Please correct the statement.	Sentence was revised to read: "The current models indicate that the YF/CM CAU is likely to meet its regulatory boundary objective, which is to verify that RN contamination from the YF/CM CAU is contained within the Yucca Flat basin, thus not impacting the Frenchman Flat LCA or downgradient receptors."
22	Page 5-4, Section 5.3, First Paragraph, First Sentence		The complete regulatory boundary objective is not proved. Please correct the statement.	The first two sentences were revised to read: "The Model Evaluation Team maintains that sufficient confidence now exists in these models that they can be used to support regulatory decisions. These decisions include developing a monitoring well network; identifying use restriction boundaries; and complying with the regulatory boundary objective to verify that RN contamination from the YF/CM CAU is contained within the Yucca Flat basin, thus not impacting the Frenchman Flat LCA or downgradient receptors."
Comments added as a result of Navarro final quality assurance review:				
23	Page 2-26, Section 2.2.6, Second Paragraph, First Sentence		^{3}H values reported for ER-2-2 should be 23,400,000 and 23,300,000 pCi/L	Text was revised to correct these values to 23,400,000 and 23,300,000 pCi/L.
24	Page 2-102, Section 2.9.3, First Paragraph, Seventh Sentence		Well name should be U-7ba PS 1AS instead of U-7ba PS AS.	Well name was corrected to U-7ba PS 1AS.
25	Page 2-102, Section 2.9.3, Fourth Paragraph, First Sentence		Well name should be U-7ba PS 1AS instead of U-7ba PS AS.	Well name was corrected to U-7ba PS 1AS.

[a]Comment Types: M = Mandatory, S = Suggested.
Return Document Review Sheets to Environmental Management Nevada Program Operations Activity, Attn: QAC, M/S NSF 505

DISTRIBUTION

	Copies
John Myers Environmental Management Nevada Program P.O. Box 98518, M/S 505 Las Vegas, NV 89193-8518	1 hard copy w/electronic media
Bill R. Wilborn Environmental Management Nevada Program P.O. Box 98518, M/S 505 Las Vegas, NV 89193-8518	UGTA website
Chris Andres State of Nevada Nevada Division of Environmental Protection 2030 E. Flamingo Road, Suite 230 Las Vegas, NV 89119-0818	1 hard copy w/electronic media
Mark McLane State of Nevada Nevada Division of Environmental Protection 2030 E. Flamingo Road, Suite 230 Las Vegas, NV 89119-0818	1 hard copy w/electronic media
Elizabeth Jacobson State of Nevada Nevada Division of Environmental Protection 2030 E. Flamingo Road, Suite 230 Las Vegas, NV 89119-0818	NDEP File Exchange
Andrew Tompson Lawrence Livermore National Laboratory 7000 East Avenue, L-286 Livermore, CA 94550-9909	UGTA website
Mavrik Zavarin Lawrence Livermore National Laboratory 7000 East Avenue, L-231 Livermore, CA 94550-9909	UGTA website

	Copies
Edward Kwicklis Los Alamos National Laboratory Hydrology, Geochemistry, and Geology Group, EES-6 Earth and Environmental Sciences Division SM-30 Bikini Atoll Rd., MS T003 Los Alamos, NM 87545	UGTA website
S. Michelle Bourret Los Alamos National Laboratory Hydrology, Geochemistry, and Geology Group, EES-6 Earth and Environmental Sciences Division SM-30 Bikini Atoll Rd., MS T003 Los Alamos, NM 87545	UGTA website
Ken Ortego Mission Support and Test Services, LLC P.O. Box 98521, M/S NLV 082 Las Vegas, NV 89193-8521	UGTA website
Charles E. Russell Desert Research Institute 755 E. Flamingo Las Vegas, NV 89119	UGTA website
Karl Pohlmann Desert Research Institute 755 E. Flamingo Las Vegas, NV 89119	UGTA website
Jeff Sanders U.S. Geological Survey Water Resources Division 160 North Stephanie Street Henderson, NV 89074	UGTA website
Rebecca Frus U.S. Geological Survey Water Resources Division 160 North Stephanie Street Henderson, NV 89074	UGTA website

	Copies
Ken Rehfeldt Navarro P.O. Box 98952, NSF 167 Las Vegas, NV 89193-8518	UGTA website
Brian Haight Navarro P.O. Box 98952, NSF 167 Las Vegas, NV 89193-8518	UGTA website
Sharad Kelkar Navarro P.O. Box 98952, NSF 167 Las Vegas, NV 89193-8518	UGTA website
Irene Farnham Navarro P.O. Box 98952, NSF 167 Las Vegas, NV 89193-8518	UGTA website
Peter Martian Navarro P.O. Box 98952, NSF 167 Las Vegas, NV 89193-8518	UGTA website
Tim deBues Navarro P.O. Box 98952, NSF 167 Las Vegas, NV 89193-8518	UGTA website
Jeffrey Wurtz Navarro P.O. Box 98952, NSF 167 Las Vegas, NV 89193-8518	UGTA website
Environmental Management Records Environmental Management Nevada Program P.O. Box 98518, M/S 505 Las Vegas, NV 89193-8518	1 hard copy w/electronic media

	Copies
Navarro Central Files P.O. Box 98952, NSF 156 Las Vegas, NV 89193-8518	1 hard copy w/electronic media
U.S. Department of Energy Office of Scientific and Technical Information P.O. Box 62 Oak Ridge, TN 37831-0062	1 electronic copy
Southern Nevada Public Reading Facility c/o Nuclear Testing Archive P.O. Box 98521, M/S 400 Las Vegas, NV 89193-8521	2 electronic copies
Manager, Northern Nevada FFACO Public Reading Facility c/o Nevada State Library & Archives 100 N. Stewart Street Carson City, NV 89701-4285	1 electronic copy